

6601306

SUBJ
GEOL
ACIAn Analysis of the Cooling of Intrusives by Ground-Water
Convection which Includes Boiling

L. M. CATHLES

Abstract

A finite difference model of the cooling of an igneous intrusive of limited volume is developed and used to investigate the relation between igneous intrusion, the formation of liquid and vapor dominated geothermal systems, and the formation of porphyry-type ore deposits. The model takes into account the properties of pure water and accommodates the phenomena of boiling and condensation. Permeability, level of intrusion, and pluton volume are systematically varied. Pressure, temperature, and fluid velocity are computed as functions of time.

It is found that a self-supported, vapor dominated steam zone is commonly (but briefly) formed above the intrusive. Condensed water bounds the steam zone above, and if the hydrothermal solutions are saline, a zone of boiling bounds the steam zone below. For pure water condensation is far more important than boiling—the solutions circulate around the critical point of water to become gaseous without boiling. Despite large temperature variations, convection causes fluid pressures throughout the whole uniform permeability system to be close to normal cold-water hydrostatic values. Thus, even in an active convecting system with moderate permeability variations, fluid pressure will tend toward normal hydrostatic values. Fluid circulation appears easily sufficient to produce a typical porphyry copper ore shell, but base metal precipitation probably must be controlled by mechanisms other than simple temperature drop.

Introduction

At the present time considerable effort is being directed toward exploitation of geothermal resources. Geothermal systems are thought to be associated somehow with magmatic intrusion. There has been considerable, highly illuminating modeling of geothermal systems such as Wairakei. However the modeling done to this point ignores the geometric details of the causative intrusive (which are usually poorly known), taking as a starting point a hot surface at depth (Mercer et al., 1975; Elder, 1965, 1966; Donaldson 1962). The temperature of the surface is steadily maintained so the models are steady state and do not evolve with time by themselves, although Mercer et al. have considered transient effects attending man's exploitation of the Wairakei geothermal area.

Geothermal systems have been classified as "vapor or liquid dominated" (White et al., 1971) and geologic examples of both types have been documented. Although it is generally felt an intrusive system may evolve from vapor dominated to wet in some cases, this intuition has not been refined into a formal model.

Finally there has been considerable discussion of the relation between mineral deposits (particularly porphyry copper deposits but also some nickel deposits) and intrusives, and the role ground-water

convection may play in the alteration of certain intrusives and in the localization of ore near those intrusives (Sheppard et al., 1971; Norton, 1972; Cheney, 1974; Fyfe and Henley, 1973; Henley, 1973; Phillips, 1973; Whitney, 1975). Further quantification of these ideas may be possible.

Consideration of how an igneous pluton of limited volume may be expected to cool through conduction and ground-water convection provides useful insight into the relation between igneous intrusion, the formation of liquid and vapor dominated geothermal systems, and the formation of porphyry-type ore deposits. The main purpose of this paper is to present the results of model computations that bear on these connections.

The model developed accounts for convective cooling of the pluton by ground-water convection, takes into account the properties of (pure) water, and accounts for the thermal effects of fluid boiling and condensation. These factors are all shown to be important if the cooling history of an igneous intrusion is to be realistically estimated; of course boiling is vital to the investigation of the relation of vapor dominated and wet geothermal systems. The pluton is of limited dimensions, so the system evolves with time in a quasi-steady-state fashion until the initial thermal anomaly is erased.

The pluton is considered to intrude suddenly (at 700°C) into a water-saturated, fractured formation

of uniform permeability and normal geothermal gradient. The pluton permeability is taken to be the same as the intruded formation from the start. No consideration is given as to how fractures develop in the intrusive (a problem considered by Lister, 1974) or of how magmatic water of high salinity may exolve from the pluton (a problem elegantly considered by Whitney, 1975). Our focus is entirely on those convective processes that will occur after the pluton has developed throughgoing fractures and thus is permeable. The cases presented are deliberately kept as simple as possible so that fundamental features are clearly revealed. Complications can be added "in the mind's eye" once the general features are understood.

The model gas reservoirs are self-supported in the sense that cooler surrounding water will not cause them to collapse (Elder, 1966, p. 36 ff). "Steaming ground" may exist at shallow depths above the overlying condensed (water) zone. No account is taken of steaming ground phenomena, whose main effect would be to increase drastically the effective thermal conductivity of the region above the steaming ground water table. This deficiency is unimportant when free flow out the top surface (hot-spring activity) is permitted. The gas pressures of the model steam reservoirs closely follow the normal hydrostatic gradient and are therefore (at depths >500 m) substantially greater than the 32 to 38 bars observed by White et al. (1971) at depths up to 3,000 m at Geysers, California. Geysers is probably a steaming ground situation of perhaps unusual depth extent (otherwise a cold water head would have collapsed the vapor system as Elder has argued).

The greatest defect in the models presented is the assumption of constant salinity. Magmatic waters exolving from the intrusive can have salinities of 3 to 4 wt percent or greater (Whitney, 1975; Kilinc and Burnham, 1972). This salinity anomaly will be dispersed by the convective flow of water through the intrusive in a manner similar to the convective dispersal of the heat anomaly associated with the pluton. By extending the critical curve, salinity permits boiling at greater depths. Salinity strongly affects the ability of hydrothermal solutions to carry minerals. A proper account of geothermal systems and mineral deposition phenomena must include the effects of salinity on boiling and the dispersal of initially high magmatic salinities by fluid convection. The salinity problem is not directly treated in this paper, although insight as to its effects is gained from the calculations presented and their discussion.

In the next section the theoretical foundations necessary to describe convection of pure water (including boiling) in a fractured rock environment are given. Account is taken of the temperature and

pressure dependence of viscosity, density, and enthalpy. The resulting mass, momentum, and energy balance equation are solved by standard finite difference methods (Alternating Direction Implicit) on a computer. In following sections several "heuristic" calculations of geological interest are presented and discussed.

Mathematical Formulation and Method of Solution¹

The mathematical formulation and methods of solution are similar to those published previously by others. Only a brief, general review will be given.

Basically the model simply conserves mass, momentum, and energy:

$$\nabla \cdot \underline{q} = 0 \quad \text{mass balance} \quad (1)$$

$$\nabla \cdot \frac{\nu}{k'} \nabla \psi_x - g_0 \frac{\partial \rho}{\partial y} = 0 \quad \text{momentum balance} \quad (2)$$

$$\rho_m (R + c_m) \frac{\partial T}{\partial t} = A - \nabla \cdot \underline{q} \gamma T + K_m \nabla^2 T \quad \text{energy balance} \quad (3)$$

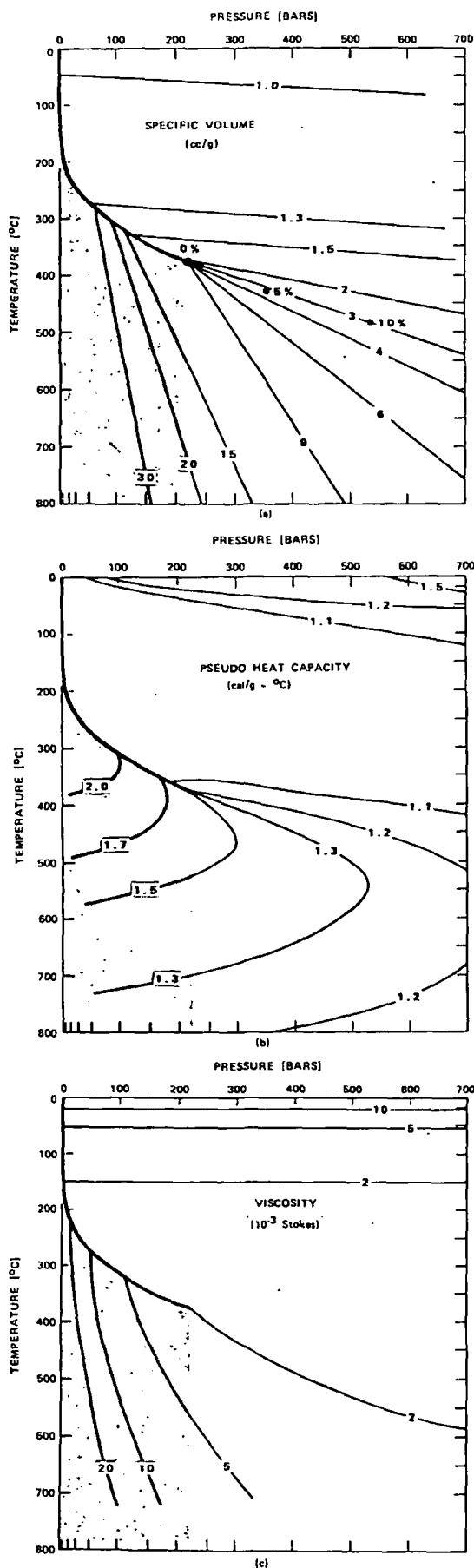
In addition, fluid pressure is given everywhere by the integral of Darcy's Law:

$$p(z) = p_s + g_0 \int_z^s \rho dz + \int_z^s \frac{\nu}{k'} q_x dz \quad (4)$$

The only new feature is that the fluid properties of density, ρ , viscosity, ν , and pseudoheat capacity, γ , are treated as functions of pressure and temperature and looked up in tables appropriate for pure water (see Fig. 1). Values of pressure and temperature halfway through any particular computational time-step are used.

This methodology allows us to account for the unusual properties of water and the effects of boiling and condensation. If the usual approximation for density were taken, $\rho = \rho_0(1 - \alpha T)$, where α is a constant coefficient of thermal expansion, ν and γ were taken to be constant, and $R = 0$, equations (1) through (3) would reduce to the equations given by Holst and Aziz (1972) and Donaldson (1962, 1968). These authors assume $\nabla \cdot \underline{q} = 0$ as we do here. The equations would also be quite similar to those given by Palm et al. (1972), Elder (1967), Lapwood (1948), and Rubin (1973), who assumed $\nabla \cdot \underline{V} = 0$ and therefore that $\rho = \text{constants}$ everywhere except in the buoyant terms of the momentum equation. The method of numerical solution we have used is described by Carnahan et al. (1969, p. 452 ff).

¹ All symbols are defined in Appendix I.



Since the treatment of boiling and condensation is novel, some further discussion might be useful. How the method of computation takes into account the heats of vaporization and condensation is best understood with reference to Figure 1b and equation (3). Suppose a packet of water is convecting upward across the critical curve in the region where γ would go from near 2 to near 1 cal/gm-°C. This crossing would occur near 300°C and 100 bars. Remembering T must be continuous across small distances, we see from (3) that the advection term, $\nabla \cdot \mathbf{q} \gamma T$ equals $(\gamma^- - \gamma^+) qT (\Delta x \Delta y / \Delta x \Delta y \Delta z)$. Since $\gamma^- - \gamma^+ \approx 1 \text{ cal/gm} = ^\circ\text{C}$, we see the advection term accounts for a latent heat of condensation of $\sim 300 \text{ cal/gm}$. The mass flux into the area $\Delta x \Delta y$ is $q \text{ gm/cm}^2$, and the volume heated by the resulting release of latent heat is $\Delta x \Delta y \Delta z$.

Thus we see the advection term, together with the data shown in Figure 1b, automatically accounts for the latent heats of vaporization and condensation. The direction of fluid motion distinguishes condensation from vaporization.

It should be stressed that the method used *assumes* that only one fluid phase (liquid or gas) is present in any given spatial volume. Boiling or condensation occur at a surface in space. The mass flux of liquid up to the base of that surface exactly equals the mass flux of steam out the top, so fluid mass is neither created nor destroyed and equation (1) is satisfied.

Of course liquid and vapor could coexist if pressure and temperature varied in such a fashion as to follow the two-phase curve of water for some distance. Thus the assumption that liquid and vapor do not coexist over an appreciable volume is equivalent to assuming that p-T variations along a streamline do not follow the two-phase curve of water (along which liquid and gas can coexist) for any appreciable distance. The results of computations

FIG. 1a. The two-phase curve for pure water is shown with isopleths of constant specific volume. The shading indicates the region on the high-temperature side of the critical curve and corresponds to shading in the figures illustrating the convective cooling of plutons. The manner in which salinity extends the critical curve is shown by percentages indicating where the end of the critical curve would be for fluids of various wt percent NaCl. The data is from Sourirajan and Kennedy (1962). Pressure and temperature values stored in tables for access by the computer programs are indicated by tick marks on the top and left border of the diagram. Values between were obtained by linear extrapolation from table entries. Tick marks are at $p = 1, 10, 25, 50, 100, 150, 200, 250, 300, 400, 500, 700, 1,000$ bars; $T = 20, 50, 100, 150, 200, 250, 300, 350, 400, 450, 500, 550, 600, 650, 700, 800^\circ\text{C}$.

FIG. 1b. Two two-phase curve for pure water is shown with isopleths of pseudoheat capacity (γ). Pseudoheat capacity is obtained by dividing the enthalpy at various temperatures and pressures by the temperature. Data are from tables 3 and 4 of Keenan et al. (1969). Shading and tick marks are as in Figure 1a.

FIG. 1c. The two-phase curve of pure water is shown with isopleths of viscosity (millistokes). The shading and tick marks are as in Figure 1a. Data is from table 8 of Keenan et al. (1969) and Bruges et al. (1966).

show that in general the streamline p-T curves intersect the critical curve of water at high angles (see Fig. 6). Thus the critical curve is crossed cleanly and the assumption of a sharp boundary between gas and liquid is appropriate.

Other details of the model that were considered during its formulation are summarized below:

1. Flow through a fractured igneous formation is described by Darcy's Law. Darcy's Law applies to flow through fractures or joints as well as flow through the pores in a sandstone and remains valid for flow rates three orders of magnitude greater than considered in this paper (for likely formation conditions). We assume there is no lower limit to the validity of Darcy's Law.

2. For a localized heat source such as would be produced by an igneous intrusive, convection will occur providing only that the intruded formation is permeable and water saturated. No critical temperature gradient (Rayleigh number) need be exceeded. The geometry of the heat source will drive forced convection not free convection. The rate of convection and the amount of fluid circulated through the intrusive will be controlled by the permeability of the intrusive and intruded formation as well as by the size, initial temperature, and location of the intrusive.

3. It is implicitly assumed that the fractures or joints through which hydrothermal solutions convect are less than 200 m apart. Provided this is true the interiors of the "matrix block" between fractures can track changes in hydrothermal solution temperature closely enough to remain essentially in thermal equilibrium with the fluid—in accord with an assumption made in modeling.

4. Heat generated by alteration reactions which occur as the convecting fluids interact with and cool the pluton are accounted for through R in equation (3). It is assumed that over the entire cooling history of the pluton 36 calories are generated in this way per gram of intrusive. This appears to be a reasonable estimate (Fyfe, 1974; Norton and Cathles, in press). For the sake of consistency it is assumed such exothermic chemical reactions occur even when the permeability is zero and the intrusive cools entirely by conduction.

5. Pressure is computed by integrating Darcy's equation and assuming the pressure at the surface is constant and known. It may be preferable to assume the pressure at some considerable depth is known (e.g., is unperturbed). If this convention is adopted the pressure contours will be altered as discussed in the last section.

6. Instabilities arise from the advection term which is given an improved treatment (Torrance,

1968, Method V) which preserves causality (heat anomalies are advected only downstream), conserves energy, and introduces only slight false conduction.

7. A variable grid spacing is used so that high surface heat flows such as are observed in geothermal areas may be accommodated. Most calculations were done on a 19 × 29 point grid.

8. Boundary conditions are written in general terms so free solution flow out the top surface can be modeled as well as the situation where no flow out the top surface is permitted. Temperature boundary conditions (insulating or fixed temperature) can also be freely specified. In Figures 2 and 3 no flow, insulating boundary conditions apply to the right and left boundaries. The base is no flow with a heat flux of 1.5 HFU (so long as the geothermal gradient is normal; near the pluton, while the pluton and its immediate environment was hot, the heat flux was taken to be zero), and the top is either no flow or free flow with a fixed temperature of 20°C.

9. The accuracy of computation is checked by inventorying the heat remaining in the computation domain, verifying that losses are accounted for by heat fluxes out of the domain and by checking that computations with denser point spacing give results similar to those with less dense spacing (e.g., computations converge).

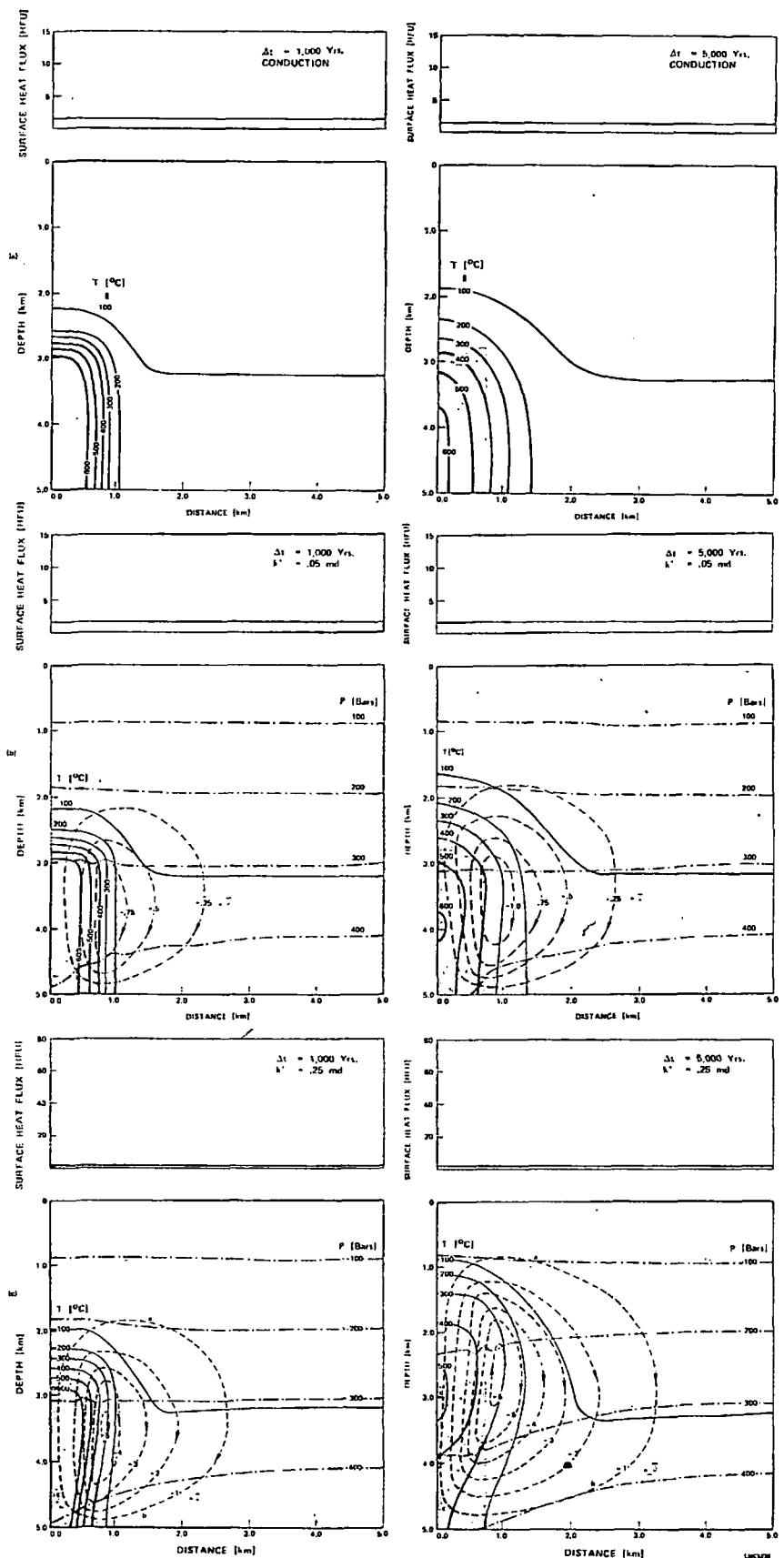
10. Model computations give the total heat flux out the top surface. For the cases where no flow out the top surface is permitted this heat flux is all conductive. In the case where free solution flow out the top surface is permitted interpretation of the proportion of heat transported across the surface by hot-spring activity through intermittent fractures and by conduction is allowed. The models presented define only the total top surface heat flux.

11. Placing the model intrusive in the middle of the computation domain gives very similar results to placing the pluton at the bottom of the domain but at the same depth. The geometry chosen for the computation domain does not appear to distort significantly the results obtained.

Results of Computations

Results of computations are given in Figures 2 through 11. Figure 2 shows the thermal evolution of a pluton 0.75 km in half-width and 2.25 km high, whose top is 2.75 km beneath the surface. The figure shows the thermal and fluid flow evolution of a system, assuming the formation and pluton permeabilities are 0, 0.05, and 0.25 millidarcies (md). In all cases the cooling of the pluton is considered to produce exothermic chemical reactions which generate, over the full course of cooling, 36 calories per gram of pluton. This is small compared to the amount of heat available from cooling, which is ap-

FIG. 2. Cooling histories for uniform 0-, 0.05-, and 0.25-md formation (and intrusive) permeabilities. In each figure temperature is indicated by isotherms (solid lines), pressure is indicated by isobars (dot dashed lines), and flow is indicated by stream lines (dashed lines). Pressure contours are computed using equation (4) and assuming the top surface pressure is 10 bars. The normalized stream function, $\bar{\psi}$, is related to the mass flux rate as indicated in Appendix I. At the top of each figure the total surface heat flux is given. In cases (such as this figure) where the top surface is impermeable to solution flow, the heat flux out the top surface is entirely conductive. Differences in cooling history are apparent. In the permeable 0.25-md case, the thermal anomaly initially associated with the intrusive rises like a hot-air balloon until it impinges on the surface. The temperature contours near the base of the pluton are pinched in. This mode of cooling is quite different from the conductive case, where the isotherms spread out symmetrically in all directions from the intrusive. Hydrostatic pressure contours are quite flat in all cases until the thermal anomaly reaches the near-surface environment. The rate of fluid circulation (given by the curl of the stream function, and approximately by the difference between the minimum in the stream function and 0) increases almost linearly with permeability (see Fig. 8a). The shaded areas in (c) above the intrusive (which is also shaded) are regions that lie on the high-temperature side of the critical curve of water. These regions correspond to similarly shaded regions in Figures 1 and 6. The top portion of the shaded zone is a zone of stream condensation. This can be seen by comparing the letters on the $\bar{\psi} = -1$ streamline of (c) at 5,000 years with the p-T loop corresponding to this streamline in Figure 6a. The conventions of Figure 3 are the same as described here.



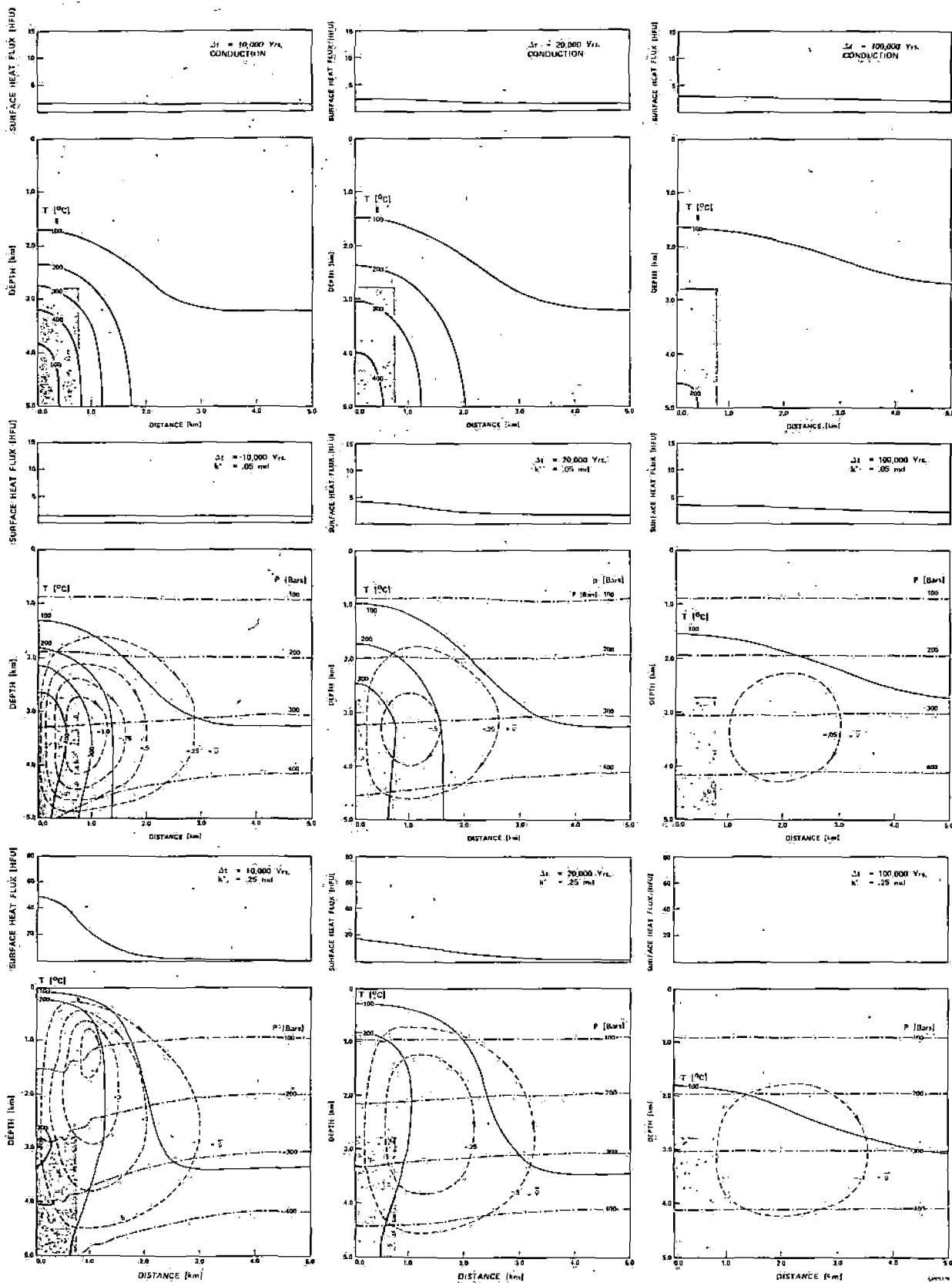
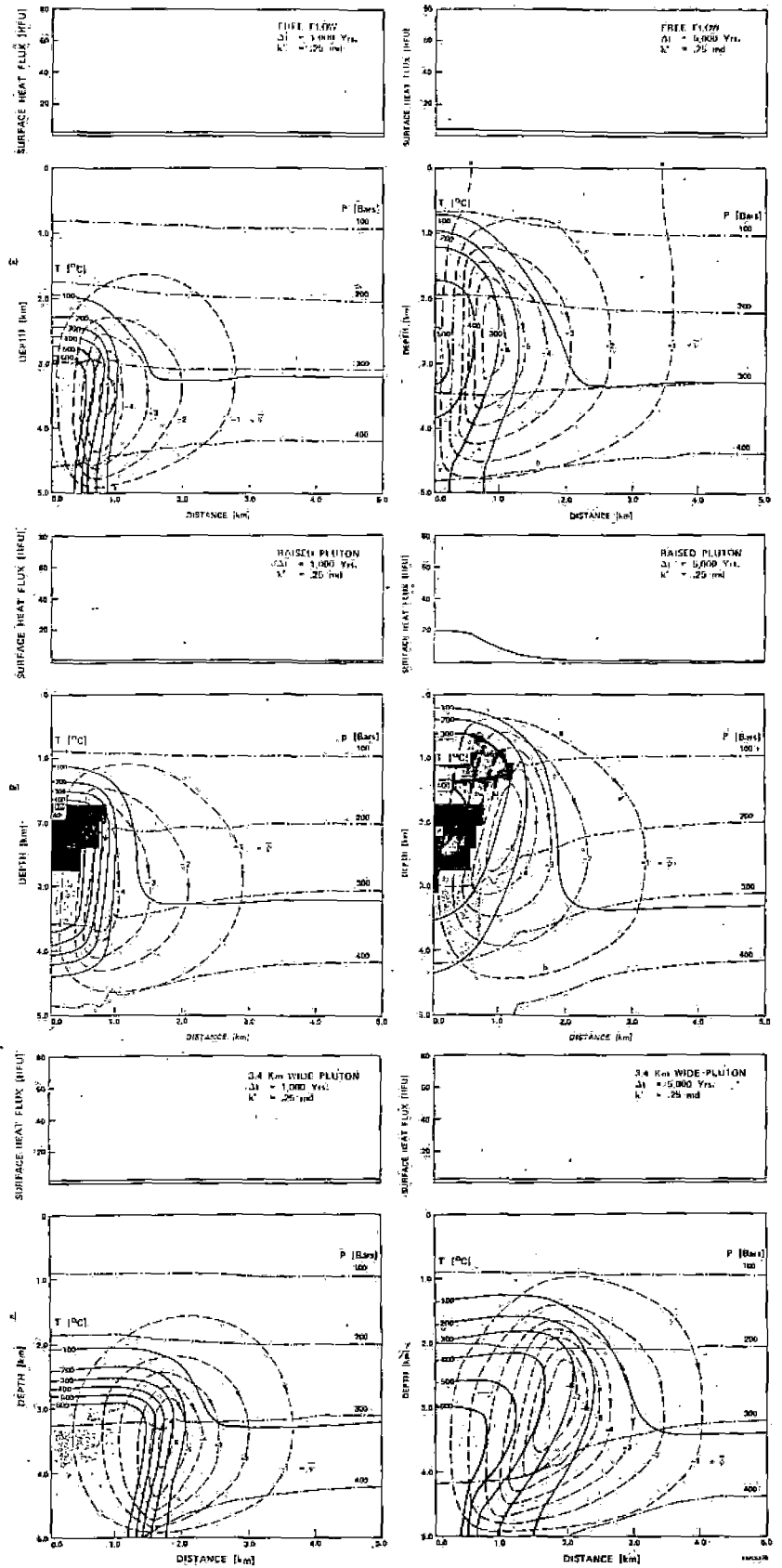
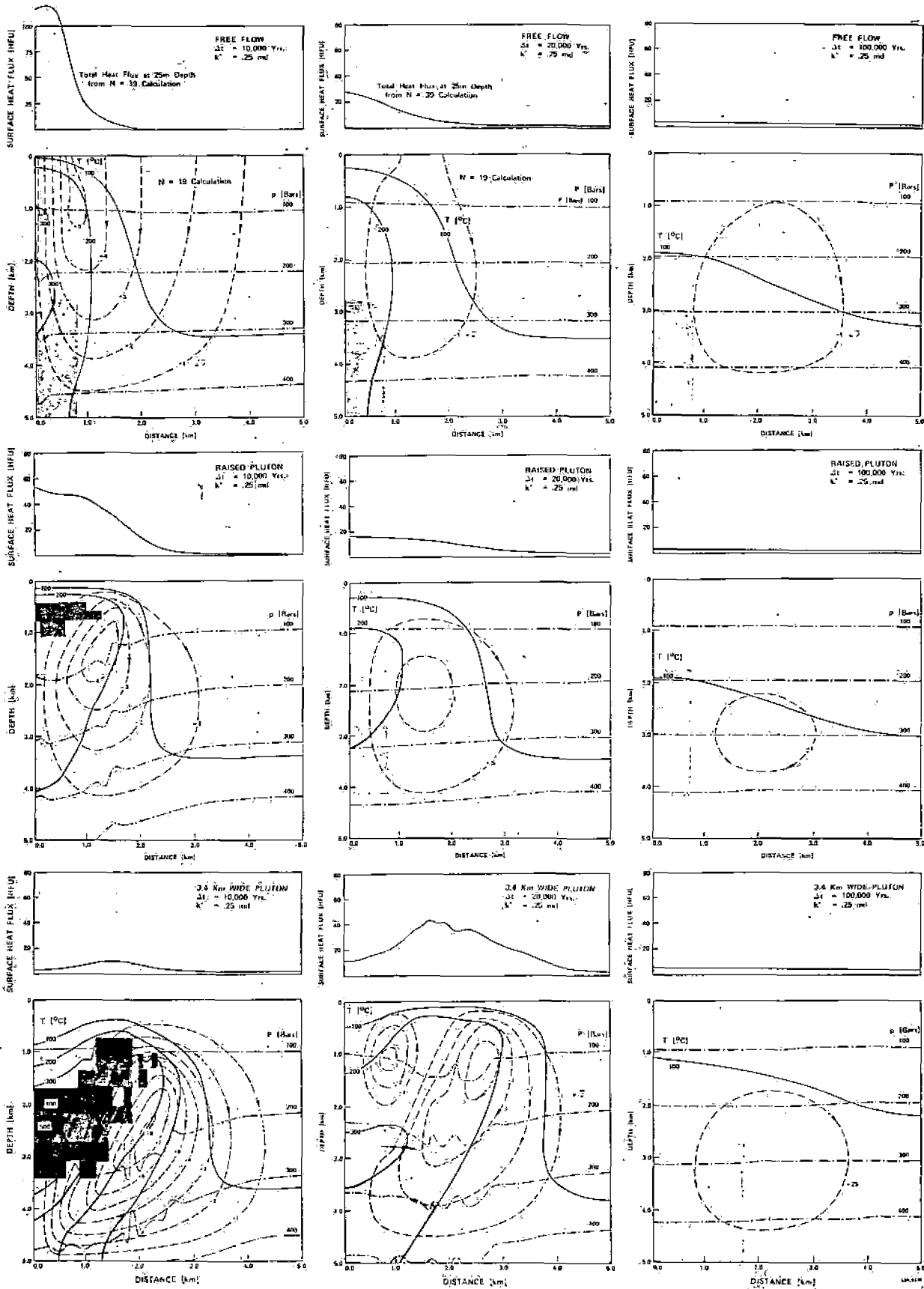


FIG. 3: The effects of free flow out the top surface, decreasing the burial depth and increasing the pluton width, are illustrated for a formation (and intrusive) permeability of 0.25 md. These cases are typical of the larger numbers of cases analyzed in Figure 9. It can be seen that if free flow out the top surface is permitted, the isobars remain flat even after the heat anomaly has reached the near surface. Also far higher surface heat fluxes are permitted. As discussed in the text, in case of free surface flow, surface heat flux may be interpreted as partly due to hot-spring activity and partly due to conductive heat transport. If the depth of burial is decreased the heat flow anomaly reaches the surface faster. If the pluton width is increased a broader surface heat anomaly results and a Bénard cell type of convection is initiated over the top of the pluton [(c) at 20,000 years]. As in Figure 2 the shaded regions above the pluton are those whose fluids lie on the high-temperature side of the two-phase curve of water and thus might be called vapor dominated. The shading of these zones corresponds to the shading in Figure 1.





proximately $600^{\circ}\text{C} \times 0.2 \text{ cal/g}^{\circ}\text{C} \times 2.7 \text{ g/cc}$ or 324/g of stock cooled.

The permeabilities 0.05 to 0.5 md are chosen to be representative of the low range of permeabilities in fractured igneous rock and the range over which convective heat transport becomes important and then dominates conductive heat transport. The permeability of crystalline rock at the Los Alamos hot-rock test site in the Jemez Mountains, New Mexico, is estimated to be about 0.002 md (Aamodt, 1976). Permeabilities of ocean-ridge basalt have been estimated at 0.45 md (Ribando et al., 1976); permeabilities in Wairakei's Waiora aquifer have been taken to be about 100 md (Mercer et al., 1975; Elder 1966).

Pure conductive cooling (Fig. 2a) of the pluton never produces a significant surface heat flow anomaly. The maximum surface heat flow occurs 65,000 years after intrusion and is only 3.4 HFU (compared to a "normal" heat flux of 1.5 HFU). The pluton cools symmetrically; the isotherms extend further from the base of the pluton than from the top of the pluton because they are superimposed on a normal geothermal gradient. The temperature of the top portion of the pluton steadily drops from a temperature of about 400°C at 1,000 years after intrusion.

If the formation permeability is 0.05 md (Fig. 2b), convective dissipation cools the intrusive more rapidly and causes the isotherms to bulge out over the top of the intrusive and pinch in near the base. The temperature of the top of the pluton remains at about 400°C for the first 10,000 years of cooling and then decreases in temperature only because the temperature of the entire pluton has dropped below 400°C . A maximum surface heat flow of 4.9 HFU occurs directly over the center of the pluton 35,000 years after intrusion.

In a formation of 0.25-md permeability, the effects of fluid flow in pinching in the isotherms at the base and ballooning them out at the top are even more apparent. The shaded area above the pluton indicates the region which lies on the high-temperature side of the critical curve (the shaded regions in Fig. 1). This area is a region of "steam" which, if discovered during its short lifetime, might be a valuable geothermal resource. The vapor dominated steam region occurs largely before the intrusive event is detectable by high heat flows at the surface. The maximum surface heat flow of 47 HFU occurs 10,000 years after intrusion. The region just above the pluton heats up to over 500°C and then cools down.

If the same pluton cools in a formation of permeability 0.5 md, the maximum heat flow anomaly is 69 HFU and occurs 6,500 years after intrusion. The

convective rise of the thermal anomaly is even more obvious than in the 0.25-md case and the surface expression of high heat flow occurs more quickly.

Figure 3 illustrates various changes on the base 0.25-md case shown in Figure 2c. If free flow out the top surface is permitted (hot-spring activity) much higher surface heat fluxes result. The maximum surface heat flow is 170 HFU 7,750 years after intrusion compared to 47 HFU 10,000 years after intrusion for the no flow case. If intrusion reaches shallower levels, the areas of vapor are larger than in the base case due to lower hydrostatic pressures and the surface heat flow is manifested sooner because the surface is closer to the intrusive. The fluid circulation is slightly less because vapor has a higher viscosity than liquid. The streamlines tend to avoid the shaded vapor zone. Finally increasing pluton half-width to 1.7 km causes convection to concentrate at the edge of the intrusive and produce a heat flow which is a maximum over the edge of the pluton rather than over the center. Because the pluton contains more heat, high temperatures can be carried to shallower depths and the vapor zone is larger. Secondary circulation cells develop after the temperature contours have been up-bowed at the edges of the intrusions. A "Rayleigh-Bénard" cell pattern is thus developed for plutons whose total width (not half-width) is comparable to the depth to the pluton.

The rate of fluid circulation can be calculated from the streamlines at any time and the total amount of fluid circulation that has occurred from the time of intrusion can be determined. Figure 4 shows the total amount of fluid that has circulated through various cases illustrated in Figures 2 and 3. In a formation with permeability of 0.05 md, 90 kg of water circulate through each sq cm of the top central portion of the intrusive in the 100,000 year cooling time computed. For a permeability of 0.25 md this figure is 250 kg per sq cm, and for a formation permeability of 0.5 md, the figure is 300 kg, per sq cm. As discussed later, the amount of fluid circulation does not go up linearly with permeability because the amount of heat in the initial thermal anomaly is limited. It can be seen that for wide plutons the maximum fluid circulation may not be in the intrusive or centrally located with respect to the pluton.

Figure 5 illustrates the fluid properties over the 200-year step between 4,800 and 5,000 years after intrusion for the 0.25-md domain shown in Figure 2. Significant variations in specific volume, pseudo-heat capacity, and viscosity are indicated. The high specific volume of the fluid above the intrusive provides the buoyant force to drive convection. The

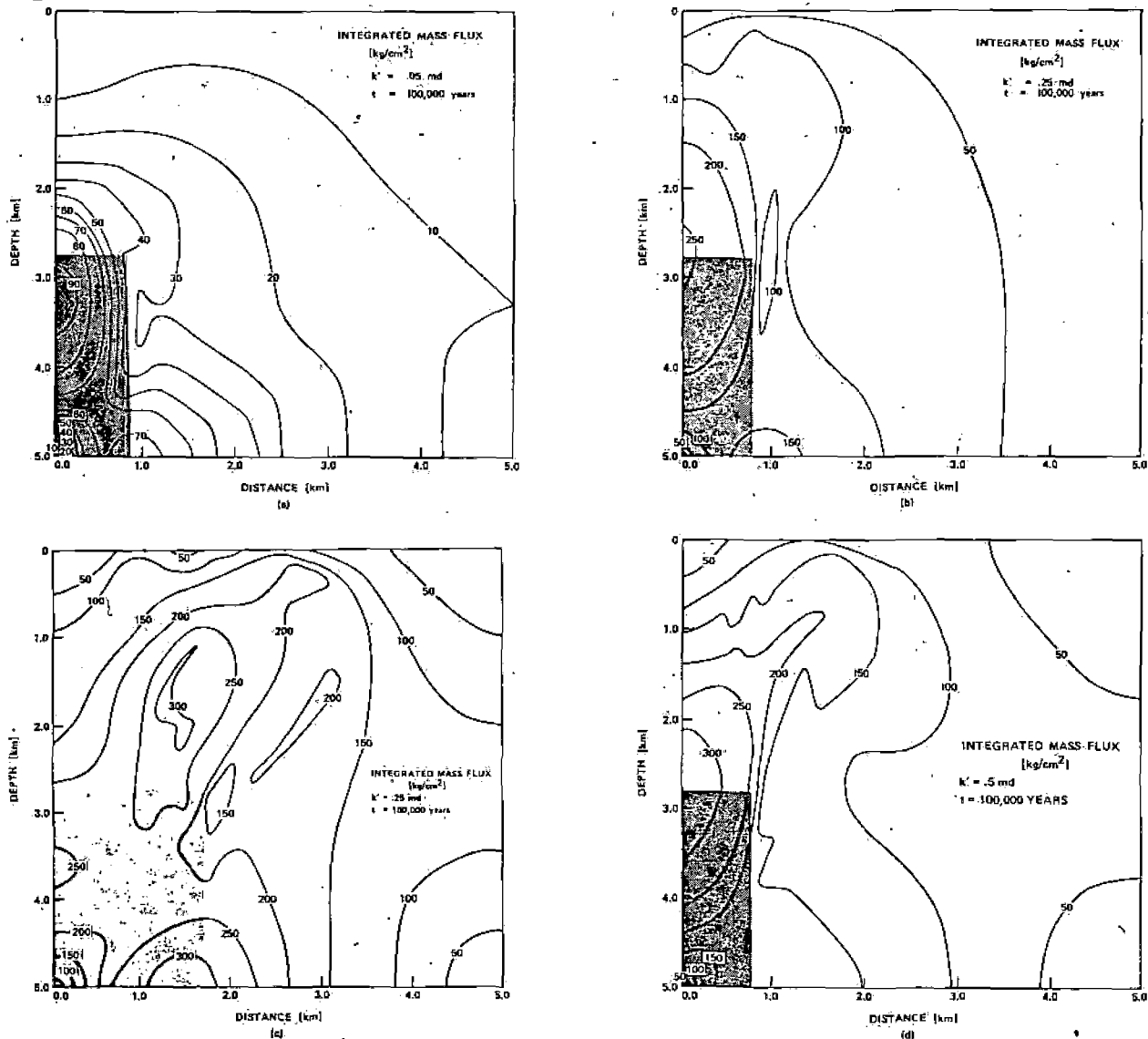


FIG. 4. The total amount of hydrothermal solution passing through each centimeter squared of surface area over 100,000 years of cooling is shown for various formation permeabilities and pluton geometries. As shown in Figures 8 and 9 this integrated mass flux is strongly dependent on permeability and pluton volume. It can be seen that for wide plutons the regions of maximum integrated mass flux are not necessarily centrally located inside the intrusive.

maximum specific volume is quite a bit larger than would be indicated by approximations usually used (specific volume = $1/(\rho_0 - .001 \rho_0 T) = 1.67$ for $T = 400^\circ\text{C}$). Variations in pseudoheat capacity show condensation will dump a significant amount of heat above the boiling zone, as the ability of the hydrothermal fluids to carry heat decreases. Variations in viscosity show a large region where the viscosity is nearly one-fifth its value at the surface. In this region, convection is five times easier than it would be if the viscosity of the fluid were constant. A high viscosity zone associated with the vapor dominated

area is also indicated (viscosity of the fluid increases as the fluid becomes gaslike).

Figure 5d shows the magnitude of fluid mass flux at 5,000 years after intrusion. The maximum mass flux rate can be seen to be about $15 \text{ g/cm}^2\text{-yr}$. That is, across the right-hand top of the pluton, about 15 grams of water will circulate on average through each sq cm surface area perpendicular to the direction of the flow in one year.

Figure 6 shows the pressure and temperature conditions encountered by fluid as it circulates around streamlines shown in Figures 2 and 3. The figure is

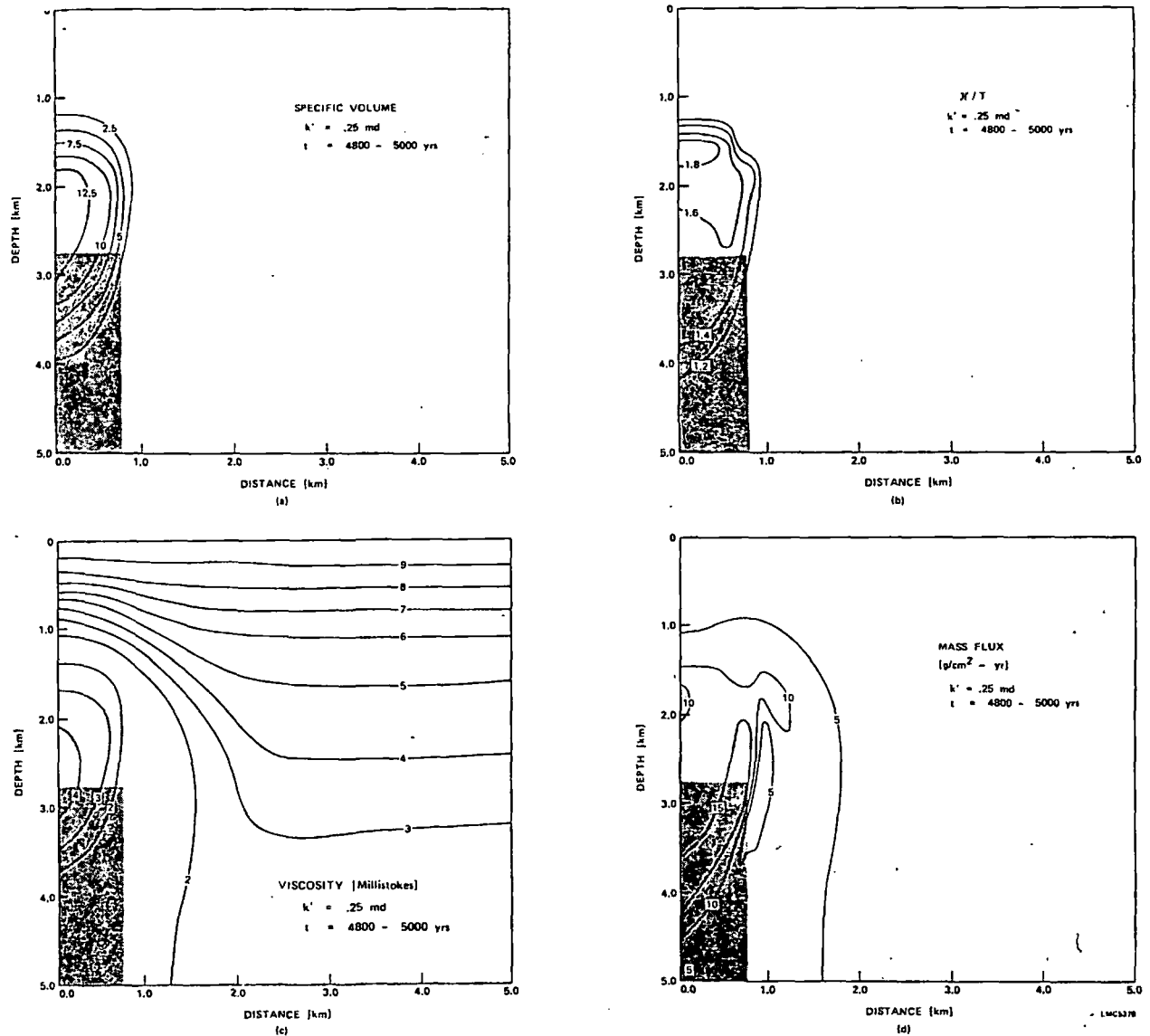


FIG. 5. Fluid properties are shown for the case of Figure 2c 4,800 to 5,000 years after intrusion. As commented in the text the combination of large specific volumes and reduced viscosity produce convection about six times faster than constant parameters models. The steep gradient in pseudoheat capacity ($\partial C/T$) strongly accelerates the upward migration of the intrusive's thermal anomaly. Fluid circulation rates are 10 to 15 g/cm^2 yearly.

arranged so that the circulation sense is the same as in Figures 2 and 3. The p - T curves may also be superimposed on the plots in Figure 1 to show the variations in specific volume, pseudoheat capacity, and viscosity along the streamlines. The fluid circulation loops rise toward lower pressures and involve increasingly smaller excursions in temperature as the pluton cools. The loops cross the critical curve from the gas to the liquid side. The solution becomes gaseous by circulating around the end of the two-phase curve. For pure water condensation is therefore a much more important phenomena than

boiling. The curves cut the two-phase curve of water at a sharp angle confirming our assumption that liquid and vapor will not coexist in the same rock volume. The return solutions follow the normal geothermal gradient as one might expect.

Figures 7, 8, 9, and 10 indicate the systematics of varying permeability, pluton burial depth, pluton half-width, and the boundary conditions for flow at the top surface. The main effect of permeability (Fig. 7a) and the convection it permits is to decrease the maximum temperature of the domain more rapidly than would be possible by conduction. The

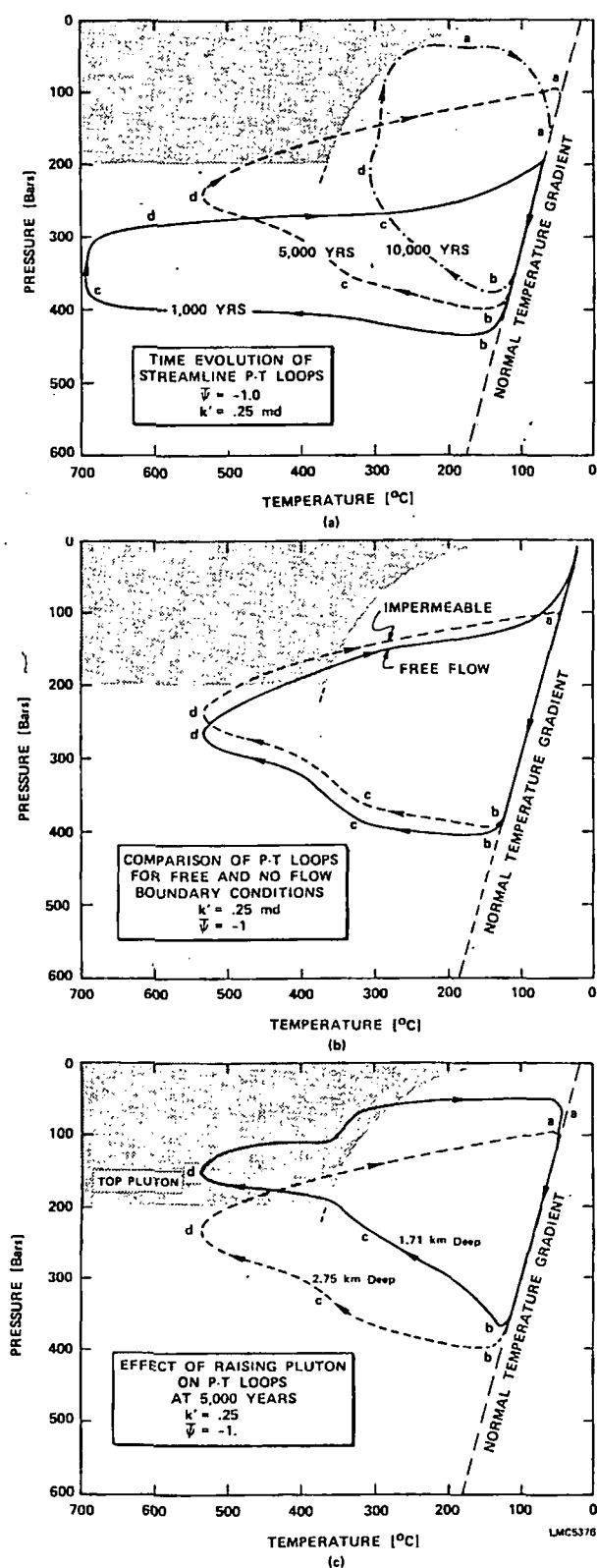


FIG. 6. The variation in pressure and temperature around selected streamlines in Figures 2 and 3. The letters key to corresponding letters in those figures. The first figure (a)

most important effects are realized in the early stages of cooling when large buoyant forces exist to drive the most rapid fluid circulation. Higher permeabilities permit higher maximum surface heat fluxes (Fig. 7c).

The maximum rate of fluid circulation is linearly proportional to permeability (Fig. 8a). Surface heat flow does not increase in such a simple way but increases sharply over a critical range of permeability between about 0.1 and 0.3 md (Fig. 8c). The maximum integrated mass flux (shown for particular cases in Fig. 4) also increases with permeability at a decreasing rate.

The last effects may be understood as follows: If the pluton were maintained at constant temperature, increasing the permeability would lead to a directly proportional increase in solution circulation rate, the integrated amount of circulation over any given time, and the surface heat flux. The last proportionality is not obvious but has been shown to be the case for Rayleigh-Bénard convection (Elder, 1967) and would also be the case for the situation just hypothesized. The pluton is not maintained at constant temperature, however, but decreases in temperature with time. The amount of fluid circulation that is possible therefore depends not only on the permeability but also on the length of time required to cool the initial intrusion. Increases in the rate of fluid circulation are cancelled to a certain extent by the shorter time required to cool the intrusive by the greater circulation. Similarly, although faster circulation rates move the thermal anomaly to the surface with less loss of heat, there is still an unavoidable loss associated with the requirement of heating the rock above the intrusive. Higher permeabilities can pro-

fers to curves in Figure 2c. The second figure refers to streamlines in Figure 3a (solid) and 2c (dotted), both 5,000 years after intrusion. Figure (c) refers to streamlines in Figure 3b (solid) and Figure 2c (dotted). The curves indicate that solutions increase rapidly in temperature at nearly constant pressure as they circulate into a pluton and decrease strongly in temperature again at nearly constant pressure upon leaving the top of the pluton. The solutions increase in temperature along the normal geothermal gradient as they circulate downward to enter the base of the intrusive. It can be seen that the flow paths cut the critical curve of water at a sharp angle; thus fluids are either liquid or gaseous and not a mixture of liquid and gas. For pure water condensation is a far more important phenomenon than boiling, which occurs only in (c). As commented in the text however, if the solution had only 10 wt percent salinity, boiling as well as condensation would occur in most of the cases shown. Salinity extends the critical curve of water (see Fig. 1a) to about 500 bars, so the p-T curves would cross the salinity-extended two-phase curve both as temperature increased and as temperature decreased. Free solution flow out the surface has only a small effect on the pressure and temperature conditions encountered around the $\psi = -1$ streamline (b), and decreasing the depth of intrusive burial decreases the pressure encountered around the streamline loop as one might expect (c).

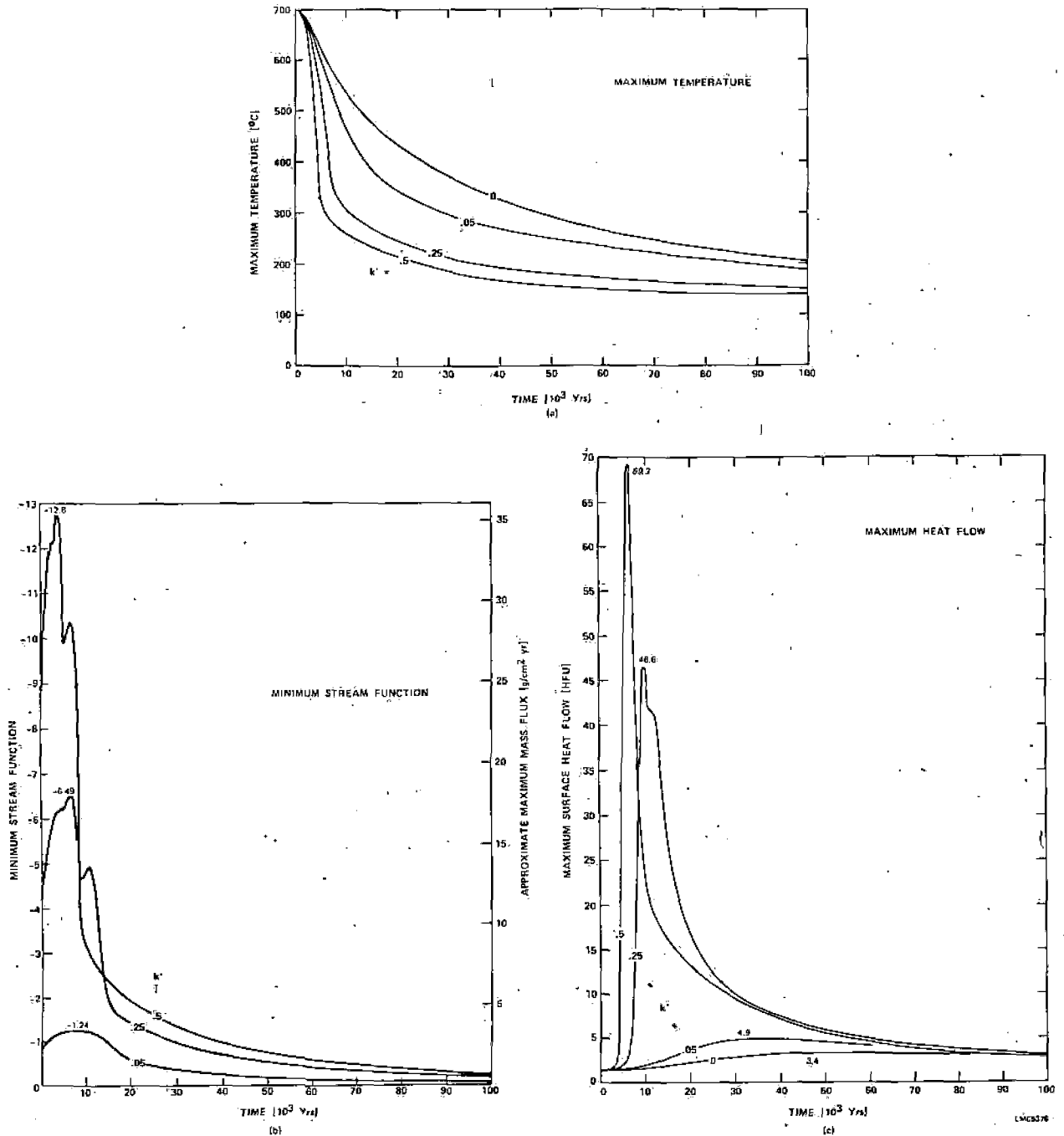


FIG. 7. The effects of permeability on cooling rate, solution circulation rate, and maximum surface heat flow. The convection allowed in permeable water-saturated formations permits a far more rapid cooling than would be allowed by conduction alone. The very steep decline in the $k' = 0.5$ - and 0.25 -md cases results from the additional cooling permitted by variable enthalpy. Most of the solution flow occurs in the first 10,000 to 20,000 years of cooling. The small secondary maxima in (b) results from the increase in the permeability that follows the disappearance of steam dominated zones. The maximum circulation rate and permeability are linearly related as indicated in Figure 8a. Maximum surface heat flow also increases as permeability increases but not proportionately (see Fig. 8c). By comparing (b) and (c) it can be seen that most of the intense fluid circulation is finished by the time strong surface heat fluxes are manifested.

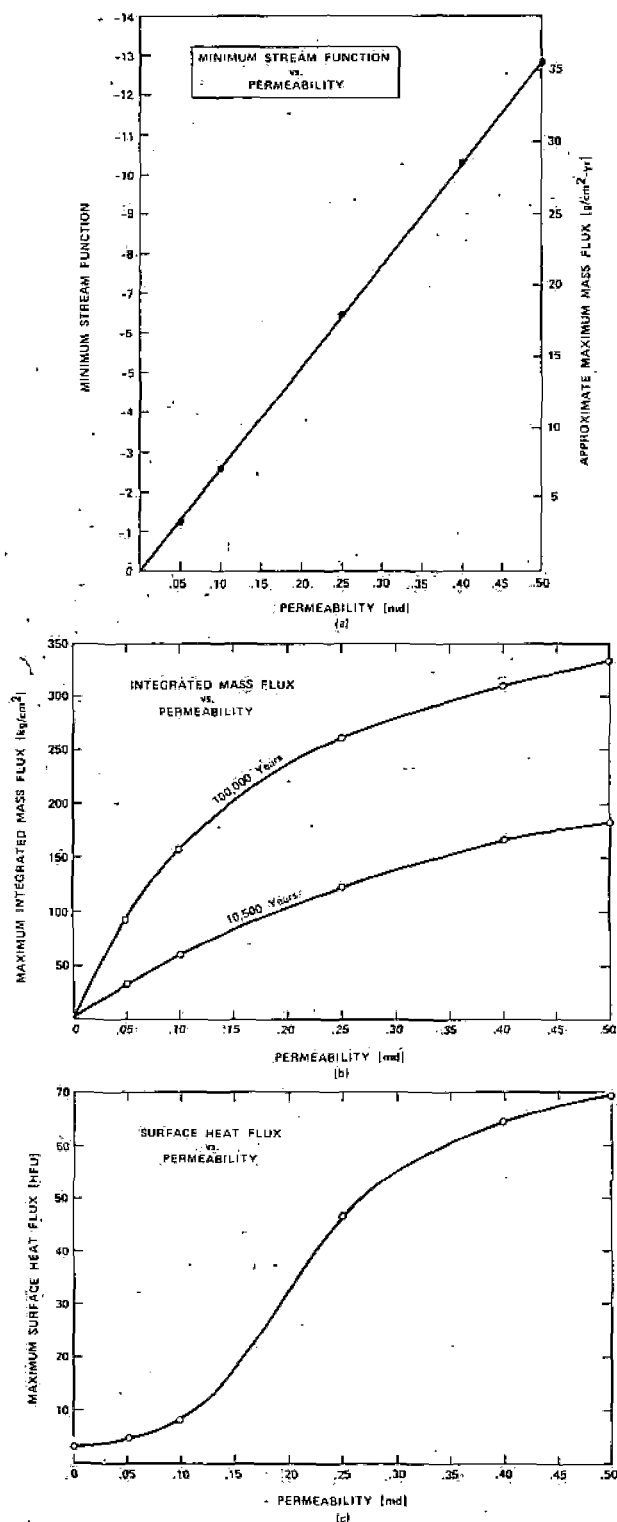


FIG. 8. The dependence of minimum stream function (approximate maximum mass flux), integrated mass flux, and maximum surface heat flux on permeability. The minimum stream function is linearly proportional to permeability. As discussed in the text, heat flow and integrated mass flux would also be linearly related to permeability if it were not for the finite heat contents of the pluton.

mote a narrower plumelike upwelling, but the constriction of the upwelling plume does not proceed rapidly enough to promote a proportional relationship between permeability and maximum surface heat flow.

Increasing the pluton half-width increases the maximum rate of fluid circulation only slightly (Fig. 9a). Similarly, as remarked previously, decreasing the depth of burial decreases the rate of fluid circulation slightly, probably as a result of the increased amount of space dominated by higher viscosity steam. The decrease for 0.05-md formation permeabilities is less noticeable than for 0.25-md formation permeabilities since substantially less volume is occupied by steam in the 0.05-md case (Fig. 9b).

The total amount of solution circulating through the pluton increases almost linearly with pluton half-width (Fig. 9c). Convection can continue longer if the initial intrusive contains more thermal energy. The increase in the duration of high surface heat flow is only about half as great as would have been expected on the basis of the increase in pluton size, however (Fig. 10a). Increasing the pluton half-width from 0.75 to 1.17 km represents a 56 percent increase in pluton volume, but the duration of 30 HFU surface heat flow is increased only 21 percent (from 5,700 to 6,900 years). Similarly, the increase from 0.75 to 1.70 km half-width increases the pluton volume by 127 percent but the duration of 30 HFU surface heat flux is increased only 68 percent. The explanation for this discrepancy is that high surface heat flows occur over a larger surface area for the wider plutons.

Allowing free solution flow out the top surface has little effect on the rate of fluid circulation (Fig. 9b) but has a very substantial effect on the total heat flux at the surface (Fig. 9f). In the 0.25-md case the maximum surface heat flux is almost quadrupled by allowing free solution flow. A substantial effect is also seen for the 0.05-md case. Even low permeability formations can produce large surface heat flow anomalies if flow out the surface occurs and intrusion reaches shallow depths (Fig. 10b).

The maximum surface heat flux increases as the depth of burial decreases for low permeability domains but is nearly independent of pluton burial depth for higher permeability domains (Fig. 9f). For the higher permeability domains, the decrease in overburden that must be heated is canceled by the decrease in solution flow rates caused by the more gaseous nature of the fluid at shallower depths.

Figure 11 illustrates the importance of taking accurate representations of fluid viscosity, specific volume, and enthalpy. Variable fluid density and viscosity allow circulation to occur much more easily. If condensation and boiling are not permitted, con-

puted results are similar to computations using the usual Bousinesq approximations [$\rho = \rho_0(1 - \alpha T)$, $\nu = \text{constant}$] provided the formation permeability is six times greater. Condensation greatly facilitates the upward migration of the heat anomaly and allows the intrusive to cool far more rapidly. Taking account of variable fluid properties makes a very substantial difference in computed results.

Geological Implications

Fluid pressure in a convecting system.

It is often of interest to know the hydrostatic or fluid pressure as a function of depth in a hydrothermal system. For example, such knowledge may be used to make a pressure correction to fluid inclusion filling temperatures. It is argued below, on the basis of the simple calculations made, that the increase in pressure with depth in a hydrothermal system may be quite close to the normal hydrostatic pressure gradient of 100 bars per kilometer, provided the permeability is reasonably uniform. This conclusion requires some interpretation of the figures given in the previous section, since in those figures the surface pressure was arbitrarily assumed to be constant and of a known value (in this case 10 bars).

Figures 2 and 3 show that in most cases the computed isobars are quite flat. In these cases a uniform normal hydrostatic gradient is indicated directly. The hydrostatic gradient is the same in the cool portions of the computation domain as it is in the hot igneous pluton. Fluid flow has compensated for the much lower fluid densities near the pluton; the resistance to upward flow increasing the pressure to normal levels.

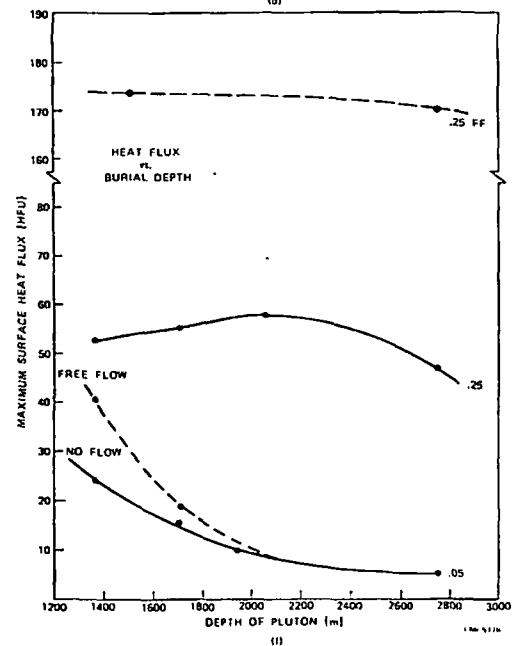
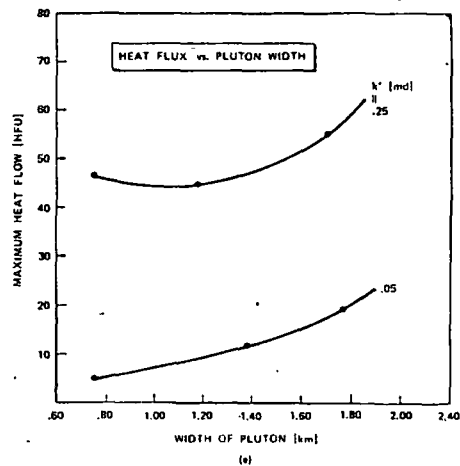
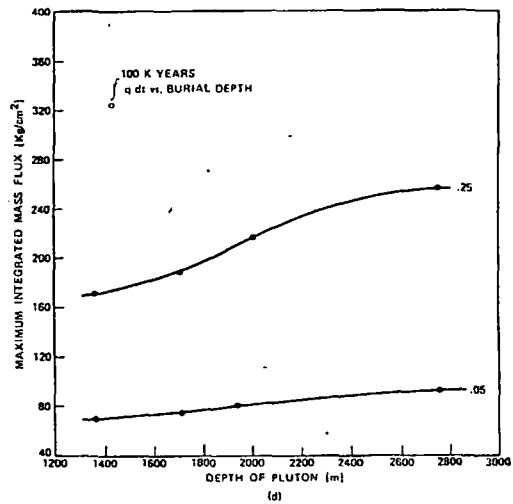
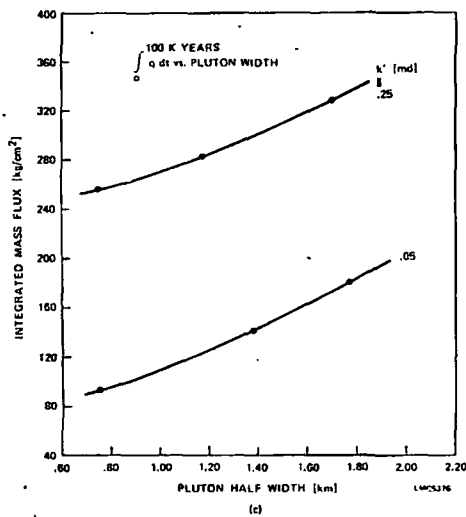
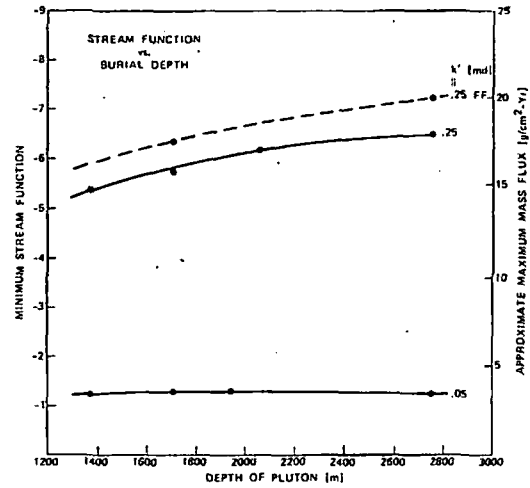
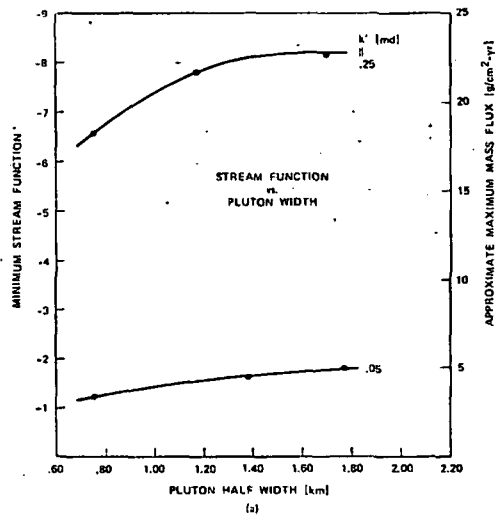
In those cases where the thermal anomaly has reached the near surface, however, the equal pressure contours are bent downward. The reason is that near the surface the upward migration of solutions cannot occur to the extent necessary to flatten the pressure contours. In the case where free solution flow out the top is permitted (Fig. 3a), however, the pressure contours remain flat even when the thermal anomaly reaches the surface. Notice that in the cases where the pressure contours are bent downward, all of the deeper pressure contours are bent downward a nearly identical amount. Apparently the pressure perturbations originating in the near-surface environment will persist downward indefinitely.

Persistence of pressure perturbations to infinite depths is not physically reasonable, and some reinterpretation of the assumptions by which pressure is calculated in these cases is indicated. As discussed in the previous section, we assume that the surface pressure is fixed and constant. This is entirely reasonable in the case where free solution flow out the surface is permitted. In this case, the pressure at the surface could be 1 bar (1 atm) or greater if the surface lay under a shallow layer of water (e.g., 10 bars). However, in the case of zero surface solution flow, maintenance of a constant surface pressure is less realistic. If the geological situation is that of a ground-water table, the ground-water table may rise in response to fluid convection. Thus, at the level which we choose to call the "surface" the pressure may change with time due to the weight of overlying pore fluids (e.g., the elevated water table). In these cases, a more reasonable convention might be that the pressure at some large depth remain constant. This will be certainly true at sufficiently large depths. In this case the deeper pressure contours would be flattened and the pressure contour at the surface ($z = 0$) would be up-bowed. In the cases of Figures 2 and 3 discussed before, this would mean an exchange of all the down-bowed pressure contours for a single up-bowed surface pressure contour whose physical interpretation would be an up-doming of the ground-water table. Since the pressure contours in Figures 2c and 3b and c are depressed about 100 bars, the up-doming of the ground-water table would be 1 km or more (more as the fluid density falls below 1 g/cc).

Since ground-water tables commonly die at depths less than 1 km, up-bowing of the ground-water table as suggested by the cases considered would cause free solution flow out the top surface. In this case, of course, the pressure contours would be flat, as indicated in Figure 3a.

Figure 12 shows pressure gradients through the axis of the pluton for some of the cases in Figures 2 and 3 and shows how solution flow reduces, and in the free flow case nearly eliminates, deviations from a normal hydrostatic pressure gradients. To reiterate: It is suggested that the pressures at the right-hand end of the curves in Figure 12 should be made coincident, whereupon deviations from normal hydrostatic pressures occur near the surface and are

FIG. 9. The dependence of minimum stream function, integrated mass flux, and maximum surface heat flow on pluton half-width and burial depth. Fluid circulation is not strongly affected by either pluton half-width or depth of burial. Integrated mass flux increases as the depth of pluton burial increases for high permeabilities. Less volume is occupied by high viscosity steam with deeper burial, and deeper burial allows larger convection cells. Integrated mass flux is nearly proportional to pluton half-widths (i.e., to the total amount of thermal energy in the initial intrusive). Free flow out the top surface does not significantly affect the rate of fluid circulation but dramatically increases the maximum surface heat flux.



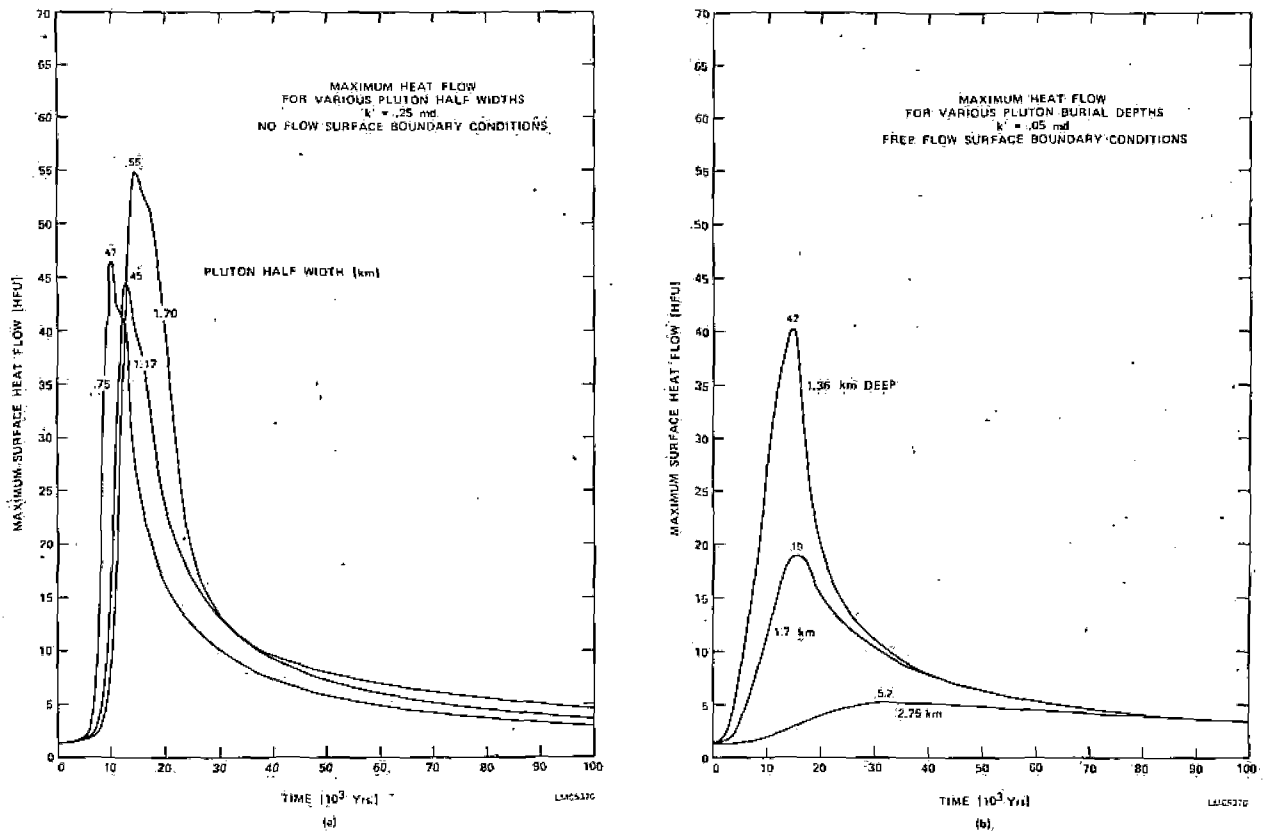


FIG. 10. Dependence of surface heat flux on pluton half-width and depth of burial. As discussed in the text wider plutons do not increase the duration of high surface heat flow proportionately because the regions of high surface heat flow are broader (see Fig. 3c). Even low permeability formations can produce significant surface heat flow anomalies if free solution flow out the top surface is permitted and if the depth of pluton burial is small.

caused by an up-bowing of the ground-water table. Computationally assuming constant pressure at great depth gives this result directly.

We conclude that for a uniformly permeable formation, pressure contours will be flat and normal hydrostatic pressure gradients may be applied to actively convecting hydrothermal systems as well as to normal cool, static ground water.

These results apply only to formations with reasonably uniform permeabilities. It is easy to imagine cases of nonuniform permeability where the fluid pressure profile would not be normal hydrostatic (e.g., flow upward through a high permeability zone with a low permeability top—most of the pressure drop would occur in the low permeability cap). Some variation in permeability can be tolerated, however, because the fluid viscosity varies by about a factor of five in different parts of the computation domain (see Fig. 5c). Even in a formation with moderate variations in permeability the results here suggest hydrostatic gradients will tend to be more normal than not.

Implications for geothermal resource formation

The consequences of the modeling presented for geothermal energy are relatively straightforward. Small plutons can generate large surface heat fluxes and substantial reservoirs of hot rock and even steam or vapor dominated reservoirs (i.e., regions which lie on the high-temperature side of the critical curve of water). The model heat fluxes are comparable to the average heat flux at Wairakei, for example, which, according to Elder (1965) is 50 HFU over an area 50 sq km with local heat fluxes up to 10^4 HFU. However, it is clear that the duration of the high surface heat fluxes (see Figs. 7c and 10a) are of short duration, generally less than 20,000 years. It can be seen from Figures 2 and 3 that the lifetimes of the vapor dominated regions are shorter still, generally less than 5,000 to 10,000 years.

Ten or even 20,000 years is geologically a very short period of time. It is unlikely that there are many conventionally exploitable intrusions of sufficiently recent vintage to have hydrothermal systems of the type modeled associated with them at the pres-

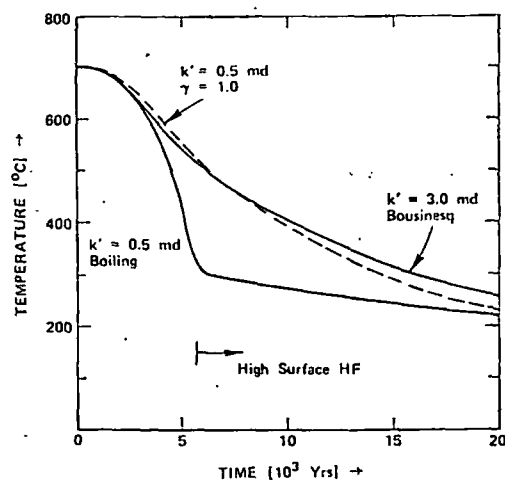


FIG. 11. The importance of taking fluid properties into account is illustrated by the differences in maximum temperature versus time. With a constant pseudoheat capacity of 1 cal/g-°C, variable fluid viscosity and density produce a cooling history similar to constant viscosity and density models with a formation permeability six times larger (dashed curve). Latent heats of condensation allow faster upward migration of the thermal anomaly and thus substantially more rapid cooling. The abrupt change of shape of this curve occurs when the heat anomaly's upward migration is arrested by the top surface. No flow out the top is permitted in this case.

ent geological instant. Permeabilities of at least 0.25 md would be required for economic flows of steam into producing wells. Unless intrusives substantially larger than 3 km in diameter are envisioned, exploration for geothermal energy would thus apparently best be devoted to areas where intrusion is thought to go on continuously, e.g., at actively rifting areas such as Wairakei, New Zealand, or near historically active volcanic systems.

For single isolated intrusives, Figures 2 and 3 suggest that the best geothermal systems may lie beneath surfaces which have yet to manifest high heat fluxes. By the time the strongest manifestation of surface heat flow occurs in the models, the vapor dominated regions have shrunk considerably in size and much of the most valuable thermal energy may have been dissipated.

Implications for porphyry-type copper deposit formation

Crerar and Barnes (1976) have shown experimentally that three important factors affecting copper solubility in hydrothermal solutions are temperature, salinity, and pH. Copper concentrations in solution of 1 gram per liter or greater are possible at temperatures of 350°C and high salinity. Changes in copper concentration of an order of magnitude (1 g/l to 100 ppm) result from changes in temperature from 350° to 250°C or from changes in salinity from

5.8 to 0.58 wt percent, or from changes in acidity from pH 3 to pH 4 (Crerar and Barnes, 1976). The models presented in the last section permit quantification of the conditions under which low-grade copper originally in the intrusive may be concentrated in a higher grade ore shell draped around the intrusive.

For a 0.4 wt percent copper cutoff, ore shells of porphyry copper deposits are typically 180 to 240 m (600 to 800 feet) thick (Lowell and Guilbert, 1970, p. 385). It is not certain the ore shell curls over the top of the intrusive with which it is associated, although this occurs in some cases (James, 1971). Typically 70 percent of the ore lies in the causative intrusive, but there are many cases where mineralization lies mostly (~80%) outside the causative intrusive (Lowell and Guilbert, 1970).

By area ratio it is quite possible to form a model ore shell 200 m thick and 1 km long draped over the model intrusive having a grade of 0.43 wt percent copper by scavenging or collecting 0.05 wt percent copper from the intrusive. The intrusive dimensions are 0.75 by 2.25 km so the area ratio is 0.75 × 2.25

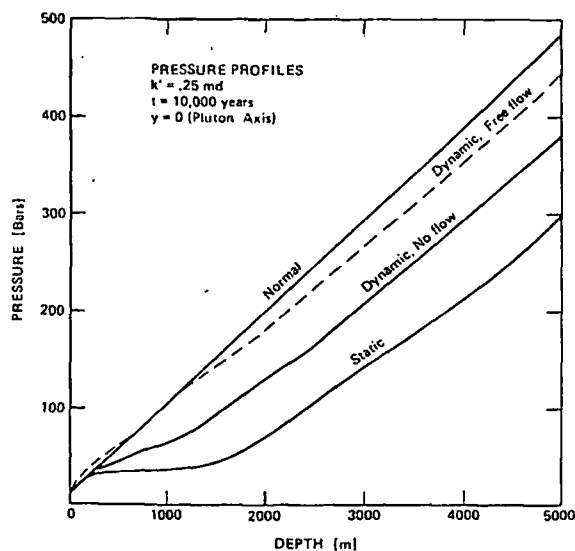


FIG. 12. Pressure as a function of depth down the pluton axis ($y=0$) is compared to the normal hydrostatic pressure increase. The curve labeled "static" indicates the increase in pressure with depth in Figure 2c due to fluid mass only. Fluid flow increases this pressure to the curve labeled "dynamic; no flow" (also from Fig. 2c but with both terms in equation (4) contributing, not just the fluid mass term). Fluid circulation reduces the deviation in hydrostatic pressure from "normal" by about a factor of two. The curve marked "dynamic; free flow" is the axial pressure from Figure 3a and shows that if free solution flow out the top surface is permitted perturbations of hydrostatic pressure from normal are nearly eliminated by fluid flow. It is suggested in the text that the "dynamic; no-flow" curve should actually be superimposed on the "normal" curve over most of its length with the perturbations toward abnormally high pressures at depths less than 1,000 meters being caused by an up-bowing of the ground-water table.

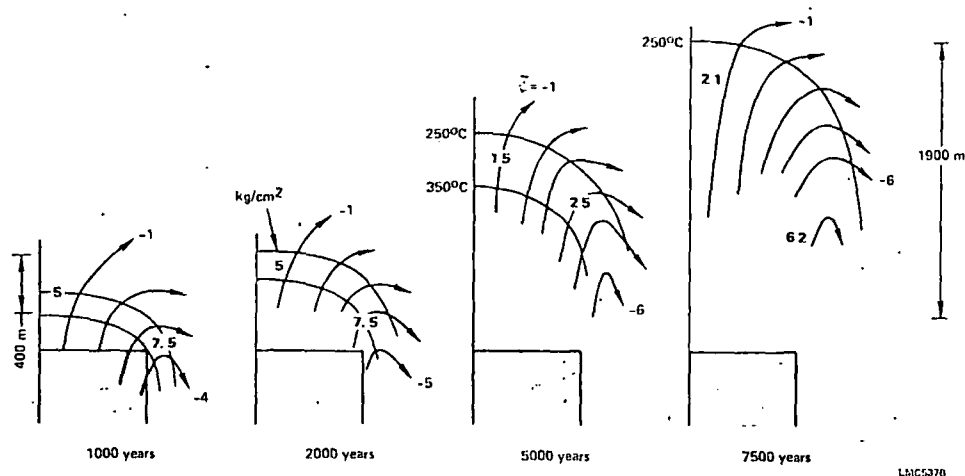


FIG. 13. The region between 250° and 350°C through which upwelling solutions flow in the case of Figure 2c is shown as a function of time. The stream lines of Figure 2c are sketched and the direction of flow indicated by arrows. The numbers between the two bounding temperature lines show the mass flux that occurs through this temperature domain over the interval of time from the last diagram. For example between 1,000 and 2,000 years 5 kg/cm² have circulated through the 250° to 350°C temperature zone immediately above the center of the pluton. As discussed in the text this figure shows that a narrow ore shell probably cannot be produced by the temperature dependence of copper solubility alone. By the time sufficient integrated solution flow has occurred to produce an ore zone similar to those observed, the critical temperature range has changed position and become too smeared out to produce a narrow ore shell.

divided by 0.2×1.0 , which is equal to 8.44; $8.44 \times 0.05 = 0.42$ wt percent. With a 1 g copper per kg water drop in solution copper concentration per pass through the ore zone, 216 kg solution is required per sq cm surface area of ore shell to form the deposit. Figures 4 and 8 show such solution fluxes are easily obtained for formation permeabilities of 0.25 md or greater. The problem, therefore, is to find a mechanism for precipitating the intrusive copper in a narrow ore shell.

One possibility is to use the temperature gradient at the top of the pluton during the early stages of intrusive cooling. Figure 13 shows that the region between 350° and 250°C forms a suitable ore shell during the first 2,000 years or so of pluton cooling. After ~2,000 years, the temperature region becomes too broad to produce a narrow ore shell or provide a relatively large concentration factor.

Unfortunately, the amount of fluid circulated through the ore shell in the first 2,000 years of cooling is too small to account for the necessary copper precipitation. For the 0.25-md case shown in Figure 13, at most about 15 kg of solution have circulated through each sq cm of surface area of the hypothesized ore shell. With a change in copper concentration of 1 g per kg, this means that at most 15 g of copper can be precipitated per sq cm of ore shell; the grade of the ore shell can at most be about 0.028 wt percent copper (equals 15 g Cu divided by $200 \times 10^2 \text{ cm} \times 2.7 \text{ g/cc}$).

Of course, if the formation were more permeable, more fluid might flow through the ore shell in the early stages of pluton cooling. Using the linear relationship between initial flow rate and permeability (see Fig. 8a), the 0.028 wt percent ore shell might be increased to 0.4 wt percent if the domain permeability were 3.5 md instead of 0.25 md. It seems unlikely, however, that 216 kg per sq cm water, the amount required to pass through the ore shell in order to produce the 0.4 wt percent grade with a 1 g Cu per kg H₂O drop per pass, could circulate through the intrusive without very substantially dispersing the initial heat anomaly. After all, the thermal anomaly is pretty well erased in 100,000 years at which time the integrated mass flux is at most only 250 kg per sq cm (see Figs. 2c and 4b). 216 kg water per sq cm will certainly smear out temperature gradients sufficiently to make thermal deposition in a 400-m shell difficult. It seems unlikely that temperature gradients alone can produce the type of porphyry ore shell commonly observed.²

As mentioned before, solution fluxes greater than required can be produced by small plutons if the formation permeability is greater than 0.25 md (Figs. 4 and 8b). Thus, there appears to be no problem

² If convection were prolonged strong temperature gradients could be maintained near the surface and substantial mineral deposition could occur there. This mechanism may well apply to kuroko-type deposits (Ohmoto and Rye, 1974). Porphyry copper ore shells are thought to have formed several kilometers beneath the surface, however.

precipitating an ore shell provided some nonthermal precipitation mechanism can be found. The best candidate is probably boiling.

The effect of salinity

Chlorine will be highly fractionated into the vapor phase as the intrusive solidifies (Kilinc and Burnham, 1972). One might therefore expect the salinity of magmatic water exsolved from the intrusive to be high. This is verified by high salinities found in fluid inclusions in many porphyry copper deposits. Salinities in fluid inclusion can be as high as 46 wt percent NaCl. (Moore and Nash, 1974; Roedder, 1971). Salinity, as previously mentioned, is an important factor affecting the ability of solution to transport copper and other base metals (Crerar and Barnes, 1976; Holland, 1972).

Although we have not explicitly taken salinity into account, several inferences are possible regarding the effects. If the intrusive initially contains magmatic waters of high salinity in addition to a heat anomaly, the salinity anomaly of the intrusive will be convected upward and dispersed in a manner similar to the way the thermal anomaly is carried upward and dispersed. There are several important differences, however.

First, unless there is surface discharge into a shallow, well-mixed sea or lake, salinity cannot escape out the top surface and will be recirculated into the surrounding formation. Low-salinity formation waters will dilute the salinity of the initial magmatic fluids, and the eventual result will be a formation at uniform temperature and salinity with the eventual salinity slightly higher than previously, reflecting the introduction of magmatic salt.

Secondly, and more importantly, if there is no boiling, the upward convection of the salt anomaly will proceed much faster than the upward convection of the thermal anomaly. This is basically because the convecting solutions can carry much more salt, relative to the ability of the formation to store salt, than they can carry heat, relative to the ability of the formation to absorb heat.

For the case where advection (fluid transport) of heat and salinity is much more important than diffusion of heat or salinity (e.g., the permeability of the formation is greater than ~ 0.1 md), the upward migration rates of heat and salinity can be quantified. If the fluid mass flux is q g/cm²-yr, the upward migration of heat, V_z^{heat} , will just be:

$$V_z^{\text{heat}} = \frac{\text{heat flux [cal/cm}^2\text{-sec]}}{\text{heat storage capacity [cal/cm}^3\text{]}} \\ = \frac{\Delta T \gamma q}{\Delta T \rho_m C_m} \text{ [cm/yr]}$$

Taking values in Appendix I, γ between 1 and 2

(Fig. 1b) and $q = 15$ g/cm²-yr, a value appropriate for the first 10,000 years of convection of a 0.25-md formation (see Fig. 7b),

$$V_z^{\text{heat}} = 0.28 \text{ to } 0.56 \text{ cm/yr}$$

The estimated time for the thermal anomaly in Figure 2c to reach the surface is therefore $2,750 \text{ m} / (0.28 - 0.56) = 5,000$ to 10,000 years. This is in good agreement with the computed initiation of high surface heat flows at about 8,000 years (Fig. 7c).

The upward migration of salinity will be given by

$$V_z^{\text{salinity}} = \frac{\text{salt flux [g NaCl/cm}^2\text{-sec]}}{\text{salt storage capacity g NaCl/cm}^3} \\ = \frac{\Delta S q / \rho}{\Delta S \phi} \text{ [cm/yr]}$$

ΔS is the magmatic salinity minus the base level formation salinity and is measured in grams NaCl/cm³ of fluid. Thus,

$$\frac{V_z^{\text{salinity}}}{V_z^{\text{heat}}} = \frac{\gamma}{\phi \rho_m C_m \rho}$$

Since $1/\rho > 1.0$, and $\gamma/\rho_m C_m > 1.85$, and $\phi < .04$,

$$\frac{V_z^{\text{salinity}}}{V_z^{\text{heat}}} > 46.$$

The salt anomaly will migrate upward toward the surface at least 46 times faster than the associated heat anomaly!

This means regions above the intrusive should increase in pore solution salinity significantly before they increase much in temperature. In fact, the intrusive's salinity anomaly may be flushed out and dispersed before the intrusive has cooled very much. Since salinity is required to carry significant base metal concentrations in solution, this suggests mineral deposition occurs soon after intrusion, while the intrusive itself is still very hot.

A final effect of salinity is that it extends the critical curve of water and thus permits fluid boiling at much greater pressures and depths. If the hydrothermal solution in Figure 2c had just 10 percent salinity, boiling as well as condensation would take place (compare extension of critical curve indicated in Fig. 1a with p-T loops in Fig. 6a). In the presence of CO₂, boiling may significantly raise the solution pH and thereby cause base metal precipitation (H. Ohmoto, pers. commun.).

Since steam can carry less dissolved salt than condensed water, the boiling salinity permits will complicate the upward convective dispersion of salinity.

Conclusions

A finite difference model has been developed that accounts for the variable properties of pure water (viscosity, specific volume, and enthalpy) and can

accommodate the effects of boiling and condensation. Variable water properties are shown to affect significantly computational results and their inclusion is therefore of interest (Fig. 11). The model is applied to the cooling of igneous intrusives to gain insight on the origin of geothermal systems and porphyry-type copper mineralization.

It is found from the modeling presented in this paper that fluid convection has the effect of carrying the initial thermal anomaly upward off the intrusive (like a hot-air balloon) until it impinges on the surface (Fig. 2c). At this point strong surface geothermal activity begins and convection practically ceases. Although there is some overlap, the geothermal reservoir tends to be "disconnected" from the intrusive in time and space. Surface heat flow reflects the cooling of a near-surface pool of hot water that migrated at an earlier time from an intrusive at depth (Fig. 7c).

Permeability, depth of burial, and pluton volume were systematically varied to study their effect on pluton cooling. Cooling is dramatically accelerated as permeability is increased (Fig. 7a). The maximum fluid circulation rate increases proportionally with permeability (Figs. 7b and 8a). The total mass of fluid circulated through the pluton during cooling increases with permeability (not linearly) and pluton volume (nearly linearly). The maximum surface heat flux depends most strongly on whether or not free solution flow (hot-spring activity) occurs out the top surface (Fig. 9f). Surface heat flux also depends importantly on permeability (Fig. 8c), depth of pluton burial (Fig. 10b), and pluton volume (Fig. 9e).

Despite the fact fluid densities are drastically reduced by the higher temperatures near the pluton, the resulting fluid circulation causes the hydrostatic pressure profile to be nearly normal in the uniform permeability cases computed. Even for formations with moderately variable permeability, hydrostatic pressures should tend to be more normal than not, due to the effects of convection.

For pure water, condensation is found to be a much more important phenomena than boiling. Hydrothermal solutions circulate around the critical point of water and hence become "gaseous" without boiling. Even for intrusives buried by 2.75 km of overburden, a vapor dominated reservoir is produced briefly beneath a condensed liquid zone for formation permeabilities ~ 0.25 md or greater. This vapor dominated region is self-supporting in the sense hydrostatic pressures within it are as great as hydrostatic pressures outside (Fig. 3a). If the fluids were saline, boiling would occur at the base of the vapor dominated steam zone as well as condensation at its top (Fig. 6a).

The duration of intense geothermal activity caused

by the model intrusives is brief ($< 20,000$ years). Unless intrusives are much bigger than those considered here, exploration for geothermal reserves may best be directed toward areas of very recent (volcanic centers) or nearly continuous (Wairakei) intrusive activity. The best geothermal resources may be those which have yet to manifest strong surface heat flows.

The amount of fluid circulation near the intrusive is accounted and shown to be sufficient to produce a typical porphyry copper ore shell. The laboratory data of Crerar (1974) are assumed to be valid and it is assumed copper originates in the intrusive. With these assumptions the natural fluid convection can account for the redistribution of copper from a porphyry intrusive into an ore shell outside the intrusive in the surrounding country rock as is frequently observed. However, it is shown that temperature gradients alone probably cannot account for the ore location (Fig. 13). Other methods of precipitation such as salinity gradients, boiling, or wall-rock reactions must be appealed to.

If the fluids evolving from the intrusive are highly saline, the intrusive's initial salinity anomaly will be convected upward by the fluid circulation and dispersed just as the heat anomaly is convected upward and dispersed. The upward advection and dispersion of the salinity anomaly will be much faster than the upward advection and dispersion of the heat anomaly, however (probably about 50 times faster). Since high fluid salinities are required to maintain high base metal solution concentrations, the dispersion of salinity may play an important role in mineral deposition. Boiling may complicate salinity dispersion.

Acknowledgments

The author would like to thank Kennecott Copper Corporation for support of the research reported in part in this paper and for permission to publish the results. Geochemical and geological discussions with Dr. Denis Norton during the early part of this work while Denis was the Kennecott, and Denis' enthusiastic support of the work during that period, are also gratefully acknowledged.

LEDGEMONT LABORATORY
KENNECOTT COPPER CORPORATION
128 SPRING STREET
LEXINGTON, MASSACHUSETTS 02173
August 31, December 28, 1976

REFERENCES

- Aamodt, R. L., 1976, Hydraulic fracturing in and communication between two adjacent wellbores [abs.]: *Am. Geophys. Union Trans.*, v. 57, p. 349.
Bruges, E. A., Latto, B., and Kay, K., 1966, New correlations and tables of the coefficient of viscosity of water and

- steam up to 1,000 bar and 1,000°C: *Internat. Jour. Heat and Mass Transfer*, v. 9, p. 465-480.
- Burnham, C. W., and Davis, N. F., 1971, The role of water in silicone melts I. P-V-T relations in the system $\text{NaAlSi}_3\text{O}_8\text{-H}_2\text{O}$ to 10 kilo-bars and 1,000°C: *Am. Jour. Sci.* v. 270, p. 54-79.
- Burnham, C. W., Holloway, J. R., and Davis, N. F., 1969, Thermodynamic properties of water to 1,000°C and 1,000 bars: *Geol. Soc. America Spec. Paper* 132, p. 96.
- Carnahan, B., Luther, H. A., and Wilkes, J. O., 1969, Applied numerical methods: New York, John Wiley & Sons, Inc., p. 604.
- Carlaw, H. S., and Jaeger, J. C., 1959, Conduction of heat in solids: Oxford, Clarendon Press, p. 510.
- Cathles, L. M., and Apps, J., 1975, A model of the dump leaching process that incorporates both physics and chemistry: *Metallurgical Trans.* v. 6B, p. 617-624.
- Cathles, L. M., Spedden, H. R., and Malouf, E. E., 1974, Tracer technique to measure the diffusional accessibility of matrix block mineralization, in Aplan, F. F., McKinney, W. A., and Pernicelli, A. D., eds., Solution mining symposium: New York, Am. Inst. Mining Metall. Petroleum Engineers, p. 129-147.
- Cheney, E. S., 1974, Examples of the application of sulfur isotopes to economic geology: *Am. Inst. Mining and Metall. Petroleum Engineers Trans.*, v. 255, p. 31-38.
- Crerar, D. A., 1974, Solvation and deposition of chalcopyrite and chalcocite assemblages in hydrothermal solutions: Ph.D. thesis, Penn. State University, p. 164.
- Crerar, D. A., and Barnes, H., 1976, Ore solution chemistry V. Solubilities of chalcopyrite and chalcocite assemblages in hydrothermal solutions at 250° to 350°C: *ECON. GEOL.*, v. 71, p. 772-794.
- Donaldson, I. G., 1968, The flow of steam water mixtures through permeable beds: A simple simulation of a natural undisturbed hydrothermal region: *New Zealand Jour. Sci.*, v. 11, p. 3-23.
- 1962, Temperature gradients in the upper layers of the earth's crust due to convective water flows: *Jour. Geophys. Research*, v. 67, p. 3449-3459.
- Elder, J. W., 1965, Physical processes in geothermal areas, in Lee, W. H. K., ed., *Terrestrial heat flow*, *Geophys. Mon. Ser. 8*: Baltimore, American Geophysical Union, p. 211-239.
- 1966, Heat and mass transfer in the earth: hydrothermal systems: New Zealand Dept. Sci. Indus. Research Bull. 169, p. 1-115.
- 1967, Steady free convection in a porous media: *Jour. Fluid Mechanics*, v. 27, p. 29-48.
- Fyfe, W. S., 1974, Heats of chemical reactions and submarine heat production: *Royal Astron. Soc. Geophys. Jour.*, v. 37, p. 213-215.
- Fyfe, W. S., and Henley, R. S., 1973, Some thoughts on chemical transport processes, with particular reference to gold: *Minerals Sci. Eng.* v. 5, p. 295-303.
- Henley, R. W., 1973, Some fluid dynamics and ore genesis: *Inst. Mining Metallurgy Trans.*, v. 82B, p. 1-8.
- Holland, H. D., 1972, Granites, solutions and base metal deposits: *ECON. GEOL.* v. 67, p. 281-301.
- Holst, P. H., and Aziz, K., 1972, Transient three-dimensional natural convection in confined porous media: *Internat. Jour. Heat Mass Transfer*, v. 15, p. 73-90.
- James, A. H., 1971, Hypothetical diagrams of several porphyry copper deposits: *ECON. GEOL.*, v. 66, p. 43-47.
- Keenan, J. H., Keyes, F. G., Hill, P. G., and Moore, J. G., 1969, Steam tables: New York, John Wiley & Sons, Inc., p. 162.
- Kilinc, J. A., and Burnham, C. W., 1972, Partitioning of chloride between a silicate melt and coexisting aqueous phase from 2 to 8 kilobars: *ECON. GEOL.*, v. 67, p. 231-235.
- Lapwood, E. R., 1948, Convection of a fluid in a porous medium: *Cambridge Philos. Soc. Proc.*, v. 44, p. 508-521.
- Lindgren, W., 1907, The relation of ore deposition to physical conditions: *ECON. GEOL.*, v. 2, p. 105-127.
- Lister, C. R. B., 1974, On the penetration of water into hot rock: *Royal Astron. Soc. Geophys. Jour.*, v. 39, p. 465-509.
- Lovering, T. S., 1935, Theory of heat conduction applied to geological problems: *Geol. Soc. America Bull.*, v. 46, p. 69-94.
- Lowell, J. D., and Guilbert, J. M., 1970, Lateral and vertical alteration-mineralization zoning in porphyry ore deposits: *ECON. GEOL.*, v. 65, p. 373-408.
- Mercer, J. W., Pinder, G. F., and Donaldson, I. G., 1975, A galerkin-finite element analysis of the hydrothermal system at Wairakei, New Zealand: *Jour. Geophys. Research*, v. 80, p. 2608-2621.
- Moore, W. J., and Nash, J. J., 1974, Alteration and fluid inclusion studies of the porphyry copper ore body at Bingham, Utah: *ECON. GEOL.*, v. 69, p. 631-645.
- Muskat, M., 1937, The flow of homogeneous fluids through porous media: New York, McGraw Hill, p. 763.
- Norton, D. L., 1972, Concepts relating anhydrite deposition to solution flow in hydrothermal systems: *Internat. Geol. Cong.*, 24th, Montreal 1972, Sec 10, p. 237-244.
- Norton, D. L., and Cathles, L. M., in press, Thermal aspects of ore deposition, in Barnes, H. L., ed., *Geochemistry of hydrothermal ore deposits*, 2nd ed.: New York, Holt, Rinehart and Winston.
- Ohmoto, H., and Rye, R. O., 1974, Hydrogen and oxygen isotopic compositions of fluid inclusions in the Kuroko deposits, Japan: *ECON. GEOL.*, v. 69, p. 947-953.
- Palm, E., Weber, J., and Kuernvold, O., 1972, On steady state convection in porous medium: *Jour. Fluid Mechanics*, v. 54, p. 153-161.
- Peaceman, D. W., and Rachford, H. H., 1955, The numerical solution of parabolic and elliptic differential equations: *Jour. Soc. Indus. Appl. Math.*, v. 3, p. 28-41.
- Phillips, W. J., 1973, Mechanical effects of retrograde boiling and its probable importance in the formation of some porphyry ore deposits: *Inst. Mining Metallurgy Trans.*, v. 82B, p. 90-98.
- Ribando, R. J., Torrance, K. E., and Turcotte, D. L., 1976, Numerical models for hydrothermal circulation in the oceanic crust: *Jour. Geophys. Research*, v. 81, p. 3007-3012.
- Roedder, E., 1971, Fluid inclusion studies on the porphyry-type ore deposits at Bingham, Utah, Butte, Montana, and Climax, Colorado: *ECON. GEOL.*, v. 66, p. 98-120.
- Rubin, H., 1973, Effect of solute dispersion on thermal convection in a porous medium layer: *Water Resources Research*, v. 9, p. 968-973.
- Schmidt, E., 1969, Properties of water and steam in SI-units: New York, Springer-Verlag, p. 205.
- Sheppard, S. M. F., Nielsen, R. L., and Taylor, H. P., Jr., 1971, Hydrogen and oxygen isotope ratios in minerals from porphyry copper deposits: *ECON. GEOL.*, v. 66, p. 515-542.
- Snow, D. J., 1968, Rock fracture spacings, openings and porosities. *Am. Soc. Civil Eng. Jour. Soil Mech. Found.*, v. SM1, p. 73-91.
- Sourirajan, S., and Kennedy, G. C., 1962, The system $\text{H}_2\text{O-NaCl}$ at elevated temperatures and pressures: *Am. Jour. Sci.*, v. 260, p. 115-141.
- Taylor, H. P., 1971, Oxygen isotope evidence for large-scale interaction between meteoric ground waters and tertiary granodiorite intrusions, western Cascade Range, Oregon: *Jour. Geophys. Research*, v. 76, p. 7855-7874.
- Torrance, K. E., 1968, Comparison of finite difference computations of natural convection: [U. S.] Natl. Bur. Standards Jour. Research, v. 72B, p. 281-301.
- Weast, R. C., 1971, Handbook of chemistry and physics, Cleveland, The Chemical Rubber Co., p. F36.
- White, D. E., Muffler, L. J. P., and Truesdell, A. H., 1971, Vapor-dominated hydrothermal systems compared with hot-water systems: *ECON. GEOL.*, v. 66, p. 75-97.
- Whitney, J. A., 1975, Vapor generation in a quartz monzonite magma: A synthetic model with application to porphyry copper deposits: *ECON. GEOL.*, v. 70, p. 346-358.
- Wooding, R. A., 1957, Steady state free thermal convection of liquid in a saturated permeable medium: *Jour. Fluid Mechanics*, v. 2, p. 273-285.

APPENDIX I

Parameter	Definition	Units	Value used	Comments
c_f	Heat capacity of water	cal/gm-°C		Variable, see \mathcal{C}
c_m	Heat capacity of the fluid saturated rock formation (media)	cal/gm-°C	0.2	See Carslaw and Jaeger (1959, appendix VI)
d	Effective fracture aperture	cm	<0.03	
g_0	Gravitational field strength	cm/sec ²	980	
H	Depth extent of system—i.e., depth to which fluid flow is permitted	cm	5.0 km	
\mathcal{C}	Enthalpy of water	cal/gm	Pure water values; see Figure 1c	
j_T	Diffusional flux of heat	calories/cm ² -sec	Computed	Wairakei's regional average over 2,500 km ² is 50 μ cal/cm ² -sec with heat flow in the more intense parts of each local area \sim 10,000 μ cal/cm ² -sec (Elder, 1965)
k'	Permeability of a porous fractured media to fluid flow	cm ²	0.05-0.5 millidarcies	10^{-11} cm ² = 1 md
K_m	Thermal conductivity of water saturated rock	cal/cm-sec-°C	6×10^{-3}	Donaldson (1968) picks mean value of 3×10^{-3} cal/cm-sec-°C
p	Hydrostatic pressure	dynes/cm ²		
p_0	Component of p that depends only on depth (z)			
q	Darcy fluid mass flux	g/cm ² -sec		Wairakei's 4×10^5 gm/sec over area of 13 km ² indicates $q = 94$ g/cm ² -yr (Donaldson, 1968)
R	Heat of reactions that alter intrusive	cal/g-°C	0.0666	See Norton and Cathles (in press) and discussion of eq. (3) in text
T	Temperature of water saturated rock or fluid that flows through it	°C		Water and rock assumed always at (essentially) the same temperature
v	Fluid velocity	cm/sec		
V	Darcy velocity	cm/sec		$V = v\phi_f$
α	Coefficient of thermal expansion	°C ⁻¹	10^{-3}	
γ	Pseudoheat capacity	cal/g-°C	Figure 3b	Ratio of enthalpy to temperature at each grid location at the previous timestep or the average value between timesteps
ν	Kinematic viscosity	cm ² -sec ⁻¹	Pure water values, see Figure 1c	
ρ	Fluid density gm/cm ³		Pure water values, see Figure 1a	
ρ_m	Density of the fluid saturated rock formation	g/cm ³	2.7	
ρ_0	Fluid density variations that are a function of depth (z) only	g/cm ³		
Φ	Total formation porosity including both flow fracture porosity and pore porosity in the impermeable matrix blocks between flow fractures	Dimensionless	$2-4 \times 10^{-2}$	
Φ_f	Flow channel or fracture porosity in the direction of flow	Dimensionless	$\sim 10^{-3}$	
$\underline{\psi}$	Vector stream function describing fluid flow	cm ² /sec		$\nabla \times \underline{\psi} = g$
ψ_x	x component of the vector stream function (appropriate for 2 dimensional flow)	cm ² /sec		$\nabla \times \psi_x \hat{x} = g$
$\bar{\psi}$	Dimensionless stream function			$\bar{\psi} = \psi \mathcal{C}^* / K_m T^*$; $\mathcal{C}^* = 1$ cal/g, $T^* = 1^\circ\text{C}$

1977, Bibliography in *Subsurface Geology*, 4th ed., LeRoy, L.W., LeRoy, D.O., and Raese, J.W.;
Colorado School of Mines.

UNIVERSITY OF UTAH
RESEARCH INSTITUTE
EARTH SCIENCE LAB.

Bibliography

- Abel, J. F., Jr., 1967, Tunnel mechanics: Colorado School Mines Quart., Golden, v. 62, no. 2, 88 p.
- Addison, W. W., 1940, Buckley oil field, Gladwin County, Michigan: Am. Assoc. Petroleum Geologists Bull., v. 24, no. 11, p. 1981.
- Ageton, R. W., 1967, Stress ellipsoid determination in rock-burst prone area at a 4000-foot depth, Galena Mine, Wallace, Idaho: U. S. Bur. Mines Rept. Inv. 6997, 23 p.
- Agnew, A. F., 1955, Facies of Middle and Upper Ordovician rocks of Iowa: Am. Assoc. Petroleum Geologists Bull., v. 39, no. 9, p. 1703-1752.
- Al-Chalabi, M., 1974, An analysis of stacking, RMS, average, and interval velocities over a horizontally layered ground: Geophys. Prospecting, v. 22, p. 458-475.
- Alexanderson, T., 1974, Carbonate cementation in coralline algae nodules in the Skagerrak, North Sea—Biochemical precipitation in undersaturated waters: Jour. Sed. Petrology, v. 44, no. 1, p. 7-26.
- Al-Hashimi, A. R. K., and Brownlow, A. H., 1970, Copper content of biotites from the Boulder batholith, Montana: Econ. Geology, v. 65, no. 8, p. 985-992.
- Allan, Andrew, Jr., Kaar, P. H., and Cooner, J. D., Sr., 1953, Measurement of loads borne by underground-roadway supports: U.S. Bur. Mines Rept. Inv. 4946.
- Allen, Terrance, 1968, Particle size measurement: Chapman and Hall, London, 248 p.
- Allman, M., and Lawrence, D. F., 1972, Geological laboratory techniques: Arco Publishing Co., New York.
- Am, K., 1972, The arbitrarily magnetized dyke—interpretation of characteristics: Geoexploration, v. 10, p. 63-90.
- American Association for Advancement of Science, 1964, Air conservation: AAAS Bull., June, p. 1.
- American Association of Petroleum Geologists, 1970, American commission on stratigraphic nomenclature: p. 1-17.
- American Petroleum Institute, 1962, Recommended practice for determining permeability of a porous media: Am. Petroleum Inst. R. P. 27.
- 1975, Recommended practice—standard procedure for the evaluation of hydraulic fracturing fluids: Am. Petroleum Inst.
- American Society of Photogrammetry, 1960, Manual of photographic interpretation: Am. Soc. Photogrammetry, Washington, D.C.
- Anderson, D. N., 1972, Geothermal development in California, SPE Paper 4180, Ann. Calif. Mtg., Bakersfield.
- Andrews-Jones, D. A., 1968, The application of geochemical techniques to mineral exploration: Colorado School Mines Mineral Industries Bull., Golden, v. 11, no. 6.
- Applied Technology Council, 1976, Working draft recommended comprehensive seismic design provisions for buildings: Prep., Applied Tech. Coun., San Francisco, California.
- Armstrong, F. C., 1970, Geologic factors controlling the uranium resources in the Gas Hills district, Wyoming: Wyoming Geol. Assoc. Guidebook, Field Conf., Casper, p. 31-44.
- Ashley, G. H., and others, 1933, Classification and nomenclature of rocks units: Geol. Soc. America Bull., v. 44, p. 423-459.
- Aufrecht, W. R., 1971, Statistical study of air and effective oil permeability for various production zones in Canada: Jour. Canadian Well Logging Soc.
- Azaroff, L. V., 1968, Elements of X-ray crystallography: McGraw-Hill Book Co., New York, 610 p.
- Azaroff, L. V., and Buerger, M. J., 1958, The powder method: McGraw-Hill Book Co., New York, 342 p.
- Back, W. R., 1966, Hydrochemical facies and groundwater flow patterns in northern part of Atlantic Coastal Plain: U.S. Geol. Survey Prof. Paper 498-A, 42 p.
- Back, W. R., and Hanshaw, B., 1965, Chemical geohydrology: in Advances in hydroscience: V. T. Chow, ed., Academic Press Inc., New York, v. 2, p. 49-109.
- Bailey, E. H., and Stevens, R. E., 1960, Selective staining of K-feldspar and plagioclase on rock slabs and thin sections: Am. Mineralogist, v. 45, p. 1020-1026.
- Baillie, A. D., 1955, Devonian system of Williston Basin: Am. Assoc. Petroleum Geologists Bull., v. 39, no. 5, p. 575-629.
- Bailey, F. H., 1952, Differential thermal analysis compared in micropaleontology for stratigraphic correlation: Am. Assoc. Petroleum Geologists Ann. Mtg., Pasadena, California.
- Baker, W. M., 1963, Waste disposal well completion and maintenance: Indust. Water and Wastes, p. 43-47.
- Balch, A. H., 1971, Color sonagrams—a new dimension in seismic data interpretation: Geophysics, v. 36, p. 1074-1098.
- Bandy, O. L., 1960a, The geologic significance of coiling ratios in the foraminifer *Globigerina pachyderma* (Ehrenberg): Jour. Paleontology, v. 34, p. 671-681.
- 1960b, General correlation of foraminiferal structure with environment: Internat. Geol. Congress, Norden, pt. 22, p. 7-19.
- Bandy, O. L., and Arnal, R. E., 1960, Concepts of foraminiferal paleoecology: Am. Assoc. Petroleum Geologists Bull., v. 44, no. 12, p. 1921-1932.
- Banks, H. O., 1961, The relationship of geologists and engineers in planning public works: GeoTimes, v. 5, no. 7, p. 16-17.
- Banks, H. O., and Richter, R. C., 1953, Sea-water intrusion into groundwater basins bordering the California coast and inland bays: Am. Geophys. Union Trans., v. 34, p. 575-582.
- Banner, F. T., and Blow, W. H., 1967, The origin, evolution and taxonomy of the foraminiferal genus *Pullentiatina* Cushman, 1927: Micropaleontology, v. 13, no. 2, p. 133-162.
- Barnes, H. L., 1967, ed., Geochemistry of hydrothermal ore deposits: Holt, Rinehart and Winston, Inc., New York, p. 166-232.
- Barnes, M. P., and Simos, J. G., 1968, Ore deposits of the Park City district with a contribution on the Mayflower lode: in Ore deposits of the United States., 1933-1967: AIMMPE, v. 2, p. 1102-1126.
- Barth, G. C., and Smith, R. M., 1940, Relative porosity and permeability of producing formations of Hugoton field as indicated by gas withdrawals and pressure decline: Am. Assoc. Petroleum Geologists Bull., v. 24, no. 10, p. 1803.
- Bastin, E. E., 1950, Interpretation of ore textures: Geol. Soc. America Mem. 45.

Bibliography

- Bateman, A. M., 1950, Economic mineral deposits: John Wiley & Sons, Inc., New York, p. 245-289.
- Be, A. W. H., Harrison, S. M., and Lott, L., 1973, *Orbulina universa* d'Orbigny in the Indian Ocean: *Micropaleontology*, v. 19, no. 2, p. 150-192.
- Bean, E. F., 1950, Engineering geology of highway location, construction, and materials: in *Berkey Volume*, Geol. Soc. America, p. 181-194.
- , 1950, Engineering geology of highway location, construction, and materials: in *Berkey Volume*, Geol. Soc. America, p. 181-194.
- Bean, R. J., 1966, A rapid graphical solution for the aeromagnetic anomaly of the two-dimensional tabular body: *Geophysics*, v. 31, no. 5, p. 963.
- Berg, L. C., 1943, Influence of salt admixtures upon dissociation of dolomite: *Acad. Sci. U. R. S. S. (Doklady) Comptes Rendus*, no. 1, p. 24-27.
- Berggren, W. A., and van Couvering, J. A., 1974, *The late Neogene*: Elsevier Publ. Co. New York, p. 1-216.
- Bergstrom, R. E., 1956, *Surface correlation of some Pennsylvanian limestones in mid-continent by thermoluminescence*: *Am. Assoc. Petroleum Geologists Bull.*, v. 40, no. 5, p. 918-942.
- Berkelhamer, L. H., 1944, Differential thermal analysis of quartz: *U.S. Bur. Mines Rept. Inv.* 3763.
- Berkey, C. P., 1929, Responsibilities of the geologist in engineering projects: *Am. Inst. Mining, Metall. Engineers Tech. Pub.* 215, p. 5.
- Bernstein R., and Ferneyhough, D. G., 1975, Digital image processing: *Photogram. Eng. and Remote Sensing*, v. 41, no. 12, p. 1465-1476.
- Beus, A. A., and Sitnin, A. A., 1972, Geochemical specialization of magnetic complexes as criteria for the exploration of hidden deposits: 24th Internat. Geol. Congress, Montreal, Canada, v. 6, p. 101-105.
- Bhappu, R. B., 1975, Economic evaluation of in-place leaching and solution mining situations: *Short course on in-place leaching and solution mining*, Mackay School Mines, Univ. Nevada, Reno.
- Biot, M. A., 1956, Theory of propagation of elastic waves in a fluid-saturated porous solid: *Jour. Acoust. Soc. America*, v. 28.
- Bird, A. G., 1975, New gold-silver discoveries at the Sunnyside mine, San Juan County, Colorado: *Mining Yearbook, Natl. West. Mining Conf. and Exhibition*, Colorado Mining Assn., p. 83-84.
- Blake, W., 1966, Application of the finite-element method of analysis in solving boundary value problems in rock mechanics: *Internat. Jour. Rock Mech. Mining Sci.*, v. 3, p. 169-180.
- Blake, W., and Duval, W., 1969, Some fundamental properties of rock noises: *AIMMPE Trans.*, v. 244, p. 288-290.
- Blake, W., and Leighton, F. W., 1970, Recent developments and applications of the microseismic method in deep mines: in *Rock mechanics—theory and practice*: AIMMPE, p. 429-443.
- Blanchard, R., 1969, Interpretation of leached outcrops: *Nevada Bur. Mines, Univ. Nevada, Reno*.
- Blanchet, P. Y., and Godwin, C. I., 1972, Geology system for computer and manual analysis of geologic data from porphyry and other deposits: *Econ. Geology*, v. 67, p. 796-813.
- Blow, W. H., 1956, Origin and evolution of the foraminiferal genus *Orbulina* d'Orbigny: *Micropaleontology*, v. 2, no. 1, p. 57-70.
- Bonham, L. C., and Spotts, J. H., 1971, Measurement of grain orientation: in *Procedures in sedimentary petrology*: Carver, R. E. ed., Wiley-Interscience, New York, p. 285-312.
- Born, W. T., 1941, The attenuation of earth materials: *Geophysics*, v. 6, p. 132-148.
- Bosworth-Smith, 1903, Report of the chief inspector of mines for January 1, 1902 to June 30, 1903: *Mysore Geol. Dept. Rept.*, 46 p.
- Bouma, A. H., 1963, Sedimentary facies model of turbidites: *Am. Assoc. Petroleum Geologists Bull.*, v. 47, no. 2, p. 351.
- Bradshaw, P. M. D., Clews, D. R., and Walker, J. L., 1970a, Detailed surveys: in *Exploration geochemistry*, pt. 2: Mining in Canada, p. 22-32.
- , 1972, Canadian problem-valley glaciated and non-glaciated areas: in *Exploration geochemistry*, pt. 7, *Canadian Mining Jour.*, v. 93, no. 5, p. 53-64.
- Bramlette, M. N., 1941, The stability of minerals in sandstone: *Jour. Sed. Petrology*, v. 11, p. 32-36.
- Bray, E. E., and Evans, E. D., 1965, Hydrocarbons in nonreservoir-rock source beds: *Am. Assoc. Petroleum Geologists Bull.*, v. 49, no. 3, p. 248-257.
- Brice, J. W., Jr., and Holmes, B. C., 1964, Engineered casing cementing programs using turbulent flow techniques: *Jour. Petroleum Tech.*, p. 503-508.
- Bristow, Q., and Jonasson, I. R., 1972, Vapor sensing for mineral exploration: *Canadian Mining Jour.*, v. 93, no. 5, p. 39-47.
- Brooks, R. R., 1972, *Geobotany and biogeochemistry in mineral exploration*: Harper and Row, New York, 290 p.
- Brown, G., 1961, ed., *The X-ray identification and crystal structures of clay minerals*: The Mineralog. Soc., London, 544 p.
- Burbank, W. S., 1941, Structural control of ore deposition in the Red Mountain, Sneffels and Telluride districts of the San Juan Mountains, Colorado: *Colorado Sci. Soc. Proc.*, v. 14, no. 5, p. 141-261.
- Buckle, F., 1965, The rock-burst hazard in Wright-Hargreaves mine in Kirkland Lake, Ontario: *Canadian Mining Jour.*, v. 86, no. 9, p. 81-87.
- Buddington, A. F., 1933, Ore deposits of the western states: in *Lindgren Volume*: AIMMPE, p. 350-385.
- Bukovansky, M., and Rodriguez, M., and Cedrun, G., 1974, Three rock slides in stratified and jointed rocks: *Internat. Soc. Rock Mechanics Cong.*, Denver, Colorado, v. 11, pt. B, p. 854-858.
- Bullard, E. C., 1975, Overview of plate tectonics: in *Petroleum and global technics*: Fischer, A. G., and Judson, S., eds., Princeton Univ. Press, p. 5-19.
- Bunte, A. S., 1939, Subsurface study of Greenwich pool, Sedgwick County, Kansas: *Am. Assoc. Petroleum Geologists Bull.*, v. 23, no. 5, p. 657.
- Burst, J. F., 1969, Diagenesis of Gulf Coast clayey sediments and its possible relation to petroleum migration: *Am. Assoc. Petroleum Geologists Bull.*, v. 53, no. 1, p. 73-93.
- Burwell, E. B., Jr., and Moneymaker, B. C., 1950, Geology in dam construction: in *Berkey Volume*, Geol. Soc. America, p. 11-43.
- Burwell, E. B., Jr., and Roberts, G. D., 1950, The geologist in the engineering organization: in *Berkey Volume*, Geol. Soc. America, p. 1-9.
- Buschbach, T. C., 1964, *Cambrian and Ordovician strata of*

Freeze core for long for
storage plastic bags for
short hauls.

Bibliography

- northeastern Illinois: Illinois Geol. Survey Rept. Inv. 218, 90 p.
- Buyce, M. R., and Friedman, C. M., 1975, Significance of authigenic K-feldspar in Cambrian-Ordovician carbonate rocks of the Proto-Atlantic shelf in North America: Jour. Sed. Petrology, v. 45, p. 808-821.
- Bynum, R. S., Jr., and Koepf, E. H., 1957, Whole-core analysis methods and interpretation of data from carbonate reservoirs: Jour. Petroleum Tech., v. 9, no. 11, p. 11-15.
- California Division of Mines and Geology, 1973, Urban geology master plan for California: California Div. Mines and Geology Bull. 198, p. 119.
- Cameron, E. N., 1961, Ore microscopy: John Wiley & Sons, Inc., New York, 293 p.
- Canadian Institute of Mining and Metallurgy, 1957, Methods and case histories in mining geophysics: Mercury Press, Montreal, 359 p.
- Cannon, H. L., 1960, The development of botanical methods of prospecting for uranium on the Colorado Plateau: U.S. Geol. Survey Bull. 1085-A, p. 1-50.
- Carpenter, R. H., Pope, T. A., and Smith, R. L., 1975, Fe-Mn oxide coatings in stream sediment geochemical surveys: Geochem. Explor. Jour., v. 4, no. 3, p. 349-364.
- Carter, L. G., and Evans, G. W., 1964, A study of cement-pipe bonding: Jour. Petroleum Tech., v. XVI, p. 157-160.
- Carter, L. G., and Slagle, K. A., 1972, A study of completion practices to minimize gas communication: Jour. Petroleum Tech.
- Carter, R. D., 1957, Derivation of the general equation for estimating the extent of the fractured area: Drilling and Production Practice, Am. Petroleum Inst., p. 267-268.
- Cartwright, Keros, 1968, Thermal prospecting for groundwater: Water Resources Research, v. 4, no. 2, p. 393-401.
- Carver, R. E., 1971, Heavy-mineral separation: in Procedures in sedimentary petrology, Carver, R. E. ed., Wiley-Interscience, New York, p. 427-452.
- Casagrande, Arthur, 1937, Seepage through dams: New England Water Works Assoc. Jour., v. LI, no. 2, p. 295-336.
- 1948, Classification and identification of soils: Am. Soc. Civil Engineers Trans., v. 113, p. 901.
- Chaffee, M. A., 1975, Geochemical exploration techniques applicable in the research for copper deposits: U.S. Geol. Survey Prof. Paper 907-B, 26 p.
- Chayes, Felix, 1952, Notes on the staining of potash feldspar with sodium cobaltinitrite in thin section: Am. Mineralogist, v. 37, p. 337-340.
- 1956, Petrographic modal analysis—an elementary approach: John Wiley & Sons, New York, 113 p.
- Cheatham, J. B., Jr., and McEver, J. W., 1964, Behavior of casing subjected to salt loading: Jour. Petroleum Tech., p. 1069-1076.
- Chebotarev, I. I., 1955, Metamorphism of natural waters in the crust of weathering: Geochim. et Cosmochim. Acta, v. 8, p. 22-48, 137-170.
- Chilingar, G. V., 1956a, Relationship between Ca/Mg ratio and geologic age: Am. Assoc. Petroleum Geologists Bull., v. 40, no. 9, p. 2256-2266.
- 1956b, Use of Ca/Mg ratio in porosity studies: Am. Assoc. Petroleum Geologists Bull., v. 40, no. 10, p. 1489-2493.
- Chisholm, W. A., 1963, The petrology of Upper Jurassic and Lower Cretaceous strata of the western interior: Wyoming Geol. Assoc. and Billings Geol. Soc., Joint Field Conf. Guidebook, Northern Powder River Basin, p. 71-86.
- Christian, W. W., Chatterji, J., and Ostroot, C. W., 1975, Gas leakage in primary cementing—a field study and laboratory investigation: SPE paper 5517, SPE-AIME Ann. Mtg., Dallas, Texas.
- Clapp, F. G., 1910, A proposed classification of petroleum and natural gas fields: Econ. Geology, v. 5, p. 503-524.
- 1917, Revision of the structural classification of petroleum and natural petroleum and natural gas fields: Geol. Soc. America Bull., v. 28, p. 553-602.
- Clark, C. R., and Carter, L. G., 1973, Mud displacement with cement slurries: Jour. Petroleum Tech., p. 775-783.
- Condit, H. R., 1970, Spectral reflectance in American soils: Photogram. Eng., v. 34, no. 9, p. 955.
- Conolly, H. J. C., 1936, A contour method of revealing some ore structures: Econ. Geology, v. 31, p. 259-271.
- Cook, N. G. W., 1963a, The seismic location of rockbursts: Rock Mechanics Symp., Pergamon Press, Oxford, p. 493-516.
- 1963b, The basic mechanics of rockbursts: South African Inst. Mining Metall. Jour., v. 64, p. 71-81.
- 1965, A note on rockbursts considered as a problem of stability: South African Inst. Mining Metall. Jour., v. 65, p. 437-446.
- Cook, N. G. W., and Hojem, J. P. M., 1966, A rigid 50-ton compression and tension testing machine: South African Mech. Eng., v. 16, p. 89-92.
- Coope, J. A., 1973, Geochemical prospecting for porphyry copper-type mineralization—a review: Jour. Geochem. Explor., v. 2, no. 2, p. 81-102.
- Cooper, D. O., and others, 1973, Simplified financial and risk analysis for minerals exploration: in Symp. on Computer Applications in the Minerals Industry: Coll. Mines, Univ. Arizona, Tucson, p. B1-B14.
- Coulson, J. R., 1972, Shear strength of flat surfaces in rock: in Stability of rock slopes: Am. Soc. Civil Engineers; Symp. Rock Mechanics, Univ. Illinois, Cording, E. J., ed.
- Crawford, C. B., 1967, Quick clays of eastern Canada: Eng. Geology, Elsevier Publ. Co., Amsterdam, v. 2, p. 239-265.
- Creasey, S. C., 1966, Hydrothermal alteration: in Geology of the porphyry copper deposits, southwestern North America: Univ. Arizona Press, Tucson, p. 51-74.
- Crowle, P. J., 1927, Notes on ground movement and methods of support in deep mines: Kolar Gold Field Mining Metall. Soc.
- 1931, Ground movements and method of support in deep mining: Inst. Mining Metall. Trans. v. 40, p. 77.
- Csatary, C. T., 1974, Application of computer programs in the review of the ventilation design of Elsburg and western areas gold mines in South Africa: Internat. Symp. on Computer Applications in the Minerals Industry, Colorado School Mines, Golden, p. G18-G62.
- Cullity, B. D., 1956, Elements of x-ray diffraction: Addison-Wesley Publ. Co., Mass., 514 p.
- Cumming, J. D., and Wicklund, A. P., 1975, Diamond drill handbook: J. K. Smit & Sons Diamond Products Ltd., Toronto, Canada.
- Cunningham, W. C., Fehrenbach, J. R., and Maier, L. F., 1972, Arctic cements and cementing: Canadian Petroleum Tech. Jour.
- Curry, J. R., 1975, Marine sediments, geosynclines and orogeny: in Petroleum and global tectonics: Fischer, A. G., and Judson, S., eds., Princeton Univ. Press, p. 157-222.

July Vol 25

Bibliography

- 922
- Curtin, G. C., King, H. D., and Mosier, E. L., 1974, Movement of elements into the atmosphere from coniferous trees in subalpine forests of Colorado and Idaho: *Jour. Geochem. Explor.*, v. 3, no. 3, p. 245-264.
- Daly, J. and Page, C. N., 1952, Seismograph interpretation as related to changes in sedimentary section in West Texas and New Mexico: *Am. Assoc. Petroleum Geologists Bull.*, v. 36, no. 4, p. 658-676.
- Daneshy, A. A., 1973, On the design of vertical hydraulic fractures: *Jour. Petroleum Tech.*, p. 83.
- Dapples, E. C., 1955, General lithofacies relationship of the St. Peter sandstone and Simpson group: *Am. Assoc. Petroleum Geologists Bull.*, v. 39, no. 4, p. 444-467.
- Dapples, E. C., Krumbein, W. C., and Sloss, L. L., 1948, Tectonic control of lithologic association: *Am. Assoc. Petroleum Geologists Bull.*, v. 32, no. 10, p. 1924-1947.
- , 1950, The organization of sedimentary rocks: *Jour. Sed. Petrology*, v. 20, no. 1, p. 3-20.
- David, M., 1973, Tools for planning—variances and conditional simulation: *Internat. Symp. on Computer Applications in the Minerals Industry*, Coll. Mines, Univ. Arizona, Tucson, p. D10-D25.
- Davidson, E. S., 1973, Geohydrology and water resources of the Tucson basin, Arizona: U.S. Geol. Survey Water-Supply Paper 1939-E, 81 p.
- Davies, D. K., Ethridge, F. G., and Berg, R. R., 1971, Recognition of barrier environments: *Am. Assoc. Petroleum Geologists Bull.*, v. 55, p. 550-565.
- Davis, R. E., and Williams, C. E., 1973, Optimization procedures for open pit mine scheduling: *Internat. Symp. on Computer Application in the Minerals Industry*, Coll. Mines, Univ. Arizona, Tucson, p. C1-C18.
- Davis, S. N., 1969, Porosity, permeability of natural materials: in *Flow through porous media*: De Wiest, R. J. M., ed., Academic Press Inc., New York, p. 53-89.
- Davis, S. N., and De Wiest, R. J. M., 1966, *Hydrogeology*: John Wiley & Sons, Inc., New York, 463 p.
- Davis, T. L., 1972, Velocity variations around Luduc reefs, Alberta: *Geophysics*, v. 37, p. 584-604.
- DeGeoffroy, J., and Wignall, T. K., 1972, A statistical study of geological characteristics of porphyry copper-molybdenum deposits in the Cordilleran Belt—application to the rating of porphyry prospects: *Econ. Geology*, p. 656-658.
- Denkhaus, H. G., 1958, The application of the mathematical theory of elasticity to problems of stress in hard rock at great depth: *South African Assoc. Mine Managers Papers*, p. 271-310.
- Denkhaus, H. G., Roux, A. J. A., and Gobbelaar, C., 1958, A study of the mechanical properties of rock with special reference to their bearing on the occurrence of rock bursts: *South African Mech. Eng.*, v. 8.
- DeRidder, E., 1972, Evaluation of magnetic depth estimation techniques: Colorado School Mines, Golden, M.Sc. thesis.
- De Sitter, L. V., 1956, *Structural geology*: McGraw-Hill Book Co., Inc., New York, 552 p.
- Deshmukh, S. S., 1974, Projects, risks, and decisions: *Internat. Symp. on Computer Applications in the Minerals Industry*, Colorado School Mines, Golden, p. A39-A55.
- Dickey, P. A., 1944, Natural potentials in sedimentary rocks: *Am. Inst. Mining Metall. Petroleum Eng. Trans.*, v. 155, p. 49.
- Dickey, P. A., and Rohn, R. E., 1955, Facies control of oil occurrence: *Am. Assoc. Petroleum Geologists Bull.*, v. 39, no. 11, p. 2306-2320.
- Diest, F. H., 1965, A nonlinear continuum approach to the problem of fracture zones and rock bursts: *South African Inst. Mining Metall. Jour.*, v. 65, p. 502-522.
- Diment, W. H., Urban, T. C., Sass, J. H., Marshall, B. V., Munroe, R. J., and Lachenbrush, A. H., 1975, Temperature and heat contents based on conductive transport of heat: in *Assessment of geothermal resources of the United States*, p. 84-103; eds. White, D. E., and Williams, D. L.: U.S. Geol. Survey Circ. 726, 155 p.
- Dinsdale, J. R., 1937, Ground failure around excavations: *Inst. Mining Metall. Trans.*, v. 46, p. 673-700.
- Dobrin, M. B., 1962, *Introduction to geophysical prospecting*: McGraw-Hill Book Co., New York, 435 p.
- Dohr, G. P., and Stiller, P. K., 1975, Migration velocity determination, Pt. 2, Applications: *Geophysics*, v. 40, p. 6-16.
- Doll, H. G., 1948, The SP log: Theoretical analysis and principles of interpretation: *AIMMPE Tech. Publ.* 2463.
- , 1949, Introduction to induction logging and application to logging of wells drilled with oil-base mud: *Jour. Petroleum Tech.* paper 2641.
- , 1950, The microlog—a new electrical logging method for detailed determination of permeable beds: *AIMMPE Trans.* v. 189.
- , 1953, The microlaterolog: *Jour. Petroleum Tech.*, v. 5.
- Domenico, S. N., 1974, Effect of water saturation on seismic reflectivity of sand reservoirs encased in shale: *Geophysics*, v. 39, p. 759-769.
- Dravo Corporation, 1974, Analysis of large-scale non-coal underground mining methods: U.S. Bur. Mines Contract Rept. S0122059, 605 p.
- Dresser-Atlas Corporation, 1970, Neutron lifetime interpretation: Dresser-Atlas Corp., Houston, Texas.
- Dryden, A. L., 1931, Accuracy in percentage representation of heavy mineral frequencies: *United States, Natl. Acad. Sci. Proc.*, v. 17, p. 233-238.
- Dueterhoeft, W. C., 1961, Propagation effects in induction logging: *Geophysics*, v. 26, no. 2.
- Dueterhoeft, W. C., Hartline, R. E., and Thomsen, H. S., 1961, The effect of coil design on the performance of the induction log: *Jour. Petroleum Tech. Paper* 1538-G.
- Dueterhoeft, W. C., and Smith, H. W., 1962, Propagation effects on radial response in induction logging: *Geophysics*, v. 27, no. 4.
- Duncan, D. M., 1974, Open pit gold mining at Cortez: 1974 Mining Yearbook, Natl. Western Mining Conf. and Exhibition, Denver, Colorado Mining Assoc., p. 92-94.
- Dupuit, J., 1863, *Etudes théoriques et pratiques sur le mouvement des eaux dans les canaux découverts et à travers les terrains perméables*: Dunod, Paris, 304 p.
- Duvall, W. I., and Stephenson, D. E., 1965, Seismic energy available from rock bursts and underground explosions: *AIMMPE Trans.*, v. 232, no. 3, p. 235-240.
- Dyck, W. and others, 1971, Comparison of regional geochemical uranium exploration methods in the Beaverlodge area, Saskatchewan: *Geochem. Explor. CIM Spec.*, v. 11, p. 132-150.
- Eckel, E. B., 1958, ed., *Landslides and engineering practice*: Highway Research Board Spec. Rept. 27, 232 p.
- Edwards, A. B., 1954, *Textures of the ore minerals*: Australian Inst. Mining Metall., 2d ed., Melbourne, 242 p.

Bibliography

- Ekström, T. K., and others, 1975, COREMAP—a data system for drill cores and boreholes: *Econ. Geology*, v. 70, p. 359-368.
- Emmons, W. H., 1940, *The principles of economic geology*: McGraw-Hill Book Co., Inc., New York, 2d ed., p. 194-197.
- Erdman, J. C., 1961, Some chemical aspects of petroleum genesis as related to the problem of source bed recognition: *Geochim. et Cosmochim. Acta*, v. 32, no. 1, p. 16-36.
- 1964, Petroleum—its origin in the earth: in Hedberg, H. D., 1964, *Geologic aspects of origin of petroleum*: Am. Assoc. Petroleum Geologists Bull., v. 48, no. 11, p. 1755-1803.
- 1975, Geochemical formation of oil: in *Petroleum and global tectonics*: Fischer, A. G., and Judson, S., eds., Princeton Univ. Press, p. 225-248.
- Erickson, A. J., Jr., 1970, Discovery and development of the north ore zone, Ontario mine, Park City district, Utah: Presented AIMMPE Ann. Mtg., Denver, Colorado.
- Erickson, R. L., Marranzino, A. P., Oda, Uteana, and Janes, W. W., 1966, Geochemical reconnaissance in the Pequop Mountains and Wood Hills, Elko County, Nevada: U.S. Geol. Survey Bull. 1198-E, 20 p.
- Erickson, R. L., and others, 1966, Gold geochemical anomaly in the Cortez district, Nevada: U.S. Geol. Survey. Circ. 534, 10 p.
- Ericson, D. B., and Wollin, G., 1964, *The deep and the past*: Alfred A. Knopf, New York, 292 p.
- Espey, H. R., 1976, Geophysical activity in 1975: *Geophysics*, v. 41, p. 780-794.
- Evamy, B. D., 1963, The application of a chemical staining technique to a study of dedolomitization: *Sedimentology*, v. 2, p. 164-170.
- Evans, C. W., and Carter, L. G., 1962, Bonding studies of cementing compositions to pipe and formations: *Drilling and Prod. Practice*, Am. Petroleum Inst. 72.
- Everett, J. E., 1974, Obtaining interval velocities from stacking velocities when dipping horizons are included: *Geophys. Prospecting*, v. 22, p. 122-142.
- Evers, J. F., and Iyer, B. C., 1975, A statistical study of the SP log in fresh-water formations of Wyoming's Big Horn and Wind River basins: *Canadian Well Logging Soc., 5th Symp.*
- Faust, C. T., 1949, Dedolomitization, and its relation to a possible derivation of a magnesium-rich hydrothermal solution: *Am. Mineralogist*, v. 34, p. 789-823.
- Feigl, Fritz, 1958, *Spot tests in inorganic analysis*: Elsevier Publ. Co. New York, 5th ed., 600 p.
- Felix, D. W., 1969, An inexpensive recording settling tube for the analysis of sands: *Jour. Sed. Petrology*, v. 39, p. 777-780.
- Feo-Codecido, Gustavo, 1956, Heavy-mineral techniques and their application to Venezuelan stratigraphy: *Am. Assoc. Petroleum Geologists Bull.*, v. 40, p. 984-1000.
- Fewings, J. H., and Pitts, J. D., 1973, Digital computing control systems application for the grinding circuits at the ASARCO Silver Bell concentrator: *Symp. on Computer Applications in the Minerals Industry*, Coll. Mines, Univ. Arizona, Tucson, p. F1-F25.
- Fischer, A. G., 1975, Origin and growth of basins: in *Petroleum and global tectonics*: Fischer, A. G., and Judson, S., eds, Princeton Univ. Press, p. 47-79.
- Fischer, R. P., 1974, Exploration guides to new uranium districts and belts: *Econ. Geology*, v. 69, no. 3, p. 362-377.
- Fitzgerald, P. E., James, J. R., and Austin, R. L., 1941, Laboratory and field observations of effect of acidizing oil reservoirs composed of sands: *Am. Assoc. Petroleum Geologists Bull.*, v. 25, no. 5, p. 850-851.
- Flawn, P. T., 1970, *Environmental geology*: Harper and Row, New York, 313 p.
- Folk, R. L., 1955, Student operator error in determination of roundness, sphericity, and grain size: *Jour. Sed. Petrology*, v. 25, p. 297-301.
- 1966, A review of grain-size parameters: *Sedimentology*, v. 6, p. 73-93.
- 1968, *Petrology of sedimentary rocks*: Hemphills, Austin, Texas, 170 p.
- Folk, R. L., and Ward, W. C., 1957, Brazos river bar—a study in the significance of grain size parameters: *Jour. Sed. Petrology*, v. 27, p. 3-26.
- Forgotson, J. M., Jr. 1954, Regional stratigraphic analysis of Cotton Valley group of upper Gulf coastal plain: *Am. Assoc. Petroleum Geologists Bull.*, v. 38, no. 12, p. 2476-2499.
- 1960, Review and classification of quantitative mapping techniques: *Am. Assoc. Petroleum Geologists Bull.*, v. 44, p. 83-100.
- 1963, How computers help find oil: *Oil and Gas Jour.*, v. 61, no. 11, p. 100-109.
- Forgotson, J. M., Jr., and Iglehart, C. F., 1967, Current uses of computers by exploration geologists: *Am. Assoc. Petroleum Geologists Bull.*, v. 51, p. 1202-1224.
- Forgotson, J. M., Jr., and Stark, P. H., 1972, Well-data files and the computer, a case history from northern Rocky Mountains: *Am. Assoc. Petroleum Geologists Bull.*, v. 56, p. 1114-1127.
- Forrester, J. D., 1948, *Principles of field and mining geology*: John Wiley & Sons, Inc., New York, p. 331-348.
- Fortescue, J. A. C., and Hornbrook, E. H. W., 1966, A brief survey of the progress made in biogeochemical prospecting research at the Geological Survey of Canada, 1962-1965: *Geol. Surv. Canada Paper 66-54*, p. 111-132.
- 1967, Progress report on biogeochemical research at the Geological Survey of Canada, 1963-1966: *Geol. Surv. Canada Paper 67-32*, pt. 1, 143 p.
- Freeman, W. E., and Visher, G. S., 1975, Stratigraphic analysis of the Navajo sandstone: *Jour. Sed. Petrology*, v. 45, p. 651-668.
- Freeze, R. A., and Witherspoon, P. A., 1966, Theoretical analysis of regional groundwater flow (1): *Water Resources Research*, v. 2, no. 4, p. 641-656.
- 1967, Theoretical analysis of regional groundwater flow (2): *Water Resources Research*, v. 3, no. 2, p. 623-634.
- 1968, Theoretical analysis of regional groundwater flow (3): *Water Resources Research*, v. 4, no. 3, p. 581-590.
- Friedman, C. M., 1958, Determination of sieve-size distribution from thin-section data for sedimentary petrological studies: *Jour. Geology*, v. 66, p. 394-416.
- 1959, Identification of carbonate minerals by staining methods: *Jour. Sed. Petrology*, v. 29, p. 87-97.
- 1961, Distinction between dune, beach, and river sands from their textural characteristics: *Jour. Sed. Petrology*, v. 31, p. 514-529.
- 1962a, Comparison of moment measures for sieving and thin section data in petrological studies: *Jour. Sed. Petrology*, v. 32, p. 15-25.
- 1962b, On sorting, sorting coefficients, and the log-normality of grain size distribution of sandstones: *Jour. Geology*, v. 70, p. 737-753.
- 1967, Dynamic processes and statistical parameters

Bibliography

- for size frequency distribution of beach and river sands: *Jour. Sed. Petrology*, v. 37, p. 327-354.
- _____. 1971, Staining: in *Procedures in sedimentary petrology*: Carver, R. E., ed., John Wiley & Sons, Inc., New York, 653 p.
- Furnas, C. C., 1929, Flow of gases through beds of broken solids: *U. S. Bur Mines Bull.* 307, 144 p.
- Gabler, R. E., Sager, R., Brazier, S., and Pourcian, J., 1975, *Introduction to physical geography*: Rinehart Press, p. 801.
- Gabriel, A., and Cox, E. P., 1929, A staining method for the quantitative determination of certain rock minerals: *Am. Mineralogist*, v. 14, p. 290-292.
- Gaither, A., 1953, A study of porosity and grain relationship in experimental sands: *Jour. Sed. Petrology*, v. 23, p. 180-195.
- Galehouse, J. S., 1967, Provenance and paleocurrents of the Paso Robles formation, California: *Geol. Soc. America Bull.*, v. 78, p. 951-976.
- _____. 1971a, Sedimentation analysis: in *Procedures in sedimentary petrology*: Carver, R. E., ed., Wiley-Interscience, New York, p. 69-94.
- _____. 1971b, Point counting, in *Procedures in sedimentary petrology*: Carver, R. E., ed., Wiley-Interscience, New York, p. 385-407.
- Gardner, G. H. F., Gardner, L. W., and Gregory, A. R., 1974, Formation velocity and density—the diagnostic basics for stratigraphic traps: *Geophysics*, v. 39, p. 770-780.
- Gates, D. M., 1965, Radiant energy, its receipt and disposal: *Meteorological Monographs*, v. 6, no. 28, p. 1-26.
- Geertsma, J., 1961, Velocity-log interpretation—the effect of rock bulk compressibility: *Soc. Pet. Engineers Jour.*
- Geertsma, J., and de Klerk, F., 1969, A rapid method of predicting width and extent of hydraulically induced fractures: *Jour. Petroleum Tech.*, SPE-AIME, Dallas, Texas, p. 1571.
- Gentry, D. W., 1974, Development of deep mining techniques: *World mineral supplies—assessment in perspective*: Elsevier Publ. Co., New York.
- Gentry, D. W., and O'Neil, T. J., 1974, A short course on financial modeling and evaluation of new mine properties: *Internat. Symp. Applications of Computers in the Mineral Industries*, Colorado School Mines, Golden, 149 p.
- Geological Survey of Canada, 1967, Mining and groundwater geophysics: Queen's Printer, Ottawa, *Economic Geology Rept.* 26, 722 p.
- Gerdemann, P. E., and Meyers, H. E., 1972, Relationships of carbonate facies patterns to ore distribution and to ore genesis in the southeast Missouri lead district: *Econ. Geology*, v. 67, no. 4, p. 426-433.
- Gibbs, M. A., 1966, Delaware basin cementing—problems and solutions: *Jour. Petroleum Tech.*, p. 1281-1285.
- Gibbs, R. J., Matthews, M. D., and Link, D. A., 1971, The relationship between sphere size and settling velocity: *Jour. Sed. Petrology*, v. 41, p. 7-18.
- Gidel, M. H., 1950, Geology in the discovery development and exploitation of mineral deposits: in *Berkey Volume*, *Geol. Soc. America*, p. 273-294.
- Ginsburg, R. N., 1956, Environmental relationships of grain and constituent particles in some south Florida carbonate sediments: *Am Assoc. Petroleum Geologists Bull.*, v. 40, no. 10, p. 2384-2427.
- Gleeson, C. F., and Hornbrook, E. H. W., 1974, Semi-regional geochemical studies demonstrating the effectiveness of till sampling at depth: *Geochem. Explor.*, Elsevier Publ. Co., New York, p. 611.
- Goddard, E. N., Trask, P. D., DeFord, R. K., Rove, O. N., Singewald, J. T., and Overbeck, R. M., 1970, *Rock-color chart*: *Geol., Soc. America*.
- Golder, H. Q., 1971, Contribution to panel discussion: in *Stability in open pit mining*: Brawner, C. O., and Milligan, V., eds., *Soc. Mining Engineers, AIMMPE*, p. 272.
- Goodwin, A. M., 1965, Mineralized volcanic complexes in the Porcupine-Kirkland Lake-Noranda region, Canada: *Econ. Geology*, v. 60, p. 955-971.
- Goodwin, A. M., and Ridler, R. H., 1970, The Abitibi orogenic belt: in *Symp. Basins and Geosynclines of the Canadian Shield*: Bae, A. J., ed., *Geol. Survey Canada Paper* 70-40, p. 1-30.
- Gott, C. B., and Botbol, 1973, Zoning of major and minor metals in the Coeur d'Alene mining district, Idaho: *Geochem. Explor.*, IMM, London, 1972, p. 1-12.
- Graf, D. L., 1952, Preliminary report on the variations in differential thermal curves of low-iron dolomites: *Illinois Geol. Survey Rept. Inv.* 161.
- Grant, F. S., and West, G. F., 1965, *Interpretation theory in applied geophysics*: McGraw-Hill Book Co., New York, 584 p.
- Graton, L. C., and Fraser, H. J., 1935, Systematic packing of spheres with particular relation to porosity and permeability: *Jour. Geology*, v. 43, p. 785-909.
- Greenman, N. N., and LeBlanc, R. J., 1956, Recent marine sediments and environments of northwest Gulf of Mexico: *Am. Assoc. Petroleum Geologists Bull.*, v. 40, no. 5, p. 813-847.
- Griffiths, D. H., and King, R. F., 1965, *Applied geophysics for engineers and geologists*: Pergamon Press, Oxford, 225 p.
- Griffiths, J. C., 1952, Grain size distribution and reservoir-rock characteristics: *Am. Assoc. Petroleum Geologists Bull.*, v. 36, p. 205-229.
- _____. 1960, Modal analysis of sediments: *Rev. Geograph. Phys. Geol. Dynamique*, v. 3, p. 29-48.
- _____. 1967, Scientific method in analysis of sediments: McGraw-Hill Book Co., New York, 508 p.
- Griffiths, J. C., and Singer, D. A., 1973, Size, shape and arrangement of some uranium ore bodies, in *Internat. Symp. on Computer Applications in the Minerals Industry*: *Coll. Mines, Univ. Arizona, Tucson*, p. B82-B112.
- Grim, R. E., 1944, Differential thermal analysis of clays and shales, control and prospecting method: *Illinois Geol. Survey Rept. Inv.* 96.
- _____. 1953, *Clay mineralogy*: McGraw-Hill Book Co., New York.
- Grim, R. E., and Rowland, R. A., 1943, Differential thermal analysis of clay minerals and other hydrous materials: *Am. Mineralogist*, v. 27, no. 11, p. 746-761.
- Grosman, M., and others, 1961, A sonic method for analyzing the quality of borehole casings: *Jour. Petroleum Tech.*, v. 13.
- Guilbert, J. M., and Lowell, J. D., 1974, Variations in zoning patterns in porphyry ore deposits: *Canadian Mining Metall. Bull.*, p. 1-11.
- Gustafson, L. B., and Hunt, J. P., 1975, Porphyry copper deposit at El Salvador, Chile: *Econ. Geology*, v. 70, no. 5, p. 857-912.
- Guyod, Hubert, 1955, *Guyod model electrical resistivity logs*: Houston, Texas, copyright Hubert Guyod, 17 volumes.

- Haas, M. W., 1969, *Frontiers in economic micropaleontology*: Jour. Geology Education, v. 17, no. 3, p. 81-86.
- Hails, J. R., and Hoyt, J. H., 1969, The significance and limitations of statistical parameters for distinguishing ancient and modern sedimentary environments of the lower Georgia coastal plain: Jour. Sed. Petrology, v. 39, p. 559-580.
- Hansen, W. R., 1965, The Black Canyon of the Gunnison—today and yesterday: U.S. Geol. Survey Bull. 1911.
- Harbaugh, J. W., 1964, A computer method for four-variable trend analysis illustrated by a study of oil-gravity variations in southeastern Kansas: Kansas State Geol. Survey Bull. 171, 58 p.
- Harbaugh, J. W., and Merriam, D. F., 1968, Computer applications in stratigraphic analysis: John Wiley & Sons, Inc., New York, 282 p.
- Hardin, J. W., 1951, Geological aspects of coastal engineering: Conf. on Coastal Engineering, Proc., p. 133-136.
- Harms, J. C., and Tackenberg, P., 1972, Seismic signatures of sedimentation models: Geophysics, v. 37, p. 45-58.
- Harris, D. P., 1973, A subjective probability appraisal of metal endowment of northern Sonora, Mexico: Econ. Geology, v. 68, p. 222-242.
- Harris, D. P., and Brock, T. N., 1973, A conceptual Bayesian geostatistical model for metal endowment: in Internat. Symp. on Computer Applications in the Minerals Industry: Coll. Mines, Univ. Arizona, Tucson, p. B113-184.
- Harshman, E. N., 1968, Uranium deposits of Wyoming and South Dakota: in Ore deposits of the United States, 1933-1967: New York, AIMMPE, v. 1, p. 815-831.
- Hartman, R. R., Teskey, D. J., and Friedberg, J. L., 1971, A system for rapid digital aeromagnetic interpretation: Geophysics, v. 36, p. 891-918.
- Hastings, J. S., 1959, Exploration and development drilling in the Uravan mineral belt: Moab, Utah, Four Corners Geol. Soc. Guidebook, p. 115-117.
- , 1963, Mining geology methods in the Uravan mineral belt: Mines Magazine, Golden, Colorado, p. 14-17.
- Haun, J. D., 1975, Methods of estimating the volume of undiscovered oil and gas resources: Am. Assoc. Petroleum Geologists Studies in Geology, no. 1.
- Hausen, D. N., and Kerr, P. F., 1968, Fine gold occurrence at Carlin, Nevada: in Ore deposits of the United States, 1933-1967: New York, AIMMPE, v. 1, p. 908-940.
- Hawkes, H. E., Bloom, Harold, Riddell, J. E., and Webb, J. S., 1960, Geochemical reconnaissance in eastern Canada: Internat. Geol. Cong., Mexico City, v. 3, p. 607-621.
- Hawkes, H. E., and Webb, J. S., 1962, Geochemistry in mineral exploration: Harper and Row, New York, 415 p.
- Haycocks, C., and Lucas, J. R., 1973, Computerized determination of mine planning data from boreholes: Mining Eng., AIMMPE, v. 25, no. 4, p. 52-56.
- Hazen, S. W., and Meyer, W. L., 1966, Using probability models as a basis for making decisions during mineral deposit exploration: U.S. Bur. Mines Rept. Inv. 6778, 83 p.
- Heald, K. C., 1950, Geologic engineering in the petroleum industry: in Berkey Volume, Geol. Soc. America, p. 251-271.
- Hedberg, H. D., 1948, Time-stratigraphic classification of sedimentary rocks: Geol. Soc. America Bull., v. 59, p. 447-462.
- Heeger, J. E., 1913, Ueber die mikrochemische Untersuchung fein verteilter Carbonate im Gesteinsschliff: Centralbl. Mineralogie, p. 44-51.
- Heiland, C. A., 1946, Geophysical exploration: Prentice Hall, New York, 1013 p.
- Henkel, J. J., 1970, Geotechnical considerations of lateral stresses: ASCE Specialty Conf. Lateral Stresses in the Ground and Design of Earth-retaining Structures, Cornell Univ., New York, p. 1-49.
- Henningsen, Dierk, 1967, Crushing of sedimentary rock samples and its effect on shape and number of heavy minerals: Sedimentology, v. 8, p. 253-255.
- Herness, S. K., 1950, Subsurface and office representation in mining geology: in Subsurface Geologic Methods, Colorado School of Mines, p. 969-1037, Golden.
- Heroy, W. B., 1941, Petroleum geology: in Geology 1888-1938, 50th Anniv. Volume: Geol. Soc. America Bull., p. 534-539.
- Hetenyi, M., 1954, Handbook of experimental stress analysis: John Wiley & Sons, Inc., New York.
- Hicks, W. C., and Berry, J. E., 1956, Application of continuous velocity logs to determination of fluid saturation of reservoir rocks: Geophysics, v. 21, p. 739-754.
- Hill, F. C., 1954, An investigation into the problem of rock bursts: South African Inst. Mining Metall. Jour., v. 55, p. 63-102.
- Hill, H. J., and Anderson, A. E., 1959, Streaming potential phenomena in SP log interpretation: AIMMPE Trans., v. 216, p. 203.
- Hill, H. J., and Milburn, J. D., 1956, Effect of clay and water salinity on electrochemical behavior of reservoir rocks: Jour. Petroleum Tech., p. 65.
- Hill, R. D., 1971, Restoration of a terrestrial environment—the surface mine: Assoc. Southeastern Biologists Bull., v. 18, no. 3, p. 107-116.
- Hoek, E., 1970, Estimating the stability of excavated slopes in open-cast mines: Inst. Mining Metall. (London) Trans., Sec. A, v. 79.
- Hoek, E., and Bray, J. W., 1974, Rock slope engineering: Inst. Mining Metall. (London).
- Hottman, C. E., and Johnson, R. K., 1965, Estimation of formation pressures from log-derived shale properties: Jour. Petroleum Tech.
- Howard, G. C., and Fast, C. R., 1970, Hydraulic fracturing: SPE-AIME Monograph (Dallas, Texas) v. 2, p. 203.
- Howard, W. V., and David, M. W., 1936, Development of porosity in limestones: Am. Assoc. Petroleum Geologists Bull., v. 20, no. 11, p. 1402.
- Hrebar, M. J., 1971, Business risk analysis applied to preliminary economic evaluation of mining properties: Univ. Arizona, Tucson, M. Sci. thesis.
- Hubbert, M. K., 1940, The theory of groundwater motion: Jour. Geology, v. 48, p. 785-944.
- Hubert, J. F., 1971, Analysis of heavy-mineral assemblages: in Procedures in sedimentary petrology: Carver, R. E., ed., Wiley-Interscience, New York, p. 453-478.
- Hunt, C. B., 1950, Military geology: in Berkey Volume, Geol. Soc. America, p. 295-327.
- Hunt, J. M., 1972, Distribution of carbon in crust of earth: Am. Assoc. Petroleum Geologists Bull., v. 56, no. 11, p. 2273-2277.
- Hunt, J. M., and Jamieson, G. W., 1956, Oil and organic matter in source rocks of petroleum: Am. Assoc. Petroleum Geologists Bull., v. 40, no. 3, p. 477-488.
- Hurd, B. C., and Fitch, J. L., 1959, The effect of gypsum on core analysis results: AIMMPE Trans., p. 216, 221.

Bibliography

926

- QE
433
H87
- Hutchinson, C. A., Jr., Dodge, C. F., and Polasek, T. L., 1961, Identification, classification, and prediction of reservoir nonuniformities affecting production operations: *Jour. Petroleum Tech.*, v. 13, p. 223-230.
- Hutchinson, C. S., 1974, *Laboratory handbook of petrographic techniques*: John Wiley & Sons, Inc., New York, 527 p.
- Hutchinson, R. W., 1973, Volcanogenic sulfide deposits and their metallogenic significance: *Econ. Geology*, v. 68, no. 8, p. 1223-1247, Dec.
- Hvorshev, M. J., 1946, Annual meeting of the Highway Research Board: 25th Ann. Mtg., Washington, D.C.
- _____, 1949, Subsurface exploration and sampling of soils for civil engineering, U.S. Army Engineers Waterways Experiment Station: Corps of Engineers, Vicksburg, Mississippi.
- _____, 1953, The unified soil classification system: *Tech. Mem. 3-357*, U.S. Army Engineers Waterways Experiment Station, Corps of Engineers, Vicksburg, Mississippi.
- Hyatt, D. E., 1973, The environmental impact statement—a new requirement in planning the mining operation: *Colorado School Mines Mineral Industries Bull.*, Golden, v. 16, no. 3, 10 p.
- Imbrie, John, 1955, Biofacies analysis: *Geol. Soc. America Spec. Paper 62*, p. 449-464.
- _____, 1964, Factor analytic model in paleoecology: in *Approaches to paleoecology*: Imbrie, John, and Newell, Norman, eds., John Wiley & Sons, Inc., New York, p. 407-422.
- Ingram, R. L., 1971, Sieve analysis: in *Procedures in sedimentary petrology*: Carver, R. E., ed., Wiley-Interscience, New York, p. 49-67.
- Inman, D. L., 1952, Measures for describing the size distribution of sediments: *Jour. Sed. Petrology*, v. 22, p. 125-145.
- Ireland, H. A., 1936, The use of insoluble residues for correlation in Oklahoma: *Am. Assoc. Petroleum Geologists Bull.*, v. 20, p. 1086-1181.
- _____, 1947, Terminology for insoluble residues: *Am. Assoc. Petroleum Geologists Bull.*, v. 31, p. 1479-1490.
- _____, 1956, Upper Pennsylvanian arenaceous foraminifera from Kansas: *Jour. Paleontology*, v. 30, p. 831-864.
- _____, 1971, Insoluble residues: in *Procedures in sedimentary petrology*: Carver, R. E., ed., Wiley-Interscience, New York, p. 479-498.
- Ives, William, Jr., 1955, Evaluation of acid etching of limestone: *Kansas Geol. Survey Bull.* 114, pt. 1.
- Jacob, C. E., 1950, Flow of groundwater: in *Engineering hydraulics*: Rouse, H., ed., John Wiley & Sons, Inc., New York, p. 321-386.
- Jackson, M. L., 1964, Soil clay mineralogy analysis: in *Soil clay mineralogy*: Rich, C. I., and Kunze, G. W., eds., North Carolina Press, Chapel Hill, p. 245-294.
- Jakosky, J. J., 1950, *Exploration geophysics*: Trija Publ. Co., Los Angeles, 1195 p.
- Jankowski, W., 1970, Empirical investigation of some factors affecting elastic wave velocities in carbonate rocks: *Geophys. Prospecting*, v. 18, p. 103-118.
- Janssens, A., 1973, Stratigraphy of the Cambrian and Lower Ordovician rocks in Ohio: *Ohio Div. Geol. Survey Bull.* 64, 197 p.
- Jenkins, R. E., and Bush, D. C., 1970, An improved method for the analysis of reservoir rocks containing clays: *Canadian Well Logging Soc.*, Paper 7053.
- Jerome, S. E., and Cook, D. R., 1967, Relation of some metal mining districts in the western United States to regional tectonic environments and igneous activity: *Nevada Bur. Mines Bull.* 69, p. 35.
- John, K. W., 1969, Graphical stability analysis of slopes in jointed rock: *Jour. Soil Mechanics and Foundations Div. Proc., ASCE*, v. 94, SM2, p. 497-526. Discussions and closure, v. 95, SM6, p. 1541-1546.
- Johns, W. D., and Shimoyama, A., 1972, Clay minerals and petroleum-forming reactions during burial and diagenesis: *Am. Assoc. Petroleum Geologists Bull.*, v. 56, no. 11, p. 2160-2167.
- Johnson, D. W., 1919, *Shore processes and shoreline development*: John Wiley & Sons, Inc., New York.
- Johnson, P. L., 1969, *Remote sensing in ecology*: Univ. Georgia Press, Athens, 244 p.
- Johnson, T. B., and Sharp, W. R., 1971, A three-dimensional dynamic programming method for optimal ultimate open pit design: *U.S. Bur. Mines Rept. Inv.* 7553, 25 p.
- Jones, C., 1968, *Economic analysis for mining ventures and projects*: Surface Mining (1st ed.), New York, AIMMPE, p. 997-1013.
- Jones, J. S., 1926, Report of the sub-committee on rockbursts—Kolar Gold Field.
- Joseph, E. H. A., 1938, Rock bursts: The mechanism of crush bursts: *South Africa Chem. Metall. Mining Soc. Jour.*, v. 39, p. 114-134.
- Jumikis, A. R., 1962, *Soil mechanics*: Van Nostrand, New York.
- Karlak, R. F., and Burnett, D. S., 1966, Quantitative phase analysis by X-ray diffraction: *Anal. Chem.*, v. 38, p. 1741-1745.
- Kastelic, W. R., 1975, Gold placer exploration, Nome, Alaska: *Mining Yearbook, Natl. West. Mining Conf., and Exhibition, Colorado Mining Assoc.*, Denver, p. 85-92.
- Katz, Amitai, and Friedman, G. M., 1965, The preparation of stained acetate peels for the study of carbonate rocks: *Jour. Sed. Petrology*, v. 35, p. 248-249.
- Keelan, D. K., 1972, A critical review of core analysis techniques: *Canadian Pet. Tech. Jour.*, v. 11, no. 2, p. 42-55.
- Kellagher, R. C., and Flanagan, F. J., 1956, The multiple-cone sample splitter: *Jour. Sed. Petrology*, v. 26, p. 213-221.
- Keller, G. V., and Frischknecht, F. C., 1966, *Electrical methods in geophysical prospecting*: Pergamon Press, New York, 517 p.
- Keller, W. D., 1956, Clay minerals as influenced by environments of the formation: *Am. Assoc. Petroleum Geologists Bull.*, v. 40, no. 11, p. 2689-2710.
- Keopf, E. H., and Granberry, R. J., 1960, The use of sidewall core analysis in formation evaluation: *Jour. Petroleum Tech.*, Oct.
- Kiersch, G. A., 1955, *Engineering geology*: Colorado School Mines Quart., Golden, v. 50, no. 3, 122 p.
- _____, 1965, Vaiont Dam disaster: *GeoTimes*, p. 9-12.
- _____, 1969, The geologist and legal cases—responsibility, preparation and the expert witness: in *Case histories in engineering geology*, no. 7: *Geol. Soc. America*, p. 1-6.
- _____, 1972, Guidelines for the engineer as an expert witness: *Natl. Soc. Prof. Engineers, Sec. on Prof. Engineers Private Practice*, Washington, D.C.
- King, F. H., 1898, Principles and conditions of the movement of groundwater: *U.S. Geol. Survey 19th Ann. Rept.* pt. 2, p. 208-218.
- Kingman, D. S. S., 1975, Rift Valley basins and sedimentary history of trailing continental margins: in *Petroleum and*
- ← New 1

Bibliography

- global tectonics, Fischer, A. G., and Judson, S., eds., Princeton Univ. Press, p. 83-126.
- Klemme, H. D., 1975, Geothermal gradients, heat flow and hydrocarbon recovery: in *Petroleum and global tectonics*, Fischer, A. G., and Judson, S., eds., Princeton Univ. Press., p. 251-304.
- Klinkenberg, J., 1941, The permeability of porous media to liquids and gases: *Drilling Prod. Practice*, p. 200.
- Klug, H. P., and Alexander, L. E., X-ray diffraction procedures for polycrystalline and amorphous materials: John Wiley & Sons, Inc., New York, 716 p.
- Koch, G. S., and Link, R. F., 1971, Statistical analysis of geological data: John Wiley & Sons, Inc., New York, v. 1 (1970), and v. 2 (1971).
- Koch, G. S., and others, 1972, Computer programs for geology: Artronic Inf. Systems, New York, 142 p.
- Koenig, J. B., 1972, *Worldwide status of geothermal exploration and development*: SPE Paper 4179, SPE-ALME Ann. Calif. Fall Mtg., Bakersfield.
- Koerperich, E. A., 1975, Utilization of Waxman-Smiths equations for determining oil saturation in low-salinity, shaly sand reservoir: *Jour. Petroleum Tech.*, p. 1204.
- Konikow, L. F., and Bredehoeft, J. D., 1974, Modeling flow and chemical quality changes in an irrigated stream-aquifer system: *Water Resources Research*, v. 10, no. 3, p. 546-562.
- Frank, K., 1972, Tidal currents of sediment distribution in Northumberland Strait, Maritime Provinces: *Jour. Sed. Petrology*, v. 42, p. 596-601.
- Krumbein, W. C., 1934, Size frequency distribution of sediments: *Jour. Sed. Petrology*, v. 4, p. 65-77.
- , 1935, Thin-section mechanical analysis of indurated sediments: *Jour. Geology*, v. 43, p. 482-496.
- , 1946, Criteria for subsurface recognition of unconformities: *Am. Assoc. Petroleum Geologists Bull.*, v. 26, no. 1, p. 36-62.
- , 1948, Lithofacies maps and regional sedimentary stratigraphic analysis: *Am. Assoc. Petroleum Geologists Bull.*, v. 32, no. 10, p. 1909-1923.
- , 1950, Geological aspects of beach engineering: in *Key Volume, Geol. Soc. America*, p. 195-223.
- , 1952, Principles of facies map interpretation: *Jour. Sed. Petrology*, v. 22, p. 200-211.
- , 1956, Regional and local components in facies maps: *Am. Assoc. Petroleum Geologists Bull.*, v. 40, p. 2163-2194.
- , 1959, Trend surface analysis of contour-type maps with irregular control-point spacing: *Jour. Geophys. Research*, v. 64, p. 823-834.
- , 1962, Open and closed number systems in stratigraphic mapping: *Am. Assoc. Petroleum Geologists Bull.*, v. 46, p. 2229-2245.
- Krumbein, W. C., and Monk, G. D., 1943, Permeability as a function of the size parameters of unconsolidated sand: *AIMMPE Trans.*, v. 151, p. 153-163.
- Krumbein, W. C., and Nagle, F. C., 1953, Regional stratigraphic analysis of "Upper Cretaceous" rocks of Rocky Mountain Region: *Am. Assoc. Petroleum Geologists Bull.*, v. 37, no. 5, p. 940-960.
- Krumbein, W. C., and Pettijohn, F. J., 1938, *Sedimentary petrology*: Appleton Century Croft, New York, 549 p.
- Krumbein, W. C., and Sloss, J. J., 1956, *Stratigraphy and sedimentation*: W. H. Freeman and Co., San Francisco, p. 1-497.
- Krynine, D. P., 1948, The megascopic study and field classification of sedimentary rocks: *Jour. Geology*, v. 56, p. 130-165.
- Krynine, P. D., and Judd, W. R., 1957, *Principles of engineering geology and geotechnics*: McGraw-Hill Book Co., New York, 730 p.
- Lafehr, T. R., 1965, The estimation of the total amount of anomalous mass by Gauss's Theorem: *Jour. Geophys. Research*, v. 70, p. 1911-1919.
- Lamar, J. E., 1950, Acid etching in the study of limestones and dolomites: *Illinois Geol. Survey Circ.* 156, p. 1-47.
- Lambe, T. W., and Whitman, R. V., 1969, *Soil mechanics*: John Wiley & Sons, Inc., New York, p. 281-292.
- Lambert, C., and Mutimansky, J. M., 1973, Applications of integer programming to effect optimum truck and shovel selection in open pit mines: in *Internat. Symp. Computer Applications in the Mineral Industry*, Coll. Mines, Univ. Arizona, Tucson, p. A75-A105.
- Lamberton, B. A., 1967, Terranier chemical grout: ASCE Structural Eng. Conf., Seattle.
- Landes, K. K., 1966, Eometamorphism can determine oil floor: *Oil and Gas Jour.*, v. 64, no. 18, p. 172-177.
- , 1967, Eometamorphism and oil and gas in time and space: *Am. Assoc. Petroleum Geologists Bull.*, v. 51, no. 6, p. 828-841.
- Langstroth, W. T., 1971, Seismic study along a portion of the Devonian salt front in North Dakota: *Geophysics*, v. 36, p. 330-338.
- Lawson, B. L., and Cook, C. L., 1970, A theoretical and laboratory evaluation of carbon logging. Pt. II—Theoretical evaluation of oxygen interference: *Log Analyst*, v. 11, no. 6.
- Lee, C. H., 1919, *Geology and ground waters of the western part of San Diego County, California*: U.S. Geol. Survey Water Supply Paper 446.
- Leeman, E. R., 1958, Some underground observations relating to the extent of fracturing around excavations in some Central Rand Mines: *South African Assoc. Mine Managers Papers*, no. 5.
- Legget, R. F., 1962, *Geology and engineering*: McGraw-Hill Book Co., New York, 884 p.
- , 1973, *Cities and geology*: McGraw-Hill Book Co., New York, 624 p.
- Leighton, F., and Blake, W., 1970, Rock noise source location techniques: *U.S. Bur. Mines Rept. Inv.* 7432, 18 p.
- Lepeltier, C., 1969, A simplified statistical treatment of geochemical data by graphical presentation: *Econ. Geology*, v. 64, no. 5, p. 538-550.
- LeRoy, D. O., and Levinson, S., 1974, A deep-water Pleistocene microfossil assemblage from a well in the northern Gulf of Mexico: *Micropaleontology*, v. 20, no. 1, p. 1-37, pls. 1-14, text-figs. 1-4.
- Levinson, A. A., 1974, *Introduction to exploration geochemistry*: Applied Publ. Ltd., Calgary, Canada, 612 p.
- Levorson, A. I., 1954, *Petroleum geology*: W. H. Freeman and Co., San Francisco, 701 p.
- , 1958, The future of subsurface exploration: in *Subsurface geology in petroleum exploration*, LeRoy, L. W., and Haun, J. D., eds.: p. 8-14.
- Lindgren, Waldemar, 1933, *Mineral deposits*: McGraw-Hill Book Co., New York, 930 p.
- Lindseth, R. O., 1974, Recent advances in digital processing of geophysical data—a review: *Soc. Expl. Geophysicists Continuing Education Program*.

copy

Bibliography

- Lindsey, H. E., Jr., and Bateman, S. J., 1973, Improved cementing of drilling liners in deep wells: *World Oil*, p. 65.
- Locke, Augustus, 1926, Leached outcrops as guides to copper ores: Williams and Wilkins, Baltimore.
- Louderback, G. D., 1950, Faults and engineering geology: in *Berkey Volume*, Geol. Soc. America, p. 125-150.
- Love, W. W., and Fitzgerald, P. E., 1937, Importance of geological data in acidizing of wells: *Am. Assoc. Petroleum Geologists Bull.*, v. 21, no. 5, p. 616.
- Lowell, J. D., and Guilbert, J. M., 1970, Lateral and vertical alteration-mineralization zoning in porphyry ore deposits: *Econ. Geology*, v. 65, p. 373-408.
- Lowell, J. D., and others, 1975, Petroleum and plate tectonics of the southern Red Sea: in *Petroleum and global tectonics*: Fischer, A. G., and Judson, S., eds., Princeton Univ. Press, p. 129-153.
- Lowman, S. W., 1949, Sedimentary facies in Gulf Coast: *Am. Assoc. Petroleum Geologists Bull.*, v. 33, no. 12, p. 1939-1997.
- Lucas, A. L., 1974, A high resolution marine seismic survey: *Geophys. Prospecting*, v. 22, p. 665-682.
- Ludwig, N. D., 1953, Portland cements and their application in the oil industry: *Drilling Production Practice*, Am. Petroleum Inst., p. 183-209.
- Luffel, D. L., and Randall, R. V., Core handling and measurement techniques for obtaining reliable reservoir characteristics: *Formation Evaluation Symp.*, Calgary, Canadian Well Logging Soc.
- Lyon, R. J. P., and Lee, K., 1970, Remote sensing in exploration for mineral deposits: *Econ. Geology*, v. 65, no. 7, p. 785-801.
- MacKenzie, D. B., and Poole, D. M., 1962, Provenance of Dakota Group sandstones of the western interior: *Symp. on Early Cretaceous Rocks of Wyoming*, Wyoming Geol. Assoc. Ann. Field Conf. Guidebook, p. 62-71.
- Malouf, E. E., 1962, New technology of leaching waste dumps: *Mining Cong. Jour.*, v. 48, no. 11, p. 82-85.
- Mangold, G. B., 1955, Differential thermal analysis, a new type of formation correlation: *World Oil*, v. 140, nos. 2, 4.
- Marr, J. D., 1971, Seismic stratigraphic exploration: *Geophysics*, pt. 1, v. 36, p. 311-329; pt. 2, v. 36, p. 533-553; pt. 3, v. 36, p. 676-689.
- Martin, H. C., 1931, Insoluble residues studies of Mississippian limestones in Indiana: Indiana Dept. Cons. Pub. 191.
- Martner, S. T., and Brigham, R. J., 1975, An interactive computer system for well log analysis: *SPWLA Ann. Logging Symp.*, 16th, Paper No. FF.
- Mason, C. C., and Folk, R. L., 1958, Differentiation of beach, dune, and aeolian flat environments by size analysis, Mustang Island, Texas: *Jour. Sed. Petrology*, v. 28, p. 211-226.
- Mayor, J. N., and Fisher, F. S., 1972, Middle Tertiary replacement ore bodies and associated veins in the northwest San Juan Mountains, Colorado: *Econ. Geology*, v. 67, p. 214-230.
- McCarthy, J. M., 1972, Mercury vapor and other volatile components in the air as guides to ore deposits: *Jour. Geochem. Explor.*, v. 1, no. 2, p. 143-162.
- McConnell, D., Mielenz, R. C., Holland, W. Y., and Greene, K. T., 1950, Petrology of concrete affected by cement-aggregate reaction: in *Berkey Volume*, Geol. Soc. America, p. 225-250.
- McDonal, F. J., Mills, R. L., Sengbush, R. L., and White, J. E., 1958, Attenuation of shear and compressional waves in Pierre shale: *Geophysics*, v. 23, p. 421-439.
- McFadden, D. H., 1968, Pit planning and design—coal mines: in *Seeley Mudd Series*, AIMMPE, Subsurface Mining, p. 211-216.
- McGregor, D. J., 1954, Stratigraphic analysis of Upper Devonian and Mississippian rocks in Michigan Basin: *Am. Assoc. Petroleum Geologists Bull.*, v. 38, no. 11, p. 2324-2356.
- McGuire, W. J., and Sikora, V. J., 1958, The effect of vertical fractures on well productivity: *AIMMPE Trans.*, v. 219, p. 401-403.
- McKee, E. D., 1949, Facies changes in the Colorado Plateau: *Geol. Soc. America Mem.* 39, p. 35-54.
- McKinstry, H. E., 1948, *Mining geology*: Prentice-Hall, Inc., New Jersey, 680 p.
- McLachie, A. S., Hemstock, R. A., and Young, J. W., 1958, The effective compressibility of reservoir rock and its effects on permeability: *AIMMPE Trans.*, v. 213, p. 386.
- McLean, R. H., Manry, C. W., and Whitaker, W. W., 1967, Displacement mechanics in primary cementing: *Jour. Petroleum Tech.*, p. 251-260.
- McMahon, B. K., 1971, Statistical methods for the design of rock slopes: *Australian-New Zealand Conf. Geomechanics 1st, Proc.*, v. 1, p. 314-321, and v. 2, p. 559.
- 1974, Design of rock slopes against sliding on pre-existing fractures: *Internat. Congress Soc. Rock Mechanics 3d, Proc.*, v. 11, pt. B, p. 803-808.
- 1975, Probability of failure and expected volume of failure in high rock slopes: *Australian-New Zealand Conf. Geomechanics, Proc.* p. 308-313.
- McQueen, H. S., 1931, Insoluble residues as a guide in stratigraphic studies: *Missouri Geol. Survey, 56th Bienn. Rept. State Geologist*, p. 103-131.
- Meinzer, O. E., 1923, *Outline of ground-water hydrology with definitions*: U.S. Geol. Survey Water Supply Paper 494, 71 p.
- 1950, Geology and engineering in the production and control of groundwater: in *Berkey Volume*, Geol. Soc. America, p. 151-179.
- Metzner, A. B., 1957, Non-Newtonian flow: *Indust. Eng. Chem.*, v. 49, p. 1429.
- Meyboom, P., 1962, Patterns of groundwater flow in the prairie profile: *Hydrology Symp.*, 3d, Groundwater, Univ. Alberta, Calgary, Canada, p. 5-20.
- Meyer, Charles, 1946, Notes on the cutting and polishing of thin sections: *Econ. Geology*, v. 41, p. 166-172.
- Meyer, C., Shea, E. P., and Coddard, C. C., Jr., 1968, Ore deposits at Butte, Montana: in *Ore deposits of the United States, 1933-1967*: AIMMPE, v. 2, p. 1373-1416.
- Mielenz, R. C., 1948, Petrography and engineering properties of igneous rocks: U.S. Dept. Interior, Bur. Reclamation Eng. Mon. 1, p. 8-9.
- Mifflin, M. D., 1968, Delineation of groundwater flow systems in Nevada: *Desert Res. Inst., Univ. Nevada, Tech. Rept.* 4, 110 p.
- Milner, H. B., ed., 1962, *Sedimentary petrography*: 3d ed., Murby, London.
- Minor, Thane, and Henderson, G. E., 1975, Regional analysis in exploration: *Formation Evaluation Symp.*, Calgary, Canadian Well Logging Soc., p. EE.
- Moiola, J. R., and Weiser, D., 1968, Textural parameters and evaluation: *Jour. Sed. Petrology*, v. 38, p. 45-53.
- Moody, J. D., 1975, Distribution and geological characteristics of giant oil fields: in *Petroleum and global tectonics*: Fischer,

#10-00
Not in Library

Bibliography

- A. G., and Judson, S., eds., Princeton Univ. Press, p. 307-320.
- Moore, R. C., 1949, Meaning of sedimentary facies: *Geol. Soc. America Mem.* 39, p. 1-14.
- Morgan, W. J., 1975, Heat flow and vertical movements of the crust: in *Petroleum and global tectonics*: Fischer, A. G., and Judson, S., eds., Princeton Univ. Press., p. 24-43.
- Morganstern, N. R., and Price, V. E., 1965, The analysis of the stability of general slip surfaces: *Geotechnique*, v. 15, p. 79-93.
- Morrow, N. R., Huppler, J. D., and Simmons, A. R., 1969, Porosity and permeability of unconsolidated, upper Miocene sands from grain-size analysis: *Jour. Sed. Petrology*, v. 39, p. 312-321.
- Morse, R. H., 1971, Comparison of geochemical prospecting methods using radium with those using radon and uranium: *Geochem. Explor. CIM Spec.*, v. 11, p. 215-230.
- Moses, Leslie, 1970, From lease to release, a guide for petroleum landmen: Am. Assoc. Petroleum Landmen, Ft. Worth, Texas.
- Motica, J. E., 1968, Geology and uranium-vanadium deposits in the Uravan mineral belt, southwestern Colorado: in *Ore deposits of the United States, 1933-1967*: AIMMPE, v. 1, p. 805-813.
- ounce, W. D., and Rust, W. M., Jr., 1944, Natural potentials in well logging: AIMMPE, v. 155, p. 39.
- Müller, L., 1964, The rock slide in the Vaiont Valley: *Rock Mech. and Eng. Geology, Internat. Soc. Rock Mech., Jour.*, v. 11, p. 148-212.
- Mutmansky, J. M., and Kim, Y. C., 1973, The use of simulation gaming for evaluation of base metals marketing strategies: *Internat. Symp. Computer Applications in the Minerals Industry*, Coll. Mines, Univ. Arizona, Tucson, p. C66-C80.
- Nanz, R. H., Jr., 1954, Genesis of Oligocene sandstone reservoir, Seeligson field, Jim Wells and Kleberg Counties, Texas: *Am. Assoc. Petroleum Geologists Bull.*, v. 38, p. 96-117.
- Nelson, K. R., 1972, Use of multi-element analysis and data processing in minerals exploration: *The Mountain Geologist, Rocky Mtn. Assoc. Geologists*, v. 9, no. 1, p. 41-53.
- Nemec, V., 1974, Space models of ore deposits—further practice achievements: in *Internat. Symp. Computer Applications in the Minerals Industry*: Colorado School of Mines, Golden, p. H40-H58.
- Nettleton, L. L., 1940, *Geophysical prospecting for oil*: McGraw-Hill Book Co., New York, 444 p.
- , 1971, Elementary gravity and magnetism for geologists and seismologists: *Soc. Expl. Geophysicists, Tulsa, Okla.*, 121 p.
- Newhouse, W. H., 1942, ed., *Ore deposits as related to structural features*: Princeton Univ. Press, 280 p.
- Nichol, I., Garrett, R. G., and Webb, J. S., 1969, The role of some statistical and mathematical methods in the interpretation of regional geochemical data: *Econ. Geology*, v. 64, p. 204-220.
- Nielsen, R. L., 1970, Mineralization and alteration in calcareous rocks near the Santa Rita stock, New Mexico: *New Mexico Geol. Soc. Field Conf. Guidebook*, p. 133-140.
- igli, Paul, 1964, *Ore deposits*: in *Park and MacDiarmid*: W. H. Freeman & Co., San Francisco, p. 222.
- Nordberg, B., 1949, Sand and gravel: in *Industrial minerals and rocks*: Seeley W. Mudd Ser., AIMMPE, p. 844-892.
- Nordgren, R. D., 1972, Propagation of a vertical hydraulic fracture: *SPE—AIME*, Dallas, p. 306.
- Norton, F. H., 1939, Critical study of the differential thermal method for the identification of the clay minerals: *Jour. Am. Ceramic Soc.*, v. 22, p. 54-63.
- Obert, Leonard, and Duvall, W. I., 1945, The microseismic method of predicting rock failure in underground mining: II. Laboratory experiments: *U.S. Bur. Mines Rept. Inv.* 3803, 14 p.
- Obert, Leonard, Duvall, W. I., and Merrill, R. H., 1960, Design of underground openings in competent rock: *U.S. Bur. Mines Bull.* 587.
- O'Brian, D. T., and Weiss, A., 1967, Practical aspects of computer methods in ore reserve analysis and ore reservation estimation in grade control: *Canadian Inst. Mining Metall. Spec.*, v. 9, p. 109-113.
- O'Doherty, R. F., and Anstey, N. A., 1971, Reflection on amplitudes: *Geophys. Prospecting*, v. 19, p. 430-458.
- Omar, S., Bishara, W. W., and Nase, M., 1974, Grain-size parameters and paleoenvironments of the Nubia sandstone: *Jour. Sed. Petrology*, v. 44, p. 136-144.
- O'Neil, T. J., 1973, Estimating minimum copper price levels through production cost protection: in *Internat. Symp. Computer Applications in the Minerals Industry*: Coll. Mines, Univ. Arizona, Tucson, p. G1-C30.
- Otto, C. H., 1933, Comparative tests of several methods of sampling heavy mineral concentrates: *Jour. Sed. Petrology*, v. 3, p. 30-39.
- Overbey, W. K., Jr., and Henniger, B. R., 1970, Disaggregation of sandstone by ultrasonic energy: *Jour. Sed. Petrology*, v. 40, p. 465-472.
- Ovchinnikov, L. N., and Grisoryan, S. V., 1971, Primary halos in prospecting for sulfide deposits: *Canadian Inst. Mining Metall. Spec.*, v. 11, p. 375-380.
- Ovchinnikov, L. N., Sokolov, V. A., Fridman, A. L., and Yanitskii, I. N., 1973, Caseous geochemical methods in structural mapping and prospecting for ore deposits: *Internat. Geochem. Symp.*, London (1972), p. 177-182.
- Page, H. C., 1955, Phi-millimeter conversion table: *Jour. Sed. Petrology*, v. 25, p. 285-292.
- Parasnis, D. S., 1972, *Principles of applied geophysics*: Chapman and Hall Ltd., London, 214 p.
- , 1975, *Mining geophysics*: American Elsevier, New York, 395 p.
- Pardue, C. H., and others, 1963, Cement bond log—a study of cement and casing variables: *Jour. Petroleum Tech.*, v. XV.
- Park, C. F., Jr., and MacDiarmid, R. A., 1975, *Ore deposits*: W. H. Freeman and Co., San Francisco, 3d ed., 529 p.
- Parks, R. D., 1949, Examination and evaluation of mineral property: Addison-Wesley Press, Inc., Cambridge, Mass.
- Pask, J. A., and Turner, M. D., 1952, *Geology and ceramic properties of the Ione formation, Buena Vista area, Amador County, California*: California Dept. Nat. Res., Div. of Mines Spec. Rept. 19.
- Passega, R., 1957, Texture as characteristic of clastic deposits: *Am. Assoc. Petroleum Geologists Bull.*, v. 41, p. 1952-1984.
- , 1964, Grain size representation by CM patterns as a geological tool: *Jour. Sed. Petrology*, v. 34, p. 830-847.
- Pattillo, P. D., 1975, A modification of Carter's equation for fracture area: *SPE-AIME, Ann. Fall Mtg.*, Dallas, Texas, SPE Paper 5630.

Bibliography

930

- Patton, F. D., 1966, Multiple modes of shear failure in rock and related materials: Univ. Illinois unpubl. Ph.D. thesis.
- Paulding, B. W., 1970, Coefficient of friction of natural rock surfaces: Am. Soc. Civil Engineers, Soil Mech. Found. Div. Jour., v. 96, SM2.
- Feele, R., Mining engineer's handbook: John Wiley & Sons, Inc., New York, 3d ed.
- Peikert, E. W., 1963, IBM 709 program for least-square analysis of three-dimensional geological and geophysical observations: Off. Naval Research, Geogr. Brch., Tech. Rept. 4, ONR Task No. 389-135, Contract Nonr-1228(26), 71 p.
- Pelto, C. R., 1954, Mapping of multicomponent systems: Jour. Geology, v. 62, p. 501-511.
- Perkins, H. C., Univ. Kansas unpubl. M.Sc. thesis.
- Perkins, T. K., and Kern, L. R., 1961, Widths of hydraulic fractures: SPE-AIME (Dallas; Texas) Jour. Petroleum Tech., p. 937.
- Perrin, P. G., 1965, Writer's guide and index to English: 4th ed. rev., Scott Foresman, Chicago, Illinois.
- Perry, V. D., 1961, The significance of mineralized breccia pipes: AIMMPE Trans., v. 220, p. 216-226.
- Peters, L. J., 1949, The direct approach to magnetic interpretation and its practical application: Geophysics, v. 14, no. 3.
- Pettijohn, F. J., 1949, Sedimentary rocks: Harper's Geoscience Series, New York, p. 436.
- , 1957, Sedimentary rocks: Harper and Brothers, 2d ed., New York, 718 p.
- Pettijohn, F. J., Potter, P. E., and Siever, R., 1973, Sand and sandstones: Springer-Verlag, New York, p. 618.
- Pfleider, E. P., 1968, ed., Surface mining: in Seeley W. Mudd Ser., AIMMPE Symp., 1061 p.
- Pfleider, E. P., and Weaton, G. F., 1968, Iron ore mining: in Seeley W. Mudd Ser., AIMMPE, Symp., p. 897-967.
- Philippi, C. T., 1965, On the depth, time and mechanism of petroleum generation: Geochim. et Cosmochim. Acta, v. 29, p. 1021-1049.
- Pickett, G. R., 1960, The use of acoustic logs in the evaluation of sandstone reservoirs: Geophysics, v. XXV, Feb.
- , 1963, Acoustic character logs and their applications in formation evaluation: Jour. Petroleum Tech., June.
- , 1966, Prediction of interzone fluid communication behind casing by use of the cement bond log: SPWLA Trans., May.
- Pickett, G. R., and Reynolds, E. B., 1969, Evaluation of fractured reservoirs: Soc. Pet. Eng. Jour., Mar.
- Piteau, D. R., and Jennings, J. E., 1970, The effects of plan geometry on the stability of natural slopes in rock in the Kimberley area: Internat. Soc. Rock Mechanics Cong., Beograd, Proc., v. 111, theme 7, p. 289-295.
- Pitman, E. D., 1972, Diagenesis of quartz in sandstones as revealed by scanning electron microscopes: Jour. Sed. Petrology, v. 42, no. 3, p. 507-519.
- Pitrat, C. W., 1956, Thermoluminescence of limestones of Mississippian Madison group in Montana and Utah: Am. Assoc. Petroleum Geologists Bull., v. 40, no. 5, p. 943-952.
- Polcyn, F. C., and Lyzenga, D. R., 1973, Multispectral sensing of water parameters: in Remote sensing and water resources management: Thompson, K. P. B., and others, eds., Am. Water Resources Assoc., Urbana, Illinois, p. 394-403.
- Potter, P. E., and Pryor, W. A., 1961, Dispersal centers of Paleozoic and later clastics of the upper Mississippi Valley and adjacent areas: Geol. Soc. America Bull., v. 72, p. 1195-1250.
- Poupon, A., Hoyle, W. R., and Schmidt, A. W., 1970, Log analysis in formations with complex lithologies: SPE-AIME Ann. Mtg., SPE paper 2925.
- Powers, M. C., 1953, A new roundness scale for sedimentary particles: Jour. Sed. Petrology, v. 23, p. 117-119.
- , 1967, Fluid-release mechanisms in compacting marine mudrocks and their importance in oil exploration: Am. Assoc. Petroleum Geologists Bull., v. 51, no. 7, p. 1240-1254.
- Preston, F. W., and Harbaugh, J. W., 1965, BALCOL programs and geologic application for single and double Fourier series using IBM 7090/7094 computers: Kansas State Geol. Survey Spec. Distr. Pub. 24, 72 p.
- Priestly, J., 1772, Directions for impregnating water with fixed air: Royal Soc. Proc., London, England.
- Pritchett, V. S., 1960, Language, literature and science: New York Literary Mag., from Jeffares, A. N., 1960, Leeds Univ. Press, England.
- Pryor, W. A., 1971, Grain shape, in Procedures in sedimentary petrology: Carver, R. E., ed., Wiley-Interscience, New York, p. 131-150.
- , 1971, Reservoir inhomogeneities of some recent sand bodies: Soc. Petroleum Engineers preprint paper SPE 3607, 24 p.
- Putnam, G. W., and Burnham, C. W., 1963, Trace elements in igneous rocks, northwestern and central Arizona: Geochim. et Cosmochim. Acta, v. 27, no. 1, p. 53-106.
- Randohr, P., 1969, The ore minerals and their intergrowths: Pergamon Press, New York, 1174 p.
- Ramsey, A. S., 1940, An introduction to the theory of Newtonian attraction: Cambridge Univ. Press, Cambridge, Mass., 184 p.
- Reed, F. S., and Mergner, J. L., 1953, Preparation of rock thin sections: Am. Mineralogist, v. 38, p. 1184-1203.
- Reilly, J. D., 1968, Coal mining: in Seeley W. Mudd Ser., AIMMPE, Subsurface Mining, p. 821-848.
- Reubens, J. B., 1965, Challenge: good scientific writing: IEEE Trans., Engineering Writing and Speech, v. 8, no. 2, p. 48.
- Reudelhuber, F. O., and Furen, J. E., 1957, Interpretation and application of sidewall core analysis data: Gulf Coast Assoc. Geol. Soc. Trans., VII, 83 p.
- Rhoades, R., 1946, Geology in civil engineering: Address, Pan American Congress, Rio de Janeiro, on mining engineering and geology.
- Ries, H., 1949, Clay—industrial minerals and rocks: in Seeley W. Mudd Ser., AIMMPE, p. 207-244.
- Roberts, R. J., Raddke, A. S., and Coats, R. R., 1971, Gold-bearing deposits in northcentral Nevada and southwestern Idaho: Econ. Geology, v. 66, no. 1, p. 14-33.
- Robinson, T. W., 1958, Phreatophytes: U.S. Geol. Survey Water-Supply Paper 1423, 84 p.
- Rockwell, D. W., and Roberts, Roger, 1973, An application-oriented exploration data-base system: Oil and Gas Jour., Feb.
- Rogers, J. J., and Head, W. B., 1961, Relationships between porosity, median size, and sorting coefficients of synthetic sands: Jour. Sed. Petrology, v. 31, p. 467-470.
- Ronov, A. B., 1958, Organic carbon in sedimentary rocks (in relation to the presence of petroleum): Geochemistry, Trans. from Geokhimiia, v. 5, p. 510-536.
- Rose, A. W., 1970, Zonal relations of wall rock alteration and sulfide distribution in porphyry deposits: Econ. Geology, v. 65, p. 920-936.
- , 1973, Statistical interpretation techniques in

Bibliography

- geochemical exploration: SME Trans., AIMME, v. 252, p. 233-238.
- Rose, D., 1965, A civil engineer reads a geology report: *GeoTimes*, v. 10, no. 1, p. 9-12.
- Roux, A. J. A., and Denkhaus, H. C., 1954, An analysis of the problem of rock bursts in deep level mining: *South African Inst. Mining Metall. Jour.*, v. 55, p. 103-124.
- Rowland, E. O., 1953, A rapid method for the preparation of thin rock sections: *Mineralog. Magazine*, v. 30, p. 254-258.
- Rowland, R. A., and Lewis, D. H., 1951, Furnace atmosphere control in differential thermal analysis: *Am. Mineralogist*, v. 36, nos. 1-2, p. 80-91.
- Rowley, D. S., Burk, C. A., and Manuel, T., 1967, Oriented cores: Christensen Diamond Products Co.
- Rubey, W. W., 1933, Settling velocities of gravel, sand and silt particles: *Am. Jour. Science*, v. 25, p. 325-338.
- Rutledge, R. B., and Bryant, H. S., 1937, Cunningham field, Kingman and Pratt Counties, Kansas: *Am. Assoc. Petroleum Geologists Bull.*, v. 21, no. 4, p. 518.
- Sabins, F. F., Jr., 1961, Grains of detrital, secondary, and primary dolomite from Cretaceous strata of the western interior: *Geol. Soc. America Bull.*, v. 73, p. 1183-1196.
- Sales, R. H., and Meyer, C., 1950, Interpretation of wall rock alteration at Butte, Montana: *Colorado School Mines Quart.*, Golden, v. 45, no. 1B, p. 261-273.
- Sanborn, J. F., 1950, Engineering geology in the design and construction of tunnels: in *Berkey Volume*, *Geol. Soc. America*, p. 45-81.
- Sanders, C. W., 1943, Stratigraphic type oil fields and proposed new classification of reservoir traps: *Am. Assoc. Petroleum Geologists Bull.*, v. 27, p. 539-550.
- Sandström, G. E., 1970, *Man the builder*: McGraw-Hill Book Co., New York, 280 p.
- Sangster, D. R., 1972, Precambrian volcanogenic massive sulfide deposits in Canada—a review: *Canadian Geol. Survey Paper* 72-22, p. 44.
- Sax, N. I., 1975, *Dangerous properties of industrial materials*: Van Nostrand Reinhold, New York, 4th ed., 1258 p.
- Scherz, J. P., and Stevens, A. R., 1970, An introduction to remote sensing for environmental monitoring: *Univ. Wisconsin, Madison*, 80 p.
- Schlee, J., 1966, A modified Woods Hole rapid sediment analyzer: *Jour. Sed. Petrology*, v. 36, p. 403-413.
- Schlumberger Well Surveying Corporation, Departure curves for gamma ray neutron tools, type CNT-F and C, Pu, Be source, long spacing: Houston.
- 1949, Document 7, Resistivity departure curves.
- 1951, Document 4, Interpretation handbook for resistivity logs.
- 1955, Document 7, Resistivity departure curves (beds of infinite thickness).
- 1962, Log interpretation chart book.
- 1974, Log interpretation, Volume II, Applications: Schlumberger Limited, New York, 116 p.
- Schmidt, H., 1936, On mapping underground geology: *Eng. and Mining Jour.*, v. 137, p. 557.
- Schneider, W. A., 1971, Developments in seismic data processing and analysis (1968-1970): *Geophysics*, v. 36, p. 1043-1073.
- Schneider, W. T., 1943, *Geology of the Wasson field, Yoakum and Gaines Counties, Texas*: *Am. Assoc. Petroleum Geologists Bull.*, v. 27, no. 4, p. 521.
- Schrayer, G. J., and Zarrella, W. M., 1963, Organic geochemistry of shales, I. Distribution of organic matter in the siliceous Mowry shale of Wyoming: *Geochim. et Cosmochim. Acta.*, v. 27, p. 1033-1046.
- Schultz, J. R., and Cleaves, A. B., 1955, *Geology in engineering*: John Wiley & Sons, Inc., New York, 592.
- Schürmann, E., 1888, *Ann. der Chemie*, v. 249, p. 326-350.
- Shah, P. M., 1973, Use of wavefront curvature to relate seismic data with subsurface parameters: *Geophysics*, v. 38, p. 812-825.
- Sharpe, C. F. S., 1960, *Landslides and related phenomena*: Columbia Univ. Press, New York, 137 p.
- Sharpe, J. A., 1942, The production of elastic waves by explosion pressures. I. Theory and empirical field observations: *Geophysics*, v. 7, p. 144-154.
- Shepard, F. P., 1948, *Submarine geology*: Harper and Brothers, New York, 348 p.
- 1963, *Submarine geology*: Harper and Row, New York, 2d ed.
- Shepard, F. P., and Young, R., 1961, Distinguishing between beach and dune sands: *Jour. Sed. Petrology*, v. 31, p. 196-214.
- Sheriff, R. E., 1973, *Encyclopedic dictionary of exploration geophysics*: Soc. Expl. Geophysicists.
- 1975, Factors affecting seismic amplitudes: *Geophys. Prospecting*, v. 23, p. 125-138.
- Short, M. N., 1940, Microscopic determination of the ore minerals: *U.S. Geol. Survey Bull.* 914, 314 p.
- Shrock, R. R., 1948, A classification of sedimentary rocks: *Jour. Geology*, v. 56, p. 118-130.
- Siegel, F. R., 1975, *Applied geochemistry*: John Wiley & Sons, Inc., New York, p. 353.
- Sillitoe, R. H., 1973, The tops and bottoms of porphyry copper deposits: *Econ. Geology*, v. 68, no. 6, p. 799-816.
- Silverman, S. R., 1973, *Petroleum geochemistry (diagenesis in organic sediments)*: *Am. Assoc. Petroleum Geologists Short Educational Course*.
- Simmons, B. D., and Falconbridge Copper, Ltd. Staff, 1973, *Geology of the Millenbach massive sulphide deposit, Noranda, Quebec*: *Canadian Inst. Mining, Ann. Mtg.*, 75th, Vancouver.
- Sinclair, W. E., 1936, Rock bursts—their cause and prevention: *South African Chem. Metall. Mining Soc. Jour.* v. 37, p. 4-11.
- Sippel, R. F., 1965, Simple device for luminescent petrography: *Sci. Instruments Rev.*, v. 36, p. 1556-1558.
- 1968, Sandstone petrology, evidence from luminescence petrography: *Jour. Sed. Petrology*, v. 38, p. 530-554.
- Skall, H., 1975, The paleoenvironment of the Pine Point lead-zinc district: *Econ. Geology*, v. 70, no. 1, p. 22-47.
- Skempton, A. W., 1961, Horizontal stresses in an over-consolidated Eocene clay: *Internat. Conf. on Soil Mechanics and Foundation Engineering, Proc.*, v. 1, Paris, p. 351-357.
- Slagle, K. A., and Smith, D. K., 1963, Salt cement for shale and bentonite sands: *Jour. Petroleum Tech.*, Feb. AIMME Trans., 228.
- Slawson, W. F., and Nackowski, M. P., 1959, Trace lead in potash feldspars associated with ore deposits: *Econ. Geology*, v. 54, p. 1543-1555.
- Sloss, L. L., Krumbain, W. C., and Dapples, E. C., 1949, Integrated facies analysis: *Geol. Soc. America Mem.* 39, p. 91-123.
- Smeeth, W. F., 1904, Airblasts and quakes on the Kolar gold field: *Mysore Geol. Survey Bull.*, no. 2.

Act in Library

Bibliography

- Smith, M. B., and Souder, W. W., 1975, Minicomputers for mass analysis: SPWLA, Ann. Logging Symp., Paper No. R. Society of Exploration Geophysicists, 1966, Mining geophysics: In Case histories: Soc. Expl. Geophysicists, Tulsa, v. I, 492 p.
- 1967, Mining geophysics: Theory Soc. Expl. Geophysicists, Tulsa, v. II, 708 p.
- Spalding, J., 1937, Theory and practice of ground control: AIMMPE Trans., v. 37, p. 71-143.
- Spangler, M. G., and Handy, R. L., 1973, Soil engineering: Intext Education Publ., New York, 3d ed.
- Speil, Sidney, Berkelhamer, L. H., Pask, J. A., and Davies, Ben, 1945, Differential thermal analysis, its application to clays and other aluminous minerals: U.S. Bur. Mines Tech. Paper 664.
- Spence, C. D., and de Rosen-Spence, A. F., 1975, The place of sulfide mineralization in the volcanic sequence at Noranda, Quebec: Econ. Geology, v. 70, p. 90-101.
- Spencer, D. W., 1963, The interpretation of grain size distribution curves of clastic sediments: Jour. Sed. Petrology, v. 33, p. 180-190.
- Spieker, E. M., 1949, Sedimentary facies and associated diastrophism in the Upper Cretaceous of central and eastern Utah: Geol. Soc. America Mem. 39, p. 55-90.
- Standing, M. B., and Hong, K. C., 1973, Productivity of perforated completions: SPE-AIME Ann. Mtg., Las Vegas, Nevada, SPE Paper 4653.
- Stanton, R. L., 1972, Ore petrology: McGraw-Hill Book Co., New York, 713 p.
- Steenland, N. C., 1965, Oil fields and aeromagnetic anomalies: Geophysics, v. 30, no. 5.
- Steineck, L. P., 1973, Paleogeography, paleobathymetry, and paleotectonism of mid-Tertiary, Jamaica: Am. Assoc. Petroleum Geologists, v. 57, no. 4, p. 806-807 (abs.).
- Stermole, F. J., 1972, Economic evaluation of mineral investment alternatives: Colorado School Mines Mineral Industries Bull., Golden, v. 15, no. 3, p. 1-16.
- Steven, T. A., and Epis, R. C., 1968, Oligocene volcanism in southcentral Colorado in Cenozoic volcanism in the southern Rocky Mountains: Colorado School Mines Quart., Golden, v. 63, no. 3, p. 241-258.
- 1975, Middle Tertiary volcanic field in the southern Rocky Mountains: Geol. Soc. America Mem. 144, p. 75-94.
- Stone, R. L., 1954, Thermal analysis of magnesite at CO₂ pressures up to six atmospheres: Am. Ceramic Soc. Jour., v. 37, no. 2, p. 46-47.
- Stone, R. L., and Rowland, R. A., 1955, DTA of kaolinite and montmorillonite and water vapor pressures up to six atmospheres: Natl. Acad. Sci. Publ. 395, Natl. Research Council.
- Strangway, D., 1970, History of the earth's magnetic field: McGraw-Hill Book Co., New York, 168 p.
- Structural Engineers Association of California, 1974, Recommended lateral force requirements and commentary: Seismology Committee, San Francisco.
- Stuart, W. H., Moneymaker, B. C., Gardner, W. I., Coombs, H. A., Monahan, C. J., Cedergren, H. R., and Roberts, C. D., 1969, Symposium on reservoir leakage and groundwater control: Assoc. Eng. Geologists Bull., v. 6, no. 1, 93 p.
- Stude, G. R., 1970, Application of paleobathymetry to exploration: Gulf Coast Assoc. Geol. Soc. Trans., v. 20, p. 194-200.
- Sultan, H. A., and Seed, H. B., 1969, Stability of sloping core earth dams: in Stability and performance of slopes and embankments: Am. Soc. Civil Engineers, Soil and Found. Div., Berkeley, California, p. 51-73.
- Sundeen, S. W., 1968, Preliminary evaluations of surface mine prospects: In Surface mining: Seeley W. Mudd Ser., AIMMPE, p. 54-65.
- Swann, D. H., Fisher, R. W., and Walters, M. J., 1959, Visual estimates of grain size distribution in some Chester sandstones: Illinois State Geol. Survey Circ. 280, 43 p.
- Swift, D. J. P., 1971, Grain mounts: in Procedures in sedimentary petrology: Carver, R. E., ed., Wiley-Interscience, New York, p. 499-510.
- Swift, D. J. P., Schubel, J. R., and Sheldon, R. W., 1972, Size analysis of fine-grained suspended sediments—a review: Jour. Sed. Petrology, v. 42, p. 122-190.
- Swiger, W. F., 1962, Construction of Rocky Reach grouted cutoff: Am. Soc. Civil Engineers Trans., v. 127, pt. 1.
- Taner, T., Cook, E. E., and Neidell, N. S., 1970, Limitations of the reflection seismic method: Lessons from computer simulations: Geophysics, v. 35, p. 551-573.
- Tanner, W. J., 1958, The zig-zag nature of type I and type IV curves: Jour. Sed. Petrology, v. 28, p. 372-375.
- Taylor, J. M., 1950, Pore-space reduction in sandstones: Am. Assoc. Petroleum Geologists Bull., v. 34, p. 701-716.
- Tennant, C. B., and White, M. L., 1959, Study of the distribution of some geochemical data: Econ. Geology, v. 54, p. 1281-1290.
- Terzaghi, Karl, 1950, Mechanism of landslides: In Berkeley Volume, Geol. Soc. America, p. 83-123.
- 1960, From theory to practice in soil mechanics: John Wiley & Sons, Inc., New York, p. 62-67.
- Terzaghi, Karl, and Peck, R. B., 1967, Soil mechanics in engineering practice: John Wiley & Sons, Inc., New York.
- Terzaghi, Karl, Proctor, M. E., and White, T. L., 1946, Rock tunneling with steel supports: Commercial Shearing and Stamping Co., Youngstown, Ohio.
- Terzaghi, Karl, and Richart, F. E., Jr., 1952, Stresses in rock around cavities: Geotechnique, v. 3, no. 2, p. 57-90.
- Theim, A., 1906, Hydrologische Methoden: Leipzig, Gebhardt, 56 p.
- Theis, C. V., 1935, The relation between the lowering of the piezometric surface and the rate and duration of discharge of a well using groundwater storage: Am. Geophys. Union Trans., v. 16, p. 519-524.
- Thornburg, W. D., 1954, Principles of geomorphology: John Wiley & Sons, Inc., New York, 618.
- Timoshenko, S., 1934, Theory of elasticity: McGraw-Hill Book Co., New York.
- 1972, Intrusion, and wall rock, porphyry copper deposits: Econ. Geology, v. 67, no. 1, p. 122-123, Jan.-Feb.
- Tichey, H. J., 1966, Effective writing: McGraw-Hill Book Co., New York.
- Titley, S. R., and Hicks, C. L., 1966, eds. Geology of the porphyry copper deposits, southwestern North America: Univ. Arizona Press, Tucson.
- Tittman, and others; 1966, The sidewall epithermal neutron porosity log: Jour. Petroleum Tech., v. 18, no. 10.
- Tixier, M. P., Alger, R. P., and Doh, C. A., 1958, Sonic logging: Jour. Petroleum Tech.
- Todd, D. K., 1959, Ground water hydrology: Wiley and Sons, Inc., New York, p. 394.
- Tolms, C. F., 1937, Ground water: McGraw-Hill Book Co., New York, 589 p.

Bibliography

- Trask, P. D., ed., 1950, *Applied sedimentation*: John Wiley & Sons, Inc., New York, 707 p.
- Travis, R. B., 1956, *Optical mineralogy techniques*: Colorado School of Mines, Golden.
- Tucker, P. M., and Yorston, H. J., 1973, Pitfalls in seismic interpretation: *Soc. Expl. Geophysicists Mon. 2*.
- Turner, A. K., 1976, Computer aided environmental impact analysis: *Colorado School Mines Mineral Industries Bull.*, Golden, v. 19, pt. 1, no. 2, 23 p.
- Turner, A. K., Coffman, D. M., 1973, *Geology for planning—a review of environmental geology*: Colorado School Mines Quart., Golden, v. 68, no. 3, 127 p.
- Twenhofel, W. H., and Tyler, S. A., 1941, *Methods of study of sediments*: McGraw-Hill Book Co., New York.
- Udden, J. A., 1898, *Mechanical composition of wind deposits*: Augustana Library Publications No. 1.
- United States Forest Service, 1975, *Anatomy of a mine from prospect to production*: Ogden, Utah, 118 p.
- United States National Aeronautics and Space Administration, Goddard Space Flight Center, 1971, *Data users handbook (for Earth Resources Technology Satellite)*: U.S. Natl. Aeronautics and Space Admin., Goddard Space Flight Center Doc. 71SD4249 (loose-leaf, variously pagéd).
- United States National Aeronautics and Space Administration, Johnson Space Center, 1971, *Skylab Earth resources data catalog*: U.S. Natl. Aeronautics and Space Admin., Johnson Space Center Doc. JSC 09016, 359 p., with maps.
- United States Department of the Navy, 1965, *Design manual soil mechanics, foundations and earth structures*: U.S. Dept. Navy, NAVDOCKS DM7, p 7-3-9 through 7-3-15.
- Urey, H. C., 1952, *The planets—their origin and development*: Yale Univ. Press, New Haven, Connecticut.
- Uytendogaardt, W., 1951, *Table for microscopic identification of ore minerals*: Princeton Univ. Press, 282 p.
- Vairoga, J., Hearn, C. L., Daring, D. W., and Rhoades, V. W., 1970, Effect of rock stress on gas production from tight reservoirs: *AIMMPE Ann. Fall Mtg.*, SPE Paper 3001.
- Valentin, H., 1952, *Die Küste der Erde*: Petermanns Geographische Mitteilungen Ergänzungsheft 246.
- Van Andel, Tj. H., 1950, *Provenance, transport and deposition of Rhine sediments: H. Veenman en Zonen, Wageningen, Netherlands*, 129 p.
- 1956, *Recent sediments of the Rhone delta, II. Sources and deposition of heavy minerals*: *Geol. Mijnbouwkundig Genootsch. Nederland Verhand.*, Géol. Série, v. 15, p. 535-556.
- Van de Graff, F. R., 1972, *Fluvial-deltaic facies of the Castlegate sandstone (Cretaceous), east-central Utah*: *Jour. Sed. Petrology*, v. 42, p. 558-571.
- Van der Vlis, A. C., Haafkens, R., Schipper, B. A., and Visser, W., 1975, *Criteria for proppant placement and fracture conductivity*: *SPE-AIME Ann. Fall Mtg.*, Dallas, Texas, SPE paper 5637.
- Van Haften, A. C., 1969, *Acute tetrabromoethane (acetylene tetrabromide) intoxication in man*: *Am. Ind. Hygiene Assoc. Jour.*, v. 30, p. 251-256.
- Visher, G. S., 1969, *Grain size distributions and depositional processes*: *Jour. Sed. Petrology*, v. 39, p. 1074-1106.
- Von der Ahe, K. L., 1953, *Operating problems in oil exploration in the Arctic*: *Pet. Eng.*, B12.
- Wadell, H., 1934, *Some new sedimentation formulas*: *Physics*, v. 5, p. 281-291.
- Wadsworth, M. E., 1975, *Physico-chemical aspects of solution mining: Short course on in-place leaching and solution mining*: Mackay School Mines, Univ.-Reno, Nevada.
- Wahl, and others, 1964, *The dual spacing formation density log*: *Jour. Petroleum Tech.*, v. 16, no. 12.
- Waldschmidt, W. A., Fitzgerald, P. E., and Lunsford, C. L., 1956, *Classification of porosity and fractures in reservoir rocks*: *Am. Assoc. Petroleum Geologists Bull.*, v. 40, p. 953-974.
- Wallace, S. R., and others, 1968, *Multiple intrusion in mineralization at Climax, Colorado: in Ore deposits of the United States, 1933-1967*: *AIMMPE*, v. 1, p. 605-640.
- Walters, R. F., 1969, *Contouring by machine*: *Am. Assoc. Petroleum Geologists Bull.*, v. 53, p. 2324-2340.
- Walton, W. R., 1964, *Recent foraminiferal ecology and paleoecology*: in Imbrie, John, and Newell, Norman, eds., *Approaches to paleoecology*: John Wiley & Sons, Inc., New York, p. 151-237.
- Warner, D. L., 1965, *Deep-well injection of liquid waste*: U.S. Dept. Health, Education Welfare, Public Service Publ. no. 99-WP-21, 55 p.
- Warren, H. V., and Delavault, R. E., 1960, *Aqua regia extractable copper and zinc in plutonic rocks in relation to ore deposits*: *Inst. Mining Metall. Bull.* 643, p. 495-504.
- 1969, *Aqua regia extractable copper and zinc in volcanic rocks in relation to copper mineralization*: *Econ. Geology*, v. 64, no. 6, p. 672-676.
- Waterman, G. C., and Hazen, S., 1968, *Development drilling and bulk sampling in surface mining*: Seeley W. Mudd Ser. *AIMMPE*, p. 69-102.
- Webster, G. M., and Dawsongrove, G. E., 1959, *The alteration of rock properties by percussion sidewall coring*: *Jour. Petroleum Tech.*, 59.
- Weiss, O., 1938, *Theory of rock bursts*: *South Africa Chem. Metall. Mining Soc. Jour.*, v. 38, p. 273-329.
- Weller, J. M., 1960, *Stratigraphic principles and practice*: Harper and Brothers, New York, p. 1-725.
- Welte, D. H., 1965, *Relationship between petroleum and source rock*: *Am. Assoc. Petroleum Geologists Bull.*, v. 49, no. 12, p. 2246-2268.
- Wentworth, C. K., 1922, *A scale of grade and class terms for clastic sediments*: *Jour. Geology*, v. 30, p. 377-392.
- Wertz, J. B., 1970, *The Texas lineament and its economic significance in southeast Arizona*: *Econ. Geology*, v. 65, p. 166-181.
- White, D. E., 1973, *Characteristics of geothermal resources*, p. 69-94, in *Geothermal energy*, Kruger, P., and Otte, C., eds., Stanford Univ. Press, Stanford, 360 p.
- White, F. L., 1952, *Setting cements in below freezing conditions*: *Petroleum Eng.*, B7, Aug.
- Whitmore, F. C., Jr., 1950, *Sedimentary materials in military geology*: in *Applied sedimentation*, Trask, P. D., ed.: John Wiley & Sons, Inc., New York, p. 707.
- Whitney, J. W., 1975, *A resource analysis based on porphyry copper deposits and the cumulative copper metal curve using Monte Carlo simulation*: *Econ. Geology*, v. 70, p. 527-537.
- Whitney, P. R., 1975, *Relationship of manganese-iron oxides and associated heavy metals to grain size in stream sediments*: *Jour. Geochem. Explor.*, v. 4, no. 2, p. 251-264.
- Williams, A. B., 1972, *Gravity and magnetic field analytic modeling program*: *Soc. Explor. Geophysicist Ann. Mtg.*, Anaheim, California.

W&M
Library
933

Bibliography

- Williams, Howel, Turner, F. J., and Gilbert, C. N., 1954, Petrography: W. H. Freeman and Co., San Francisco.
- Wilson, L. R., 1956, Composite micropaleontology and its application to Tertiary and near-Recent stratigraphy: *Micropaleontology*, v. 2, no. 1, p. 1-6.
- Wilson, P. B., 1924, Report on the collection, recording, and economic application of geological data: Am. Mining Cong., Ann. Convention.
- Wilson, W. B., 1934, Proposed classifications of oil and gas reservoirs, problems of petroleum geology: *Am. Assoc. Petroleum Geologists Bull.*, p. 433-445.
- Winland, H. D., 1971, Nonskeletal deposition of high-Mg calcite in the marine environment and its role in the retention of textures: in *Carbonate cements*: Bricker, O. P., ed., Johns Hopkins Univ. Press, Baltimore, 376 p.
- Winograd, I. J., 1971, Hydrogeology of ash-flow tuff: A preliminary statement: *Water Resources Research*, v. 7, no. 4, p. 994-1006.
- Withers, J. H., Sliding resistance along discontinuities in rock masses: Univ. Illinois Civil Eng. Ph.D. thesis.
- Witwatersrand Rock Burst Committee Report, 1926: Govt. Printers, Capetown, South Africa.
- Woodbury, H. O., Murray, I. B., Jr., Pickford, P. J., and Akers, W. H., 1973, Pliocene and Pleistocene depocenters, outer continental shelf, Louisiana and Texas: *Am. Assoc. Petroleum Geologists Bull.*, v. 57, no. 12, p. 2428-2439.
- Woods, J. P., 1956, The composition of reflections: *Geophysics*, v. 21, p. 261-276.
- Woods, K. B., and others, 1960, Highway engineering handbook: McGraw-Hill Co., New York.
- Worthington, P. F., 1975, Procedures for the optimum use of geophysical methods in groundwater development programs: *Assoc. Eng. Geologists Bull.*, v. 12, no. 1, p. 23-38.
- Wyllie, M. R. J., Gregory, A. R., and Gardner, L. W., 1956, Elastic wave velocities in heterogeneous and porous media: *Geophysics*, v. 21.
- Wyllie, M. R. J., Gregory, A. R., and Gardner, G. H. F., 1958, An experimental investigation of factors affecting elastic wave velocities in porous media: *Geophysics*, v. 23.
- Zemanek, J., and others, 1969, The borehole televiewer—a new logging concept for fracture location and other types of borehole inspection: *Jour. Petroleum Tech.*, June.
- Ziegler, J. M., and Gill, B., 1959, Tables and graphs for the settling velocity of quartz in water, above the range of Stokes law: Woods Hole Oceanographic Inst., Ref. No. 59-36, 67 p.
- Zingula, R. P., 1968, A new breakthrough in sample processing: *Jour. Paleontology*, v. 42, no. 4, p. 1092.

Bibliography from Volcanology

by Howell Williams (UC Berkeley), and
Alexander R. McBirney (U of Ore)

1979. San Francisco, Freeman, Cooper & Co.

- Allen, C. R., St. Armand, P., Richter, C. F., and Nordquist, J. M., 1965, Relationship between seismicity and geologic structure in the southern California region: *Bull. Seis. Soc. Amer.*, *55*, 753-797.
- Allen, E. T., and Day, A. L., 1927, Steam wells and other thermal activity at "The Geysers," California: *Carnegie Inst. Wash. Pub.*, *378*, 106 pp.
- , and Day, A. L., 1935, Hot springs of the Yellowstone National Park: *Carnegie Inst. Wash. Pub.*, *466*, 525 pp.
- , and Zies, E. G., 1923, A chemical study of the fumaroles of the Katmai region: *Nat. Geog. Soc., Contr. Tech. Papers, Katmai Ser.*, no. 2, 75 pp.
- Almond, D. C., 1971, Ignimbrite vents in the Sabaloka cauldron, Sudan: *Geol. Mag.*, *108*, 159-176.
- , 1977, The Sabaloka igneous complex, Sudan: *Phil. Trans. Roy. Soc. London, A*, *287*, 595-633.
- Anderson, A. T., 1975, Some basaltic and andesitic gases: *Rev. Geoph. and Space Phys.*, *13*, 37-55.
- Anderson, C. A., 1933, The Tuscan formation of Northern California: *Univ. Calif. Pub. Geol. Sci.*, *23*, 215-276.
- , 1941, Volcanoes of the Medicine Lake Highlands, California: *Univ. Calif. Pub. Bull. Dept. Geol. Sci.*, *25*, 347-422.
- Anderson, R. N., 1972, Petrologic significance of low heat-flow on the flanks of slow-spreading mid-ocean ridges: *Geol. Soc. Amer. Bull.*, *83*, 2947-2956.
- Anderson, Tempest, and Flett, J. S., 1903, Report on the eruption of the Soufrière in St. Vincent in 1902: *Phil. Trans. Roy. Soc. London, A*, *22*, 354-553.
- Aramaki, Shigeo, 1956, The 1783 activity of Asama Volcano: *Jap. Jour. Geol. and Geog.*, *27*, 189-229, and 1957, *28*, 11-33.
- Armstrong, R. L., Ekren, E. B., McKee, E. H., and Noble, D. C., 1969, Space-time relations of Cenozoic silicic volcanism in the Great Basin of the western United States: *Amer. Jour. Sci.*, *267*, 478-490.
- Arnason, B., and Sigurgeirsson, T., 1968, Deuterium content of water vapour and hydrogen in volcanic gas at Surtsey, Iceland: *Geoch. et Cosmoch. Acta*, *32*, 807-814.
- Atwater, T., 1970, Implications of plate tectonics for the Cenozoic tectonic evolution of Western North America: *Geol. Soc. Amer. Bull.*, *81*, 3513-3536.
- Ault, W. U., Eaton, J. P., and Richter, D. N., 1961, Lava temperatures in the 1959 Kilauea eruption and cooling lake: *Geol. Soc. Amer. Bull.*, *72*, 791-794.
- Aumento, F., 1968, The Mid-Atlantic Ridge near 45° N—Pt. 2, Basalts from the area of Confederation Peak: *Can. Jour. Earth Sci.*, *5*, 1-21.
- , 1969, The Mid-Atlantic Ridge near 45° N. V. Fission track and ferro-manganese chronology: *Can. Jour. Earth Sci.*, *6*, 1431-1440.
- Baak, J. A., 1949, A comparative study on Recent ashes of the Java volcanoes, Smeru, Kelut, and Merapi: *Meded. alg. Proefstn. Landb., Buitenzorg*, *83*, 1-60.
- Bailey, D. K., 1974, Melting in the deep crust, in Sørensen, H., ed., *The alkaline rocks*: John Wiley & Sons, Inc., New York, 436-442.
- Bailey, E. B., and Maufe, H. B., 1960, The geology of Ben Nevis and Glen Coe and the surrounding country: *Mem. Geol. Surv. Scotland*, 307 pp.
- Bailey, E. H., Irwin, W. P., and Jones, D. L., 1964, Franciscan and related rocks, and their significance in the geology of western California: *Calif. Div. Mines and Geol. Bull.*, *183*.
- Bailey, R. A., Dalrymple, G. E., and Lanphere, M. A., 1976, Volcanism, structure, and geochronology of Long Valley Caldera, Mono County, California: *Jour. Geoph. Res.*, *81*, 725-744.
- Baker, B. H., 1975, Geology and geochemistry of the Ol Doinyo Nyokie trachyte ignimbrite vent complex, South Kenya Rift Valley: *Bull. Volc.*, *39*, 1-21.
- , Mohr, P. A., and Williams, L. A., 1972, Geology of the Eastern Rift system of Africa: *Geol. Soc. Amer. Sp. Paper* 136, 67 pp.

- , and Wohlenberg, J., 1971, Structure and evolution of the Kenya Rift valley: *Nature*, 229, 538-542.
- Baker, P. E., 1968, Comparative volcanology and petrology of the Atlantic island-arcs: *Bull. Volc.*, 32, 189-206.
- Ballard, R. D., Bryan, W. B., Heirtzler, J. R., Keller, G., Moore, J. G., Van Andel, Tj., 1975, Manned submersible observations in the FA-MOUS area: Mid-Atlantic Ridge: *Science*, 190, 103-108.
- Barazangi, M., and Isacks, B. L., 1976, Spatial distribution of earthquakes and subduction of the Nazca plate beneath South America: *Geology*, 4, 686-692.
- Barberi, F., Borsi, S., Ferrara, G., Marinelli, G., and Varet, J., 1970, Relations between tectonics and magmatology in the northern Danakil Depression: *Phil. Trans. Roy. Soc. London, A*, 267, 293-311.
- Barth, T. F. W., 1950, Volcanic geology, hot springs and geysers of Iceland: *Carnegie Inst. Wash. Pub.*, 587, 174 pp.
- Bartlett, R. W., 1969, Magma convection, temperature distribution, and differentiation: *Amer. Jour. Sci.*, 267, 1067-1082.
- Belousov, V. V., 1962, Basic problems in Geotectonics, McGraw-Hill, N. Y., 809 pp.
- , and Ruditch, E. M., 1961, Island arcs in the development of the earth's structure (especially in the region of Japan and the Sea of Okhotsk): *Jour. Geol.*, 69, 647-658.
- Bemmelen, R. W. van, 1929, The origin of Lake Toba: *Proc. 4th Pac. Sci. Congress, Batavia*, 2A, 115-124.
- , 1931, Het boekje Mapas-Pematang Semoet vulkanisme: *Verh. Mijn. Genoot. Ned. Kol., Geol. Ser. 9*, 57-76.
- , 1939, The volcano-tectonic origin of Lake Toba, N. Sumatra: *De Mijningenieur*, No. 9, 126-140.
- , 1949, The geology of Indonesia, Vol. 1A: Gov't. Printing Office, The Hague, 732 pp.
- , 1954, Mountain building, Martinus Nijhoff, The Hague, 177 pp.
- , and Rutten, M. G., 1955, Tablemountains of northern Iceland: *Leiden*, 217 pp.
- Bentor, Y., 1955, La Chaîne des Puys: *Bull. Carte Geol. de France*, No. 242.
- Bertrand, M., 1887, Sur la distribution géographique des roches éruptives en Europe: *Bull. Soc. Geol. France*, Ser. 3, V. 16, 573-617.
- Best, M. G., 1975, Migration of hydrous fluids in the upper mantle and potassium variation in Calc-alkaline rocks: *Geology*, 3, 429-432.
- Birch, F., 1965, Speculations on the earth's thermal history: *Geol. Soc. Amer. Bull.*, 76, 133-154.
- Bjornsson, S., 1968, Radon and water in volcanic gas at Surtsey, Iceland: *Geoch. et Cosmoch. Acta*, 32, 815-822.
- Blot, C., and Priam, R., 1964, Une nouvelle éruption du Volcan de Lopevi (Nouvelles Hébrides) et son analogie sismique avec les éruptions précédentes: *Bull. Volc.*, 27, 341-345.
- Bodvarsson, G., and Palmason, G., 1961, Exploration of subsurface temperature in Iceland: U. N. Conf. on New Sources of Energy, Rome.
- , and Walker, G. P. L., 1964, Crustal drift in Iceland: *Geoph. Jour. Roy. Astro. Soc.*, 8, 285-300.
- Bonatti, E., 1967, Mechanism of deep-sea volcanism in the South Pacific: in Abelson, P. H., Editor, *Res. in Geoch.*, 2, 453-491.
- Bond, A., and Sparks, R. S. J., 1976, The Minoan eruption of Santorini, Greece: *Jour. Geol. Soc. London*, 132, 1-16.
- Booth, B., and Self, S., 1973, Rheological features of the 1971 Mount Etna lavas: *Phil. Trans. Roy. Soc. London, A*, 274, 99-106.
- Borchardt, G. H., Harward, M. E., and Schmitt, R. A., 1971, Correlation of volcanic ash deposits by activation analyses of glass separates: *Quat. Res.*, 1, 247-260.
- Bordet, P., Marinelli, G., Mittempergher, M., and Tazieff, H., 1963, Contribution à l'étude volcanologique du Katmai et de la Vallée des Dix Mille Fumées: *Soc. Belge Geol., Paleont. et Hydrol., Mem., Ser. 8*, 7-70.
- Bostok, Derek, 1973, The holmium-thulium ratio of kuselite and seafloor spreading: *Trans. Phil. Soc. Agua Blanca*, 97, 892-897.
- Bottinga, Y., and Weill, D. F., 1970, Densities of liquid silicate systems calculated from partial molar volumes of oxide components: *Amer. Jour. Sci.*, 269, 169-182.
- , and Weill, D. F., 1972, The viscosity of magmatic silicate liquids: a model for calculation: *Amer. Jour. Sci.*, 272, 438-475.
- Bowes, D. R., and Wright, A. E., 1961, An explosion-breccia complex at Back Settlement, near Kentallen Argyll: *Trans. Edinburgh Geol. Soc.*, 18, 293-314.
- Boyd, F. R., 1961, Welded tuffs and flows in the rhyolite plateau of Yellowstone Park, Wyoming: *Geol. Soc. Amer. Bull.*, 72, 387-426.
- Bradley, J., 1965, Intrusion of major dolerite sills: *Trans. Roy. Soc. New Zealand*, 3, 27-55.
- Branch, C. D., 1966, Volcanic cauldrons, ring complexes, and associated granites of the Georgetown Inlier, Queensland: *Bull. Miner. Res. Geol. Geoph. Australia*, 76, 159 pp.
- , 1966a, The structure and evolution of the volcanic cauldrons, ring complexes, and associated granites of the Georgetown Inlier, Queensland: *Nature*, 209, 606-607.

- , 1967, The source of eruption for pyroclastic flows: cauldrons or calderas: *Bull. Volc.*, 30, 41-5.
- Buch, L. von, 1825, *Physikalische Beschreibung der Canarischen Inseln*. Berlin.
- Bunsen, R., 1847, *Über den inneren Zusammenhang der pseudovulkanischen Erscheinungen Islands: Liebigs Ann. Chem. u Pharm.*, 62, 1-59.
- , 1851, *Ueber die Prozesse der vulkanischen Gesteinbildungen Islands: Pogg. Ann.*, Vol. 83, pp. 197-272.
- Burk, C. A., 1965, The Aleutian Arc and Alaska continental margin: *Geol. Surv. Can. Paper* 66-15, 206-215.
- Carlisle, D., 1963, Pillow breccias and their aquagene tuffs, Quadra Island, British Columbia: *Jour. Geol.*, 71, 48-71.
- Carmichael, I. S. E., Nicolls, J., Spera, F. J., Wood, B. J., and Nelson, S. A., in press, High temperature properties of silicate liquids: applications to the equilibration and ascent of basic magma: *Phil. Trans. Roy. Soc. London*, A.
- , Turner, F. J., and Verhoogen, J., 1974, *Igneous petrology*: McGraw-Hill, N.Y., 739 pp.
- Carr, M. J., and Stoiber, R. E., 1973, Intermediate depth earthquakes and volcanic eruptions in Central America, 1961-1972: *Bull. Volc.*, 37, 326-337.
- Carron, J., 1969, *Recherches sur la viscosité et les phénomènes de transport des ions alcalins dans les obsidiennes granitiques*: Paris, Ecole Normale Supérieure, Travaux Lab. Geol., No. 3, 112 pp.
- Chaigneau, M., Tazieff, H., and Fabre, R., 1960, Composition des gaz volcaniques du lac de lave permanent du Nyiragongo (Congo belge): *Acad. Sci. (Paris) Comptes Rendus*, 250, 2482-2485.
- Chamberlin, R. T., 1908, The gases in rocks: Carnegie Inst. Wash. Pub., 106, 80 pp.
- Chouet, B., Hamisevicz, N., and McGetchin, T.R., 1974, Photoballistics of volcanic jet activity at Stromboli, Italy: *Jour. Geoph. Res.*, 79, 4961-4976.
- Christensen, M. N., and Gilbert, C. M., 1964, Basaltic cone suggests constructional origin of some guyots: *Science*, 143, 240-242.
- Christiansen, R. L., and Lipman, P. W., 1966, Emplacement and thermal history of a rhyolite lava flow near Fortymile Canyon, southern Nevada: *Geol. Soc. Amer. Bull.*, 77, 671-684.
- , and Lipman, P. W., 1972, Cenozoic volcanism and plate tectonic evolution of the Western United States. II. Late Cenozoic: *Phil. Trans. Roy. Soc. London*, A, 271, 249-284.
- Clacy, G. R. T., 1968, Geothermal ground noise amplitude and frequency spectra in the New Zealand volcanic region: *Jour. Geoph. Res.*, 73, 5377-5383.
- Clark, R. H., and Cole, J. W., 1976, Prediction studies on White Island volcano, Bay of Plenty, New Zealand: in *Volcanism in Australasia*, R. W. Johnson, editor, 375-384.
- Clark, S. P., Jr. and Ringwood, A. E., 1964, Density distribution and constitution of the mantle: *Rev. Geophys.*, 2, 35-88.
- Clarke, W. B., Beg, M. A., and Craig, H., 1969, Excess ^3He in the sea: evidence for terrestrial primordial helium: *Earth Plan. Sci. Ltrs.*, 6, 213-220.
- Cloos, Hans., 1941, *Bav. und Tatigkeit von Tuffschloten*: *Geol. Rundschau*, 32, 705-800.
- Coats, R. R., 1936, *Intrusive domes of the Washoe district, Nevada*: Univ. Calif. Pub. Bull. Geol. Sci., 24, 71-84.
- , 1962, Magma type and crustal structure in the Aleutian arc, in *The Crust of the Pacific Basin*: *Geoph. Mon.*, 6, 92-109.
- Coe, K., 1966, *Intrusive tuffs of West Cork, Ireland*: *Quart. Jour. Geol. Soc. London*, 122, 1-28.
- Colgate, S. A., and Sigurgeirsson, T., 1973, Dynamic mixing of water and lava: *Nature*, 244, 552-555.
- Condie, K. L., and Potts, M. J., 1969, Calc-alkaline volcanism and the thickness of the early Precambrian crust in North America: *Can. Jour. Earth Sci.*, 6, 1179-1184.
- Cook, H. E., 1968, *Ignimbrite flows, plugs, and dikes in the southern part of the Hot Creek Range, Nye Co., Nevada*: *Geol. Soc. Amer., Memoir* 116, 107-152.
- Corwin, G. and Foster, Helen., 1959, *The 1957 explosive eruption of Iwo-jima, Volcano Islands, Japan*: *Amer. Jour. Sci.*, 257, 161-171.
- Cotton, C. A., 1969, The pedestals of oceanic volcanic islands: *Geol. Soc. Amer. Bull.*, 80, 749-760.
- Craig, H., 1963, The isotopic geochemistry of water and carbon in geothermal areas: in *Nuclear Geology of Geothermal Areas*, Pisa, 17-53.
- , Boato, G., and White, D. E., 1956, Isotopic geochemistry of thermal waters: *Natl. Acad. Sci. - Natl. Res. Coun. Pub. No.* 400, 29-38.
- , Clarke, W. G., and Beg, M. A., 1975, Excess ^3He in deep water on the East Pacific Rise: *Earth Plan. Sci. Ltrs.*, 26, 125-132.
- Crandell, D. R., and Mullineaux, D. R., 1967, Volcanic hazards at Mount Rainier, Washington: *U. S. Geol. Surv. Bull.*, 1238, 26 pp.
- , Mullineaux, D. R., and Sigafoos, R. S., 1974, Chaos Crags eruptions and rock-fall avalanches, Lassen Volcanic National Park, California: *Jour. Research, U. S. Geol. Surv.*, 2, 49-59.
- , and Waldron, H. H., 1956, A Recent volcanic mudflow of exceptional dimensions from Mt. Rainier, Washington: *Amer. Jour. Sci.*, 254, 349-362.

- Curtis, G. H., 1954, Mode of origin of pyroclastic debris in the Mehrten formation of the Sierra Nevada: *Univ. Calif. Pub. Geol. Sci.*, 29, 435-502.
- , 1968, The stratigraphy of the ejecta from the 1912 eruption of Mount Katmai and Novarupta, Alaska: *Geol. Soc. Amer., Mem.* 116, 153-210.
- Dalrymple, G. B., Silver, E. A., and Jackson, E. D., 1973, Origin of the Hawaiian Islands: *Amer. Scientist*, 61, 294-308.
- Daly, R. A., 1933, *Igneous rocks and the depths of the earth*: McGraw-Hill, N.Y., 598 pp.
- Dana, J. D., 1890, *Characteristics of volcanoes*: Dodd, Mead & Co., N. Y., 399 pp.
- Danes, Z. F., 1972, Dynamics of lava flows: *Jour. Geoph. Res.*, 77, 1428-1432.
- Darwin, C. R., 1844, Geological observations on the volcanic islands visited during the voyages of HMS Beagle, with brief notices on the geology of Australia and the Cape of Good Hope, being the second part of the geology of the voyage of the Beagle: London.
- Dawson, J. B., 1964, Carbonate tuff cones in northern Tanganyika: *Geol. Mag.*, 101, 129-137.
- Decker, R. W., 1973, State-of-the-art in volcano forecasting: *Bull. Volc.*, 37, 372-393.
- , and Hadikusumo, 1961, Results of the 1960 expedition to Krakatau: *Jour. Geoph. Res.*, 66, 3497-3511.
- Delaney, F. M., 1955, Ring structures in the northern Sudan: *Ecl. Geol. Helv.*, 48, 133-148.
- Desmarest, N., 1771, Sur l'origine et la nature du basalte à grandes colonnes polygmes, déterminées par l'histoire naturelle de cette pierre observée en Auvergne: *Mem. Acad. Sci., Paris*, Vol. 87, pp. 705-775.
- Dickinson, W. R., 1969, Evolution of calc-alkaline rocks in the geosynclinal system of California and Oregon: *Proceedings of the Andesite Conf.*, A. R. McBirney, ed., Oregon Dept. Geol. Min. Ind. Bull., 65, 151-156.
- , 1970, Relations of andesites, granites, and derivative sandstones to arc-trench tectonics: *Rev. of Geoph. and Space Phys.*, 8, 813-860.
- , 1976, Sedimentary basins developed during evolution of Mesozoic-Cenozoic arc-trench systems in western North America: *Can. Jour. Earth Sci.*, 13, 1268-1287.
- , and Hatherton, T., 1967, Andesitic volcanism and seismicity around the Pacific: *Science*, 157, 801-803.
- Dieterich, J. H., and Decker, R. W., 1975, Finite element modeling of surface deformation associated with volcanism: *Jour. Geoph. Res.*, 80, 4094-4102.
- Duncan, R. A. and McDougall, I., 1976, Linear volcanism in French Polynesia: *Jour. Volc. Geoth. Res.*, 1, 197-227.
- Durrell, Cordell, 1944, Andesite breccia dikes near Blairsden, California: *Geol. Soc. Amer. Bull.*, 55, 255-272.
- Du Toit, A. I., 1920, The Karroo dolerites: *Trans. Geol. Soc. S. Africa*, 33, 1-42.
- Dymond, J. and Hogan, L., 1973, Noble gas abundance patterns in deep-sea basalts—primordial gases from the mantle: *Earth Plan. Sci. Ltrs.*, 20, 131.
- Eaton, G. P., 1963, Volcanic ash deposits as a guide to atmospheric circulation in the geologic past: *Jour. Geoph. Res.*, 68, 521-528.
- , 1964, Windborne volcanic ash: a possible index to polar wandering: *Jour. Geol.*, 72, 1-35.
- , Christiansen, R. L., Iyer, H. M., Pitt, A. M., Mabey, D. R., Blank, H. R., Zietz, I., and Gettings, M. E., 1975, Magma beneath Yellowstone Park: *Science*, 188, 787-796.
- Eaton, J. P., and Murata, K. J., 1960, How volcanoes grow: *Science*, 132, 925-938.
- Eckel, E. B., 1959, Geology and mineral resources of Paraguay—a reconnaissance: *U.S. Geol. Survey, Prof. Paper* 327, 110 pp.
- Edman, J., 1976, Lithosphere thickness, subsidence of aseismic ridges, and volcano height: *Jour. Volc. Geoth. Res.*, 1, 363-379.
- Eggers, A., Krausse, J., Rush, H., and Ward, J., 1976, Gravity changes accompanying volcanic activity at Pacaya Volcano, Guatemala: *Jour. Volc. Geoth. Res.*, 1, 229-236.
- Eggler, D. H., 1972, Water-saturated and under-saturated melting relations in a Paricutin andesite and an estimate of water content in the natural magma: *Contr. Min. Petr.*, 34, 261-271.
- Einarsson, T., 1949, The eruption of Hekla, 1947-1948, Pt. IV, 3: The flowing lava: *Soc. Sci. Islandica*.
- , 1950, The basic mechanism of volcanic eruptions and the ultimate causes of volcanism: *Visindafelag Islandinga*, IV, 5, 30 pp.
- , 1956, Studies of the mechanism of explosive activity in the Hekla eruption: *Visindafelag Islandinga*, V, 2, 1-54.
- , 1966, Studies of temperature, viscosity, density and some types of materials produced in the Surtsey eruption: *Surtsey Research Prog. Rpt.*, 2, 163-179.
- Ellis, A. J., 1957, Chemical equilibrium in magmatic gases: *Amer. Jour. Sci.*, 255, 416-431.
- , 1962, Investigations in hydrothermal chemistry: *New Zealand Sci. Rev.*, 20, 95-99.
- , and Mahon, W. A. J., 1964, Natural hydrothermal systems and experimental hotwater/rock interactions: *Geoch. Cosmoch. Acta*, 28, 1323-1357.
- Elskens, I., Tazieff, H., and Tonani, F., 1964, A new method for volcanic gas analyses in the field: *Bull. Volc.*, 27, 1-4, 347-350.

- , 1969, Investigations nouvelles sur les gas volcaniques: *Bull. Volc.*, 32, 523-574.
- Emeleus, T. G., 1977, Thermo-magnetic measurements as a possible tool in the prediction of volcanic activity in the volcanoes of the Rabaul caldera, Papua, New Guinea: *Jour. Volc. Geoth. Res.*, 2, 343-359.
- Ewart, A., 1963, Petrology and petrogenesis of the Quaternary pumice ash in the Taupo area, New Zealand: *Jour. Petrology*, 4, 392-431.
- , Hildreth, W., and Carmichael, I. S. E., 1975, Quaternary acid magma in New Zealand: *Contrib. Min. Petrol.*, 51, 1-27.
- Facca, G., and Tonani, F., 1964, Theory and technology of a geothermal field: *Bull. Volc.*, 27, 143-189.
- Fedotov, S. A., 1974, Magmatic chambers of East Kamchatka volcanoes by the seismological data: Nauka Pub. House, Novosibirsk, 88 pp.
- , 1975, Mechanism of magma ascent and deep feeding channels of island arc volcanoes: *Bull. Volc.*, 39, 1-14.
- Fenner, C. N., 1923, The origin and mode of emplacement of the great tuff deposit of the Valley of Ten Thousand Smokes: *Nat. Geog. Soc., Contrib. Technical Papers, Katmai Series, No. 1*.
- , 1948, Incandescent tuff flows in southern Peru: *Geol. Soc. Amer. Bull.*, 59, 879-893.
- Finch, R. H., 1930a, Mud flow eruption of Lassen volcano: *Volcano Letter No. 266, Hawaiian Volcano Observ.*, Jan., 1930.
- , 1930a, Rainfalls accompanying explosive eruptions of volcanoes: *Amer. Jour. Sci.*, 19, 147-150.
- Fisher, N. H., 1939, Geology and vulcanology of Blanche Bay and the surrounding area, New Britain: *Terr. New Guinea Geol. Bull.* 1, Canberra.
- Fisher, R. V., 1960, Criteria for recognition of laharic breccias, southern Cascade Mts., Washington: *Geol. Soc. Amer. Bull.*, 71, 127-132.
- , 1961, Proposed classification of volcanoclastic sediments and rocks: *Geol. Soc. Amer. Bull.*, 72, 1409-1414.
- , 1964, Maximum size, median diameter, and sorting of tephra: *Jour. Geoph. Res.*, 69, 341-355.
- , 1966, Rocks composed of volcanic fragments and their classification: *Earth-Sci. Rev.*, 1, 287-298.
- , 1966a, Mechanism of deposition from pyroclastic flows: *Amer. Jour. Sci.*, 264, 350-363.
- , and Waters, A. C., 1970, Base surge bed forms in maar volcanoes: *Amer. Jour. Sci.*, 268, 157-180.
- Fiske, R. S., 1963, Subaqueous pyroclastic flows in the Ohanapecosh Formation, Washington: *Geol. Soc. Amer. Bull.*, 74, 391-406.
- Mount Rainier National Park, Washington: U.S. Geol. Surv., Prof. Paper 444.
- , and Jackson, E. D., 1972, Orientation and growth of Hawaiian volcanic rifts: the effect of regional structure and gravitational stresses: *Proc. Roy. Soc. London, A*, 329, 299-326.
- , and Kinoshita, W. T., 1969, Inflation of Kilauea volcano prior to its 1967-1968 eruption: *Science*, 165, 341-349.
- , and Matsuda, T., 1964, Submarine equivalents of ash flows in the Tokiwa formation, Japan: *Amer. Jour. Sci.*, 262, 76-106.
- Floyd, D. A., and Winchester, J. A., 1975, Magma type and tectonic setting discrimination using immobile elements: *Earth Plan. Sci. Ltrs.*, 27, 211-218.
- Forbes, R. B., Ray, D. K., Katsura, T., Matsumoto, H., Haramura, H., and Furst, M. J., 1969, The comparative chemical composition of continental vs. island arc andesites in Alaska: *Proc. Andesite Conf. (McBirney, A. R., editor)*, pp. 111-120.
- Foster, H. L., and Mason, A. C., 1955, 1950 and 1951 eruptions of Mihara Yama, O-Shima volcano, Japan: *Geol. Soc. Amer. Bull.*, 66, 731-762.
- Fouqué, Ferdinand, 1879, Santorin et ses eruptions: Paris, 440 pp.
- Fournier, R. O., and Rowe, J. J., 1966, Estimation of underground temperatures from the silica content of water from hot springs and wet-steam wells: *Amer. Jour. Sci.*, 264, 685-697.
- , and Truesdell, A. H., 1973, An empirical Na-K-Ca geothermometer for natural waters: *Geochim. Cosmochim. Acta*, 37, 1255-1275.
- Francis, E. H., 1959, A volcanic vent in the Bogside Mines, Fife: *Geol. Mag.*, 96, 457-469.
- , 1961, Volcanism in relation to sedimentation in the Carboniferous rocks of the Saline District, Fife: *Bull. Geol. Surv. Gr. Brit.*, No. 17, 116-144.
- , 1967, A review of Carboniferous-Permian volcanicity in Scotland: *Geol. Rund.*, 57, 219-246.
- , 1968, Effect of sedimentation on volcanic processes, including neck-sill relationships, in the British Carboniferous: XXIII Int. Geol. Cong., V, 2, 163-174.
- , and Howells, M. F., 1973, Transgressive welded ash-flow tuffs among the Ordovician sediments of the NE Snowdonia, N. Wales: *Jour. Geol. Soc.*, 129, 621-641.
- Friedlaender, I., 1918, Regelmässigkeit der Abstände vulkanischer Eruptions-zentren: *Zeitschr. für Vulk.*, 4, 15-32.
- Friedman, I., Lipman, P. W., Obradorich, J. D., Gleason, J. D., and Christiansen, R. L., 1974, Meteoric water in magmas: *Science*, 184, 1069-1072.
- Friend, J. P., 1973, The global sulfur cycle in *Chemistry of the Lower Atmosphere*: S. I. Rasool, ed., Plenum, New York.
- Fries, C. Jr., 1953, Volumes and weights of pyroclastic material, lava and water erupted by Parícutin Volcano, Michoacán, Mexico: *Amer. Geophys. Un. Trans.*, 34, 603-616.

- Fudali, R. F., and Melson, W. G., 1970, Ejecta velocities, magma chamber pressure and kinetic energy associated with the 1968 eruption of Arenal volcano: *Bull. Volc.*, 35, 383-401.
- Fujii, N., and Uyeda, S., 1974, Thermal instabilities during flow of magma in volcanic conduits: *Jour. Geoph. Res.*, 79, 3367-3369.
- Fuller, R. E., 1928, The Asotin Craters of the Columbia River basalt: *Jour. Geol.*, 36, 56-74.
- , 1931, The aqueous chilling of basaltic lava on the Columbia River plateau: *Amer. Jour. Sci.*, 21, 281-300.
- , 1939, Gravitational accumulation of olivine during the advance of basaltic flows: *Jour. Geol.*, 47, 303-313.
- Fyfe, W. S., 1970, Some thoughts on granitic magmas: in *Mechanics of igneous intrusions*, G. Newall and N. Rast, editors, Gallery Press, Liverpool.
- Gass, I. G., Harris, P. G., and Holdgate, M. W., 1963, Pumice eruption in the area of the South Sandwich Islands: *Geol. Mag.*, 100, 321-330.
- Gauthier, F., 1973, Field and laboratory studies of the rheology of Mount Etna lava: *Phil. Trans. Roy. Soc. London, A*, 274, 83-98.
- Gautier, A., 1906, La genèse des eaux thermales et ses rapports avec le volcanisme: *Ann. Mines (Paris) Mem.*, Ser. 6, 9, 316-370. (Translated and condensed by F. L. Ransome: *Econ. Geol.*, 1, 688-697.)
- Geikie, A., 1897, *Ancient volcanoes of Great Britain*, 2 vol., Macmillan, London, 969 pp.
- , 1902, The geology of East Fife: *Mem. Geol. Surv. Scotland*.
- Gerth, H. 1955, *Der geologische Bau der Sudamerikanischen Kordillera*: Gebrüder Borntraeger, Berlin, 264 pp.
- Gèze, Bernard, 1964, Sur la classification des dynamismes volcaniques: *Bull. Volc.*, 27, 237-257.
- Goff, F. E., Donnelly, J. M., Thompson, J. M., 1977, Geothermal prospecting in the Geysers-Clear Lake area, northern California: *Geology*, 5, 509-515.
- Goguel, J., 1953, Le Regime thermique de l'eau souterraine: *Ann. Mines, Min. Ind. Ener.*, 10, 3-32.
- Gonzalez, R. J., and Foshag, W. F., 1946, The birth of Parícutin: *Smithsonian Inst. Ann. Rpt.*, 223-234.
- Goranson, R. W., 1931, The solubility of water in granitic magmas: *Amer. Jour. Sci.*, 22, 481-502.
- Gorshkov, G. S., 1956, On the deep magmatic hearth of Klyuchevskoi Volcano: *Dok. Akad. Nauk. USSR*, 106, No. 4.
- , 1959, Gigantic eruption of the volcano Bezymianny: *Bull. Volc.*, 20, 77-112.
- , 1960, Determination of the explosion energy in some volcanoes according to barograms: *Bull. Volc.*, 23, 141-144.
- , 1962, Petrochemical features of volcanism in relation to the types of the earth's crust: in *The Crust of the Pacific Basin*, *Geoph. Mon.* 6, 110-115.
- , and Dubik, Y. M., 1970, Gigantic directed blast at Shiveluch volcano, Kamchatka: *Bull. Volc.*, 34, 261-288.
- Gottini, Violetta, 1963, Sur l'origine des roches pipernoïdes de la région phlégréenne: *Bull. Volc.*, 25, 263-276.
- Grapes, R. H., Reid, D. L., and McPherson, J. G., 1974, Shallow dolerite intrusion and phreatic eruption in the Allan Hills region, Antarctica: *New Zealand Jour. Geol. Geoph.*, 17, 563-577.
- Greeley, R., 1971, Observations of actively forming lava tubes and associated structures, Hawaii: *Mod. Geol.*, 2, 207-223.
- Griggs, D. T., 1972, The sinking lithosphere and the focal mechanism of deep earthquakes: in *The nature of the solid earth*, Robertson, E. C., editor, McGraw-Hill, N. Y., 361-384.
- Grout, F. F., 1945, Scale models of structures related to batholiths: *Amer. Jour. Sci.*, 243A, 260-284.
- Gruntfest, I. J., 1963, Thermal feedback in liquid flow; plane shear at constant stress: *Trans. Soc. Rheol.* 7, 195-207.
- Guettard, M., 1752, *Memoire sur quelques montagnes de France qui ont été des volcans*: *Mem. Acad. Sci. Paris*.
- Gunn, B. M., 1974, Systematic petrochemical differences in andesitic suites: *Bull. Volc.*, 38, 481-490.
- Hall, James, 1805, Experiments on whinstone and lava: *Trans. Roy. Soc. Edinburgh*, 5, 43-75.
- Hamilton, D. L., and Anderson, G. M., 1967, Effects of water and oxygen pressure on the crystallization of basaltic magmas: in *Basalts*, H. H. Hess and Poldervaart, ed., Vol. 1, 445-482.
- , Burnham, C. W., and Osborn, E. F., 1964, The solubility of water and effects of oxygen, fugacity and water content on crystallization in mafic magmas: *Jour. Petrol.*, 5, 21-39.
- Hamilton, E. L., 1957, Marine geology of the southern Hawaiian ridge: *Geol. Soc. Amer. Bull.*, 68, 1011-1026.
- Harris, P. G., 1957, Zone refining and the origin of potassic basalts: *Geochim. Cosmoch. Acta*, 12, 195-208.
- , 1974, Anataxis and other processes within the mantle: in *Sørensen, H.*, ed. *The alkaline rocks*, John Wiley & Sons, Inc., N.Y., 427-436.

- Harrison, J. C., and Brisbin, W. C., 1959, Gravity anomalies off the west coast of North America, 1, Seamount Jasper: *Geol. Soc. Amer. Bull.*, 70, 929-934.
- Hay, R. L., 1959, Formation of the crystal-rich glowing avalanche deposits of St. Vincent, B. W. I.: *Jour. Geol.*, 67, 540-562.
- Hayes, T. J., 1938, *Elements of ordnance*, New York, 715 pp.
- Heald, E. F., Naughton, J. J., and Barnes, I. L., 1963, The chemistry of volcanic gases. Use of equilibrium calculations in the interpretation of volcanic gas samples: *Jour. Geoph. Res.*, 68, 546-567.
- Healy, James, 1962, Structure and volcanism in the Taupo volcanic zone, New Zealand: *Crust of the Pacific*, *Geoph. Mono. No. 6*, 151-157.
- Hearn, B. C. Jr., 1968, Diatremes with kimberlitic affinities in North-central Montana: *Science*, 159, 622-625.
- Heiken, G., 1976, Depressions surrounding volcanic fields: a reflection of underlying batholiths: *Geology*, 4, 568-573.
- Higgins, M. W., 1973, Petrology of Newberry volcano, central Oregon: *Geol. Soc. Amer. Bull.*, 84, 455-488.
- Hildreth, W. and Spera, F., 1974, Magma chamber of the Bishop Tuff: gradients in T, P_{Total} and P_{H₂O}: *Geol. Soc. Amer. Abstr. Programs*, 6, 795.
- Holland, H. D., 1962, Model for the evolution of the earth's atmosphere: *Geol. Soc. Amer., Bulletin* Vol., 447-477.
- Hopgood, A. M., 1962, Radial distribution of soda in a pillow of spilitic lava from the Franciscan, California: *Amer. Jour. Sci.*, 260, 383-396.
- Howorth, R., and Rankin, P. C., 1975, Multi-element characterization of glass shards from stratigraphically related correlated rhyolitic tephra units: *Chem. Geol.*, 15, 239-250.
- Hubbert, M. K., and Willis, D. G., 1957, Mechanics of hydraulic fracturing: *Amer. Inst. Mining Metall. and Petrol. Eng. Trans.*, 210, 153-166.
- Hulme, G., 1974, The interpretation of lava flow morphology: *Geoph. Jour. Roy. Astr. Soc.*, 39, 361-383.
- Hunt, C. B., 1938, A suggested explanation of the curvature of columnar joints in volcanic necks: *Amer. Jour. Sci.*, 36, 142-149.
- Hurst, A. W., and Christoffel, D. A., 1973, Surveillance of White Island Volcano, 1968-1972, 3. Thermo-magnetic effects due to volcanic activity: *N. Z. Jour. Geol. Geoph.*, 16, 965-972.
- Iddings, J. P., 1920, Relative densities of igneous rocks calculated from their norms: *Amer. Jour. Sci.*, 49, 363-366.
- Iida, K., 1938, The mud flow that occurred near the explosion-crater of Mt. Bandai on May 9 and 15, 1938: *Bull. Earthquake Res. Inst.*, 16, 681.
- Isacks, B., Oliver, J., and Sykes, L. R., 1968, Seismology and the new global tectonics: *Jour. Geoph. Res.*, 73, 5855-5899.
- Ishikawa, T., Minato, M., Kuno, H., Matsumoto, T., and Yagi, K., 1957, Welded tuffs and deposits of pumice flow and *nuée ardente* in Japan: *Proc. Internat. Geol. Congress, 20th Session, Mexico. Sección 1—Vulcanología del Cenozoico*, 137-150.
- Iwasaki, I., 1951, The 1950-51 eruption of Mihara-yama; geochemical investigations of the volcano: *Jour. Geogr. (Tokyo)*, 60, 140-143.
- Jaeger, J. C., 1959, Temperatures outside a cooling intrusive sheet: *Amer. Jour. Sci.*, 257, 44-54.
- , 1964, Thermal effects of intrusions: *Rev. Geoph. Space Phys.*, 2, 443-466.
- Jaggard, T. A., 1917, Thermal gradient of Kilauea lava lake, *Jour. Wash. Acad. Sci.*, 7, 397-405.
- , 1940, Magmatic gases: *Amer. Jour. Sci.*, 238, 313-353.
- , 1949, Steam blast volcanic eruptions: *Fourth Spec. Rep. Hawaiian Volcano Observ., Honolulu*, 133 pp.
- , and Finch, R. H., 1924, The explosive eruption of Kilauea in Hawaii in 1924: *Amer. Jour. Sci.*, 8, 353-374.
- James, R., 1968, Wairakei and Larderello; geothermal power systems compared: *New Zealand Jour. Sci. and Tech.*, 11, 706-719.
- Johnston, M. J. S., and Stacey, F. D., 1969, Volcano-magnetic effect observed on Mt. Ruapehu, New Zealand: *Jour. Geoph. Res.*, 74, 6541-6544.
- Joly, J., 1930, *The surface-history of the earth*: Clarendon Press, 211 pp.
- Kadik, A. A., Lukanin, O. A., Lebedev, Ye. B., and Korovushkina, E. Ye., 1972, Solubility of H₂O and CO₂ in granite and basalt: *Geoch. Internat.*, 9, 1041-1050.
- , and Lukanin, O. A., 1973, The solubility dependent behavior of water and carbon dioxide in magmatic processes: *Geoch. Internat.*, 10, 115-129.
- Kane, M. F., Mabey, D. R., and Brace, R. L., 1976, A gravity and magnetic investigation of the Long Valley Caldera, Mono County, California: *Jour. Geoph. Res.*, 81, 754-762.
- Kani, K., and Hosokawa, K., 1936, On the viscosities of silicate rock-forming minerals and igneous rocks: *Res. Electrotech. Lab.*, 391, 1-105.
- Karig, D. E., 1970, Ridges and basins of the Tonga-Kermadec Island arc system: *Jour. Geoph. Res.*, 75, 239-254.

- , and Sharman, G. F. III, 1975, Subduction and accretion in trenches: *Geol. Soc. Amer. Bull.*, *86*, 377-389.
- Kato, I., Muroi, I., Yamazaki, T., and Abe, M., 1971, Subaqueous pyroclastic flow deposits in the upper Donzurubo formation, Nijo-san District, Osaka, Japan: *Jour. Geol. Soc. Japan*, *77*, 193-206.
- Kaula, W. M., 1963, Elastic models of the mantle corresponding to variations in the external gravity field: *Jour. Geoph. Res.*, *68*, 4967-4978.
- Kawada, K., 1966, Studies of the thermal state of the earth. The 17th paper: Variation of thermal conductivity of rocks. Pt. 2: Tokyo Univ. Earthquake Research Inst. Bull., *44*, 1071-1091.
- Keller, W. D., and Reesman, A. L., 1963, Dissolved products of artificially pulverized silicate minerals and rocks, Part 2: *Jour. Sed. Pet.*, *33*, 426-437.
- Kemmerling, G. L. L., 1919, De Kloetramp: *De Ingenieur*, *34* e., Jaarg., 804-813.
- Kennedy, G. C., 1955, Some aspects of the role of water in rock melts: *Geol. Soc. Amer.*, Sp. Paper 62, 489-504.
- , and Holser, W. T., 1966, Pressure-volume-temperature and phase relations of water and carbon-dioxide, *Geol. Soc. Amer.*, Mem. 97, Sect. 16.
- , and Nordlie, B. E., 1968, The genesis of diamond deposits: *Econ. Geol.*, *63*, 498-499.
- Kennedy, W. Q., 1931, On composite lava flows: *Geol. Mag.*, *68*, 166-176.
- , 1933, Composite auto-intrusion in a Carboniferous lava flow: Summary of Progress, *Geol. Surv.*, Great Britain for 1932, 83-93.
- Kennett, J. P., McBirney, A. R., and Thunell, R. C., 1977, Episodes of Cenozoic volcanism in the Circum-Pacific region: *Jour. Volc. Geoth. Res.*, *2*, 145-163.
- , and Thunell, R. C., 1975, Global increase in Quaternary explosive volcanism: *Science*, *187*, 497-503.
- Kieffer, S. W., 1976, Geysers: a hydrodynamic model for the early stages of eruption (abstract): *Geol. Soc. Amer. Ann. Mtg.*, *7*, 1146.
- Kingery, W. D., 1959, Surface tension of some liquid oxides and their temperature coefficients: *Jour. Amer. Ceram. Soc.*, *42*, 6-10.
- Kinoshita, W. T., 1965, A gravity survey of the island of Hawaii: *Pacific Sci.*, *19*, 339-340.
- , and Okamura, R. T., 1965, A gravity survey of the Island of Maui: *Pacific Sci.*, *19*, 341-342.
- Kjartansson, G., 1951, Eruption of Hekla, 1947-1948: Part 2, No. 4, Water flood and mud flows: *Soc. Scient. Islandica, Reykjavik*.
- , 1959, The Moberg formation: *Geog. Annlr.*, *41*, 135-169.
- Koczy, F. F., 1956, Specific salinity: *Deep Sea Res.*, *3*, 279-288.
- Koenig, J. B., 1967, The Salton-Mexicali geothermal province: *Calif. Div. Mines and Geol., Min. Inf. Serv.*, *20*, 75-81.
- Koide, H., and Bhattacharji, S., 1975, Formation of fractures around magmatic intrusions and their role in ore localization: *Econ. Geol.*, *70*, 781-799.
- and —, 1975, Mechanistic interpretation of rift valley formation: *Science*, *189*, 791-793.
- Koyanagi, R. Y., Swanson, D. A., and Endo, E. T., 1972, Distribution of earthquakes related to mobility of the south flank of Kilauea Volcano, Hawaii: *U. S. Geol. Surv., Prof. Paper 800-D*, 89-97.
- Kozu, S., 1934, The great activity of Komagatake in Hokkaido in 1929: *Tschermak's min. w. pet. Milt.*, *45*, 133-174.
- Krauskopf, K. B., 1948, Mechanism of eruption at Parícutin volcano, Mexico: *Geol. Soc. Amer. Bull.*, *59*, 711-732.
- , 1948, Lava movement at Parícutin volcano, Mexico: *Geol. Soc. Amer. Bull.*, *59*, 1267-1283.
- Krivoy, H. L., Baker, M., and Moe, E. E., 1965, A reconnaissance gravity survey of the island of Kauai, Hawaii: *Pacific Sci.*, *19*, 354-358.
- Kuno, Hisashi, 1941, Characteristics of deposits formed by pumice flows and those by ejected pumice: *Bull. Earthquake Res. Inst.*, *19*, 144-148.
- , 1959, Origin of Cenozoic petrographic provinces of Japan and surrounding areas: *Bull. Volc.*, *20*, 37-76.
- , 1962, Frequency distribution of rock types in oceanic, orogenic and kratogenic volcanic associations: *Amer. Geoph. Un., Monogr.* *6*, 135-139.
- , 1962, Catalogue of the active volcanoes of the world, Part II—Japan, Taiwan, and Marianas: *Internat. Assoc. Volc., Rome*.
- , 1968, Origin of andesite and its bearing on the island arc structure: *Bull. Volc.*, *32*, 141-176.
- , *et al.*, 1964, Sorting of pumice and lithic fragments as a key to eruptive and emplacement mechanism: *Jap. Jour. Geol. and Geog.*, *35*, 223-238.
- Kushiro, I., 1976, Changes in viscosity and structure of melt of NaAlSi₂O₆ composition at high pressures: *Jour. Geoph. Res.*, *81*, 6347-6350.
- , Yoder, H. S. Jr., and Mysen, B. O., 1976, Viscosities of basalt and andesite melts at high pressures: *Jour. Geoph. Res.*, *81*, 6351-6356.
- Lachenbruch, A. M., Sass, J. H., Monroe, R. J., and Moses, T. H. Jr., 1976, Geothermal setting and simple heat-conduction models for the Long Valley Caldera: *Jour. Geoph. Res.*, *81*, 769-784.

- Lacroix, Alfred., 1904, *La Montagne Pelée et ses éruptions*: Paris, Masson et Cie., 662 pp.
- La Fehr, T. R., 1965, Gravity, isostasy and crustal structure in the southern Cascade Range: *Jour. Geoph. Res.*, 70, 5581-5597.
- Lamb, H. H., 1970, Volcanic dust in the atmosphere; with a chronology and assessment of its meteorological significance: *Proc. Roy. Soc. London*, 266, 425-533.
- Larson, R. L., and Spiess, F. N., 1969, East Pacific Rise crest: a near-bottom geophysical profile: *Science*, 163, 68-71.
- Larsson, Walter, 1936, Vulkanische Asche vom Ausbruch des chilenischen Vulkans Quizapu (1932) in Argentina gesammelt. Eine Studie über aolische Differentiation: *Bull. Geol. Inst. Upsala*, 26, 27-52.
- Leyden, R. von, 1936, Staukuppen und verwandte Bildungen: *Zeitschr. für Vulk.*, 16, 225-247.
- Lingenfelter, R. E. and Schubert, G., 1974, Hot spot and trench volcano separation: *Nature*, 249, 820.
- Lipman, P. W., 1966, Water pressures during differentiation and crystallization of some ash-flow magmas from southern Nevada: *Amer. Jour. Sci.*, 264, 810-826.
- , 1967, Mineral and chemical variations within an ash-flow sheet from Aso caldera, southwestern Japan: *Contr. Mineral. and Petr.*, 16, 300-327.
- , Christiansen, R. L., and O'Connor, J. T., 1966, A compositionally zoned ash-flow sheet in southern Nevada: *U. S. Geol. Surv., Prof. Paper* 524-F.
- , Prostka, H. J., and Christiansen, R. L., 1972, Cenozoic volcanism and plate-tectonic evolution of the Western United States. I. Early and Middle Cenozoic: *Phil. Trans. Roy. Soc. London, A*, 271, 217-248.
- Lirer, L., Pescatore, T., Booth, B., and Walker, G. P. L., 1973, Two Plinian pumice-fall deposits from Somma-Vesuvius, Italy: *Geol. Soc. Amer. Bull.*, 84, 759-772.
- Lloyd, E. F., 1959, The hot springs and hydrothermal eruptions of Waioatapu: *N. Z. Jour. Geol. and Geoph.*, 2, 141-176.
- Lorenz, V. W., 1970, Origin of Hole-in-the-Ground, a maar in Central Oregon: Unpublished NASA rept., 113 pp.
- Ludden, J. N., 1977, Eruptive patterns for the volcano Piton de la Fournaise, Reunion Island: *Jour. Volc. Geoth. Res.*, 2, 385-395.
- Luyendyk, B. P., 1970, Origin and history of abyssal hills in the northeast Pacific: *Geol. Soc. Amer. Bull.*, 81, 2237-2260.
- Lydon, P. A., 1968, Geology and lahars of the Tuscan formation, California: *Geol. Soc. Amer., Mem.* 116, 441-475.
- Macdonald, G. A., 1939, An intrusive peperite at San Pedro Hill, Calif.: *Univ. Calif. Pub. Bull. Geol. Sci.*, 24, 329-338.
- , 1943, The 1942 eruption of Mauna Loa, Hawaii: *Amer. Jour. Sci.*, 241, 241-256.
- , 1944, The 1840 eruption and crystal differentiation in the Kilauean magma column: *Amer. Jour. Sci.*, 242, 177-189.
- , 1953, Pahoehoe, aa and block lava: *Amer. Jour. Sci.*, 251, 169-191.
- , 1956, Structure of Hawaiian volcanoes: *Gedenboek H. A. Brouwer; Kon. Ned. Geol. Mijnbouw. Gen.*, 16, 274-295.
- , 1958, Barriers to protect Hilo from lava flows: *Pacific Sci.*, 12, 258-277.
- , 1962, The 1959 and 1960 eruptions of Kilauea volcano, Hawaii, and the construction of walls to restrict the spread of the lava flows: *Bull. Volc.*, 24, 249-294.
- , 1972, *Volcanoes*: Prentice-Hall, N. J., 510 pp.
- , and Alcaraz, A., 1956, Nuées ardentes of the 1948-1953 eruption of Hibok Hibok: *Bull. Volc.*, 18, 169-178.
- MacKenzie, J. K., 1950, The elastic constants of a solid containing spherical holes: *Proc. Phys. Soc.*, B63, 2-11.
- Mackin, J. H., 1961, A stratigraphic section in the Yakima basalt . . . in south-central Washington: *Rep. of Investigations No. 19, Div. Mines and Geol., State of Washington*.
- MacLeod, N. S., Walker, G. W., and McKee, E. H., 1977, Geothermal significance of eastward increase in age of upper Cenozoic rhyolitic domes in Southeastern Oregon: *Second United Nations Symp. Dev. and Use of Geoth. Res.*, 465-474.
- Mahon, W. A. J., 1966, Silica in hot water discharged from drill holes at Wairakei, New Zealand: *N. Z. Jour. Sci.*, 9, 135-144.
- , 1976, The hydrogeochemistry of geothermal systems: prospecting and development and use: *Proc. 2nd United Nations Symp. Dev. and Use of Geoth. Res.*, 1, 775-783.
- Mansfield, G. R., and Ross, C. S., 1935, Welded rhyolitic tuffs in southeastern Idaho: *Trans. Amer. Geoph. Union*, 308-321.
- Marhinin, E. K., and Stratula, D. S., 1973, Relationship between chemical composition of volcanic rocks and depth of the seismofocal layer as shown by the Kliuchevskaya volcanic group (Kamchatka) and the Kurile-Kamchatka Island arc: *Bull. Volc.*, 37, 175-182.
- Marler, G. D. and White, D. E., 1975, Seismic Geyser and its bearing on the origin and evolution of geysers and hot springs of Yellowstone National Park: *Geol. Soc. Amer. Bull.*, 86, 749-759.
- Marsh, B. D., 1975, Plume spacing and source: *Nature*, 256, 240.

- , and Carmichael, I. S. E., 1974, Benioff zone magmatism: *Jour. Geoph. Res.*, *79*, 1196-1206.
- Marshall, M., and Cox, A., 1971, Magnetism of pillow basalts and their petrology: *Geol. Soc. Amer. Bull.*, *82*, 537-552.
- Martin, R. F., and Piwinski, A. J., 1972, Magmatism and tectonic settings: *Jour. Geoph. Res.*, *77*, 4966-4975.
- Mason, A. C., and Foster, H. L., 1956, Extruded mudflow hills of Nirasaki, Japan: *Jour. Geol.*, *64*, 76-83.
- Mathews, W. H., 1947, "Tuyas," flat-topped volcanoes in northern British Columbia: *Amer. Jour. Sci.*, *245*, 560-570.
- Mathez, E. A., 1976, Sulfur solubility and magmatic sulfides in submarine basaltic glass: *Jour. Geoph. Res.*, *81*, 4269-4276.
- Matsuo, S., 1960, On the origin of volcanic gases: *Jour. Earth Sci., Nagoya Univ.*, *8*, 222-245.
- , 1961, The behavior of volatiles in magma: *Jour. Earth Sci., Nagoya Univ.*, *9*, 101-113.
- , 1962, Establishment of chemical equilibrium in the volcanic gas obtained from the lava lake of Kilauea, Hawaii: *Bull. Volc.*, *24*, 59-71.
- , Suzuoki, T., Kusakabe, M., Wada, H., and Suzuki, M., 1974, Isotopic and chemical compositions of volcanic gases from Satsuma-Iwojima, Japan: *Geoch. Jour.*, *8*, 165-173.
- Matumoto, T., 1971, Seismic body waves observed in the vicinity of Mount Katmai, Alaska, and evidence for the existence of molten chambers: *Geol. Soc. Amer. Bull.*, *82*, 2905-2920.
- Mayo, E. B., 1944, Rhyolite near Big Pine, California: *Geol. Soc. Amer. Bull.*, *55*, 599-620.
- McBirney, A. R., 1955, Thoughts on the eruption of the Nicaraguan Volcano Las Pilas: *Bull. Volc.*, *17*, 113-117.
- , 1963, Breccia pipe near Cameron, Arizona, discussion: *Geol. Soc. Amer. Bull.*, *74*, 227-232.
- , 1963, Factors governing the nature of submarine volcanism: *Bull. Volc.*, *26*, 455-469.
- , 1968, Second additional theory of origin of fiamme in ignimbrites: *Nature*, *217*, 938.
- , 1971, Thoughts on some current concepts of orogeny and volcanism: *Comments on Earth Sciences: Geophysics*, *2*, 69-76.
- , 1976, Some geologic constraints on models for magma generation in orogenic environments: *Can. Min.*, *14*, 245-254.
- , 1978, Volcanic evolution of the Cascade Range: *Ann. Rev. Earth Planet Sci.*, *6*, 437-456.
- , and Aoki, K., 1968, Petrology of the island of Tahiti: *Geol. Soc. Amer., Mem.* *116*, 523-556.
- , Sutter, J. F., Naslund, H. R., Sutton, K. G., and White, C. M., 1974, Episodic volcanism in the central Oregon Cascade Range: *Geology*, *2*, 585-589.
- , and Williams, H., 1969, Geology and petrology of the Galápagos Islands: *Geol. Soc. Amer., Mem.* *118*, 197 pp.
- McCall, G. J. H., 1963, Classification of calderas: Krakatoan and Glencoe types: *Nature*, *197*, 136-138.
- , and Bristow, C. M., 1965, An introductory account of Suswa volcano, Kenya: *Bull. Volc.*, *28*, 333-367.
- McGetchin, T. R., Settle, M., and Chouet, B. A., 1974, Cinder cone growth modeled after North-east Crater, Mount Etna, Sicily: *Jour. Geoph. Res.*, *79*, 3257-3272.
- , and Ullrich, G. W., 1973, Xenoliths in maars and diatremes with inferences for the Moon, Mars and Venus: *Jour. Geoph. Res.*, *78*, 1833-1853.
- McLaughlin, R. J., and Stanley, W. D., 1975, Pre-Tertiary geology and structural control of geothermal resources, the Geysers steam field, California: *Second UN Symp. on Dev. and Use of Geoth. Res., San Francisco*, *1*, 475-485.
- McNitt, J. R., 1961, Geology of the Geysers thermal area, California: *United Nations Conf. on New Sources of Energy, Rome*, *2*, 292-303, United Nations, N.Y.
- , 1963, Exploration and development of geothermal power in California: *Calif. Div. Mines and Geol., Spec. Rept.* *75*, 45 pp.
- McTaggart, K. C., 1960, The mobility of *nuées ardentes*: *Amer. Jour. Sci.*, *258*, 369-382.
- , 1962, *Nuées ardentes* and fluidization: a reply: *Amer. Jour. Sci.*, *260*, 470-476.
- Mehring, P. J. Jr., Blinman, E., and Peterson, K. L., 1977, Pollen influx and volcanic ash: *Science*, *198*, 257-261.
- Melson, W. G., and Saenz, R., 1973, Volume, energy and cyclicity of eruptions of Arenal volcano, Costa Rica: *Bull. Volc.*, *37*, 416-437.
- Menard, H. W., 1956, Archipelagic aprons: *Bull. Amer. Assoc. Petr. Geol.*, *40*, 2195-2210.
- , 1964, *Marine Geology of the Pacific*: McGraw-Hill, N.Y., 271 pp.
- , 1969, Growth of drifting volcanoes: *Jour. Geoph. Res.*, *74*, 4827-4837.
- , and Mammerickx, J., 1967, Abyssal hills, magnetic anomalies and the East Pacific Rise: *Earth and Planetary Sci. Ltrs.*, *2*, 465-472.
- Mercalli, Giuseppe, 1907, *I vulcani attivi della terra*: Milan.
- Michard, G., and Foullac, C., 1976, Remarques sur le geothermomètre Na-Ca-K: *Jour. Volc. Geoth. Res.*, *1*, 297-304.
- Minakami, T., 1950, The explosive activities of volcano Asama in 1935: *Bull. Earthq. Res. Inst.*, *13*, 629-644, 790-800.

- , 1950, On explosive activities of andesite volcanoes and the forerunning phenomena: *Bull. Volc., Ser. II, 10*, 59-87.
- , 1951, On the temperature and viscosity of the fresh lava extruded in the 1951 Oo-sima eruption: *Bull. Earthq. Res. Inst., 29*, 487-498.
- , Ishikawa, T., and Yagi, K., 1951, The 1944 eruption of volcano Usu in Hokkaido, Japan: *Bull. Volc., 11*, 45-157.
- Mizutani, Y., 1978, Isotopic compositions of volcanic steam from Showashinzan Volcano, Hokkaido, Japan: *Geoch. Jour., 12*, 57-63.
- Mogi, K., 1958, Relations between the eruptions of various volcanoes and the deformation of the ground surface around them: *Bull. Earthquake Res. Inst., 36*, 99-134.
- Molnar, P. and Sykes, L. R., 1969, Tectonics of the Caribbean and Middle America regions from focal mechanisms and seismicity: *Geol. Soc. Amer. Bull., 80*, 1639-1684.
- Moore, J. G., 1962, K/Na ratio of Cenozoic igneous rocks of the western United States: *Geochim. Cosmochim. Acta, 26*, 101-130.
- , 1965, Petrology of deep-sea basalt near Hawaii: *Am. Jour. Sci., 263*, 40-52.
- , 1967, Base surge in recent volcanic eruptions: *Bull. Volc., 30*, 337-363.
- , 1970, Water content of basalt erupted on the ocean floor: *Contr. Miner. Petr., 28*, 272-279.
- , 1970, Relationship between subsidence and volcanic load, Hawaii: *Bull. Volc., 34*, 562-576.
- , 1975, Mechanism of formation of pillow lava: *Amer. Sci., 63*, 269-277.
- , Batchelder, J. N., and Cunningham, C. G., 1977, CO₂-filled vesicles in mid-ocean basalt: *Jour. Volc. Geoth. Res., 2*, 309-327.
- , and Fabbri, B. P., 1971, An estimate of the juvenile sulfur content of basalt: *Contr. Miner. Petr., 33*, 118-127.
- , and Fiske, R. S., 1969, Volcanic substructure inferred from dredge samples and ocean-bottom photographs, Hawaii: *Geol. Soc. Amer. Bull., 80*, 1191-1202.
- , Fleming, H. S., and Phillips, J. D., 1974, Preliminary model for extrusion and rifting at the axis of the Mid-Atlantic Ridge, 36°48' North: *Geology, 2*, 437-440.
- , and Melson, W. G., 1969, Nuées ardentes of the 1968 eruption of Mayon volcano, Philippines: *Bull. Volc., 33*, 600-620.
- , Nakamura, K., and Alcaraz, A., 1966, The 1965 eruption of Taal Volcano: *Science, 151*, 955-960.
- , and Peck, D. L., 1962, Accretionary lapilli in volcanic rocks of the western continental United States: *Jour. Geol., 70*, 182-193.
- , Phillips, R. L., Grigg, R. W., Peterson, D. W., and Swanson, D. A., 1973, Flow of lava into the sea, 1969-1971, Kilauea Volcano, Hawaii: *Geol. Soc. Amer. Bull., 84*, 537-546.
- , and Schilling, J.-G., 1973, Vesicles, water, and sulfur in Reykjanes Ridge basalts: *Contr. Miner. Petr., 41*, 105-118.
- Moore, E. M., and Vine, F. J., 1970, The Troodos Massif, Cyprus and other ophiolites as oceanic crust, evaluation and implications: *Proc. Roy. Soc. London, A, 268*, 443-466.
- Morgan, W. J., 1972, Deep mantle convection plumes and plate motions: *Amer. Assoc. Petrol. Geol. Bull., 56*, 203-213.
- Mroz, E. J., and Zoller, W. H., 1975, Composition of atmospheric particulate matter from the eruption of Heimaey, Iceland: *Science, 190*, 461-464.
- Muenow, D. W., 1973, High temperature mass spectrometric gas-release studies of Hawaiian volcanic glass: Pele's tears: *Geochim. Cosmochim. Acta, 37*, 1551-1561.
- Murai, I., 1960, Pumice-flow deposits of Komagatake Volcano, southern Hokkaido: *Bull. Earthq. Res. Inst., 38*, 451-466.
- , 1961, A study of the textural characteristics of pyroclastic flow deposits in Japan: *Bull. Earthq. Res. Inst., Tokyo Univ., 39*, 133-248.
- Murase, T., 1962, Viscosity and related properties of volcanic rocks at 800° to 1400° C., *Jour. Fac. Sci., Hokkaido Univ., Ser. VII, V. 1*, 487-584.
- , and McBirney, A. R., 1970, Viscosity of lunar lavas: *Science, 167*, 1491-1493.
- , and —, 1973, Properties of some common igneous rocks and their melts at high temperatures: *Geol. Soc. Amer. Bull., 84*, 3563-3592.
- Murata, K. J., 1960, Occurrence of CaCl emission in volcanic flames: *Amer. Jour. Sci., 258*, 769-772.
- , 1966, An acid fumarolic gas from Kilauea Iki, Hawaii: *Geol. Surv. Prof. Paper 537-C*, 6 pp.
- , Dondoli, C., and Saenz, R., 1966, The 1963-65 eruption of Irazú Volcano, Costa Rica (The period of March, 1963 to October, 1964): *Bull. Volc., 29*, 765-796.
- , and Richter, D. H., 1966, The settling of olivine in Kilauean magma as shown by lavas of the 1959 eruption: *Amer. Jour. Sci., 264*, 194-203.
- Mysen, B. O., Egger, D. H., Seitz, M. G., and Holloway, J. R., 1976, Carbon dioxide in silicate melts and crystals. Part I. Solubility measurements: *Amer. Jour. Sci., 276*, 455-479.
- Nakamura, K., 1965, Energies dissipated with volcanic activities—classification and evaluation: *Bull. Volc. Soc. Japan, 10*, 81-90.

- , 1977, Volcanoes as possible indicators of tectonic stress orientation—principle and proposal: *Jour. Volc. Geoth. Res.*, 2, 1-16.
- Naughton, J. J., Heald, E. F., and Barnes, I. L., 1963, The chemistry of volcanic gases I. Collection and analysis of equilibrium mixtures by gas chromatography: *Jour. Geoph. Res.*, 68, 539-544.
- Nayudu, Y. R., 1962, A new hypothesis for the origin of guyots and seamount terraces: *Amer. Geoph. Un., Geoph. Mon.* 6, 171-180.
- Neeb, G. A., 1943, The composition and distribution of the samples: *The Snellius Expedition*, 5, Pt. 3, Leyden.
- Neumann van Padang, M., 1929, Goenoeng Papandajan: *Exc. Guide, Fourth Pac. Sci. Cong., Java*.
- , 1931, Der Ausbruch des Merapi (Mittel Java) im Jahre 1930: *Zeitschr. fur Vulk.*, 14, 135-148.
- , 1934, Die Eruptionsregenfrage in Bezug auf den grossen Krakatau-Ausbruch vom 26, und 27, August, 1883: *Proc. Kon. Akad. van Wetensch, te Amsterdam*, 37, 3-8.
- , 1934a, Haben bei den ausbruchen des Slametvulkans Eruptionsregen stattgefunden? *Leidsche. geol. Med.*, 6, 79-97.
- , 1935, Eenige opmerkingen naar aanleiding van Hartmann's beschouwingen over eruptie-regens: *De Ingenieur in Ned.-Indie*, 8, 71-78.
- , 1936, Over de verplaatsing van de Kraters der Vulkanen Slamet, Lamongan, Merapi en Smeroe: *De Ingenieur in Ned.-Indie*, 4, 1-6.
- Nielson, D. R., and Stoiber, R. E., 1973, Relationship of potassium content in andesitic lavas and depth to the seismic zone: *Jour. Geoph. Res.*, 78, 6887-6892.
- Noe-Nygaard, A., 1940, Sub-glacial volcanic activity in ancient and recent times: *Fol. Geogr. Dan.*, 1, no. 2, 1-67.
- , 1968, On Extrusion forms in plateau basalts. Shield volcanoes of "scutulum" type: *Scientia Islandica, Anniversary Vol.*, 10-13.
- Noguchi, K., and Kamiya, H., 1963, Prediction of volcanic eruption by measuring the chemical composition and amounts of gases: *Bull. Volc.*, 26, 367-378.
- Nordlie, B. E., 1971, The composition of the magmatic gas of Kilauea and its behavior in the near surface environment: *Amer. Jour. Sci.*, 271, 417-463.
- Nordyke, M. D., 1961, Nuclear craters and preliminary theory of the mechanics of explosive crater formation: *Jour. Geoph. Res.*, 66, 3439-3459.
- Norton, D., and Knight, J., 1977, Transport phenomena in hydrothermal systems: Cooling plutons: *Amer. Jour. Sci.*, 277, 937-981.
- Oftedahl, C., 1978, Cauldrons of the Permian Oslo rift: *Jour. Volc. Geoth. Res.*, 3, 343-372.
- O'Hara, M. J., 1973, Non-primary magmas and dubious mantle plume beneath Iceland: *Nature*, 243, 507-508.
- Omori, F., 1911 and 1920, The Usu-san eruption and earthquake and elevation phenomena: *Bull. Imp. Earthq. Inv. Com.*, 5, 101-107, 9, 41-76.
- Oxburgh, E. R. and Turcotte, D. L., 1968, Problem of high heat flows and volcanism associated with zones of descending mantle convective flow: *Nature*, 218, 1041-1043.
- , and —, 1970, Thermal structure of island arcs: *Geol. Soc. Amer. Bull.*, 81, 1665-1688.
- Parker, R. B., 1963, Recent volcanism at Amboy Crater, California: *Calif. Div. Mines and Geol., Spec. Rep.*
- Parsons, W. H., 1958, Origin, age, and tectonic relationships of the volcanic rocks in the Absaroka-Yellowstone-Beartooth region, Wyoming-Montana: *Billings Geol. Soc. Guidebook*, 9th Ann. Field Conf., 36-43.
- , 1967, Manner of emplacement of pyroclastic andesitic breccias: *Bull. Volc.*, 30, 177-187.
- Pearce, J. A., and Cann, J. R., 1973, Tectonic setting of basic volcanic rocks determined using trace element analyses: *Earth Plan. Sci. Ltrs.*, 19, 290-300.
- Peck, D. L., 1966, Lava coils of some recent historic flows: *U. S. Geol. Surv., Prof. Paper* 550-3, 148-151.
- Peckover, R. S., Buchanan, D. J., and Ashby, D.E.T.F., 1973, Fuel-coolant interactions in submarine vulcanism: *Nature*, 245, 307-308.
- Perlaki, E., 1966, Pumice and scoria: their notion, criteria, structure, and genesis: *Acta Geologica Hung.*, 10, 13-29.
- Perret, F. A., 1924, The Vesuvius eruption of 1906: Study of a volcanic cycle: *Carnegie Inst. of Wash., Pub.* 339, 151 pp.
- , 1937, The eruption of Mt. Pelée in 1929-1932: *Carnegie Inst. of Wash., Pub.* 458, 126 pp.
- , 1950, Volcanological observations: *Carnegie Inst. of Wash., Pub.* 549, 162 pp.
- Peterson, D. W., 1961, Flattening ratios of pumice fragments in an ash-flow sheet near Superior, Arizona: *U. S. Geol. Surv., Prof. Paper* 424-D, 82-84.
- , and Tilling, R. I., 1978, The transition of lava from pahoehoe to aa at Kilauea Volcano, Hawaii (abstract): *Geol. Soc. Amer. Cord. Sect. Mtg.*, 10, 142.
- Pollack, J. G., Toon, J. B., Sagan, C., Summers, A., Baldwin, B., and Van Camp, W., 1976, Volcanic explosions and climatic change; a theoretical assessment: *Jour. Geoph. Res.*, 81, 1070-1085.

- Powers, H. A., 1955, Composition and origin of basaltic magma of the Hawaiian Islands: *Geoch. Cosmoch. Acta*, 7, 77-107.
- Press, F., 1972, The earth's interior as inferred from a family of models: in *The Nature of the solid earth*, McGraw-Hill, N. Y., 147-171.
- Ragan, D. M., and Sheridan, M. F., 1972, Compaction of the Bishop Tuff, California: *Geol. Soc. Amer. Bull.*, 83, 95-106.
- Ramberg, H., 1967, Gravity deformation and the earth's crust as studied by centrifuged models: Academic Press, London and N. Y.
- , 1968, Instability of layered systems in the field of gravity: in *Phys. Earth Planet. Interiors I*, 427-474.
- , 1970, Model studies in relation to intrusion of plutonic bodies: in *Mechanics of igneous intrusions*, G. Newall and N. Rast, editors, Gallery Press, Liverpool.
- Rankama, K., and Sahama, Th. G., 1950, *Geochemistry*: Univ. Chicago Press, 912 pp.
- Rasmussen, J., and Noe-nygaard, A., 1969, Beskrivelse til geologisk kort over Faeroerne: *Danmarks Geol. Under.*, Series 1, No. 24, 370 pp.
- Ratté, J. C., and Steven, T. A., 1967, Ash flows and related volcanic rocks associated with the Creede caldera, San Juan Mts., Colorado: *U. S. Geol. Surv.*, Prof. Paper 524-H.
- Reck, Hans, 1910, Islandische Masseneruptionen: *Geol. v. pal. Abh.*, 9, 41-103 and 121-183.
- Reyer, E., 1888, *Theoretische Geologie*: Stuttgart.
- Reynolds, D. L., 1954, Fluidization as a geological process: *Amer. Jour. Sci.*, 252, 577-613.
- Richards, A. F., 1958, Transpacific distribution of floating pumice from Isla San Benedicto, Mexico: *Deep-Sea Research*, 5, 29-35.
- , 1959, Geology of the Islas Revillagigedo, Mexico: *Bull. Volc.*, 22, 73-123.
- , 1965, Linear relationship between energy and pressure of volcanic explosions: *Nature*, 207, 1382-1383.
- Richardson, D., and Ninkovich, D., 1976, Use of K_2O , Rb, Zr, and Y versus SiO_2 in volcanic ash layers of the eastern Mediterranean to trace their source: *Geol. Soc. Amer. Bull.*, 87, 110-116.
- Richey, J. E., 1938, The rhythmic eruptions of Ben Hiant, Ardnamurchan: *Bull. Volc.*, 3, 3-21.
- , and Thomas, H. H., 1930, The geology of Ardnamurchan, north-west Mull and Coll: *Mem. Geol. Surv.*, Scotland.
- Richter, C. F., 1958, *Elementary seismology*: Freeman, San Francisco, 768 pp.
- Riehle, J. R., 1973, Calculated compaction profiles of rhyolitic ash-flow tuffs: *Geol. Soc. Amer. Bull.*, 84, 2193-2216.
- Rikitake, T., and Yokoyama, I., 1955, Volcanic activity and changes in geomagnetism: *Jour. Geoph. Res.*, 60, 165-172.
- Ringwood, A. E., 1962, A model for the upper mantle: *Jour. Geoph. Res.*, 67, 857-867.
- Rittman, A., 1930, *Geologie von Ischia*: *Zeitschr. fur Vulk.*, Ergänzungsband 6.
- , 1931, Der Ausbruch des Stromboli am 11 Sept., 1930: *Zeitschr. fur Vulk.*, 14, 47-77.
- , 1933, Beitrag zur Kenntnis des Stromboli-Kraters: *Zeitschr. fur Vulk.*, 16, 184-190.
- , 1933, Die geologisch Bedingte Evolution und Differentiation des Somma-Vesuvmagmas: *Zeitschr. fur Vulk.*, 15, 8-94.
- , 1938, Die Vulkane am Myvatn in Nordost-Island: *Bull. Volc.*, 4, 3-38.
- , 1962, *Volcanoes and their activity*: John Wiley & Sons, N. Y. 305 pp.
- , 1973a, Explosive volcanic eruptions—a new classification scheme: *Geol. Rundsch.*, 62, 431-446.
- Roberts, J. L., 1963, Source of the Glencoe ignimbrites: *Nature*, 199, 901.
- , 1966a, Emplacement of the main Glencoe fault-intrusion: *Geol. Mag.*, 103, 299-316.
- , 1966b, Ignimbrite eruptions in the volcanic history of the Glencoe cauldron subsidence: *Geol. Jour.*, 5, 173-184.
- , 1970, The intrusion of magma into brittle rocks: in *Mechanism of igneous intrusion*, G. Newall and N. Rast, editors, *Geol. Jour. Spec. Issue 2*, 287-338.
- Robson, G. R., 1967, Thickness of Etnean lavas: *Nature*, 216, 251-252.
- , and Barr, K. G., 1964, The effect of stress on faulting and minor intrusions in the vicinity of a magma body: *Bull. Volc.*, 27, 1-16.
- , and Tomblin, J. F., 1966, Catalogue of active volcanoes of the world, Part 20, West Indies: *Internat. Assoc. Volc.*, Rome.
- Roedder, E., 1965, Liquid CO_2 inclusions in olivine bearing nodules and phenocrysts from basalts: *Amer. Min.*, 50, 1746-1782.
- Rose, W. I. Jr., 1973, Pattern and mechanism of volcanic activity at the Santiaguito volcanic dome, Guatemala: *Bull. Volc.*, 37, 73-94.
- , Bonis, S., Stoiber, R. E., Keller, M., and Bickford, T., 1973, Studies of volcanic ash from two recent Central American eruptions: *Bull. Volc.*, 37, 338-364.
- Rutten, M. G., 1964, Formation of a plateau basalt series (from the example of Iceland): *Bull. Volc.*, 27, 93-111.

- Sahama, T. G., and Meyer, A., 1958, A study of the volcano Nyirangongo; Progress report: Explor. Parc Nat. Albert: Miss. d'études volcanologiques, 2.
- Sainte Claire, Deville, 1857, Sur la composition chimique des gas rejetés par les événements volcaniques de l'Italie meridionale: C. R. Acad. Sci., n. 4, 4 pp.
- Sakuma, S., 1954, Effect of thermal history on viscosity of Oosima lavas (Elastic and viscous properties of volcanic rocks. Pt. 4): Bull. Earthq. Res. Inst., 32, 215-230.
- , and Murase, T., 1957, Some properties of natural gasses at high temperature-viscosity and the growth of bubbles: Bull. Volc. Soc. Japan, 2nd ser., 2, 6-16.
- Sapper, K., 1927, *Vulkankunde*: Stuttgart, 424 pp.
- Scarfe, C. M., 1973, Viscosity of basic magmas at varying pressure: *Nature*, 241, 101-102.
- Schilling, J. G., 1973, Iceland mantle plume: geochemical evidence along Reykjanes Ridge: *Nature*, 242, 565-571.
- Schimke, G. R., and Bufe, C. G., 1968, Geophysical description of a Pacific Ocean seamount: *Jour. Geoph. Res.*, 73, 559-569.
- Schmincke, H. U., 1967, Stratigraphy and petrography of four upper Yakima basalt flows in south-central Washington: *Geol. Soc. Amer. Bull.*, 78, 1385-1422.
- , and Swanson, D. A., 1967, Laminar viscous flowage structures in ash-flow tuffs from Gran Canaria, Canary Islands: *Jour. Geol.*, 75, 641-664.
- Scholl, D. W., Marlow, M. S., MacLeod, N. W., and Buffington, E. C., 1976, Episodic Aleutian Ridge igneous activity: implications of Miocene and younger submarine volcanism west of Buldir Island: *Geol. Soc. Amer. Bull.*, 87, 547-554.
- Sclater, J. G., 1972, Heat flow and elevation of the marginal basins of the western Pacific: *Jour. Geoph. Res.*, 77, 5705-5719.
- , Von Herzen, R. P., William, D. L., Anderson, R. N., and Klitzord, K., 1974, The Galápagos spreading center: heat-flow low on the north flank: *Geoph. Jour. Roy. Astron. Soc.*, 38, 609-626.
- Scott, R. B., 1965, Tertiary geology and ignimbrite petrology of the Grant Range, east-central Nevada: Ph. D. thesis, Rice University.
- , Rona, P. A., McGregor, B. A., and Scott, M. R., 1975, The TAG hydrothermal field: *Nature*, 251, 301-302.
- Scrope, G. P., 1825, Considerations on volcanoes: W. Phillips and G. Yard Pub., London, 270 pp.
- , 1862, *Volcanoes*: 2nd ed., London.
- Searle, E. J., 1958, A note on the formation of native iron and other effects associated with contact of basalt and carbonized wood at Auckland, N. Z.: *N. Z. Jour. Geol. and Geoph.*, 1, 451-458.
- Secor, D. T. Jr., 1965, Role of fluid pressure in jointing: *Amer. Jour. Sci.*, 263, 633-646.
- Segerstrom, Kenneth, 1966, Parícutin, 1965—aftermath of eruption: U. S. Geol. Surv., Prof. Paper 550-C, 93-101.
- Sekiya, S., and Kikuchi, Y., 1890, The eruption of Bandai-san: *Jour. Coll. Sci., Imp. Univ. Tokyo*, 3, 91-172.
- Settle, M., 1978, Volcanic eruption clouds and the thermal power output of explosive eruptions: *Jour. Volc. Geoth. Res.* 3, 309-324.
- Shaw, H. R., 1963, Obsidian-H₂O viscosities at 1000 and 2000 bars in the temperature range 700° to 900°C: *Jour. Geoph. Res.*, 68, 6337-6342.
- , 1969, Rheology of basalt in the melting range: *Jour. Petr.*, 10, 510-535.
- , 1972, Viscosities of magmatic silicate liquids: an empirical method of prediction: *Amer. Jour. Sci.*, 272, 870-893.
- , 1974, Diffusion of H₂O in granitic liquids: Part I. experimental data; Part II. mass transfer in magma chambers: in *Geochemical transport and kinetics*, Hofmann, A. W., Giletti, B. J., Yoder, H. S. Jr., and Yund, R. A., eds., Carnegie Inst. Wash., Publ. 634, 139-170.
- , Peck, D. L., and Okamura, R., 1968, The viscosity of basaltic magma: an analysis of field measurements in Makaopuhi lava lake, Hawaii: *Amer. Jour. Sci.*, 266, 120-152.
- , and Swanson, D. A., 1970, Eruption and flow rates of flood basalts: *Proc. Second Columbia R. Bas. Symp.*, East. Wash. State College Press, 271-299.
- Shepherd, E. S., 1925, The analysis of gases obtained from volcanoes and from rocks: *Jour. Geol.*, 33, 289-370.
- , 1938, The gases in rocks and some related problems: *Amer. Jour. Sci.*, 35-A, 311-351.
- Sheridan, M. F., 1970, Fumarolic mounds and ridges of the Bishop Tuff, California: *Geol. Soc. Amer. Bull.*, 81, 851-868.
- , and Ragan, D. M., 1976, Compaction of ash-flow tuffs: in *Compaction of coarse-grained sediments*, Chilingarian, G. V. and Wolf, K. H., eds., 2, 677-713.
- , and Updike, R. G., 1975, Sugar loaf Mountain tephra—a Pleistocene rhyolitic deposit of base-surge origin in northern Arizona: *Geol. Soc. Amer. Bull.*, 86, 571-581.
- Sherwood, A. E., 1967, Effect of air drag on particles ejected during explosive cratering: *Jour. Geoph. Res.*, 72, 1783-1791.

- Shimazu, Y., 1960, A thermodynamical aspect of volcanic gas: *Jour. Earth Sci., Nagoya Univ.*, 8, 197-221.
- , 1961, Physical theory of generation, upward transfer, differentiation, solidification and explosion of magmas: *Jour. Earth Sci., Nagoya Univ.*, 9, 185-223.
- Shimozuru, D., 1968, Discussion on the energy partition of volcanic eruption: *Bull. Volc.*, 32, 383-394.
- Shoemaker, E. M., and Moore, H. J., 1956, Diatremes on the Navajo and Hopi reservation: *U. S. Geol. Surv., Trace Elements Inv. Rpt.* 640, 197-203.
- , Roach, C. H., and Byers, F. M. Jr., 1962, Diatremes and uranium deposits in the Hopi Buttes, Arizona: *Geol. Soc. Amer., Buddington Vol.*, 327-355.
- Sigurdsson, H., 1977, Chemistry of the crater lake during the 1971-72 Soufrière eruption: *Jour. Volc. Geoth. Res.*, 2, 165-186.
- Sigvaldason, G. E., and Elisson, G., 1968, Collection and analysis of volcanic gases at Surtsey, Iceland: *Geochim. et Cosmochim. Acta*, 32, 797-805.
- Simkin, T., 1970, Origin of some flat-topped volcanoes and guyots (abstract): *Ann. Mtg. Geol. Soc. Amer.*, p. 685.
- , and Howard, K. A., 1970, Caldera collapse in the Galápagos Islands, 1968: *Science*, 169, 429-437.
- Simmons, G., 1967, Interpretation of heat flow anomalies, 2, Flux due to initial temperature of intrusives: *Rev. Geoph. Space Phys.*, 5, 109-120.
- Sleep, N. H., 1974, Segregation of magma from a mostly crystalline mush: *Geol. Soc. Amer. Bull.*, 85, 1225-1232.
- Smith, R. L., 1960a., Ash flows: *Geol. Soc. Amer. Bull.*, 71, 795-842.
- , 1960a, Zones and zonal variations in welded ash flows: *U.S. Geol. Surv., Prof. Paper* 354 F, 149-159.
- , and Bailey, R. A., 1966, The Bandelier Tuff: a study of ash-flow eruption cycles from zoned magma chambers: *Bull. Volc.*, 29, 83-104.
- Snyder, G. L., and Fraser, G. D., 1963, Pillowed lavas: *U. S. Geol. Surv., Prof. Paper* 454 B and C.
- Sonder, R. A., 1937, Zur Theorie und Klassifikation der eruptiven vulkanischen Vorgänge: *Geol. Rundschau*, 27, 499-548.
- Sparks, R. S. J., 1978, The dynamics of bubble formation and growth in magmas: a review and analysis: *Jour. Volc. Geoth. Res.*, 3, 1-37.
- , Pinkerton, H., and Hulme, G., 1976, Classification and formation of lava levees on Mount Etna, Sicily: *Geology*, 4, 269-271.
- , and Sigurdsson, H., 1977, Magma mixing: a mechanism for triggering acid explosive eruptions: *Nature*, 267, 315-318.
- , and Wilson, L., 1976, A model for the formation of ignimbrite by gravitational column collapse: *Jour. Geol. Soc.*, 132, 441-452.
- Spieß, F. N. and Mudie, J. D., 1971, Small scale topographic and magnetic features: *The Sea*, J. C. Maxwell, ed., 4, 205-250.
- Spry, Alan, 1962, The origin of columnar jointing, particularly in basalt flows: *Jour. Geo. Soc. Australia*, 8, 191-216.
- Stanley, D. J., and Taylor, P. T., 1977, Sediment transport down a seamount flank by a combined current and gravity process: *Marine Geol.*, 23, 77-88.
- Stearns, H. T., 1925, The explosive phase of Kilauea volcano, Hawaii, in 1924: *Bull. Volc.*, 5, 1-16.
- Steeple, D. W., and Iyer, H. M., 1976, Low velocity zone under Long Valley, California: *Jour. Geoph. Res.*, 81, 841-848.
- Stefani, C. de, 1907, Die phlegraischen Felder bei Neapel: *Petermann's Mitt., Ergänzungsheft* No. 156.
- Stehn, Ch. E., 1934, Die semivulkanischen Explosionen des Pematang Bata in der Soeh-Senke (Sud-Sumatra) im Jahre 1933: *Natuurk. Tijdschr. voor Ned.-Indie*, 94, 46-69.
- Stephenson, P. J., and Griffin, T. J., 1976, Some long basaltic lava flows in north Queensland: in *Volcanism in Australasia*, R. W. Johnson, ed., 41-51.
- Steven, T. A., and Lipman, P. W., 1976, Calderas of the San Juan volcanic field, Southwestern Colorado: *U. S. Geol. Surv., Prof. Paper* 958, 35 pp.
- Stewart, M. K., and Hulston, J. R., 1976, Stable isotope ratios of volcanic steam from White Island, New Zealand: *Bull. Volc.*, 39, 28-46.
- Stille, H., 1940, Einführung in den Bau Amerikas: *Borntraeger, Berlin*.
- Stoiber, R. E., and Jepsen, E., 1973, Sulfur dioxide contributions to the atmosphere by volcanoes: *Science*, 182, 577-578.
- , and Rose, W. I. Jr., 1969, Recent volcanic and fumarolic activity at Santiaguito volcano, Guatemala: *Bull. Volc.*, 33, 475-502.
- Strange, W. E., Woolard, G. P., and Rose, J. C., 1965, An analysis of the gravity field over the Hawaiian Islands in terms of crustal structure: *Pacific Sci.*, 19, 381-389.
- Stuart, Wm. D., and Johnston, M. J. S., 1975, Intrusive origin of the Matsushiro earthquake swarm: *Geology*, 3, 63-67.

- Sugimura, A., 1965, Distribution of volcanoes and seismicity of the mantle in Japan: *Jour. Volc.*, 2: 37-58 (in Japanese).
- , 1966, Complementary distributions of epicenters of mantle earthquakes and of loci of volcanoes in island arcs: *Jour. Seism. Soc. Japan*, 19, 96-106.
- , Matsuda, T., Chinzei, K., and Nakamura, K., 1963, Quantitative distribution of late Cenozoic volcanic materials in Japan: *Bull. Volc.*, 26, 125-140.
- Sutherland, F. L., 1965, Dispersal of pumice, supposedly from the March, 1962 South Sandwich Islands eruption, on Southern Australian shores: *Nature*, 207, 1332-1335.
- Swanson, D. A., 1972, Magma supply rate at Kilauea volcano, 1952-1971: *Science*, 175, 169-170.
- , Wright, T. L., and Helz, R. T., 1975, Linear vent systems (and estimated rates of magma production and eruption) for the Yakima Basalt of the Columbia Plateau: *Amer. Jour. Sci.*, 275, 877-905.
- Sykes, L. R., 1966, The seismicity and deep structure of island arcs: *Jour. Geoph. Res.*, 71, 2981-3006.
- Szekely, J., and Reitan, P. H., 1971, Dike filling by magma intrusion and by explosive entrainment of fragments: *Jour. Geoph. Res.*, 76, 2602-2609.
- Talwani, M., Windisch, C. C., and Langseth, M. G., 1971, Reykjanes Ridge Crest: a detailed geophysical study: *Jour. Geoph. Res.*, 76, 473-517.
- Tanakadate, H., 1935, Evolution of a new volcanic islet near Io-zima: *Proc. Imper. Acad.*, 9, 152-154.
- Taubeneck, W. H., 1967, Notes on the Glen Coe cauldron subsidence, Argyllshire, Scotland: *Geol. Soc. Amer. Bull.*, 78, 1295-1316.
- Taverne, N. J. M., 1925, De Gunung Papandajan: *Vulk. Berichten*, No. 42, *Natuurk. Tijdschr. v. Ned.-Indie*, 81.
- Taylor, G. A. M., 1958, The 1951 eruption of Mount Lamington, Papua: *Australian Bur. Min. Res., Geol. and Geoph.*, Bull. 38.
- Taylor, H. P. Jr., 1968, The oxygen isotope geochemistry of igneous rocks: *Contr. Mineral. Petr.*, 19, 1-71.
- , 1971, Oxygen isotope evidence for large-scale interaction between meteoric ground waters and Tertiary granodiorite intrusions, Western Cascade Range, Oregon: *Jour. Geoph. Res.*, 76, 7855-7874.
- , 1977, Water/rock interaction and the origin of H₂O in granitic batholiths: *Jour. Geol. Soc.*, 133, 509-558.
- , and Epstein, S., 1962, Relationship between O¹⁸/O¹⁶ ratios in coexisting minerals of igneous and metamorphic rocks: *Geol. Soc. Amer. Bull.*, 73, 461-480, 675-694.
- Taylor, P. S., and Stoiber, R. E., 1973, Soluble material on ash from active Central American volcanoes: *Geol. Soc. Amer. Bull.*, 84, 1031-1042.
- Taylor, S. R., 1969, Trace-element chemistry of andesites and associated calc-alkaline rocks: *Oregon Dept. Geol. Min. Ind. Bull.* 65, 43-63.
- Tazieff, H., 1969, Volcanisme sous-marin de l'Afar (Ethiopie): *Com. Rend., Acad. Sci. Paris*, 268, 2657-2660.
- , 1970, New investigations on eruptive gases: *Bull. Volc.*, 34, 1-18.
- , 1977, La Soufrière, volcanology and forecasting: *Nature*, 269, 96-97.
- , Boulay, J. L., Garand, M., and Maulard, J., 1968, Mesure des variations rapides des paramètres thermiques des gaz éruptifs: *Compt. Rend., Acad. Sci. Paris*, 267, 1253-1256.
- , and Jatteau, M., 1969, Mesure dans l'infrarouge des paramètres physiques des gaz éruptifs: *Compt. Rend., Acad. Sci. Paris*, 268, 767-770.
- , Marinelli, G., Barberi, F., and Varet, J., 1970, Géologie de l'Afar Septentrional: *Bull. Volc.*, 33, 1039-1072.
- Thorarinsson, S., 1950, The eruption of Mt. Hekla, 1947-1948: *Bull. Volc.*, Ser. 2, 10, 157-168.
- , 1954, The eruption of Hekla, 1947-1948, Part II 3. The tephra-fall from Hekla on March 29th, 1947: *Visindafelag Islendinga*, 68 pp.
- , 1967, Some problems of volcanism in Iceland: *Geol. Rundschau*, 57, 1-20.
- , 1969, The Lakagigar eruption of 1783: *Bull. Volc.*, Ser. 2, 33, 910-927.
- , and Sigvaldason, G. E., 1962, The eruption of Askja 1961: *Amer. Jour. Sci.*, 260, 641-651.
- Tikhonov, A. N., Lubimova, E. A., and Vlasov, V. K., 1970, On the evolution of melting zones in the thermal history of the earth: *Phys. Earth Planet. Inter.*, 2, 326-331.
- Tjia, H. D., 1968, Volcanic lineaments in the Indonesian island arcs: *Pac. Geol.*, 1, 175-182.
- Tomkeieff, S. I., 1940, Basalt lavas of the Giant's Causeway: *Bull. Volc.*, 6, 89-143.
- Truesdell, A. H., 1976, Summary of Section III, Geochemical techniques in exploration: *Proc. 2nd U. N. Symp. on Dev. and Use of Geoth. Res.*, San Francisco, 1, LIII - LXXIX.
- Tsuya, H., 1930, The eruption of Komagatake, Hokkaido, in 1929: *Bull. Earthquake Res. Inst.*, 8, 238-270.
- , 1933, Explosive activity of volcano Kusatu-Sirane in October, 1932: *Bull. Earthquake Res. Inst.*, 11, 82-112.
- Turcotte, D. L., and Oxburgh, E. R., 1969, Convection in a mantle with variable physical properties: *Jour. Geoph. Res.*, 74, 1458-1474.
- Tyrrell, G. W., 1931, *Volcanoes*: Holt & Co., N. Y. 252 pp.
- , 1937, Flood basalts and fissure eruption: *Bull. Volc.*, 1, 89-111.

- , 1955, Distribution of igneous rocks in space and time: *Geol. Soc. Amer. Bull.*, 66, 405-426.
- Uffen, R. J., and Jessop, A. M., 1963, The stress release hypothesis of magma formation: *Bull. Volc.*, 26, 57-66.
- U.N.E.S.C.O., 1971, The surveillance and prediction of volcanic activity, a review of methods and techniques: Paris, 166 pp.
- Verhoogen, J., 1938, *Les volcans Virunga et l'éruption du Nyamagira de 1938*: *Ann. Soc. Geol. de Belg.*, 42, 326-353.
- , 1939, New data on volcanic gases: the 1938 eruption of Nyamagira: *Amer. Jour. Sci.*, 237, 656-672.
- , 1948, *Les éruptions 1938-1940 du volcan Nyamuragira: Exploration du Parc National Albert, Fascicule 1*, Brussels, 186 pp.
- , 1951, Mechanics of ash formation: *Amer. Jour. Sci.*, 249, 239-246.
- Vogt, P. R., 1974, Volcano height and plate thickness: *Earth Planet. Sci. Ltrs.*, 23, 337-348.
- Volarovich, M. P., and Tolstoi, D. M., 1936, The simultaneous measurement of viscosity and electrical conductivity of some fused silicates at temperatures up to 1400°: *Jour. Soc. Glass Tech.*, 20, 54-60.
- Volz, F. E., 1975, Burden of volcanic dust and nuclear debris after injection into the stratosphere at 40°-58°N.: *Jour. Geoph. Res.*, 80, 2649-2652.
- Wadge, G., 1976, Deformation of Mount Etna, 1971-1974: *Jour. Volc. Geoth. Res.*, 1, 237-263.
- , 1977, The storage and release of magma on Mount Etna: *Jour. Volc. Geoth. Res.*, 2, 361-384.
- , Walker, G. P. L., and Guest, J. E., 1975, The output of the Etna volcano: *Nature*, 255, 385-387.
- Waff, H. S., 1975, Pressure-induced coordination changes in magmatic liquids: *Geophys. Res. Ltrs.*, 2, 193-196.
- Walker, G. P. L., 1959, *Geology of the Reydarfjörður area, eastern Iceland*: *Wuart. Jour. Geol. Soc. London*, 114, 367-393.
- , 1965, Some aspects of Quaternary volcanism in Iceland: *Trans. Leicester Lit. and Philos. Soc.*, 59, 25-40.
- , 1965a, Evidence of crustal drift from Icelandic geology: *Phil. Trans. Roy. Soc. London*, 258, 199-204.
- , 1967, Thickness and viscosity of Etnean lavas: *Nature*, 213, 484-485.
- , 1971, Grain-size characteristics of pyroclastic deposits: *Jour. Geol.*, 79, 696-714.
- , 1973, Lengths of lava flows: *Phil. Trans. Roy. Soc. London*, 274, 107-118.
- , 1974, Eruptive mechanisms in Iceland: in Kristjansson (ed.), *Geodynamics of Iceland and the North Atlantic area*, 189-201.
- , 1974, Volcanic hazards and the prediction of volcanic eruptions: *Geol. Soc. London Misc. Pub.* 3, 23-41.
- , and Blake, D. H., 1966, The formation of a palagonite breccia mass beneath a valley glacier in Iceland: *Quart. Jour. Geol. Soc. London*, 122, 45-61.
- , and Croasdale, R., 1972, Characteristics of some basaltic pyroclastics: *Bull. Volc.*, 35, 303-317.
- , Wilson, L., and Bowell, E. L. G., 1971, Explosive volcanic eruptions—I the rate of fall of pyroclasta: *Geoph. Jour. Roy. Astr. Soc.*, 22, 377-383.
- Walker, G. W., and Swanson, D. A., 1968, Laminar flowage in a Pliocene soda rhyolite ash-flow tuff, Lake and Harney Cos., Oregon: *U. S. Geol. Surv., Prof. Paper 600-B*, 37-47.
- Walsh, J. B., and Decker, R. W., 1971, Surface deformation associated with volcanism: *Jour. Geoph. Res.*, 76, 3291-3302.
- Waring, G. A., Blankenship, R. R., and Bentall, R., 1965, Thermal springs of the United States and other countries of the world—a summary: *U. S. Geol. Surv., Prof. Paper 492*, 383 pp.
- Warrick, R. A., 1975, Volcano hazard in the United States: A research assessment: *Inst. Behavioral Sci., Univ. Colorado*, 144 pp.
- Waters, A. C., 1955, Volcanic rocks and the tectonic cycle: *Geol. Soc. Amer., Spec. Paper 62*, 703-722.
- , 1961, Stratigraphic and lithologic variations in the Columbia River basalt: *Amer. Jour. Sci.*, 259, 583-611.
- Watkins, N. D., and Baksi, A. K., 1974, Magnetostratigraphy and oroclinal folding of the Columbia River, Steens and Owyhee basalts in Oregon, Washington, and Idaho: *Amer. Jour. Sci.*, 274, 148-189.
- Weertman, J., 1971, Theory of water-filled crevasses in glaciers applied to vertical magma transport beneath oceanic ridges: *Jour. Geoph. Res.*, 76, 1171-1183.
- Wentworth, C. K., 1954, The physical behavior of basaltic lava flows: *Jour. Geol.*, 62, 425-438.
- , and Macdonald, G. A., 1953, Structures and forms in basaltic rocks in Hawaii: *U. S. Geol. Surv. Bull.*, 994, 98 pp.
- , and Williams, H., 1932, The classification and terminology of the pyroclastic rocks: *Natl. Res. Council Bull.* 89, 19-53.
- Westgate, J. A., and Smith D. G. W., 1969, Electron probe technique for characterizing pyroclastic deposits: *Earth Planet. Sci. Ltrs.*, 5, 313-319.
- White, C. M., and McBirney, A. R., 1978, Some quantitative aspects of orogenic volcanism in the Oregon Cascades: *Geol. Soc. Amer., Mem.*, 1979.
- White, D. E., 1955, Violent mud-volcano eruption of Lake City hot springs, northeastern California: *Geol. Soc. Amer. Bull.*, 66, 1109-1130.
- , 1967, Some principles of geyser activity, mainly from Steamboat Springs, Nevada: *Amer. Jour. Sci.*, 265, 641-684.

- , 1968, Hydrology, activity, and heat flow of the Steamboat Springs thermal system, Washoe County, Nevada: U. S. Geol. Survey, Prof. Pap. 458-C, 109 pp.
- , Anderson, E. T., and Grubbs, D. K., 1963, Geothermal brine well: mile-deep drill hole may tap ore-bearing magmatic water and rocks during metamorphism: *Science*, *139*, 919-922.
- , Fournier, R. O., Muffler, L. J. P., and Truesdell, A. H., 1975, Physical results of research drilling in thermal areas of Yellowstone National Park, Wyoming: U. S. Geol. Surv., Prof. Paper 892.
- , Muffler, L. J. P., and Truesdell, A. H., 1971, Vapor-dominated hydrothermal systems compared with hot-water systems: *Econ. Geol.*, *66*, 75-97.
- , and Waring, G. A., 1963, Data of geochemistry, Sixth Edition, Chapter K. Volcanic emanations: U. S. Geol. Surv., Prof. Paper 440-K, 29 pp.
- Wilcox, R. E., 1944, Rhyolite-basalt complex on Gardiner River, Yellowstone Park, Wyoming: *Geol. Soc. Amer. Bull.*, *55*, 1047-1080.
- , 1954, Petrology of Parícutin volcano, Mexico: U. S. Geol. Surv. Bull., *965-C*, 281-353.
- Williams, Howel, 1927, The geology of Snowdon, North Wales: *Quart. Jour. Geol. Soc. London*, *83*, 346-431.
- , 1928, A recent volcanic eruption near Lassen Peak, California: *Univ. Calif. Pub. Bull. Geol. Sci.*, *17*, 241-263.
- , 1932, The history and character of volcanic domes: *Univ. Calif. Pub. Geol. Sci.*, *21*, 51-146.
- , 1935, The Newberry volcano of central Oregon: *Geol. Soc. Amer. Bull.*, *46*, 253-304.
- , 1936, Pliocene volcanoes of the Navajo-Hopi country: *Geol. Soc. Amer. Bull.*, *47*, 111-172.
- , 1942, Geology of Crater Lake National Park, Oregon: *Carnegie Inst. Wash.*, Pub. 540.
- , 1950, Volcanoes of the Parícutin region, Mexico: U. S. Geol. Surv. Bull., *965-B*, 279 pp.
- , 1952, Geologic observations on the ancient human footprints near Managua, Nicaragua: *Carnegie Inst. Wash.*, Pub. No. 596.
- , 1952a, The great eruption of Coseguina, Nicaragua, in 1835: *Univ. Calif. Pub. Geol. Sci.*, *29*, 21-46.
- , 1952b, Volcanic history of the Meseta Central Occidental, Costa Rica: *Univ. Calif. Pub. Geol. Sci.*, *29*, 145-180.
- , 1960, Volcanic history of the Guatemalan Highlands: *Univ. Calif. Pub. Geol. Sci.*, *38*, 1-86.
- , and Curtis, G. H., 1976, The Sutter Buttes of California: a study of Plio-Pleistocene volcanism: *Univ. Calif. Pub. Geol. Sci.*, *116*, 1-56.
- , McBirney, A. R., and Dengo, G., 1964, Geologic reconnaissance of southeastern Guatemala: *Univ. Calif. Pub. Geol. Sci.*, *50*, 1-56.
- , and McBirney, A. R., 1969, Volcanic history of Honduras: *Univ. Calif. Pub. Geol. Sci.*, *85*, 1-101.
- Wilson, J. T., 1963, Evidence from islands on the spreading of ocean floors: *Nature*, *197*, 536-538.
- , 1963, A possible origin of the Hawaiian Islands: *Can. Jour. Phys.*, *41*, 863-870.
- Wilson, L., 1972, Explosive volcanic eruptions. II. The atmospheric trajectories of pyroclasts: *Geoph. Jour. Roy. Astr. Soc.*, *30*, 381-392.
- , 1976, Explosive volcanic eruptions. III. Plinian eruption columns: *Geoph. Jour. Roy. Astr. Soc.*, *45*, 543-556.
- , Sparks, R. S. J., Huang, T. C., and Watkins, N. D., 1978, The control of volcanic column heights by eruption energetics and dynamics: *Jour. Geoph. Res.*, *83*, 1829-1836.
- Wisser, Edward, 1927, Oxidation subsidence at Bisbee, Arizona: *Econ. Geol.*, *22*, 761-790.
- Wolery, T. J., and Sleep, N. H., 1976, Hydrothermal circulation and geochemical flux at mid-ocean ridges: *Jour. Geol.*, *84*, 249-275.
- Woolsley, T. S., McCallum, M. E., and Schumm, S. A., 1975, Modeling of diatreme emplacement by fluidization: *Phys. Chem. of the Earth*, *9*, 29-42.
- Wright, H. E., 1943, Cerro Colorado, an isolated non-basaltic volcano in central New Mexico: *Amer. Jour. Sci.*, *241*, 43-56.
- Yamazaki, T., Kato, I., Muroi, I., and Abe, M., 1973, Textural analysis and flow mechanism of the Donzurubo subaqueous pyroclastic flow deposits: *Bull. Volc.*, *37*, 231-244.
- Yoder, H. S. Jr., 1976, Generation of basaltic magma: *Nat. Acad. Sci.*, 265 pp.
- Yokoyama, I., 1963, Structure of caldera and gravity anomaly: *Bull. Volc.*, *26*, 67-72.
- Young, G. A., 1965, The physics of the base-surge: White Oak, Md., U. S. Naval Ordnance Lab., AD-618733, 294 pp.
- Zies, E. G., 1938, The concentration of the less familiar elements through igneous and related activity: *Amer. Jour. Sci.*, *35-A*, 385-404.

Discoveries of cinnabar in the Tamani Neogene deposits

M.G. Shishkunov and V.N. Trufanov

In recent years, widespread development of mercury mineralization has been identified in the Northwestern Caucasus and neighboring regions. The mercury shows (in commercial concentrations in individual sectors) have been localized in various sequences of sand-clay, carbonate, and volcanogenic sedimentary rocks, having an age ranging from Early Jurassic to Neogene, inclusive.

The prospective estimate of the individual mercury shows and the mercury mineralization of the Northwestern Caucasus as a whole is regarded at present as one of the pressing problems of geological investigation in this region. In this respect, in addition to the prospecting-exploration work, carried out with the object of assessing the mercury shows and clarifying their general distribution patterns, the solution to the problem of the age of the mercury mineralization is also of great importance. Special interest in this respect centers around the Borisogleb mercury show, discovered in Neogene sands at Tamani by N. T. Butov (1967).

During 1969-1970, the Borisogleb sector was investigated as a mercury show by the authors of the present report. As a result, new data were obtained on the localization of the cinnabar not only in the bituminous sands, but also in the sands which had not been bituminized, and in conglomerates, with the presence of allothigenic cinnabar also identified in the latter in the form of well-rounded aggregates, covered with thin films of iron hydroxides.

The Borisogleb mercury show is located in the eastern portion of the Kerch-Tamani transverse downwarp (4), which separates the Northwestern Caucasus from the High Crimea. The geologic structure of the downwarp is characterized by the development of zones of diastrophic and dome-like brachyfolds with northeasterly trend, consisting of Neogene sand-clay deposits. Mercury mineralization also occurs in the arch of the Borisogleb brachyfold, which comprises the eastern termination of the Fanariyskoye anticlinal zone (3).

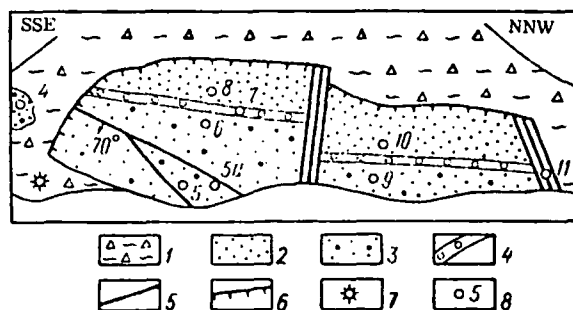
Translated from *O nakhodkakh kinovari v neogenovykh porodakh Tamani, Sovetskaya Geologiya*, 1974, no. 6, p. 141-143. Shishkunov is with the North Caucasian TGU, Trufanov with Rostov State University.

The sector of manifestation of mercury mineralization consists of fine- and medium-grained quartzose and quartz-feldspar sands of the Kuyal'nik stage of the Neogene, which crops out along the western margin of the Akhtanizovo estuary for 250 m, with a visible thickness of up to 30 m (see figure). The sands are overlain by old hilly deposits of an extinct mud volcano, which form the summit of Borisogleb hill. The sands lie very gently, at 5-10° (dip direction 310-320° at 5-10°), and bedding is weakly defined in them.

Approximately in the middle part of the outcrop along a series of closely spaced joints with steep southwesterly dip (210° at 80-85°), the sand sequence is broken into two blocks, vertically displaced by 10-15 m. This is clearly observed on the basis of a thin (0.4-0.6 m) seam of finely clastic conglomerates, in which compressed, well-rounded clasts of limestones, siderites, and siltstones predominate, cemented by iron hydroxides. Below, lie quartzose sands, and above are quartz-feldspar sands. In the former, the quartz grains occupy more than 99% of the volume; garnets, tourmaline, zircon, and epidote are present in insignificant amounts (less than 0.1%). The quartz-feldspar sands contain 20-25% quartz and 70-75% feldspars; kyanite, muscovite, chlorite, and hydrobiotite have been recorded as additives (up to 0.1% in amount).

The quartz sands have been bituminized, bituminization has affected the conglomerates very weakly, and is completely absent in the quartz-feldspar sands. Their visible thickness exceeds 20 m, with bitumen coating the quartz grains, weakly cementing them, as a result of which the sands acquire a yellowish-brown tint and appear like friable sands.

The most intense bituminization of the sands has been observed in a block of closely spaced steeply dipping joints (dip direction 270-290° at < 70-75°). These joints evidently have a deep-seated origin and are tectonic in nature, since in addition to the clear control of the bitumen mineralization, the maximum amounts of cinnabar and abundant accumulations of natural gases are confined to them. In the northern part of the sector, the bituminization is restricted by joints, which dip at 60-70° (dip direction 10-20°).



Diagrammatic section of Borisogleb ore show.

1 - mud-volcano deposits; 2 - non-bituminized quartz-feldspar sands; 3 - bituminized quartz sands; 4 - conglomerates; 5 - joints; 6 - boundary of soil creep; 7 - natural-gas shows; 8 - sampling locality and number.

Mineralogical composition of heavy fractions of concentrates*

Sample No.	Weight of concentrate, mg	Weight contents of minerals (per kg of rock), mg											
		amphiboles	garnets	kyanite	ilmenite	cinnabar	leucosene	pyrite	rutile	tourmaline	chromite	zircon	epidote
Quartzose, strongly bituminized sands													
5	250	—	5	2.5	25	0.23	0.25	0.20	25	0.02	—	12	0.02
5a	630	—	32	32	63	0.38	0.20	0.60	12	0.60	—	6.30	0.10
Quartzose, weakly bituminized sands													
4	2070	0.20	103	103	1035	0.14	2.70	0.25	207	20	—	107	0.25
6	1600	—	160	80	800	0.11	1.60	—	—	3.20	0.15	32	0.20
9	850	—	8.50	0.90	595	0.01	1.60	—	43	0.80	0.20	0.20	—
Quartz-feldspar non-bituminized sands													
8	3340	5	3.50	4.50	950	0.19	0.50	0.50	15	1.00	0.50	1.00	10
10	710	0.02	360	0.06	110	0.05	1.40	—	14	0.30	0.06	7.10	0.70
11	530	0.25	265	1.50	110	0.01	—	—	1.50	0.30	—	0.50	0.20
Conglomerates													
7	5350	0.37	3745	—	535	16.00	—	1.20	0.35	1.50	—	0.37	—

* Analyses completed by mineralogist L. A. Lyamkina in the Laboratory of the Krasnodar Geological Expedition.

The bituminized quartz-feldspar sands have been silted from the surface by mud-volcano deposits creeping downslope (see figure) and enriched in friable ochreous-yellow aggregates of jarosite and twinned gypsum crystals.

On the basis of results from a mineralogical analysis of concentrates (see Table), relatively large amounts of cinnabar (up to 4 mg/kg) have been observed in the conglomerates, and its aggregates have a different color and rounding, and dimensions from 0.1 to 0.5 mm. The

larger aggregates (0.3-0.5 mm) are colored dark cherry-red and dark claret, and are well rounded; the latter undoubtedly indicate their allothigenic nature. Like the main clastic components of the rocks, they have been cemented by iron hydroxides. The smaller cinnabar segregations (0.1-0.3 mm) are colored raspberry- or aloe-red. They have not been completely rounded and have an irregular near-rhombohedral shape. They are extremely insignificant in number among the allothigenic cinnabar, and have been recorded in the concentrates almost as single grains.

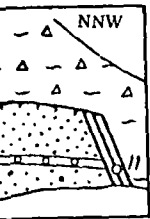
Cinnabar is present in the sands in the form of non-rounded finely crystalline (0.1-0.4 mm) aggregates of irregularly shaped penetration twins of rhombohedra. Occasionally, small solitary rhombohedra (0.3 mm) have been recorded, having other cinnabar aggregates, a raspberry-like color. The amount of cinnabar is from 0.4 mg/kg in the bituminous sands to 0.05 mg/kg in the non-bituminized (see table).

The cinnabar aggregates in the bituminized sands, like the sand grains, have been covered with a thin film of bitumen. In the sands affected by bituminization, cinnabar is present in the form of monomineralic aggregates clearly recognized under the binocular microscope against a background of light-colored well-rounded quartz grains. It is interesting to note that the numerous pores in the conglomerates and quartz sands are frequently filled with well-formed cinnabar crystals, but also with sheaf-like aggregates of zeolites. Ilmenite, rutile, pyrite, and tourmaline have been identified as other minerals in the sands and conglomerates. However, their amount is quite insignificant (see Table). They are present in the rocks as clastic minerals.

The general geologic features of the occurrence of cinnabar recorded and the morphology of its crystals even by themselves, indicate the presence of two genetic types of cinnabar in the Borisogleb ore show. The dark-claret cinnabar in every way may be assigned to the normal clastogenic (allothigenic) cinnabar, whereas its light-tinted, raspberry-like varieties were most probably formed in situ. This information emphasizes this conclusion that is they are typically authigenic. The information obtained during a thermobarometric study of the varieties of cinnabar.

A visual-polythermic study of the cinnabar has shown that in the dark-claret (allothigenic) cinnabar, there is a complex of inclusions. The mercury-forming solutions identical to those of the mercury deposits of the Pervomaysk type in the Northwest Caucasus (2). These are mainly gas-liquid inclusions with homogenization temperatures up to 150°.

In the dark-aloe (authigenic) cinnabar, the assemblage of inclusions is different. The main bulk consists of liquid or gas inclusions. The liquid relicts of traces of mineral formation. The gas bubble occupies not more than 10% of the volume of the inclusion, and the remaining space is filled with light-colored, brownish bitumen. The temperatures of homogenization of such inclusions are usually 50-60°C, and sometimes up to 70-90°. Their low temperatures



ore show.
minized quartz-
ands; 4 - cong-
oil creep; 7 -
ly and number.

of concentrates*

mg of rock), mg				
rutile	tourmaline	chromite	zircon	epidote
ands				
25	0.02	—	12	0.02
12	0.60	—	6.30	0.10
nds				
207	20	—	107	0.25
—	3.20	0.15	32	0.20
43	0.80	0.20	0.20	—
ands				
15	1.00	0.50	1.00	10
14	0.30	0.06	7.10	0.70
1.50	0.30	—	0.50	0.20
0.35	1.50	—	0.37	—

laboratory of the Krasnodar Geo-

agates (0.3-0.5 mm) are colored
-red and dark claret, and are well
e latter undoubtedly indicate their
nature. Like the main clastic con-
he rocks, they have been cemented
oxides. The smaller cinnabar
s (0.1-0.3 mm) are colored rasp-
loe-red. They have not been com-
ded and have an irregular near-
al shape. They are extremely in-
n number among the allothigenic
nd have been recorded in the con-
most as single grains.

Cinnabar is present in the sands only in the form of non-rounded finely crystalline (0.1-0.4 mm) aggregates of irregular shape or penetration twins of rhombohedra. Occasionally, small solitary rhombohedra (0.2-0.3 mm) have been recorded, having, as in other cinnabar aggregates, a raspberry- or aloe-red color. The amount of cinnabar ranges from 0.4 mg/kg in the bituminous sands down to 0.05 mg/kg in the non-bituminized sands (see table).

The cinnabar aggregates in the bituminized sands, like the sand grains, have been covered with a thin film of bitumen. In the sands not affected by bituminization, cinnabar is present in the form of monomineralic aggregates, clearly recognized under the binocular microscope against a background of light-colored, well-rounded quartz grains. It is interesting to note that the numerous pores in the conglomerates and quartz sands are frequently incrustated not only with well-formed cinnabar crystals, but also with sheaf-like aggregates of zeolites. Ilmenite, rutile, pyrite, and chromite have been identified as other ore minerals in the sands and conglomerates. However, their amount is quite insignificant (see table). They are present in the rocks as clastogenic minerals.

The general geologic features of localization of cinnabar recorded and the morphology of its crystals even by themselves, indicate the presence of two genetic types of this mineral in the Borisogleb ore show. The rounded, dark-claret cinnabar in every way must be assigned to the normal clastogenic (allothigenic) minerals, whereas its light-tinted, non-rounded varieties were most probably formed in place, that is they are typically authigenic. Additional information emphasizing this conclusion was obtained during a thermobarometric analysis of the varieties of cinnabar.

A visual-polythermic study of the samples has shown that in the dark-claret (allothigenic) cinnabar, there is a complex of inclusions of pre-forming solutions identical to that typical of the mercury deposits of the Pereval' or Belokamenny type in the Northwestern Caucasus (2). These are mainly gas-liquid vacuoles with homogenization temperatures of 120-130°.

In the dark-aloe (authigenic) cinnabar, the assemblage of inclusions is different: the main bulk consists of liquid or essentially liquid relicts of traces of mineral formation (the gas bubble occupies not more than 3-5% of the volume of the inclusion), and also vacuoles filled with light-colored, brownish-red bitumen. The temperatures of homogenization of such inclusions are usually 50-60°, sometimes up to 70-90°. Their low temperature

may be judged on the results of vacuum decrepitation, which agree with the homogenization data. The maxima for the decrepitation of the inclusions of authigenic cinnabar do not exceed 100°, whereas for the inclusions of allothigenic cinnabar, they reach 150° and more.

The data obtained suggest that the formation of the nonrounded crystalline aggregates of aloe-red (authigenic) cinnabar is genetically associated with bituminization of the quartzose sands and conglomerates during the effect on them of the weakly mineralized gas-liquid products of mud volcanism. The possible association between the mercury shows in the Northwestern Caucasus and mud volcanism was pointed out earlier by Poyarkov and Netroba (1).

The age of the nonrounded authigenic cinnabar, judging by the stratigraphic position of the surrounding sands and conglomerates, has been convincingly determined as Late Pliocene, possibly even early Quaternary, which corresponds to the maximum manifestation of mud volcanism.

The presence of allothigenic cinnabar in the conglomerates of the Kuyal'nik stage of the Pliocene, similar on the basis of thermobaric indices to its aggregates in the commercial deposits of the Northwestern Caucasus, enables us to discuss the significance of the scale of their denudation in the Neogene. This is also suggested by the presence of manifestations of allothigenic cinnabar covering substantial areas in the "ore" strata of the Kimmerian stage, discovered by K. V. Platonov (1967) near Krymsk.

REFERENCES

1. Poyarkov, V. E., and Netroba, A. V., 1967, POSSIBILITY OF AN ASSOCIATION BETWEEN MUD VOLCANOES AND THE FORMATION OF CERTAIN MERCURY DEPOSITS: Alma-Ata.
2. Shamray, I. A., et al., 1972, MINERALOGY AND THERMODYNAMICS OF THE MERCURY ORE-SHOWS OF THE NORTHERN CAUCASUS: Izd-vo Rostov Univ., Rostov-on-Don.
3. Shardanov, A. N., and Peklo, V. P., 1961, NEW DATA ON THE TECTONICS OF THE WESTERN FALL OF THE CAUCASUS AND TAMANI: Geol. Sb. VNII, vyp. 6, p. 207-221.
4. Shardanov, A. N., 1966, TECTONICS OF WESTERN CIS-CAUCASIA AND THE NORTHWESTERN CAUCASUS. In PROBLEMS OF GEOLOGY AND PETROLEUM OCCURRENCES OF THE KRASNODAR REGION, p. 15-32. Izd-vo Nedra, Moscow.

SUBJ
GEOL
EGS17

Sky Schaff p 295
Proceedings of the Seventeenth Annual

ENGINEERING GEOLOGY AND SOILS ENGINEERING SYMPOSIUM

Sponsors

IDAHO TRANSPORTATION DEPARTMENT
DIVISION OF HIGHWAYS

UNIVERSITY OF IDAHO
Department of Geology
Department of Civil Engineering

IDAHO STATE UNIVERSITY
Department of Geology
Department of Engineering

BOISE STATE UNIVERSITY
Department of Geology
& Geophysics
Department of Physics
& Engineering



UNIVERSITY OF UTAH
RESEARCH INSTITUTE
EARTH SCIENCE LAB.

HELD AT THE UNIVERSITY OF IDAHO MOSCOW, IDAHO
APRIL 4, 5 & 6, 1979

CONTENTS

SEVENTEENTH ANNUAL SYMPOSIUM
ON
ENGINEERING GEOLOGY
AND
SOILS ENGINEERING

-C-O-N-T-E-N-T-S-

Page	
1	The Destructive Tabas Earthquake of September 16, 1978, East Iran-A Preliminary Report. A. Haghypour, M. Amidi and A. Aghanabati, Geological Survey of Iran, Saleem M. Farooqui, Shannon & Wilson, Inc.
13	Design, Construction, and Performance Hatwai Creek Embankment. Patrick J. Lightfield, Idaho Transportation Department and Robert M. Smith, Converse-Ward-Davis-Dixon.
35	Analysis Techniques for Low Reinforced Soil Retaining Walls and Comparison of Strip and Sheet Reinforcements. William Whitcomb and J.R. Bell, Oregon State University.
63	Chain-Link Retaining Walls. Daryl R. Greenway, Siskiyou National Forest and Bruce C. Vandre, U.S. Forest Service.
81	Ground Water Flow Systems in the "Phosphate Sequence" of South-eastern Idaho. Gerry V. Winter and Dale R. Ralston, University of Idaho.
95	The Use of Resistivity Soundings in a Ground Water Problem at Elk River, Idaho. Rainer Blum, University of Idaho.
109	Mathematical Modeling Approach for Delineating Landslide Hazards in Watersheds. Timothy J. Ward, Ruh-Ming Li and Daryl B. Simons, Colorado State University.
143	Surficial Investigation of the Perpetual Landslide Summerland, British Columbia. Linda Riglin, U.S. Forest Service.
161	Effect on Groundwater of the Cavalier, North Dakota, Sanitary Landfill. Alan E. Kehew, North Dakota Geological Survey and Gerald W. Knudsen, North Dakota State Department of Health.
181	Seepage from Partially Saturated Mine Waste Disposal Systems. G.L. Bloomsburg, University of Idaho and R.A. Bloomfield, Bureau of Mines, U.S. Department of Interior.
197	Geophysical Investigations of the Pullman, Washington - Moscow, Idaho Ground-Water Basin. Muriel S. Robinette, University of Idaho.
219	Simple Statistics for Elastic Properties from Seismic Analysis. Lee Robinson, Idaho State University.
235	Soil Classification by Seismic Refraction. Michael L. Hiner, Andres Garcia and Dan Herold, Boise State University.

Page	
249	A Simplified Preload Design. Thomas M. Gurtowski and Thomas E. Kirkland, Shannon & Wilson, Inc.
275	Active Fault Zones and Regional Seismicity in Western Nevada. David K. Rogers and John Stellar, Converse-Ward-Davis-Dixon and David B. Simon, Harding Lawson Associates.
295	Vibratory Core Sampling in the Missouri River. Marvin W. Taylor, U.S. Army Corps of Engineers.
303	Inventory and Classification of Abandoned Mine Tailings. Mike Gross, Christos Ioannou and Dale R. Ralston, University of Idaho.
317	Design Considerations for Embankment Construction on a Loess Foundation in Southeastern Idaho. Fred Y.M. Chen and Stanley H. Kline, International Engineering Company, Inc.
347	Tunnel Boring Machines for Aqueducts and Subways. Richard J. Proctor, The Metropolitan Water District of Southern California.
359	Rock Engineering at Brownlee Dam. Nestor T. Mirafuente, International Engineering Company, Inc.

AUTHORS

SEVENTEENTH ANNUAL SYMPOSIUM
ON
ENGINEERING GEOLOGY
AND
SOILS ENGINEERING

	Page
Aghanabati, A., Geological Survey of Iran. The Destructive Tabas Earthquake of September 16, 1978, East Iran-A Preliminary Report.	1
Amidi, M., Geological Survey of Iran. The Destructive Tabas Earthquake of September 16, 1978, East Iran-A Preliminary Report.	1
Bell, J.R., Oregon State University. Analysis Techniques for Low Reinforced Soil Retaining Walls and Comparison of Strip and Sheet Reinforcements.	35
Bloomfield, R.A., Bureau of Mines, U.S. Department of Interior. Seepage from Partially Saturated Mine Waste Disposal Systems.	181
Bloomsburg, G.L., University of Idaho. Seepage from Partially Saturated Mine Waste Disposal Systems.	181.
Blum, Rainer, University of Idaho. The Use of Resistivity Soundings in a Ground Water Problem at Elk River, Idaho.	95
Chen, Fred Y.M., International Engineering Company, Inc. Design Considerations for Embankment Construction a Loess Foundation in Southeastern Idaho.	317
Farooqui, Saleem M., Shannon & Wilson, Inc. The Destructive Tabas Earthquake of September 16, 1978, East Iran-A Preliminary Report.	1
Garcia, Andres, Boise State University. Soil Classification by Seismic Refraction.	235
Greenway, Daryl R., Siskiyou National Forest. Chain-Link Retaining Walls.	63
Gross, Mike, University of Idaho. Inventory and Classification of Abandoned Mine Tailings.	303
Gurtowski, Thomas M., Shannon & Wilson, Inc. A Simplified Preload Design.	249
Haghipour, A., Geological Survey of Iran. The Destructive Tabas Earthquake of September 16, 1978, East Iran-A Preliminary Report.	1
Herold, Dan, Boise State University. Soil Classification by Seismic Refraction.	235
Hiner, Michael L., Boise State University. Soil Classification by Seismic Refraction.	235

	Page
Ioannou, Christos, University of Idaho. Inventory and Classification of Abandoned Mine Tailings.	303
Kehew, Alan E., North Dakota Geological Survey. Effect on Groundwater of the Cavalier, North Dakota, Sanitary Landfill.	161
Kirkland, Thomas E., Shannon & Wilson, Inc. A Simplified Preload Design.	249
Kline, Stanley H., International Engineering Company, Inc. Design Considerations for Embankment Construction on a Loess Foundation in Southeastern Idaho.	317
Knudsen, Gerald W., North Dakota State Department of Health. Effect on Groundwater of the Cavalier, North Dakota, Sanitary Landfill.	161
Li, Ruh-Ming, Colorado State University. Mathematical Modeling Approach for Delineating Landslide Hazards in Watersheds.	109
Lightfield, Patrick J., Idaho Transportation Department. Design, Construction, and Performance Hatwai Creek Embankment.	13
Mirafuente, Nestor T., International Engineering Company, Inc. Rock Engineering at Brownlee Dam.	359
Proctor, Richard J., The Metropolitan Water District of Southern California. Tunnel Boring Machines for Aqueducts and Subways.	347
Ralston, Dale R., University of Idaho. Ground Water Flow Systems in the "Phosphate Sequence" of Southeastern Idaho.	81
Ralston, Dale R., University of Idaho. Inventory and Classification of Abandoned Mine Tailings.	303
Riglin, Linda, U.S. Forest Service. Surficial Investigation of the Perpetual Landslide Summerland, British Columbia.	143
Robinette, Muriel S., University of Idaho. Geophysical Investigations of the Pullman, Washington - Moscow, Idaho Ground-Water Basin.	197
Robinson, Lee, Idaho State University. Simple Statistics for Elastic Properties from Seismic Analysis.	219
Rogers, David K., Converse-Ward-Davis-Dixon. Active Fault Zones and Regional Seismicity in Western Nevada.	275
Simon, David B., Harding Lawson Associates. Active Fault Zones and Regional Seismicity in Western Nevada.	275

-A-U-T-H-O-R-S-

	Page
Simons, Daryl B., Colorado State University. Mathematical Modeling Approach for Delineating Landslide Hazards in Watersheds.	109
Smith, Robert M., Converse-Ward-Davis-Dixon. Design, Construction, and Performance Hatwai Creek Embankment.	13
Stellar, John, Converse-Ward-Davis-Dixon. Active Fault Zones and Regional Seismicity in Western Nevada.	275
Taylor, Marvin W., U.S. Army Corps of Engineers. Vibratory Core Sampling in the Missouri River.	295
Vandre, Bruce C., U.S. Forest Service. Chain-Link Retaining Walls.	63
Ward, Timothy J., Colorado State University. Mathematical Modeling Approach for Delineating Landslide Hazards in Watersheds.	109
Whitcomb, William, Oregon State University. Analysis Techniques for Low Reinforced Soil Retaining Walls and Comparison of Strip and Sheet Reinforcements.	35
Winter, Gerry V., University of Idaho. Ground Water Flow Systems in the "Phosphate Sequence" of Southeastern Idaho.	81

COMMITTEE

SEVENTEENTH ANNUAL SYMPOSIUM
ON
ENGINEERING GEOLOGY
AND
SOILS ENGINEERING

SEVENTEENTH ANNUAL SYMPOSIUM
ON ENGINEERING GEOLOGY AND SOILS ENGINEERING

ANNUAL SYMPOSIUM COMMITTEE

PARTICIPATING AGENCY

Boise State University

Donaldson, Paul R.

Chairman, 1980 Symposium

Applegate, James K.

Coordinating Sec., 1980 Symposium

Idaho State University

Robinson, Lee

Strawn, Mary B.

Idaho Transportation Department,
Division of Highways

Humphrey, C.B.

Charboneau, Robert G.

University of Idaho

Howard, Terry

Chairman, 1979 Symposium

Hardcastle, James

Coordinating Sec., 1979 Symposium

EDITOR. C. B. HUMPHREY

ASSOCIATE EDITOR. R. G. CHARBONEAU

PUBLICATION SECRETARY. Betty M. Herendeen

PUBLISHER. Idaho Transportation Department,
Division of Highways

REGISTRANTS

SEVENTEENTH ANNUAL SYMPOSIUM
ON
ENGINEERING GEOLOGY
AND
SOILS ENGINEERING

SEVENTEENTH ANNUAL SYMPOSIUM ON
ENGINEERING GEOLOGY AND SOILS ENGINEERING

REGISTRANTS

<u>NAME</u>	<u>REPRESENTING</u>	<u>ADDRESS</u>
Anderson, Carol J.	U.S. Forest Service	615 W. Ravalli Hamilton, MT 59840
Applegate, James K.	Boise State University	Department of Geology & Geophysics Boise State University Boise, ID 83725
Bain, Gayton L.		405 NE 103 Ave. Portland, OR 97220
Beemer, Jack D.	Century Testing Laboratories	20448 Bullblock Rd. Bend, OR 97701
Bell, J.R.	Oregon State University	420 N.W. Ponderosa Corvallis, OR 97330
Biggane, John H.	Student, Washington State University	N.E. 685 Maple Pullman, WA 99163
Bilderback, James	Oregon Department of Transportation Highway Division	Star Route 1, Box 482 Winston, OR 97496
Bidondo, Charlie	Student, Boise State University	1030 E. 5th Meridian, ID 83642
Bliss, Douglas A.	Student, University of Idaho	Department of Geology University of Idaho Moscow, ID 83843
Bloomfield, Roger A.	U.S. Bureau of Mines	Bureau of Mines U.S. Dept. of Interior Washington, D.C.
Bloomingdale, John D.	U.S. Forest Service	76487 Portal Dr. Oakridge, OR 97463
Bloomsburg, George L.	University of Idaho	Department of Agricultural Engineering University of Idaho Moscow, ID 83843
Blount, Charles W.	Idaho State University	274 Hyde Pocatello, ID 83201

<u>NAME</u>	<u>REPRESENTING</u>	<u>ADDRESS</u>
Blum, Rainer	University of Idaho	College of Mines & Earth Resources University of Idaho Moscow, ID 83843
Bowers, Peter W., Jr.	Oregon Department of Transportation	P.O. Box 473 Myrtle Creek, OR 97457
Breckenridge, Roy	Student, University of Idaho	Rt. 1, Box 208 Moscow, ID 83843
Brooks, Eugene M.	ITD-Division of Highways	8725 Shellie Lane Boise, ID 83704
Brooks, Tom	Student, University of Idaho	University of Idaho Moscow, ID 83843
Brown, Mike A.	Student, University of Idaho	University of Idaho Moscow, ID 83843
Bumala, Tom	Slope Indicator Co.	3668 Albion Pl. North Seattle, WA 98103
Burrows, Josh	Diamond Drill Contracting Co. and Blue Bore Inc.	P.O. Box 11307 Spokane, WA 99211
Buu, Tri	ITD- Division of Highways	503 D Hale Boise, ID 83706
Charboneau, Robert G.	ITD- Division of Highways	2404 Weaver Circle Boise, ID 83704
Chen, Fred Y.M.	International Engineering Co.	220 Montgomery St. San Francisco, CA 94104
Christiansen, Robert	International Engineering Co.	220 Montgomery St. San Francisco, CA 94104
Clark, Charlie H.	U.S. Forest Service	Drawer D Florence, MT 59833
Coffman, Max L.	ITD-Division of Highways	Box 92 Shoshone, ID 83352
Cohen, Philip L.	Student, University of Idaho	Rt. 1, Box 468 Pullman, WA 99163
Corbet, Tom	Student, University of Idaho	419 1/2 N. Jefferson Moscow, ID 83843

<u>NAME</u>	<u>REPRESENTING</u>	<u>ADDRESS</u>
Cox, Willard E.	Montana Tech, Department of Geological Engineering	Montana Tech Butte, MT 59701
Crosby, James W. III	Washington State University	1467 Alpowa Moscow, ID 83843
Davis, H.E. (Hank)	Mobil Drilling Co., Inc.	P.O. Box 461 Aptos, CA 95003
Davoren, Anthony	Student, Washington State University	J2 Kamiak Apts. Pullman, WA 99163
Dewey, Craig S.	U.S. Forest Service	P.O. Box 147 Kalispell, MT 59901
Didrichsen, William G.	Petur Instrument Co., Inc.	1700 Lake Washington Blvd. South Seattle, WA 98144
Donaldson, Paul R.	Boise State University	Department Geology & Geophysics Boise State University Boise, ID 83725
Eckwright, Terry A.	Student, University of Idaho	Park Village #83 Moscow, ID 83843
Egan, Philip	The Reinforced Earth Co.	3333 Quebec St. Suite 2200 Denver, CO 80207
Elvin, Robert R.	ITD-Division of Highways	2311 7th Street Lewiston, ID 83501
Eshelman, Clarence J.	Oregon Department of Transportation	1316 S.W. Sherri Ct. West Linn, OR 97068
Farooqui, Saleem M.	Shannon & Wilson, Inc.	Shannon & Wilson, Inc. Portland, OR 97201
Gadbois, Laurence J.	Washington State Department of Transportation	P.O. Box 1717 Vancouver, WA 98663
Gailbt, Gary	Student, University of Idaho	705 Lewis St. Moscow, ID 83843
Garcia, Andres	Student, Boise State University	1831 W. Boise Ave. #E Boise, ID 83706
Garrabrand, Gary W.	Student, University of Idaho	E.E. Department University of Idaho Moscow, ID 83843

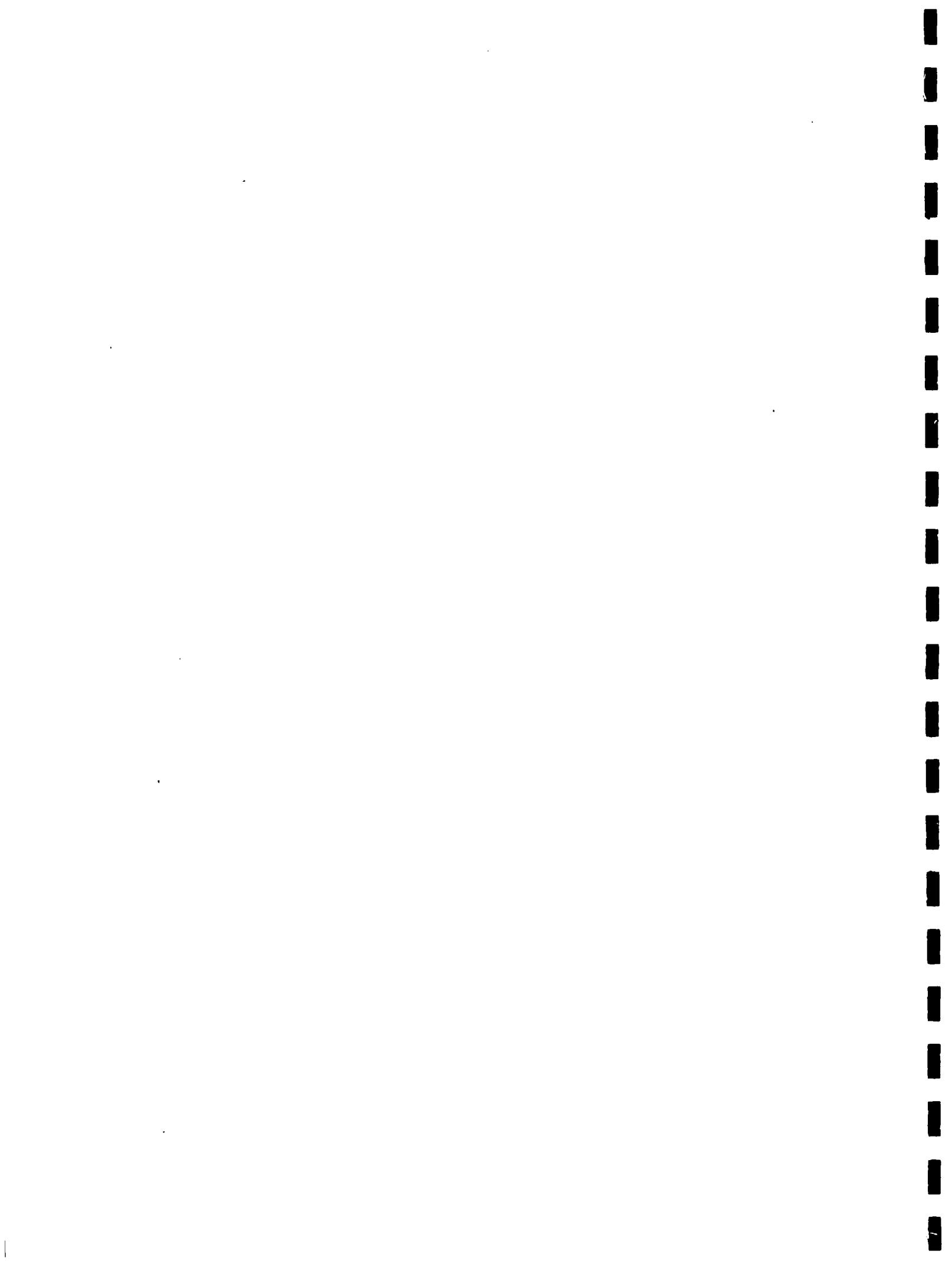
<u>NAME</u>	<u>REPRESENTING</u>	<u>ADDRESS</u>
Gilani, Behrooz B.	Student, University of Idaho	200 S. Asbury #5 Moscow, ID 83843
Graham, Dave	Student, University of Idaho	University of Idaho Moscow, ID 83843
Greenway, Daryl R.	U.S. Forest Service	Siskiyou Natl. Forest Gold Beach OR 97444
Gross, Mike	University of Idaho	Department of Geology University of Idaho Moscow, ID 83843
Gurtowski, Thomas M.	Shannon & Wilson, Inc.	1105 N. 38th St. Seattle, WA 98103
Hanna, Bruce E.	The Reinforced Earth Co.	4661 Carter Trail Boulder, CO 80301
Hardcastle, James H.	University of Idaho	Department of Civil Engineering University of Idaho Moscow, ID 83843
Hardin, Dwight J.	Dames & Moore	Dames & Moore 1220 S.W. Morrison Portland, OR 97205
Hasbrouck, James	Nimbus Instruments- Geometrics, Inc.	395 Java Drive, Sunnyvale, CA 94086
Hays, Ron	Student, University of Idaho	Department of Geology University of Idaho Moscow, ID 83843
Hazleton, Bart C.	Bison Instruments	5708 W. 36th St. Minneapolis, MN 55416
Herold, Dan	Student, Boise State University	Sweet, ID 83670
Higgins, James A.	Simplot Minerals & Chemical Division	P.O. Box 912 Pocatello, ID 83201
Higgs, Nelson B.		P.O. Box 8434 Moscow, ID 83843
Hiner, Michael	Student, Boise State University	352 Greensboro Boise, ID 83706
Holcomb, James R.	Pacific Scientific	12607 S.E. 11 St. Vancouver, WA 98664

<u>NAME</u>	<u>REPRESENTING</u>	<u>ADDRESS</u>
Honsinger, David A.	Washington State Department of Transportation	P.O. Box 98 Wenatchee, WA 98801
Hood, John L.		505 N.W. 76th St. Vancouver, WA 98665
Howard, Terry R.	University of Idaho	Department of Geology University of Idaho Moscow, ID 83843
Hulse, Steve	Sprague & Henwood, Inc.	3189 S. 4140 W. Salt Lake City, UT 84120
Ingraham, Peter C.	Student, University of Idaho	305 N. Washington #1 Moscow, ID 83843
Ioannou, Christos	Student, University of Idaho	Department of Geology University of Idaho Moscow, ID 83843
Janacek, Otto	Janacek Testing Apparatus, Inc.	2317 S.W. Vermont, Portland, OR 97219
Johnsen, Edgar L.	Oregon Department of Transportation	502 Executive House Salem, OR 97310
Johnson, Bill	Longyear Company	E. 11304 17th St. Spokane, WA 99206
Jones, William W.	Acker Drill Company, Inc.	P.O. Box 830 Scranton, PA 18501
Joolazadeh, Mohammad	Student, University of Idaho	P.O. Box 3163 Moscow, ID 83843
Kehew, Alan E.	North Dakota Geological Survey	University Station, Grand Forks, ND 58202
Kennedy, Richard A.	U.S. Forest Service	Kootenai N.F. Box AS Libby, MT 59923
Kuper, Herman T.	Century Testing Laboratories, Inc.	535 Penn St. Bend, OR 97701
Kinzer, Wayne R.	Bechtel Power Corp.	231 W. Middle St. Chelsea, MI 98118
Lahabi, Ali	Student, University of Idaho	Department of Geology University of Idaho Moscow, ID 83843

<u>NAME</u>	<u>REPRESENTING</u>	<u>ADDRESS</u>
Lankston, Robert W.	G - Cubed, Inc.	E. 509 Parkhill Dr. Spokane, WA 99208
Larson, Richard L.	Washington State Department of Transportation	Rt. 6, Box 84 Spokane, WA 99207
Laudon, Kate	Student, Washington State University	
LePard, David D.	Idaho Department of Water Resources	3108 Bogus Basin Rd. Boise, ID 83702
Lightfield, Patrick J.	ITD-Division of Highways	629 Park Avenue Lewiston, ID 83501
Linder, Gary	Student, University of Idaho	Department of Geology University of Idaho Moscow, ID 83843
Lofgren, David C.	Federal Highway Admin.	1533 S.W. Harrison, #12 Portland, OR 97201
Luttrell, Stuart P.	Student, University of Idaho	1320 Linda Lane Moscow, ID 83843
Markland, Thomas R.	ITD-Division of Highways	3418 Lake Boise, ID 83704
Marshall, Larry G.	Oregon Institute of Technology	1335 Pacific Terrace Klamath Falls, OR 97601
Martin, Kathleen R.	Student, University of Idaho	Rt. 2 Box 77 Genesee, ID 83832
Martin, Larry	Student, University of Idaho	608 S. Jefferson #3 Moscow, ID 83843
Maughan, Gerald C.	American Testing Laboratories	711 East Pioneer Drive Soda Springs, ID 83276
McClelland, Douglas E.	U.S. Forest Service	319 Main St. Grangeville, ID 83530
McCowan, Donald P.	Bonneville Power Admin.	15933 N.W. Siskiyou Portland, OR 97230
McGee, W. Denis	Argonne National Laboratory	778 Raymond Idaho Falls, ID 83401
McKillip, Richard L.	Associated Pile & Fitting Corporation	P.O. Box 636 - Rt. #2 Cadiz, KY 42211

<u>NAME</u>	<u>REPRESENTING</u>	<u>ADDRESS</u>
Mercer, Mark A.	U.S. Forest Service	P.O. Box AS Libby, MT 59923
Moore, Beth	Student, University of Idaho	Department of Geology University of Idaho Moscow, ID 83843
Morris, Robert E.	ITD-Division of Highways	Rt. 4, Box 4 Rigby, ID 83442
Nelson, Dave E.	Cascade Surveying & Engineering, Inc.	P.O. Box 326 Arlington, WA 98223
Newton, David J.	Century Testing Laboratories, Inc.	P.O. Box 1174 Bend, OR 97701
Nieman, Jim M.	U.S. Forest Service	Box 383 Sandpoint, ID 83864
Olivo, Agustin	Student, University of Idaho	Department of Geology University of Idaho Moscow, ID 83843
Oneida, Frank A.	ITD-Division of Highways	1670 Ammon Pocatello, ID 83201
Parker, Elliott	Oregon Department of Transportation	P.O. Box 1128 Roseburg, OR 97470
Pereus, Steven C.	Student, University of Idaho	1315 Linda Lane #5 Moscow, ID 83843
Pilz, Hugo A.	Washington State Department of Transportation	1414 Oak Wenatchee, WA 98801
Prellwitz, Rodney W.	U.S. Forest Service	Rt. 2, Box 164 Stevensville, MT 59870
Prinkki, Larry D.	U.S. Forest Service	Box AS Libby, MT 59923
Proctor, Richard J.	Metropolitan Water District of Southern California	327 Fairview Arcadia, CA 91006
Pusc, Steve	Student, University of Idaho	Department of Geology University of Idaho Moscow, ID 83843
Ralston, Dale R.	University of Idaho	Department of Geology University of Idaho Moscow, ID 83843

<u>NAME</u>	<u>REPRESENTING</u>	<u>ADDRESS</u>
Raymond, Larry C.	J.R. Simplot Co.	P.O. Box 67 Conda, ID 83230
Reiland, Drue N.	Student, Washington State University	P.O. Box 62 Enumclaw, WA 98022
Riglin, Linda D.	U.S. Forest Service	Box 340 Choteau, MT 59422
Robinette, Muriel S.	University of Idaho	Department of Geology University of Idaho Moscow, ID 83843
Robinson, Lee	Idaho State University	Box 8371 Idaho State University Pocatello, ID 83209
Rogers, David K.	Converse, Ward, Davis, Dixon, Inc.	101 Howard St. San Francisco, CA 94105
Ross, Larry W.	U.S. Forest Service	121 E. 1st St. Grangeville, ID 83530
Sanchez, Dick O.	ITD-Division of Highways	634 East B. St. Moscow, ID 83843
Sherman, Frank B.	Idaho Department of Water Resources	1316 N. 7th Boise, ID 83702
Shorey, Edwin F.	CH2M Hill Inc.	200 SW Market St. 12th Fl. Portland, OR 97201
Sidle, Roy C.	Oregon State University Forestry Extension	1178 NW Country Crt. Corvallis, OR 97330
Smith, Brian L.	ITD-Division of Highways	401 Sykes Idaho Falls, ID 83401
Smith, Donald A.	Student, University of Idaho	847 Kenneth Moscow, ID 83843
Smith, Paul G.	Student, Washington State University	
Smith, Robert M.	Converse, Ward, Davis, Dixon, Inc.	101 Howard St. San Francisco, CA 94105
Smith, Rodney D.	Student, Washington State University	1505 Valley Rd. #8 Pullman, WA 99163



<u>NAME</u>	<u>REPRESENTING</u>	<u>ADDRESS</u>
Smith, Roger N.	Student, Washington State University	1610 NE Wheatland Dr. Apt. 18 Pullman, WA 99163
Sorensen, Richard K.	ITD-Division of Highways	P.O. Box 2A Shoshone, ID 83352
Spencer, Susan G.	EG&G, Idaho	Box 1625 Idaho Falls, ID 83401
Spofford, Rob	Student, University of Idaho	Rt. 2, Box 26 Kimberly, ID 83341
Steele, Gray L.	Mobile Drilling Co.	Rt. 3, Box 164 Central City ID 52214
Steffy, David	Student, Washington State University	
Swaine, Gail P.	Cascade Surveying and Engineering, Inc.	P.O. Box 326 Arlington, WA 98223
Swanson, Jeannie	Student, University of Idaho	Department of Geology University of Idaho Moscow, ID 83843
Sylvies, William A.	ITD-Division of Highways	10855 Onondaga Dr. Boise, ID 83705
Tatman, Don C.	Student, University of Idaho	481 Boyde Moscow, ID 83843
Taylor, Marvin	U.S. Army Corps of Engineers	4572 Shirley Omaha, NE 68106
Torgeson, David N.	Tudor Engineering Co.	4980 Wildrye Dr. Boise, ID 83703
Tubbs, Donald W.	Roger Lowe Associates, Inc.	508 Lakeside Ave. S. Seattle, WA 98144
Underwood, Joan	Student, University of Idaho	Department of Geology University of Idaho Moscow, ID 83843
Vining, Mark R.	Roger Lowe Associates, Inc.	15713 SE 26th St. Bellevue, WA 98008
Vukelich, Edward K.	U.S. Forest Service	110 1st Ave. Hamilton, MT 59840

<u>NAME</u>	<u>REPRESENTING</u>	<u>ADDRESS</u>
Wagner, S. R. "Peter"	U.S. Forest Service	596 2nd Ave. W.N. Kalispell, MT 59901
Ward, Tim J.	Colorado State University	Department of Civil Engineering Colorado State University Ft. Collins, CO 80521
Warfield, William S.	Montana Department of Highways	Geology Section of Materials Bureau Montana Dept. of Highways 2701 Prospect Ave. Helena, MT 59601
Washburn, Bob L.	Washington State Department of Transportation	612 No. 38th St. Yakima, WA 98901
Watts, Fred J.	University of Idaho	489 Paradise Dr. Moscow, ID 83843
Whitcomb, W.G.	Oregon State University	Department of Civil Engineering Oregon State University Corvallis, OR 97330
Williams, George A.	University of Idaho	Department of Geology University of Idaho Moscow, ID 83843
Williams, Roy E.	University of Idaho	College of Mines & Earth Resources University of Idaho Moscow, ID 83843
Winter, Gerry V.	Student, University of Idaho	738 Second St. Clarkston, WA 99403
Youell, James R.	Mobile Drilling Co.	P.O. Box 338 Wenden, AR 85357
Young, Steves	Student, University of Idaho	Department of Geology University of Idaho Moscow, ID 83843
Zimmerman, Tom V.	Washington State Department of Transportation	P.O. Box 7128 Olympia, WA 98507

THE DESTRUCTIVE TABAS EARTHQUAKE OF SEPTEMBER 16, 1978, EAST IRAN-A PRELIMINARY REPORT

By

A. Haghypour¹, Saleem M. Farooqui², M. Amidi¹,
and A. Aghanabati¹

ABSTRACT

The most devastating earthquake of this century in Iran occurred on the evening of September 16, 1978, near Tabas in east Iran. The earthquake killed more than 19,000 people and completely destroyed the ancient desert town of Tabas and several surrounding villages.

Tabas is located on a narrow playa basin. The basin is underlain by thick Neogene and Quaternary sedimentary deposits and bordered by mountain ranges underlain by complexly deformed pre-Tertiary rocks. The earthquake was accompanied by a north-trending zone of surface rupture more than 55 km long and 100 to 250 m wide. This zone of surface rupture, which is located about 2 km southeast of Tabas, near the Quaternary/Neogene contact was dominated by low-angle thrust displacements with a minor component of right-lateral slip.

Because most of the houses in the epicentral area were constructed of adobe walls and domed roofs, none were left standing in the epicentral area.

INTRODUCTION

A major earthquake occurred in east Iran on the evening of September 16, 1978. Preliminary determinations by the U.S. Geological Survey placed the epicenter at latitude 33.21°N and longitude 57.35°E with a shallow focal depth. The magnitude was 7.7, based on surface waves. Approximately 100,000 square kilometers of the central Iran plateau was shaken by this earthquake. It was felt in Tehran, at a distance of 650 km northwest of the epicenter.

The earthquake totally destroyed the ancient desert town of Tabas and several surrounding villages. Because the earthquake occurred at 7:30 in the evening, almost all of the population were indoors for dinner. As a result, more than 19,000 were killed by the earthquake.

The history of Tabas goes back more than one thousand years. During modern times Tabas has been a remote and obscure desert town, virtually unknown outside Iran; but it was well known throughout much of the civilized world in the Middle Ages. Located near the center of the Great Salt Desert, Tabas grew up around a green oasis and became an important junction on the ancient Silk

¹ Geological Survey of Iran, Tehran, Iran

² Shannon & Wilson, Inc., Portland, Oregon

Route linking China with the West. Many of the historic monuments were destroyed, including Baghe Golsham, Zarak, Khosrowabad and Pirhajat shrines, and the Jomeh Mosque.

Iran was undergoing a massive political turmoil when the earthquake occurred. Only a few weeks before, a dawn to dusk martial-law had been declared. As a consequence, lines of communications were disrupted, and travel to the epicentral region severely curtailed. Despite these problems, however, the Geological Survey of Iran quickly put together a reconnaissance team, and subsequently dispatched a detailed investigative team into the field. The writers of this report, who were part of the reconnaissance team, visited the epicentral region 8 days after the destructive event had occurred. A gigantic rescue operation was already underway, with an air strip and a field camp established and functioning approximately 5 km away from the devastated town. Transport planes and helicopters of the Iranian Air Force were bringing in much needed supplies and carrying the wounded to safety. The army units were trying to restore the communications, electric lines and water supplies, and spraying chemicals to reduce the danger of an epidemic that could result from the decaying bodies buried under the mounds of rubble. The stench of death was everywhere.

Because of the difficult situations in the area and because of pressing business commitments in Tehran, the writers could only spend a total of 2 days in the field. This report presents the results of our reconnaissance investigation. The detailed investigations are being accomplished by members of the Geological Survey of Iran and Ferdowsi University, Meshad.

Earthquake Damage

The Tabas earthquake was one of the most destructive events in the history of Iran. The damage is shown in Plates I and II. The destruction in the epicentral region was almost total. The building construction techniques in Tabas, as elsewhere in Iran, have not changed in centuries. The buildings in the Tabas region are predominantly constructed of massive adobe (Plate I, Photo A and B), with thick walls and domed roofs. The 1/2 to 1 meter thick walls generally rise straight up to a height of 2.5 to 3 meters and then curve into arches, forming domed roofs. The destruction of the adobe structures produced extensive mounds of rubble that consisted of a highly fragmented and pulverized conglomeration of particle sizes (Plates I and II). Even more modern structures of steel frame and kiln-dried bricks also were heavily damaged. These frame buildings were twisted, rotated and partly collapsed.

The qanats, or underground water galleries that transported water to Tabas and surrounding villages also were heavily damaged, but the overhead utility lines and poles were not damaged; nor were they out of plumb wherever observed. Consequently, the massive destruction and death toll in contrast to the undisturbed utility lines indicated that the earthquake struck the region with a massive vertical punch with no perceptible foreshocks or warning.



A. TABAS BEFORE ITS DESTRUCTION. THE BUILDINGS CONSISTED OF MASSIVE ADOBE WALLS AND DOMED ROOFS, WITH DATE PALMS IN THE COURTYARDS.



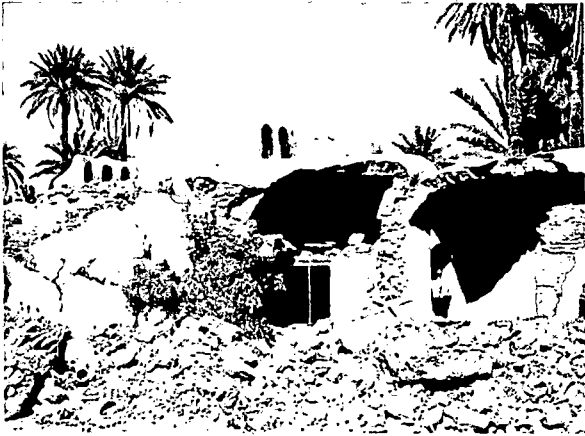
B. A TYPICAL ADOBE VILLAGE IN CENTRAL IRAN. SIMILAR VILLAGES NEAR TABAS TURNED INTO MOUNDS OF RUBBLE DURING THE EARTHQUAKE.



C. AERIAL VIEW OF TABAS AFTER ITS DESTRUCTION BY THE SEPTEMBER 16 EARTHQUAKE.



D. THE ADOBE BUILDINGS WERE COMPLETELY RAZED TO THE GROUND.



A. A VIEW OF A PARTIALLY COLLAPSED ADOBE DOME.



D. PILES OF RUBBLE AND DEBRIS MARK THE SITE OF BUILDINGS.



B. AN ANCIENT (CIRCA A.D. 1300) CARAVAN SERAI (TRAVELERS' LODGE) WAS DESTROYED BY THE EARTHQUAKE. THIS SERAI IS LOCATED ABOUT 25 KILOMETERS WEST OF TABAS.



C. THE COLLAPSE OF ADOBE BUILDINGS PRODUCED HIGHLY FRAGMENTED MOUNDS OF RUBBLE.



E. MAN (UPPER RIGHT) SEARCHES THE REMAINS OF HIS HOME FOR HIS FAMILY.

PLATE II - Photographs of the Earthquake Damage

Seismicity

The Tabas region is in a part of central Iran whose seismic activity is markedly different compared to the adjacent more seismically active Zagros, Alborz and Kopet Dagh regions. The seismicity of the Tabas region, and its relationship to geologic structures, are shown in Figure 1. Historical seismicity (pre-1900) (Ambraseys, 1968; 1974) shows that the ancient cities of Iran have experienced recurring, major destructive earthquakes since 4th century B.C. The town of Tabas was a major trade junction on the ancient Silk Route that linked the towns of Qom, Kashan and Esfahan to the west, Kerman to the south and Qaen, Khaf and Nazad to the east. All of these ancient towns of central Iran have suffered severe damage from major earthquakes. However, major destruction owing to an earthquake is not evident from the approximately 1000-year old history of Tabas as preserved in its historic monuments and from travelers' accounts. The Tabas area has experienced only 2 moderate events of $M=5\pm$ (Berberian, 1976) since 1900, neither of which apparently caused any noticeable damage. These events were located approximately 40 km to the northeast.

The nearest clusters of instrumentally recorded moderate to major earthquakes occur approximately 200 km from Tabas. These clusters are located in the vicinity of Bahabad, 200 km to the southwest, and Qaen and Dasht-e-Bayaz, 200 km northeast of the Tabas. The destructive earthquake of September 16, 1978, thus, was a unique event in the history of Tabas.

Geology

Tabas is located near the east margin of the Great Kavir Desert where it merges with the Dasht-e-Lut. The physiography of these extensive deserts are characterized by playa basins bounded by mountain ranges. The Tabas playa is a triangular-shaped feature approximately 60 km long and 20 km wide with an average elevation of approximately 750 m. The bordering mountain ranges rise to elevations of 3,200 m. The nearest mountain range, the Shatori Range, trends northerly about 10 km east of Tabas. The surface drainage in the area is closed and internal. Water to the town and surrounding villages is transported from near the mountain front by means of ancient underground system of water galleries called "qanats". The depth of groundwater beneath the playa is unknown.

The geology of the Tabas area is known only from reconnaissance studies (Ruttner, et. al., 1968; Stocklin, et. al., 1965; and Aghanabati, 1977). The major geologic elements of the area are shown in Figure 2. The mountain ranges surrounding the playa basin are composed of a complex mixture of different lithologies ranging from Pre-cambrian to Cretaceous in age. These lithologies include metamorphosed and non-metamorphosed marine shale, sandstone, marl, limestone, and oceanic volcanic rocks and tuffs. Continental syntectonic clastic deposits of Neogene age, occur along the flanks of these ranges. These younger deposits are also tightly folded and faulted. Towards the basin, these folded

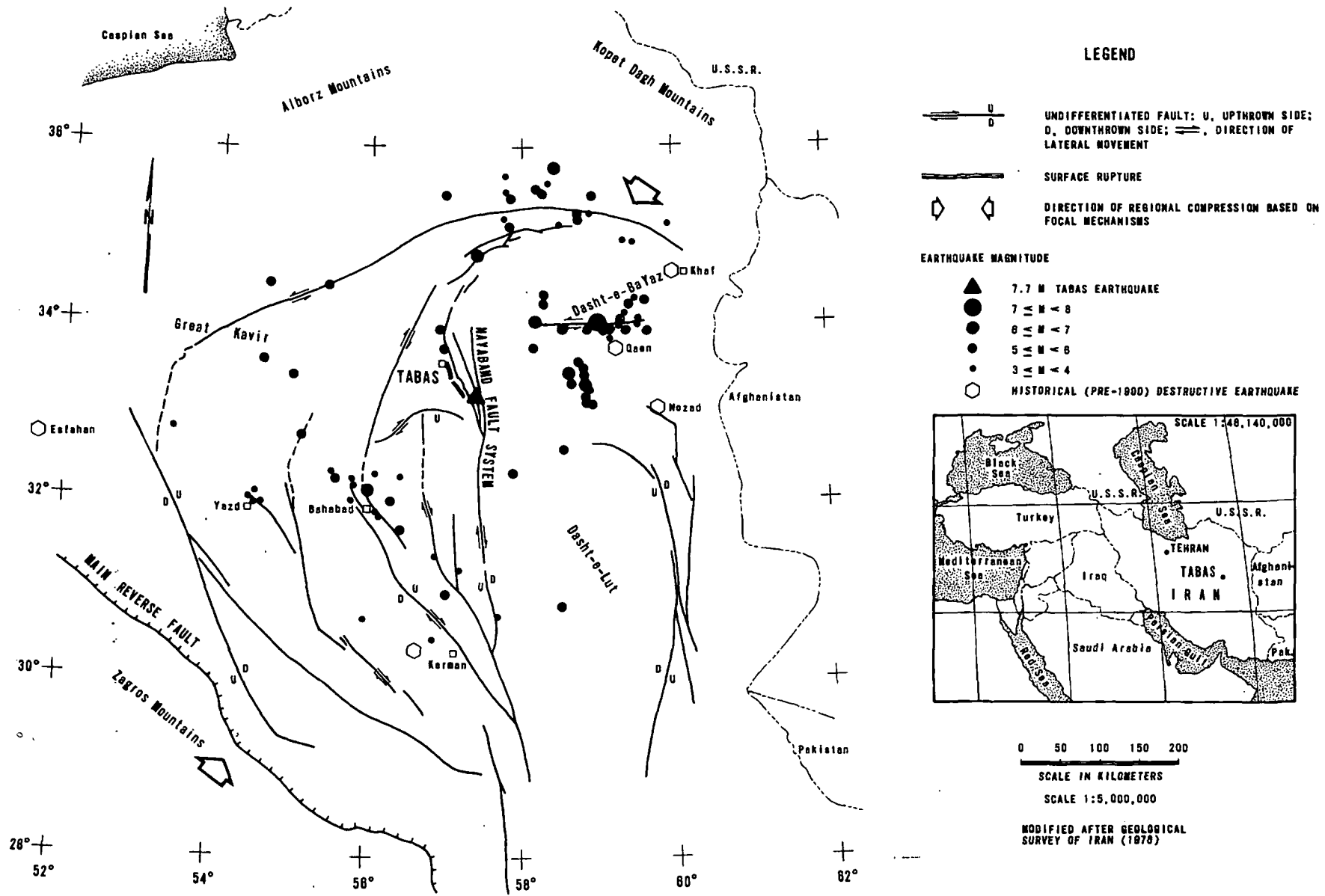


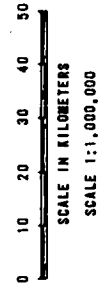
FIGURE 1 - Tectonic Map of East Part of Central Iran



LEGEND

- Holocene salt and mud flats.
- Quaternary gravel deposits of coalescing bahades.
- Quaternary basalt flows.
- Mesozoic clastic rocks and red beds.
- Paleogene andesitic volcanics and tuffs.
- Mesozoic shales, sandstone, marl and limestone, locally metamorphosed.
- Paleozoic shales, sandstone and limestone, locally metamorphosed, includes some pre-Cambrian metamorphic rocks.
- ALLUVIAL FANS
- ANTICLINES (INTERVENING SYNCLINES ARE OMITTED)
- UNDIFFERENTIATED FAULTS
- SURFACE RUPTURE - TABAS EARTHQUAKE
- EPICENTRAL LOCATION (U.S.G.S.) OF THE TABAS EARTHQUAKE

MODIFIED AFTER NATIONAL IRANIAN OIL CO. MAP (1978)



GEOLOGY OF TABAS

FIGURE 2

and faulted clastic deposits of Neogene age are overlain by coarse clastic deposits of coalescing bahadas, and playa silt and salt.

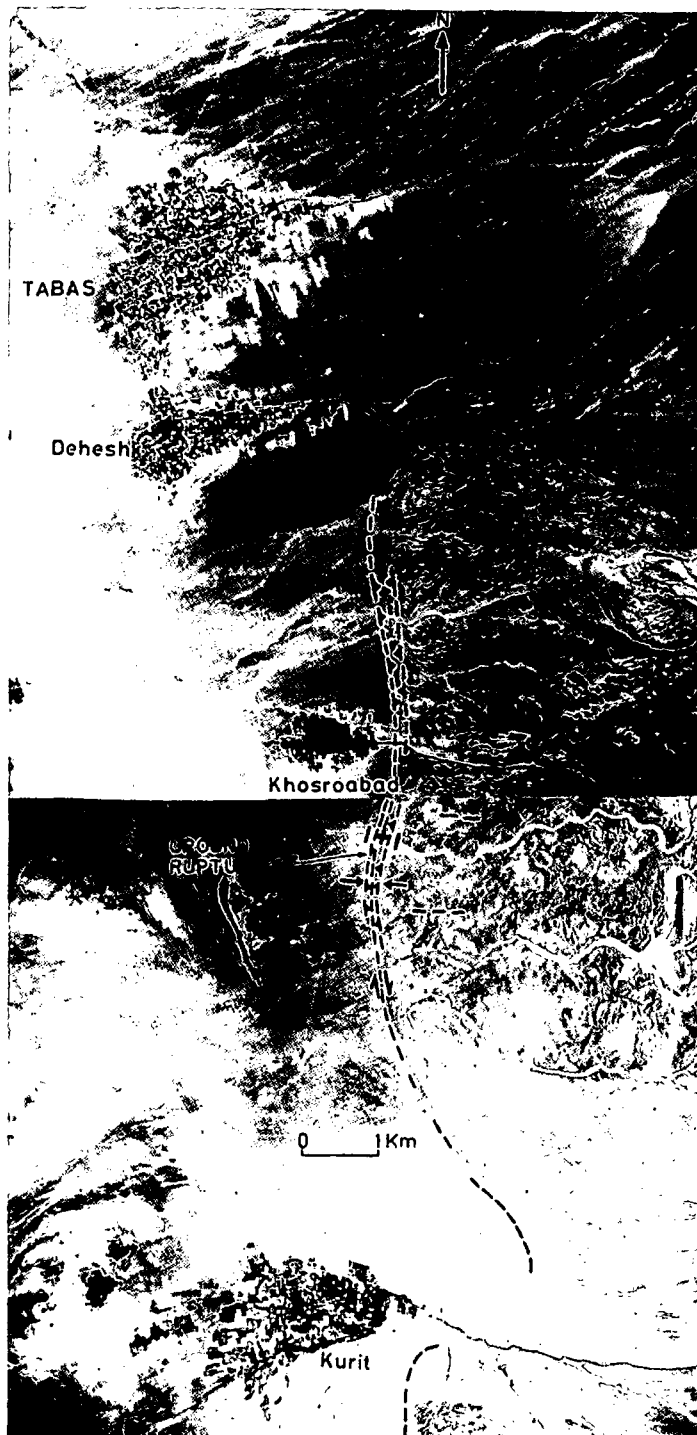
The regional tectonic structures trend northerly across the Tabas area. These major tectonic elements bow around anomalous east-west tectonic elements south of Tabas basin and converge again to the north and south. Faults in the area are generally high-angle reverse with some right-lateral strike-slip component. Numerous secondary sets of northwesterly and northeasterly trending faults have dissected the area into a complex mosaic.

The Nayaband fault system, one of the major regional features, appears to be the source of the September 16, Tabas earthquake. This fault system is more than 400 km long, and branches of it have cut the Shatori Range into numerous linear blocks. The nearest mapped branch is approximately 25 km east of Tabas. Barbarian (1976) indicates that the latest deformation of this fault system is of Quaternary age. Preliminary determinations by the USGS place the epicenter near the south end of the Shatori Range, approximately 75 km south-east of Tabas.

Surface Rupture

The Tabas earthquake was associated with a complex north-trending zone of surface rupture. This zone of surface rupture lies about 2 km east of the Tabas, and it could be traced for a distance of 10 km before it disappeared in the young alluvium of a dry wash. The ruptures could not be traced farther because of lack of time; however, the surface ruptures continue southward for a distance of 55 km (Sharp and Orsini, 1978). The topography and the extent of the rupture mapped is shown in Plate III.

The surface ruptures occurred along the contact between the Quaternary bahada and the Neogene clastic rocks (Plate III). Thrust-type movement predominated. The rupture zone, which was 100 m to 250 m wide, included 3 prominent, low-angle thrust faults with small displacement. Lack of prominent marker horizons precluded precise determinations of fault parameters. However, it was estimated that the thrust angles and displacements at the surface ranged from 0 to 10 degrees and 10 to 20 cm, respectively. The morphological features of the rupture included undulating, serrated and branching fault traces and associated pressure ridges on the upper plate. These features are shown in Plates IV and V. Although the surface ruptures were dominated by thrust faulting, they also showed some evidence of minor right-lateral strike-slip movement, such as crude enclon nature of pressure ridges and short segments of branch faults. The three thrust fault segments were separated by 70 to 150 m wide zones in which numerous north-trending linear tension cracks had developed. Locally these tension cracks showed as much as 1 cm normal displacement. Because of the seesaw motion of fault planes, it was very difficult to estimate whether the east block moved over the west or vice versa. The surface rupture kinematically, may be related to the Nayaband fault system (Figures 1 and 2).



VERTICAL AERIAL PHOTO-
MOSAIC (PRE-EARTHQUAKE)
OF TABAS AREA. ARROWS
SHOW THE WIDTH OF THE
RUPTURE AND THE SENSE
OF MOVEMENT. THE RUPTURE
OCCURRED ALONG THE CONTACT
BETWEEN NEOGENE DEPOSITS
(RIGHT SIDE) AND QUATERNARY
DEPOSITS (LEFT SIDE).

AERIAL PHOTOMOSAIC
OF TABAS AREA

PLATE III



A. A PANORAMA OF THE SURFACE RUPTURE.



B. THE RUPTURE ZONE WHICH INCLUDED SEVERAL PARALLEL SEGMENTS OF THRUST FAULTING. UNDISTURBED STREAM BANKS SHOW LACK OF STRIKE-SLIP MOVEMENT.

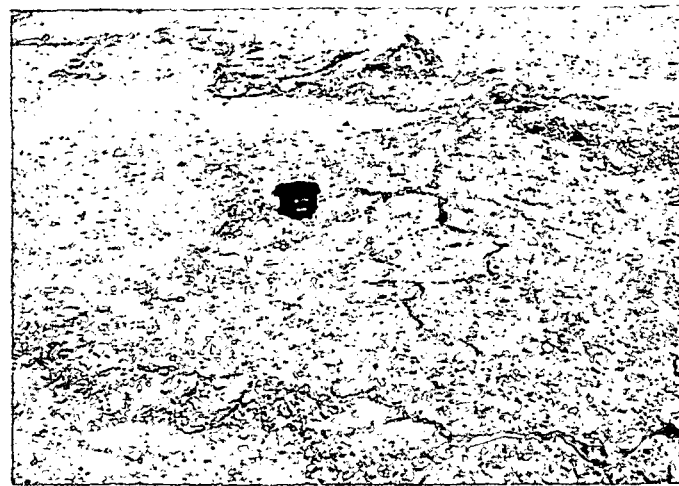


C. TYPICAL MORPHOLOGICAL FEATURES OF ONE OF THE SEGMENTS OF THE THRUST FAULT.

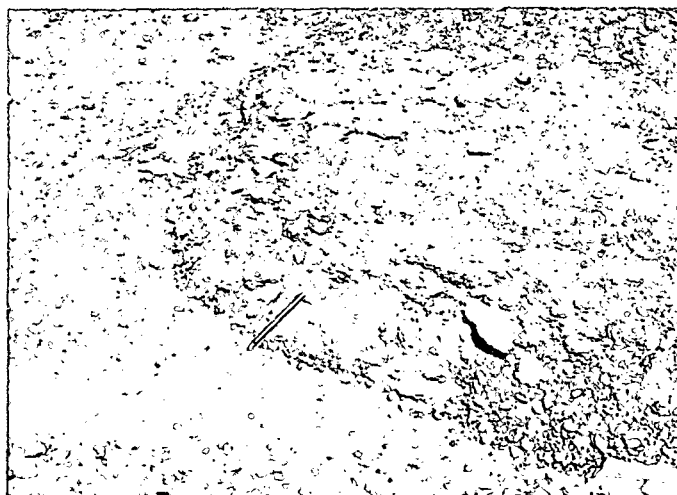
PLATE IV - Oblique Aerial Photographs of the Surface Rupture



A. TYPICAL SERRATED AND BRANCHED NATURE OF THE GROUND RUPTURE. THE GROUND TO THE LEFT OF THE RUPTURE THRUSTED OVER THE GROUND TO THE RIGHT OF THE RUPTURE.



B. A PRESSURE RIDGE WITH TENSION CRACKS NEAR ITS CREST. NUMEROUS SIMILAR PRESSURE RIDGES HAVE DEVELOPED ON THE UPPER THRUST PLATE.



C. THE EDGE OF THE THRUST PLATE, SHOWING SLUMPING AND SLIDING ALONGS ITS FRONT.

PLATE V - Close-up Photographs of the Surface Rupture

The Destructive Tabas Earthquake of September 16,
1978, East Iran-A Preliminary Report
By A. Haghypour, Saleem M. Farooqui,
M. Amidi, and A. Aghanabati
Page 12

ACKNOWLEDGEMENTS

The authors wish to thank H.H. Waldron, R.J. Deacon and R.C. Couch for reviewing the manuscript and providing several helpful suggestions, and Margaret C. Lewis for the illustrations.

REFERENCES

- Aghanabati, S.A. 1977, "Etude Geologique de la Region de Kalmard (West Tabas) Stratigraphie et Tectonique," Geol. Surv. Iran, Report 35.1.
- Ambraseys, N.N., 1968, "Early Earthquakes, North-Central Iran" Bull. Seis. Soc. Am. Vol. 58, No. 2.
- Ambraseys, N.N., 1974, "Historical Seismicity of North-central Iran." Geol. Surv. Iran, Report 29.
- Berberian, M., 1976, "Contribution to the Seismotectonics of Iran." Geol. Surv. Iran, Report 29.
- Ruttner, A., Nabavi, M.H., Hajian, J., 1968, "Geology of the Shirgesht Area." (Tabas Region) Geol. Surv. Iran, Report 4.
- Sharp, Robert, and Orsini, Nicholas, 1978, "Preliminary Report on the Tabas, Iran, Earthquake of September 16, 1978," Newsletter, Earthquake Engineering Research Institute, Vol. 12, No. 6.
- Stocklin, J., Eftekhar - Nezhad, J., Hushmand-zadeh, A., 1965, "Geology of the Shotori Range," Geol. Surv. Iran, Report 3.
- Stocklin, J., 1968, "Structural History and Tecontics of Iran - A Review", The Am. Assoc. of Pet. Geol. Bull., Vol. 52, No. 7.

DESIGN, CONSTRUCTION, AND PERFORMANCE HATWAI CREEK EMBANKMENT

By

Patrick J. Lightfield¹ and Robert M. Smith²

ABSTRACT

The Hatwai Creek crossing presented a major obstacle in completing the realignment of U.S. 95 on Lewiston Grade in North Central Idaho. Hatwai Creek is deeply incised into the basalt flows which underlie the Palouse Loess. A steeply sloping drainage and limited available right of way imposed severe geometric constraints, and required an embankment approximately 230 feet high with side slopes on the order of 1.75 horizontal to 1 vertical. The material economically available consisted of loess from adjacent excavation with only minor amounts of basalt.

Conventional slope stability analyses and finite element stress deformation analyses, using the computer program ISBILD, were performed to investigate the feasibility of the embankment and to develop the design. The recommended design parameters included 1.75 horizontal to 1 vertical slopes which were to be armored with a blanket of "shot" rock and a series of "shot" rock stiffening layers within the lower 100 feet of the embankment.

Construction began in January, 1978 with excavation of the embankment foundation and backfilling with 78,000 cubic yards of "shot" rock. Placing of the soil portion of the fill began in early April, 1978, and continued through mid-October, 1978. A total of 1.3 million cubic yards of soil was placed at an average rate of 16,000 cubic yards per day.

Embankment instrumentation included three slope inclinometers, five total stress cells and nine pore pressure transducers. Instruments were read and evaluated during construction to monitor stresses and deformations and to control placement rate if necessary. Post construction readings will be continued periodically to develop information on long term behavior of the compacted loess soil.

The design parameters and results of the finite element analysis are presented. The data, obtained from the instrumentation are compared to the predicted stresses and deformations.

INTRODUCTION

The Hatwai Creek crossing presented a major obstacle in completing the realignment of U.S. 95 on the Lewiston Grade in North Central Idaho. An outline

¹ Idaho Transportation Department, Lewiston, Idaho

² Converse - Ward - Davis - Dixon, San Francisco, California

map of the State of Idaho and vicinity map of the project area are shown on Figure 1.

Hatwai Creek is deeply incised into the basalt flows which underlie the Palouse Loess; the wind blown soil which blankets the region. The steeply sloping drainage, and limited available right of way imposed severe geometric constraints, and required an embankment approximately 230 feet high with side slopes on the order of 1.75 horizontal to 1 vertical. The economically available material for embankment construction consisted of loess from adjacent excavation with only minor amounts of basalt.

Preliminary design began in early 1976 and the geotechnical design reports were completed in June 1977. Conventional slope stability analyses and finite element stress and deformation analyses were performed to investigate the feasibility of the embankment and to develop the design features. The recommended design included 1.75 horizontal to 1 vertical slopes which were to be armored with a blanket of "shot" rock and a series of "shot" rock layers within the lower 100 feet of the embankment.

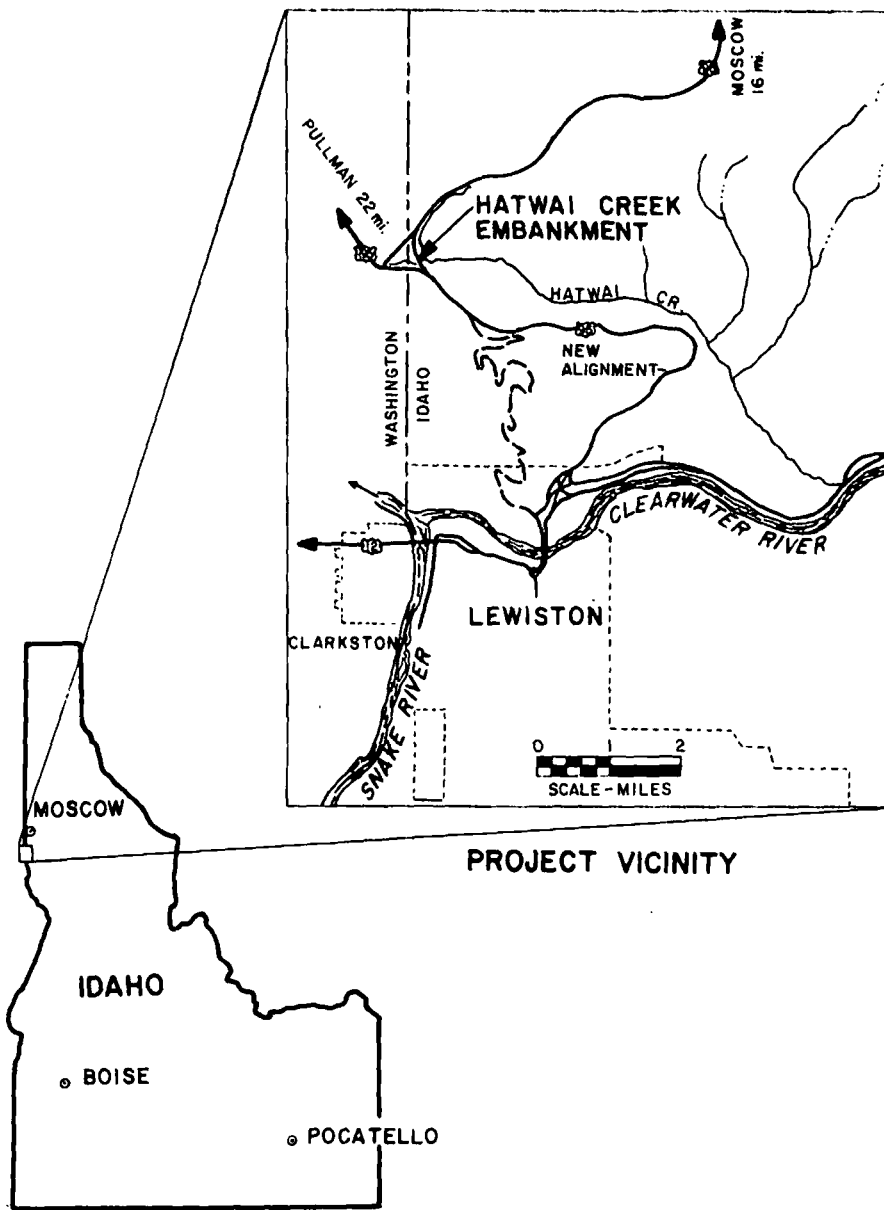
Construction began in January, 1978 with excavation of the embankment foundation and backfilling with 78,000 cubic yards of "shot" rock. Placing of the soil portion of the embankment began in early April, 1978, and continued through mid-October, 1978. A total of 1.3 million cubic yards (c.y.) of fill, including 200,000 c.y. of "shot" basalt rock, was placed at an average rate of 16,000 c.y. per day.

Embankment instrumentation included three slope inclinometers, five total stress cells and nine pore pressure transducers. Instruments were read and evaluated during construction to monitor stresses and deformations. Post construction readings are being continued periodically to develop information on long term behavior of the steep embankment slopes.

REGIONAL AND LOCAL SITE GEOLOGY

Hatwai Creek lies within the Clearwater Embayment of the Miocene age Columbia River Basalts. The individual basalt flows within the embayment are typically separated by highly indurated clayey interbed sediments. Following deposition, the basalt flows and interbed sediments were folded and faulted into their present attitudes. During the Pleistocene, the folded and faulted basalts in the central and northern portions of the embayment were covered with eolian deposits of silts and clays locally known as Palouse Loess.

The new alignment for U.S. 95, north of Lewiston, Idaho, climbs across the embayment basalts on the north limb of the Lewiston Syncline from elevation about +760 near the Clearwater River to elevation about +2730 at the rim of the Hatwai Creek Canyon. The basalt flows in the lower part of the slope dip south but are generally flat lying at the top.



PROJECT LOCATION AND VICINITY MAP

Figure 1

Hatwai Creek is deeply incised into the flat lying basalts near the top of the slope. Three distinct flows and two interbeds were observed in the canyon walls. The canyon follows a normal fault which appears to be associated with the Pre-Pleistocene Vista House Fault. The south block is up thrown offsetting the beds 40 to 50 feet across the canyon.

The lithology observed from top to bottom in the canyon walls follows:

- o Palouse Soil Up to 50 feet thick
- o Columnar to Diced Basalt 20 to 60 feet thick
- o Interbed and Flow Top Indurated, highly weathered red-colored clayey interbed, 20 feet thick
- o Vesicular Diced Basalt Open joints, 40 feet thick
- o Columnar Basalt 80 feet thick
- o Interbed Indurated hard blue clay baked top, jointed, iron staining in joints, 20 to 40 feet thick

The canyon bottoms in columnar basalt except near the toe of the proposed embankment where the blue clay interbed is exposed in the canyon bottom.

DESIGN CONSTRAINTS

Available right of way, topography and materials availability were constraints on the design of the Hatwai Creek crossing. The available right of way was limited on the upstream side by the Idaho-Washington State Boundary. Approximately 600 to 700 feet downstream from the proposed centerline, the bottom gradient of Hatwai Creek Canyon became abruptly steeper than the approximately 12 percent slope at the crossing site.

On the order of 1,000,000 cubic yards of excavation were to be generated on both sides of the canyon and no economically suitable waste area was available. The soils to be excavated were predominantly the eolian silts and clays. Only small quantities of rock were encountered in the exploratory borings.

Few, if any, embankments higher than 100 feet have been constructed of Palouse soils. Side slopes have been generally constructed two horizontal to one vertical or flatter due to the high erodibility characteristic

of the Palouse soils. To construct an embankment across the 230 foot-deep canyon within the available right of way and which would be founded on the flatter (12 percent) bottom slope necessitated side slopes steeper than two horizontal to one vertical.

DESIGN PARAMETERS

Prior to analysis, a laboratory testing program was initiated to develop strength and compressibility parameters for the soils which would be used to construct the embankment. Test borings in the proposed cuts south of and adjacent to the Hatwai Creek Canyon encountered predominantly silty clays and clayey silts. The range of index properties measured in these soils is as follows:

Liquid Limit	31-33%
Plasticity Index	9-12%
Finer than No. 200 Sieve	97-98%

Layers of low plasticity to non-plastic silts were encountered but these appeared to be generally below grade in the cuts or of limited extent.

Direct shear, triaxial compression, and one dimensional consolidation tests were performed on laboratory compacted specimens of the clayey soils. Compaction levels were varied from approximately 95 to 100 percent of AASHTO T-99. Tests were performed at as compacted and saturated moisture contents, and at varying strain rates.

Effective stress strength parameters were developed using consolidated drained direct shear tests. Total stress strength parameters were developed using the results from relatively undrained direct shear and unconsolidated undrained triaxial compression tests. The results of the laboratory strength tests are summarized in Table 1. Strain rates used in drained direct shear tests were chosen such that the time to failure would be greater than 50 times the time required for 50 percent consolidation. The "undrained" direct shear test specimens were subjected to shear stress immediately after applying normal stress, and strain rates of 0.05 inches per minute were used to minimize drainage. Consolidation occurred very rapidly in the compacted samples at normal stresses less than about 8 ksf, so samples were at least partially consolidated prior to testing.

Based on the results of the consolidation tests and an assumed six month construction time, 50 to 70 percent of the consolidation was expected to occur during construction. In one series of undrained triaxial compression tests, the specimens were allowed to consolidate for ten minutes (approximately 65 percent consolidation) prior to testing, to provide strengths considered representative of the as constructed embankment.

TABLE 1 SUMMARY OF LABORATORY STRENGTH TESTS

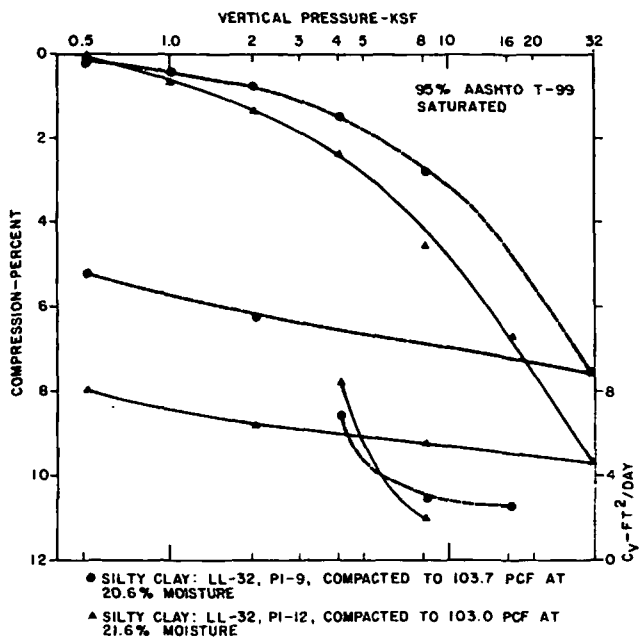
MATERIAL	DRY DENSITY PCF	MOLDING MOISTURE %	TEST TYPE	TEST MOIST. COND.	TEST SPEED IN/MIN	ϕ_u	C_u KSF	ϕ'	C' KSF	RANGE σ_3 or σ_n KSF
SILTY CLAY LL-33 PI-12	102	21.6	DIRECT SHEAR	21.6	0.05	19°	0.95			2-8
				21.6	0.0035		28.5°	0.28		
				SAT.	0.0035		29.5°	0		
SILTY CLAY LL-32 PI-9	103/104	20.6		20.6	0.05	24°	0.75			2-8
				SAT.	0.0035		30.5°	0.20		
SILTY CLAY 107/108	19.8	19.8		19.8	0.05	24.5°	1.30			2-15
				19.8	0.0035		27°	0.90		
				SAT.	0.008		30°	0.25		
SILTY CLAY	108	19.5	UU(1)	19.5	0.015	14.4°	3.41			2-10
			UU(2)	19.5	0.015	18.6°	3.66			
CLAYEY SILT	105.5	18.8	UU	18.8		31°	1.58			
SILTY CLAY	107	18.8	UU	18.8	0.005	13.5°	4.18			

- (1) Consolidated 10 min. - 10% strain
 (2) Consolidated 10 min. - 15% strain

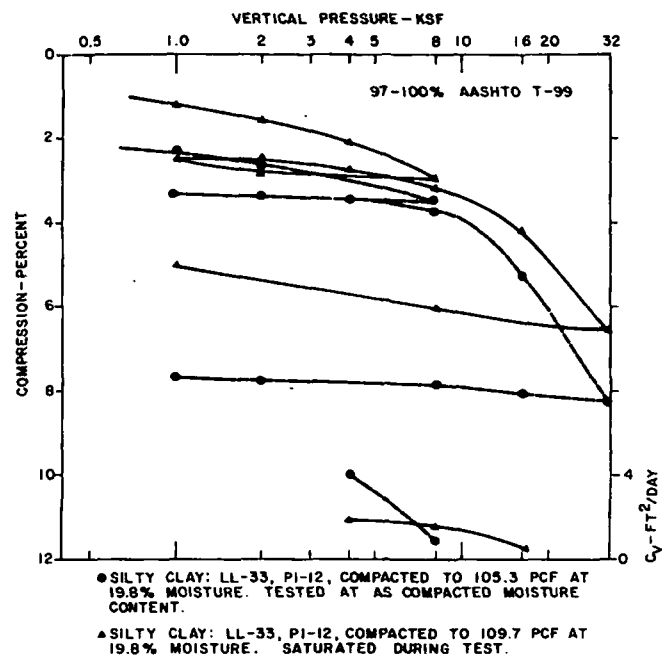
Consolidation tests were performed on specimens which were compacted to densities representing 95, 97, and 100% of AASHTO T-99. Consolidation test results were illustrated in Figures 2 and 3.

STABILITY ANALYSIS

Conventional stability analyses using the modified Bishop method were performed with the aid of the computer program ICES LEASE 1 (Bailey and Christian 1969). The end of construction condition was analyzed using the results of the "undrained" direct shear tests and partially consolidated undrained triaxial compression tests as shown in Table 1. Minimum factors



CONSOLIDATION TEST RESULTS
 Figure 2



CONSOLIDATION TEST RESULTS
 Figure 3

of safety against slope failure in the maximum embankment section (190 feet above the rockfill base and 1.75 horizontal to 1.0 vertical slopes) were computed to be 1.1 at 95 percent compaction and 1.4 for 100 percent compaction.

The apparent cohesion measured in the direct shear tests was found to decrease significantly in saturated tests. Saturation of the surface due to rainfall or snowmelt was therefore considered to be the critical condition for long term stability of the slope surface. Analyses were performed to determine the thickness of rockfill needed to confine the slope surface and provide resistance to shallow slope failure. A planar potential failure surface at the interface between the rockfill and the soil embankment was assumed to occur along the entire height of the slope. Resistance to sliding was assumed to be provided by friction in the embankment soil and by a passive wedge in the rockfill. Shear strength parameters used were:

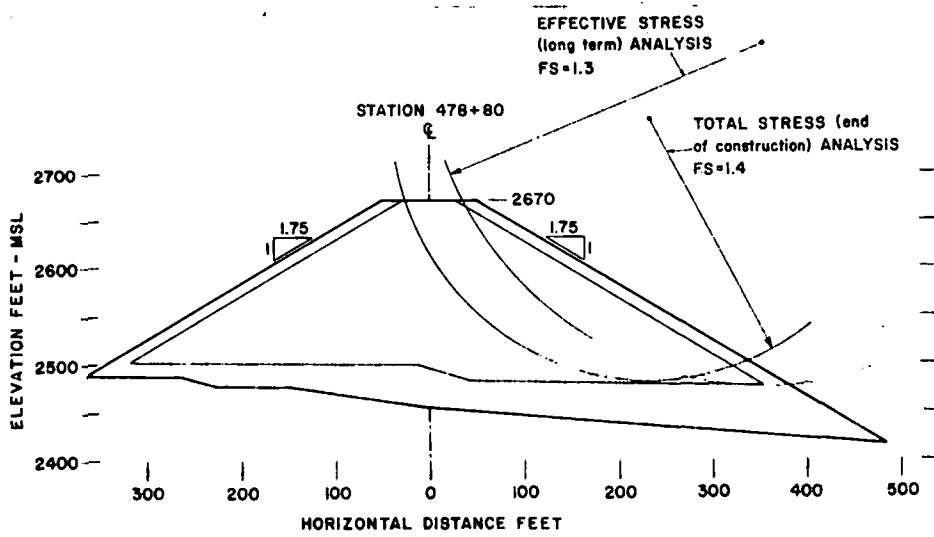
Rockfill -	$\phi = 42^\circ$	C = 0
Soil -	$\phi = 30^\circ$	C = 0

For a 1.75 horizontal to 1.0 vertical slope, rockfill placed ten feet thick (measured normal to the slope) was found to provide factors of safety against failure of the entire downstream slope of 1.06 and 1.1 respectively for 95 and 100 percent compaction in the embankment. The computed factors of safety are very low. However, the analysis is judged to represent the lower bound conditions, since the internal angle of friction for basalt rockfill under low confining pressures is expected to be more nearly 50 degrees according to values published by Wong and Duncan (1974). Also, drainage in the rockfill will be rapid and the saturation conditions necessary for failure will be of short duration and are not expected to occur along the entire slope simultaneously.

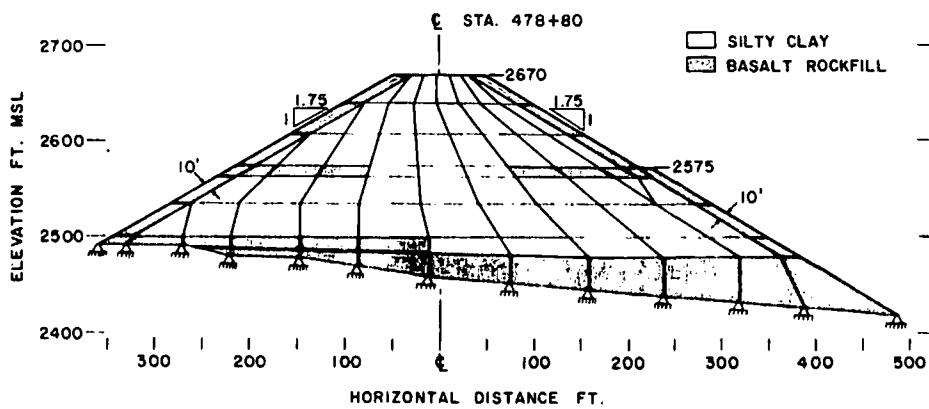
Long term stability analysis utilizing the results of the saturated drained direct shear tests yielded a minimum factor of safety of 1.3. Figure 4 illustrates the trail embankment section and locations of critical failure arcs.

FINITE ELEMENT ANALYSIS

Since factors of safety computed using conventional analyses were less than 1.5, additional analyses were made using non-linear elastic finite element methods. Finite element analyses provided estimates of the long term embankment stresses and deformations, and provided a basis for comparison with performance. The computer program ISBILD developed by Ozawa and Duncan (1973) was used in these analyses. Embankment construction is simulated in the ISBILD program by applying layers of elements incrementally, and computing stresses and deformations due to each increment. The finite element mesh used is shown in Figure 5. Non linear hyperbolic stress-



RESULTS OF STABILITY ANALYSIS
 Figure 4



FINITE ELEMENT MESH FOR HATWAI CREEK EMBANKMENT
 Figure 5

strain parameters were developed for the silty clay and rockfill materials with the methods outlined by Wong and Duncan (1974) using the results of drained direct shear tests and consolidation tests. The parameters assigned to the embankment materials are shown in Table 2.

TABLE 2 PROPERTIES OF EMBANKMENT MATERIALS FOR USE IN FINITE ELEMENT ANALYSIS

MATERIAL	TOTAL DENSITY PCF	INITIAL VOID RATIO	ϕ'	C' KSF	K	K_{UR}	N	RF	G	F (3)	d (3)
SILTY CLAY (1)	125	0.66	28.5°	0.28	95	178	1.00	0.75	0.40	0.08	2.5
SILTY CLAY (2)	129	0.59	30°	0.12	165	330	0.70	0.75	0.39	0.08	2.5
ROCK FILL (3)	133	0.30	42°	0.00	450	585	0.37	0.65	0.34	0.16	4.8

(1) 95% of AASHTO T-99

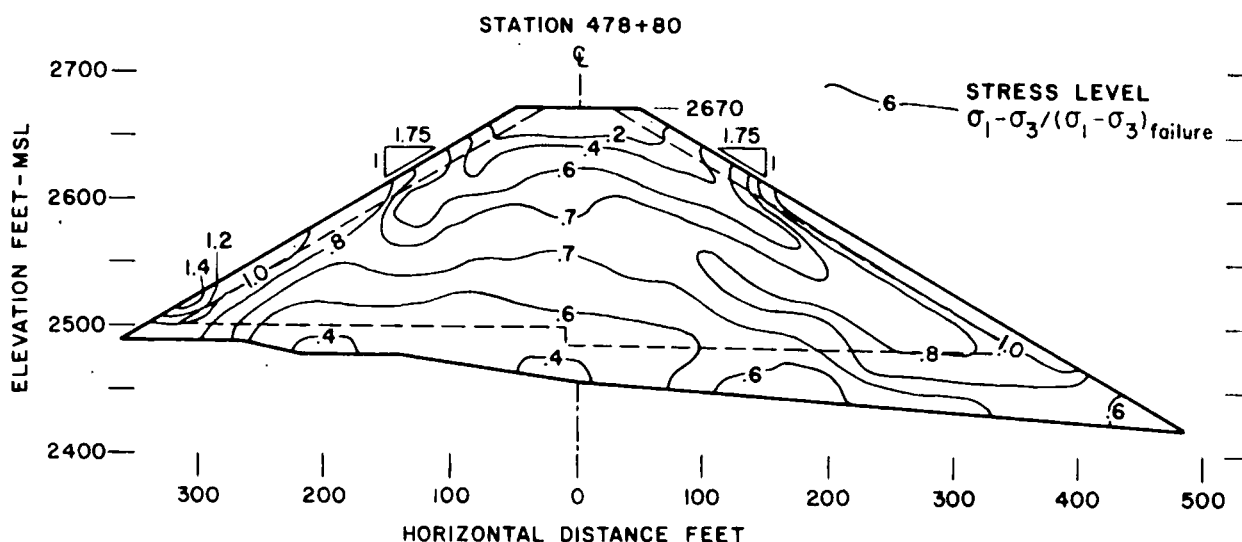
(2) 100% of AASHTO T-99

(3) Assumed, based on published values (Wong and Duncan, 1974)
 ϕ' adjusted for confining pressure

Modulus numbers K and K_{UR} represent the initial stiffness or modulus of elasticity for initial loading, and reloading curves. The parameter N relates the increase in elastic modulus with increasing confining pressure. Actual stress-strain relationships deviate from the hyperbolic curve near failure and the failure ratio (RF) relates the deviator stress at failure for the material to the computed hyperbolic curve. Parameters G, F, and D represent initial Poisson's ratio, the decrease in initial Poisson's ratio with increasing confining pressure, and rate of increase of Poisson's ratio with increasing strain.

Initially, soil parameters representing 95 percent compaction were input and interior rock layers were not included. Figure 6 presents the stress levels computed for each element for a 95 percent compaction level.

The discontinuity represented by the rockfill-silty clay interface is evident from the stress level contours. High stress levels at the interface with the rockfill and the location of the 80 percent stress level generally agree with the results of the conventional stability analyses.



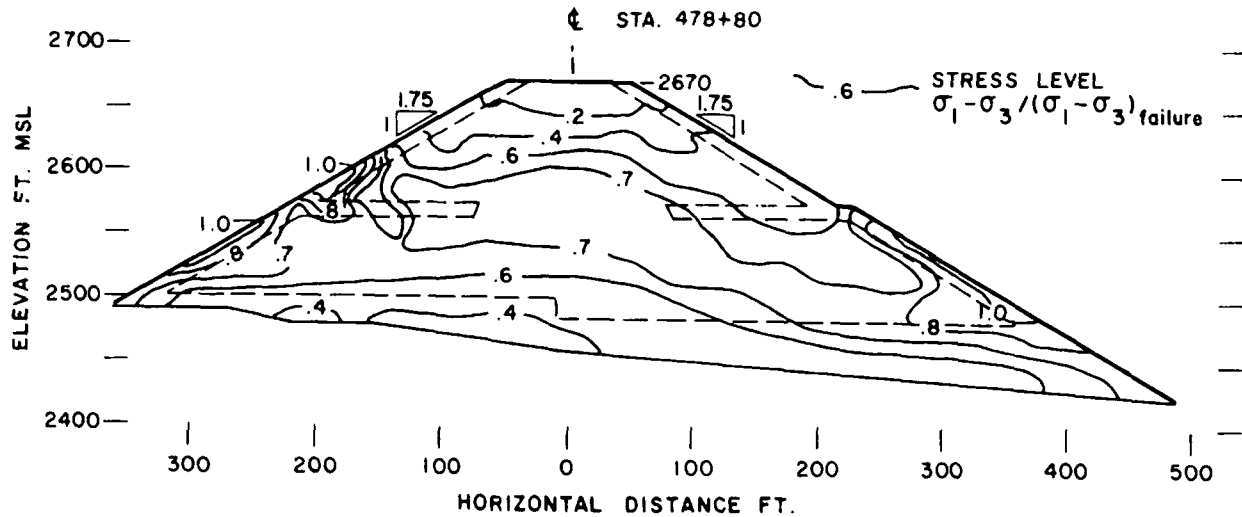
MAXIMUM STRESS LEVELS - 95 PERCENT COMPACTION WITHOUT
 INTERNAL ROCK STIFFENING LAYER

Figure 6

The facing elements are poorly shaped, relative movement cannot occur and the internal friction angle assigned to the rockfill was reduced about 10 degrees from that which could be expected under low confining pressure. Therefore, high stress levels computed in the rockfill slope facing are not of great concern.

The program was rerun using stress-strain parameters representative of 100 percent compaction. To provide more rapid pore pressure dissipation and consequently a more rapid strength increase, an internal rockfill layer was added at about elevation 2570. The resulting stress levels are illustrated on Figure 7. The discontinuity at the base of the rockfill facing is again evident, however, the internal stress levels have been reduced by about 12 percent beneath the downstream slope and are more uniform along the foundation. Stress levels in the rockfill slope facing are reduced by as much as 40 percent with overstress occurring only in localized areas.

The finite element analysis provides a "picture" of the stresses and displacements occurring within the embankment which can be used to locate probable critical areas. The picture was used in this study to aid in locating instrumentation and to illustrate the effect of compaction level on the internal stresses.

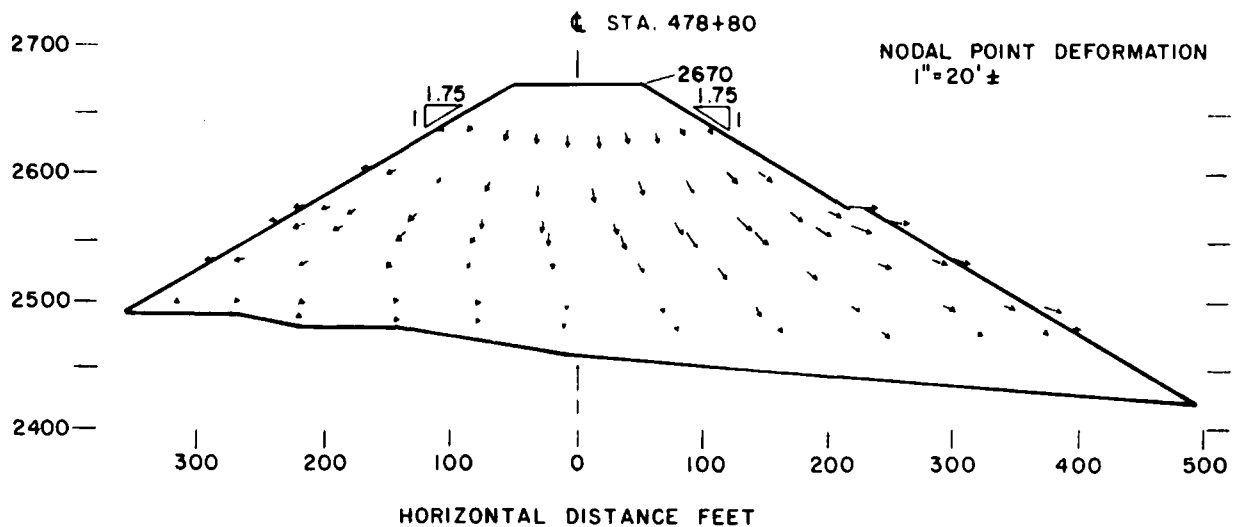


MAXIMUM STRESS LEVELS-100 PERCENT COMPACTION WITH
 INTERIOR ROCK STIFFENING LAYER

Figure 7

Figure 8 illustrates the approximate magnitude and direction of the nodal point deflections computed for 100 percent embankment compaction. The computed deflections are elastic and the assumption is made that the deflections occurring due to an increment of fill are complete before the next increment or layer is placed. The computer output therefore, cannot be directly used to estimate time dependent deformations. Time-consolidation data from the laboratory tests were used to estimate the degree of vertical deformation (consolidation) occurring during construction. The estimates of horizontal and vertical deformation developed from this analysis are presented in the discussion of embankment performance.

Finite element analyses using undrained strength and modulus parameters were not performed since the long term stability was judged to be more critical. The results of an undrained or partially drained analysis would however, provide a better comparison with short term or end of construction performance.



TOTAL DEFORMATION-100 PERCENT COMPACTION WITH INTERIOR ROCK LAYER

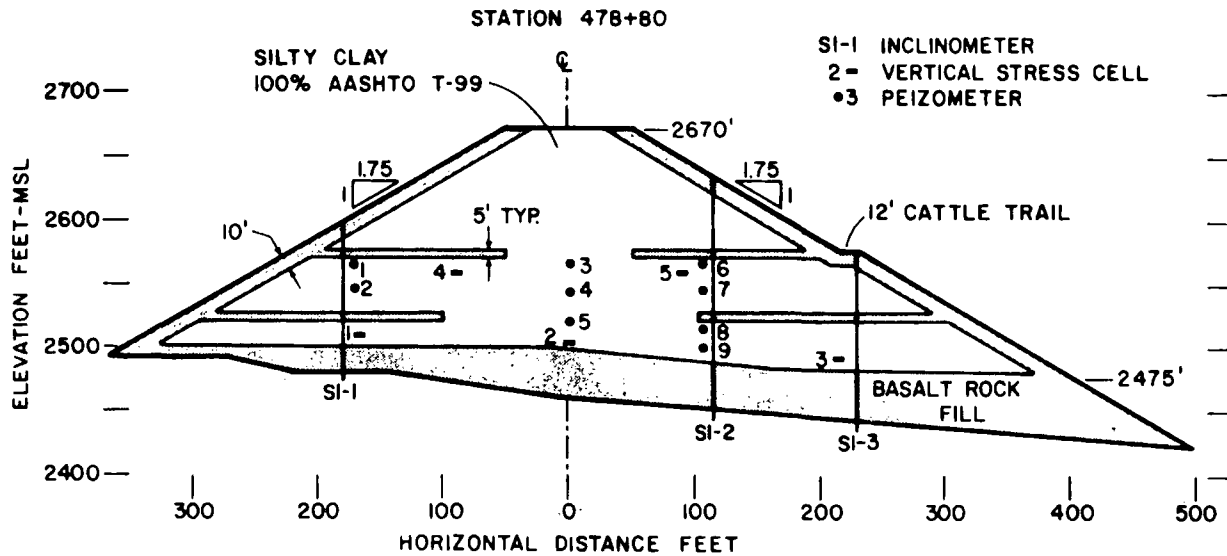
Figure 8

DESIGN SECTION

Based on the results of the conventional stability analyses and the finite element analyses, the design section was established as shown in Figure 9. Since the volume of internal drainage was expected to be relatively small, the internal rock layer was reduced to a five foot thickness. A second five foot thick layer was added at about elevation +2520 to further increase the rate of pore pressure dissipation. Instrumentation was proposed as shown in Figure 9 to monitor the performance of the embankment.

CONSTRUCTION

Foundation excavation and clearing began in January, 1978. Foundation excavation extended to rock except near the downstream toe of the embankment where the lower interbed was encountered at the south side of the canyon bottom. Approximately 20 feet of clay interbed was overexcavated to construct a key way.



DESIGN SECTION SHOWING INSTRUMENTATION

Figure 9

By early April, 1978, 78,000 cubic yards of rockfill had been placed in the base of the embankment. During the placement of the embankment base, the six foot diameter multiplate pipe was installed in a trench in the rockfill. Loose rockfill was placed over the pipe to a depth of at least two feet to act as a partially imperfect trench reducing the vertical stress on the pipe. The rockfill was also placed to provide drainage for seepage areas encountered on the north side of the channel about 20 feet above the foundation. Since the rockfill contained appreciable fines, the creek flow was diverted through the rockfill for nearly 4 weeks to confirm that permeability was adequate.

The contractor began placing the silty clay embankment in April, 1978. Initially, the work area was restricted in the narrow canyon and placement was slow. Material was excavated from the cut section adjacent to and north of the canyon. The uppermost six to ten foot thick layer of silty clay appeared to be equivalent to the soils in the cut immediately south of the canyon which were tested to provide the strength parameters used in the analyses. This layer was near optimum moisture content, and presented little difficulty in compaction. Beneath the silty clay, a 15 to 25 foot thick layer of clayey silt containing caliche was encountered which extended to rock. The moisture content in the silt was below optimum and considerably more compactive effort was required to break down the caliche and achieve

the minimum compaction level. Actual densities achieved in both the laboratory and field tests were about two pounds per cubic foot lower than those representative of the laboratory strength tests.

The contractor requested that additional laboratory maximum density tests be performed on the clayey silt to confirm the maximum density achieved in the field. Three laboratories performed additional tests in accordance with both AASHTO T-99 and T-180. The results were comparable or higher than the maximum density curve previously developed in the field. Additional compactive effort was provided and the embankment was completed on October 18, 1978. A total of 1.3 million cubic yards of fine grained soil was placed at an average rate of 16,000 cubic yards per day.

The rockfill facing was brought to grade along with the silty clay embankment. The embankment section in Figure 9 depicts the rock-soil fill interface as a plane. The interface as constructed consists of a series of benches approximately five feet high with a ten foot minimum thickness of rockfill. The basalt rockfill contained appreciable fines and the ten foot thickness was expected to adequately retain the finer grained soil under the intermittent wetting, therefore, no filter layer was judged necessary.

INSTRUMENTATION

Instrumentation which was installed during embankment construction is shown on Figure 9 and consisted of three inclinometers, nine pneumatic porous stone piezometers, and five total pressure cells. Additional settlement monitoring points were established at the tops of the inclinometer casings and on steel rods driven at the outside shoulders of the maximum fill section.

Inclinometers were drilled into bedrock following completion of the rockfill foundation. As the embankment was placed, the inclinometer casings were extended in five foot sections. Long couplings and settlement flanges were attached to provide a means of monitoring internal settlement. Inclinometer measurements were initiated once the embankment reached the elevation of the top of the casing. Settlement was to be monitored using a USBR type probe, but measurements were discontinued early in construction when the probe was lost in the inclinometer casing.

Piezometer tips were encased with a canvas bag filled with saturated fine sand prior to placement. Pneumatic piezometers and total pressure cells were installed in hand excavations as the embankment was being placed. The instruments were backfilled with sand and hand compacted soil was mounded over the excavation. Pore pressures and embankment pressures were monitored throughout construction of the embankment.

PERFORMANCE

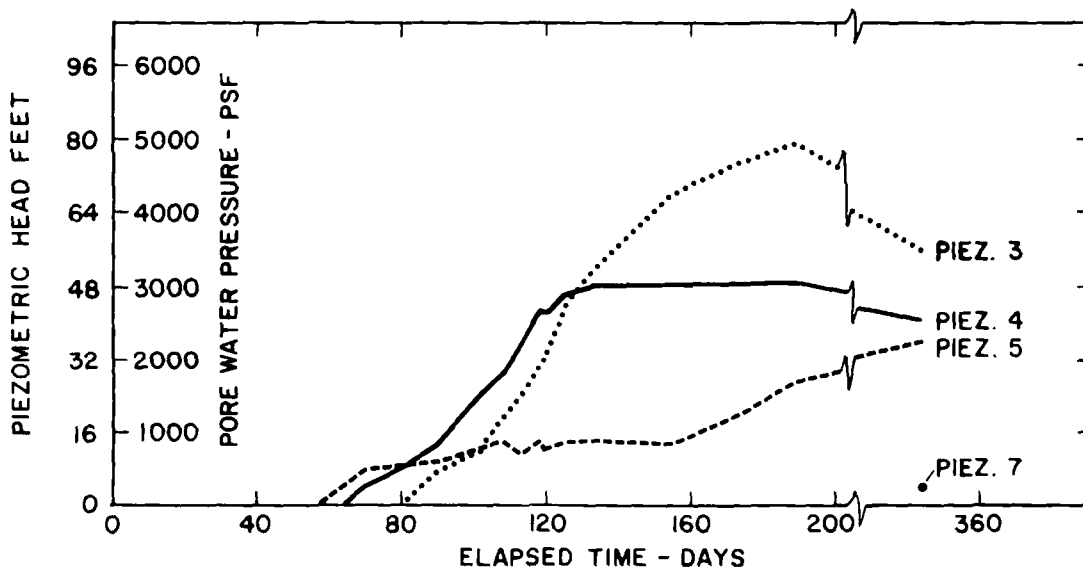
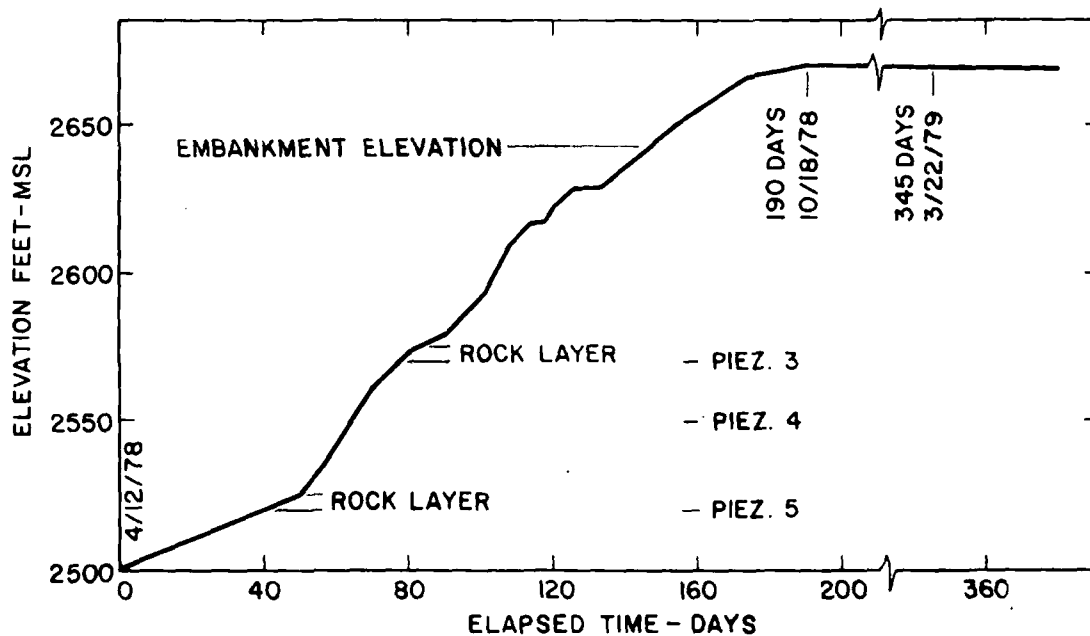
Figure 10 illustrates the rate of embankment construction and the corresponding porewater pressures measured in Piezometers 3, 4, 5 and 7. Pore pressures were observed to be zero during construction in all piezometers except 3, 4, and 5. These piezometers were located near the center of the embankment as shown on Figure 9. With the exception of Piezometers 2, 3, 4, 5 and 7, all others were located relatively near the internal rockfill layers.

In Piezometer 3, the ratio of pore pressures measured during construction to vertical soil pressure (based on soil densities) was calculated at 0.4, which is a commonly assumed value for compacted fill. Immediately upon completion of the embankment the pore pressure was observed to diminish, dropping approximately 300 psf in 10 days. Pore pressures in Piezometer 4 increased for the first 60 days and then no increase or decrease was observed until the embankment was completed. A malfunction or air trapped in the piezometer tip is suspected. Piezometer 5 responded in a similar manner for about 10 days but the rate of increase slowed resulting in nearly flat response for about 80 days. During the last 30 days of construction the rate of pore pressure increase was only slightly flatter than Piezometer 3, and the pressure was still increasing slowly five months after completion. An air bubble may have slowed the response such that the actual pore pressure was not being recorded, and the recorded pore pressure had not yet reached equilibrium. Piezometer 7 registered a small pore pressure for the first time about 5 months after completion. Pore water is apparently migrating laterally more rapidly than it is dissipating into the internal rock layers.

Five pneumatic steel diaphragm type total pressure cells were installed at the locations shown in Figure 9. All cells were oriented to measure vertical pressure. None of the five operated satisfactorily. The measured vertical pressures bore little resemblance to the calculated vertical pressure and in some cases the cell pressure was measured to be as high as 10 ksf with as little as two feet of cover. Potential causes of the malfunction are being studied by the manufacturer.

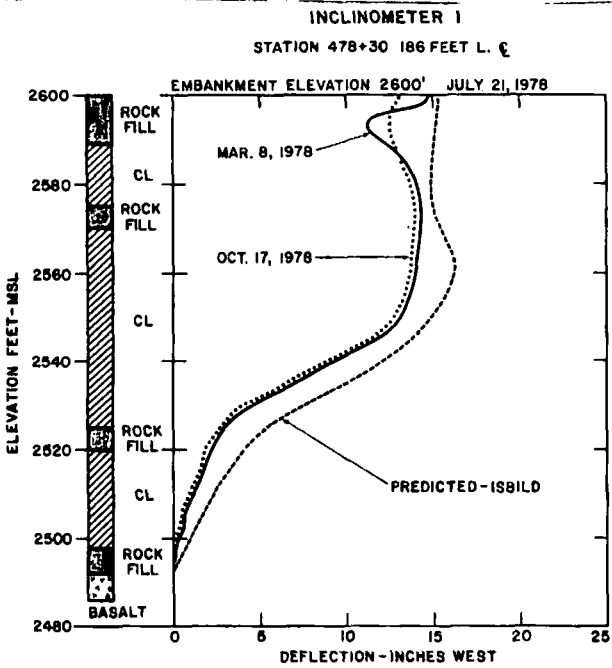
Deflections in the three inclinometers were consistent even though the slip jointed couplings complicated reproducing the depths between sets of measurements. Figures 11, 12 and 13 illustrate the measured deflections and those predicted from the finite element analysis. Stratigraphic sections showing the positions of the rockfill zones are located along the left side of the figures.

Restricted movement at the levels of the interior rockfill layers is apparent, particularly in Inclinometers 1 and 3. Relatively larger deflection in the rockfill facing is evident in Inclinometers 1 and 3, and the March 8 reading shows the increased deflection in the facing which occurred during snow melt.



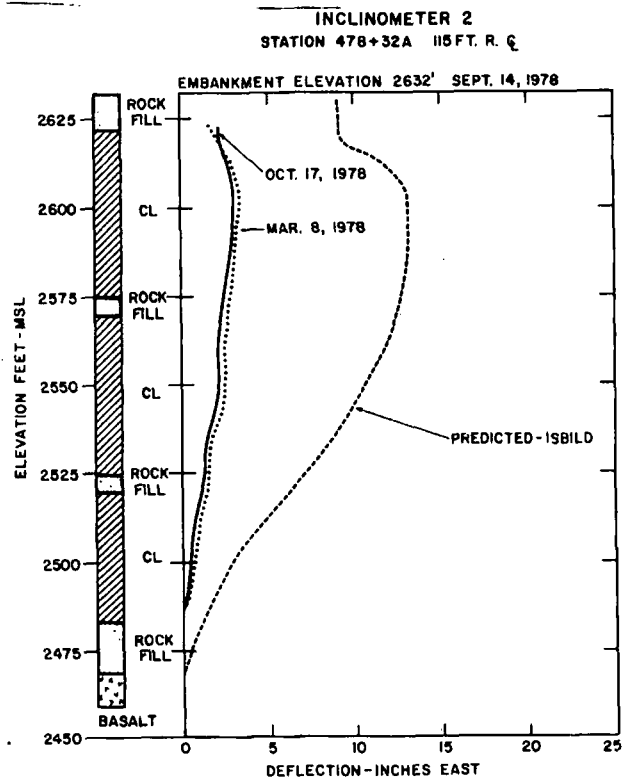
EMBANKMENT ELEVATION AND PORE PRESSURE
 VARIATION WITH TIME

Figure 10



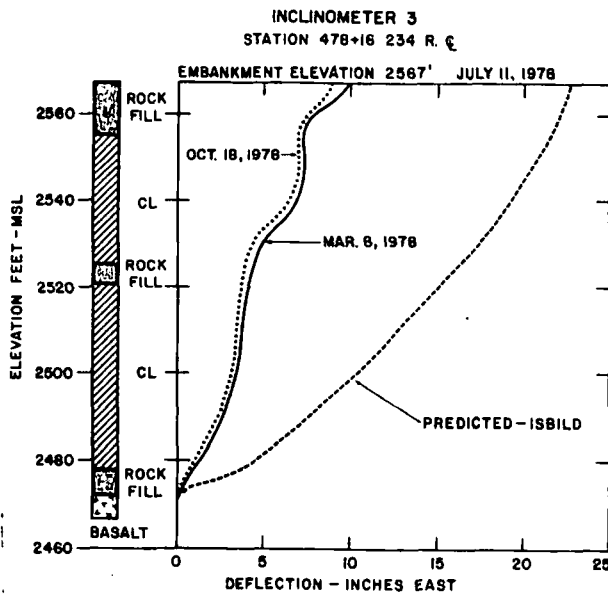
MEASURED VERSUS PREDICTED DEFLECTION

Figure 11



MEASURED VERSUS PREDICTED DEFLECTION

Figure 12



MEASURED VERSUS PREDICTED DEFLECTION

Figure 13

Measured deflections in Inclinator 1 unexpectedly agreed exceptionally well with those predicted. Deflections in Inclinator 2 and 3 were however only 30 to 40 percent of the predicted values. The finite element analysis does not account for time effects and therefore the predicted deflections are "ultimate". The measured deflections therefore were expected to be somewhat less than the predicted values. In all three inclinometers, the general shape of the observed deflection curve was similar to that predicted. The difference in performance between the downstream and upstream slopes has not been explained. Monitoring will continue for at least another 6 to 12 months.

Vertical deformation (settlement) was measured at the collars of the inclinometers and at two monuments at the shoulders of the roadway. Table 3 is a summary of the predicted and measured settlements. As settlement computed in the finite element analysis does not account for time effects, predicted settlements were therefore adjusted to reflect the consolidation rate. Total settlement values in Table 3 represent the amount which would occur at each point if the embankment was placed in one lift, i.e. instantaneous "gravity turn on".

TABLE 3
 PREDICTED AND OBSERVED VERTICAL DEFORMATION

POINT	REF. ELEV.	PREDICTED DEFORMATION - FT.		OBSERVED DEFORMATION - FT.			
		TOTAL	(1)	10/20/78	12/18/78	3/1/79	3/22/79
PAVEMENT C	2670	4.9	1.2 - 1.6	-	-	0.34	0.37
COLLAR SI-1	2600	1.5	1	0.28	0.33	-	0.97
COLLAR SI-2	2632	3.2	2	0.6	0.72	-	1.14
COLLAR SI-3	2567	1.6	1	0.84	0.98	-	1.49

(1) Deformation expected to occur after embankment reaches reference elevation

In early March, the actual settlement of the tops of the inclinometer casings was observed to rapidly increase, exceeding the predicted values. The increase appeared to coincide with the end of the snow melt period. During the same period the settlement at the top of the embankment increased on the order of 0.04 feet. Downslope movement of the facing and migration of the clayey silt into the rockfill facing in response to saturation of the slope may have been the causes of the differential settlement experienced between the tops of

the slope indicators and the embankment crest. Pore pressure dissipation and corresponding settlement of the crest is occurring slowly. Approximately 25 percent pore pressure dissipation occurred in the first five months following completion of the embankment.

CONCLUSIONS

Based on the analyses performed during design and the observed performance in the first five months following completion of the embankment, the following conclusions have been made.

- (1) Conventional slope stability analysis methods provide reasonable results for the design of the embankment section. The finite element analysis however, provides a more complete "picture" of the effect of variables such as stiffness (density, compaction level, strength) on the stress levels and deformations developed in the interior of the embankment. Instrumentation can be located more effectively using the results of the finite element analysis.
- (2) Finite element analyses performed using "undrained" or partially drained strength and modulus parameters would more closely approximate the conditions during and at the end of construction.
- (3) Laboratory test results used to develop the strength and modulus parameters may not be representative of the soils from the north side of the canyon which were actually placed in the embankment. Average compaction levels were slightly higher than the 100 percent minimum specified, and actual densities were lower than those developed for analysis. Laboratory testing of samples recovered from the constructed embankment would provide data on the density increase which has occurred within the embankment and the accompanying settlement and would provide stress-strain parameters representative of the soil in place.
- (4) The internal drainage layers functioned as anticipated. Pore pressures in the areas of the embankment near the internal rock-fill layers dissipated as fast as they were generated. Lateral deflections were reduced at the levels of the rockfill layers in Inclinerometers 1 and 3.
- (5) Based on the pore pressure dissipation rate observed in Piezometer 3, deflections may not be substantially complete for five years or more. If settlement of the crest of the embankment is proportional to the pore pressure dissipation, settlement will approach 1.3 feet after about five years, which agrees well with that predicted, from finite element analysis and consolidation tests.

- (6) Measured deflections in Inclinometers 2 and 3 are 30 to 40 percent of those predicted by the finite element analysis. Since predicted deflections are ultimate or long term, measured deflections may not approach predicted values even after several years.
- (7) The settlement observed at the tops of the inclinometer casings and the deflections measured in the upper 10 feet appear to result, at least in part, from the downslope movement of the rockfill facing and softening of the underlying silty clay during snowmelt. In addition, more rapid settlement has probably occurred beneath the embankment slopes due to dissipation of pore pressures into the internal rockfill layers.
- (8) Knowledge of the amount and distribution of internal settlement is valuable in documenting performance. Measurement made at the joints in inclinometer casing is the simplest and least expensive method of measuring internal settlement, and a simple hook type probe is preferred. Additional pneumatic or hydraulic settlement devices will provide supplemental data but will require long leads which can be expected to have a high failure rate. Total stress cells have limited value in assessing performance, require very careful installation and in the authors' experience have a high rate of failure.

REFERENCES

- Bailey, W.A., and Christian, J.T.: "ICES LEASE-I, A Problem Oriented Language for Slope Stability Analysis," User's Manual, Soil Mechanics Division and Civil Engineering Systems Laboratory, Department of Civil Engineering Massachusetts Institute of Technology, Cambridge, Massachusetts, April 1969.
- Materials Section Correspondence to District 4, Project TQ-F-4114(32) dated: 11, June 1976; 1 March, 1977; 5 April, 1977; 3 June, 1977; and 17 June, 1977. Idaho Transportation Department, Division of Highways, Boise, Idaho.
- Ozawa, Y. and Duncan, J.M.: "ISBILD: A Computer Program for Analysis of Static Stresses and Movements in Embankments," Report TE-73-4, Department of Civil Engineering, University of California, Berkeley, California, July 1974.

Design, Construction, and Performance
Hatwai Creek Embankment
By Patrick J. Lightfield and Robert M. Smith
Page 22

Wong, K.S. and Duncan, J.M.: "Hyperbolic Stress-Strain Parameters for Non-linear Finite Element Analyses of Stresses and Movements in Soil Masses," Report TE-74-3, Department of Civil Engineering, University of California, Berkeley, California, July 1974.

ANALYSIS TECHNIQUES FOR LOW REINFORCED SOIL RETAINING WALLS AND COMPARISON OF STRIP AND SHEET REINFORCEMENTS

By

William Whitcomb and J.R. Bell
Department of Civil Engineering, Oregon State University
Corvallis, Oregon

ABSTRACT

As the concept of reinforced soil becomes better known and more widely accepted, reinforced soil walls are being increasingly used to support narrow secondary roads in steep terrain. In these applications, it is difficult to obtain a balanced design which utilizes the full strength of the conventional metal reinforcing strips without embedment lengths which require excessive, costly excavation. It appears that this problem can be overcome by using continuous reinforcements, rather than strip reinforcements.

This paper presents an analysis of walls with strip and continuous sheet reinforcement elements over a range of conditions. Traditional methods of analysis and appropriate design parameters found in the literature are reviewed. Selection of the design parameters and the analysis approach is described. The results of example designs indicate that live loading of low walls significantly changes the design of the reinforcement in the upper portion of the wall, and that traditional analysis methods may be inadequate to accurately account for this effect.

In the example designs, continuous reinforcement permits the use of weaker, and therefore possibly less expensive materials and allows a more balanced design. In addition, the continuous reinforcement does have a tendency to reduce the required embedment lengths; however, this advantage may be substantially offset by the reinforcement length requirement for an adequate factor of safety against sliding of the entire wall.

INTRODUCTION

The concept of adding materials to soil for added strength or erosion control is not new and other researchers (1, 2)³ have provided excellent documentation of the use of straw, logs, wooden beams, metal and other materials to improve the engineering properties of the soil-reinforcement system. In 1966, rational design procedures for incorporating tension reinforcing elements into soil to produce a desirable composite material applicable for important engineering structures was introduced by the French engineer, Henri Vidal (3, 4, 5, 6). It soon became apparent that when compared to conventional retaining walls, reinforced soil structures could offer many advantages, including speed and relative ease of construction, flexibility of the resulting structure, and economy.

Analysis Techniques for Low Reinforced Soil Retaining Walls
and Comparison of Strip and Sheet Reinforcements
By William Whitcomb and J.R. Bell
Page 2

Because of these advantages, a growing interest has developed in the Pacific Northwest in using reinforced soil retaining walls for the construction of low standard roads through steep and relatively unstable terrain in remote areas. The U.S. Forest Service has constructed a number of trial walls (7,8,9,10), using various types of reinforcement, including fabric and chain link metal. In addition, at least one wall has been built in Southwestern Oregon using concrete facing elements and steel strips in the process patented by the Reinforced Earth Company.

Use of reinforced soil walls in these applications can pose several problems not normally encountered in the discussions of analysis techniques for design found in the literature. For example, in steep terrain, overall wall width becomes an important consideration in the achievement of an economical design. In certain situations, as wall width becomes slightly greater, excavation quantities can increase dramatically. Also, heavy live loading due to log truck traffic can be an important consideration in the overall wall design, and could possibly be the overriding factor in the design of tension elements in the uppermost portion of the wall. It is not inconceivable to expect loaded log trucks to be operating nearly at the wall edge.

It appears at first glance that the problem of excavation in steep terrain can be minimized by using continuous reinforcement. There exists a need to determine whether or not there are indeed significant advantages of continuous reinforcement over strip reinforcement in reinforced soil walls used in the construction of low standard roads. This paper investigates this question. Presently available analysis techniques used in the design of reinforced soil walls are reviewed, together with a discussion of appropriate parameters to be used in calculation. As a result of this review, an analysis technique similar to that presented by Lee (1), but with several significant modifications, is used in the design of example walls with strip and sheet reinforcement. Based on these designs, factors important in the design of reinforced soil walls are highlighted.

Figure 1 presents a sketch of the basic elements in reinforced soil walls. The major components are the wall skin and the reinforcements, in this particular instance, strip reinforcements. In addition to strip reinforcing, continuous reinforcement, such as geotextiles, chain link fencing, or welded wire fabrics can be used.

The basic mechanism of reinforced soil is that the soil transmits stress to the reinforcement through soil-reinforcement friction. The amount of stress transmitted is related to several factors, including overburden pressure, live load, and soil and reinforcement material properties.

The exact mechanism functioning in the reinforced soil wall to give it the stability to support both the backfill soil and any surcharges placed upon it is not fully understood. Three approximate analyses have been used, including the tie back method described by Lee (1), the standard design method

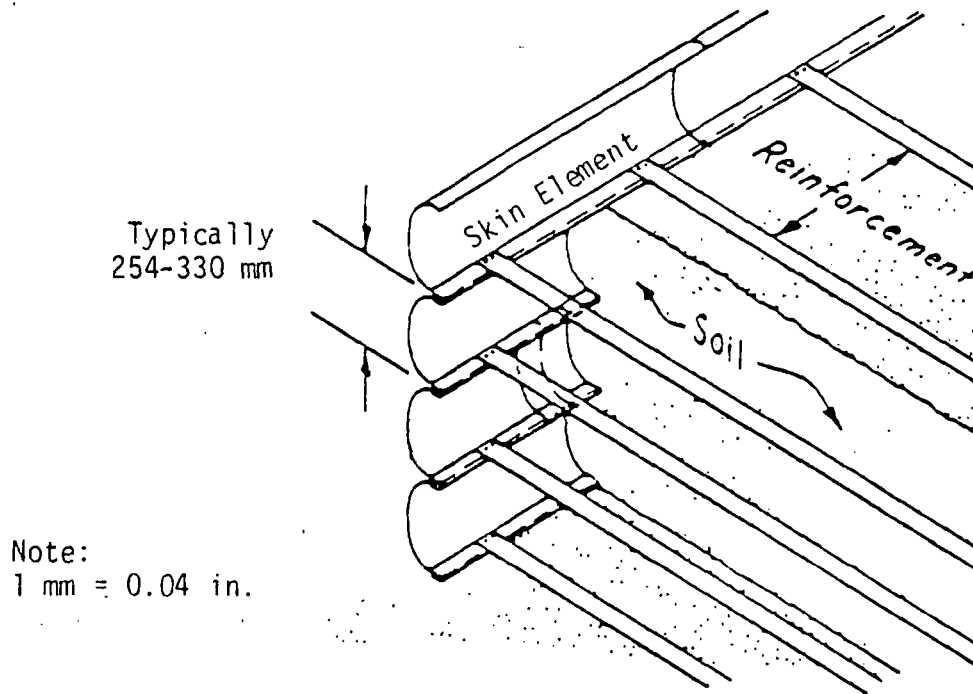


FIGURE 1 - Components of Reinforced Soil Walls (2)

described by Schlosser (11), the Coulomb method described by Vidal and Schlosser (3). These have been summarized by Hausmann (12), together with typical methods for dealing with non-uniform surcharges. Prior to discussions of the methods of analysis, a discussion of appropriate design parameters to be used in the analyses is presented.

DESIGN PARAMETERS

Soil Properties

The soil properties used for the example reinforced soil walls are included in Table 1. The backfill is considered cohesionless and free-draining, and is assumed to meet all gradation specifications usually required, i.e. less than 15% passing the 0.074 mm (#200) sieve.

Live Loadings

The wheel loadings assumed are presented in Figure 2. To apply the conventional design methods, it is necessary to transform the three-dimensional

TABLE 1
 SUMMARY OF DESIGN PARAMETERS

DESIGN PARAMETERS	VALUES USED IN CALCULATIONS
Soil Properties	$\phi = 30^\circ$ $\gamma = 19 \text{ kN/m}^3$
Live Loadings	Line Loads 87.6 kN/m at 1.1 m (For Horizontal Pressure Distribution) 2 - 36.5 kN/m at 1 m and 2.8 m (For Vertical Pressure Distribution)
Earth Pressure	K_0 used
Soil Tie Friction	$\delta = 2/3 \phi$
Minimum Reinforcement Lengths	Greater of 3.1 m or $1/3 H$
Factors of Safety	Reinforcement Rupture - 2.0 Reinforcement Pullout - 2.0 Sliding - 1.5

Note: 1 m = 3.3 ft.

1 kN/m = 68.5 lb./ft.

live loading as shown, into an equivalent two-dimensional system. Line loadings are chosen to represent this condition. The problem is two-fold: first it is necessary to determine the appropriate line loading to give a horizontal pressure distribution at the wall similar to that resulting from the point loads and second, to select a line loading to give appropriate vertical stress distributions. Each of these problems was solved using a trial and error procedure.

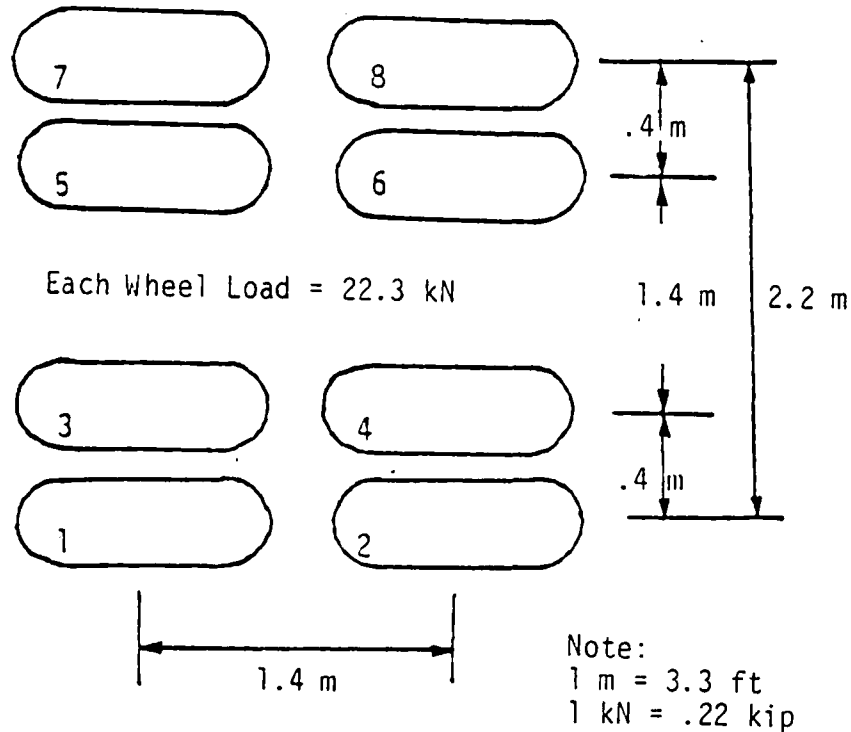


FIGURE 2 - Log Truck Wheel Loadings for Assumed Design Problem

The horizontal stress distributions for the wheel loads treated as point loads were calculated using the procedure outlined by Spangler (13), which incorporates a modified form of the Boussinesq equations. The horizontal stress distribution due to the line loading and the vertical stress distributions for both point and line loadings were also determined using Boussinesq equations (14). The stress distributions for the eight point loads were plotted together with the stress distributions from several assumed line loads. The resulting line loads giving the "best" match of stress distribution with the point loads were selected. The horizontal stress distribution at the wall due to actual truck loading is approximated by the stress distribution resulting from the application of an 87.6 kN/m (6,000 lb./ft.) line load, located 1.1 m (3.5 ft.) from the face of the wall. The vertical stress distributions are best approxi-

mated by two 36.5 kN/m (2,500 lb./ft.) line loads located 1.0 m (38 in.) and 2.8 m (110 in.) from the wall face. These equivalent line loadings were used in all subsequent calculations.

Coefficient of Earth Pressure and Pressure Distributions

Both the standard design method and the tie back model assume that the vertical and horizontal earth pressures are related through the coefficient of earth pressure, K . The appropriate K value to use remains a moot point, however. The standard design method given by Schlosser (11) and the tie back model presented by Lee (1) assume that Rankine's coefficient of active earth pressure, K_a , is appropriate. This conclusion is based mainly on assumptions regarding wall movement. In his discussion closure (1) however, Lee proposes that the at-rest earth pressure, K_0 , rather than the active earth pressure, K_a , be used in the tie back design model. Chang (2) indicates that field measurements show that the earth pressure coefficient approaches K_0 . Vidal and Schlosser (3) indicate that, theoretically, the coefficient of earth pressure, K , should be K_0 at the top of the wall due to lack of wall movement. In all cases, the distributions are assumed to be hydrostatic.

It is assumed that because of construction compaction and traffic vibration, earth pressures will probably approach or exceed K_0 . Since this has been substantiated by measurements in actual walls, it is believed that this is the best assumption. Hence, K_0 is used for all calculations in this paper.

Soil-Reinforcement Friction and Embedment Length

The angle of friction between the soil and the reinforcement material is normally designated as δ . Schlosser and Long (15) have performed research relating the angle δ to the internal friction of the soil, ϕ . The results of that work indicate that for a variety of soils with various percentages of fines, the angle δ varies between $1/2 \phi$ and ϕ . Chang (16) has performed a significant amount of research on the behavior of earthwork reinforcement in soil and indicates that δ can be estimated as 0.9ϕ . Bell (7) suggests $2/3 \phi$ for soil-fabric friction. For the purposes of this investigation, it is assumed that δ is equal to $2/3 \phi$ in all cases.

Chang (2) has found from pull tests made on steel strips following the construction of a reinforced soil wall in California, that for strips less than 3.1 m (10 ft.) in length, the peak force necessary to remove the tie is sometimes actually less than would be predicted theoretically. In view of this fact, he suggests that the length for steel strips be no less than 3.1 m (10 ft.) in walls 3.1 m (10 ft.) or less in height.

In addition, Vidal and Schlosser (3) have suggested that a horizontal shear failure within the wall can be prevented if the ratio $L:H$ (where L is the total length of the reinforcement strip and H is the wall height) is no less than 1:3 for backfill material with $\phi = 30^\circ$.

The authors believe that these are reasonable requirements, based on available knowledge. Therefore, the length of strip reinforcement in walls is restricted to no less than 3.1 m (10 ft.), and the length of strip or sheet reinforcement will be no less than one-third of the wall height.

Factors of Safety

Selection of reasonable and accurate factors of safety in the design of any earth retaining structure is a significant process. Over conservative estimates can lead to safe but costly designs. Design of reinforced soil is by approximate methods, and many suggested factors of safety can be found in the literature, with several methods of applying them (1,2,9,11). The factors of safety believed to be appropriate for this paper are the following.

The factor of safety with respect to reinforcement rupture is 2.0, and is applied using the allowable stress of the reinforcement material. This is believed to be appropriate because of the various types of reinforcement materials currently being introduced. These materials can exhibit significantly different strains and creep susceptibilities at given fractions of their ultimate stress. A factor of safety of 2.0 with respect to tie pullout has been proposed by Schlosser and Long (11) and is considered acceptable in this investigation. Schlosser (17) also suggests a factor of safety of 1.5 against sliding of the reinforced soil mass, and this will also be used in this investigation.

DESIGN OF REINFORCED SOIL WALLS

Three possible analysis techniques are discussed: the tie back model, as outlined by Lee (1); the Coulomb analysis outlined by Vidal and Schlosser (3); and the standard analysis described by Schlosser and Long (11) and Hausmann (12). An appropriate model for the design of low reinforced soil walls for low standard roads is developed. The development of the design equations and a detailed description of the design procedure used is found following the "Conclusions" and "Recommendations" sections at the end of the paper.

Analysis Techniques Available

Tie Back Model

In the tie back model, illustrated in Figure 3, Lee (1) assumes that a failure surface inclined at an angle of $\theta = 45^\circ + \phi/2$ from the horizontal at the base of the wall develops behind the wall. The tensile force which must be resisted by any tie is found by examining the pressure distribution at the wall face and summing that distribution over the area of influence of the tie. Only that portion of the tie behind the failure surface is assumed to contribute friction which resists the tensile force developed at the face of the wall. This method of analysis is quite popular and has been used in the design of walls continuously reinforced with fabrics in the Pacific Northwest (7,8,9).

Lee (1) did not discuss the incorporation of non-uniform surcharges into the analysis. The authors assume that this would be done by determining the horizontal pressure distribution due to the live load and adding that to the horizontal pressure distribution resulting from the soil only.

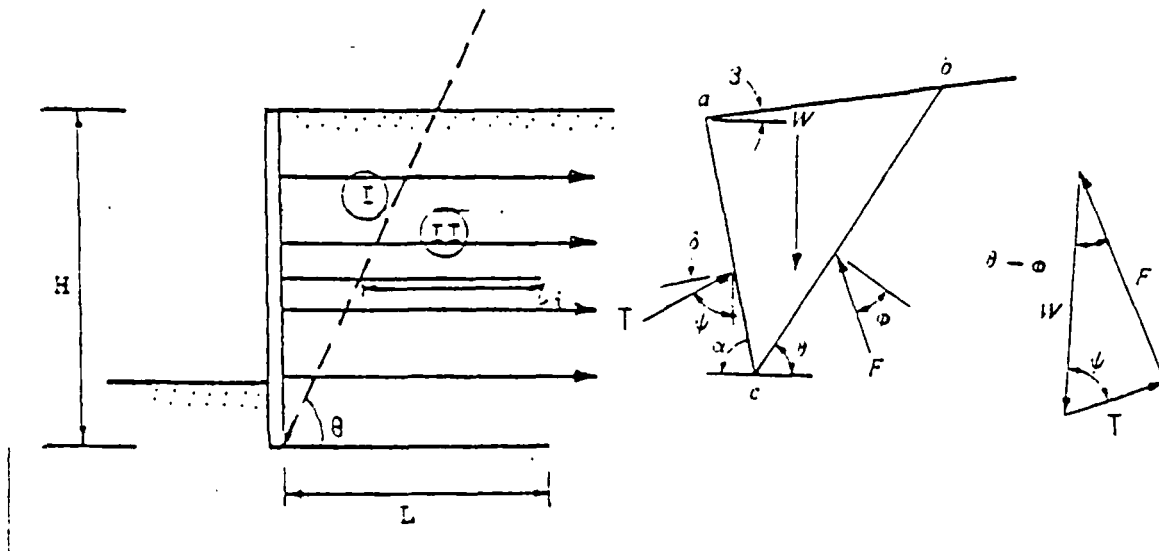


FIGURE 3 - Tieback and Coulomb Models for Reinforced Soil Walls

Coulomb Method

The Coulomb method of analysis is also shown in Figure 3 and is basically the determination of the total tensile force "T" which must be developed at the failure wedge to resist a sliding failure. The analysis is performed using the graphical procedure given by Culmann (14). Use of this procedure easily allows the incorporation of line loading into the analysis.

Vidal and Schlosser (3) have suggested that this total tensile force is distributed in a triangular fashion with the lowest reinforcements most heavily loaded. If "i" is the level of the reinforcements, then:

$$T_i = \frac{2i}{N(N+1)} T \quad \{1\}$$

where: T_i = the tensile force in the "i"th layer
 i = the level of the reinforcement ($i=1$ for highest reinforcement level)
 N = total number of reinforcement levels
 T = total tensile force, determined from Coulomb Analysis

Standard Analysis (Reinforced Earth)

The standard analysis technique used by the Reinforced Earth Company in the design of strip reinforcements has been described in the literature (11, 12). In this method, the lateral pressure on the wall is assumed to be the vertical pressure multiplied by an appropriate coefficient of lateral earth pressure. The vertical pressures may include live loads and may be increased to account for overturning moment. In determining the value of embedment necessary to resist pullout, the entire length of the strip is used.

Application of Live Loadings

For design purposes, the non-uniform surcharges represented by the equivalent line loadings can be handled in a variety of ways. Hausmann (12) discusses some of the possible methods of handling non-uniform surcharges due to line, point or rectangular surcharges. Note that in all cases, while the horizontal pressure against the wall will increase and tends to cause pullout, there is a corresponding increase in vertical stress, which increases pullout resistance.

Stress increases computed by elastic theory (Boussinesq equations) can be used directly and the total increase in horizontal or vertical stress can be found by directly integrating the appropriate stress distribution, as illustrated in Figure 4b. Schlosser and Long (11) suggest a simplified procedure to estimate the increase in vertical stress, illustrated in Figure 4c. The horizontal stress increase at any level is simply the vertical stress increase multiplied by the appropriate coefficient of earth pressure.

Although the computations are more time-consuming, this investigation will use the stress distributions calculated by Boussinesq Theory and integrated over the appropriate intervals. This is preferred over the approximate method proposed by Schlosser and Long (11), because the horizontal pressure increases given by Schlosser do not appear to adequately represent the conditions in the top three or four feet of the wall, and because the equivalent line loads were developed using Boussinesq theory, making it more consistent to use the Boussinesq stress distributions in the determination of horizontal and vertical stresses within the reinforced soil structure.

Design for External Stability

Researchers (3,8,17) have identified several modes of failure for the entire reinforced earth mass acting as a single unit. These have included

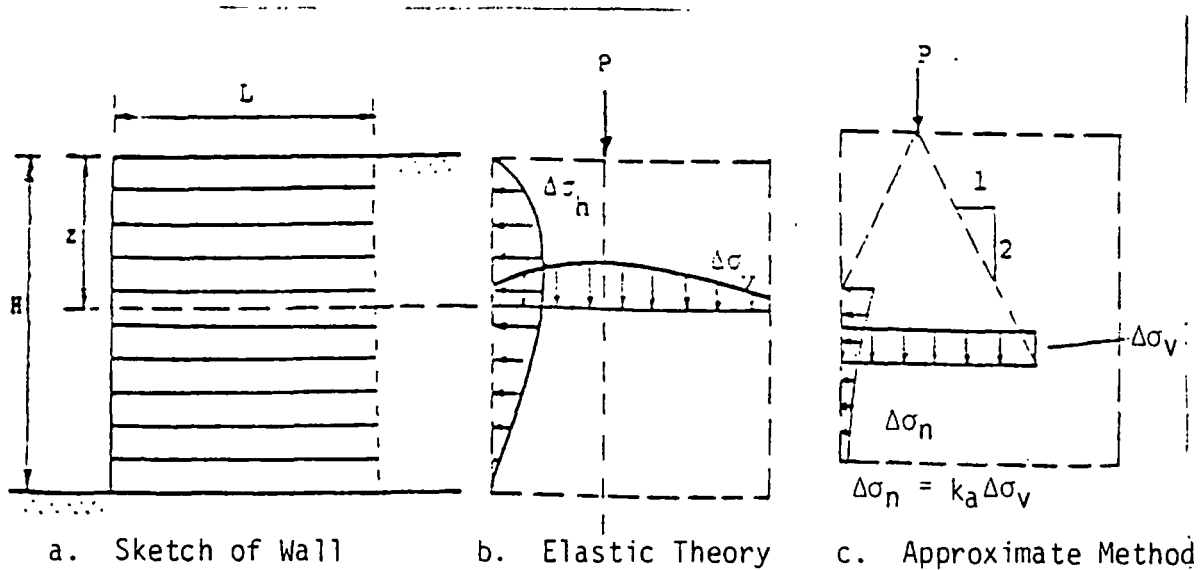


FIGURE 4 - Methods for Incorporating Non-Uniform Surcharges into the Analysis of Reinforced Soil Walls (12)

bearing capacity, sliding at the base of the structure, overturning and general stability of the slope on which the wall is placed. It is assumed that the bearing capacity and the slopes are adequate to support the wall. Also, for the walls considered, failure by overturning of the entire mass is unlikely. Consequently, in the present study, only the investigation of resistance to sliding is investigated. The determination of a factor of safety against sliding will parallel the calculations performed for a gravity retaining structure. The reinforced soil mass will be assumed rigid and will extend the full length of the reinforcements.

Since all strip reinforcements will be a minimum of 3.1 m (10 ft.) long, the live loads will lie within the reinforced soil mass and their loads will be assumed to assist in providing sliding resistance. For sheet reinforcements, each case will be examined individually. The pressure distribution at the rear of the wall will be assumed to be hydrostatic and the material will be assumed to have properties identical to the backfill material within the reinforced soil mass.

Evaluation of Available Techniques

It was first assumed that the tie back model would be a reasonable one for comparing strip and sheet reinforcements for low walls with heavy live loadings close to the wall edge. As previously mentioned, this design has

been successfully used in the construction of several fabric retaining walls in the Pacific Northwest (7,8,9). However, an initial design incorporating conventional metal strips, 60 mm wide and 3 mm thick (2.36 in. by 0.12 in.) spaced 0.30 m (1 ft.) vertically and 0.90 m (3 ft.) horizontally yielded rather startling embedment lengths when used in the design of a 3.2 m (10.5 ft.) wall. Using design parameters as discussed in the previous section, the necessary embedment lengths were nearly 20 m (65.6 ft.) at the top of the wall.

Clearly, this embedment length is excessive and is inconsistent with experience with successful walls. Assuming that only the length of embedment extending past the failure plane contributes to pullout resistance is conservative when the live loads are included in the design and probably contributed to this inconsistency. In this respect, the standard design method appeared most promising in providing for a pullout due to the total pressure on the wall. However, the standard method did not specifically consider internal failure of the reinforced soil mass.

The Coulomb method was also considered; however, the major question was the allocation of the total tension force among the available levels of reinforcement. As previously mentioned, Vidal and Schlosser (3) have suggested proportioning this force assuming that the force against the wall is triangular in nature. This is a reasonable assumption for walls experiencing only soil loading. With the application of heavy live loadings, the problem becomes more complicated.

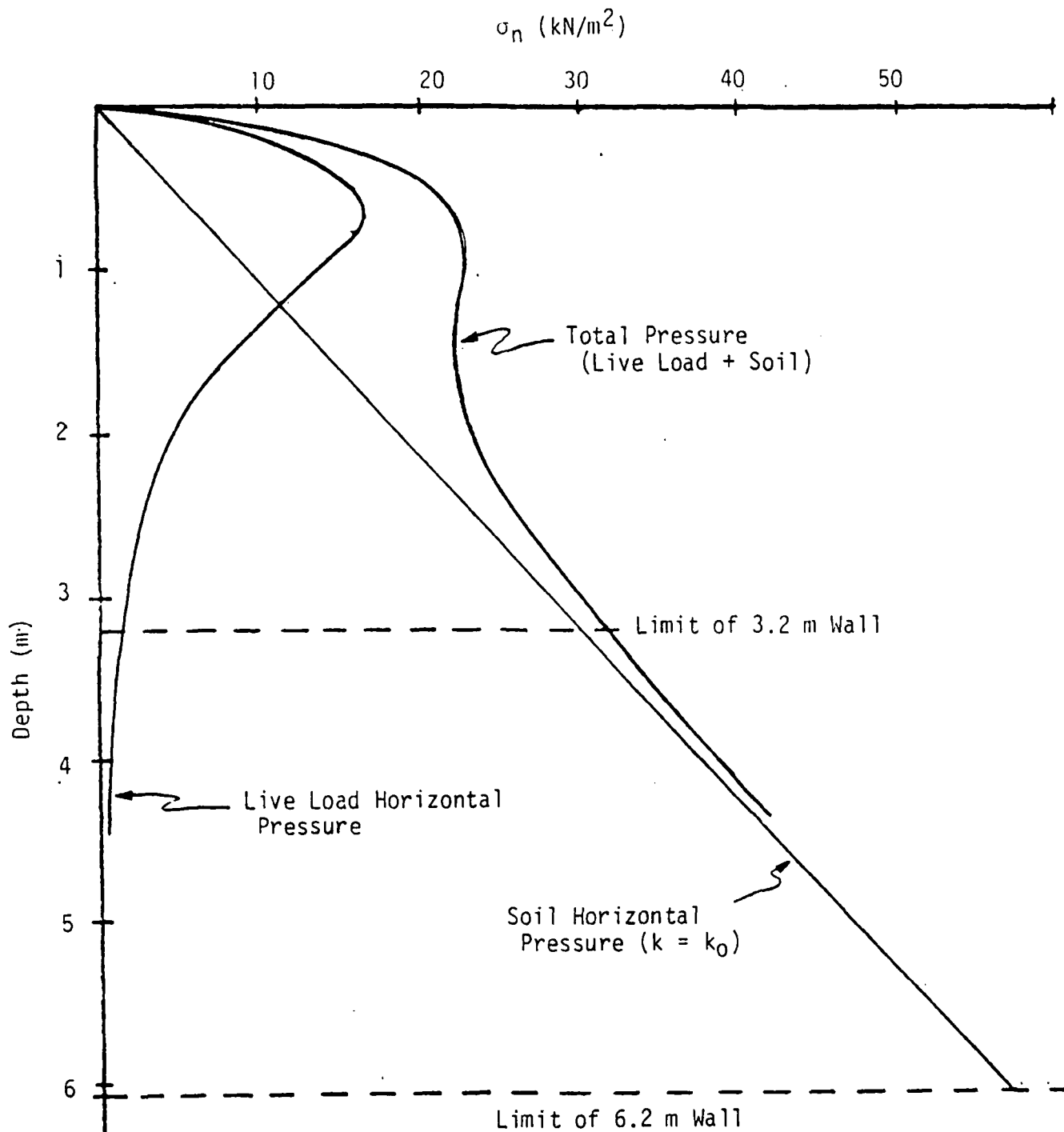
Figure 5 shows the horizontal loads against the wall for soil loading, live loadings, and the total of the two. The plot shown for the total pressure illustrates the problem with assuming a triangular pressure distribution. This plot is almost rectangular for low (3.2 m) walls.

None of the methods appeared satisfactory by itself, but each has desirable features. These features are incorporated into a recommended analysis technique, described in the following section.

Recommended Analysis Technique

The design of reinforced soil walls is a rather complicated task with a multitude of choices available to the designer. Basically, however, the design of a wall is the process of providing a reinforcement material which has adequate strength, and embedding it in a sufficient amount of soil so that it resists the tensile force developed because of horizontal pressures placed against the wall face.

The recommended analysis technique is a composite of the three previously mentioned design techniques. Three different cases are considered, which represent possible internal failure modes. The cases are described. The wall is also tested for stability against sliding.



Note: 1 m = 3.3 ft
1 kN/m² = 20.9 psf

FIGURE 5 - Horizontal Pressure Distributions as a Function of Depth

Loaded Design - Case I

In Case I, the wall is investigated with the live loading included. The reinforcement is subjected to tensile forces resulting from the horizontal pressure due to both the soil loads and the live loads. The horizontal live loads are determined through integration of the Boussinesq equation.

The tensile forces in the reinforcement are resisted by soil-reinforcement friction developed over the entire length of the reinforcement. The normal forces acting on the reinforcement include both the soil above the level of reinforcement and the live loadings at the ground surface. The live load vertical force on the reinforcement is determined through integration of the Boussinesq equation.

Unloaded Design - Case II

In Case II, the wall is investigated without the live loadings. The horizontal tensile forces in the reinforcement result from the soil loads at the wall face. The length of reinforcement which is considered effective in resisting pullout is that extending behind an assumed failure surface which develops at the base of the wall. Friction is developed along the reinforcement due to the normal forces from the soil weight above the level of reinforcement.

Coulomb Method - Case III

Case III is an investigation of the development of a failure surface in the soil mass behind the wall, as determined by the Coulomb Analysis, with both soil and live loads acting. The Coulomb analysis of the loaded wall is performed and a total tensile force is determined. However, because of the nearly rectangular distribution of the total pressure with depth (Figure 5), it is assumed that the total force is uniformly distributed among the levels of reinforcement. This assumption appears quite reasonable for low walls. For higher walls, perhaps the distribution is more triangular. Care should be exercised to assume a distribution which does not result in underdesigning the upper levels of reinforcement for pullout failure. The effective length of embedment which resists pullout is assumed to be that extending behind the failure surface.

RESULTS OF EXAMPLE DESIGNS

Using the procedure outlined in the previous section, one wall utilizing strip reinforcement and one with sheet reinforcement was designed for heights of 3.1 m (10 ft.) and 6.2 m (20 ft.). Sketches of the wall designs are given in Figures 7 and 8. Each figure shows the vertical spacing and reinforcement lengths to scale and tabulates the required reinforcement strength, f_s . The value, f_s , does not represent the stress which the reinforcement will experience at each level, but represents the strength required at the most highly stressed level. It is assumed that the same material will be used in the construction of the wall. For the strip reinforcement, the ratio of strip width, b , to horizontal strip spacing, ΔB , is also tabulated.

DISCUSSION OF RESULTS

The results of the designs for each wall are briefly discussed in this section. Controlling factors for the values of $b/\Delta B$ for strip reinforcement and ΔH for sheet reinforcement are presented, and important results are highlighted.

Walls 3.1 m (10 ft.) High

Strip Reinforcement

The required length of embedment is controlled by the recommendation that the length of strip reinforcement be no less than 3.1 m (10 ft.). At the top of the wall, $b/\Delta B$ is controlled by the Coulomb analysis (Case III) for tie pullout. From 0.46 m (1.5 ft.) to 2.0 m (6.5 ft.), Case II (the unloaded condition) controls. Finally, from 2.3 m (7.5 ft.) to 3.2 m (10.5 ft.), the reinforcement strength, f_s , controls $b/\Delta B$.

Sheet Reinforcement

The sheet reinforcement actually required a somewhat longer amount of embedment, 3.2 m (10.25 ft.), in order to meet the unloaded condition, Case II, which controlled the design of the top-most reinforcement. The value of ΔH is rather large at 1.07 m (3.5 ft.) but the required allowable stress, f_s , is almost 33% less than that required for the strip reinforcement.

Discussion

The designs shown represent only one of the many possible for both types of reinforcement. The controlling factor for the strip reinforcement length is the 3.1 m (10 ft.) minimum length recommendation reported in the literature, and developed from pullout tests performed on relatively narrow strips. The $b/\Delta B$ ratios necessary for the internal stability of the wall are much greater than common values reported in the literature, and consequently, it is uncertain whether this modification of $b/\Delta B$ (increasing the width or decreasing the spacing or both) would have some effect in modifying the 3.1 m (10 ft.) minimum length requirement.

During the design of the sheet reinforcement in the unloaded design (Case III), it was necessary to make a choice which affected the minimum reinforcement length requirement. The authors chose to lengthen the reinforcement, rather than decrease the vertical spacing in an attempt to conserve reinforcement material. If embedment length was extremely critical, then ΔH could be reduced to reduce the embedment length required. However, under no circumstances could the total sheet reinforcement length have been less than 2.3 m (7.4 ft.). At this length, ΔH would have been 0.61 m (2 ft.) instead of 1.1 m (3.5 ft.).

Walls 6.2 m (20 ft.) High

Strip Reinforcement

The embedment length is controlled in this case by the external stability due to sliding and 4.3 m (14 ft.) is necessary. To accommodate this minimum length requires a significantly large value of $b/\Delta B$ in the top levels of reinforcement. The levels from 0.15 m to 1.4 m (0.5 ft. to 4.5 ft.) are controlled by the Coulomb Analysis (Case III) for tie pullout. In the midpart of the wall, from depths 1.7 m to 4.1 m (5.5 ft. to 13.5 ft.), the $b/\Delta B$ ratio is controlled by the unloaded design (Case II). The final 1.8 m (6 ft.) from 4.4 m to 6.3 m (13.5 ft. to 20.5 ft.) is controlled by the strength of the reinforcement, f_s .

Sheet Reinforcement

In this case, the embedment length for sheet reinforcement is also controlled by sliding and is equal to that for the strips. The total number of reinforcement levels is controlled by the Coulomb Analysis (Case III) for reinforcement pullout. The required strength of material, f_s , is significantly less than with the strip reinforcement.

Discussion

The 6.2 m (20 ft.) wall designs shown represent only two of the many possible. However, both designs represent the minimum reinforcement lengths which can be achieved using the soil properties and design parameters, as shown in Table 1. In both cases, the embedment length is controlled by the external stability necessary to resist sliding.

The Coulomb method of analysis, Case III, becomes very important in the design of the topmost levels of reinforcement in walls higher than 3.1 m (10 ft.) and its effect becomes greater as the height of wall becomes greater. As the wall height increases, the total tensile force as determined by the Coulomb analysis increases and the assumption regarding the allocation of this force becomes more and more important. If a uniform distribution is assumed, then this portion of the analysis (Case III) becomes the overriding consideration in the top levels of reinforcement.

Because of the importance of this assumption and its effect on design, the authors suggest that an important modification to the procedure proposed in this paper would be the allocation of total tensile force based on a trial and error procedure of moment calculation, using all the forces involved.

General Discussion of Example Walls

The designs shown are only four of the many which could have been developed using the same soil properties and design parameters. The values of f_s , ΔB , ΔH , and L can all be varied by the designer to meet the requirements of a specific application. Situations may exist in which any one or combination of the

following factors may be most important: the amount or availability of reinforcement material, strength of the reinforcement material, amount of excavation, quantity of backfill material, or quality of backfill material.

The particular designs in this paper were developed on the basis of limiting reinforcement embedment length and thereby minimizing the excavation and backfill quantities. Three of the four designs represent the minimum possible reinforcement lengths possible for the soil properties and design parameters assumed.

One of the major difficulties encountered in the design of reinforced soil walls is the achievement of a reasonable, balanced, economical design. Theoretically, a more balanced design is possible by specifying different values of f_s , ΔB , b and L at each level of reinforcement. This would not appear economical from the standpoint of construction, however.

CONCLUSIONS

As a result of the initial investigation for low retaining walls with high live loads, where minimizing the length of embedment is of primary importance, the following preliminary conclusions can be drawn.

- (1) Low reinforced soil retaining structures subjected to significant non-uniform live loads appear outside the realm of past experience in presently used design methods for reinforced soil walls, as reported in the literature.
- (2) Most design methods imply that the effect of live loads is usually small or is considered "offsetting" (i.e. the increased horizontal pressure is offset by increased vertical pressure on the reinforcement.) This may be true for continuous reinforcement or relatively wide reinforcement strips spaced closely together. However, for widely spaced, narrow strips, the increased vertical pressure does not assist significantly in resisting the increased horizontal pressure.
- (3) With heavy truck traffic, the live loads on walls designed for low standard roads are indeed extremely important in the design of the top 3.1 m (10 ft.), and are critically important in the top 1.5 m (5 ft.).
- (4) A coherent design technique with reasonable design parameters for situations involving significant live loading, such as that discussed in this paper, is lacking in the literature.
- (5) There is disagreement in the literature relative to earth pressure distributions, lateral earth pressure coefficients, and soil-reinforcement friction appropriate for wall designs.

(6) Low retaining walls utilizing strip reinforcement and rather short embedment lengths can be successfully designed. However, significantly wider strips than values reported in the literature are required.

(7) The apparent advantage of shorter embedment lengths for sheet reinforcements does not appear to be significantly great. However, much weaker materials can be utilized in the construction of walls using sheet reinforcement than in walls using strip reinforcement, resulting in more nearly balanced designs.

RECOMMENDATIONS

Research is needed to define the failure mechanisms and to further develop and validate a coherent design technique for low reinforced soil walls with heavy live loads.

DEVELOPMENT OF DESIGN EQUATIONS

Equations which simplify the design process and yet allow sufficient latitude to the designer in the choice of soil parameters and reinforcement materials are developed in the following sections. The notation common to all of the wall designs is illustrated in Figure 6.

Strip Reinforcement

The development of design equations for strip reinforcement for Cases I, II and III follows.

Case I

For a unit length of wall:

$$T' = \left[\int_{d_1}^{d_2} \sigma_h + \left\{ 1/2 (d_1 + d_2) \gamma K \right\} \Delta H \right] \quad (2)$$

where: d_1, d_2 = the upper and lower limits of the influence of reinforcement
 $\int \sigma_h$ = the integral of the horizontal live load pressure distribution
 γ = the unit weight of the soil
 K = an appropriate value for coefficient of lateral earth pressure.

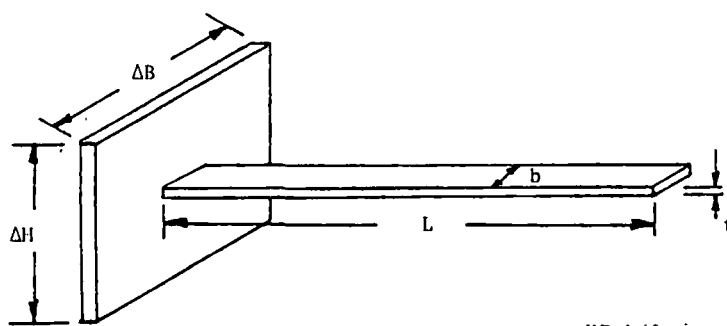
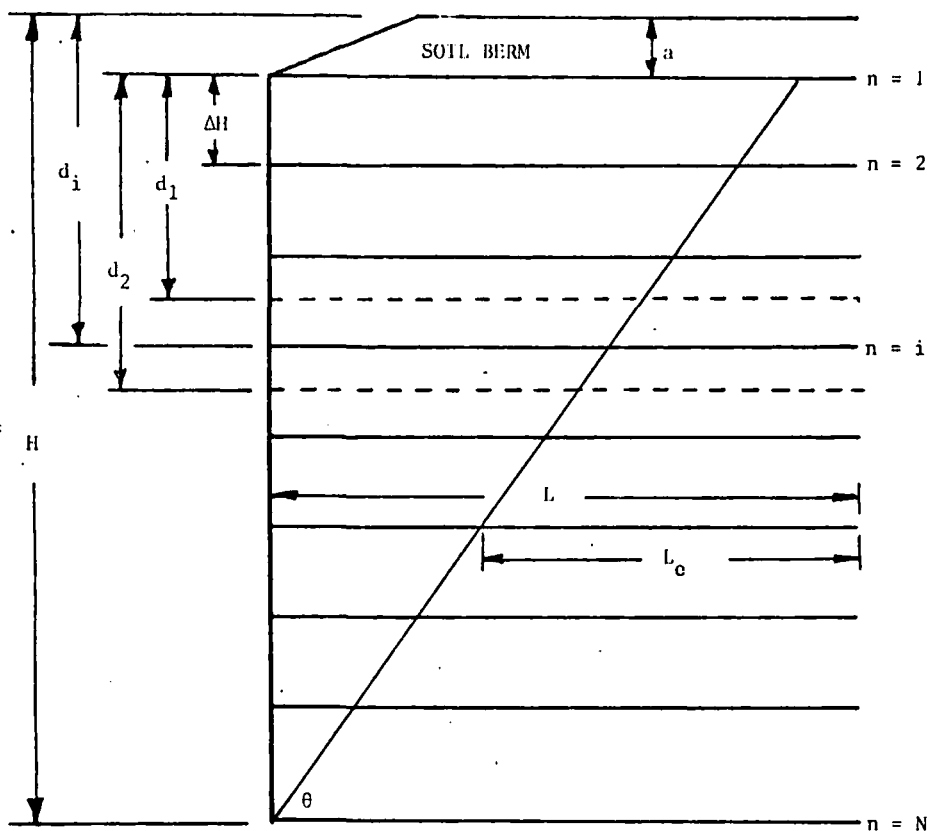


FIGURE 6 - Common Notation for Reinforced Soil Walls Utilizing Strip and Sheet Reinforcement

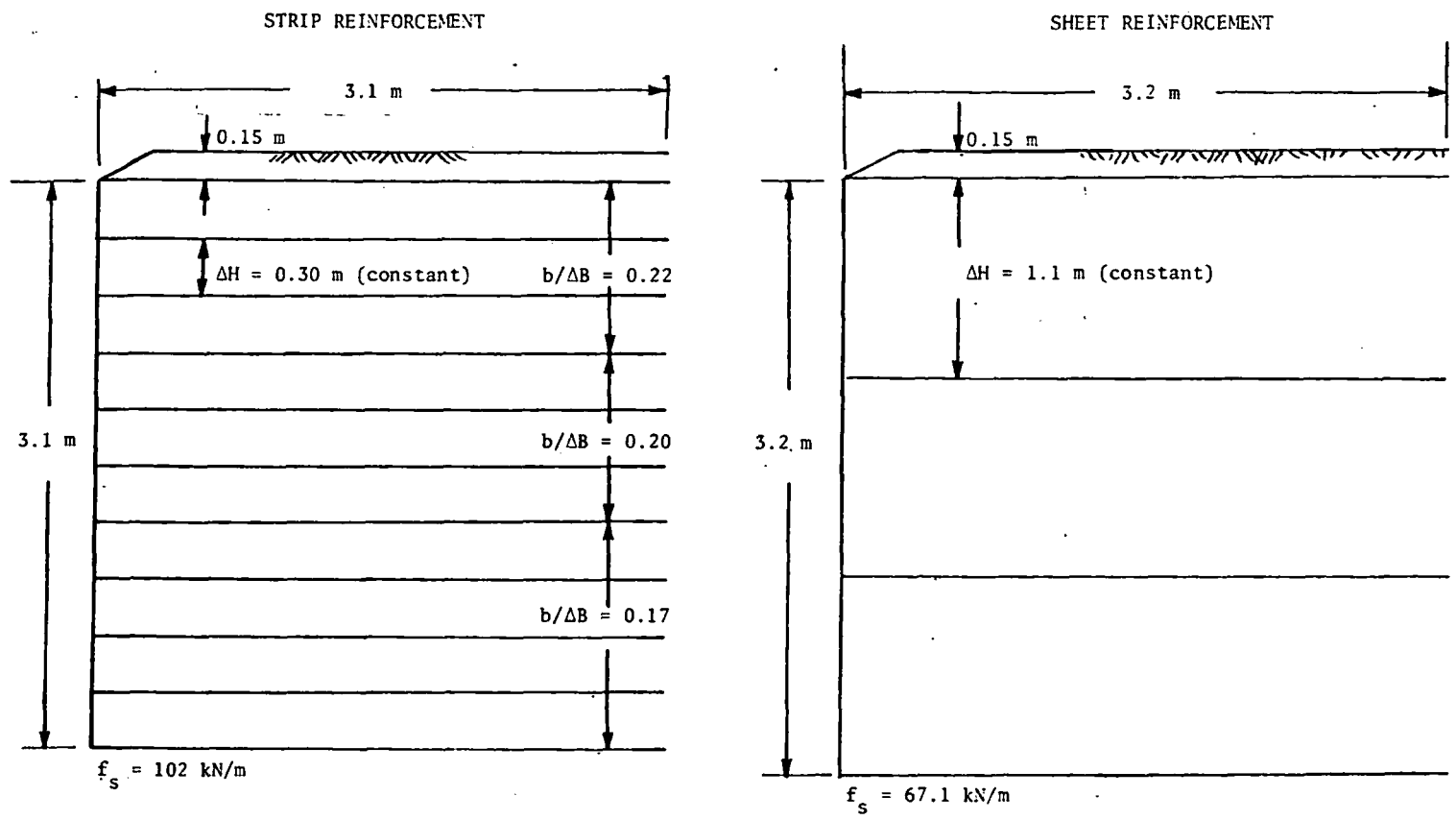
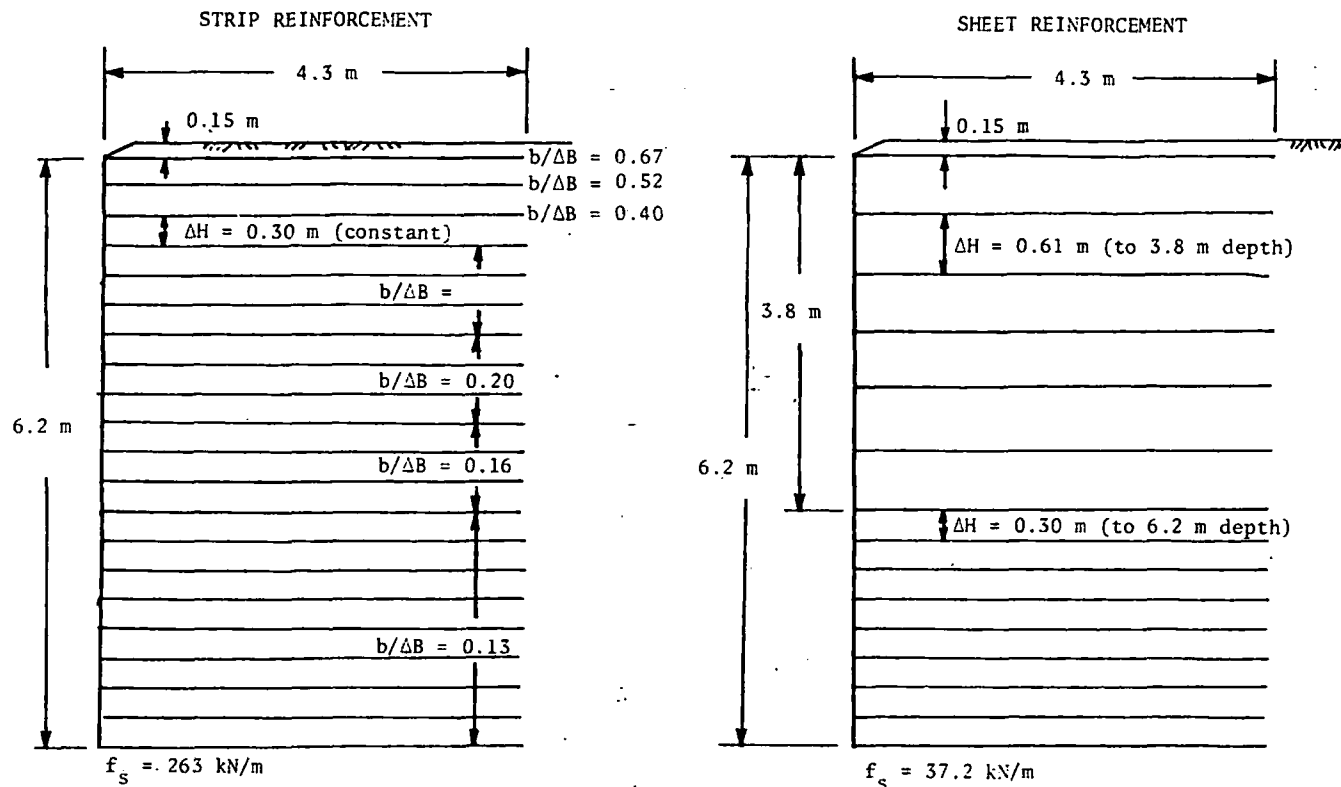


FIGURE 7 - Final Wall Configurations for 3.1 m (10 ft.) Walls Utilizing Sheet and Strip Reinforcement



NOTE: 1 m = 3.3 ft.
 1 kN/m = 68.5 lb.ft.

FIGURE 8 - Final Wall Configurations for 6.2 m Walls Utilizing Strip and Sheet Reinforcement

Analysis Techniques for Low Reinforced Soil Retaining Walls
 and Comparison of Strip and Sheet Reinforcements
 By William Whitcomb and J.R. Bell
 Page 21

If the strip reinforcements are spaced horizontally some distance, ΔB , apart, then the total horizontal force applied to one reinforcement strip, F_h , is:

$$F_h = T' \Delta B \quad \{3\}$$

The value of F_h is limited both by the strength of the reinforcement material and by the pullout resistance which can be mobilized by the strip reinforcement.

If f_s is the allowable stress in the reinforcement, expressed in terms of some value of force per unit of strip width, then the thickness of the reinforcement, t , can be eliminated from consideration in any design equations and is implicit in the designation of f_s .

With the application of an appropriate factor of safety against reinforcement rupture, FS_{RR} , then:

$$F_h \leq \frac{f_s b}{FS_{RR}} \quad \{4\}$$

Substituting from Equation {3} :

$$T' \Delta B \leq \frac{f_s b}{FS_{RR}} \quad \{5\}$$

$$T' \leq \frac{f_s}{FS_{RR}} \frac{b}{\Delta B} \quad \{6\}$$

The limitation of F_h due to embedment requirements can be expressed in the following manner:

$$F_h \leq 2 b \left[\int_0^L \sigma_{vd} + \gamma d L \right] \tan \delta \quad \{7\}$$

where: $\int_0^L \sigma_{vd}$ = the integral of the live load vertical pressure distribution on the strip between the wall face and the distance L from the wall face at depth d .

δ = the angle of friction between the soil and the reinforcement.

If:

$$L_f = \left(\int_0^L \sigma_{vd} + \gamma d L \right) \tan \delta \quad \{8\}$$

Then:

$$F_h \leq 2 b L_f \quad \{9\}$$

Recall:

$$F_h = T' \Delta B$$

Therefore:

$$T' \leq \frac{2 b}{\Delta B} L_f \quad \{10\}$$

If an appropriate factor of safety for pullout resistance, FS_{PR} , is applied, then:

$$T' \leq \frac{2}{FS_{PR}} \frac{b}{\Delta B} L_f \quad \{11\}$$

Note that $b/\Delta B$ can also be expressed as a function of the parameters given previously. From Equations {6} and {11} :

$$b/\Delta B \geq \frac{T' (FS_{RR})}{f_s} \quad \{12\}$$

$$b/\Delta B \geq \frac{T' (FS_{PR})}{2 L_f} \quad \{13\}$$

Case II

For Case II, the live loads are not taken into account and the equations are much simpler. If the case of pullout is investigated, the horizontal force, F_h , acting on one reinforcement strip, can be written as:

$$F_h = \gamma (d - a) K \Delta H \Delta B \quad \{14\}$$

This is resisted in pullout by the force F_{p0} , where:

$$F_{p0} = 2 b (\gamma d L_e) \tan \delta \quad \{15\}$$

Analysis Techniques for Low Reinforced Soil Retaining Walls
 and Comparison of Strip and Sheet Reinforcements
 By William Whitcomb and J.R. Bell
 Page 23

The factor of safety against pullout must be less than the ratio of Equations {14} and {15} :

$$FS_{PR} \leq \frac{2 b (\gamma d L_e) \tan \delta}{\gamma (d - a) K \Delta H \Delta B} \quad \{16\}$$

Therefore:

$$b/\Delta B \geq \frac{(d - a) K \Delta H}{d L_e \tan \delta} \times \frac{FS_{PR}}{2} \quad \{17\}$$

Tie-breaking does not have to be considered in Case II because any configuration of reinforcement which is sufficient to withstand the horizontal forces due to both line loads and soil loads is sufficient for soil loads only.

Case III

The development of equations for Case III is very similar to that for Cases I and II. In Case III, the horizontal force acting on any reinforcement strip is:

$$F_h = \frac{T}{N} \Delta B \quad \{18\}$$

where: T = the total tensile force, as determined by the Coulomb analysis
 N = the total number of levels of reinforcement

At certain reinforcement levels, the tensile force, F_h , calculated from Equation {18} may be greater than that calculated from the Case I analysis and determined in Equation {3}. Consequently, the adequacy of the reinforcement material strength must be rechecked using the following equations:

$$F_h \leq \frac{f_s b}{FS_{RR}} \quad \{19\}$$

$$\frac{T \Delta B}{N} \leq \frac{f_s b}{FS_{RR}} \quad \{20\}$$

$$b/\Delta B \geq \frac{T}{N} \frac{FS_{RR}}{f_s} \quad \{21\}$$

In addition, the horizontal force, F_h , is resisted by a shear force developed along both sides of the strip, extending past the failure plane. If the force resisting pullout is termed F'_{p0} , then:

$$F'_{p0} = 2 b \left[\begin{array}{c} L_2 \\ f \\ L_1 \end{array} \sigma_{vd} + \gamma d L_e \right] \tan \delta \quad \{22\}$$

where: L_1 = the distance from the wall to the failure plane at depth "d"
 L_2 = the total length of the reinforcement strip
 $L_e = L_2 - L_1$ = the effective length of the reinforcement behind the failure plane.

If the factor of safety against pullout is termed FS_{PR} , then:

$$FS_{PR} \leq \frac{2 b \left[\begin{array}{c} L_2 \\ f \\ L_1 \end{array} \sigma_{vd} + \gamma d L_e \right] \tan \delta}{\frac{T}{N} \Delta B} \quad \{23\}$$

and if:

$$L_{ef} = \left[\begin{array}{c} L_2 \\ f \\ L_1 \end{array} \sigma_{vd} + \gamma d L_e \right] \tan \delta$$

then:

$$b/\Delta B \geq \frac{FS_{PR} T/N}{2 L_{ef}} \quad \{24\}$$

Sheet Reinforcement

The development of equations for determining the functional relationship of the design parameters proceeds in a manner similar to that for strip reinforcement. This development is not necessary, however, if one recognizes the fact that $b/\Delta B$ is one for sheet reinforcement. Using Equations {12}, {13}, {17}, {21}, and {24} and setting $b/\Delta B$ equal to one yields the following equations for sheet reinforcement.

Case I

$$\text{Reinforcement Rupture:} \quad 1 \geq \frac{T' (FS_{RR})}{f_s} \quad \{25\}$$

$$\text{Reinforcement Pullout:} \quad 1 \geq \frac{T' (FS_{PR})}{2 L_f} \quad \{26\}$$

Case II

$$\text{Reinforcement Pullout:} \quad 1 \geq \left(\frac{d - a}{d} \right) \left(\frac{K \Delta H}{L_e \tan \delta} \right) \left(\frac{FS_{PR}}{2} \right) \quad \{27\}$$

Case III

$$\text{Reinforcement Rupture:} \quad 1 \geq \frac{T}{N} \frac{FS_{RR}}{f_s} \quad \{28\}$$

$$\text{Reinforcement Pullout:} \quad 1 \geq \frac{FS_{PR} T/N}{2 L_{ef}} \quad \{29\}$$

DESIGN PROCEDURE FOR EXAMPLE WALLS

The parameters used in the design of the example reinforced soil walls in this paper are given in Table 1. In addition, the thickness of the soil berm above the top of the wall (Figure 6) is assumed to be 0.15 m (6 in.), the value of f_s is assumed to be constant for all reinforcement layers, and ΔH for the strip reinforcements is assumed constant at 0.30 m (1 ft.).

The limitation of embedment length was considered one of the most important factors in design and therefore, minimization of the reinforcement embedment length was achieved in all but one of the designs presented. Minimization of reinforcement material was achieved in the 3.1 m (10 ft.) wall, using sheet reinforcement.

Calculator programs were developed which evaluated T' (Equation {2}) for any one line load located at any distance from the wall face between any values of d_1 and d_2 . Calculator programs were also developed to evaluate L_f (Equation {8}) at any depth for two line loads located any distance from the wall. In addition, the program determined L_{ef} for any L_1 , L_2 and d .

The design procedure included the following steps:

(1) The length of embedment for both strip and sheet reinforcement was minimized based on the requirements for external wall stability (sliding resistance).

(2) A range of L_f values was determined for the depths encountered in the problem (See Equation {8}).

(3) For strip reinforcement, ΔH was fixed; therefore, T' was known at various depths. By using T' values and L_f values at similar depths, a range of $b/\Delta B$ values were determined, using Equation {13}. For sheet reinforcement, knowing that $2 L_f \geq T' F_{SPR}$, reasonable values of ΔH were determined, using Equation {26}.

(4) The necessary value of f_s was determined by use of Equation {6}.

(5) For sheet reinforcement, the values of ΔH and f_s were then adjusted until a reasonably balanced design was determined. For strip reinforcement, the values of $b/\Delta B$ and f_s were adjusted.

(6) The unloaded condition (Case II) was then checked using Equations {17} and {27} for strip and sheet reinforcement, respectively. The failure surface used was assumed to be inclined at an angle of $45^\circ + \phi/2$ at the base of the wall.

(7) A Coulomb analysis was performed using the Culmann graphical procedure and "T" was determined. Case III was then investigated using Equations {21} and {24} for strip reinforcement, and {28} and {29} for sheet reinforcement.

(8) A final design which met all criteria was selected.

REFERENCES

1. Lee, K.L., Adams, B.D. and Vagneron, J.M.J., "Reinforced Earth Retaining Walls," Journal of the Soil Mechanics and Foundation Engineering Division, ASCE, SM10, October 1973, pp. 745-764.
2. Chang, Jerry C. Earthwork Reinforcement Techniques, Final Report CA-DOT-TL-2115-9-74-37, California Department of Transportation, October 1974.

Analysis Techniques for Low Reinforced Soil Retaining Walls
and Comparison of Strip and Sheet Reinforcements
By William Whitcomb and J.R. Bell
Page 27

3. Vidal, H. and Schlosser, F., "Reinforced Earth," English Translation of "La Terre Armee," Bulletin de Liaison des Laboratoires Routiers - Ponts et Chaussees, No. 41, November 1969.
4. Vidal, H., "The Principle of Reinforced Earth," Highway Research Record, No. 282, 1969, pp. 1-16.
5. Vidal, H., "Reinforced Earth," (French) Annalis de l'Institute Technique du Batiment et des Travaux Publics, Paris France, Nos. 223-229, July-August, 1966, pp. 888-938.
6. Vidal, H., "Reinforced Earth Steel Retaining Wall," Civil Engineering, ASCE, Volume 40, No. 2, February 1970, pp. 72-73.
7. Bell, J.R., Stilley, A.N., Vandre, B., "Fabric Retained Earth Walls," Proceedings, 13th Annual Engineering Geology and Soils Engineering Symposium, Moscow, Idaho, 1975.
8. Steward, J.E., Williamson, R., Mohney, J., Chapter 5, "Earth Reinforcement," Guidelines for Use of Fabrics in Construction and Maintenance of Low Volume Roads, U.S. Forest Service, Portland, Oregon, June, 1977.
9. Bell, J.R., Steward, J.E., "Construction and Observations of Fabric Retained Soil Walls," Proceedings, International Conference on the Use of Fabrics in Geotechnics, Ecole Nationale Des Ponts et Chaussees, Paris, Volume I, April 1977, pp. 123-128.
10. Greenway, D.R., Vandre, B.C., "Chain-Link Retaining Walls," Presented at the 17th Annual Engineering Geology and Soils Engineering Symposium, Moscow, Idaho, April 1979.
11. Schlosser, F., Long, N.T., "Recent Results in French Research on Reinforced Earth," Journal of the Construction Division, ASCE, Volume 100, No. C03, September 1974, pp. 223-237.
12. Hausmann, M.R., "Behavior and Analysis of Reinforced Soil," thesis in partial fulfillment of degree of Doctor of Philosophy, New South Wales Institute of Technology, Australia, Draft Copy.
13. Spangler, M.G., Handy, R.L., Soil Engineering, Third Edition, Intex Education Publishers, 1973, pp. 566-572.
14. Wu, T.H., Soil Mechanics, Second Edition, Allyn and Bacon, Inc., 1976, pp. 136-137.

Analysis Techniques for Low Reinforced Soil Retaining Walls
and Comparison of Strip and Sheet Reinforcements
By William Whitcomb and J.R. Bell
Page 28

15. Schlosser, F., Long, N.T., "Fonctionnement et Comportement de la Terre Armee," DOTA, 1975, pp. 47-62.
16. Chang, J.C., Harmon, J.B., Forsyth, R.A., "Pull Resistance and Interaction of Earthwork Reinforcement and Soil," Transportation Research Record, No. 640, Transportation Research Board, National Academy of Sciences, Washington, D.C., 1977.
17. Schlosser, F., "Reinforced Earth," (English Translation), Note D-Information Technique, Laboratoire Central Des Ponts et Chaussees, April 1976.

CHAIN-LINK RETAINING WALLS

By

Daryl R. Greenway¹ and Bruce C. Vandre²

ABSTRACT

Construction of low volume, low budget roads in mountainous terrain continues to be a major challenge. Steep and frequently unstable side-slopes, coupled with environmental concerns, create a need for earth retaining structures that are inexpensive, easy to construct, and esthetic. Recent experience on the Siskiyou National Forest indicates that chain-link retaining walls may be one solution to this problem.

Chain-link retaining walls utilize chain-link fabric layered with compacted backfill in a manner similar to synthetic fabric (geotextile) retained earth walls. The chain-link fabric provides continuous, flexible high strength reinforcement to stabilize the soil mass. This paper describes the design, construction, and performance of four low chain-link walls and the supporting laboratory pull-out resistance tests. Cost data is also presented, documenting as-built construction costs.

INTRODUCTION

Four experimental chain-link retaining structures were constructed on the Siskiyou National Forest during 1977 and 78. The four low retaining walls were constructed within a three mile section of an existing road to regain width lost from fill erosion. These installations provided the opportunity to develop construction procedures, check selected design assumptions, monitor performance, and compile cost data for chain-link structures, as well as providing an economic solution to a specific problem.

Two earlier retaining walls on the Siskiyou National Forest provided impetus for these structures. A polypropylene fabric (geotextile) wall was constructed in 1974 on the Illinois River Rd. 3504 at Snailback Creek. The design and construction of this wall was reported by Bell (1). Then, a chain-link wall with "half culvert" facing elements was constructed in 1975 at the north abutment of Winchuck River Bridge 3907-1.0. The construction feasibility of the chain-link walls was evaluated during construction of these earlier walls.

The chain-link walls, built 15 miles east of Brookings, Oregon, were approved Forest Service trial-use installations (3,7). These walls were instrumented with strain gages and pressure cells to evaluate the nature of load transfer from the soil to the chain-link fabric. Large scale laboratory pull-out tests were performed on the chain-link fabric at the California

¹ Siskiyou National Forest, Gold Beach, Oregon

² Intermountain Region, USFS, Ogden, Utah

Department of Transportation "CALTRANS" Materials Laboratory at Sacramento. The corrosion potential of these sites was studied by a corrosion consultant. Data obtained during construction and testing are summarized herein, and the design procedures and short term performance are discussed.

WALL DESIGN

The design procedure used for the chain-link walls relative to internal stability was based on the reinforced soil analysis method developed by Lee (4) and adapted to fabric reinforcement by Bell (1). The internal stability is dependent on the fabric not rupturing or pulling out. External stability of the wall, including overturning, base sliding, and foundation bearing, was assessed following standard procedures (6). These structures were designed with a minimum safety factor of 2.0 under full live load. The critical live load used was a logging yarder-tower combination (gross weight 205,000 pounds) passing one foot from the wall face. This vehicle loading was used to evaluate chain-link stresses only. For fabric layers directly beneath the vehicle, added pull-out stresses are cancelled by higher confinement of the fabric; design for adequate pull-out resistance was therefore based on a dead load condition. Sacrificial steel was provided for safety against corrosion over the design life of the structure.

A typical wall cross section is shown in Figure 1. The salient feature of the design is that only chain-link and earth materials were used in the structure. The chain-link fabric provides structural (internal) stability as well as retaining backfill materials at the wall face. Coarse rock, 2 inch to 6 inch size, was placed near the wall face to prevent loss of particles through the openings in the chain-link mesh. Where coarse rock fill is expensive or unavailable, a finer mesh or synthetic fabric could be used at the face of the wall to retain the backfill. The finer mesh should be placed between the backfill and the chain-link.

Wall dimensions are summarized in Table I. Because of the experimental nature of the project, the chain-link walls were arbitrarily limited to 14 feet or less, necessitating a steel binwall be constructed beneath the chain-link wall at site 3. It should be noted that no intrinsic height limitations otherwise exist in the design procedure.

Two types of 6 gage chain-link fabric were used in three of the walls. The principle type used was zinc coated steel, while a small amount of vinyl coated steel was used. (These fabrics correspond to AASHTO M 181-74 types I and IV, respectively.) The fourth wall was constructed of 9 gage zinc coated chain-link. All the chain-link used had 2 inch mesh openings.

TABLE I
 CHAIN-LINK WALL DIMENSIONS

Wall Site	Mile Post	Wall Length (ft.)	Maximum Height (ft.)	Face Area (sq. ft.)
1	1.35	130	10	1,040
2	1.70	65	12	500
3	2.80	115	12*	1,110
4	0.36	78	14	650

* total height, including steel binwall, was 22 feet.

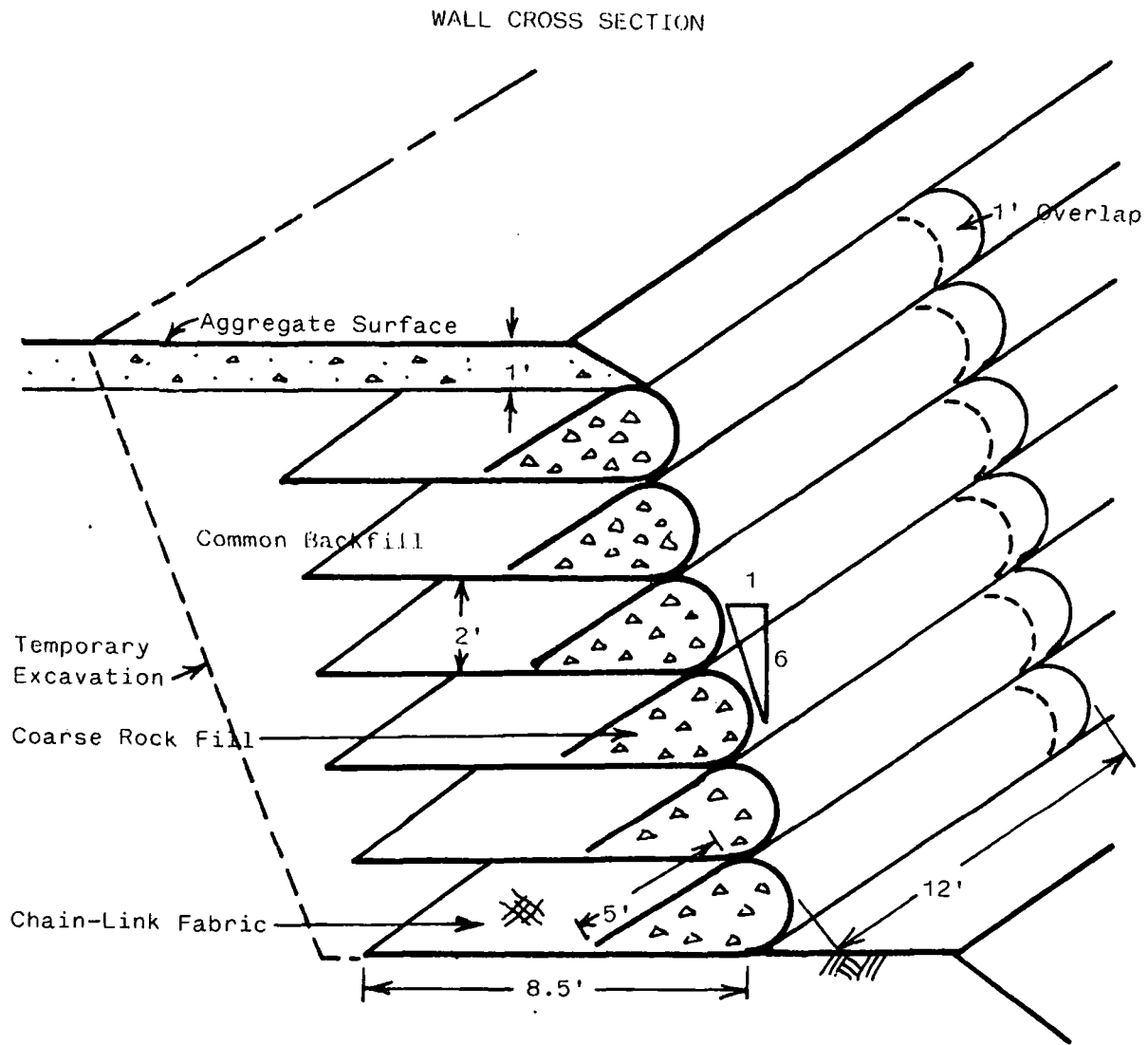
WALL CONSTRUCTION

Three chain-link walls were constructed on Mt. Emily Road 3983 in August, 1977, to restore road width where sidecast fill material had eroded or slid downslope. A fourth wall was constructed in September, 1978, to repair a similar failure that occurred in December, 1977.

The construction sequence involved excavation of a foundation bench, layer placing the chain-link fabric and backfill, and compaction. Twelve foot wide chain-link segments were placed transverse to the roadway on the approved foundation, allowing for a 1 foot overlap between pieces. Coarse rock fill was then placed along the face of the wall, the chain-link fabric was folded over the rock berm, and common backfill was placed to complete the layer. Details of construction and three completed walls are shown on Plates 1 and 2.

Two of the walls (at sites 1 and 2) were backfilled with weathered dacite fragments. Weathered dacite bedrock, from an intrusive igneous formation, is exposed adjacent to these wall sites. The backfill varied from a well graded silty gravel (Unified Soils Classification GW-GM) to a silty sand (SM). The other two walls were backfilled with silty gravel (GM) composed of weathered sandstone fragments. Compaction to 95 percent of AASHTO T 99 was accomplished by repeatedly tracking the area with a front loader.

The contractor developed a simple method for forming the wall face as shown on Plate 1. A row of steel fence posts were driven along the wall alignment initially. Plywood sections two feet high were then placed against the posts, and a 2x4 (not shown) was fastened to the top of the posts. This arrangement supported the chain-link and rock fill until the backfill was



NOTE: Maximum Height for Section Shown=12'

FIGURE 1



WALL CONSTRUCTION

PLATE I



SITE 2



SITE 3



SITE 4

COMPLETED
CHAIN-LINK WALLS

PLATE 2

in place. The contractor placed the rock berm approximately 6 inches above the plywood form to allow for settlement when the form was removed. On succeeding layers the fence posts were driven into the outermost edge of the layer below. This method entirely circumvented the need for exterior bracing supported from the steep slope below the wall, but the resulting batter was closer to 4:1 than the 6:1 designed.

An important advantage to this wall type was evident during construction when the contractor was able to open the road to pickup traffic at nearly any intermediate stage of wall construction. After any layer was completed, the ends of the work area could be gently ramped, and light trucks could be accommodated through the site.

CONSTRUCTION COSTS

The contract bid price for the chain-link walls was \$12.00 per square foot of face area compared to \$20.00 per square foot for steel binwalls included in the same contract. (Bid date was June 16, 1977). This contract price included the wall materials and installation costs. The total wall cost, including structural excavation and backfill was \$18.30 and \$29.40 per square foot for chain-link and binwall, respectively.

The total "as-built" cost was estimated to be \$11.60 and \$21.80 per square foot for chain-link and binwall, respectively. This estimate was prepared considering materials cost, equipment used, and installation time. A tracked loader, backhoe, and dump truck were used during construction.

These comparative costs may have been somewhat more favorable to binwall had equal amounts of the two wall types been installed. Under this contract, approximately ten times more chain-link wall was constructed than binwall.

FIELD INSTRUMENTATION

Two of the chain-link walls were instrumented to obtain performance data. The instrumentation program included strain gages welded to the chain-link, and earth pressure cells and corrosion monitoring coupons embedded in the backfill.

The strain gages were Ailtech Weldable Flexlead gages (model SG16S), and were spot welded to the top of the chain-link wires. A file was used to make a small flat spot, free of zinc coating, for each gage. This method precluded quantitative interpretation of the data as it was not possible to separate bending effects from the measured tensile strains. A pair of gages attached to opposite sides of the same wire, would be required to differentiate tension from bending. Qualitatively, the strain gages aided in the interpretation of the earth pressure data and soil-structure interaction.

Three Slope Indicator Company "SINCO" total earth pressure cells (model 51482) were installed to measure horizontal pressures and two cells were installed to measure vertical pressures. The pressure cell readings for various depths of overburden are plotted on Figures 2 and 3 for vertical and horizontal pressures, respectively.

The measured vertical pressures were equal to or less than the predicted earth pressures in all cases. Values less than theoretical may be attributed to localized arching around the pressure cell. The coarse granular backfill and the presence of angular rock fill nearby in the face of the wall could readily create such arching effects.

The measured horizontal pressures, Figure 3, were largely equal to or less than the theoretical "at rest" lateral earth pressures. (An effective friction angle of 41° was selected for the backfill based on laboratory tests). Measured pressures considerably less than theoretical can also be attributed to arching in the backfill. For Cell D, for which pressures increased from "active" to "at rest" with increasing overburden, adjacent strain gages indicated the surrounding chain-link was intension, suggesting load transfer to the fabric had occurred. For Cells C and E, which measured decreases in pressure, the surrounding strain gages had negative (bending) readings, suggesting arching was caused by fill settlement.

The classification of earth pressures as being either "active" or "at rest" based on field instrumentation is complicated by variations in shear strength within the backfill, particularly the occurrence of apparent cohesion. Localized arching caused by backfill settlement also complicated data interpretation. Earth pressure "at rest" appears to be a safe assumption for the design of chain-link walls, however. Chang (2) and others have recommended "at rest" design pressures based on field studies of Reinforced Earth. A design based on "active" pressures would not result in a significant economy in the construction of low retaining walls, in any case.

LABORATORY TESTS

Laboratory tests performed included direct shear and triaxial strength tests on the common backfill, and pull-out resistance tests on the chain-link fabric.

Direct shear tests were performed on 1/4-inch minus fraction of the fill soil compacted to approximately 90% of AASHTO T 99 maximum density at moisture contents between 8 and 12 percent. The results are plotted on Figure 4 for tests which peaked at 15 percent strain or less. Two direct shear strength envelopes are also plotted on Figure 4 which bracketed the observed data. These envelopes have friction angles of 42° and cohesion of 950 to 1,600 psf.

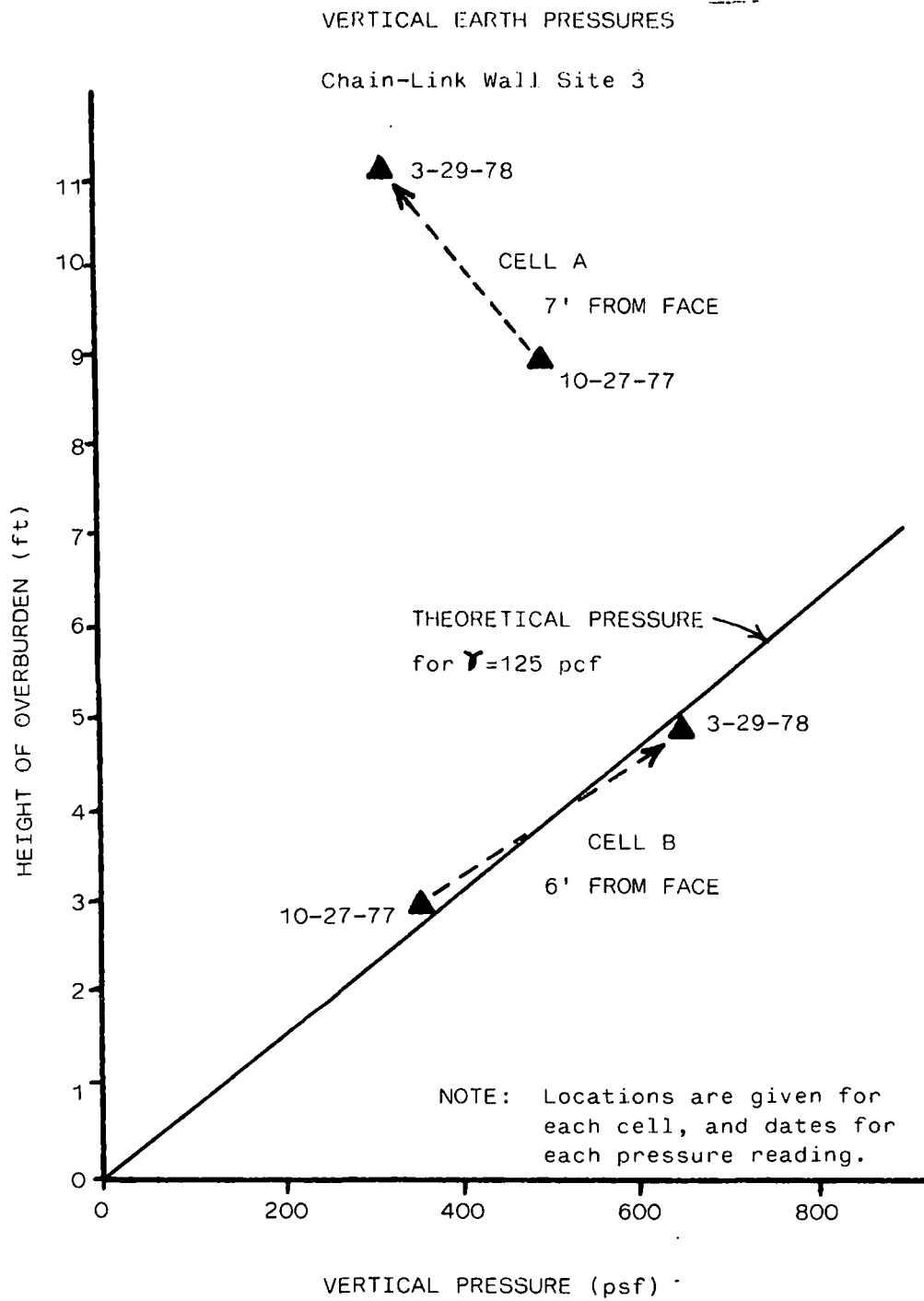


FIGURE 2

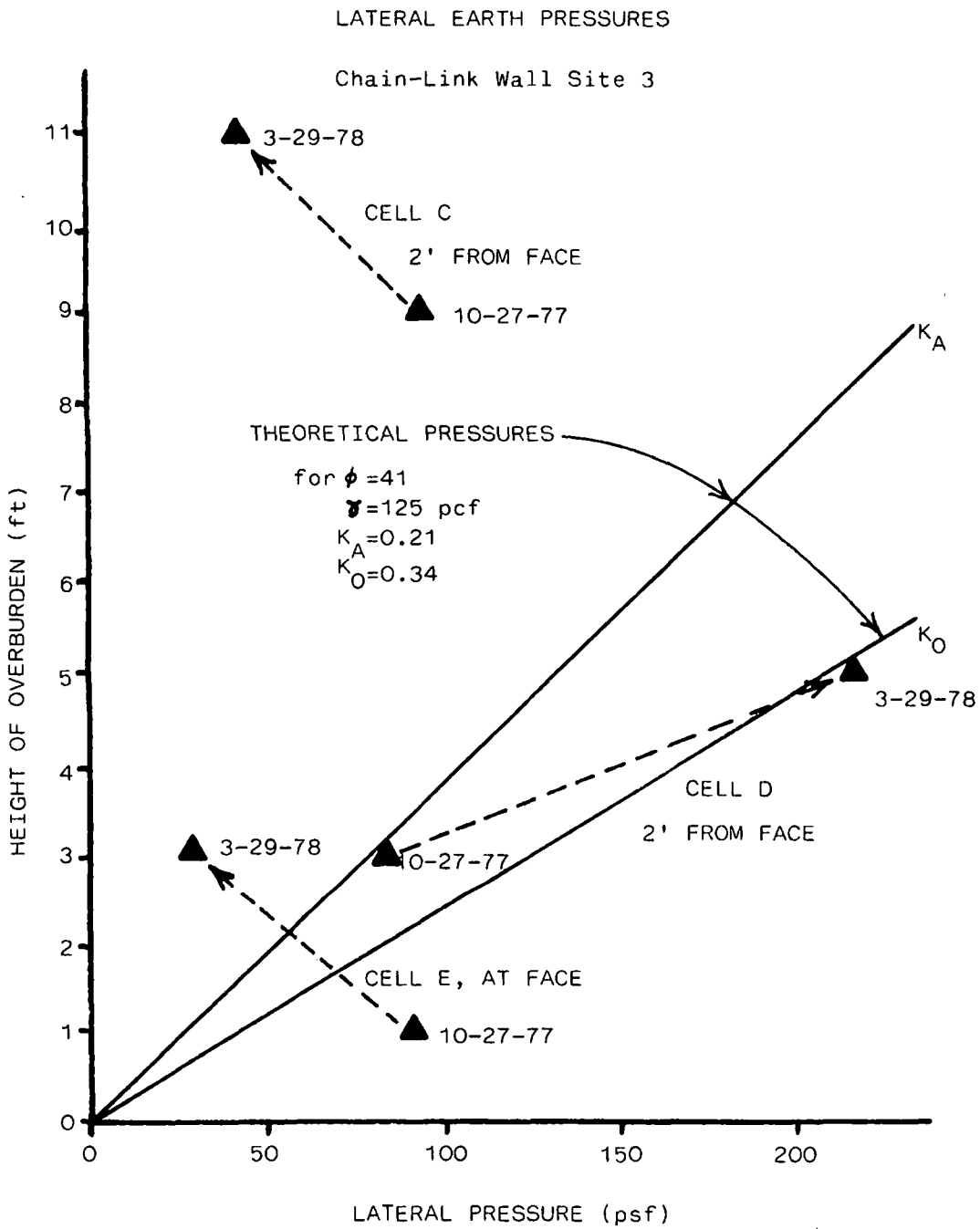


FIGURE 3

A consolidated-undrained triaxial test with pore pressure measurements was also run on the backfill soil. The resulting strength envelope is included on Figure 4. The effective friction angle from this envelope is 41° , with zero cohesion.

Three laboratory pull-out tests were performed to evaluate pull-out resistance and ultimate strength characteristics of the chain-link fabric. The test device consisted of a rigid steel box 18 inches high, 36 inches wide, and 54 inches long. Backfill soil was compacted in the box, with a 24 inch wide by 48 inch long piece of 6 gage chain-link fabric placed at mid-height of the box. (Compacted soil densities were slightly higher than that of the samples tested for shear strength.) Vertical pressure was applied to simulate overburden. The chain-link was gripped in a vise and pulled at variable rates of deformation.

For pull-out tests 1 and 3, the front face of the box was removed during the entire test. The front face was left in place during test 2 until the chain-link wire broke at the bise grip. The chain-link fabric was regripped, the front face plate was removed, and pulling was continued. Normal pressures of 600, 300 and 1,000 psf were applied to tests 1, 2 and 3, respectively.

Load-deformation curves for tests 1 and 3, and the confined portion of test 2, are plotted on Figure 5. The high deformations obtained were caused by the narrowing of the mesh. Figure 6 shows the deformed chain-link segment and the effective embedded area after test 1. The chain-link width reduced from 24 inches to approximately 9 inches under the pulling load of tests 1 and 3.

A highly disturbed soil zone caused by the fabric deformation was observable as a cone shaped cavity. Estimates of the effective embedded fabric area resisting pull-out were made based on the location of the disturbed soil cone, the looseness of the soil, and the distorted width of the fabric. Strain gages mounted on the fabric during the pull-out tests indicated the pull-out load was not being transferred to the chain-link until the peak shear resistance of the adjacent soil had been reached.

The envelope for the estimated pull-out stress versus normal pressure is included on Figure 4. The pull-out resistance is approximately twice as great as the soil shear strength. This suggests that a thin soil layer, extending above and below the wire mesh, is sheared on both surfaces. This might be termed a "double shear" condition. For mesh openings considerably greater than two inches, this condition may not exist.

From Figure 5, the ultimate strength of the 6 gage chain-link fabric was determined to be 5,000 pounds per foot of fabric; Figure 5 also clearly illustrates the two modes of chain-link failure (i.e. breaking and pull-out).

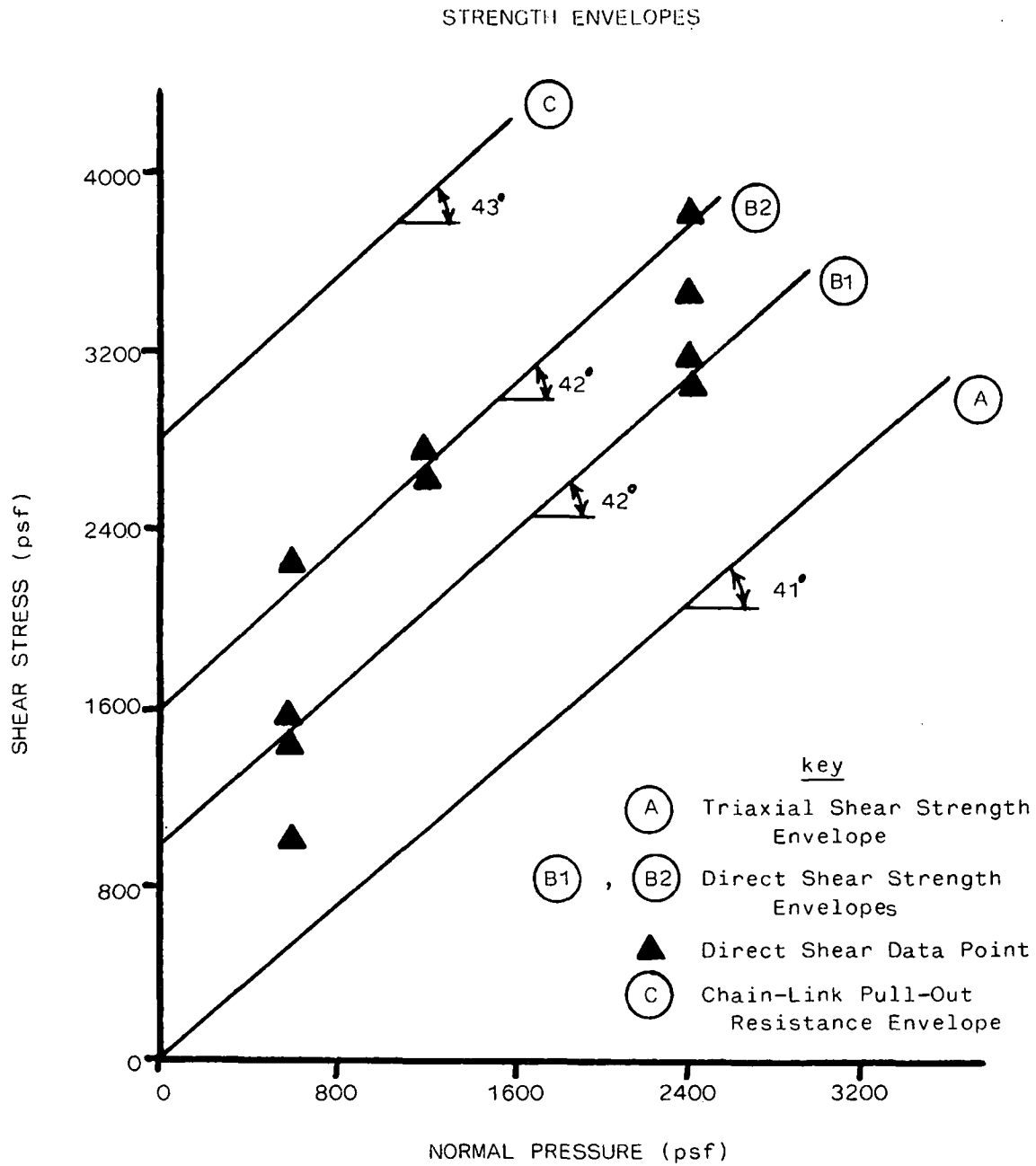


FIGURE 4

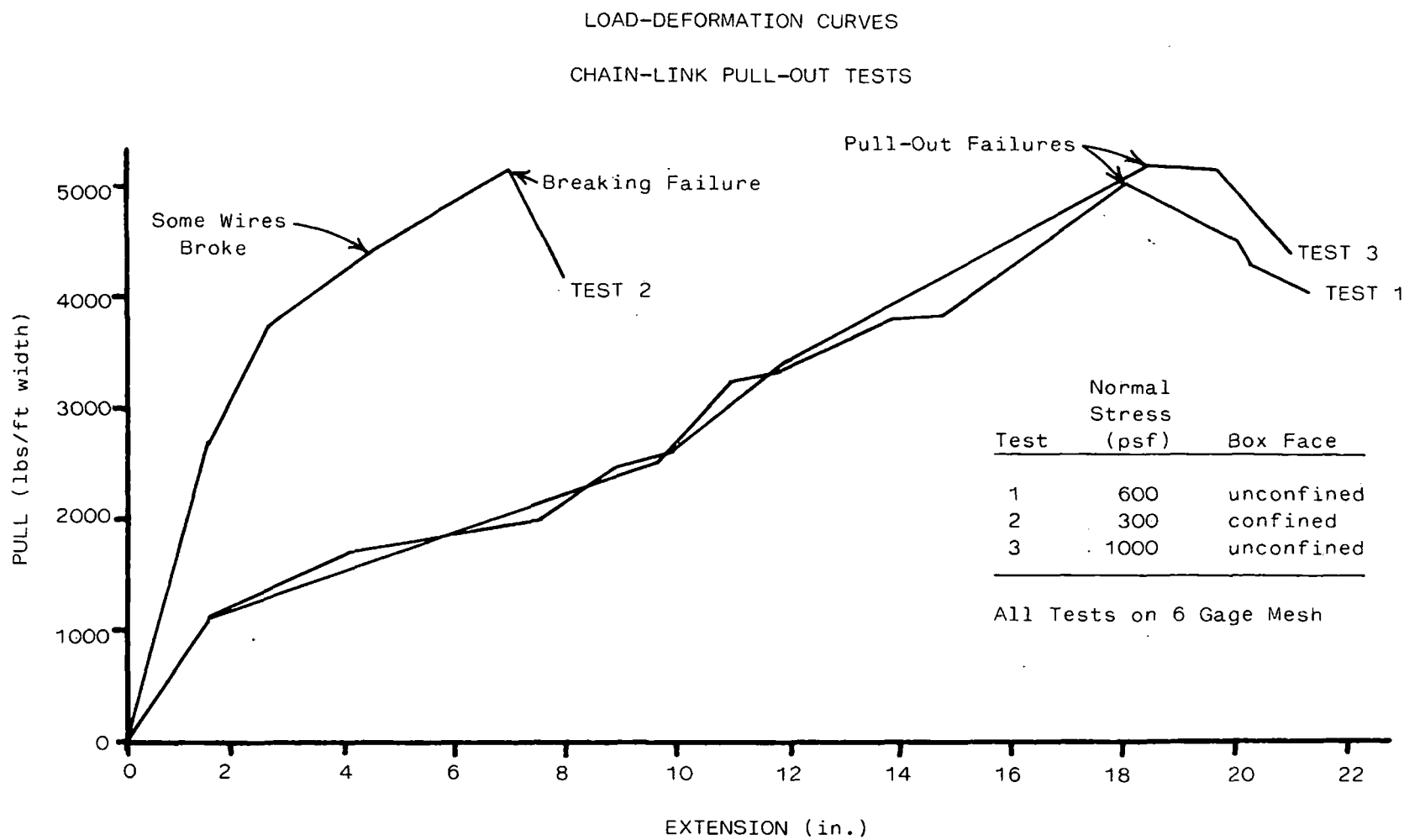
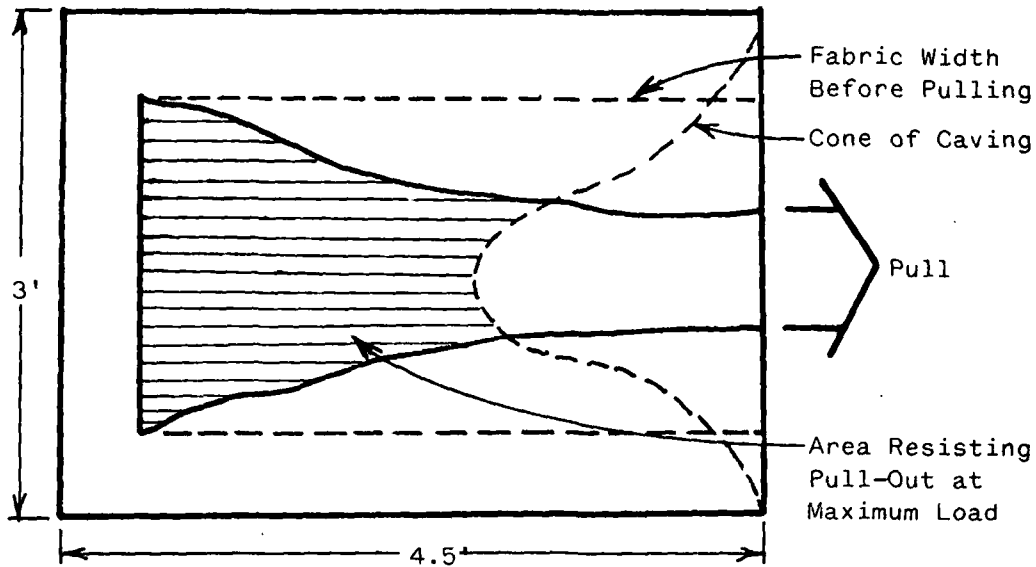


FIGURE 5

PULL-OUT TEST 1



DEFORMED CHAIN-LINK



FIGURE 6

CORROSION CONSIDERATIONS

Corrosion of the buried chain-link is of concern, as it directly affects the design life of the structure. The relative corrosion resistance of the two types of chain-link fabric was investigated, zinc coated (Type I) and vinyl coated (Type IV-bonded). (Fabric types follow AASHTO M 181-74). One hundred fifty square feet of wall at site 1 was constructed with vinyl coated; all other fabric used was zinc coated (galvanized). Corrosion monitoring coupons were also installed at site 1 for long term monitoring.

The chain-link walls were designed to provide sacrificial steel to corrosion attack while providing a safety factor relative to wire breakage. The design life was originally calculated to be 24 years assuming a corrosion rate of 0.004 inches per year acting on the wire diameter. A corrosion consultant, Norton Corrosion Limited, was engaged to refine the assumed corrosion rate.

The corrosion rate initially assumed was 200 to 400 times greater than the rates recommended by Norton for zinc coated chain-link at these sites (8). While increasing the projected design life 200 to 400 times (to 4,450 or 8,900 years, respectively) seems unreasonable, it does appear that satisfactory performance could be expected from the chain-link structures with respect to corrosion. For this reason, less sacrificial steel was provided in the fourth wall constructed; 9 gage wire was used rather than 6 gage at wall site 4. Norton also pointed out that vinyl coated chain-link, although initially more corrosion resistant than zinc coated, would not perform as well in the long run. They reasoned that the vinyl coating could be damaged by the backfill, providing bare spots where corrosion would concentrate its attack on the wire. In view of the construction procedures utilized, this appears entirely possible.

Inspection of the exposed chain-link on the face of the completed walls in March, 1979, revealed three small spots of iron oxide staining and apparent corrosion at site 3. These stained spots, which are from 3 to 6 inches in diameter, appear to be occurring where rock fragments containing iron pyrite are in direct contact with the fabric. Weathering and oxidation of the iron pyrite produces an acidic condition which could greatly increase the corrosion rate of both zinc and steel. The effect of weathering and oxidation on the backfill away from the wall face will probably be much less than that observed at the face. These spots will be observed periodically as part of the long term corrosion monitoring program.

The corrosion potential of any specific site is related to the composition of the soil and groundwater. The resistivity of the soil, the pH (acidity or alkalinity) of the soil and groundwater, and the presence of chlorides and sulfates have been identified as significant factors in corrosivity (5). Soils to be suspected as highly corrosive include clays, cinders, and organic "mucks".

CONCLUSIONS

The as-built costs of the chain-link walls indicate they are competitive to synthetic fabric (geotextile) walls, and a considerable savings over steel binwalls or other standard types. The walls were simple and expedient to construct, and the esthetic qualities were judged to be excellent once the contractor had perfected his construction technique.

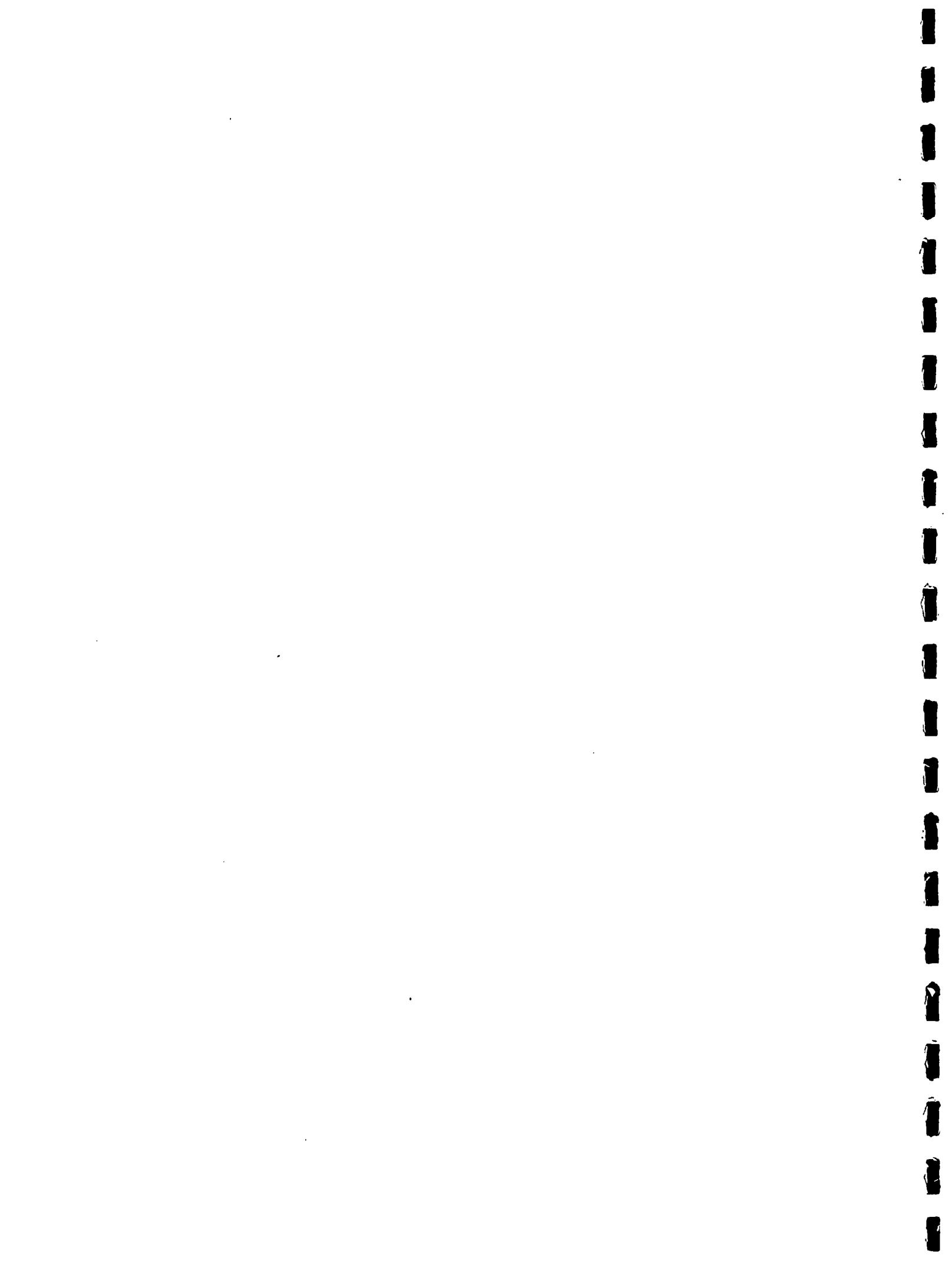
In light of the short term performance data collected, the design assumptions have been met. The existing design procedure appears to be adequate for this construction method. Available data on chain-link characteristics is limited at this time, and warrants further investigation. Design economies could be achieved by further study of the optimum wall batter relative to excavation costs and fabric embedment lengths.

From the foregoing data, the Mt. Emily chain-link walls were highly successful based on economics, construction expediency, predicted design life, and esthetics. It is recommended that future designs be based on the existing procedures, utilizing the chain-link strength and pull-out data contained herein. The corrosion potential of each proposed site should also be properly evaluated.

REFERENCES

- (1) Bell, J.R., Stille, A.N., and Vandre B., "Fabric Retained Earth Walls," Proceeding, 13th Annual Engineering Geology and Soils Engineering Symposium, Moscow, Idaho, 1975.
- (2) Chang, J.C., "Earthwork Reinforcement Techniques," Final Report CA-DOT-TL-2115-9-74-37, California Department of Transportation, October, 1974.
- (3) Greenway, D.R., "Trail-Use Proposal for Chain-Link Retaining Structure," Siskiyou National Forest, U.S. Forest Service, Grants Pass, Oregon, May 1977.
- (4) Lee, K.L., Adams, B.D., and Vagneron, J.M.J., "Reinforced Earth Retaining Walls," Journal of the Soil Mechanics and Foundation Engineering Division, ASCE, SM10, October, 1973, pp. 745-764.
- (5) Romanoff, M., "Underground Corrosion," Circular 597, National Bureau of Standards, U.S. Department of Commerce, April, 1957.

- (6) Terzaghi, K., and Peck, R.B., Article 46, "Retaining Walls," Soil Mechanics in Engineering Practice, John Wiley and Sons, 1967, pp. 361-378.
- (7) Vandre, B.C., and Greenway, D.R., "Construction and Evaluation of Chain-Link Retaining Structures," Siskiyou National Forest, U.S. Forest Service, April, 1979.
- (8) Williams, K.L., and Simon, P.D., "Corrosion Engineering Survey, Emily Road Reconstruction, Siskiyou National Forest, U.S. Forest Service," Norton Corrosion Limited, Woodinville, Washington, June, 1977.



GROUND WATER FLOW SYSTEMS IN THE "PHOSPHATE SEQUENCE" OF SOUTHEASTERN IDAHO

By

Gerry V. Winter and Dale R. Ralston
University of Idaho
Moscow, Idaho

ABSTRACT

The complex geologic framework of the Western Phosphate Field in southeastern Idaho produces an equally complex pattern of ground water flow. Knowledge of this flow pattern is of importance in minimizing water resource impacts on and from open pit phosphate mining.

Previous research at the University of Idaho has indicated that individual geologic formations produce patterns of ground water flow that are consistent over a large part of the potential mining area. Data were gathered on stream gain and loss and spring location and discharge during the "drought" summer of 1977 to test these hypotheses of ground water flow.

The "phosphate sequence" of geologic units, the Dinwoody, Phosphoria and Wells Formations, exhibit a predictable pattern of ground water flow systems in the areas examined. The Phosphoria Formation, particularly the Meade Peak Member, appears to severely limit water movement from the Dinwoody Formation into the Wells Formation. Most of the gaining streams and the springs are from the Dinwoody and Thaynes Formations stratigraphically above the Phosphoria Formation. Most of the streams lose flow into the stratigraphically lower Wells Formation.

This pattern of ground water flow has important implications for mine operation and water resource impacts from such operation.

INTRODUCTION

Phosphate has been surface mined in southeastern Idaho since 1945 but additional demands for the ore will require that new areas be mined. A comprehensive understanding of the hydrogeology and hydrology of the area is required both from a mining and a regulatory standpoint. The interception of a significant ground water flow system by a mining operation could be very costly due to pit flooding. A prior knowledge of the ground water flow system regimen could provide a means of circumventing such a problem, as with drainage well. Regulatory agencies are also concerned with the possible disappearance of existing springs and gaining reaches of streams from the alteration of ground water flow systems.

Past hydrogeologic research efforts have been site specific but the results are similar. Ground water flow systems exist in the Thaynes and Dinwoody Formations that occur stratigraphically above the Phosphoria Formation that contains the phosphatic ore beds. The Phosphoria Formation

was not found to support any major ground water flow system but the Wells Formation that underlies it was found to support such a system (Ralston and others, 1977).

The general objective of this study was to test the hypothesis that similar ground water flow systems exist within the phosphate sequence throughout a large area of the Western Phosphate Field in Caribou County, Idaho. The location of this study area is shown on Figure 1. Specifically, the objectives were to test the hypotheses that major ground water flow systems exist in both the upper and lower members of the Dinwoody and Wells Formations and that no major ground water flow systems exist in the members of the Phosphoria Formation.

Stream gain-loss measurements across formation members provided the bulk of the data used for this study. These data were analyzed in conjunction with existing geologic maps to determine whether the formation member has either a low or high hydraulic conductivity. A significant change in streamflow across a formation member indicates that the member has a high hydraulic conductivity. Geologic conditions must be evaluated if there is no change in streamflow to determine if the lack of change is due to a low hydraulic conductivity or geologic conditions. The basic concepts of stream gain-loss conditions are illustrated on Figure 2.

A reconnaissance survey was also made of numerous springs in the study area. The existence of a spring indicates that the formation it issues from has a high hydraulic conductivity and supports a ground water flow system.

Field work was conducted during the summer of 1977 which was particularly advantageous for this type of study. Precipitation during the recharge period prior to this summer was well below normal as illustrated by Figure 3. Streamflow for the Blackfoot River is also plotted on Figure 3 which more accurately reflects the effects of the low precipitation period. Only those ground water flow systems of significant length or storage capability would continue to discharge during this period.

This study was funded through the Water Resources Research Institute located at the University of Idaho. This paper was derived from a Master of Science thesis (Winter, 1979) at the University of Idaho.

HYDROGEOLOGY

The formations comprising the ground water flow systems encountered in this study are sedimentary in origin as described in Table 1. The Dinwoody Formation consists of an upper and lower member that is occasionally mapped with the Woodside Shale separating the members. Three members comprise the Phosphoria Formation but frequently the cherty shale and Rex Chert Members are mapped as one unit. The Meade Peak Phosphatic Shale Member contains the phosphatic ore beds of economic interest in the area.

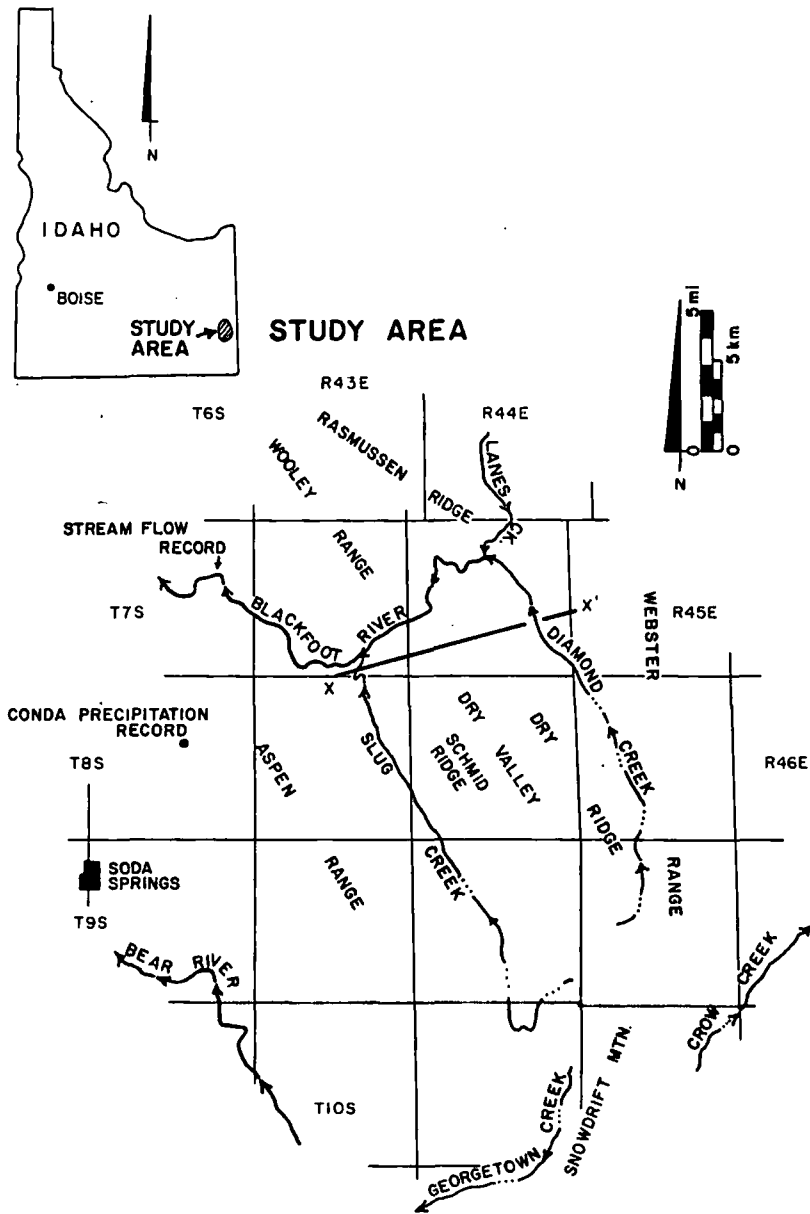


FIGURE 1 - Location Map of Study Area

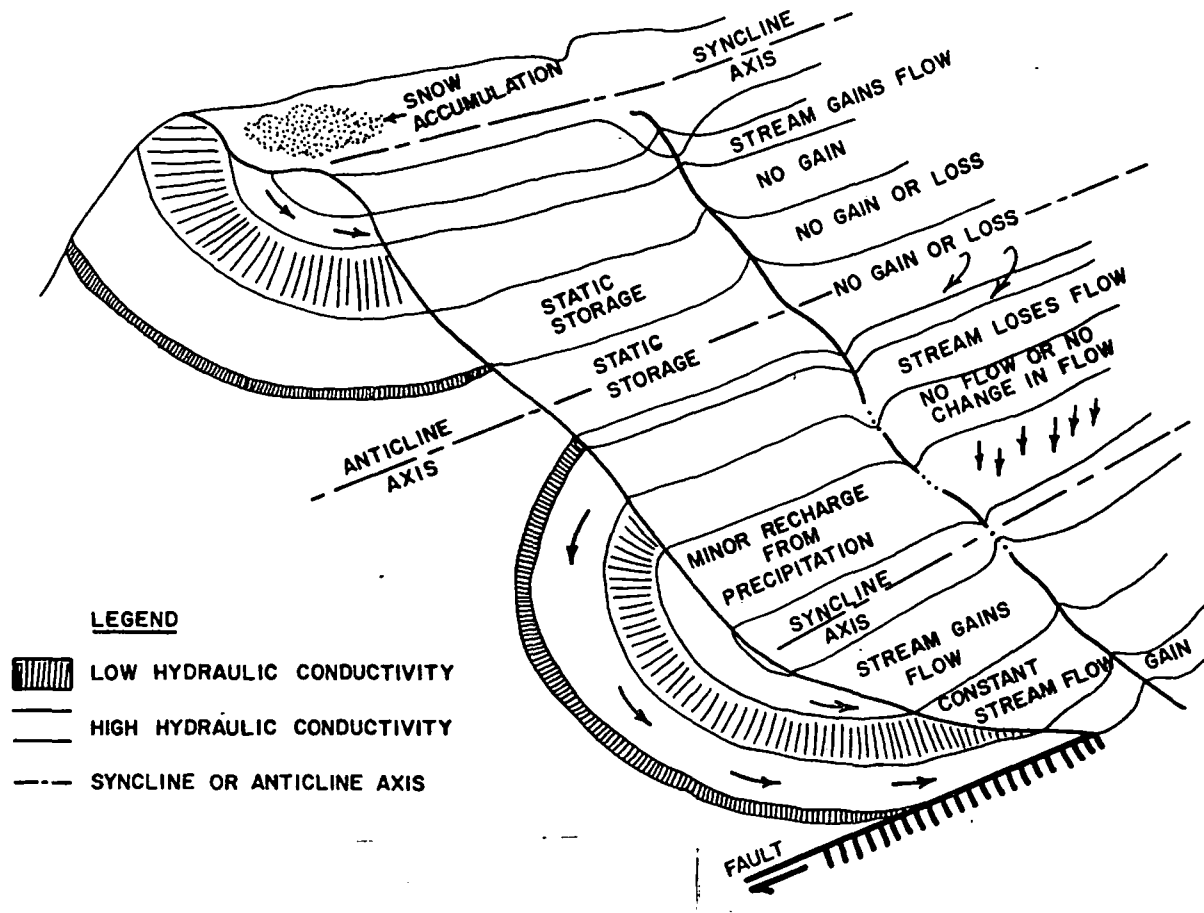
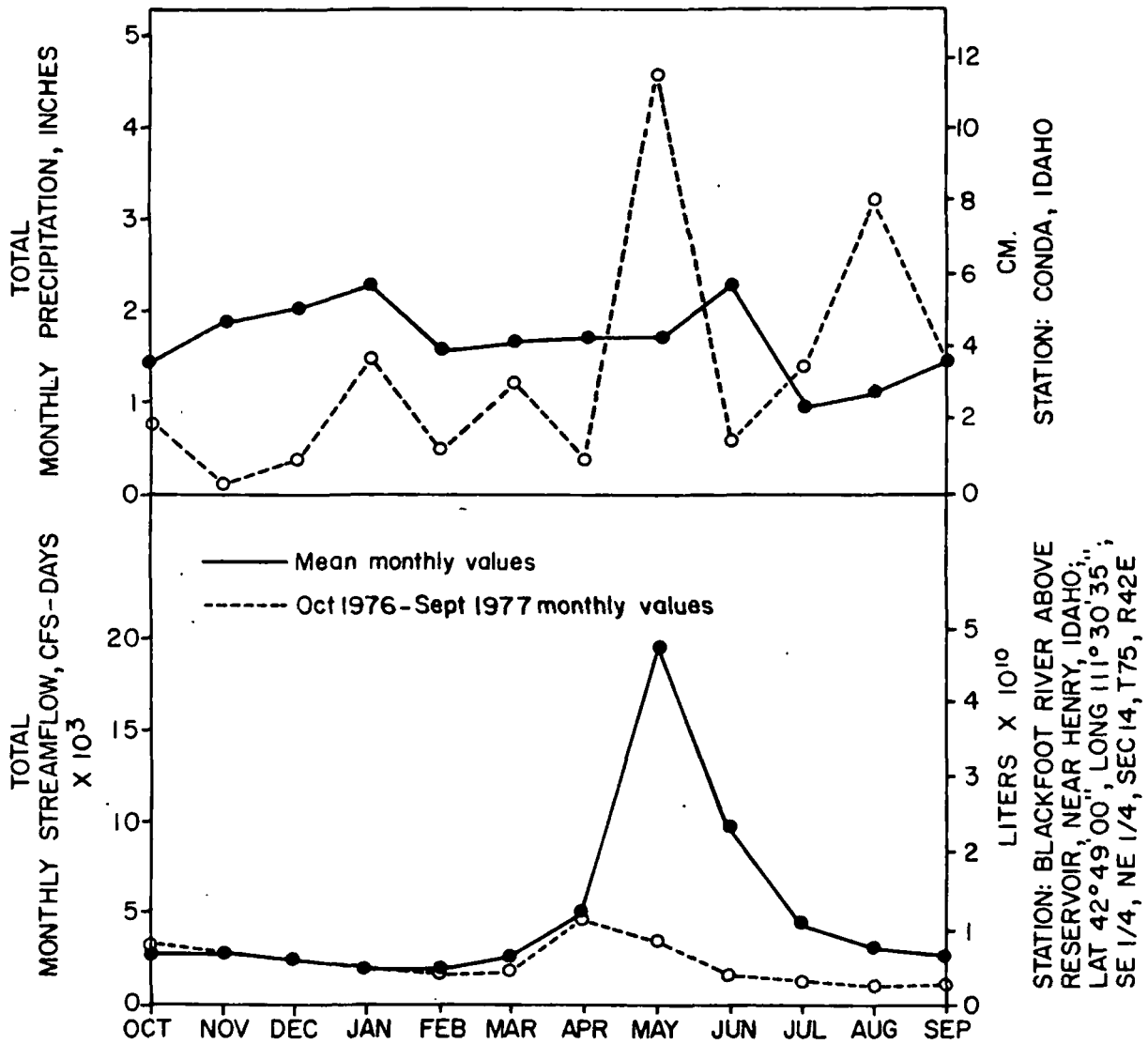


FIGURE 2 - Typical Stream Gain-loss Characteristics



PRECIPITATION DATA SOURCE: U.S. DEPT. OF COMMERCE, NATIONAL OCEANIC AND ATMOSPHERIC ADMINISTRATION

STREAM FLOW DATA SOURCE: U.S. DEPT. OF INTERIOR, GEOLOGIC SURVEY

MEAN VALUES, PERIOD OF RECORD; PRECIPITATION = 1-1960 TO 12-1976
 STREAMFLOW = 4-1914 TO 9-1925 & 8-1967 TO 9-1976

FIGURE 3 - Monthly Precipitation and Streamflow, October, 1976, Through September, 1977

TABLE 1. Geologic Section

Age	Formation Name	Unit Name	Symbol	Thickness		Description
				(ft)	(m)	
Quaternary			Qa1			Alluvium or colluvium
Quaternary or Tertiary	Basalt		Qtb	Varies		Olivine basalt
Tertiary	Salt Lake		Ts1			Light-gray fine-grained pebble conglomerate mostly chert and limestone
Upper Triassic	Higham Grit ^{*1}		Trh	200 to 250		Sandstone-conglomeratic, light-gray, pink, buff and pale green, medium to coarse grained
Lower Triassic	Thaynes	Timothy Sandstone Member	Trtt	200 to 250		Buff to gray and maroon sandstone
		Upper Part of Portneuf Limestone Member	Trtpv	250 to 300		Dark-gray and gray limestone, thin to thick bedded with yellowish-gray to yellowish-brown sandstone
Lower Triassic	Ankareh ^{*1}	Lanes Tongue	Tral	500		Red to reddish brown, very fine grained to fine grained, thin bedded sandstone
Lower Triassic	Thaynes	Lower Part Portneuf Limestone Member	Trtp1	300 to 400		Gray, finely crystalline, massive limestone and gray to yellowish-gray and fine grained sandstone
		Nodular Siltstone Member	Trtn	400		Olive to brownish-gray siltstone and shale, contains small dark-gray limestone nodules; interbedded with sandstone and limestone
		Black Shale Member	Trtb	300		Gray to black, fissile, hard platy shale; interbedded with thin dark-gray limestone and brownish-gray siltstone in lower part; a few thin bedded shaly and silty black limestone beds in upper part
		Platy Siltstone Member	Trts	650 to 750		Yellowish-brown to olive-gray, calcareous, thin bedded, platy siltstone; a few thin beds of shale and limestone
		Black Limestone Member	Trtl	550 to 800		Dark-gray to black shale and siltstone interbedded with dark-gray to black limestone over dark-gray

TABLE 1. (Continued)

Age	Formation Name	Unit Name	Symbol	Thickness		Description
				(ft)	(m)	
Lower Triassic (cont'd)	Thaynes (cont'd)	Black Limestone Member (cont'd)	Trtl (cont'd)	550 (cont'd)		to black limestone with a few thin beds of dark-gray shale over dark-gray to black shale and siltstone over gray limestone with Meekoceras ammonite zone at base
	Dinwoody ^{*2}	Upper Member	Trdu	700		Gray fossiliferous limestone interbedded with soft olive-brown calcareous siltstone, contains tongues of Woodside Formation as red siltstone or green and maroon shale
	Woodside		Trw	150		
	Dinwoody	Lower Member	Trdl	500 to 900		Olive-brown calcareous siltstone and shale with thin bedded limestone
Permian	Phosphoria	Cherty Shale ^{*3} Member	Ppc	170		Thin-bedded dark brown to black cherty mudstone, siliceous shale and argillaceous chert
		Rex Chert Member ^{*3}	Ppr	80		Thick-bedded black to white chert with some mudstone, some limestone lenses near top and bottom
		Meade Peak Phosphatic Shale Member	Ppm	100 to 200		Dark-brown to black mudstone, limestone, and phosphorite
		Park City	Grandeyr Tongue ^{*4}	Ppg	100	
Permian and Pennsylvanian	Wells	Upper Member	PPwu	1000 to 1400		Light-gray to reddish-brown sandstone, some interbedded gray limestone and dolomite
		Lower Member	Pwl	500 to 950		Medium bedded gray cherty limestone, some interbedded sandstone
Mississippian	Monroe Canyon Limestone (also referred to as Brazer Limestone)		Mb	800 to 1600		Light-gray limestone with interbedded sandstone, occasionally with gray and green shale
		Madison Limestone (or Lodgepole Limestone)	Mn	1000		Dark-gray to black finely crystalline to aphanitic limestone in thin beds

Note: *1 = Appear on geologic maps, not of importance to study.
 *2 = Occasionally mapped as one unit (Trd).
 *3 = Occasionally mapped as one unit.
 *4 = Usually mapped as part of upper Wells.

(Armstrong, F., 1969, 2 plates; Cressman, E., 1964, 105 p.; Cressman, E. and Gulbrandsen, R., 1955, 18 p.; Gulbrandsen, R., and others, 1956, 23 p.; Lowell, W., 1952, 53 p.; Montgomery, K. and Cheney, T., 1967, 63 p.; Rioux, R., and others, 1975, 6 p.)

No distinction was made between the Grandeur Tongue of the Park City Formation in this study.

Geologic structure viewed today is the result of major overthrusting associated with the Bannock Thrust Zone. The synclinal-anticlinal folds and faulting that occurred during the Upper Cretaceous and Paleocene periods are a result of this thrusting. Additional faulting since the Oligocene combined with differential subsidence and erosion has resulted in the current major valleys and ridges seen today (Cressman, 1964, p. 62-91).

STREAM GAIN-LOSS CHARACTERISTICS

Data for Wood Canyon is presented as Figure 4 and Table 2 as an example of a typical gain-loss situation.

TABLE 2. Wood Canyon, Stream Gain-loss Measurements

Measuring Point	Flow Measurement	
	GPM	liter/sec.
A	12	0.76
B	10	0.63
C	1.6	0.10
D	95	6.0
E	99	6.2
F	95	6.0
G	88	5.6
H	4.2	0.26
I	0	0

The lack of a significant change in stream flow across the black limestone member (Trt1) of the Thaynes Formation cannot be attributed to the formation having a low hydraulic conductivity since a static storage condition may exist. Stream flow decreased significantly across the upper member (Trdu) of the Dinwoody and then increased very significantly across the lower member (Trdl) of the Dinwoody Formation. Both members therefore, have a high hydraulic conductivity and can support ground water flow systems. There was no significant change in stream flow across the members (Ppc, Ppr and Ppm) of the Phosphoria Formation; hence it has a low hydraulic conductivity and cannot support a ground water flow system. All stream flow was lost across the upper member (PPwu) of the Wells Formation indicating that this member has a high hydraulic conductivity and can support a ground water flow system. The stream gain-loss characteristics of all the streams studied are shown on Table 3.

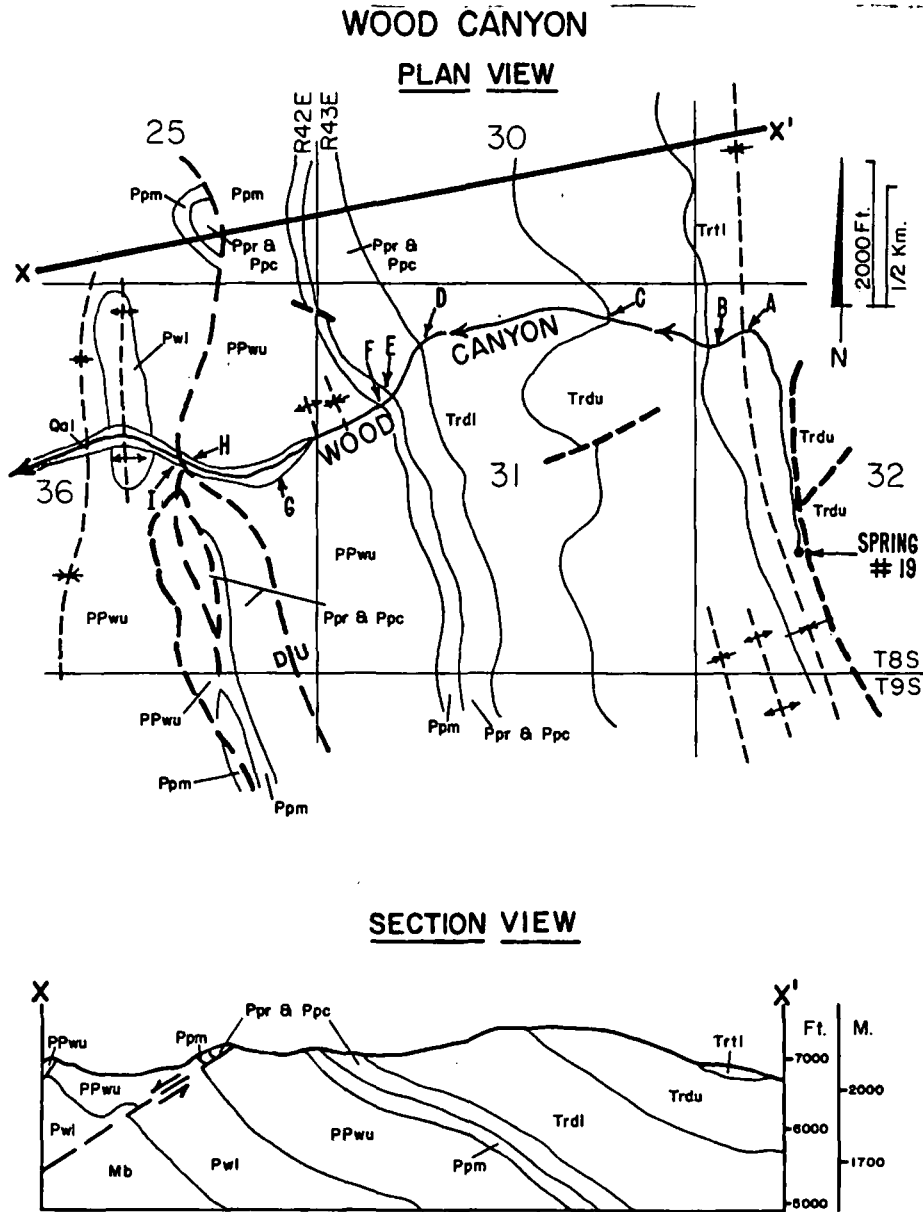


FIGURE 4 - Geologic Plan and Section Views of Wood Canyon
 Showing Stream Measurement Sites and Spring
 Locations (Modified After Gulbrandsen and
 Others, 1956 Plate 1)

TABLE 3. Stream Gain-loss Characteristics

Subarea	Site	Formation Evaluated	Unit Evaluated	Stream Gain-Loss Characteristics	Comments
Aspen Range	Wood Canyon T8S, R42 & 43E	Thaynes	Black Limestone Member - Trt1	Indeterminate	
		Dinwoody	Upper Member - Trdu	Losing	
		Dinwoody	Lower Member - Trd1	Gaining	
		Phosphoria	Cherty Shale & Rex Chert Members - Ppc & Ppr	No gain or loss	
		Phosphoria	Meade Peak Phosphatic Shale Member - Ppm	No gain or loss	
		Wells	Upper Member - Ppwu	Losing	Lost all surface flow in the vicinity of a fault
	Unnamed Tributary to Johnson Creek T9S, R43E	Dinwoody	Lower Member - Trd1	Gaining	Fault intercepts part of stream channel
Wooley Range	Sheep Creek T6S, R44E	Dinwoody	Upper Member - Trdu	Gaining	
		Thaynes	Black Limestone Member - Trt1	Losing	Validity of measurement questionable at Trt1-Trts contact
			Platy Siltstone Member - Trts	Gaining	Validity of measurement questionable at Trt1-Trts contact
			Black Shale Member - Trtb	No gain or loss	
			Nodular Siltstone Member - Trtn	Gaining	Fault intercepts Stream
Webster Range	Smoky Canyon T8S, R45 & 46E	Dinwoody	Upper Member - Trdu	Gaining	
		Woodside -Trw		Indeterminate	Magnitude of change in flow insignificant
		Dinwoody	Lower Member - Trd1	Gaining and losing	
		Phosphoria	Cherty Shale Member - Ppc	No gain or loss	
	Phosphoria	Rex Chert Member - Ppr	Losing		
	Sage Creek T9S, R45 & 46E	Dinwoody	Upper Member - Trdu	Gaining	
		Woodside -Trw		Unknown	Unable to measure flow at Trw-Trd1 contact

TABLE 3. (Continued)

Subarea	Site	Formation Evaluated	Unit Evaluated	Stream Gain-Loss Characteristics	Comments
Webster Range (cont'd)	Sage Creek (cont'd)	Dinwoody	Lower Member Trd1	Gaining	
		Phosphoria	Cherty Shale Member - Ppc	No gain or loss	
		Phosphoria	Rex Chert Member - Ppr	No gain or loss	
		Phosphoria	Meade Peak Phosphatic Shale Member - Ppm	No gain or loss	
		Wells	Upper Member - PPwu	Losing	
	Unnamed Tributary to Deer Creek T9S, R45E	Dinwoody	Upper Member - Trdu	Gaining	
			Lower Member - Trd1	Gaining	
		Phosphoria	Cherty Shale Member - Ppc	No gain or loss	
		Phosphoria	Rex Chert Member - Ppr	No gain or loss	
		Phosphoria	Meade Peak Phosphatic Shale Member - Ppm	No gain or loss	Flow measurement made approximately midway through member
		Wells	Upper Member - PPwu	Losing	Lost all surface flow crossing this member
			Lower Member - Pw1	Unknown	No stream flow
		Monroe Canyon Limestone -Mb		Unknown	No stream flow
		Wells	Lower Member - Pw1	Unknown	No stream flow
		Wells	Upper Member - PPwu	Unknown	No stream flow
Phosphoria	Cherty Shale Member - Ppc	Gaining	Contact between Ppr and Ppc was estimated in field, member assignment not definite		
		-and- Losing	Thin (?) exposure		
Phosphoria	Rex Chert Member - Ppr	Losing and gaining			
Phosphoria	Meade Peak Phosphatic Shale Member - Ppm	No gain or loss			
Wells	Upper Member - PPwu	Losing			
Wells Canyon T10S, R45E	Phosphoria	Rex Chert Member - Ppr	Gaining		
	Phosphoria	Meade Peak Phosphatic Shale Member - Ppm	No gain or loss	Alluvium at site may have created low surface flow	
	Wells	Upper Member - PPwu	Losing	All surface flow lost approximately 1,100 feet downstream of Ppm-PPwu contact	

Note: Formations listed in sequence proceeding downstream.

SPRING CHARACTERISTICS

Numerous springs were located during this study, a number of which are not shown on existing topographic maps. The primary information derived is the formation that supports the spring. Figure 5 summarizes the formations that were found to support springs and hence ground water flow systems. The majority of the springs occur in the Thaynes and Dinwoody Formations and have a mean discharge of 25 gallons per minute (1.6 liter/sec.). Few springs were found in the Phosphoria Formation and the Wells Formation but the mean discharge from the Wells Formation was 130 gpm (8.0 liter/sec).

CONCLUSIONS

The original hypotheses were basically confirmed by this study. The upper and lower members of the Dinwoody and Wells Formations support major ground water flow systems, but no major ground water flow system exists in the cherty shale or Meade Peak Phosphatic Member of the Phosphoria Formation. The Rex Chert Member supported a ground water flow system in a few instances.

Ground water flow systems in the area are separated by the Phosphoria Formation into one of two categories due to its low hydraulic conductivity. Those formations above the Phosphoria Formation support short ground water flow systems and numerous springs and gaining reaches of streams. Stream flow was always lost to the Wells Formation that underlies the Phosphoria Formation.

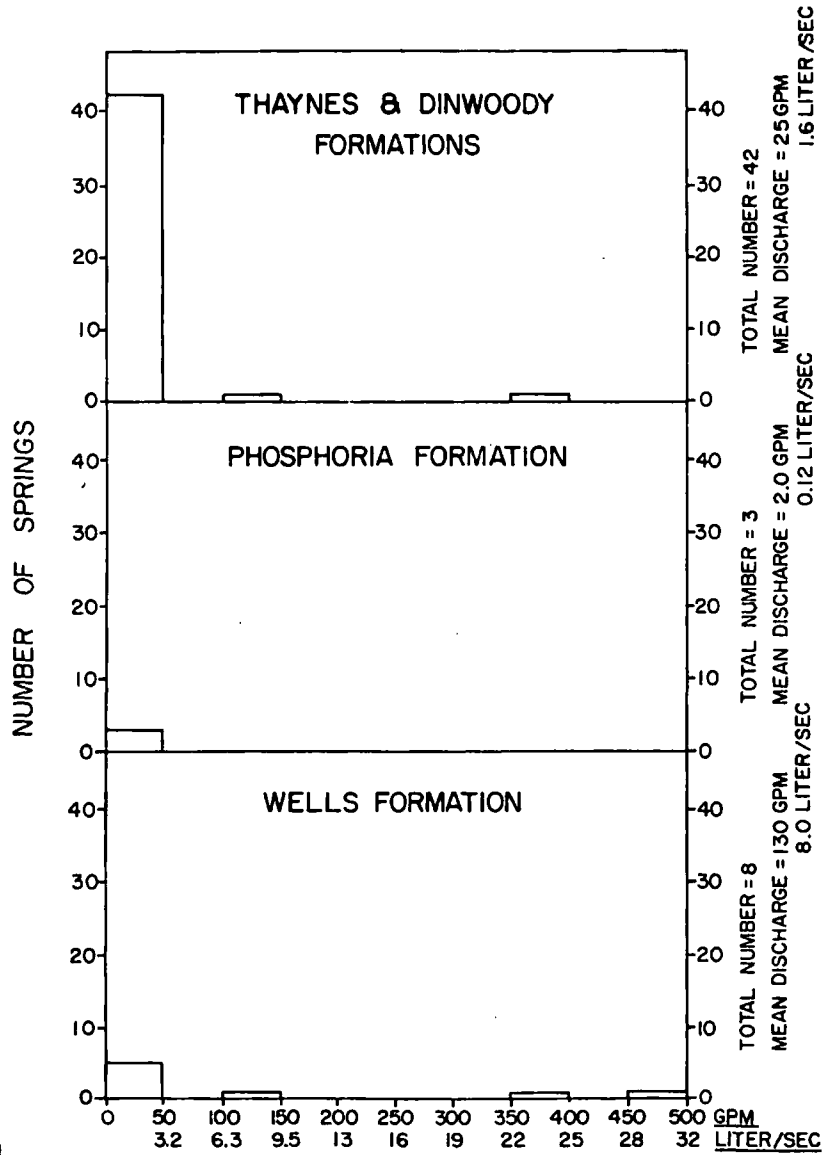


FIGURE 5 - Spring Discharge Histograms by Formation

REFERENCES

- Armstrong, Frank C., 1969, Geologic Map of the Soda Springs Quadrangle Southeastern Idaho: U.S. Department of the Interior, Geological Survey Map I-557, 2 plates.
- Cressman, Earle R., 1964, Geology of the Georgetown Canyon-Snowdrift Mountain Area, Southeastern Idaho: U.S. Department of the Interior, Geological Survey, Bulletin 1153, 105 p.
- Cressman, Earle R. and Gulbrandsen, Robert A., 1955, Geology of the Dry Valley Quadrangle, Idaho: U.S. Department of the Interior, Geological Survey, Bulletin 1015-I, 18 p.
- Gulbrandsen, R.A., McLaughlin, K.P., Honkala, F.S., and Clabaugh, S.E., 1956, Geology of the Johnson Creek Quadrangle, Caribou County, Idaho: U.S. Department of the Interior, Geological Survey, Bulletin 1042-A, 23 p.
- Lowell, Wayne Russell, 1952, Phosphatic Rocks in the Deer Creek-Wells Canyon Area, Idaho: U.S. Department of the Interior, Geological Survey, Bulletin 982-A, 52 p.
- Montgomery, Kathleen M. and Cheney, T.M., 1967, Geology of the Stewart Flat Quadrangle, Caribou County, Idaho: U.S. Department of the Interior, Geological Survey, Bulletin 1217, 63 p.
- Rioux, Robert L., Hite, Robert J., Dyni, John R., and Gere, Willard C., 1975, Geologic Map of the Upper Valley Quadrangle, Caribou County, Idaho: U.S. Department of Interior, Geological Survey, Map G0-1194, 6 p. and 1 plate.

THE USE OF RESISTIVITY SOUNDINGS IN A GROUND WATER PROBLEM AT ELK RIVER, IDAHO

By

Rainer Blum
College of Mines and Earth Resources
University of Idaho
Moscow, Idaho

ABSTRACT

The purpose of the investigation was to help the city of Elk River, Idaho find a new water well. The aquifer was believed to be closely related with an ancient valley bottom, now being covered by clays of an average thickness of 70 m. The resistivity method was chosen to determine the bedrock topography. Observations at an existing well, were used for the interpretation of 5 sounding profiles parallel to the striking direction of the valley. The resulting cross section is presented. Its significance with respect to the underlying ground water problem as well as correlations with drilling results will be discussed.

INTRODUCTION

Elk River is a small town located about 50 miles east of Moscow. Geologically, this puts it on the eastern margin of the Columbia Plateau Basalts. Since one year, Elk River lacks a satisfying water supply. At this time, the old city well, drilled in 1966, stopped functioning. Despite various engineering efforts, it couldn't be brought back into production. A new well, drilled 15 m aside the old one, did not find water. This led to a more detailed investigation of the geohydrology of the area.

The general geologic setting is typical for the marginal area of the Columbia Plateau Basalts. Some basalt flow entered the historical Elk Creek valley and dammed the stream. Thus, a lake was created and slowly filled up with sediments. Meanwhile, this lake has dried out and only its clayey and sandy sediments are remaining. They are up to 70 m thick. The geohydrologist's assessment of this situation is that the safest place for finding water is the ancient, now buried stream bed (D. Ralston, personal communication). There the river gravels could act as an aquifer. Thus, the problem of finding a suitable location for a well was reduced to the problem of determining the bedrock topography, or simply to find the deepest point of the granite surface. To those ends, a geophysical approach should be used.

APPLIED METHOD

The setting seemed to be ideal for any geophysical method, due to the simple, at least partly understood structure, which consists of two clearly contrasting materials, clayey sediments above granitic bedrock. The decision which method to apply was partly based on the equipment being available. Partly, however, it was hoped that an electrical resistivity sounding would not only

yield the bedrock contact but additional information, with respect to the transition from clay to granite, especially whether there are any hints for a possible aquifer.

The resistivity unit used was a regular, battery-powered ABEM Terrameter. Generally, electrical sounding means that a current is fed into the ground through two electrodes while the voltage between two other electrodes is observed. The reading gives a kind of spatial resistance of the ground. By considering for the geometry of the electrode set-up, this may be transformed into an apparent resistivity. The way how this apparent resistivity changes with increasing electrode spacing allows one to draw conclusions about the distribution of electrical resistivity in the subsurface. For simple structures, like horizontal two or three layer cases, the depth-resistivity function is found by comparing the observations with master curves. For more complicated cases, an indirect interpretation is applied whereby apparent resistivity-distance functions are computed for geologically reasonable models. Those models then are improved or adjusted until a satisfactory match is reached between the observed values and the computed model curve. This model is then accepted as the resistivity-depth distribution at the center point of the profile. A computer program has been developed to calculate such model curves for horizontally layered structures. It is based on the method given by Mooney et al. (1966), which was discussed and checked for its reliability by Inman et al. (1973). The such determined best model, however, only yields information concerning the depth-resistivity distribution. Resistivity, however, is not typical for a specific material. Generally, each material may vary widely in its resistivity, mainly due to its grade of consolidation and properties of its water content. In the case presented here, additional information helped to override this drawback. This information was contained in the driller's log, recorded for the old city well. By observing one sounding profile across this well, it could be determined which material belongs to which resistivity, a valuable help for interpreting five profiles, which were to be observed in the valley (Figure 1), parallel to the striking direction.

The costs for the project included two field days for two persons, half a day of processing and interpreting the data, and equipment rental. They remained well below \$1,000, which has to be compared with the price of \$10,000 for one drill hole.

RESULTS

The test profile at the old city well could only be observed over a length of ± 100 m from the center point, due to buildings. Figure 2 shows the best model chosen as an interpretation in the lower part. It consists of 2 m with a resistivity of $170 \Omega\text{m}$ followed by 3 m with $20 \Omega\text{m}$, then 60 m with $70 \Omega\text{m}$, then the end value of $500 \Omega\text{m}$ is reached. The low resistivities of 20 and $70 \Omega\text{m}$ are typical for clayey sediments. The bottom of the sediments is marked by a sharp increase in resistivity. The match between

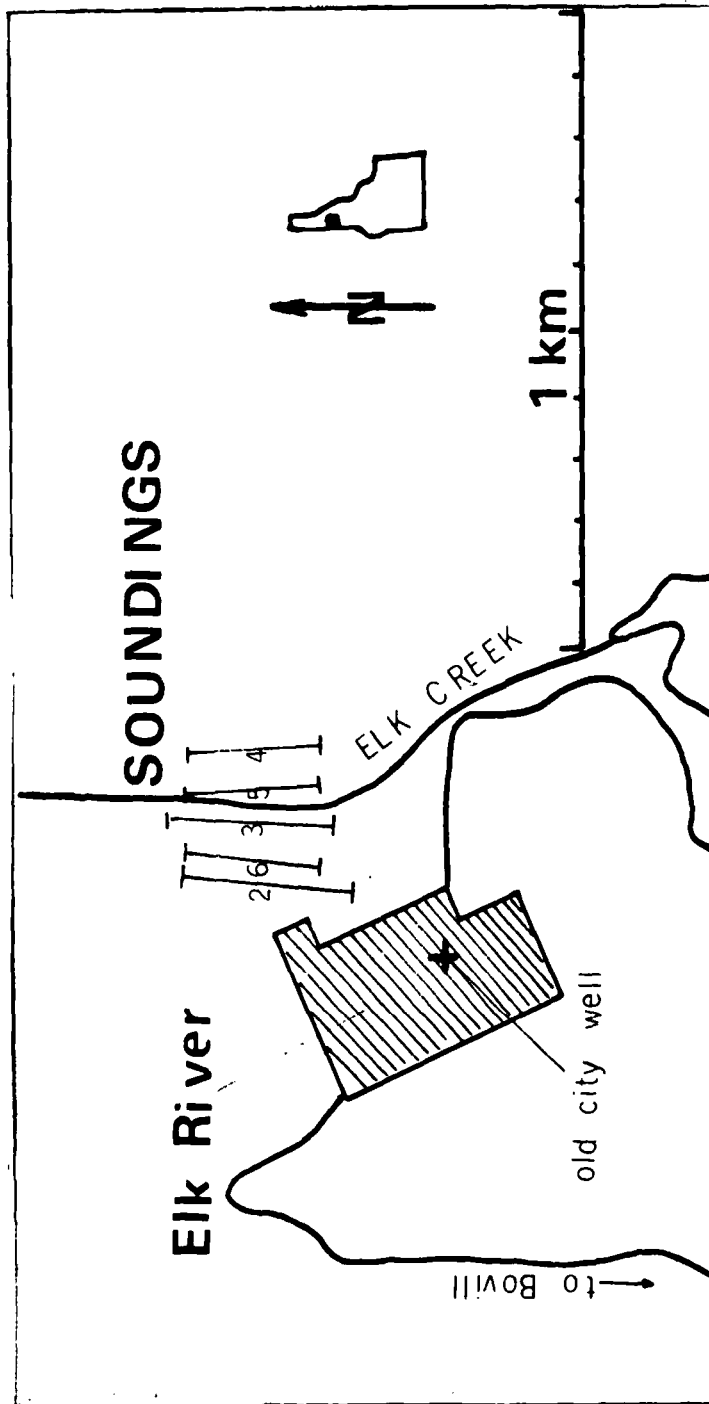


FIGURE 1

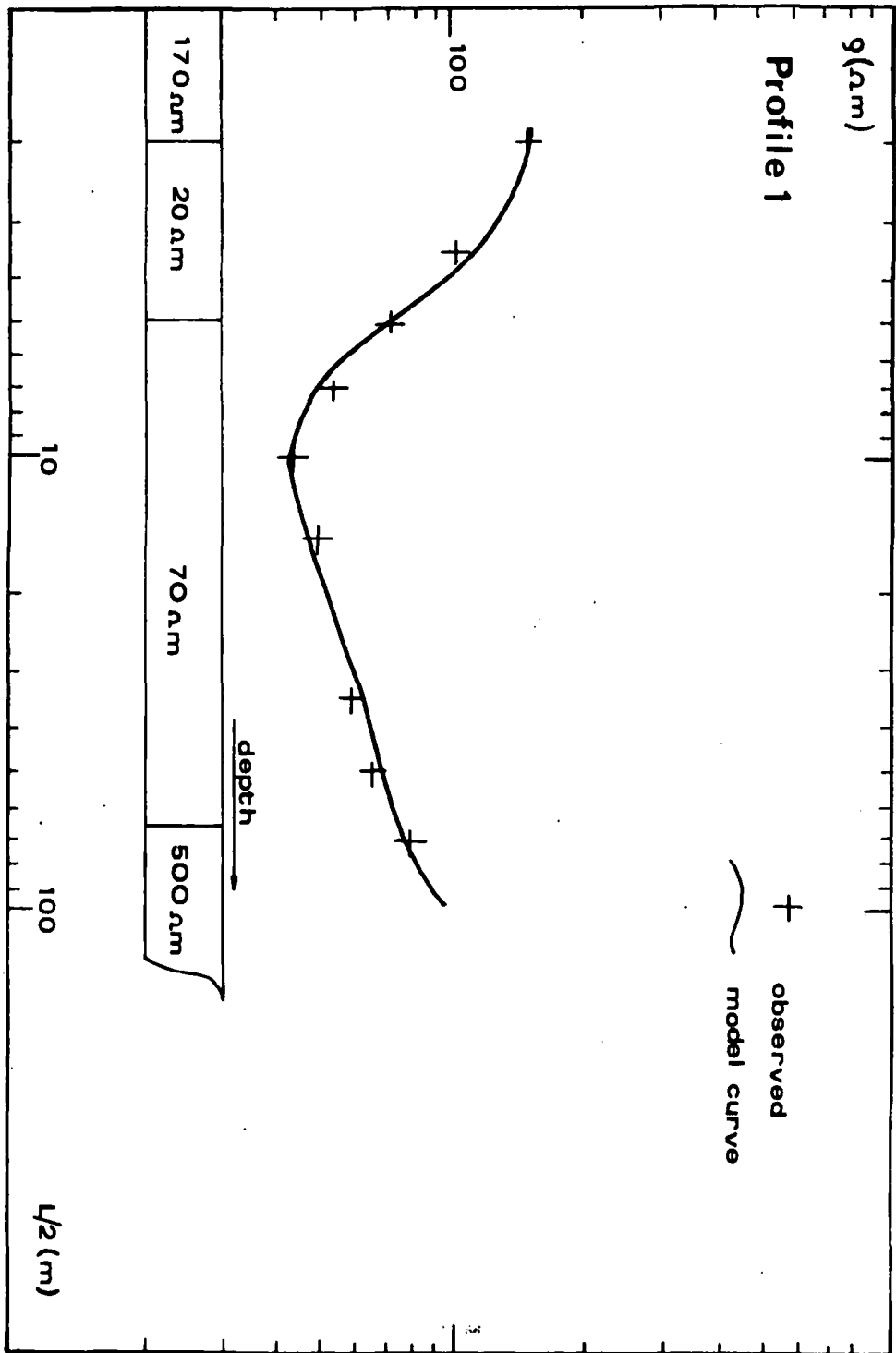


FIGURE 2

The Use of Resistivity Soundings
in a Ground Water Problem at Elk River, Idaho
By Rainer Blum
Page 5

observations and model curve is excellent in this case, indicating that the model represents a realistic possibility. Because of the profile's limited length, no conclusions can be drawn with respect to the structure below the granite surface. The model simply assumes the 500 Ωm extending infinitely deep. The effect of this layer, however, is only weakly visible at the very end of the model curve.

The value of this sounding interpretation becomes clear when compared to the driller's log of the well, as shown in Figure 3. The driller's classification of dirt and clay for the top 2 m coincides nicely with the 170 Ωm layer of equal thickness. Below this zone, the driller's log reports one layer of fine sand and clay, 65 m thick, interrupted only once by a thin bed of coarse sand. The resistivity sounding yields a similar picture, beneath 3 m of obviously rather pure clay (20 Ωm) the whole clay and sand zone is lumped together into a single 70 Ωm layer. Of course, this sediment zone is well structured as described e.g. by Jones (personal communication). He lists up 13 different layers - sandy clays and clayey sands - for this zone. As this sedimentary filling itself is of no interest for the investigation, it is a special advantage that it can be treated as one homogeneous layer. The bottom of this overburden, the beginning of the water zone in the driller's log and the resistivity increase to 500 Ωm coincide in depth. So the significance of this test profile for the investigation is that it shows what type of resistivity-depth structure is to be expected at the sounding sites in the valley: a varying cover (soil, sand or gravel) above a consistent 70 Ωm - layer, the bottom of which should be marked by a sharp increase in resistivity. A bedrock aquifer should show up as a resistivity around 500 Ωm . For dry, sounder bedrock materials even higher values are to be expected.

Figure 4 to 8 show the results for the sounding sites. Profile 2 (Figure 4) is described by a model consisting of 2 m with 350 Ωm and 2 m with 700 Ωm overlaying 35 m of clay sediments. The transition to the bedrock here is sharper than at the city well. The 1,000 Ωm resistivity indicates that the granite here is in a sounder condition and probably doesn't act as an aquifer. The match between model curve and observations is quite satisfactory, deviations at medium distances could be controlled by varying the top materials. The contact between clay and granite is well determined in depth as well as in sharpness.

A similar structure is found at profile 3 (Figure 5). Under 2 m of 120 Ωm , 5 m of 400 Ωm , and 35 m of 70 Ωm , a sharp increase to 1,000 Ωm explains the observations.

The model at site 4 (Figure 6) varies in overburden and in the transition to the bedrock. It consists of 1 m with 6,500 Ωm (dry sand), 5 m of 2,500 Ωm (gravel), 5 m of 700 Ωm (clayey gravel), 5 m of 70 Ωm (clay zone) above a 500 Ωm material. A nearby Forest Service well reported cemented conglomerate under "muck" and called it an aquifer. This kind of material could explain a resistivity of 500 Ωm , it could however, as well be a fractured granite which increases in quality with depth.

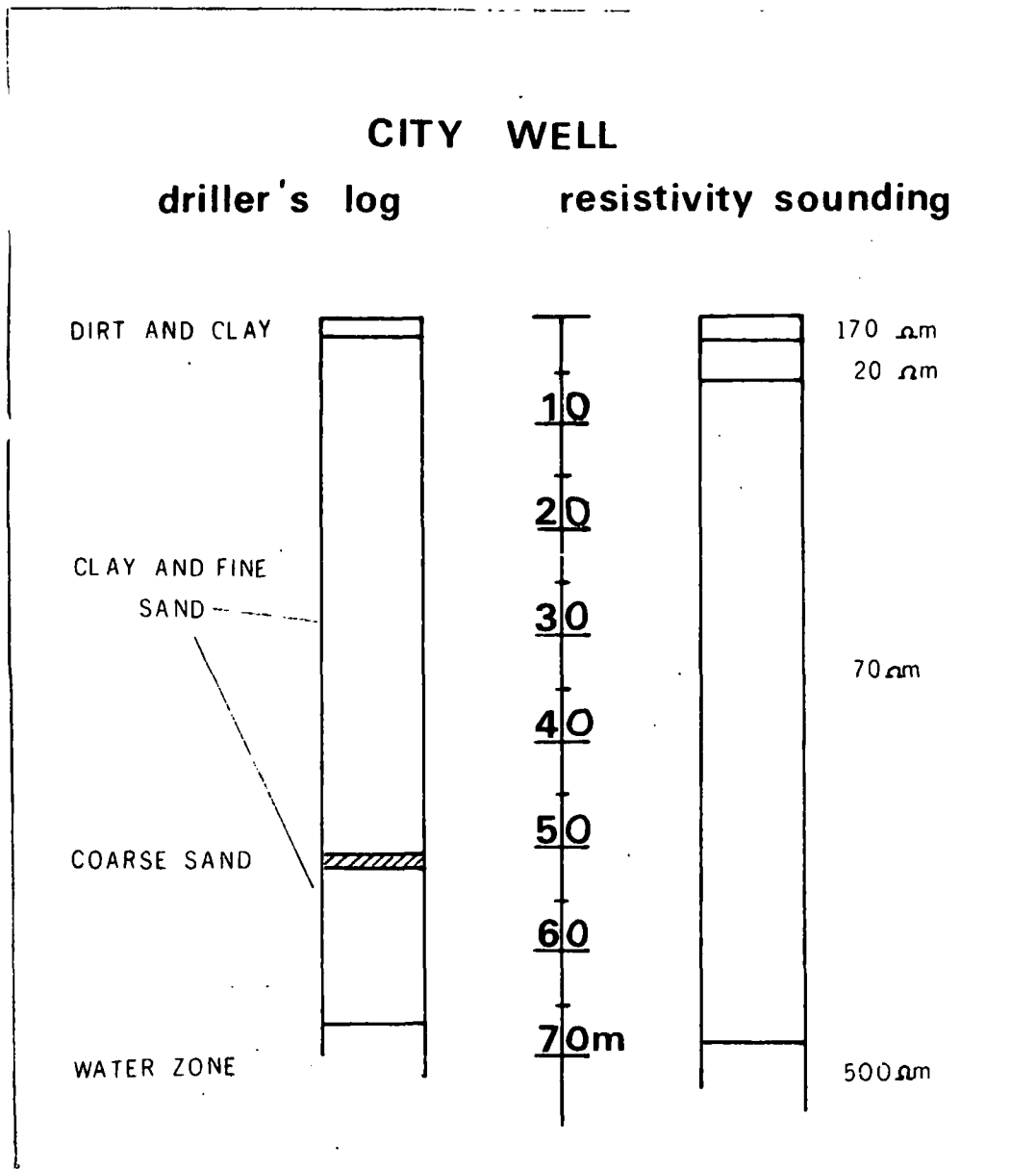


FIGURE 3

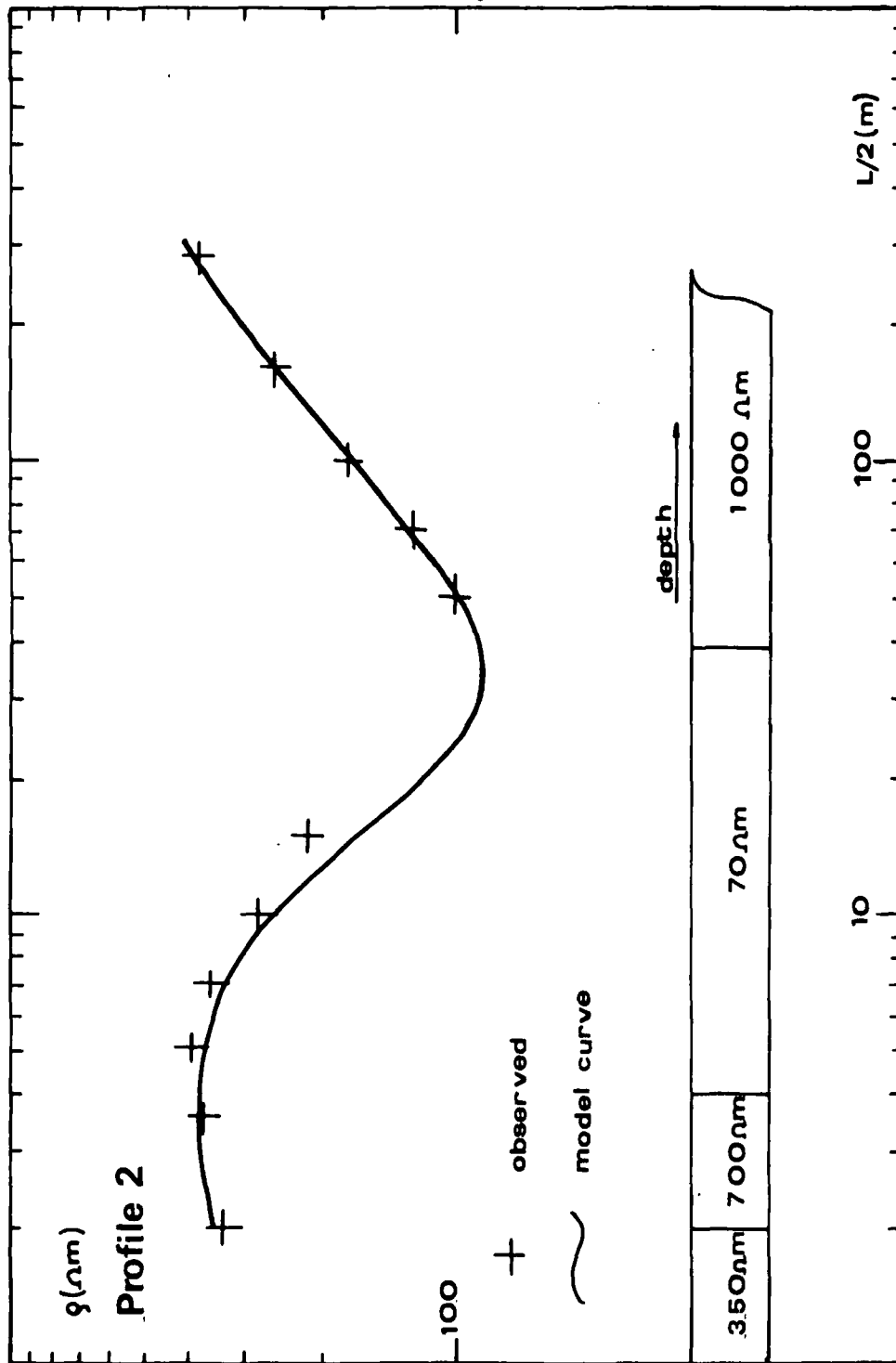


FIGURE 4

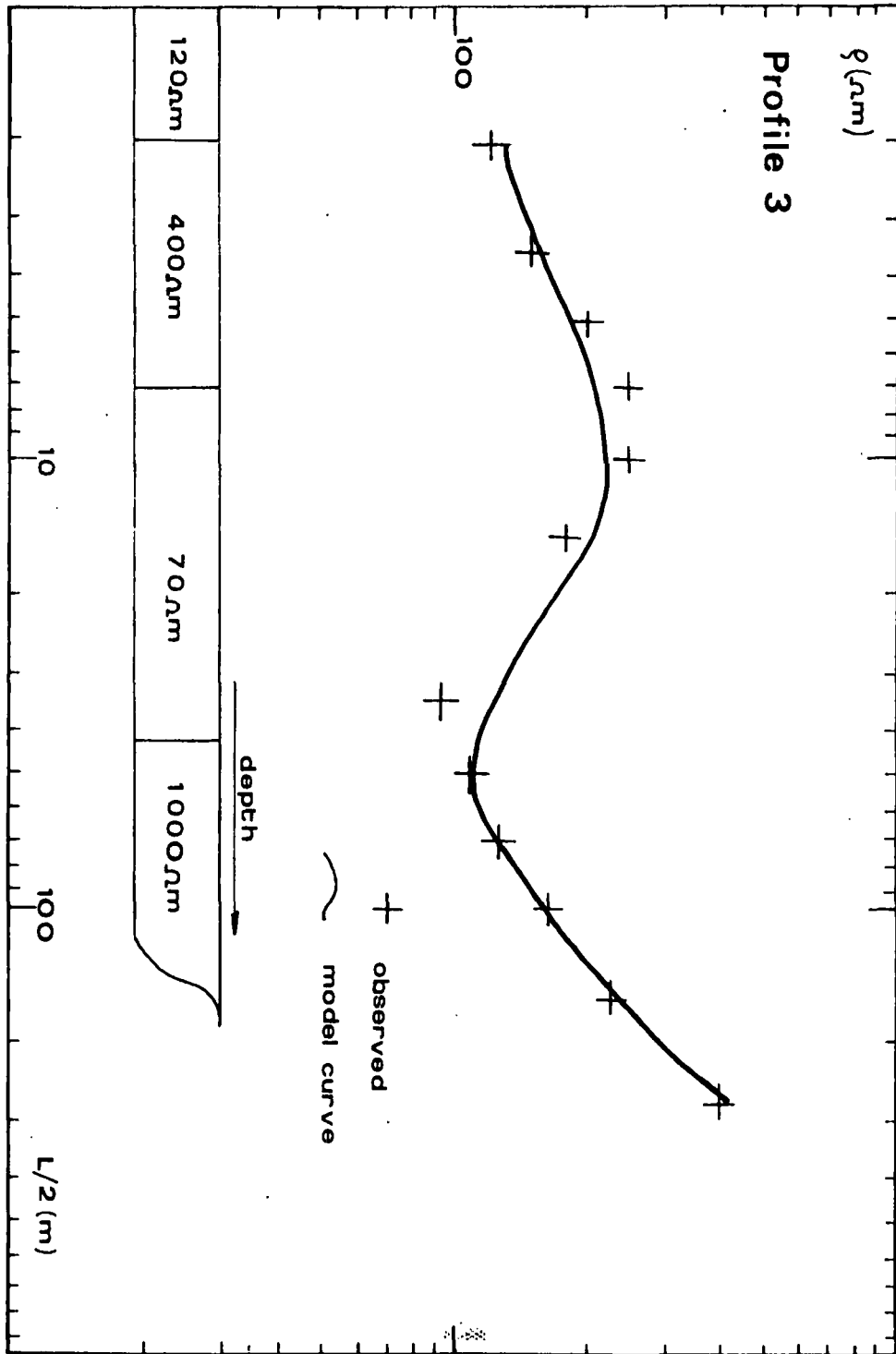


FIGURE 5

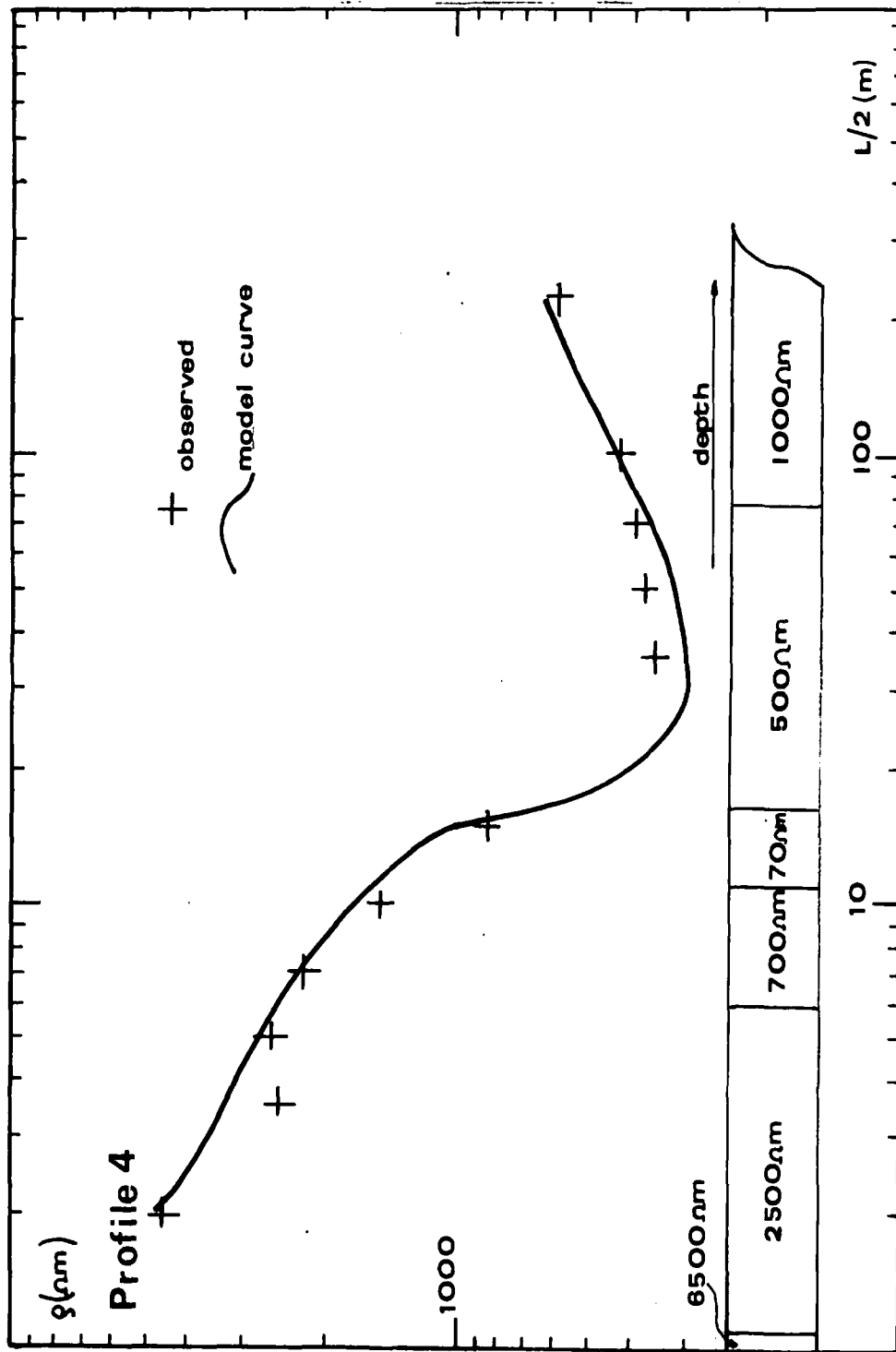


FIGURE 6

A similar transition is encountered at profile 5 (Figure 7). Here, under 4 m of 2,000 Ωm (gravel), 2 m of 300 Ωm (clayey gravel), 15 m of 70 Ωm (clay zone), 5 m of 500 Ωm are reached. At a depth of 26 m, the sound granite starts with a resistivity of 1,000 Ωm . The above mentioned Forest Service well, located close to this profile, gives a depth of 25 m to the conglomerate. The model curve further shows the influence of a variation in the bedrock resistivities between 1,000 and 2,000 Ωm .

Profile 6 (Figure 8) is explained by 3 m of 2,500 Ωm , 40 m of 70 Ωm and again, 5 m of 500 Ωm above the 1,000 Ωm material. Despite the poor fit of observations at short distances, the character and depth of this 500 Ωm transition is well secured. Because the profile is located on the same side of the valley as the city well, it is assumed that here 500 Ωm mark the surface of the granite, jointed as at the city well.

JOINT INTERPRETATION

The models for all profiles are combined in the cross section shown in Figure 9. The various covers are left white as they are not significant for the goal of the interpretation. The clay zone is marked by black. Below this sediment filling an extrapolation is proposed for the bedrock surface by the black line. The resulting deepest point of the granite surface is located right beneath the center of profile 6 and 3. Choosing the upper boundary of the 500 Ωm material at profile 5 as granite surface, the extrapolated deepest point would be shifted slightly towards profile 3. An additional sounding over the here assumed deepest point of the bedrock, would help to confirm the exact location and also the character of the transition. It was not observed because of terrain conditions.

The results presented in Figure 9 were regarded as reliable enough to recommend the center point between profiles 6 and 3 as a drilling site. An encouraging confirmation for the findings came from a later found well log for an abandoned well at profile 3. The log reports a depth of 42-45 m to the granite, the prediction given by the sounding model is 42 m. The final value of this resistivity interpretation will be determined as soon as the well will be drilled.

CONCLUSIONS

Concluding it shall be pointed out that an electrical resistivity survey gave good and inexpensive results in this environment of highly contrasting materials. The depth penetration to more than 50 m did not pose a difficulty. The interpretation was largely facilitated by incorporating information from an existing well.

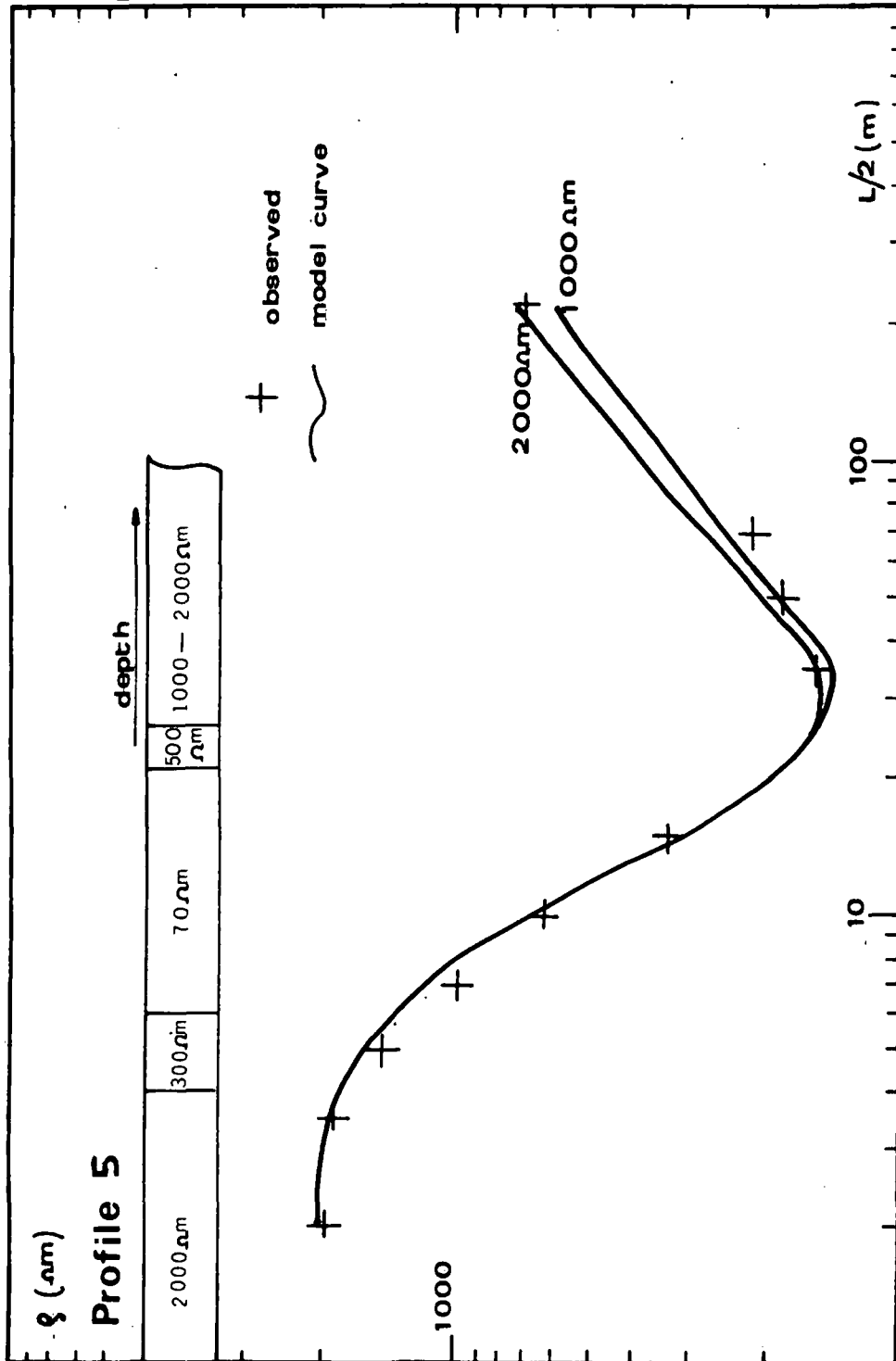


FIGURE 7

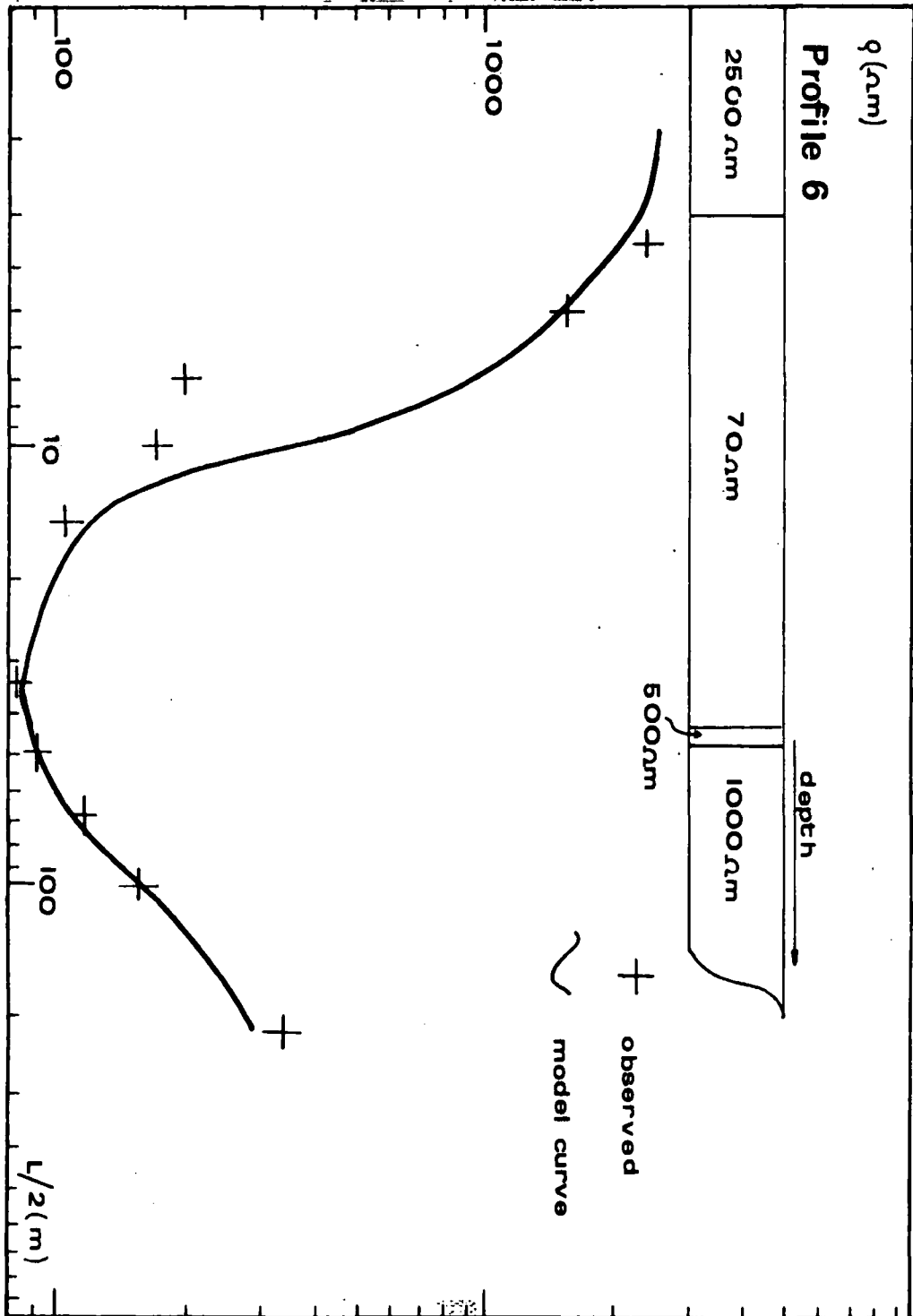


FIGURE 8

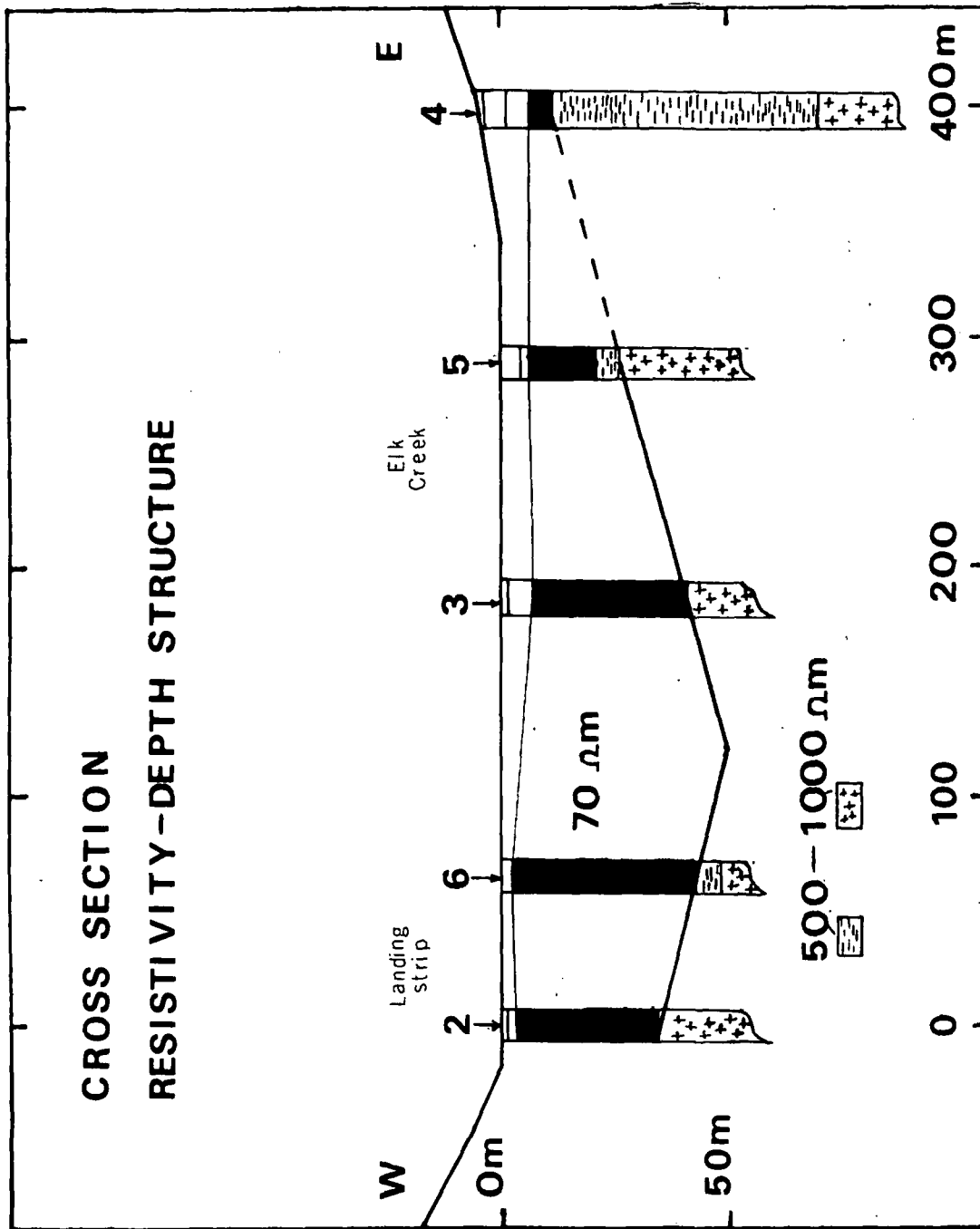


FIGURE 9

The Use of Resistivity Soundings
in a Ground Water Problem at Elk River, Idaho
By Rainer Blum
Page 14

ACKNOWLEDGEMENTS

Dale Ralston helped the author towards a basic understanding of the geologic background. Mike Allen helped with the field work and Elaine Utter typed the manuscript.

REFERENCES

- Inman, J.R., J. Ryn, and S.H. Ward. Resistivity Inversion, Geophysics, Vol. 38 No. 6, 1088-1108, 1973.
- Mooney, H.M., E. Orellana, H. Picket and L. Tornheim. A Resistivity Computation Method for Layered Earth Models, Geophysics, Vol. 31, 192-203, 1966.

MATHEMATICAL MODELING APPROACH FOR DELINEATING LANDSLIDE HAZARDS IN WATERSHEDS

By

Timothy J. Ward, Ruh-Ming Li and Daryl B. Simons
Department of Civil Engineering
Colorado State University
Fort Collins, Colorado

ABSTRACT

A physically based mathematical model has been developed that estimates landslide potential. Because uncertainty exists in the input variables, a probability of failure reflecting this situation is also computed. The model was applied to a forested watershed in Oregon. Results indicate the model provides a realistic approach for determining landslide hazards. A limitation of this method is encountered in providing actual input data for soil parameters and vegetative strength. Although these values are often hard to obtain, realistic estimates can provide a relative classification of landslide hazards in the watershed. Examples demonstrate the use of the model in delineating hazards under varying groundwater conditions and timbering activities. The landslide hazard delineation model can provide an effective methodology for assessing the relative stability of a watershed under various dynamic conditions.

INTRODUCTION

Landslides pose an ever present threat to man's activities in hilly or mountainous watersheds. In addition to interfering with timbering, road building, mining, recreation, or second home development, landslides can provide large amounts of sediment to stream channels. This sediment can then lower water quality, increase flood hazards, and affect fisheries. Landslides are often initiated by man's activities or by natural events such as rainfall or earthquakes. In order to avoid triggering landslides and provide better scheduling of watershed activities to bypass potential landslide sites, methodologies are needed for delineating landslide hazards.

Landslides in watershed soils are a result of a combination of several interacting factors including soil strength, soil depth, groundwater, slope inclination, and vegetative influences. This paper presents an approach for delineating potential landslide areas based on such factors using a common geotechnical model. Using a watershed modeling approach the model, based on physical characteristics is developed and applied to a selected watershed. The results are encouraging suggesting that this approach may prove useful to the land use manager.

CURRENT APPROACHES

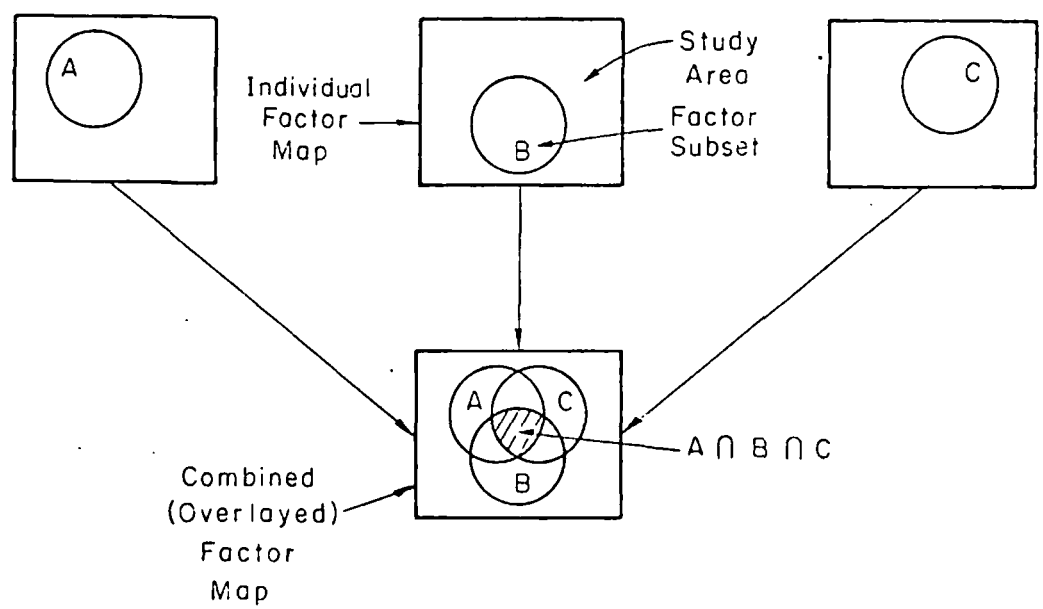
There are many approaches to landslide potential delineation. These approaches include on-ground monitoring, remote sensing techniques, factor overlay methods, statistical models, and geotechnical process models.

On-ground monitoring consists of utilizing installed measuring devices such as strain gages and down hole tilt meters. This type of approach is extremely useful for checking suspected landslide zones but is limited in aerial coverage because of cost of installation and maintenance. Chang (1971) summarized many of these techniques. Takada (1968) and Takeuchi (1971) provided two examples of applications of different methods.

Remote sensing coupled with pattern recognition techniques provide a means for surveying large areas. In this approach, remotely sensed data, particularly aerial photography such as black and white, color infrared, and multiband spectral, can be analyzed for features distinctive of landslide hazards (Liang and Belcher, 1958; Poole, 1969, 1972; McKean, 1977). This analysis, a type of the more general pattern recognition, can be quite effective if landslide hazards are manifested in surface characteristics that can be photographed. However, it is not always the situation since landslides often result from deep seated factors not visible on the ground surface.

The most common delineation method concurrently in use is factor overlay or a combination of landslide producing elements. Krynine and Judd (1957) noted that landslides occur in a regional framework, or that certain factors common to a region contribute to landsliding. Baker and Chieruzzi (1959) expanded this concept to develop a physiographic classification of landslide hazards based on topography, erosional development, and associated rock types. Blanc and Cleveland (1968) were two of the first to attempt delineating landslides by use of selected factors. Evans and Gray (1971) presented a methodology for mud slide risk delineation in Southern Ventura County, California. Cleveland (1971) summarized and presented those factors important in regional landslide prediction. His factors include precipitation, rock strength, vegetation effects, slope, and stream pattern. The approaches described by Nilsen and Brabb (1973) and the Building Research Advisory Board (1974) follow this systematic methodology using landslide factors. In this approach, certain factors related to landslide occurrence are individually delineated. For example, if landslides occur where steep slopes, weak earth materials, and water are all coincident, then these factors should be used as slope stability indicators. Areas where factors coincide can then be classified as a hazard potential. Simons and Ward (1976) summarized this approach as the factor overlay method or set theory approach to hazard delineation as presented in Figure 1. Although not explicitly stated in delineation schemes, this idea is the basis for most techniques.

The factor overlay approach is conceptually correct since it recognizes that landslides are a combination of different factors. However, this approach is subjective and nonsensitive to dynamic inputs. Subjectivity results from a lack of defined guidelines for developing and weighting various factors. Nonsensitivity occurs because static factors are usually considered while dynamic factors, such as groundwater fluctuations, are excluded. Factor overlay can be improved if standardized guidelines are developed, dynamic factors are incorporated, and realistic weighting functions are used. Simons and Ward (1976)



<u>Potential</u>	<u>Set</u>
High	$A \cap B \cap C$
Medium	$A \cap B; B \cap C; A \cap C; A; B; C$
Low	$A \cup B \cup C$ (i.e. not in A, B, or C)

\cap - Intersection of Subsets
 \cup - Union of Subsets

FIGURE 1 - Set Theory Approach to Landslide Potential Classification
 (From Simons and Ward, 1976)

presented a numerical approach to the factor overlay technique that may help quantify the relative importance of each factor.

Another method of potential delineation is use of empirically developed models. These models, developed through statistical analyses of measurable data, attempt to provide a numerical value related to slope stability. Multiple regression and discriminant function analyses are common techniques for developing such relationships (Jones, Embody and Peterson, 1961; Waltz, 1971). Empirically derived relationships have a major drawback since they require large amounts of data to develop the equations. Such data is usually temporally and spatially static. Temporally static implies the developed relationship is applicable to

a limited time span during which data was collected and, therefore, does not represent changing conditions. Spatially static implies the method is applicable to a limited area and transfer to other areas may not be warranted.

A final type of landslide hazard delineation methodology is based on geotechnical models. Geotechnical models are derived from observed natural phenomena and basic laws of physics, and are representative of the physical process being studied. Geotechnical models of slope stability relate the forces acting on the hill slope. One set of forces, predominated by gravity, acts to move earth materials downslope. The other set of forces, predominated by the shear strength of the earth materials, resists the driving gravity forces. When driving forces exceed resisting forces, a landslide occurs. Geotechnical models have been developed and modified to account for primary factors in landslide occurrence such as soil strength, groundwater influences, vegetative effects, and slope inclination. Because geotechnical models represent actual field conditions they can be used to analyze the response of a hill slope to temporally and spatially varying factors. Simplifying assumptions can yield a method for determining the probability of a landslide. Because of the ability to account for several temporally and spatially varying contributing factors in a nonsubjective, physically meaningful manner, geotechnical models are promising methods for landslide potential delineation.

FACTOR OF SAFETY DELINEATION MODEL

Model Selection

The analysis presented in this paper is applicable to translational or planar types of landslides in soil masses. Rock masses require a more complex analysis because of their response to the geometry of failure planes, and are not considered here.

Various types of slope stability models exist. Two basic types are the infinite slope and finite slope models, each derived by a different set of assumptions (Lambe and Whitman, 1969). Common to both types is the formation of a factor of safety equation that consists of a ratio of resisting to driving forces of

$$FS = \frac{R}{D} \quad (1)$$

where FS = factor of safety; R = resistive forces; and D = driving forces.

Resistive forces are related to soil strength and vegetative parameters while the primary driving force is the downslope weight of the soil mass. If resistance is less than the driving force, then the factor of safety is less than one indicating failure.

The infinite slope model of slope stability is primarily applicable to failure occurring along planar type surfaces such as translational slides. The model presented in this paper consolidates and refines ideas presented by several researchers (Brown and Sheu, 1975; O'Loughlin, 1974; Simons, Ward, and Li, 1976; Swanson, et al., 1973). These developments were further studied by Ward (1976) to yield the model's present form. Because finite slope formulations also relate the same resisting and driving force elements, the model can estimate the failure potential for other landslide types such as rotational slumps.

Derivation of Model Equations

Derivation of the equations of static equilibrium for an infinite slope is relatively easy (Brown and Shen, 1975; Lambe and Whitman, 1969; O'Loughlin, 1974). The derivation presented here is similar to those given by previous authors but with changes in the formulation and simplification of the basic model. An idealized infinite slope consisting of a single soil type with isotropic properties resting on a bedrock interface is shown in Figure 2. This situation is similar to residual soil slopes found in forested watersheds and most hilly or mountainous terrain.

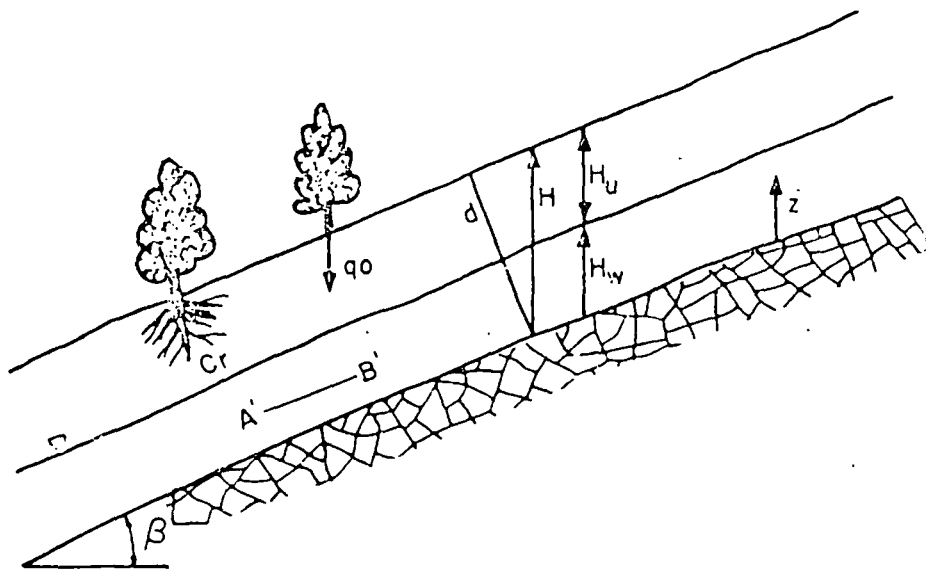


FIGURE 2 - Idealized Infinite Slope

The shear strength of a soil can be represented by the Coulomb equation of

$$\tau = \bar{c} + \bar{\sigma} \tan \bar{\phi} \quad (2)$$

where τ = shear strength; \bar{c} = effective cohesion intercept; $\bar{\sigma}$ = effective normal stress; and $\bar{\phi}$ = effective angle of internal friction.

Equation 2 is applicable to drained soil strength conditions and represents resisting forces contributed by the soil mass. Components of \bar{c} and $\bar{\phi}$ (hereafter, the overbar will be dropped) are intrinsic strength characteristics of soil and represent interaction of soil factors.

Analysis of Figure 2 aids evaluation of $\bar{\sigma}$. Normal stress on plane A' - B' located at a distance, Z, above the bedrock surface in the soil mass can be easily solved if the plane is assumed parallel to soil and bedrock surfaces and is located between Z = 0 and Z = H_w. The total normal stress, σ , on this plane can be written as

$$\sigma = \sum_{i=1}^n \gamma_i \Delta z_i \quad (3)$$

where γ_i = unit weight of layer i; and Δz_i = thickness of layer i.

In this case n = 2 for the saturated and unsaturated soils but can be expanded to a multilayer case. However, in many residual soils, assumption of a single soil type is often valid (Lumb, 1970). The geometry and other important factors can be used to evaluate σ . The normal stress on plane A' - B' is composed of stresses from soil weight and tree surcharge. Soil weight per area component is (H_u cos β γ) for the soil above water table level and [(H_w-Z) cos β γ_{sat}] for soil below water table level. Normal force per area supplied by tree surcharge is (q₀ cos β). Assuming the contact surface as a unit squared the area enables the normal stress to be written as

$$\sigma = [q_0 \cos \beta + (H_w - Z) \cos \beta \gamma_{sat} + H_u \cos \beta \gamma] \cos \beta \quad (4)$$

In Equation 4 the area upon which the normal force acts is defined as cos β times a unit area. Since H_u = H - H_w, Equation 4 can be converted to

$$\sigma = H \cos^2 \beta [q_0/H + \gamma_{sat} (M - Z^*) + \gamma (1 - M)] \quad (5)$$

where $M = \frac{H_w}{H}$ = relative groundwater height and $Z^* = \frac{Z}{H}$ = relative position from bedrock surface.

Because groundwater is present, the buoyancy effect of pore water pressures must be considered in Equation 4. From the effective stress concept the relationship between total and effective normal stress in soil mass components is

$$\bar{\sigma} = \sigma - u \quad (6)$$

where u = the pore water pressure. Hydrostatic pressure can be formulated as

$$u = H(M-Z^*) (\cos^2\beta)\gamma_w \quad (7)$$

Combining and simplifying Equations 5, 6, and 7 yields

$$\bar{\sigma} = H\cos^2\beta [q_0/H + (\gamma_{sat} - \gamma_w) (M-Z^*) + \gamma(1-M)] \quad (8)$$

Consequently, the shear resistance equation becomes

$$\tau = c + H\cos^2\beta [q_0/H + (\gamma_{sat} - \gamma_w) (M-Z^*) + \gamma(1-M)] \tan\phi \quad (9)$$

The cohesion term, c , in Equation 9 has two components in forested watersheds -- soil cohesion and tree root cohesion. Gray (1970, 1978) described several ways that vegetation enhances slope stability. One of these is anchoring soil to underlying strata. Endo and Tsuruta (1968) and O'Loughlin (1974) showed that anchoring can be represented in the FS equation as a cohesion term, C_r . The cohesion term, c , can then be replaced by terms for soil cohesion, C_s , and root cohesion, C_r .

A similar analysis can be made for shear stress induced on the plane. Shear stress is composed of loads resulting from the weight of the soil mass, tree surcharge, and wind shear in trees imparted to the soil mass. Seismic loading is not considered. Because air flow usually conforms to ground surfaces or treetops, adverse wind shear will be directed downslope parallel to the failure plane. Downslope components of tree and soil loadings are used except when groundwater flow is assumed parallel to the failure plane; then pore water pressure does not enter shear force computation. Shear stress can then be represented as

$$\tau' = H\sin\beta \cos\beta \left[\frac{q_0}{H} + \frac{T_{sw}}{H\sin\beta \cos\beta} + \gamma_{sat} (M-Z^*) + \gamma(1-M) \right] \quad (10)$$

If τ = overall shear resistance and τ' = overall shear stress, the factor of safety equation can be written as

$$FS = \frac{R}{D} = \frac{\tau}{\tau'} \quad (11)$$

Substituting shear strength (Equation 9) and shear stress (Equation 10) into Equation 11 yields a factor of safety equation of

$$FS = \frac{Cs+Cr+H\cos^2\beta\left\{\frac{q_0}{H}\right\} + (\gamma_{sat} - \gamma_w)(M-Z^*) + \gamma(1-M)}{H\left\{\frac{q_0}{H}\right\} + (Tsw/H\sin\beta\cos\beta)+\gamma_{sat}(M-Z^*)+\gamma(1-M)} \tan\phi \quad (12)$$

Parameters in Equation 12 can be placed into nondimensional groups as

$$FS = \frac{\frac{2(Cs+Cr)}{\gamma_w H \sin 2\beta} + \left[\frac{q_0}{\gamma_w H} + \frac{(\gamma_{sat} - 1)(M-Z^*)}{\gamma_w} + \frac{\gamma}{\gamma_w}(1-M)\right] \frac{\tan\phi}{\tan\beta}}{\frac{q_0}{\gamma_w H} + \frac{2Tsw}{\gamma_w H \sin 2\beta} + \frac{(\gamma_{sat})}{\gamma_w}(M-Z^*) + \frac{\gamma}{\gamma_w}(1-M)} \quad (13)$$

As Equation 13 shows, the basic model contains variables for four factors present in a forested area. Representing soil factors are γ , γ_{sat} , Cs , and ϕ ; all controlled by soil type, while H = a measure of soil depth. Topography is included as slope inclination, β . Vegetative factors are q_0 , Cr , and Tsw . Finally, a dynamic factor for relative groundwater level is included as M . This basic equation is used to derive a more simplified form.

Using sensitivity and order of magnitude analysis techniques, Ward (1976) showed the factor of safety (Equation 13) could be reduced to an accurate, simpler form by determining that certain variables were relatively unimportant and others could be assumed as constants. Relative depth, Z^* , was set at zero for the worst case. Wind shear, Tsw , was determined insignificant in magnitude, and soil mass and tree loading terms had little effect on the sensitivity of the equation. Soil and tree loading could have either positive or negative effects on slope stability depending on other factors. The simplified infinite slope factor of safety model used in this study for estimating landslide potential is then

$$FS = \frac{2(C_s + C_r)}{\gamma_w H \sin 2\beta} + \frac{\left[\frac{q_0}{\gamma_w H} + \left(\frac{\gamma_{sat}}{\gamma_w} - 1 \right) M + \frac{\gamma}{\gamma_w} (1-M) \right] \frac{\tan \phi}{\tan \beta}}{\frac{q_0}{\gamma_w H} + \left(\frac{\gamma_{sat}}{\gamma_w} \right) M + \frac{\gamma}{\gamma_w} (1-M)} \quad (14)$$

Equation 14 defines the landslide potential of a slope in terms of a factor of safety value. For relative rankings of hazards, limits of factor of safety values can be established considering possible errors in the variables. Relative errors in factor of safety values can be approximately 20 to 30 percent (Ward, 1976), comparable to results of others (Feld, 1965; Singh, 1971). A realistic set of relative hazard levels is given in Table 1, Column 2. Although other limits could be selected, these values were considered most appropriate for the cases under examination.

TABLE 1

Model Classification of Landslide Potential and Probability		
Classification (1)	Landslide Potential FS (2)	Landslide Probability P[FS < 1] (3)
High	< 1.2	> 60%
Medium	1.2-1.7	30-60%
Low	> 1.7	< 30%

Derivation of Probability Delineation

Soil and root strength parameters are highly variable or uncertain. Other parameters such as soil depth, slope angle, unit weight of soil, and groundwater depth can be estimated and set at some conservative value. If groundwater level, M, is assumed at a steady state, and H, β, and γ are known, the factor of safety equation can be simplified to

$$FS = L_1(C_s) + L_1(C_r) + L_2(\tan \phi) \quad (15)$$

where

$$L_1 = \frac{2}{\gamma_w H \sin 2\beta \left[\left(\frac{q_0}{\gamma_w H} \right) + \left(\frac{\gamma_{sat}}{\gamma_w} \right) M + \left(\frac{\gamma}{\gamma_w} \right) (1-M) \right]} \quad (16)$$

and

$$L_2 = \frac{\left(\frac{q_0}{\gamma_w H}\right) + \left(\frac{\gamma_{sat}}{\gamma_w} - 1\right)M + \left(\frac{\gamma}{\gamma_w}\right) (1-M)}{\left[\left(\frac{q_0}{\gamma_w H}\right) + \left(\frac{\gamma_{sat}}{\gamma_w}\right) M + \frac{\gamma}{\gamma_w} (1-M)\right]} \tan \beta \quad (17)$$

If Equation 14 is rewritten in terms of random variables, it becomes

$$S = L_1 X + L_1 Y + L_2 Z \quad (18)$$

where S, X, Y, and Z are the random variables. The expected value, $E[\cdot]$, or the mean of a linear equation such as Equation 18 is (Benjamin and Cornell, 1970)

$$E[S] = L_1 E[X] + L_1 E[Y] + L_2 E[Z] \quad (19)$$

If the strength parameters are considered independent (Holtz and Krizek, 1971; Lumb, 1970), the variance, $\text{Var}[\cdot]$, or standard deviation squared becomes

$$\text{Var}[S] = E[(S - E[S])^2] \quad (20)$$

or

$$\text{Var}[S] = E[S^2 - 2E[S]S + E^2[S]] \quad (21)$$

Following the form of Equation 19, Equation 21 becomes

$$\text{Var}[S] = E[S^2] - 2E[S] \cdot E[S] + E^2[S] \quad (22)$$

because

$$E[E[S]] = E[S]$$

Equation 22 reduces to

$$\text{Var}[S] = E[S^2] - E^2[S] \quad (23)$$

The term S^2 is defined as

$$S^2 = L_1^2 [X^2 + 2XY + Y^2] + L_1 L_2 2Z[X + Y] + L_2^2 Z^2 \quad (24)$$

Substitution of Equation 24 into Equation 23 yields

$$\text{VAR}[S] = L_1^2 [E[X^2] + 2E[X] E[Y] + E[Y^2]] + 2L_1 L_2 E[Z] [E[X] + E[Y]] + L_2^2 E[Z^2] - E^2[S] \quad (25)$$

Following the form of Equation 22, the substitution for $E[X^2]$ can be made as

$$E[X^2] = \text{Var}[X] + E^2[X] \quad (26)$$

Similar substitutions are made for Y and Z yielding

$$\begin{aligned} \text{Var}[S] = & L_1^2[\text{Var}[X] + E^2[X] + 2E[X]E[Y] + \text{Var}[Y] + E^2[Y]] \\ & + 2L_1L_2E[Z] [[E[X] + E[Y]] + L_2^2 [\text{Var}[Z] + E^2[Z]] - E^2[S] \end{aligned} \quad (27)$$

The mean and variance computed from Equations 9 and 26 can be used to estimate failure probability. This is written as

$$P[FS \leq 1] = p \quad (28)$$

where p = probability of failure and $P[FS \leq 1]$ = cumulative probability that FS is less than or equal to one. A reasonable distribution of failure probabilities is a normal or Gaussian distribution. Making this choice allows computation of the failure of probability. First, a nondimensional variate, U , is computed as

$$U = \frac{1 - \overline{FS}}{(\text{Var} [FS])^{1/2}} \quad (29)$$

The value of U is used to compute cumulative failure, p , as

$$p \approx 0.4 U \text{ if } U \leq 0.13 \quad (30)$$

or

$$p \approx -0.01314 + 0.49494 U - 0.15804 U^2 + 0.01661 U^3 \text{ if } U > 0.13 \quad (31)$$

Equations 29 and 30 are approximations with errors less than one percent.

From U and B the failure probability is found as

$$P[FS \leq 1] = 0.5 + p \text{ if } U > 0 \quad (32)$$

$$P[FS \leq 1] = 0.5 - p \text{ if } U < 0 \quad (33)$$

$$P[FS \leq 1] = 0.5 \text{ if } U = 0 \quad (34)$$

Similar to potential rankings, probabilities can be grouped into three hazard classes, as shown in Table 1, Column 3. These limits can be modified depending upon the case under examination. Please note, however, that a high potential is not necessarily identical with high probability. The levels in Table 1 are not one-to-one correlations.

Mathematical Modeling Approach for Delineating
Landslide Hazards in Watersheds

By Timothy J. Ward, Ruh-Ming Li and Daryl B. Simons
Page 12

The means and variances of C_s , C_r , and $\tan \phi$ must be known or estimated to find failure probability. Usually this type of information is not available to the engineer without extensive measurements. Ward (1976) and Ward, Li, and Simons (1978) suggest that input variables be assumed as uniformly distributed random values. With this assumption, the mean of a random number is found as

$$E[X] = \frac{X_a + X_b}{2} \quad (35)$$

and the variance as

$$\text{Var } [X] = \frac{(X_b - X_a)^2}{12} \quad (36)$$

where X_a and X_b = lower and upper limits on the variable X .

Ward, Li, and Simons (1978) used Monte Carlo generation techniques to demonstrate that the assumption of a uniform distribution provided a more conservative estimate or overestimate of failure probability. Another appealing aspect of the uniform distribution assumption is that a range of values can be chosen as the input. Ward (1976) presented tentative sets of ranges for C_s , ϕ , and C_r based on the Uniform Soil Classification and vegetative characteristics. These values are guidelines and are subject to modification by the user.

Tree root cohesion represents the tensile and shear resistance of the roots and may vary significantly. Although some research indicates values up to 250 psf, Burroughs and Thomas (undated) suggest tree root strengths of 2856 psf for Douglas fir growing in Tye sandstone basins. However, tree roots are only effective if the failure surface intersects them. In deep seated slides, the failure surface is often below the roots. In instances of planar type landslides, the roots are effective only if they connect the soil mass to the underlying stable strata. Although considered as a beneficial influence to slope stability, tree roots only enhance stability under certain conditions.

Model Sensitivity

An important aspect of any mathematical model is its sensitivity to various input variables. Often it is desirable to know how accurately an input must be measured or the effect of changing the value of a variable on a model's output. Ward (1976) used partial differentiation of the factor of safety equation to demonstrate model response to changes in each input variable.

Under certain conditions, an increase in the value of an input variable can produce positive, negative, or no change in the FS value. These types of relationships occur for γ , γ_{sat} , q_0 , and H . The soil depth measure, H , usually has a negative influence on FS except for a dry cohesionless slope

where $FS = \frac{\tan\phi}{\tan\beta}$. It can be demonstrated mathematically that increasing γ , γ_{sat} , and q_0 may beneficially effect slope stability under certain conditions. Mathematically, this would occur when

$$C_s + C_r < \gamma_w H_w \tan\phi \cos^2\beta \quad (37)$$

Theoretically, when conditions exist that satisfy this inequality, uniform loading of a slope should increase stability. This result suggests that in some cases forests aid stability by adding a uniform load to the soil. The relative importance of each variable can be graphically displayed through numerical computation of FS values using different variable values. For a selected set of conditions, some inputs have a linear effect on FS values while others, notably H and β , have strong nonlinear effects. Graphs are useful for showing the relative importance of each variable as compared to others (Figure 3). Although this figure is for a selected set of values, computations for other input sets show the same relative shapes. Sometimes C_s and C_r reverse their relative importance and q_0 , not shown, becomes slightly more important. In most cases, γ has only a slight affect as do γ_{sat} and q_0 . These three variables have smaller effects for reasons previously explained but also because they are included in the numerator (resisting force) and denominator (driving force) of Equation 14. This type of analysis is important in studying a new area since it indicates which input variables are most important to measure and what variable changes most affect stability.

COMPUTER MAPPING OF WATERSHED LANDSLIDE HAZARDS

Background

The landslide potential and probability model together with a realistic range of input values allows analysis of slope stability. Such an approach is adequate for small areas but large areas require computer-based models to process extensive quantities of input data and simulate short- and long-term changes. Another desirable feature of computer-based system response models is the ability to process and utilize information from remote sensing sources.

In the landslide mapping model, watersheds are segmented and digitized for analysis using a watershed segmentation model developed by Simons and Li (1975). With this model, a grid system subdivides the watershed into square or rectangle response units, also called cells. Cell size depends on the accuracy required for the output data, size of the area to be mapped, quality of input data, use of the output, and whether mapping will reflect land-use changes.

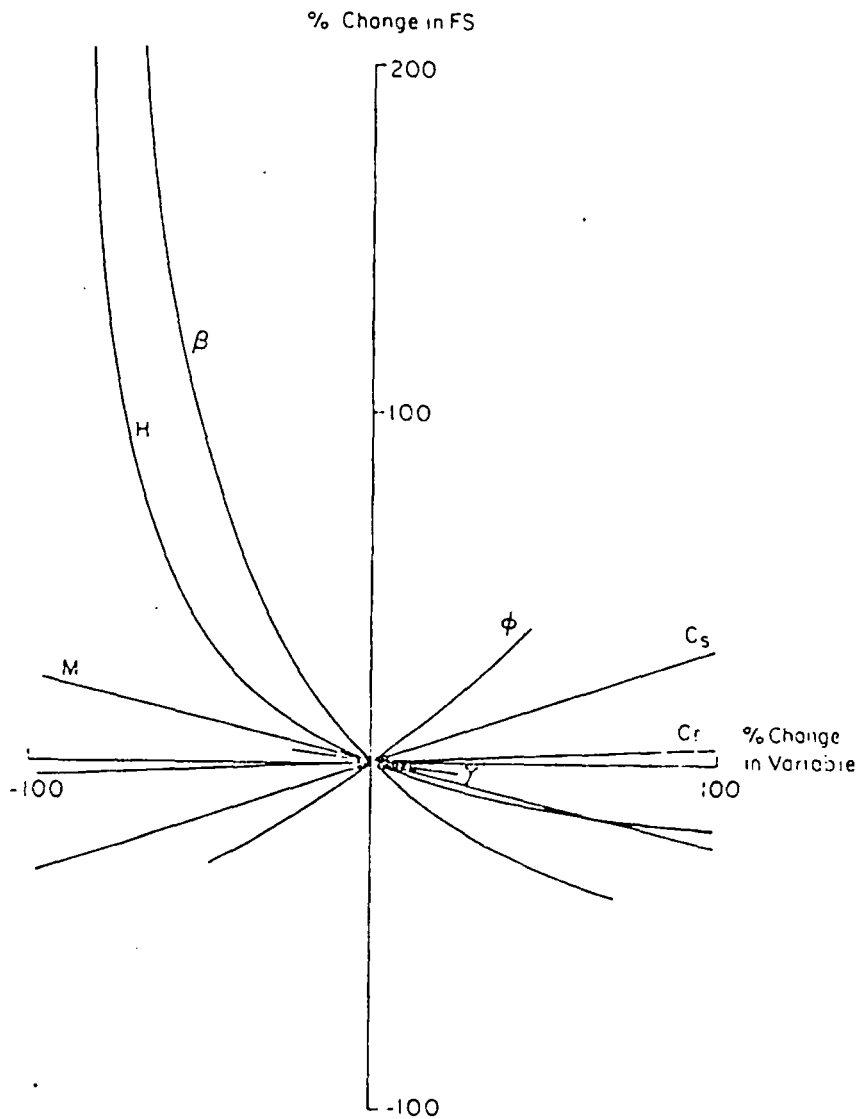


FIGURE 3 - Percent Change in Factor of Safety, FS, as Compared to Percent Change in Variable

Data input is fairly general. A cell size is selected and the corresponding grid is overlaid on the raw data maps (Figure 4). Some maps are composed entirely of code numbers that designate various characteristics. For example, if the raw data shows vegetation, code number 1 may indicate high root strength while number 2 may indicate low root strength. Code data input at the grid line intersections or nodes allows assignation of values to the respective variables. This procedure is followed for vegetation and soil but other data such as elevation or canopy density (the relative amount of vegetation) are input as raw numbers and are not coded. With data input and stored, the segmentation model computes several useful quantities. Elevation data is used to compute slope inclination and aspect of the cell. Slope aspect indicates the direction the cell slopes; that is, the direction of landslide movement in the cell. The watershed segmentation program organizes data on a cell-by-cell basis for the watershed. The organized, coded, and averaged values are then output to a mass storage device or permanent file where they are accessed by the landslide hazard mapping program.

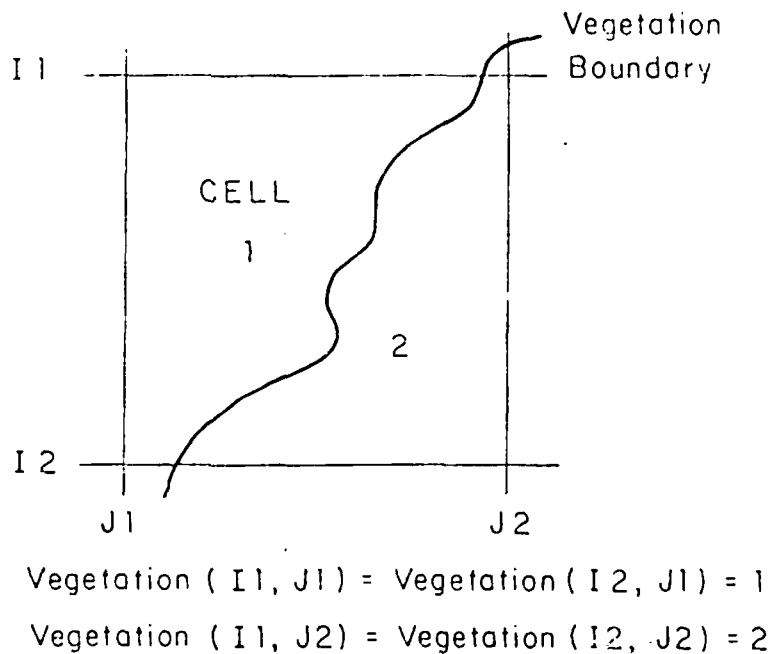


FIGURE 4 - Input Format to Segmentation Model

Landslide Hazard Mapping

Output from the segmentation model (WASEG) is input to the landslide hazard mapping program (LSMAP). In the basic version, LSMAP requires input from program WASEG and the user. A more detailed version incorporates WASEG, LSMAP, and gray map printing routines into a method for delineating landslide hazards as well as other watershed characteristics.

Program LSMAP analyzes the watershed on a cell-by-cell basis. Soil and root strength values and soil depths are averaged for each cell. Consequently, the factor of safety is based on the averaged values for each cell, rather than the average of the factors of safety at each node point.

The landslide hazard mapping model presented here can provide a rapid means of assessing the impacts of various land-use changes on slope stability. An application using actual field data is presented in the following section.

APPLICATION OF MODEL

Site Selection

A heavily forested, landslide-prone watershed was selected for analysis. The selected watershed is located in the H.J. Andrews Experimental Forest about 50 miles east of Eugene, Oregon on the western edge of the Cascade Range and is shown in the topographic map supplied by Fred Swanson, USDA Forest Service, Oregon State University (Figure 5). Watershed 2 with an area of approximately 149 acres is located in the southwest corner of the Experimental Forest. Elevations in the area range from about 1,730 to 3,500 feet above mean sea level with slopes often in excess of 80 percent.

Vegetation of the watershed is typical of the area. The canopy is primarily Douglas-fir in the 125-year age class (second-growth), 450-year age class (old-growth), or a combination of the two classes (Hawk and Dyrness, undated). In some locations, however, Western Red cedar and Hemlock are present. The geology of the watershed has been characterized as lava flows, welded and unwelded tuffs and pyroclastic flows, and water-worked volcanic sediments (Swanson and James, 1975). Almost all of the landslide activity is confined to the altered volcanoclastic rocks with little activity occurring in the lava flows (Swanson and Dyrness, 1975). Soils in this area are weathered from the underlying volcanic rocks (Dyrness, 1969; Hawk and Dyrness, undated; Paeth, et al., 1971) and can be grouped into five broad classes. Five groups were used to account for subtle but important variations in soil depth and relative stability that produced unrealistic results when only three groupings were used.

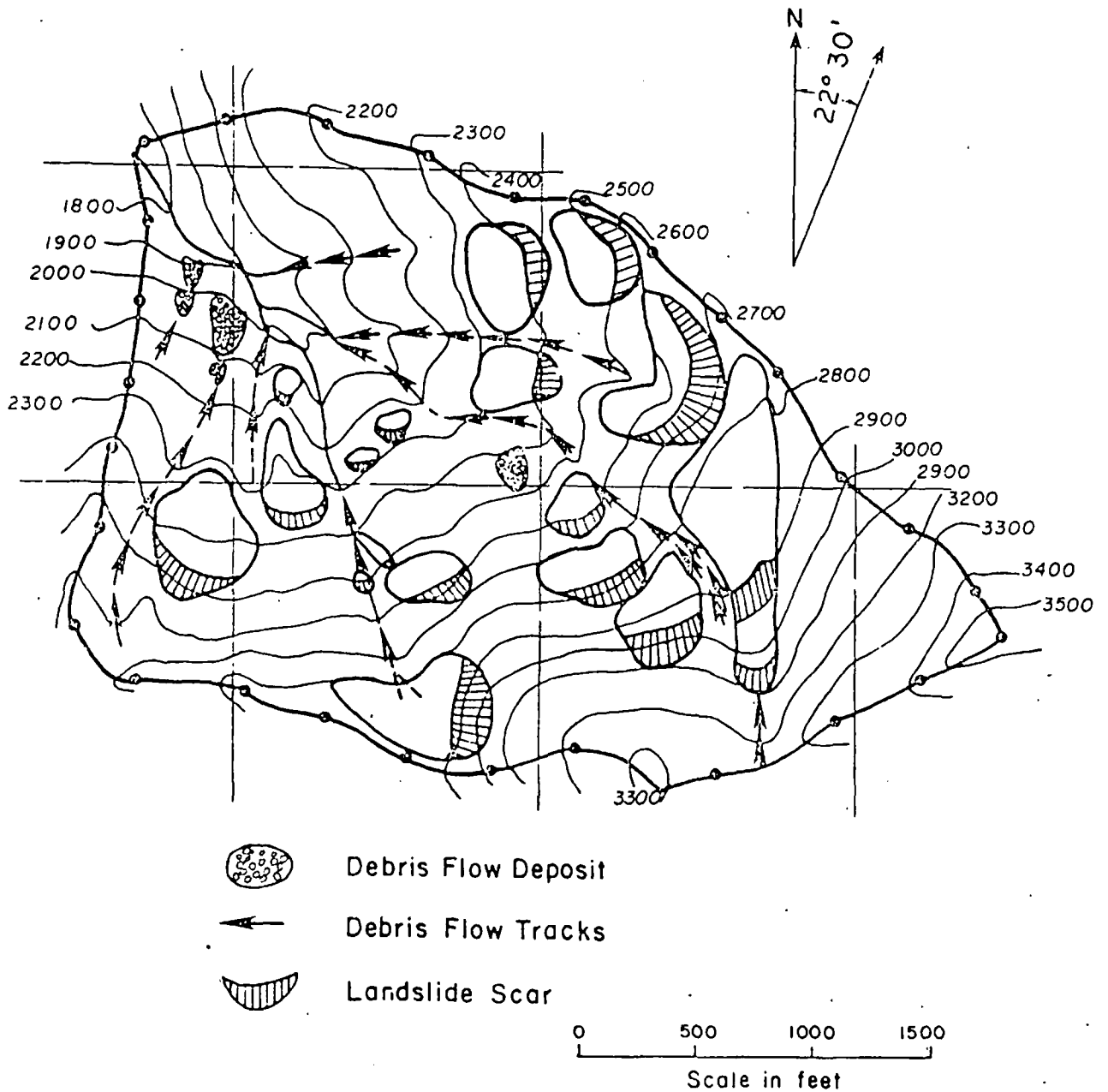


FIGURE 5 - Topographic Map of Watershed 2 Showing Landslide Scars and Deposits

The estimated Unified Soil Classifications for the soils were ML, CL, and CH. These assumed classifications were used for initial estimates of soil strength parameters as outlined by Ward (1976). Distribution of these soils indicates that two groups predominate in the watershed (Figure 6).

A vegetation grouping was conducted on Watershed 2. Because the canopy is well developed, it was assumed the root system was also well developed. Therefore, classification of vegetation with respect to characteristic root strength was based on a combination of the canopy cover densities of the larger overstory trees and the smaller understory trees and brush. Cover percentages provided a method of classification for root strength. Most of Watershed 2 was characterized by vegetation groups of second and old growth plant communities (Figure 7).

Runoff from the watershed is controlled by groundwater discharge. Precipitation averages nearly 90 inches per year with about 90 percent of the total occurring as rainfall from October to April. Storms may last several days producing rainfall of several inches. Rainfall intensities are usually low and soil infiltration rates high, therefore, overland flow seldom occurs. Streamflow is fed primarily by saturated and unsaturated groundwater flow. Because of the importance of groundwater in slope stability, it was recognized that fluctuations in the groundwater table during a storm were important. Unfortunately, an acceptable, easily applied groundwater model was not available for use in this application, therefore, only selected levels were utilized for comparison.

The segmented watershed with the superimposed grid system is shown in Figure 8. Code values were input for the five soil classes and vegetation types along with elevations and cover densities. These codes start in the lower left corner and continue counterclockwise. For example, the vegetation code in Figure 4 is 1221.

In Watershed 2, 78.5 cells (0.5 cells for a cell near a stream channel) of 181 cells in the segmented watershed were denoted as having mappable landslide scars and deposits. These hazard cells were used as a guide to model performance and adjustment. If the model predicted a potential landslide hazard in these cells, it is accepted as a correct result. Overestimation or underestimation of the number of hazardous cells indicates: a) some hazardous cells may have negative characteristics and consequently are mapped as non-hazardous, b) cells mapped as hazardous but not containing landslides may be near failure, or c) the model is incorrect due to erroneous data. Comparison of the number of correct classifications with incorrect classifications for initial runs indicated the physical process model reflected the correct slope stability conditions.

The model was adjusted through soil and root strength parameters to better match the observed data. Two criteria were established to this adjustment. First, under typical soil moisture conditions no cell should fail.

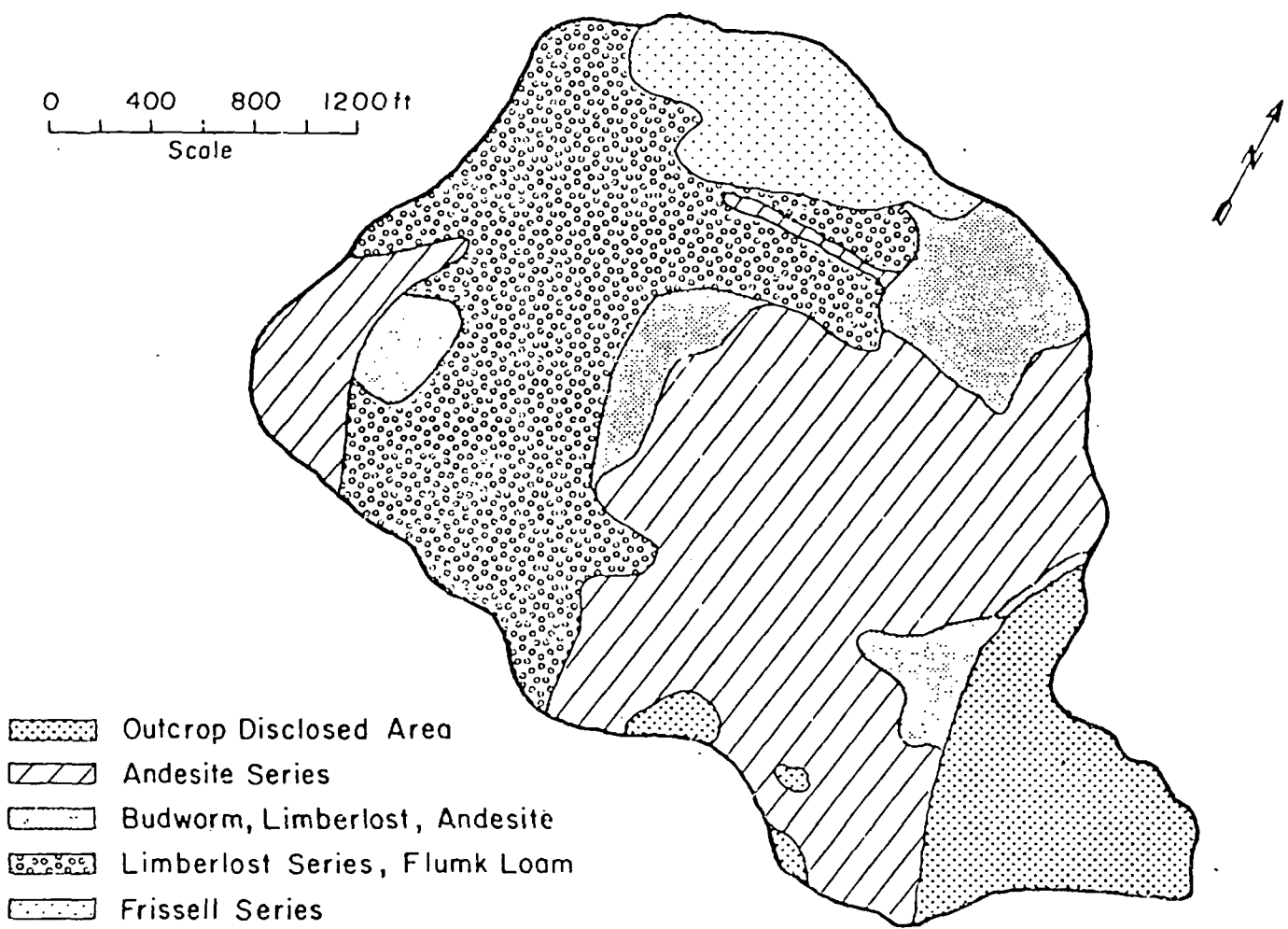


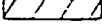

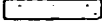


FIGURE 6 - Soil Classification Map of Watershed 2 (After Hawk and Dyrness, Undated)

-  Second and Old Growth Mix Cover $\geq 75\%$
-  Old Growth Cover 50-75%
-  Second Growth Community Cover
-  Old Growth Less than 25%
-  Vine Maple Open

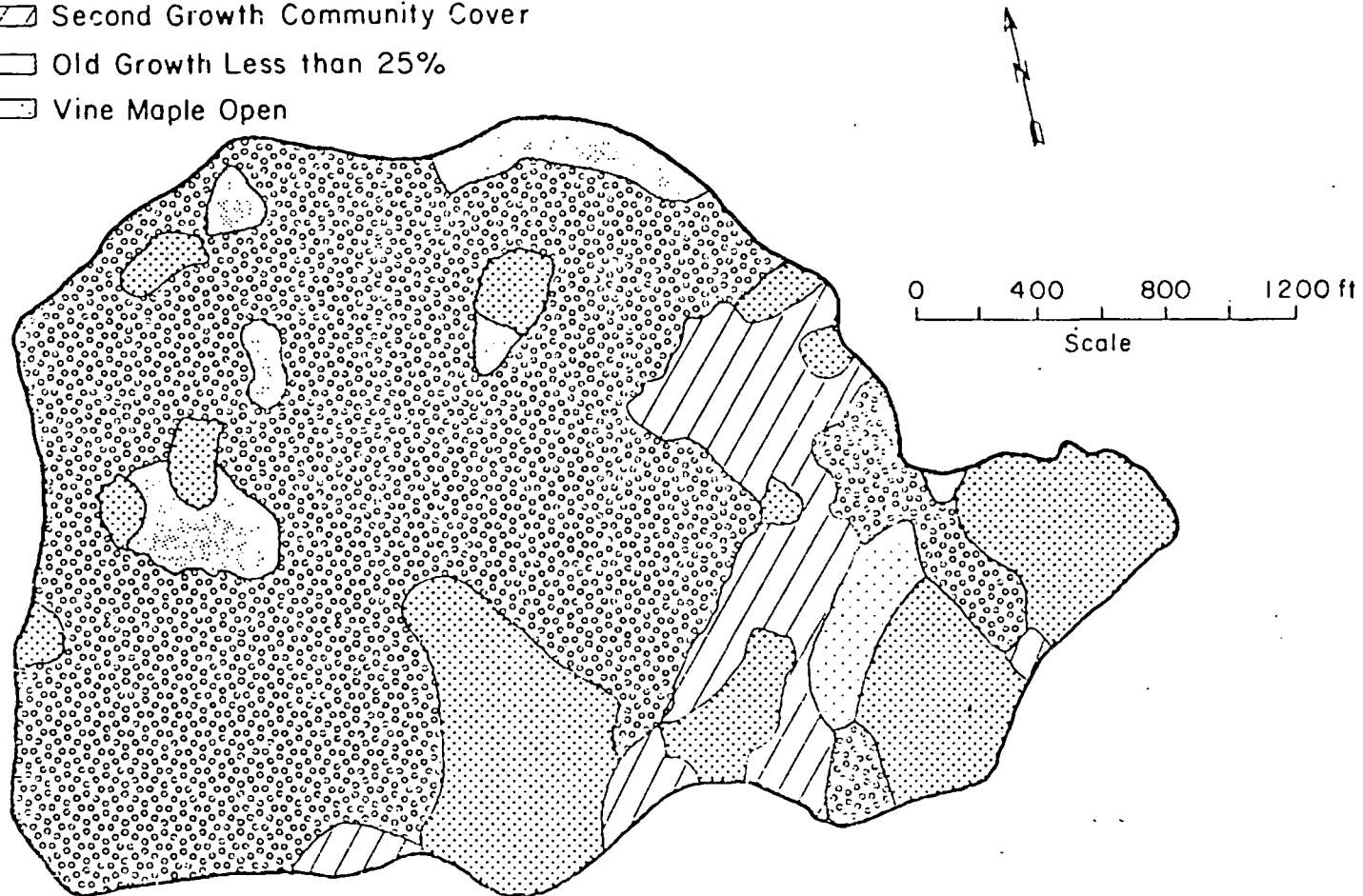


FIGURE 7 - Vegetation Map of Watershed 2 (After Hawk and Dyrness, Undated)

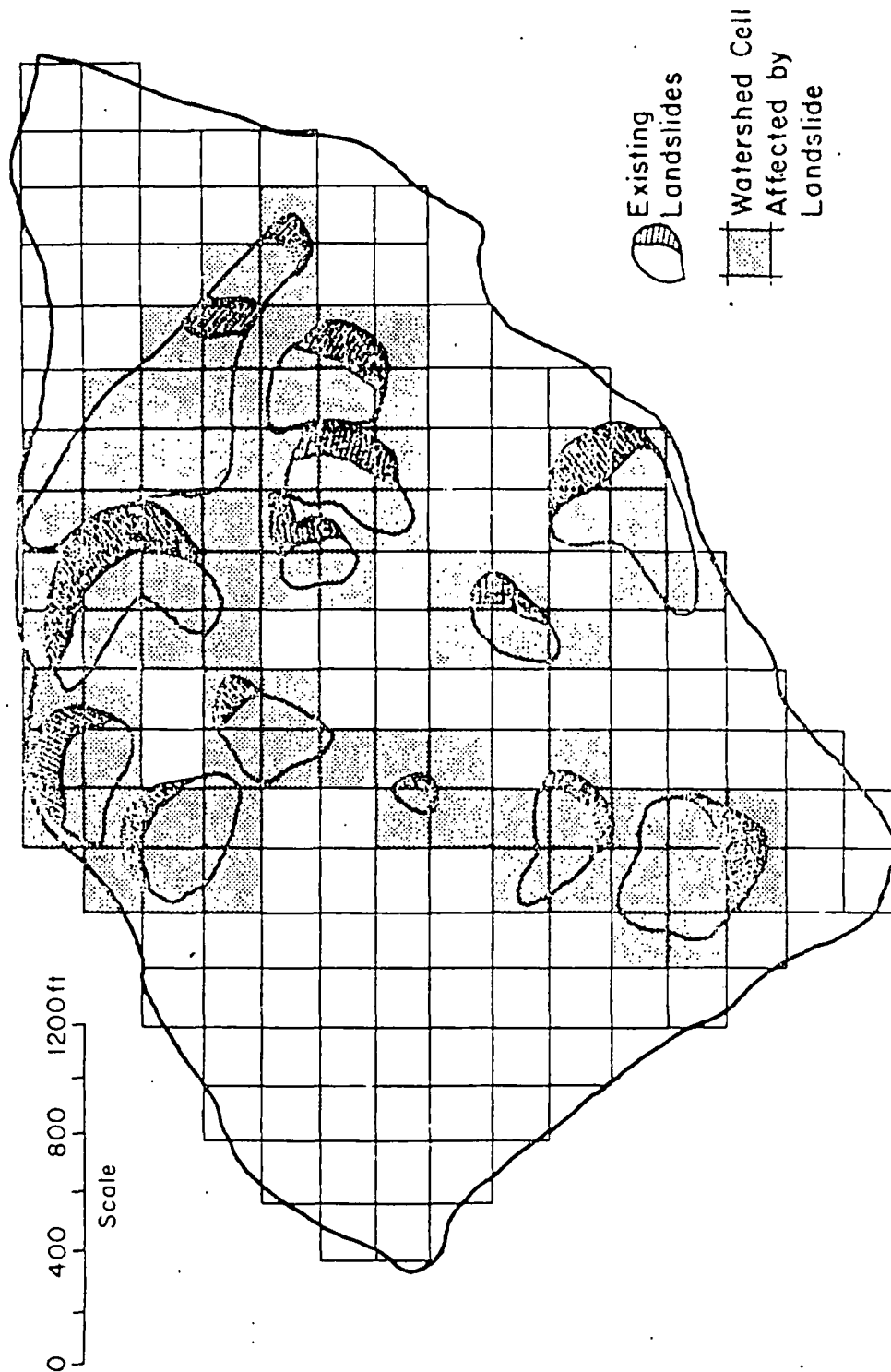


FIGURE 8 - Watershed Number 2: Existing Landslides and Watershed Cell System

Mathematical Modeling Approach for Delineating
Landslide Hazards in Watersheds

By Timothy J. Ward, Ruh-Ming Li and Daryl B. Simons

Page 22

Second, under saturated conditions all the landslide cells should fail. Although failure may occur in all the landslide cells before saturation, data does not indicate at what level failure occurred. Using these two criteria, the input values were adjusted over realistic ranges. These values plus others used in the model are listed in Table 2.

Low values of cohesion and friction angle for soil classes 2 and 3 were consistent with field observations of failures in these soils. Higher values for the other three soil classes reflect the relative stability associated with those groupings. Similar considerations were used when selecting proper ranges of root strengths. No formal methodology was used for arriving at the adjusted values in Table 2. The values do, however, reflect the relative stability of groups they represent.

The adjusted model indicated a total of 81.5 hazardous cells, 69 of which corresponded with the assumed hazardous cells, an 87.9 percent match. A total of 9.5 cells were classed as safer than assumed and 12.5 were classed as more hazardous. This is encouraging since it indicates the model represents the physical processes controlling landslide occurrence.

The adjusted model was then used to study dynamic changes in the watershed. The first application showed the change in landslide hazards under varying groundwater conditions. The potentially hazardous landslide areas and their estimated failure probabilities for a relative groundwater level of 0.5 are shown in Figures 9 and 10. Even under these conditions there are numerous areas of high potential because of the overwhelming driving forces brought about by the steep terrain. As expected, rising groundwater levels increase landslide hazards (Figures 11 and 12). If a real-time groundwater level model were available, daily or seasonal fluctuations in landslide hazards could be determined. Use of the model in determining relative hazards with respect to groundwater levels is important in planning watershed activities. Based on model results, scheduling of activities may be better determined to coincide with lower landslide hazards. Roadways may also be better planned to avoid hazardous areas or indicate where stability enhancement is required.

Timbering is another dynamic watershed activity that can be assessed with the model. Landslide potential for a 50 percent clearing of the canopy cover is shown in Figure 13. Comparison of Figure 13 with Figure 9 shows adverse effects on slope stability produced by vegetation removal. Similarly, if the watershed is clear-cut, even more instability is produced (Figure 14). However, an instantaneous drop in root strength is assumed, which is incorrect. A more realistic approximation would be loss of strength with time. The model provides a method for assessing impact of this type of timbering activity on the watershed.

An important aspect of the model is estimating landslide probability. Use of both the potential and probability maps provides the land use manager with another means for analyzing impacts of watershed activities. In addition, the probability map aids interpretation of the potential map.

TABLE 2
 Input Values for LSMAP

Soil porosity = 0.60
 Dry unit weight of soil = 66.1 pounds per cubic foot
 Saturated unit weight of soil = 103.6 pounds per cubic foot
 Vegetative surcharge = 50 pounds per square foot

Soil Group (1)	Soil Names (2)	Cohesion Range, in pounds per square foot (3)	Friction Angle Range, in degrees (4)	Typical Depth in feet (5)
1	Rock outcrop	1000-2000	35-40	5
2	Andesite series	20-50	5-20	8
3	Budworm, Limberlost, Andesite (slope < 20%)	0-5	2-5	10
4	Limberlost, Flunky	150-200	25-28	5
5	Frissell	350-400	30-33	4

Vegetation Group (1)	Root Strength Range, in pounds per square foot (2)
1	290-360
2	220-260
3	5-25
4	100-125
5	15-65

H.J. Andrews Experimental Forest, Oregon

Watershed 2

Relative Groundwater Depth .500

Map Scale 1 to 4800

Symbol Set Used for this Gray Map Indicates:

- Safety Factor Less than or Equal to 1.2 W
- Safety Factor Greater than 1.2 and Less than 1.7 I
- Safety Factor Greater than 1.7 .

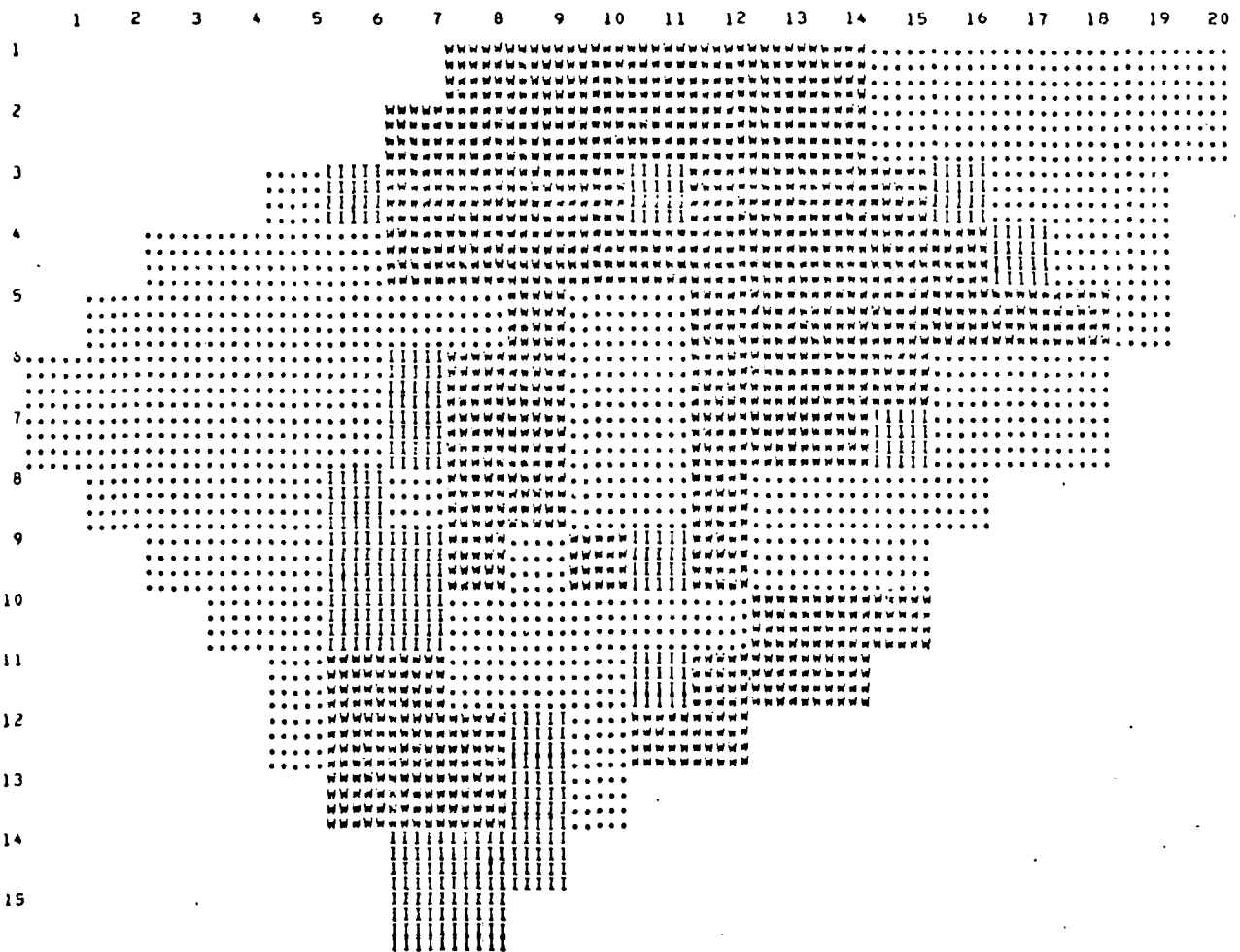


FIGURE 9 - Gray Map of Potentially Hazardous Landslide Areas for Watershed 2 with Relative Groundwater Level of 0.5

Mathematical Modeling Approach for Delineating
 Landslide Hazards in Watersheds
 By Timothy J. Ward, Ruh-Ming Li and Daryl B. Simons
 Page 25

H.J. Andrews Experimental Forest, Oregon Watershed 2
 Relative Groundwater Depth .500 Map Scale 1 to 4800

Symbol Set Used for this Gray Map Indicates:
 Probability of Sliding Higher than 60 Percent W
 Probability Higher than 30 Percent and less or
 Equal to 60 Percent I
 Probability of Sliding less than 30 Percent .

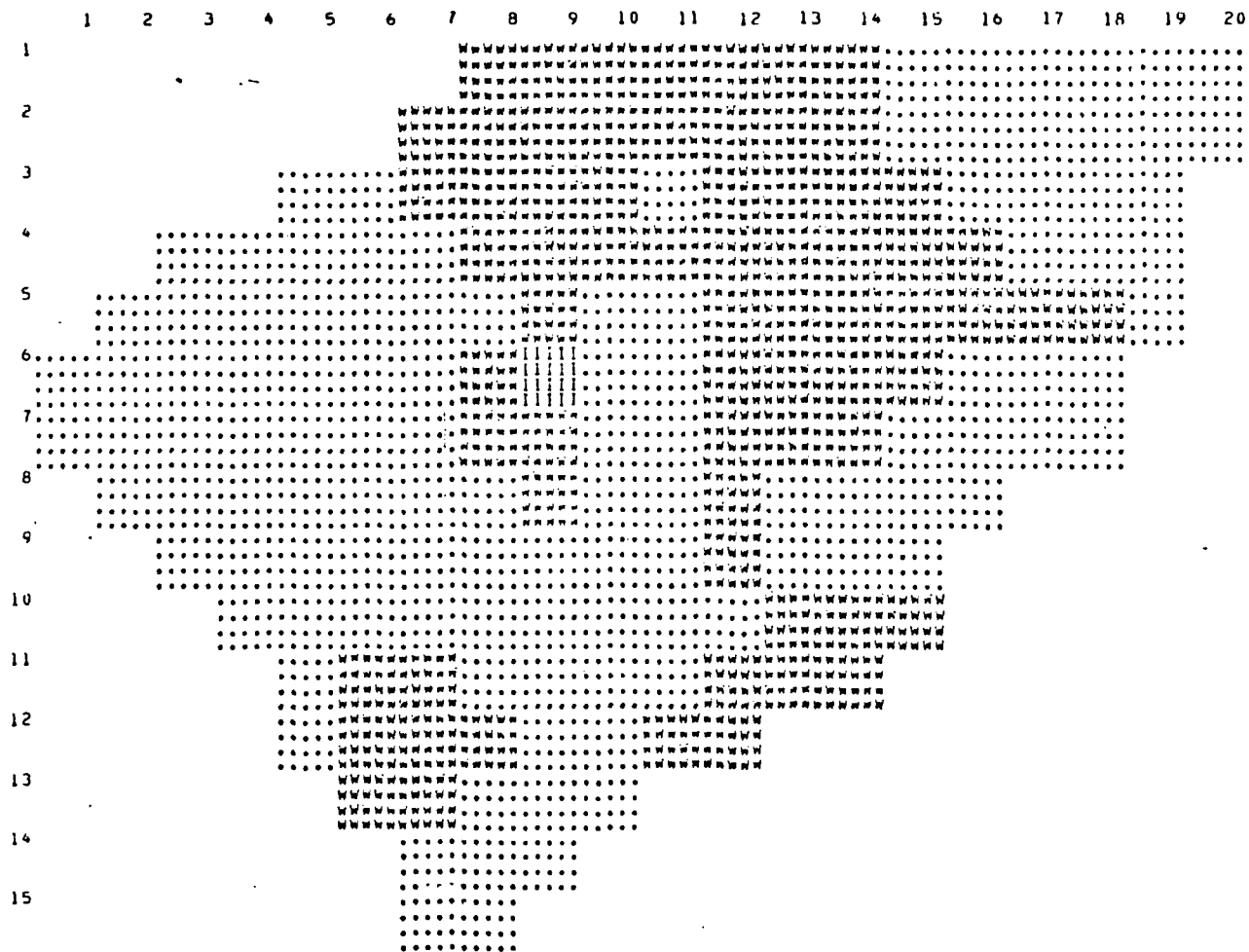


FIGURE 10 - Gray Map of Estimated Failure Probabilities of Landslide Areas
 for Watershed 2 with Relative Groundwater Level of 0.5

Mathematical Modeling Approach for Delineating
 Landslide Hazards in Watersheds
 By Timothy J. Ward, Ruh-Ming Li and Daryl B. Simons
 Page 26

H.J. Andrews Experimental Forest, Oregon Watershed 2
 Relative Groundwater Depth 1.000 Map Scale 1 to 4800

Symbol Set Used for this Gray Map Indicates:
 Safety Factor Less than or Equal to 1.2 W
 Safety Factor Greater than 1.2 and Less than 1.7 I
 Safety Factor Greater than 1.7 .

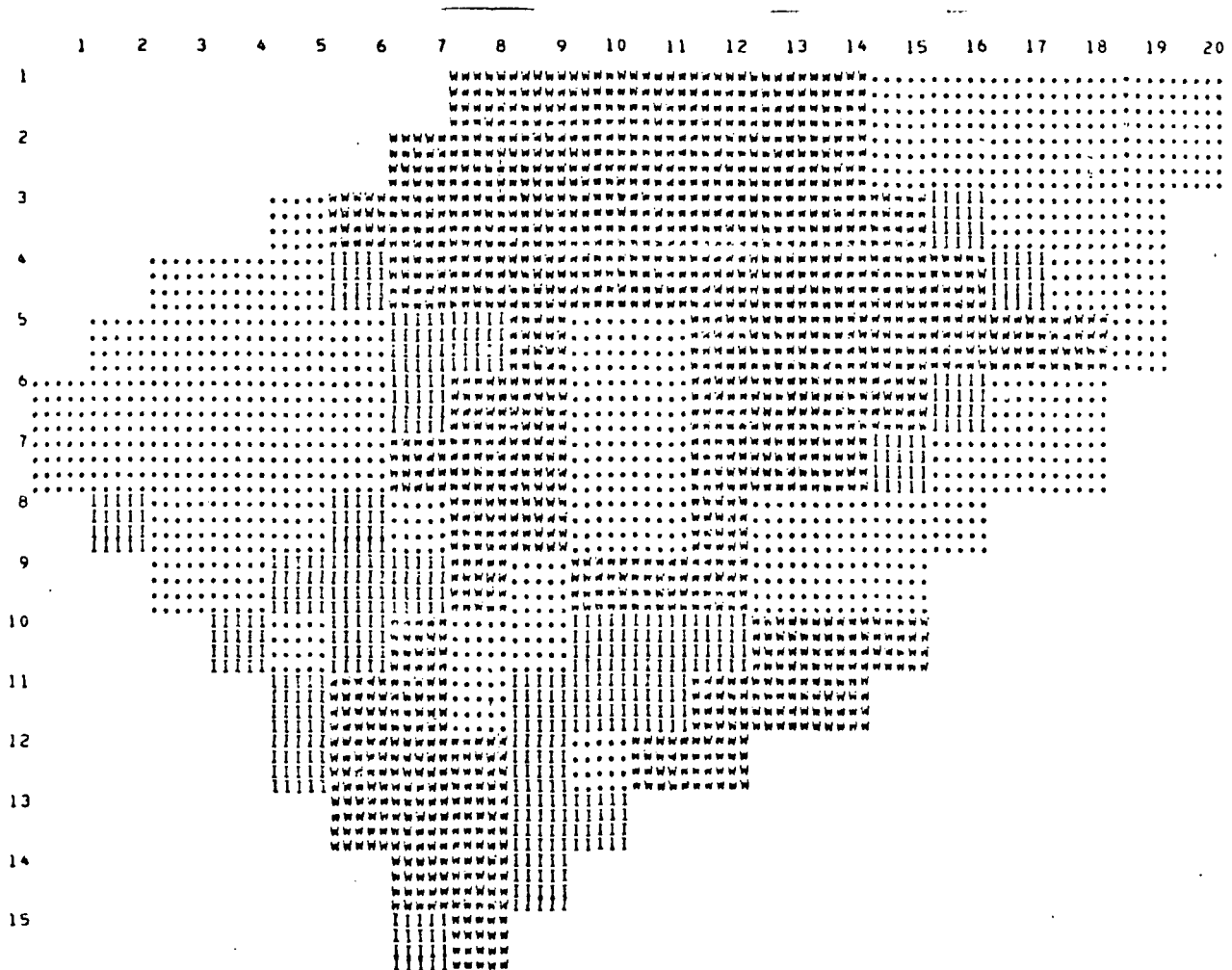


FIGURE 11 - Gray Map of Potentially Hazardous Landslide Areas for Watershed 2 with Relative Groundwater Level of 1.0

Mathematical Modeling Approach for Delineating
 Landslide Hazards in Watersheds
 By Timothy J. Ward, Ruh-Ming Li and Daryl B. Simons
 Page 27

H.J. Andrews Experimental Forest, Oregon Watershed 2
 Relative Groundwater Depth 1.000 Map Scale 1 to 4800

Symbol Set Used for this Gray Map Indicates:
 Probability of Sliding Higher than 60 Percent W
 Probability Higher than 30 Percent and Less or
 Equal to 60 Percent I
 Probability of Sliding Less than 30 Percent .

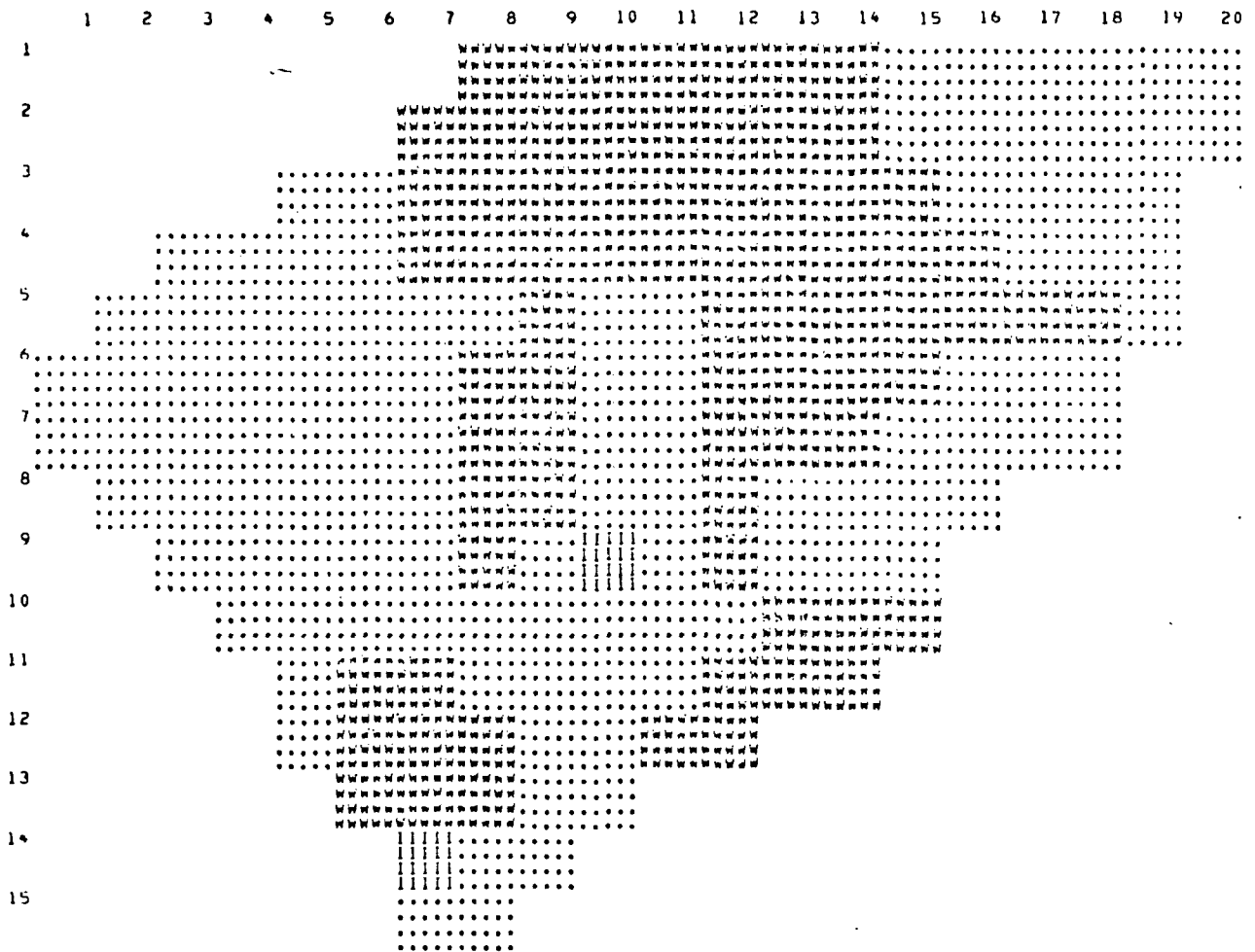


FIGURE 12 - Gray Map of Estimated Failure Probabilities of Landslide Areas
 for Watershed 2 with Relative Groundwater Level of 1.0

Mathematical Modeling Approach for Delineating
Landslide Hazards in Watersheds
By Timothy J. Ward, Ruh-Ming Li and Daryl B. Simons
Page 28

H.J. Andrews Experimental Forest, Oregon Watershed 2
Relative Groundwater Depth .500 Map Scale 1 to 4800

Symbol Set Used for this Gray Map Indicates:
Safety Factor Less than or Equal to 1.2 W
Safety Factor Greater than 1.2 and Less than 1.7 I
Safety Factor Greater than 1.7 .

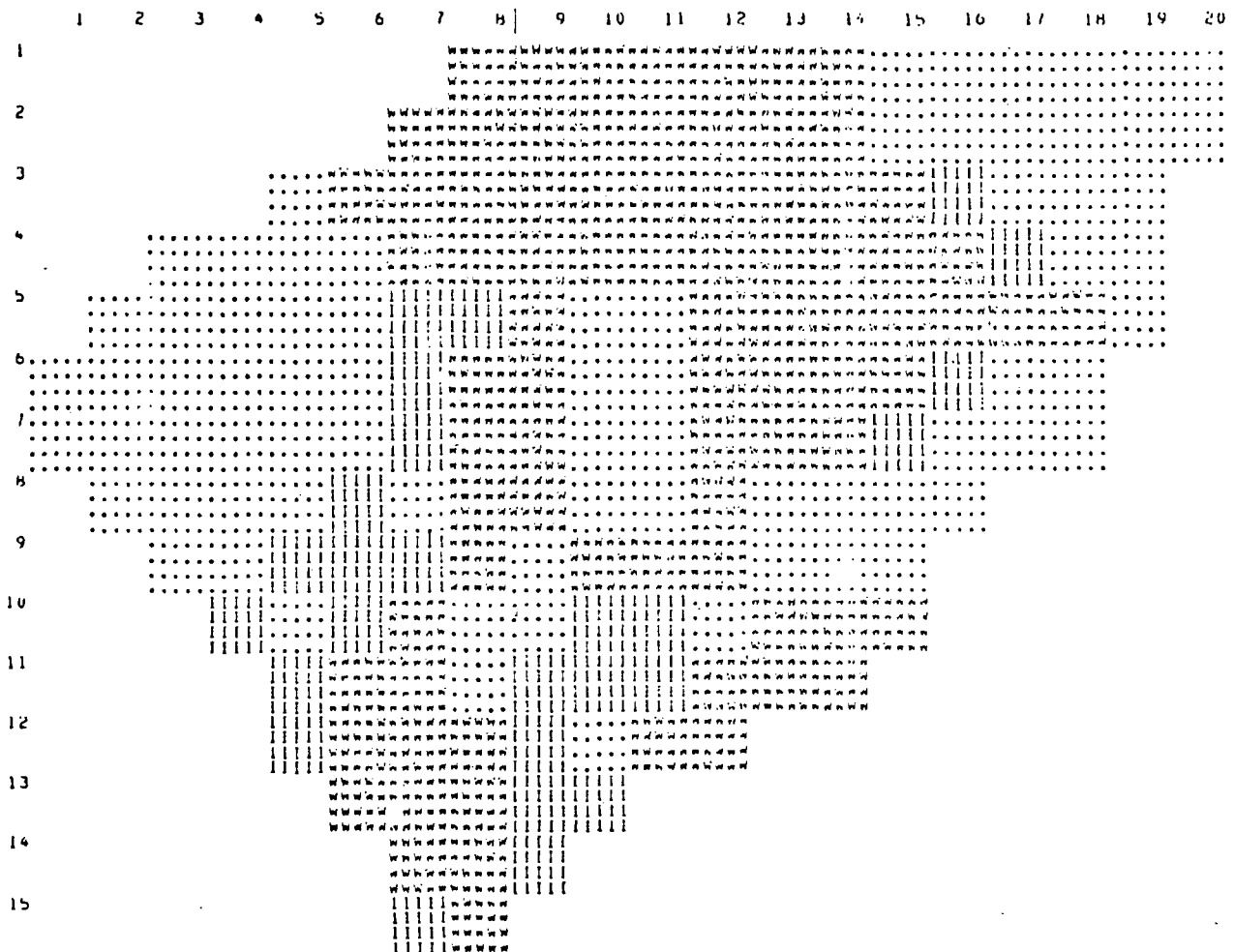


FIGURE 13 - Gray Map of Potentially Hazardous Landslide Areas for a 50 Percent Clearing of Canopy Cover with Relative Groundwater Level of 0.5

Mathematical Modeling Approach for Delineating
Landslide Hazards in Watersheds
By Timothy J. Ward, Ruh-Ming Li and Daryl B. Simons
Page 29

H.J. Andrews Experimental Forest, Oregon

Watershed 2

Relative Groundwater Depth .500

Map Scale 1 to 4800

Symbol Set Used for this Gray Map Indicates:

Safety Factor Less than or Equal to 1.2	W
Safety Factor Greater than 1.2 and Less than 1.7	I
Safety Factor Greater than 1.7	.

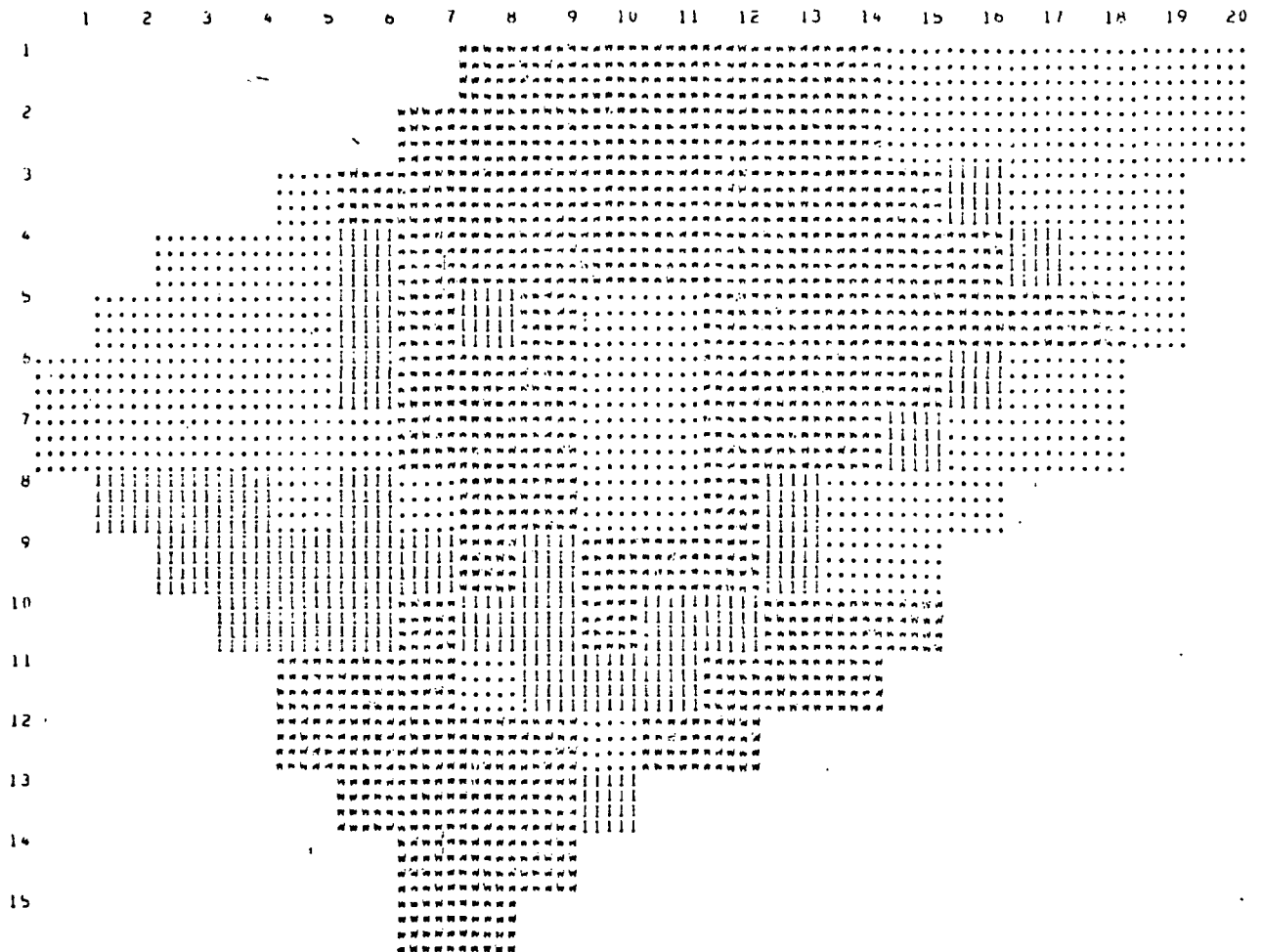


FIGURE 14 - Gray Map of Potentially Hazardous Landslide Areas for Clear Cut Watershed with Relative Groundwater Level of 0.5

SUMMARY AND CONCLUSIONS

This paper has presented the need for delineating the hazardous landslide areas. Delineation techniques were discussed and a mathematical modeling approach was detailed. Application of the approach indicates its usefulness for determining landslide hazards in a watershed under varying natural and man caused conditions.

ACKNOWLEDGEMENTS

The authors wish to thank the U.S. Department of Agriculture, Rocky Mountain Forest and Range Experiment Station, Flagstaff, Arizona and the Colorado State University Experiment Station for sponsoring projects from which this paper was derived.

REFEREMCES

- Baker, R.F., and Chieruzzi, R., "Regional Concept of Landslide Occurrence," Bulletin No. 216, Highway Research Board, 1959, pp. 1-16.
- Benjamin, J.R., and Cornell, C.A., Probability, Statistics, and Decision for Civil Engineers, McGraw-Hill, New York, N.Y., 1970, pp. 147-150.
- Blanc, R.P., and Cleveland, G.B., "Natural Slope Stability as Related to Geology, San Clemente Area, Orange, and San Diego Counties, California," Special Report 98, California Division of Mines and Geology, 1968.
- Brown, C. and Sheu, M.S., "Effects of Deforestation on Slopes," Journal of the Geotechnical Engineering Division, ASCE, Vol. 101, No. GT2, Feb., 1975, pp. 147-165.
- Building Research Advisory Board, National Research Council, National Academy of Sciences, "Methodology for Delineating Mudslide Hazard Areas," 1974.

Mathematical Modeling Approach for Delineating
Landslide Hazards in Watersheds
By Timothy J. Ward, Ruh-Ming Li and Daryl B. Simons
Page 31

- Burroughs, E.R., and Thomas, B.R., "Initial Report for the Identification of Landslide Hazard Areas in Fyee Sandstone with Slope Gradients Exceeding Sixty Percent," Draft Report, U.S. Forest Service, unpublished, undated.
- Chang, T.P., "Landslide Investigation Techniques," Colorado State University, Science Series No. 1, Department of Watershed Sciences, 1971.
- Cleveland, G.B., "Regional Landslide Prediction," Open File Release 72-73, California Division of Mines and Geology, Sacramento, California, 1971.
- Dyrness, C.T., "Hydrologic Properties of Soil on Three Small Watersheds in the Western Cascades of Oregon," Research Note PNW-111, U.S. Forest Service, Sept., 1969.
- Endo, T., and Tsuruta, T., "On the Effect of Tree Roots Upon the Shearing Strength of Soil," Annual Report of the Hokkaido Branch Forest Experiment Station (In Japanese, English Summary), 1968.
- Evans, J.R. and Gray, C.H., Jr., Eds., "Analysis of Mudslide Risk in Southern Ventura County, California," Open File Release 72-73, California Division of Mines and Geology, 1971.
- Feld, J., "The Factor of Safety in Soil and Rock Mechanics," Proceedings, Sixth International Conference on Soil Mechanics and Foundation Engineering, Vol. 111, 1965, pp. 185-197.
- Gray, D.H., "Effects of Forest Clearcutting on the Stability of Natural Slopes," Association of Engineering Geologists Bulletin, Vol. 7, Nos. 1 and 2, 1970, pp. 45-65.
- Gray, D.H., "The Role of Woody Vegetation in Reinforcing Soils and Stabilizing Slopes," Proceedings, Symposium on Soil Reinforcing and Stabilizing Techniques in Engineering Practice, Sydney, Australia, October 13-16, 1978.
- Hawk, G., and Dyrness, C.T., "Vegetation and Soils of Watershed 2 and 3," Internal Report 49, U.S. Department of Agriculture Forest Service, H.J. Andrews Experimental Forest, review copy, undated.
- Holtz, R.D., and Krizek, R.J., "Statistical Evaluation of Soils Test Data," Proceedings, the First International Conference on Applications of Statistics and Probability to Soil and Structural Engineering, 1971, pp. 230-266.
- Jones, F.O., Embody, D.R., and Peterson, W.L., "Landslides Along the Columbia River Valley, Northeastern Washington," Survey Professional Paper 367, 1961.

- Krynine, D.P., and Judd, W.R., Principles of Engineering Geology and Geotechnics, McGraw-Hill, New York, N.Y., 1957, pp. 639
- Lambe, T.W., and Whitman, R.V., Soil Mechanics, John Wiley and Sons, New York, N.Y., 1969, pp. 352-373.
- Liang, F. and Belcher, J.D., "Air Photo Interpretation in Landslides and Engineering Practice," Highway Research Board, Special Report No. 29, Publication 544, 1958.
- Lumb, P., "Safety Factors and the Probability Distribution of Soil Strength," Canadian Geotechnical Journal, Vol. 17, No. 3, 1970, pp. 225-242.
- McKean, J., "Density Slicing of Aerial Photography Applied to Slope Stability Studies," M.S. Thesis, Department of Earth Resources, Colorado State University, Fort Collins, Colorado, 1977.
- Nilsen, T.H., and Brabb, E.E., "Current Slope-Stability Studies in the San Francisco Bay Region," Journal of Research, U.S. Geological Survey, Vol. 1, No. 4, July-Aug., 1973, pp. 431-437.
- O'Loughlin, C., "The Effect of Timber Removal on the Stability of Forest Soils," Journal of Hydrology, Vol. 13, No. 2, New Zealand, 1974, pp. 121-134.
- Paeth, R.C., et al., "Factors Affecting Mass Movement of Four Soils in the Western Cascades of Oregon," Proceedings, Soil Science Society of America, Vol. 35, No. 6, 1971, pp. 943-947.
- Poole, D.H., "Slope Failure Forms: Their Identification, Characteristics and Distribution as Depicted by Selected Remote Sensor Returns," Proceedings, Sixth International Symposium on Remote Sensing of the Environment, Ann Arbor, Michigan, 1969.
- Poole, D.H., "An Evaluation of the Utility of Remote Sensor Returns for a Study of Slope Failure Phenomena," Remote Sensing Institute Technical Report 14, East Tennessee State University, Johnson City, Tennessee, 1972.
- Simons, D.B. and Li, R.M., "Watershed Segmentation by a Digital Computer for Mathematical Modeling of a Watershed," Draft Report, Rocky Mountain Forest and Range Experiment Station, Flagstaff, Arizona, Dec., 1975.
- Simons, D.B. and Ward, T.J., "Landslide Potential Delineation," Civil Engineering Department, Engineering Research Center, Colorado State University, Fort Collins, Colorado, Feb., 1976.
- Simons, D.B., Ward, T.J., and Li, R.M., "Computer Application in Mapping Potential Landslide Sites," Proceedings, Summer Computer Simulation Conference, held at Washington, D.C., 1976.

Mathematical Modeling Approach for Delineating
Landslide Hazards in Watersheds
By Timothy J. Ward, Ruh-Ming Li and Daryl B. Simons
Page 33

- Singh, A., "How Reliable is the Safety Factor in Foundation Engineering?" Proceedings, First International Conference on Applications of Statistics and Probability to Soil and Structural Engineering, Hong Kong University Press, 1971, pp. 390-424.
- Swanson, F.J. and Dyrness, C.T., "Impact of Clear-cutting and Road Construction of Soil Erosion by Landslides in the Western Cascade Range, Oregon," Geology, Vol. 3, No. 7, 1975, pp. 393-396.
- Swanson, F.J. and James, M.E., "Geology and Geomorphology of the H.J. Andrews Experimental Forest, Western Cascades, Oregon," Research Paper PNW-188, U.S. Department of Agriculture Forest Service, 1975.
- Swanson, F.J., et al., "A Conceptual Model of Soil Mass Movement, Surface Soil Erosion, and Stream Channel Erosion Processes," Internal Report 72, Erosion Modeling Group, 1973.
- Takada, Y., "A Geophysical Study of Landslides," Bulletin Disaster Prevention Research Institute, Kyoto University, Vol. 18, Part 2, No. 137, 1968.
- Takeuchi, A., "Fractured Zone Type Landslide and Electrical Resistivity Survey - 1," Bulletin Disaster Prevention Research Institute, Kyoto University, Vol. 21, Part 1, No. 185, 1971.
- Waltz, J.P., "An Analysis of Selected Landslides in Alameda and Contra Costa Counties, California," Association of Engineering Geologists Bulletin, Vol. 3, No. 2, 1971.
- Ward, T.J., "Factor of Safety Approach to Landslide Potential Delineation," thesis presented to Colorado State University, at Fort Collins, Colorado, in August, 1976, in partial fulfillment of the requirements for the degree of Doctor of Philosophy.
- Ward, T.J., Li, R.M., and Simons, D.B., "Landslide Potential and Probability Considering Randomness of Controlling Factors," Proceedings International Symposium on Risk and Reliability in Water Resources, University of Waterloo, Waterloo, Canada, June 26-28, 1978, pp. 592-608.

LIST OF SYMBOLS

C_r = root cohesion
 C_s = soil cohesion
 c = cohesion term
 \bar{c} = effective cohesion
 D = driving forces
 $E[\]$ = expected value or mean of linear equation
 FS = factor of safety
 H = measure of soil depth
 H_u = unsaturated soil height
 H_w = saturated soil height or height to groundwater table
 L_1 = dimensionless grouping of parameters
 L_2 = dimensionless grouping of parameters
 M = relative groundwater height
 n = number of soil layers
 p = cumulative probability
 P = probability of failure
 q_0 = vegetative surcharge
 R = resistive forces
 S = random variable
 T_{sw} = wind shear in trees
 U = nondimensional variate
 u = pore water pressure
 $Var[\]$ = variance
 x = variable
 \bar{x} = mean of variable x
 Y = random variable
 Z = height above bedrock surface or random variable
 Z^* = relative position above bedrock surface
 β = slope inclination
 γ = unit weight
 ΔZ = thickness
 Σ = summation sign
 σ = total normal stress
 $\bar{\sigma}$ = effective normal stress
 τ = overall shear resistance
 τ' = overall shear stress
 ϕ = angle of internal friction
 $\bar{\phi}$ = effective angle of internal friction

Subscripts

a = area; lower limit
 b = upper limit
 i = layer i
 sat = saturated
 w = water

SURFICIAL INVESTIGATION
OF THE PERPETUAL LANDSLIDE
SUMMERLAND, BRITISH COLUMBIA

By

Linda Riglin
U.S. Forest Service, Lewis & Clark National Forest
Choteau, Montana

ABSTRACT

Between 1914 and 1917 early settlers of the area referred to as Paradise Flats (near Summerland, British Columbia) noticed an incipient slope failure. Subsequent movement in the area has continued for some sixty years and the failure has become known as the Perpetual Landslide. Questions have been raised about the slide as it affects watershed quality as well as land-use in the area. Hence, a study was undertaken to determine degree of instability of the slide and factors conducive to its failure.

The Perpetual Landslide is located in the Okanagan Valley of British Columbia about 260 miles east of Vancouver. The slide spills into Trout Creek Canyon about 3-1/2 miles upstream from Okanagan Lake. Slide dimensions are 1,390 feet in length, 1,370 feet in width, and 260 feet in estimated depth. Volume is estimated to be 7×10^6 cubic yards.

Analysis of the slide included study of surficial geomorphology, geology, and hydrology to assist in slope stability interpretations. Geomorphic study related landform feature to type of movement. Geologic study was carried out primarily to determine what materials were likely to form the failure plane(s). Because of the demonstrated historical significance of ground water flow to failure, a hydrologic study of the slide's drainage basin was also conducted. Finally, slope stability was analyzed in order to understand the mechanics of the slide. This analysis included monitoring of seasonal movement, measuring shear strength of gouge, and modeling equilibrium. However, any interpretations about stability were limited by lack of subsurface data.

Results of the study demonstrate that surficial investigation of a slide can indicate type of movement and causes for instability. It is concluded that the Perpetual Slide is a composite landslide displaying slump movement in the body with a transition to flow in the toe area. The failure surface lies within Tertiary sedimentary rocks, primarily, claystone. The rocks have been remolded into a clayey gouge, likely near residual strength. The hydrologic and stability analysis indicate that ground water has critical influence on slope stability. Investigation of this slide has served to define the environment for failure and would serve to guide any more comprehensive subsurface analysis.

INTRODUCTION

The Perpetual Landslide (Figure 1) is predominantly a slump failure. It has continued to move for some 60 years since its initiation between 1914



FIGURE 1 - Overview of the Perpetual Landslide

and 1917. Concern has been expressed about safety of developed land and deterioration of water quality in the slide area. As a result, a surficial investigation of the slide was undertaken in 1975. The purpose of the investigation was to understand the degree of instability of the slide and its environment of failure. It is hoped that the results of this study may guide remedial action and may confirm the importance of geologic and hydrologic studies to prevent slope failure in similar situations.

Location

The Perpetual Landslide is located in the Southern Interior of British Columbia. It lies just west of the town of Summerland, about 260 miles (420 km) east of Vancouver (Figure 2). The slide spills into Trout Creek Canyon about 3-1/2 miles (6 km) upstream from the mouth of the creek on Okanagan Lake.

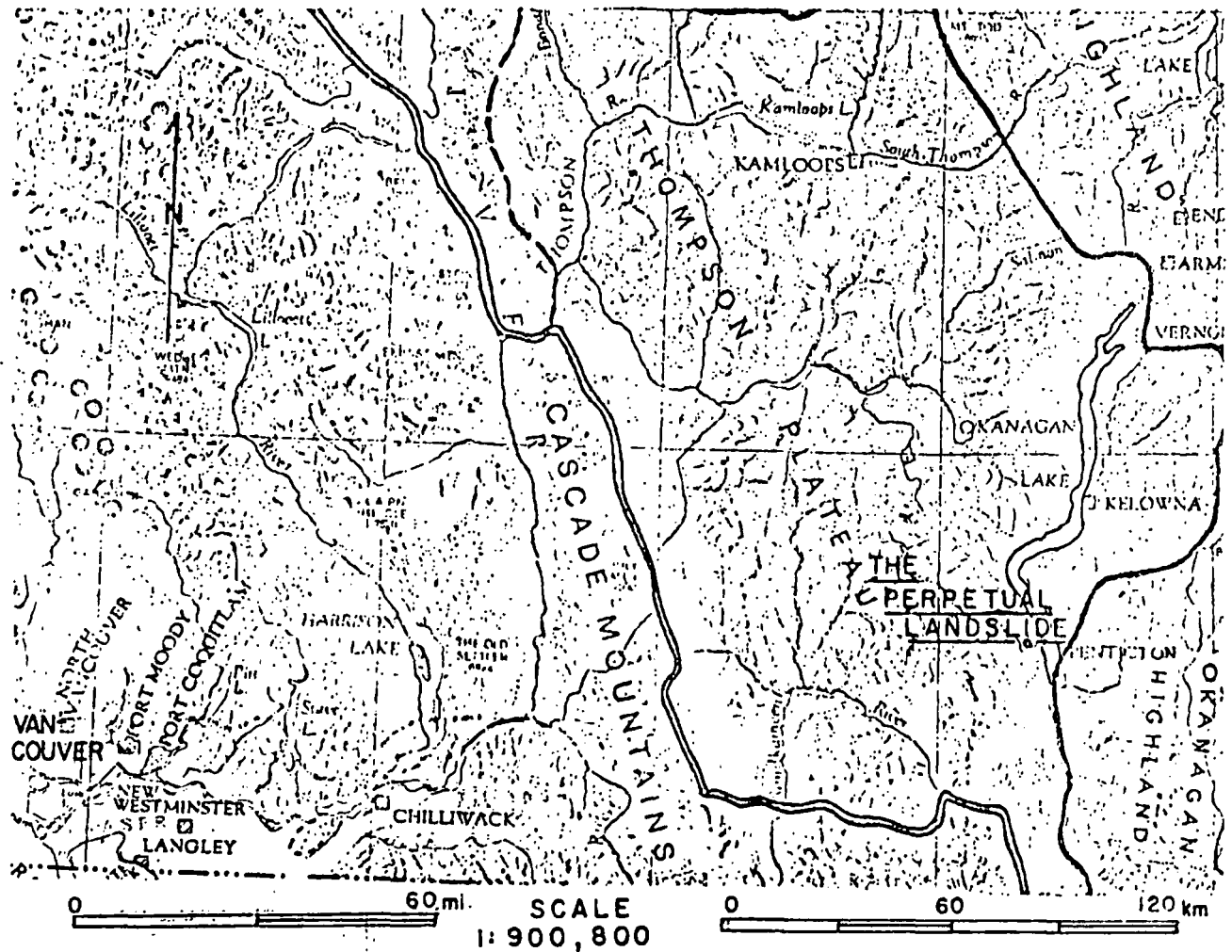


FIGURE 2 - Physiography of Southwestern British Columbia Showing Relative Location of the Perpetual Landslide (after Holland, 1964)

Description

Slide dimensions are 1,390 feet (424 meters) in length, 1,370 feet (418 meters) in width, and 260 feet (79 meters) in estimated depth. Volume is estimated to be 7×10^6 yards³ (5.4×10^6 meters³).

LANDSLIDE CLASSIFICATION AND GEOMORPHOLOGY

The type of failure is that of a slide in the strict sense. The Highway research Board Landslide Committee in their Classification of Landslides

(1958, Plate 1) describe a slide as follows: "Movement caused by finite shear failure along several surfaces which are visible or whose presence may be reasonably inferred". In the Perpetual Slide, slickensided gouge surfaces are visible at the toe and flanks. Major faults divide the body of the slide into successive blocks. From these exposed shear surfaces the failure surface at depth can be inferred as shown in Figure 3.

Further, because the slide has a dominant rotational character, it may be classified as a slump: "Movement only along internal slip surfaces which are commonly concave upward. Backward tilting of units is common." (Highway Research Board Landslide Committee, 1958, Plate 1). Many of the landform features in the Perpetual Slide are typical of slump failure (as described by Ritchie, 1958). The geomorphic map, Figure 4, shows concave scarps breaking the slide up into blocks. These blocks are commonly backward tilted with grabens or depressions at their heads. In the toe section, upthrust, impermeable gouge causes pond formation. As is common in slumps, break-up of coherent blocks and flow motion occurs in this toe area. Here, movement may be a combination of shear on bounding slip surfaces and actual flow which is described as "Movement within the displaced mass such that the form taken by the moving material, or the apparent distributions of velocities and displacements resemble those of viscous fluids." (Highway Research Board Landslide Committee, 1958, Plate 1). Relatively dry sand and gravel flows bound the toe section of the Perpetual Slide and are caused by springs undercutting loose bank material. Wet flows involve water-saturated sand and gravel masses pouring out from the toe and down along the slope below the slide. Another type of wet flow is in saturated gouge (exposed along the lip of the canyon) as it may flow rather than move with shear displacement. The clay masses which flow down the canyon wall fit Skempton's (1969) description of mudflow material, commonly consisting of unsorted, clay-rich debris in a soft clayey matrix. Deposition of flow debris results in formation of fans along Trout Creek Canyon and degradation of water quality.

GEOLOGY

The geologic study was carried out to determine what materials were likely to form the failure plane(s). Geology in the immediate vicinity of the slide was mapped. (Refer to Figure 3 for location of units within slide longitudinal section). Deposits were divided into three basic groups; an older crystalline group (units 11 and 12, which are mainly Jurassic according to Peto and Armstrong, (1976), and younger volcanic and sedimentary sequence (units 6 and 7, Eocene according to Mathews and Rouse (pers. Comm.), and overlying unconsolidated deposits (unit 3, 4, and 5, of Quaternary age).

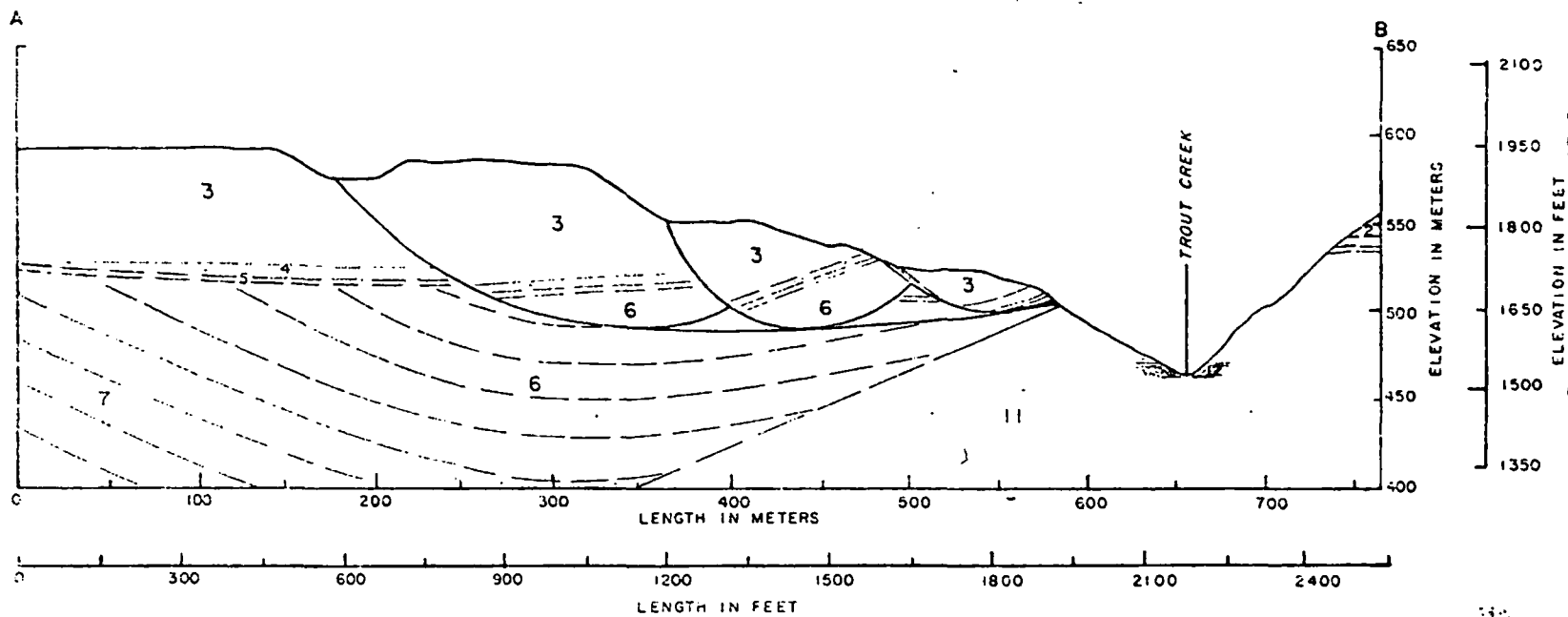


FIGURE 3 - Longitudinal Profile of the Perpetual Landslide Along Line A-B (See Figure 2-1b)

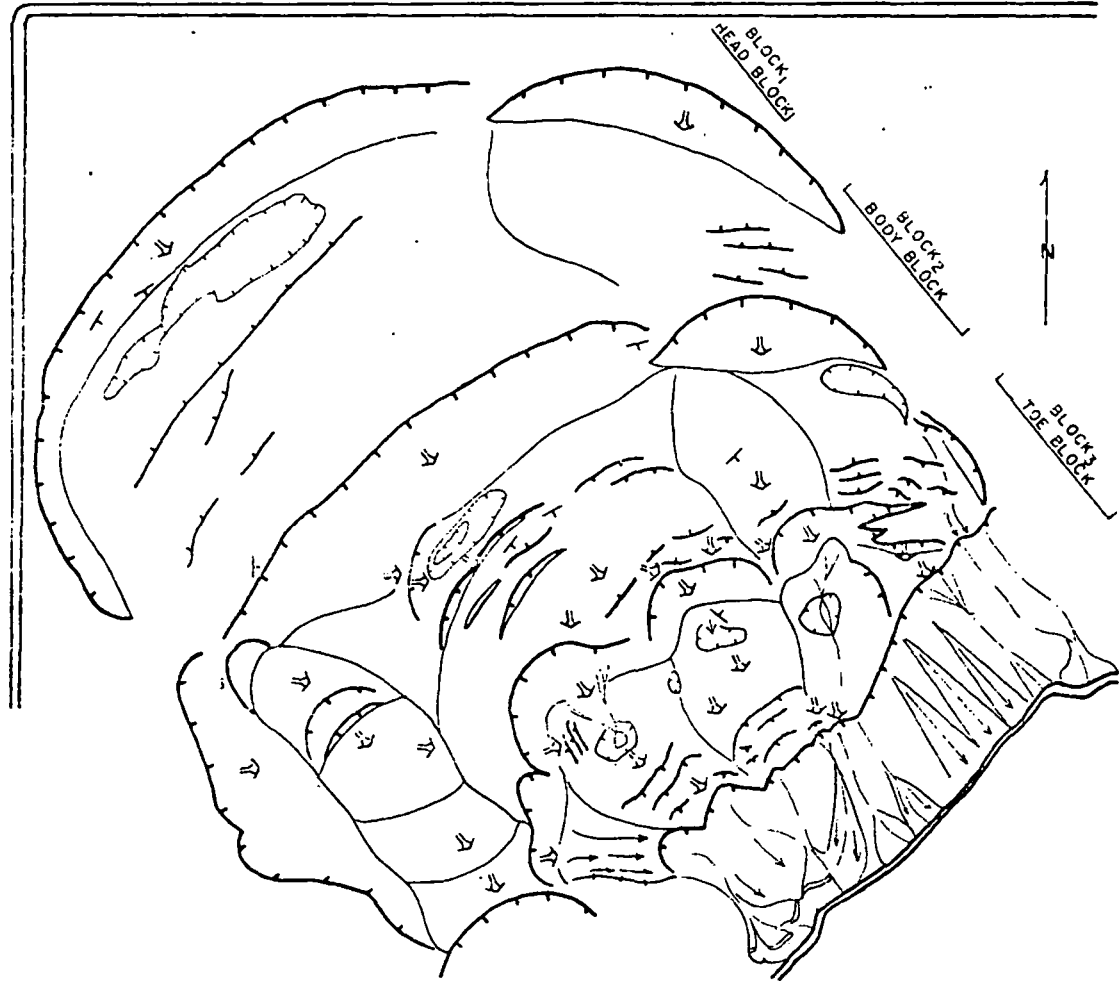
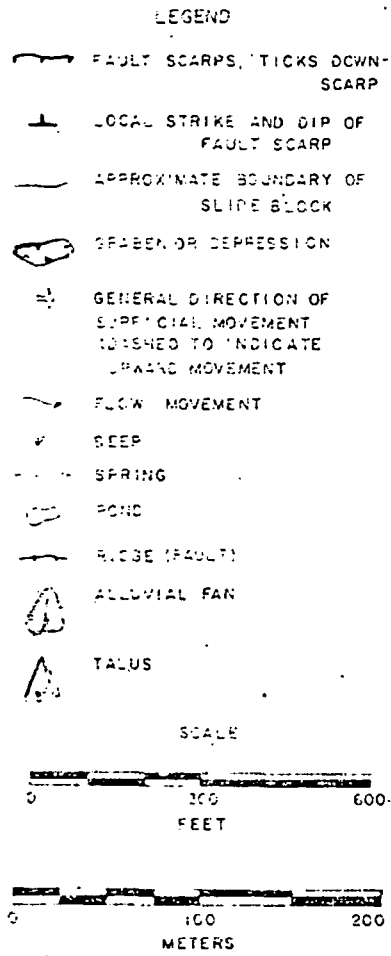


FIGURE 4 - Geomorphology of the Perpetual Landslide

Crystalline Rocks & Tertiary Volcanic Rocks

Exposed in Trout Creek Canyon, underlying and bounding the slide, is a massive body of granodiorite (unit 11) and a vein and dike complex, both of which enclose a competent unit of limestone-sandstone (unit 12). The granodiorite is commonly very friable and hydrothermally altered at vein contacts, jointed in exposure, and weathered on its upper surface (to form a saprolite and a weathered rock zone). Parts of these heterogeneities form conduits for ground water discharge in Trout Creek Canyon. Overlying the crystalline unit are Tertiary volcanic rocks (unit 7) which crop out on topographic highs surrounding the slide. Because the volcanics are commonly intensely brecciated, their strength is decreased and secondary permeability may be developed. However, neither the volcanics nor the crystalline rocks are observed to actually be part of the sliding mass.

Tertiary Sedimentary Rocks

The Tertiary sedimentary rocks (unit 6) form the failure plane of the slide and influence slope stability both hydrologically and lithologically. They consist of volcanic sandstone, claystone, and coal. At the present time, the sedimentary rocks are exposed only in the lower slide area. They are commonly intensely deformed as they are upthrust to the surface as a result of slide movement. Lack of strength in these rocks and their contrasts in conductivities produce a situation detrimental to stability.

Quaternary Deposits

The Quaternary deposits are divided into glacial till (unit 5), glaciolacustrine silt and fine sand (unit 4), glacial fluvial deltaic sands and gravels (unit 3), and terrace (or raised channel) gravels (unit 2). The till is involved in failure at depth and consists of unsorted cobbles in a clay-rich matrix. Because of this matrix, the till has low permeability relative to the other unconsolidated deposits. The clay's weakness is demonstrated by failure within the till in a strike slip fault on the southern boundary of the slide toe. This slip surface, laterally confines the slide and show mudcracks, slickensides, and brecciation.

Late Glacial & Recent History

In glacial and recent times, erosion operated to bring about slope failure of the Perpetual Slide. The downcutting of Trout Creek influenced stability in two ways:

(1) It unloaded the toe of the potential slide by eroding part of the terrace deposits on the north side of Trout Creek.

(2) It removed lateral support with downcutting and steepening of the valley walls. This excavated the unconsolidated deposits to a greater depth as well as exposed underlying Tertiary sedimentary rocks which became the failure material. The two mechanisms disrupted equilibrium and changed stress concentrations.

Slide Gouge

Gouge is apparent at the toe of the slide along the canyon lip and also in an upward rotational thrust of the failure surface. It is a heterogeneous mixture of claystone, coal, sandstone fragments, and till gravels. Its gritty, clay matrix is derived from remolded claystone and clay-rich till. As the consolidated rock, predominantly the claystone, is progressively and repeatedly sheared, it is remolded into this gouge of lower strength. Because of its clay fraction, the gouge is commonly mud-cracked on its surface. In places an abundance of cracks indicate marked volume change in the clay with change in water content. X-ray diffraction established the presence of an expanding mixed-layered clay in three samples tested. Expansive clays readily absorb water (swell), with a consequent decrease in strength. However, the extent to which this takes place is not known, as the percentage of expanding clay in the failure material of the Perpetual Slide is not defined. Generally, the gouge is evidenced to be relatively impermeable. This affects ground water flow in two ways. The gouge promotes formation of an intermediate flow system, by forcing flow through overlying unconsolidated deposits. In addition, it confines the upward discharge from any underlying aquifers (likely weathered granodiorite, volcanic sandstone, and perhaps jointed claystone and coal), thereby allowing high pore water pressures to be transmitted to the base of the slide.

HYDROLOGY

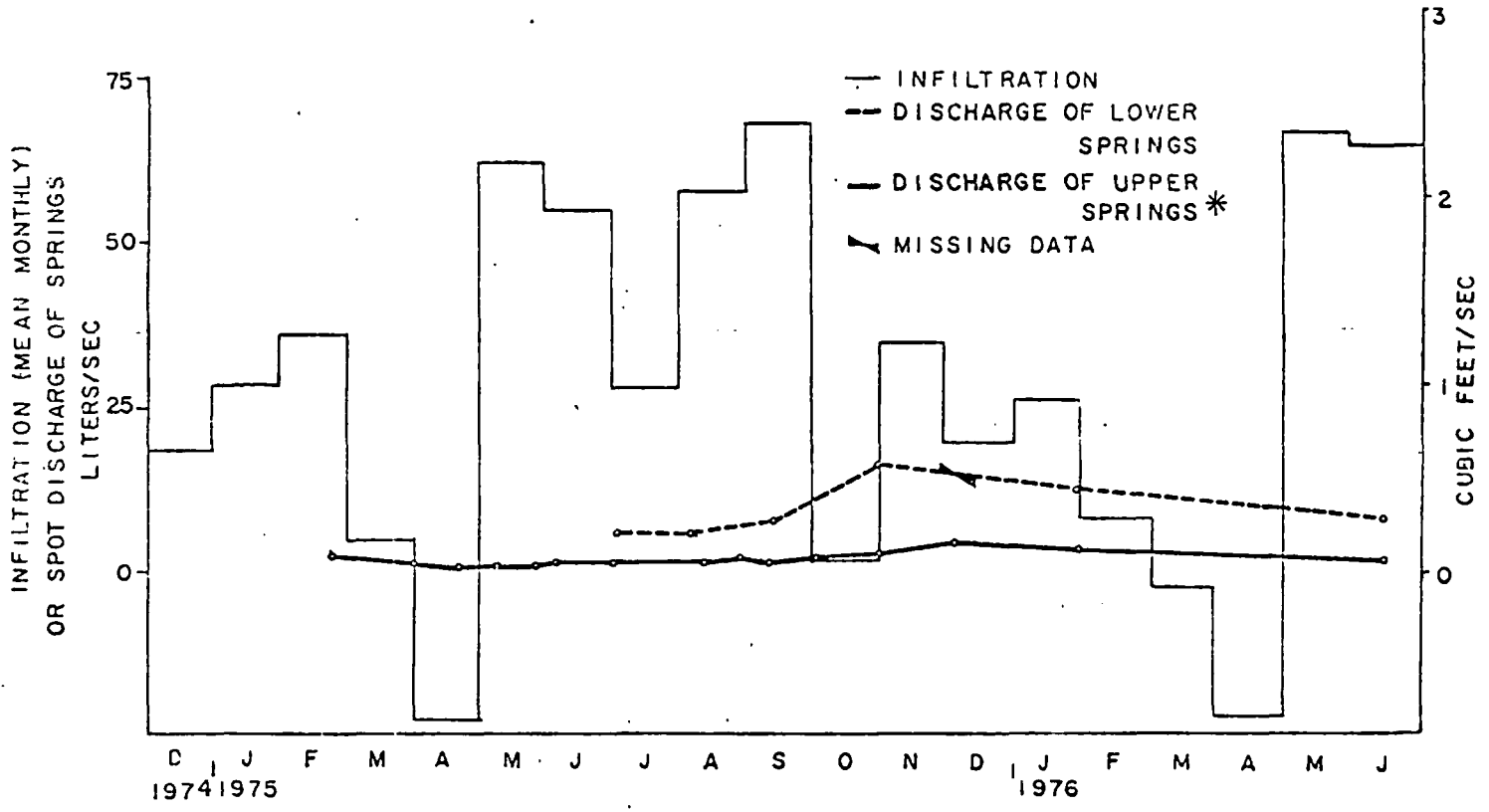
The ground water flow system exerts critical influence on slope stability. In the case of the Perpetual Slide, a change in the flow system resulting from initial irrigation of the terrace area above the slide (1903-1906) was followed by incipient ground water discharge and failure in the slide area (sometime during the period from 1914 to 1917). Because of the demonstrated significance of ground water flow to failure of the slide, a study of hydrology in its drainage basin was carried out. The main objective of this study was to quantify water inflow and outflow and to attempt to find a correlation between them.

A simplified equation:

$$\text{Precipitation} + \text{Irrigation} - \text{Evapotranspiration} = \text{Infiltration}$$

can be used to calculate the slide's hydrologic budget. Input and output parameters in the equation are expressed as rates (cubic feet/sec and liters/sec) over the catchment basin. By substitution of known parameters (precipitation, irrigation, and evapotranspiration) into the above expression, the infiltration rate is determined (Figure 5).

A portion of the infiltration increases rates of ground water recharge and consequent discharge. This casual relationship is observed as a



*included in discharge of lower springs

FIGURE 5 - Infiltration and Spring Discharge

Large water input above the slide results in several, high-discharge springs (Figure 4) occurring where gouge and bedrock are exposed below (in the slide). In Figure 5, overlain on the histogram of infiltration, are the spot discharges for the upper and lower springs. The high infiltration or recharge in the summer month, most of which is due to irrigation, is followed by maximum spring discharge in November-December. In other words, irrigation recharge creates a water table rise which is responsible for increased flow through and discharge from the system. There is a two to three month time lag between fluctuations in this input and response of spring discharge to these changes.

STABILITY ANALYSIS

Two projects were undertaken in order to understand the mechanics of the Perpetual Slide. The first involved evaluation of short-term movement by surveying the slide during a period from the summer of 1975 to the summer of 1976. The second project, actual slope stability analysis was undertaken to gain insight into the conditions responsible for observed movement or failure. This analysis included testing the shear strength of gouge and equilibrium modeling the slide.

Surficial Movement Survey

The record of short-term movement was obtained from transit survey of the slide. Figure 6 shows the deflection of stakes off lines set across the upper part of the slide. These deflections were recorded by a stadia survey. Triangulation survey evaluated directional movement of stakes set on lines in the slide toe (Figure 7).

Departures of stakes from the survey lines are listed in Table I. Reliable survey measurements demonstrate that slide movement is a function of location within the slide and time of year.

The general trend of increased rate of movement downslope may be attributed to conditions at the toe: (1) the mudflow type movement, (2) the maintenance of steep slopes by headward erosion of gullies, (3) the addition of flow and surficial movement on steep toe slopes (sloughing) to movement along the failure plane at depth, and (4) the large driving force behind, and lack of frictional resistance at the toe.

Movement rates also increase toward the interior of the slide, as illustrated by Figures 6 and 7, and directions of movement vary within the slide. Modification of the general southeasterly trend of movement is observed (Figure 7) at the toe. Lower lines are found to converge toward gullies created by the springs. Short-term upward movement is displayed by the eastern section of the toe and may result from backward tilting of coherent blocks.

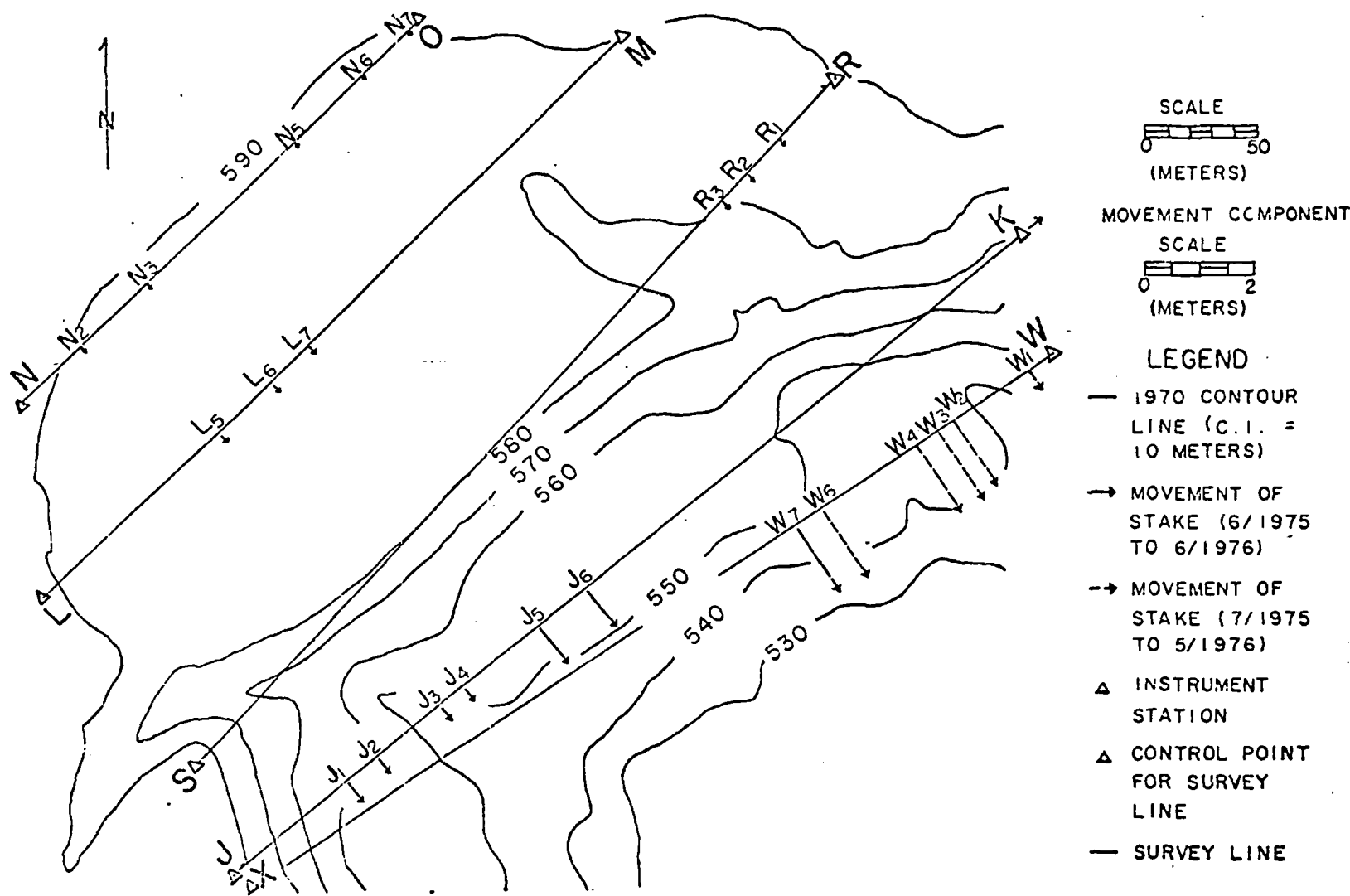


FIGURE 6 - Diagram of Horizontal Movements of Stakes Showing Components Normal to Survey Lines (Upper Part of Slide)

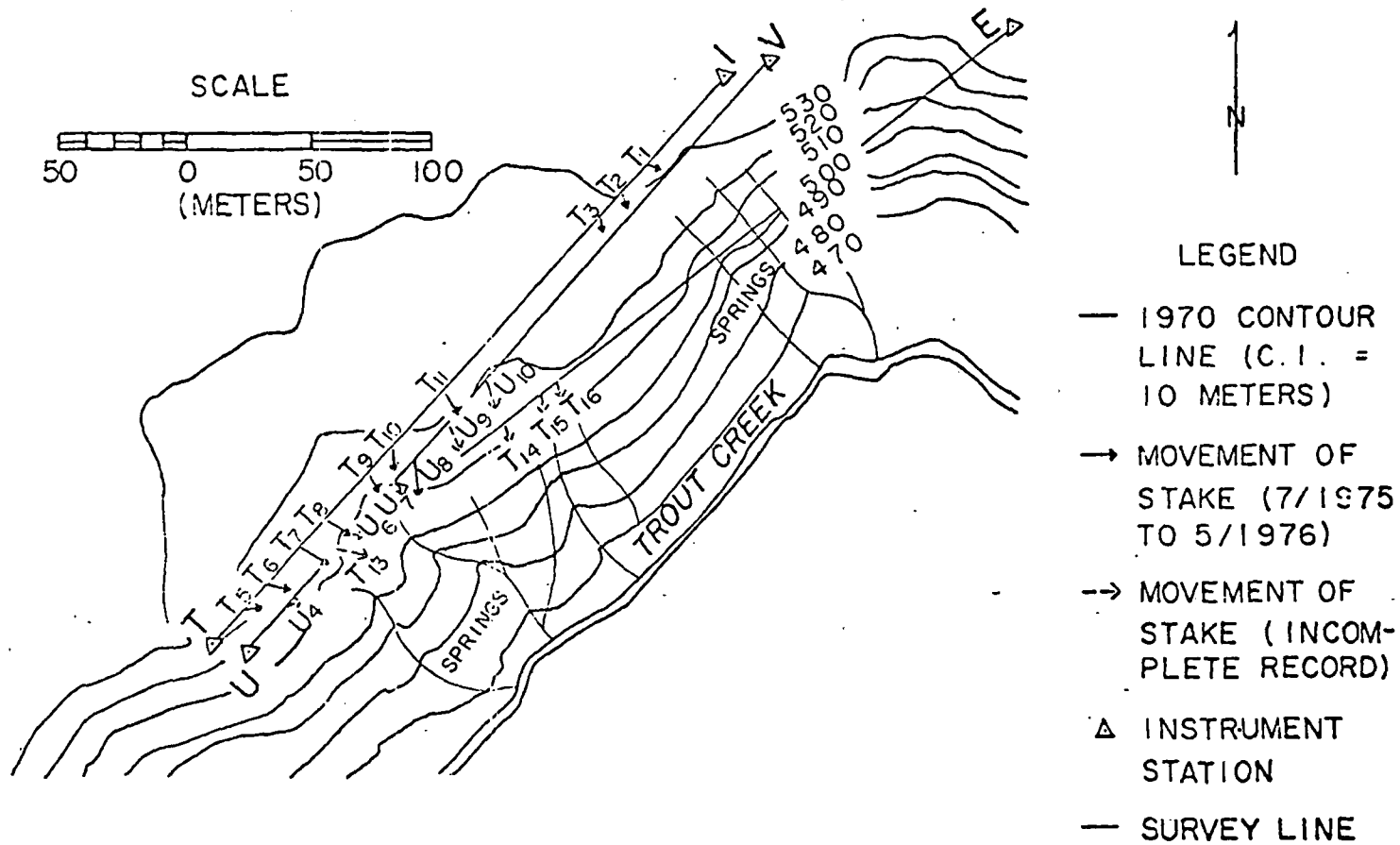


FIGURE 7 - Vector Diagram of Horizontal Movement of Stakes in True Direction (Toe of Slide)

TABLE I
 Horizontal Movement Rates of Stakes
 (Given as Averages for Each Line of Stakes)

Line		Apparent Downslope Movement Rate (Perpendicular to Survey Line)	Actual Downslope Movement Rate (True Direction)
Upper Part of Slide:			
NO	6/75 to 6/76	= .08 m/yr	
LM	"	= .18 m/yr	
RS	"	= .13 m/yr	
JK	"	= .51 m/yr	
WX	"	= 1.49 m/yr	
Toe of Slide:			
TI'	7/75 to 5/76	8.12 m/yr	9.01 m/yr
UV	"	13.09 m/yr	15.90 m/yr
TE	7/75 to 2/76	15.69 m/yr	18.30 m/yr

Seasonal fluctuations are particularly evident in toe stakes. Their average monthly movement is at maximum in November. This correlates closely to the time of maximum discharge of the springs during November and December. The back-lines, also show increased movement beginning in October-November. This increase in movement with discharge reaffirms the earlier conclusion that ground water flow has critical influence on stability.

Strength and Stability Evaluation

In the second phase of the stability analysis, shear strength of the slide gouge was evaluated. This strength, as a constant, and assumed environmental parameters, as variables, were incorporated into equilibrium models. In this way an attempt was made to find the most critical situation for failure.

The residual shear strength of the slide gouge was determined by reversible, drained, direct shear tests. Under expected loading conditions, ϕ residual was found to be equal to 18.5 degrees. This seems to be a reasonable value for the gouge when considering that its plasticity index is equal to 18 (Kanji 1970).

The shear strength was incorporated into a slope stability analysis to define a reasonable environment for failure. Limit equilibrium methods were used. Rotational (moment) equilibrium was analyzed by the Simplified Bishop Method of Slices. Stability was also evaluated using a translational analysis developed by the Civil Engineering Department at the University of British Columbia. Trial phreatic, piezometric, and slip surfaces were delineated by known geology and hydrology. The most critical combination found is shown in Figure 8, and is, at best a probable situation for failure. However, the analysis does indicate that a high piezometric surface is critical for instability.

CONCLUSIONS

(1) From geomorphic considerations, it is concluded that the Perpetual Slide is a composite landslide consisting of slump failure with a transition to flow, in the toe section. Both types of failure were confirmed by the movement survey.

(2) The geologic study shows that the failure surface lies within Tertiary sedimentary rocks, primarily claystone.

(3) From the hydrologic and stability analysis it is concluded that ground water seems to be the controlling factor initiating slope instability.

Investigation of this slide has served to define the environment for failure and would serve to guide any more comprehensive subsurface analysis.

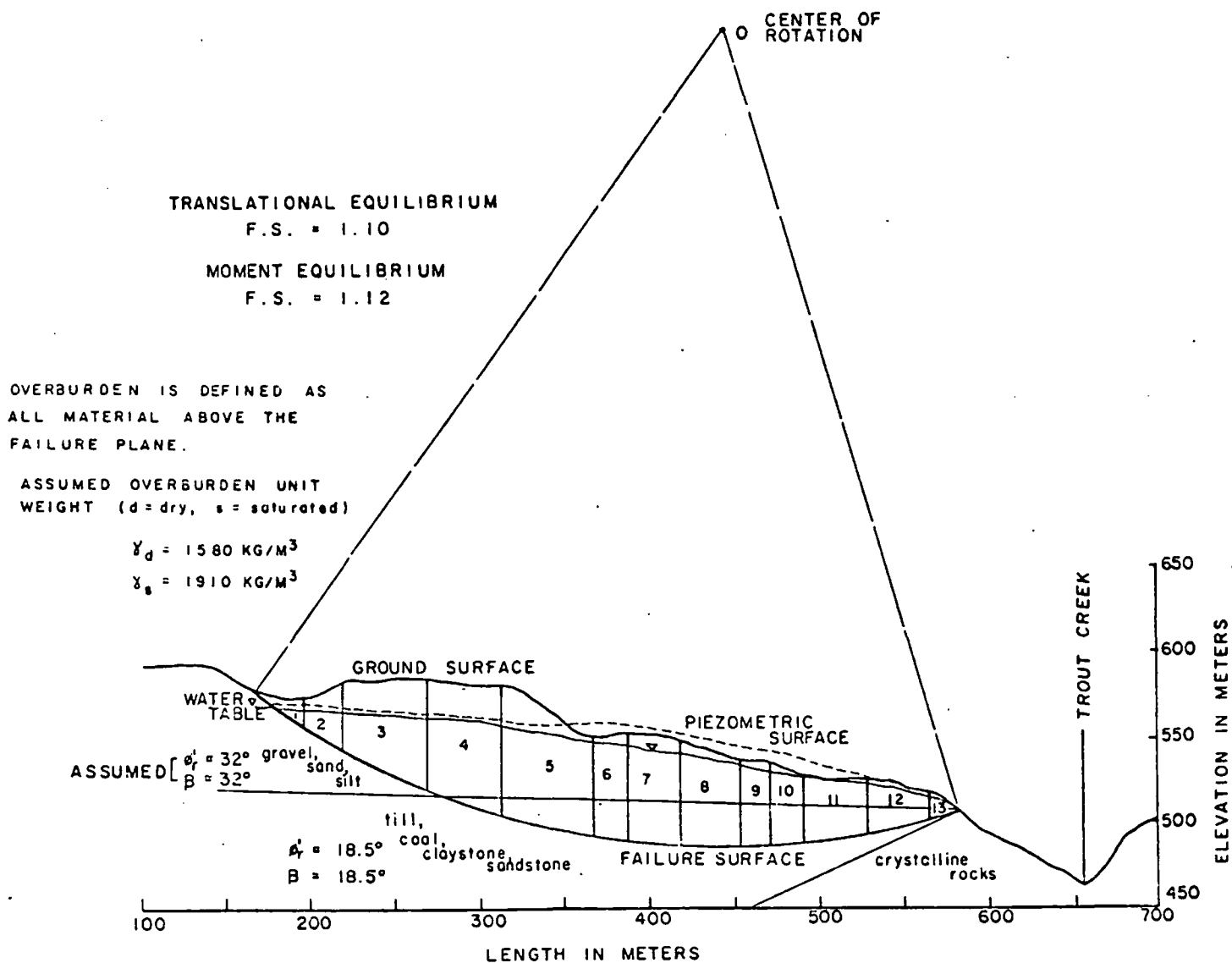


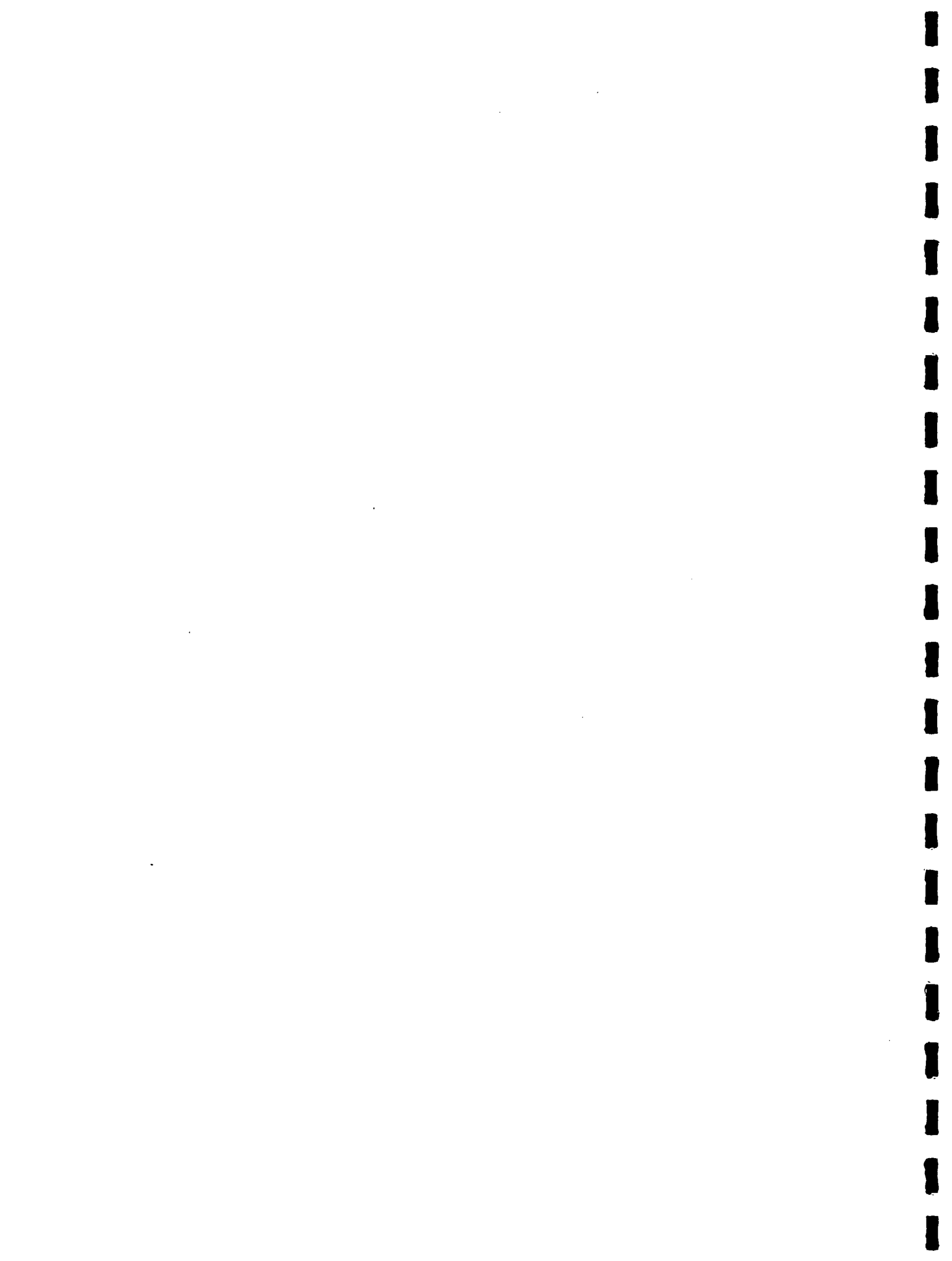
FIGURE 8 - Case 1, Failure Model for Entire Slide (Cross Section Along Line A-B of Figure 1-2b)

REFERENCES

- Agriculture Canada, 1974-1976, Weather Observations: Research Station, Summerland, B.C.
- Anderson, J.D., 1975, Slope Stability by Non-Circular Analysis: Dept. of Civil Engineering, Univ. of British Columbia, Vancouver, B.C.
- B.C. Dept. of Lands, Forests, and Water Resources, May 1975, Perpetual Slide, Trout Creek, Summerland: Water Investigations Branch, Water Resources Service, Victoria, B.C.
- Canada Dept. of Energy, Mines, and Resources, Surveys and Mapping Branch, 1968, Summerland, B.C.: Map 82E/12E, Edition 1MCE, Series A 721.
- Coligado, M.C., 1968, Risk Analysis of Weekly Climatic Data for Agricultural and Irrigation Planning, Summerland, B.C.: Prepared for the Canada Land Inventory, Dept. of Forestry & Rural Development.
- Freeze, R.A., and Witherspoon, P.A., 1967. Theoretical Analysis of Regional Ground Water Flow. 2. Effect of Water-Table Configuration and Sub-surface Permeability Variation: Water Resources Research, V. 3, No. 2. pp. 623-634.
- Highway Research Board Landslide Committee, 1958. Classification of Landslides: Landslides and Engineering Practice, (ed. E.B. Eckel), Highway Research Board Special Report 29, Plate 1.
- Hodge, R.A.L., 1976, Regional Geology, Ground Water Flow Systems and Slope Stability: Master of Applied Science Thesis, Dept. of Geological Sciences, Univ. of British Columbia, 98 pp.
- Holland, S.S., 1964, Landforms of British Columbia - A Physiographic Outline: B.C. Dept. of Mines and Petroleum Resources, Bull. 48, Figure 1.
- Kanji, M.A., 1970, Shear Strength of Soil-rock Interfaces: M.S. Thesis, Dept. of Geology, University of Illinois, Urbana, Illinois, 69 pp.
- Lambe, W.T., 1951, Soil Testing for Engineers: New York, John Wiley and Sons, Inc., 165 pp.
- Lambe, T.W., and Whitman, R.V., 1969, Soil Mechanics: New York, John Wiley and Sons, Inc., pp. 357-366.
- Mathews, W.H., 1958, Guidebook for Geological Field Trips in Southwestern British Columbia: Dept. of Geology, University of British Columbia, Report No. 6, pp. 19 and 20.

Surficial Investigation of the Perpetual
Landslide Summerland, British Columbia
By Linda Riglin
Page 17

- Patton, F.D., and Hendron, A.J., 1974, General Report on Mass Movements: Proceedings of the 2nd Internat. Congress of the Internat. Assoc. of Eng. Geology, San Paulo, Brazil, V. 2, V-Gr, 57 pp.
- Peto, Peter and Armstrong, R.L., 1976, Strontium Isotope Study of the Composite Batholith Between Princeton and Okanagan Lake: Canadian Journal of Earth Sciences, v. 13, No. 11, p. 1577-1583.
- Ritchie, A.M., 1958, Recognition and Identification of Landslides: Landslides and Engineering Practice, (ed. E.B. Eckel), Highway Research Board Special Report 29, pp. 48-68.
- Skempton, A.W., 1964, Long-term Stability of Clay Slopes: Geotechnique, V. 14, No. 2, pp. 77-102.
- Skempton, A.W., and Hutchinson, J.N., 1969, Stability of Natural Slopes and Embankment Foundations: Proc. of the 7th Internat. Conf. on Soil Mech. and Found. Eng., Mexico, State-of-the-Art, pp. 291-340.
- Summerland Development Company, 1904, Plan of Subdivision of Lots 439,440, 2195 and 2196, Osoyoos Div. - Yale Dist., Sept. 1904.
- Summerland Development Company, 1907, Plan of Subdivision of Lots 1073 and 3194G1, Osoyoos Div. - Yale Dist., May 1907.
- Terzaghi, Karl and Peck, R.B., 1967, Soil Mechanics in Engineering Practice: 2nd ed., New York, John Wiley and Sons, Inc. p. 121.
- Varnes, D.J., 1958, Landslides Types and Processes: Landslides and Engineering Practice, (ed. E.B. Eckel), Highway Research Board Special Report 29, pp. 20-47.
- Personal Communication: W.H. Mathews, 1977, Dept. of Geol. Sciences, University of British Columbia, Vancouver, B.C.



EFFECT ON GROUNDWATER OF THE CAVALIER, NORTH DAKOTA,
SANITARY LANDFILL

By

Alan E. Kehew¹ and Gerald W. Knudsen²

ABSTRACT

The Cavalier, North Dakota, sanitary landfill is located near the distal margin of an area of sandy silt (ML) and silty sand (SM) deposited as a hooked spit by longshore currents in glacial Lake Agassiz. The water table at the site ranges from 6-12 ft. (2-4 m) below land surface, with highest levels in the spring and summer resulting from recharge from snowmelt and precipitation. Groundwater in the aquifer is of calcium magnesium bicarbonate type with median hardness and TDS values of 192 mg/L and 251 mg/L respectively (Hutchinson, 1977).

Unlined trenches filled with solid waste intersect the water table during at least part of the year, thus providing optimum conditions for contamination of groundwater. Fourteen piezometers were installed around the site in order to sample groundwater from the waste cells and both up and downgradient from the cells. Eleven of the wells are screened at the water table and three others with screened intervals 15-20 ft. (5-6 m) below the water table are situated adjacent to shallow wells in various downgradient positions. Single well response tests indicate an approximate hydraulic conductivity for the site of 1.6 ft/day (5.6×10^{-4} m/sec). Using an average gradient of .008, an average groundwater velocity can be calculated as 16 ft/yr. (5 m/yr). Greater sand percentages from the vicinity of the water table suggest that hydraulic conductivity in the shallow zone of the aquifer may be greater than the approximate value given above.

Water samples are analyzed for major ions and trace metals. Results of the monitoring indicate that shallow groundwater beneath the covered waste cells is highly polluted with specific conductances ranging from 3000-5000 micromhos/cm. Downgradient from the cells, a shallow leachate plume extends beyond the landfill boundary. Conductivity values in the shallow wells decrease rapidly downgradient, reaching approximately 1000 micromhos/cm 50 ft. (15 m) from the edge of the waste cells, and approximately 800 micromhos/cm 170 ft. (52 m) from the edge of the waste cells at the landfill boundary. Major ion concentrations in the three deeper wells show no probable influence of contamination and are probably very close to background levels for this part of the aquifer. Therefore, the leachate plume probably consists of a concentrated front moving at the average groundwater velocity with a thin dispersed extension at the water table moving more rapidly than the concentrated front.

¹ North Dakota Geological Survey, University Station, Grand Forks, North Dakota 58202

² North Dakota State Dept. of Health, 1200 Missouri Ave., Bismarck, North Dakota 58505

Earth resistivity surveys detected the contaminated groundwater near the edge of the covered waste cells but indicated normal resistivities 150 ft. (46 m) downgradient.

INTRODUCTION

North Dakota is a sparsely populated agricultural state which is highly dependent upon its groundwater resources. Approximately 45 percent of water supplied to urban communities and nearly all water obtained by the rural population is groundwater (U.S. Bureau of Reclamation, 1973). Therefore, it is important to protect this resource from contamination by poor waste disposal practices. Pleistocene glacial deposits, which cover about three-fourths of the state contain some of the most important aquifers. While most of the glacial sediment is relatively impermeable till, several types of permeable glacial deposits form aquifers of regional or local importance. These semi-confined to unconfined Pleistocene aquifers constitute the highest potential for contamination by waste disposal practices.

In order to evaluate the effect of solid waste disposal in landfills, a cooperative program between the North Dakota State Department of Health and the North Dakota Geological Survey was initiated to assess the hydrogeological setting and pollution potential of sanitary landfills in the state. First, all existing sites were rated by use of existing geologic and hydrologic information and reconnaissance field visits. Individual sites, such as the Cavalier landfill were selected for more detailed field investigations.

The objectives of this study were to determine the geologic and hydrologic setting of the Cavalier sanitary landfill and to evaluate the chemical composition and movement of leachate produced at the site.

HISTORY OF LANDFILL

The Cavalier landfill was operated as a typical burning open dump for over twenty years. The normal operation for the dump was to place refuse in an excavated trench and burn daily. The trenches were 10-15 ft. (3-4.5 m) deep. The pattern of filling of trenches was probably from west to east because current trenches are now approaching the east boundary of the landfill. Based on population estimates for the city and surrounding rural area and average waste production figures, approximately 1,400 tons of uncompacted refuse was placed in the trenches each year of operation.

In order to comply with the North Dakota Solid Waste Management Regulations the city has discontinued its practice of burning the refuse. The landfill is now operated in the usual trench-fill method. The waste deposited at the site consists of residential and commercial waste. Pesticide containers have been observed in the pits but the volume of such material is not known.

GEOLOGIC SETTING

The landfill is located in Pembina County, in the extreme northeast corner of North Dakota (Figure 1). Geologically, the site occupies a position near the distal margin of an area of sandy silt (ML) and silty sand (SM) deposited as a hooked spit by longshore currents in glacial Lake Agassiz (Hutchinson, 1977). Grain size in the nearshore deposits decreases eastward, grading into offshore clay and silt deposits. At the Cavalier landfill, the material consists of yellow-brown, thin-bedded, well-sorted, fine silty sand to sandy silt. The upper 5 to 10 ft. (1.5-3 m) of material are generally more sandy, ranging from 40-70 percent sand. The sediment becomes more silty with depth with sand approximately 20-40 percent and silt 50-70 percent. Test holes nearby indicate that the sandy silt is underlain by clay at an approximate depth of 30 to 45 ft. (9-14 m) (Hutchinson, 1973), but test drilling for this project was too shallow to encounter the contact.

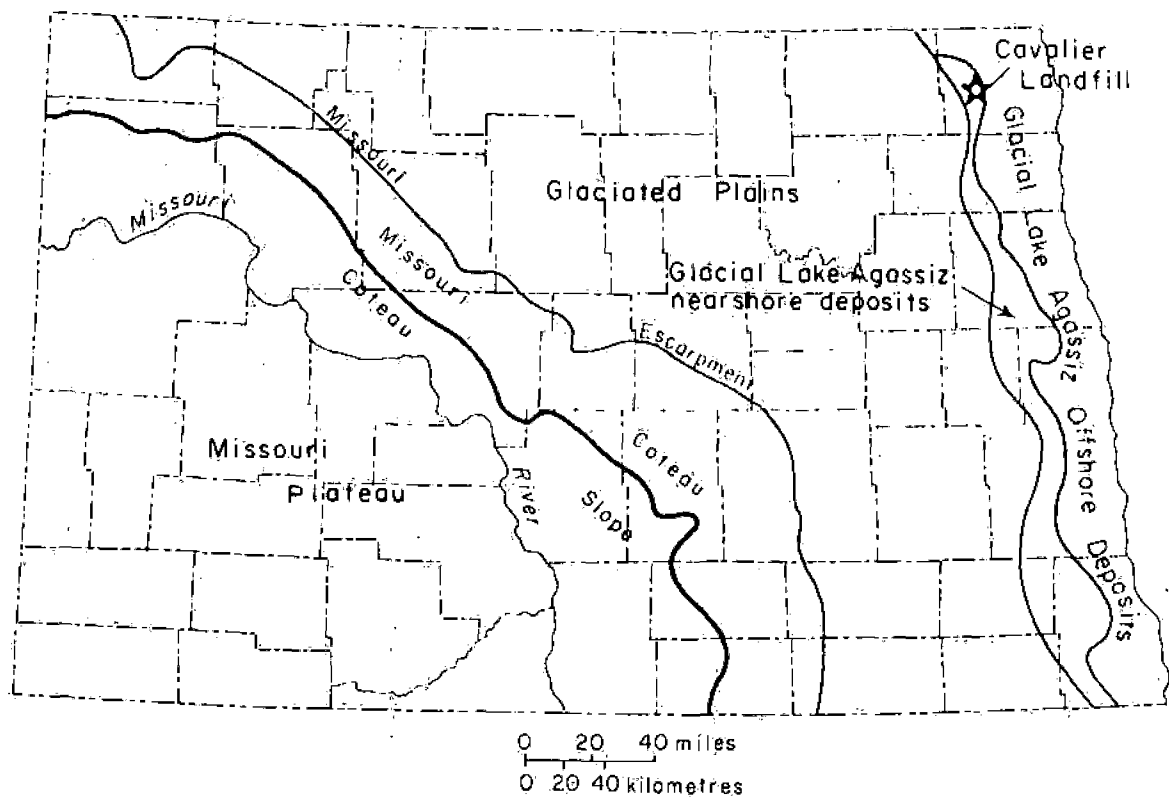


FIGURE 1 - Map of North Dakota Showing Location of Cavalier Landfill Near the Boundary of Glacial Lake Agassiz Nearshore and Offshore Deposits

METHODS

In order to investigate the hydrogeology of the site, 14 piezometers were installed at the landfill. Initially, 11 piezometers were installed in November, 1977 with a truck-mounted power auger. These were screened at the water table due to inability to keep the hole open below the water table in the wet sandy silt. In June, 1978, three deeper piezometers were installed using a hollow stem auger. The piezometers consist of 2 in. (5.08 cm) schedule 40 PVC pipe with 5 ft. (1.5 m) sections of .020 in. (.05 cm) PVC screen at the bottom. After the piezometers were placed in the open hole or through the hollow stem auger, sand from the cuttings was backfilled in the hole to several feet above the top of the screen. The hole was then filled with grout to the surface.

The landfill and the piezometer locations were surveyed with plane table and alidade (Figure 2). The topography of the landfill changes continually during operation of the site.

Resistivity profiles were made using a Soiltest R-50 Resistivity Meter. The Wenner electrode configuration was used with electrode spacings as indicated in Figures 6 and 7.

Hydraulic conductivity was measured using single well response tests analyzed by the Hvorslev (1951) method.

Water sampling began during the spring of 1978 and will be continued on a quarterly basis. Wells are bailed several days prior to sampling so that representative groundwater samples can be obtained. Bailing immediately before sampling is also done if the well contains sufficient water for the sample. Conductivity, temperature, and pH are measured in the field. The samples are then taken to a motel room and filtered through .45 micron Gelman filters which have been double rinsed with distilled water to minimize possible interferences. Preservation, transportation, and analysis of samples are performed according to standard EPA procedures (U.S. Environmental Protection Agency, 1974).

The parameters measured are shown in Table 1. Some of the samples shown on Table 1 are indicated as unfiltered. These samples were from the initial sampling period. When sampling began using the procedure described above, some of the shallow wells did not contain sufficient water to obtain a sample. Therefore, earlier unfiltered analyses were included in the table. The unfiltered analyses should not be considered accurate, but most of the major ion values are probably close to their true values because the relationship of TDS to conductivity compares well in both the unfiltered and filtered samples. The unfiltered analyses are thought to be reliable as a general indication of major ion concentrations.

Effect on Groundwater of the Cavalie
North Dakota, Sanitary Landfill
By Alan E. Kehew and Gerald W. Knuds
Page 5

Well No.	Sp. Cond.	TDS (mg/L)	pH	COD (mg/L)
1*	560	348	7.7	15.3
2*	630	393	7.4	12.7
3*	650	358	7.4	10.1
4*	880	475	7.5	19.1
4a	620	391	7.4	72.0
5	765	461	7.3	26.0
5a	650	408	7.1	70.0
6*	415	213	7.6	6.4
7*	480	262	7.6	20.2
8*	670	-	7.7	8.2
9*	5500	3777	7.4	78.2
10	4400	3417	7.1	121.0
11	1080	735	7.2	63.0
11a	600	380	7.0	39.0

* Samples Unfiltered

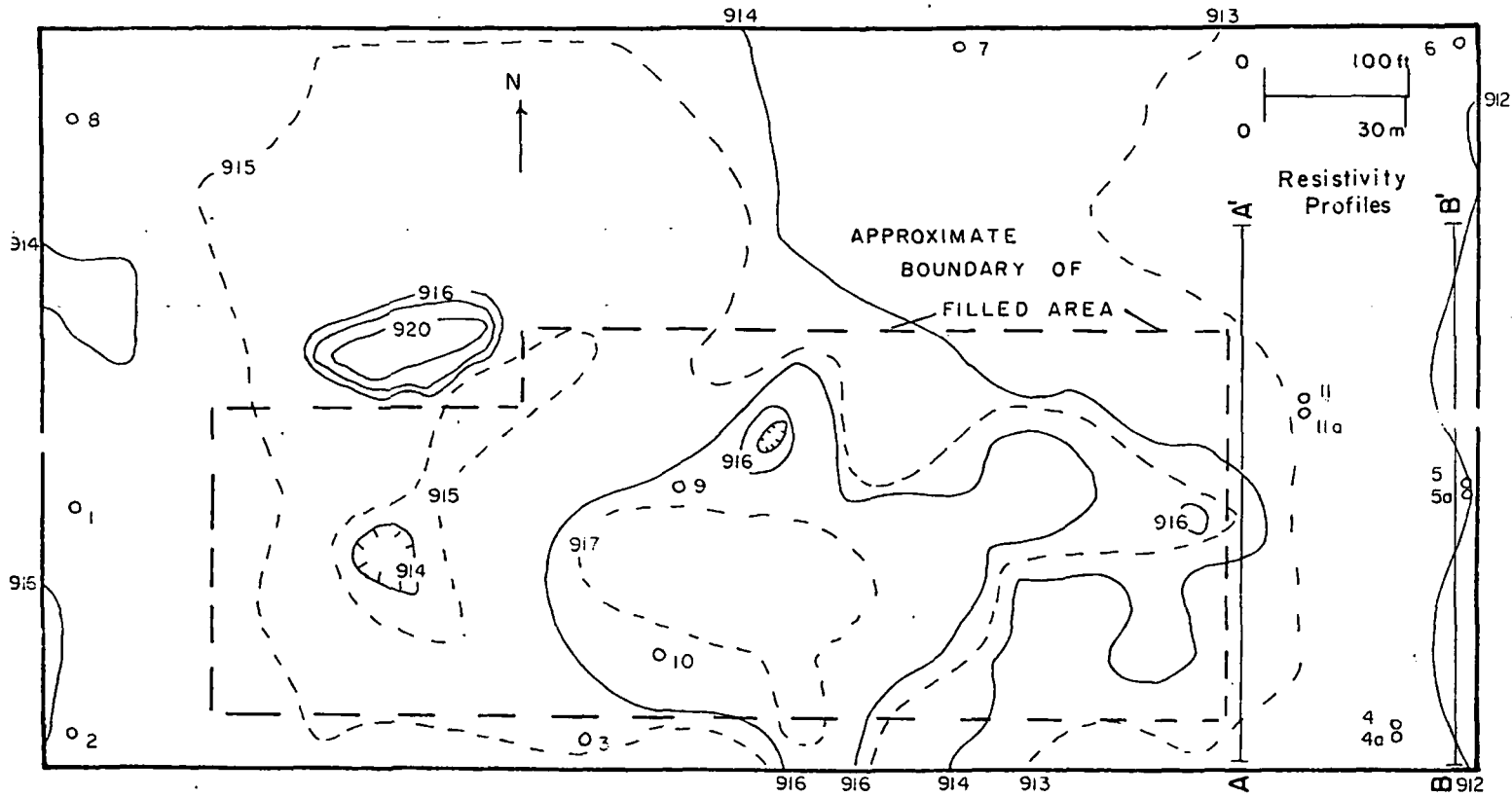


FIGURE 2 - Map of the Cavalier Landfill Showing Topography, Locations of Piezometers, and Locations of Resistivity Profiles. Topography Shown in 2 ft. (.6 m) Contour Intervals and Selected 1 ft. (.3 m) Contours.

HYDROGEOLOGICAL SETTING

The Cavalier landfill is located about one-half mile (1 km) east of the boundary of the Icelandic aquifer (Figure 3), as described by Hutchinson (1977), who interpreted the aquifer as a spit deposit in glacial Lake Agassiz. The surficial material at the landfill is continuous with and of the same origin as the Icelandic aquifer; however, the landfill is within the transition zone between nearshore and finer grained offshore lake deposits.

The Icelandic aquifer is unconfined with maximum saturated thickness of 70 ft. (21 m) (Hutchinson, 1977). Recharge to the aquifer is the result of rainfall and snowmelt over the surface of the aquifer. Water table fluctuations measured in test wells correspond closely to precipitation variations with maximum water table levels in the spring. Groundwater movement in the southern part of the aquifer is from west to east with discharge into adjacent lake deposits and by evapotranspiration and pumpage from wells.

Groundwater from the Icelandic aquifer is of calcium, magnesium, bicarbonate type with median concentrations of TDS, 251 mg/L; sodium, 4 mg/L; sulfate, 20 mg/L; chloride, 3 mg/L; and hardness, 192 mg/L (Hutchinson, 1977).

The groundwater flow system at the landfill is illustrated in Figure 4 with 2 ft. (.6 m) contour interval equipotential lines on the water table surface. Local flow at the landfill has a greater southeasterly component than the easterly regional flow in the aquifer. The average gradient at the site is about .008. Seasonal variations probably occur in the gradient. The significance of the water table depression in the vicinity of wells 9 and 10 is not known. It may represent a permeability variation due to the refuse buried at that point or an error in elevation measurement.

Head measurements of adjacent piezometers screened at different depths in the saturated zone are identical within the errors of surveying and water level measurement. Therefore, the vertical component of groundwater flow is extremely small. Groundwater moves downgradient essentially parallel to the slope of the water table.

Depth to the water table ranges from 6-12 ft. (2-4 m) at the landfill with the highest levels during the spring and summer resulting from recharge from precipitation and lowest levels during the late fall and winter. Solid waste cells therefore intersect the water table during at least part of the year bringing groundwater directly in contact with the refuse. This situation constitutes the greatest potential for generation and movement of leachate. The trenches contain no lining to isolate the waste from groundwater.

Effect on Groundwater of the Cavalier,
North Dakota, Sanitary Landfill
By Alan E. Kehew and Gerald W. Knudsen
Page 9

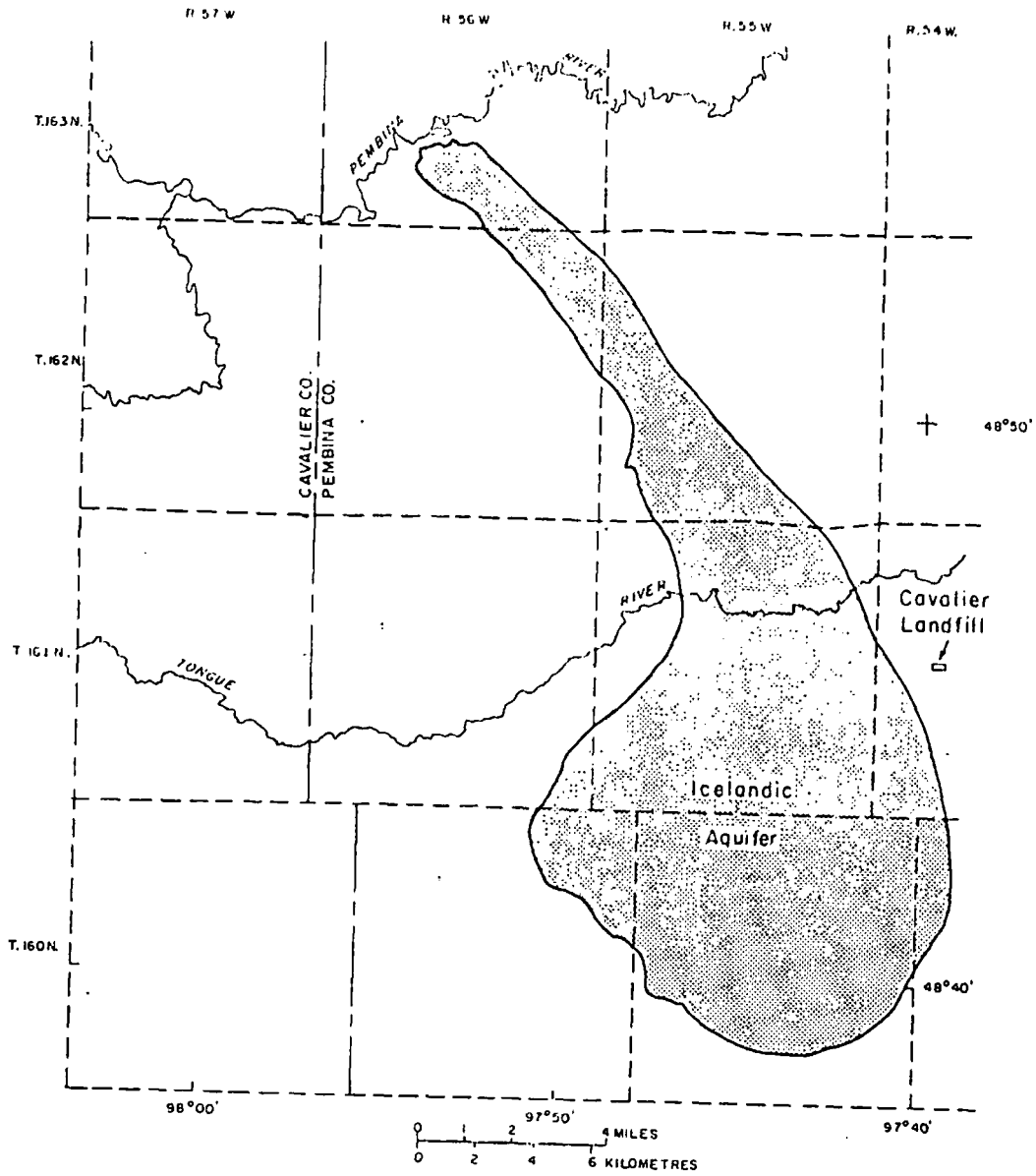


FIGURE 3 - Location of Cavalier Landfill with Respect to Icelandic Aquifer. (Modified from Hutchinson, 1977)

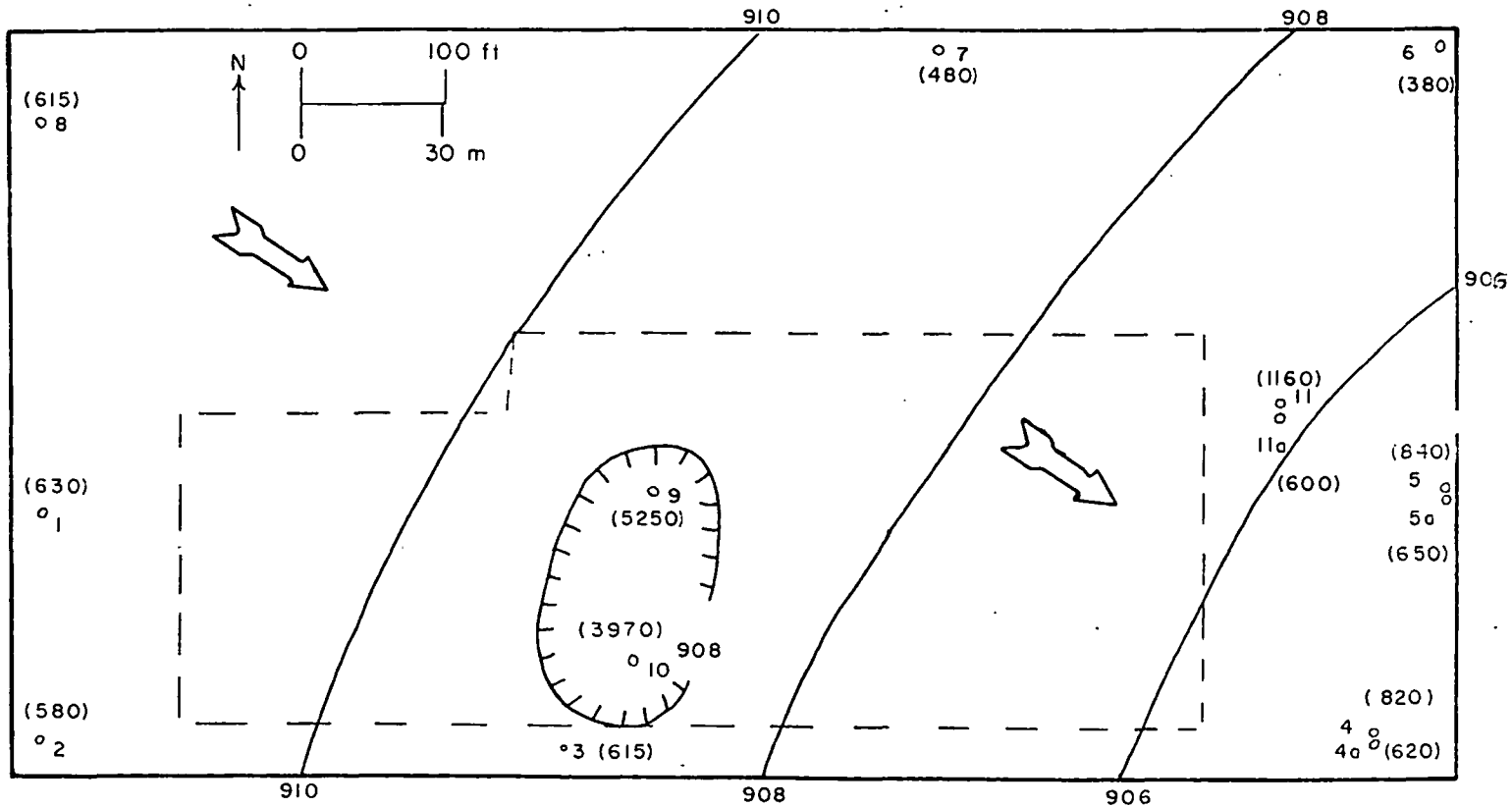


FIGURE 4 - Groundwater Flow at the Cavalier Landfill Shown by 2 ft. (.6 m) Contour Interval Equipotential Lines on the Water Table. Arrows Indicate Direction of Groundwater Movement. Average Conductivity Values in Micromhos/cm Shown for Each Piezometer.

In order to evaluate the movement of contaminants in groundwater, it is necessary to determine the hydraulic conductivity of the material. Estimates of permeability are available from the county soil survey (Thompson and Hetzler, 1977). For the soil series involved, permeability was estimated at 12-40 ft/day (4.2×10^{-3} - 1.4×10^{-2} cm/sec). This is actually an estimate of velocity or flux because it estimates "the rate at which a saturated soil transmits water in a vertical direction under a unit head of pressure" (Thompson and Hetzler, 1977). The approximate hydraulic conductivity can be calculated from these estimates as 3.7-12 ft/day (1.3×10^{-3} - 4.2×10^{-3} cm/sec), assuming a porosity of .3. This estimate may reflect the higher sand percentages in the upper 5-10 ft. (1.5-3 m) of material. For the purposes of this study, a single well response test was performed using well 11a and analyzed with the methods described by Hvorslev (1951). The value obtained in this test was 1.6 ft/day (5.6×10^{-4} cm/sec). While single well response tests measure only the hydraulic conductivity of a small area in the vicinity of a piezometer screen, we consider the value obtained to be a more realistic estimate for the overall average hydraulic conductivity at the landfill site than the soil survey estimate. Once an estimate for hydraulic conductivity is obtained, groundwater velocity can be calculated using the Darcy equation. Assuming a porosity of .3 and an average gradient of .008, groundwater velocity is estimated to be 4.3×10^{-2} ft/day (1.5×10^{-5} cm/sec). Disregarding the effects of heterogeneity upon the flow system, groundwater and associated plume of leachate should be moving at an average of 16 ft/yr. (5 m/yr).

Construction and filling of trenches during the landfill operation has proceeded from west to east, which is approximately the downgradient direction. Over the 20 year life of the landfill, the disposal operation has moved in the downgradient direction at an average rate of 30 ft/yr. (10 m/yr). Therefore, movement of leachate since the landfill began has probably been confined mostly within the filled areas. The leachate plume which can be detected downgradient from the most recent trenches probably originates from those trenches and not from older waste cells to the west.

INTERPRETATION OF CHEMICAL RESULTS

The effect of the landfill upon the hydrogeologic environment is assessed by a variety of field and laboratory measurements. Figure 4 shows the position of the filled area, locations of the wells, and average conductivity of the groundwater samples in relation to the flow system. Eleven of the piezometers are screened at the water table and three (11a, 5a, 4a) are screened 15-20 ft. (5-6 m) below the water table. Conductivity values from wells along the west and north sides of the landfill are interpreted to represent background conditions of the shallow groundwater. Piezometers 9 and 10 are completed in refuse and indicate that groundwater in the refuse cells is grossly polluted with dissolved solids. Finally, a group of two-level piezometer nests exists downgradient from the refuse cells. The three shallow wells (4, 5, 11) all indicate contamination with reduced levels of leachate concentration compared to

those completed in refuse. Piezometer 11, the well closest to the waste cells has the highest conductivity of the downgradient wells, a value of about 20 percent of the piezometers in the refuse. Shallow piezometers 4 and 5 both have conductivity values slightly above background levels, indicating that the leachate plume has reached those wells. The three deeper piezometers (4a, 5a, 11a) have nearly identical low conductivity values. This contrast is most evident in piezometer 11a which has a conductivity of about one half of the shallow well 16 ft. (5 m) directly above it (piezometer 11). In addition, there is no downgradient decrease in conductivity between wells 11a and 5a to correspond with the conductivity decrease between wells 11 and 5. Therefore, leachate is limited to the shallow zone of the aquifer downgradient from the waste cells. The reason for this may be the lack of a significant vertical component in the groundwater movement. Alternatively, hydraulic conductivity may be greater in the upper part of the aquifer because of depositional factors, thus causing more rapid horizontal movement.

Chemical analyses of water samples from the piezometers (Table 1) support the pattern of conductivity values as being an accurate indication of contaminant distribution. TDS values for all the wells averaged 62 percent of specific conductances in micromhos/cm with a range of 51 to 77 percent.

The test indicators of leachate are chloride, sulfate, and sodium. These ions show the greatest increases over background concentrations in the aquifer and also are the most conservative species, that is, are least affected by adsorption, exchange, and biochemical conversion reactions. The high levels of chloride, sulfate, and sodium present in wells completed in refuse are almost entirely derived from the refuse. Significant increases over background concentrations are also present with calcium, magnesium, potassium, and bicarbonate. These ions, however, are the principal ions present in natural groundwater in the Icelandic aquifer.

The change in concentration for selected parameters in the downgradient direction is plotted in Figure 5. This interpretation assumes that leachate produced in the youngest waste cells at the eastern edge of the landfill is of approximately the same chemical composition as the water in wells 9 and 10. The values for chloride, sodium plus potassium, and sulfate indicate an extremely low percentage of the assumed original value at a distance of 50 ft. (15 m) from the leachate source (piezometer 11). Because these ions are conservative and are not significantly attenuated by mechanisms other than mechanical dispersion, it is concluded that the actual front of the contaminant plume has not yet reached well 11. This interpretation agrees with the assumed groundwater velocity of 16 ft./yr. (5 m/yr) and an approximate age of the recent waste cells of two years or less. The low concentrations of leachate which do reach wells 11 and 5 (Figure 5) are most likely the result of a dispersed part of the leachate front which is moving more rapidly than the average groundwater velocity because of heterogeneities in the geologic medium.

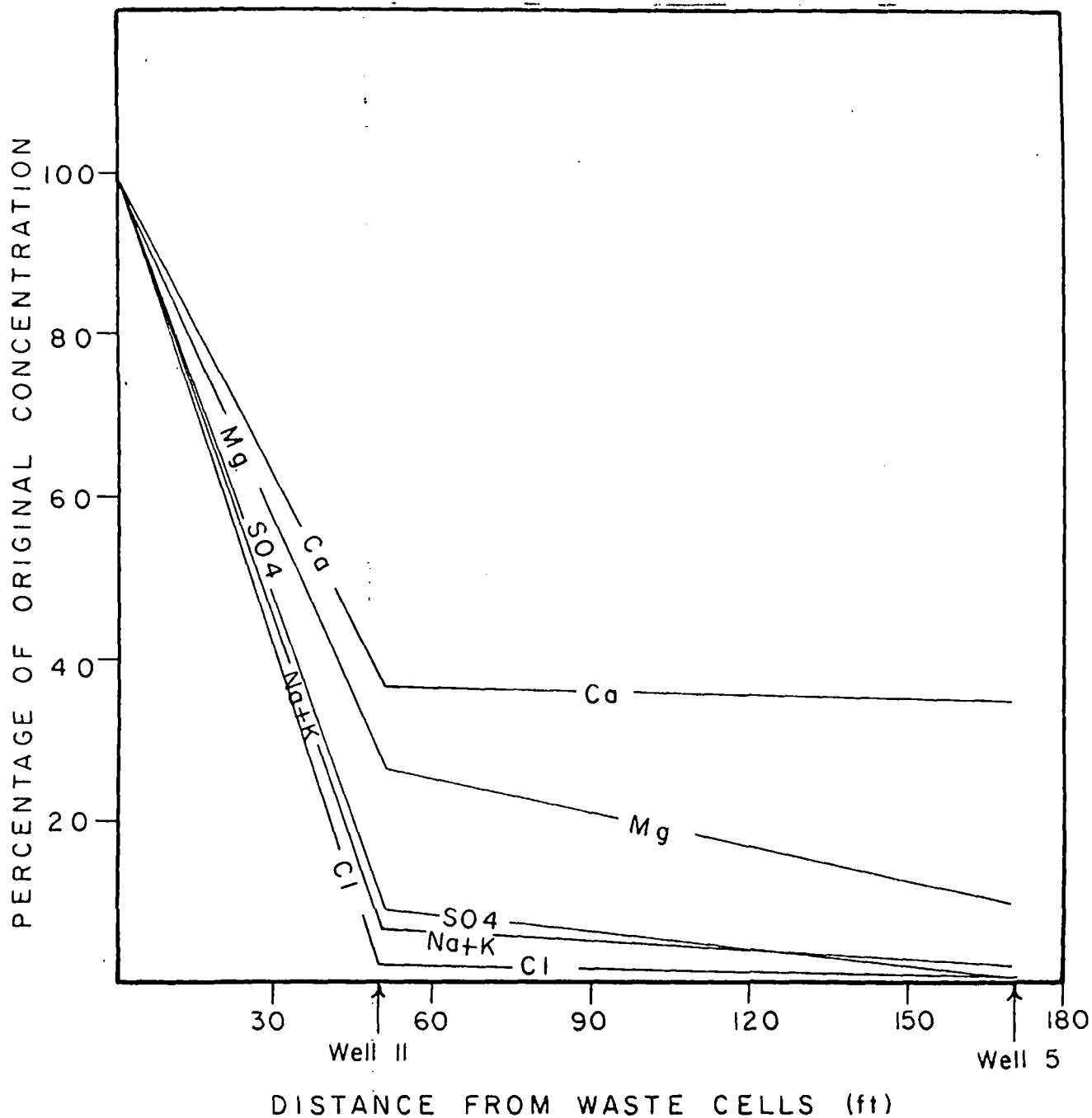


FIGURE 5 - Attenuation of Leachate Concentration Between Waste Cells and Down-gradient Piezometers. One Hundred Percent Concentration is that of Wells Completed in Refuse and is Assumed to be Similar to the Concentration of Leachate in the Most Recent Waste Cells at Eastern Edge of Filled Area. Concentrated Front of Leachate Plume has not yet Reached Piezometer 11.

The more gentle decrease in calcium and magnesium concentrations shown in Figure 5 is probably the result of cation exchange reactions along the flow path in which calcium and magnesium are desorbed from clay particles in exchange for other leachate cations (U.S. EPA, 1977). The slight declining trend in solute concentration present between wells 11 and 5 (Figure 5, Table 1) is not indicated in the corresponding deeper wells 11a and 5a. In fact, the deep wells have very similar concentrations of all major ions. Therefore, the process which is causing leachate to reach the shallow down-gradient wells is not affecting the corresponding wells. Possible explanations for this observation will be presented later.

Concentrations of other parameters listed in Table 1 do not conform to the pattern described above. Nitrate is high in one of the refuse wells but not in the other. This suggests that nitrate levels may vary greatly within the refuse area. Trace metals are not enriched in the leachate samples. This indicates either low solubility of these ions or extremely rapid attenuation.

RESISTIVITY PROFILES

Two resistivity profiles were run (Figures 6 and 7) in the positions shown in Figure 2. Readings were taken every 25 ft. (8 m) along the profile at several electrode spacings. Results support the conclusions drawn from the chemical analyses. Profile A-A' was made immediately downgradient from the edge of the most recent trenches. The results (Figure 6) indicate the presence of highly conductive groundwater (low resistivity) along the profile. A difference in conductivity was also evident between trenches which were in the process of being filled at the time of the survey and those which had been previously completed. The older trenches would be expected to have better developed, farther advanced, and more highly concentrated leachate plumes than those under construction. This trend was noted using both the 10 ft. (3 m) and 20 ft. (6 m) electrode spacings.

Figure 7 shows the results of profile B-B', made across the extreme downgradient end of the landfill site. The results of this profile again support conclusions drawn from the water analyses in that no consistent trends of low resistivity suggesting the presence of a leachate plume were detected with any of the electrode spacings. The small concentrations of leachate present in wells 4 and 5 are not high enough to be detected by the resistivity method. This profile also confirms that a concentrated leachate plume is not present either below the levels of the shallow wells or between the wells.

DISCUSSION AND CONCLUSIONS

Contaminant plumes resulting from landfills are usually considered to move as discrete masses at the average groundwater velocity with relatively

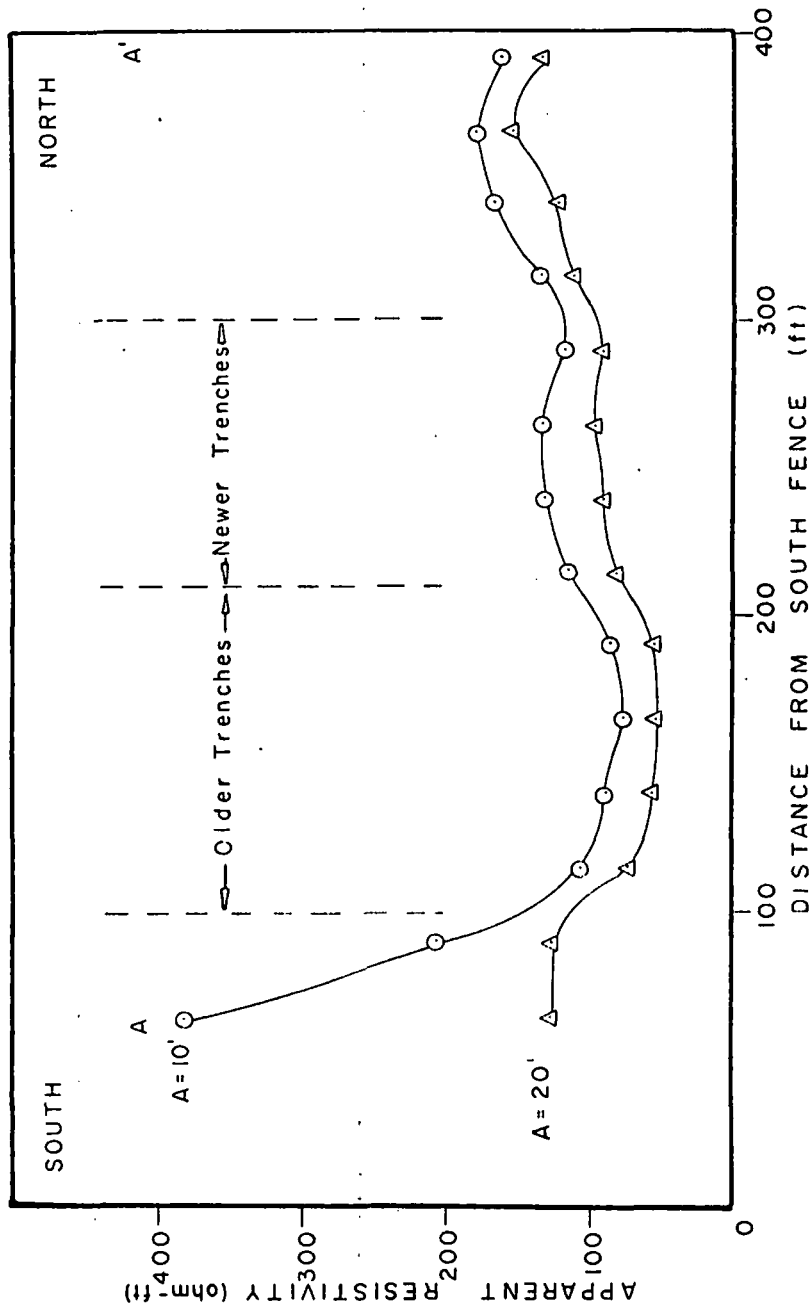


FIGURE 6 - Resistivity Profile A-A'

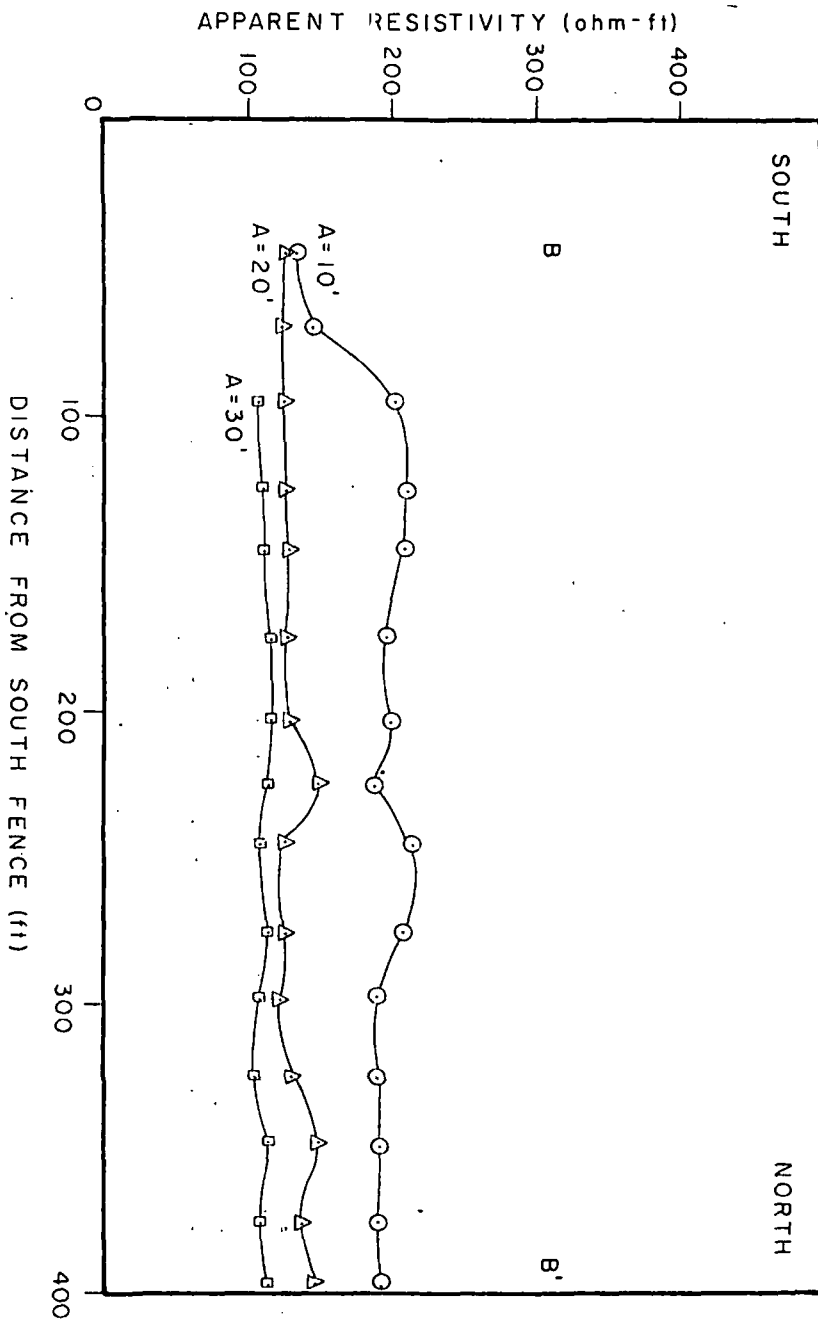


FIGURE 7 - Resistivity Profile B-B'

minor dispersion (U.S. EPA, 1977). Data gathered in this investigation indicate that the Cavalier landfill is causing gross pollution of groundwater in the vicinity of the waste cells. Shallow wells downgradient from the edge of the most recently filled trenches indicate the presence of leachate, although in greatly reduced concentrations, especially of conservative ions such as chloride and sulfate. Assuming that the groundwater velocity is 16 ft/yr. (5 m/yr) and that leachate has been moving downgradient from the recent trenches for 2 years or less, the leading edge of the plume should be approximately 32 ft. (10 m) from the edge of the trenches. Well 11, located 50 ft. (15 m) from the edge of the trenches, and well 5, located 170 ft. (52 m) from the trenches, both indicate that leachate has reached these respective positions. Therefore, some of the contaminants must be moving at a higher rate than the plume front. Dispersion of the leachate plume is occurring by some mechanism.

Cherry and others (1975) describe situations in which dispersion greater than that predicted by laboratory tracer experiments can occur as a result of inhomogeneity in the aquifer. The presence of lenses or beds of higher hydraulic conductivity than average for the material could explain the observed pattern at the Cavalier landfill. Material with a hydraulic conductivity less than one order of magnitude greater than the 1.6 ft/day (5.6×10^{-4} cm/sec) value assumed as average for the site could result in leachate movement as far downgradient as wells 4 and 5. Because the near surface material at the site is more sandy than the deeper sediment, hydraulic conductivity in the vicinity of the water table is probably greater than at the depths of the deep wells. This permeability contrast can explain the higher solute concentrations in the shallow downgradient wells relative to the deep wells. The plume may therefore consist of a concentrated front moving at the average groundwater velocity with a thin finger of dilute leachate at or near the water table moving at a higher velocity in advance of the main front (Figure 8).

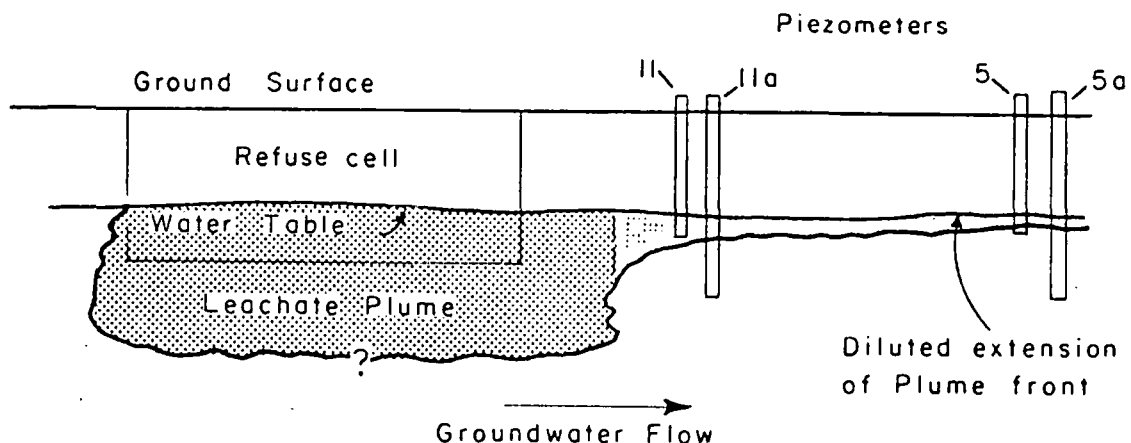


FIGURE 8 - Diagrammatic Interpretation of Leachate Plume (not to scale)

This hypothesis assumes that the solute concentrations measured in wells 11 and 5 represent the groundwater quality over the entire screened area of the wells. If, however, the leachate were entering the well through a small portion of the screened area only, water analyses from that well would represent a mixture of the leachate and natural groundwater in the well. The analysis would suggest a level of contamination less than the actual leachate concentration entering the well through the thin zone of leachate movement, because of dilution in the well bore. With existing instrumentation, the thickness of the contaminated zone in the near surface material cannot be determined. Because there is a small but significant decline in solute concentration between wells 11 and 5, dispersion is probably occurring to some extent in the material in the vicinity of the water table. Therefore, the thin diluted extension of the plume front (Figure 8) is the result of higher hydraulic conductivity in that zone and dispersion of the leachate components.

As the concentrated front of the leachate plume moves downgradient at the average groundwater velocity of 16 ft/yr. (5 m/yr), leachate concentrations will increase in the shallow and perhaps the deep wells. If no additional trenches are excavated in the downgradient direction, the concentrated front should reach well 11 in the next year or two and wells 5 and 4 in ten to twelve years.

ACKNOWLEDGEMENTS

We would like to thank Ken Harris, Gerald Groenewold, and Erling Brostuen of the North Dakota Geological Survey, and Bernd Rehm of the University of North Dakota Engineering Experiment Station for assistance in various phases of instrumentation and interpretation of data.

The chemical analyses were funded under a grant from EPA as authorized under Section 208 of the Water Pollution Control Act Amendments of 1972 (PL 92-500).

Effect on Groundwater of the Cavalier,
North Dakota, Sanitary Landfill
By Alan E. Kehew and Gerald W. Knudsen
Page 19

REFERENCES

- Cherry, J.A., Gilham, R.W., and Pickens, 1975, Contaminant Hydrogeology, Part I, Physical Processes: Geoscience Canada, V. 2, No. 2, P. 76-84.
- Hutchinson, R.D., 1973, Ground-water Basic Data of Cavalier and Pembina Counties: North Dakota Geological Survey, Bulletin 62, Part II, 606 p.
- Hutchinson, R.D., 1977, Ground-water Resources of Cavalier and Pembina Counties, North Dakota: North Dakota Geological Survey, Bulletin 62, Part III, 68 p.
- Hvorslev, M.J., 1951, Time Lag and Soil Permeability, in Groundwater Observations: U.S. Army Corps of Engineers, Waterways Experiment Station, Bulletin No. 36, 50 p.
- Thompson, K.W., and Hetzler, R.L., 1977, Soil Survey of Pembina County, North Dakota: U.S. Department of Agriculture, Soil Conservation Service, in Cooperation with North Dakota Agricultural Experiment Station, 117 p.
- U.S. Bureau of Reclamation, 1973, Water Resource Development in North Dakota, in Mineral and Water Resources of North Dakota: North Dakota Geological Survey, Bulletin 63, 252 p.
- U.S. Environmental Protection Agency, 1974, Methods for Chemical Analysis of Water and Wastes: U.S. Environmental Protection Agency (EPA-625-/6-74-003).
- U.S. Environmental Protection Agency, 1977, Procedures Manual for Ground-water Monitoring at Solid Waste Disposal Facilities: U.S. Environmental Protection Agency (SW-616), 269 p.

SEEPAGE FROM PARTIALLY SATURATED MINE WASTE DISPOSAL SYSTEMS

By

G.L. Bloomsburg¹ and R.A. Bloomfield²

ABSTRACT

A finite element computer program, UNSAT2, simulating unsaturated flow conditions is described and applied to three types of mine waste disposal systems. The first case involves the analysis of seepage from a typical tailings pond through a partially saturated foundation soil, resulting in the creation of a ground water mound above the water table. In the second case, seepage from a filtration pond constructed of oil shale waste was simulated under conditions of normal ponding and infiltration due to rainfall, and the results compared to field measured values. The last case describes seepage related to a hypothetical shale waste pile under conditions of rainfall and ponding. Hydraulic properties for the last two cases include saturated permeability and relationships between relative permeability, capillary pressure, and degree of saturation, which were determined from laboratory experiments on both field cores and laboratory packed samples.

INTRODUCTION

During the past decade, disposal of mine and mill waste material has become an increasingly important issue. Problems of structural stability and seepage effects on stability have been well addressed, and significant technological advances have been achieved (1, 2, 3). The primary problem currently facing industry in the waste disposal area is environmental protection. The greatest environmental concern is over the amount of seepage or leachate entering the ground or surface water systems. Methods to determine the quantity of water seeping from a tailings pond has been covered in the literature (1, 4). This type of analysis, however, is only applicable to situations where fully saturated conditions exist.

The partially saturated method of analysis which is discussed here is applicable to most situations involving seepage from waste piles. In a conventional type of tailings pond, a slime layer is ordinarily built up under the ponded area. This material will consolidate to some extent due to seepage forces and the weight of material deposited above it. In situations where this consolidation results in a slime layer of lower permeability than the native foundation soil, a partially saturated flow condition is likely to exist in the native soil. This will result in a smaller quantity of water entering the ground water system than would be predicted by saturated flow analysis.

¹ Agriculture Engineering Department, University of Idaho, Moscow, Idaho

² Bureau of Mines, U.S. Department of Interior, Washington, D.C.

Another common situation where partially saturated conditions occur is in a dry waste pile subject to rainfall. Depending on the material properties and geometry of the pile, the rainwater will either result in surface runoff, seepage through the pile, or seepage only into the upper layer which may later be evaporated.

The finite element program used in this study was originally developed by Neuman (5) and is called UNSAT2. The program will analyze problems of saturated or unsaturated, steady or non-steady flow and can be used with a variety of boundary conditions such as constant flux, constant pressure, maximum flux, minimum pressure, and infiltration, evaporation and seepage surfaces. The maximum flux and minimum pressure boundaries are used when maximum or minimum conditions are controlled by exterior factors such as atmospheric conditions, but the actual flow in the porous media is determined by properties of the porous media.

PRINCIPLES OF PARTIALLY SATURATED FLOW

Richards (1931) was first to combine the Darcy equation

$$\text{Flow} = q = -K \frac{\partial H}{\partial X_i}$$

with the continuity equation

$$\frac{\partial q}{\partial X_i} = -\phi \frac{\partial S}{\partial t}$$

to obtain an equation describing the unsteady flow of water under partially saturated conditions,

$$\frac{\partial}{\partial X_i} \left[K \frac{\partial H}{\partial X_i} \right] = \phi \frac{\partial S}{\partial t}$$

In the "Richards equation," K is effective hydraulic conductivity (a function of capillary pressure or saturation), H is hydraulic head, ϕ is porosity of the porous material, S is saturation, the X_i are the spatial variable (cartesian coordinates) and t is time. This equation describes the movement of a single fluid in a multifluid system if there is no resistance from the other fluid. In the case of the air-water system in the soil, it is commonly assumed that air does not affect the flow of water. This assumption in some cases is not valid but in the problems considered here it is reasonably valid. The form of the Richards equation used for the formulation of UNSAT2 differs from that above in the addition of a source or sink term and a term for compressibility of the soil matrix.

The value of effective conductivity is given by $K = K_S K_r$, where K_S is the saturated conductivity and K_r is the relative conductivity at saturations less than 1.0.

Empirical or semi-empirical equations have often been used for the functional relationship between relative hydraulic conductivity, capillary pressure and saturation or moisture content. In UNSAT2, however, data values are used in a table of relative conductivity versus moisture content and capillary pressure versus moisture content. Intermediate values of relative conductivity or capillary pressure are then determined by linear interpolation.

HYDRAULIC PROPERTY REQUIREMENTS

In addition to the table of capillary pressure - moisture content - relative conductivity values previously mentioned, it is necessary to have values of porosity and saturated conductivity for each material. Nodal point information includes initial pressures, boundary conditions and spatial coordinates. Element information includes soil identification number and direction of anisotropy.

Capillary pressure - moisture content data are relatively easy to obtain. The method used here was essentially the "pressure cell" method described by Corey (7). In this method the sample of porous material is placed in contact with a capillary barrier connected to a pressure measuring device such that capillary pressure in the soil water may be measured. Starting with the sample saturated and then weighing the amount of water which flows out at various capillary pressures gives the saturation as a function of capillary pressure.

Relative conductivity - moisture content data are more difficult to obtain, particularly in fine grained material such as retorted shale. The method used for the measurements was the "Richards" method described by Corey (7). This is a steady flow method in which water flows downward through a vertical cylindrical sample. Inflow, outflow and all pressure measurements are made through capillary barriers. Flow must be at a hydraulic gradient of 1.0 so that the capillary pressure is uniform throughout the sample, giving uniform saturation and conductivity. As inflow and outflow are adjusted to give greater capillary pressure, the sample desaturates and values of relative conductivity are obtained as a function of capillary pressure. Since this process is very time consuming, methods have been developed for calculating relative conductivity from capillary pressure - saturation data. The program given by Sinclair, et al., (8) was used for that purpose in the present work. If the relative conductivity is calculated, it is still necessary to measure the saturated conductivity.

The values of saturated conductivity used in the simulation of flow in retorted oil shale were determined in the field. The other hydraulic properties were determined in the laboratory. This procedure should work well in many field applications because the hydraulic conductivity of natural materials varies

over many orders of magnitude while the capillary pressure - saturation - relative conductivity relationships vary much less between different materials. In fact, it is more realistic in most cases to assume values for the capillary pressure - saturation - relative conductivity relationships and use unsaturated flow analysis than to use saturated flow analysis.

UNSAT2 PROGRAM DESCRIPTION

A complete description of the program, including input-output description and a program listing is given by Neuman (5). The program can be used to investigate problems involving two spatial dimensions in the horizontal or vertical plane. Three-dimensional problems can be handled provided that the flow pattern retains an axial symmetry about the vertical coordinate. The flow region may have any complex shape and it may consist of different soil materials arranged in arbitrary patterns. Each soil material may exhibit an arbitrary degree of local anisotropy, with the principal hydraulic conductivities oriented at any desired angle with respect to the coordinates.

A wide range of time-dependent boundary conditions can be treated: prescribed pressure head, prescribed flux normal to the boundary, seepage faces, and evaporation and infiltration boundaries where the maximum rate of flux is prescribed by atmospheric or other external conditions, whereas the actual rate is initially unknown. A RESTART feature is included in the program which allows boundary conditions to be changed at any stage of the computation. Atmospheric conditions controlling maximum evaporation rate can also be changed at any time.

The input used for the program is well defined. Material properties are assigned to each element by a material code number on the element input cards. Boundary conditions are imposed through a code number on the nodal point input cards. The initial value of positive head or capillary pressure is also input on the node cards.

The printed output of the program consists of a listing of all input information, a complete description of the finite element network, the boundary codes of all nodes, and the properties of each material. During each step, the program prints a listing of total head values, pressure head values, moisture content values, and discharge into or out of the system at each node. The rate of convergence of the iterative procedure is printed during each time step together with additional information pertaining to the particular problem at hand. Output information on pressure or moisture content at any particular time can be used as input for a plotting program.

SEEPAGE FROM A TAILINGS POND

In situations such as tailings pond where there is low permeability material at the bottom of the pond and more permeable material below, it is

very common to have unsaturated flow in the more permeable material. This type of problem is shown in Figure 1. This is a tailings pond located about 1,524 m (5,000 ft.) from an open pit mine. The pond consists of 0.9 m (3 ft.) of slime with 6.0 m (20 ft.) of ponded water. An approximate analysis of this problem was made by considering only the flow downward through the slime layer and determining how long would be required for this flow to saturate the region beneath the pond. Neglecting the spread of the ground water mound and the outflow at the open pit mine this time would be approximately 20 years.

To run the problem with UNSAT2, a mesh consisting of 120 node points and 85 elements, as shown in Figure 2, was used. The initial conditions were a water table at an elevation of 42.7 m (140 ft.), a negative pressure of 27.4 m (90 ft.) at the bottom of the slime layer, and a water depth of 6.1 m (20 ft.) in the pond.

The problem was studied for a period of five years. The region beneath the pond was still unsaturated at that time but the water table beneath the pond had increased in elevation approximately 2.7 m (8.9 ft.) due to downward flow. The original water table and final water table are also shown in Figure 2.

The seepage at the open pit mine affected the water table for a distance of only about 304 m (1,000 ft.). This shows that the assumption made in the approximate analysis above that the flow into the open pit would have no effect on the flow under the seepage pond is certainly valid.

SEEPAGE FROM A FILTRATION POND

Several cases of seepage were analyzed using data from field permeability test ponds constructed of spent shale under a U.S. Bureau of Mines contract. Results of two tests on the pond are given here. The bottom area of the pond was 187 m² (2,017 ft.²), and the shale was about 1.1 m (4 ft.) thick. The construction, test procedures, and field results are described in detail by Holtz (6).

The finite element mesh for this pond is shown in Figure 3. The axis of symmetry for the pond is at the left side, and there are 130 node points and 106 elements.

This pond had a wide range of boundary conditions. At various times, as shown in Table 1, the upper boundary had conditions of constant potential, no flow, infiltration, or evaporation. The lower boundary was either a seepage surface or a no-flow boundary at all times. The seepage surface extended from node 1 to node 103.

The hydraulic properties of the shale were not considered constant over the entire period of simulation. When the pond was initially filled, the average moisture content on a volume basis was .054 and the average porosity was .453 which would indicate considerable trapped air in the shale.

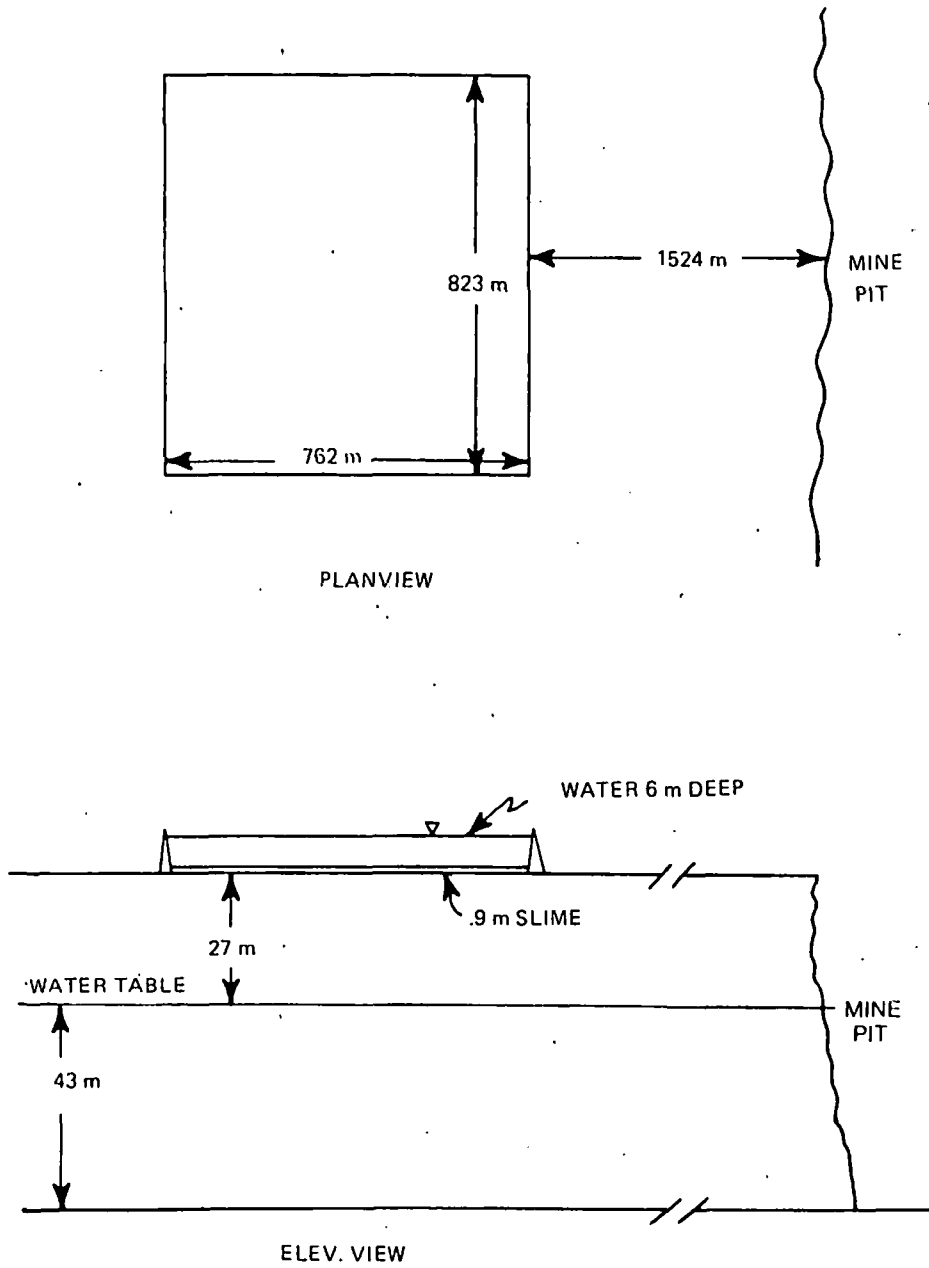
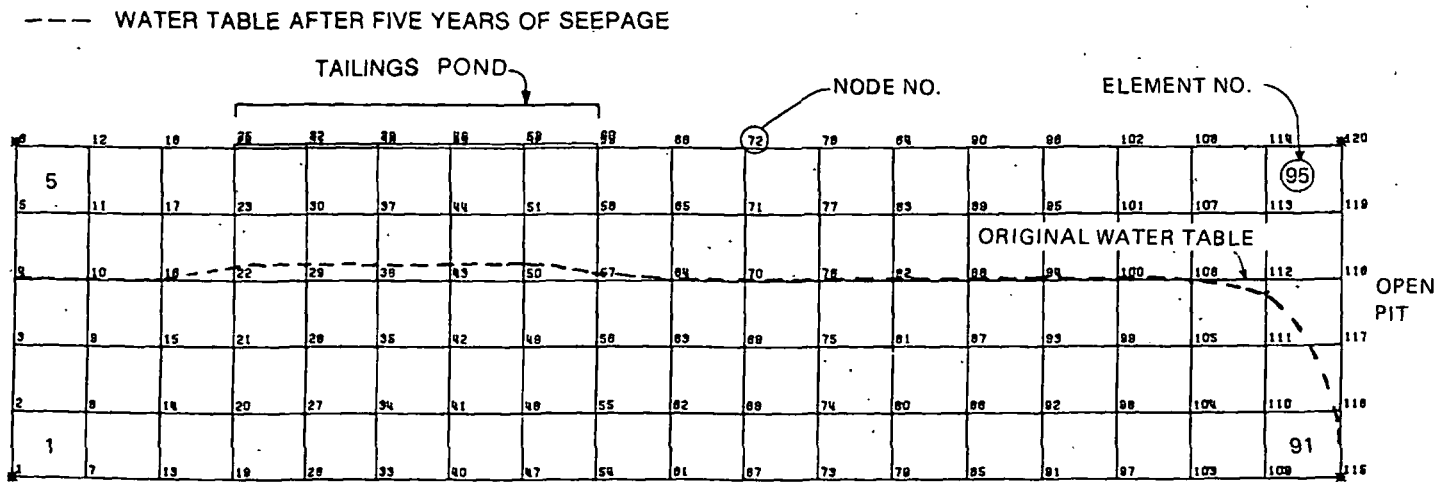


FIGURE 1 - Tailings Pond



HORIZONTAL SCALE 1 cm = 120 m
 VERTICAL SCALE 1 cm = 12 m

FIGURE 2 - Water Table Profile - Tailings Pond Example

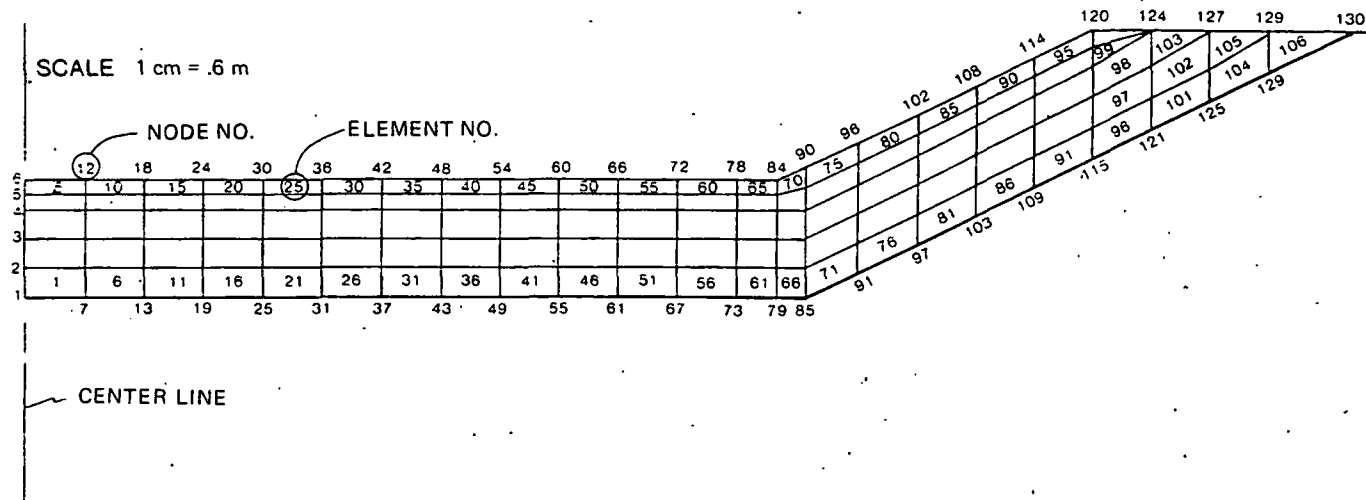


FIGURE 3 - Finite Element Mesh for Oil Shale Filtration Pond

Seepage From Partially Saturated Mine
Waste Disposal Systems
By G.L. Bloomsburg and R.A. Bloomfield
Page 9

TABLE 1

BOUNDARY CONDITIONS AND VALUES OF PARAMETERS FOR SIMULATION OF POND 2					
Date	ΔT	Top Boundary Condition	Bottom Boundary Condition	Conductivity Used m/yr.	Porosity
Dec. 10, 1975	30 hours	H = 0.277 m	Seepage Surface	37.9	0.412
Dec. 11, 1975	120 hours	0.357 m	No Flow	44.8	All other porosities were 0.453
Dec. 16, 1975	21 hours	0.282 m	Seepage Surface	52.9	
Dec. 17, 1975	21 hours	0.183 m	No Flow	60.6	
Dec. 18, 1975	50 hours	0.171 m	No Flow	60.6	
Dec. 20, 1975	21 hours	0.366 m	No Flow	60.6	
Dec. 21, 1975	24 hours	0.259 m	Seepage Surface	68.0	
Dec. 22, 1975					
May 11, 1976	196 hours	0.817 m	No Flow	All other conductivities were 200 m/yr.	
May 19, 1976	7 hours	0.817 m	Seepage Surface		
May 19, 1976	7 hours	0.488 m	Seepage Surface		
May 20, 1976	6 hours	0.223 m	Seepage Surface		
May 20, 1976					
June 8, 1976	170 hours	0.924 m	No Flow		
June 15, 1976	6 hours	0.677 m	Seepage Surface		
June 15, 1976	16 hours	0.283 m	Seepage Surface		
June 16, 1976	8.5 hours	0.030 m	Seepage Surface		
June 16, 1976	961 hours	No Flow	Seepage Surface		
June 26, 1976	2,424 hours	Evaporation	No Flow		
Nov. 4, 1976	95 hours	Infiltration	Seepage Surface		
Nov. 6, 1976					

During the initial period of simulation, imbibition (rewetting) data for the shale were used. From laboratory data on imbibition, the moisture content was estimated to go to 0.412 without any influence of trapped air. Thus, the porosity used with the imbibition data was 0.412 for the first 30 hours. After this time, a porosity of 0.453 was used so that the shale could become completely saturated.

The value of hydraulic conductivity used varied from 37.9 m/yr. to 68.0 m/yr. over the initial simulation period of 287 hours. The reasoning for this is the same as above, initially the material contained trapped air but eventually it became completely saturated. The value of 68.0 m/yr. was the value actually measured in the field in December when the water temperature was 1°C.

Figure 4 shows the comparison of field measured and simulated flows into the pond during December, 1975. The agreement between simulation and field data is excellent except after 265 hours when the measured flow was less than predicted. Thus, during the periods of 30 to 150 hours and 180 to 270 hours when the outlet valve was closed there is still water moving into the shale increasing the saturation. This particular flow situation cannot be simulated with a saturated flow program.

During 1976 several other conditions were simulated as previously shown in Table 1. In general, the agreement between simulation and field data was very good. The last test run on this pond was seepage under rainfall conditions. The pond was sprinkled with 17,400 liters (4,600 gal.) over a 30 minute period (4 inches per hour). The pond had not contained water for about 4 months, so the moisture content of the shale was very low. This evaporation period was simulated to estimate the moisture content at the start of the rainfall test. Table 2 shows the values for the cumulative seepage measured in the field and calculated by the simulation. When considering that 17,400 liters of water was applied to a volume of about 680 m³ (24,000 ft.³) of shale, and the difference of simulated seepage to measure was only 6.28 liters (1.66 gal.), the correlation is quite good.

SPENT SHALE WASTE PILE

A series of computer simulations was carried out on a hypothetical spent shale embankment using a valley fill profile as shown in Figure 5. The overall size was 573 m (1,880 ft.) horizontally and 91 m (300 ft.) vertically. The right side (to the right of nodes 76-84) consisted of shale compacted to 95 pcf. To the left of this line was 85 pcf shale and under the entire pile was a 1.5 m (5 ft.) layer of free draining material. The initial moisture conditions (on dry weight basis) were 25%, 20% and 13% respectively. This

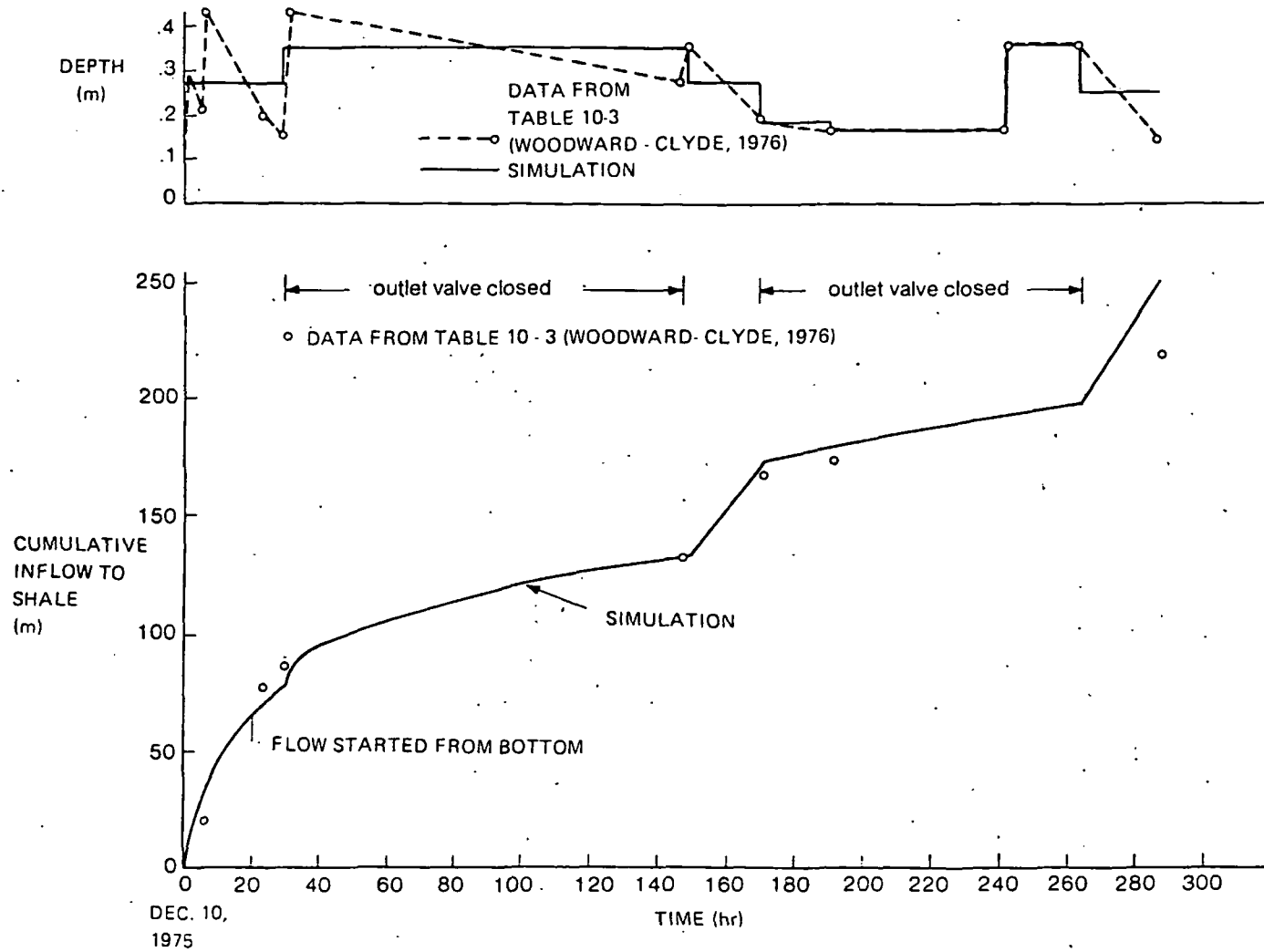


FIGURE 4 - Simulation of Oil Shale Pond - Dec., 1975

TABLE 2
CUMULATIVE LEACHING AFTER SPRINKLING

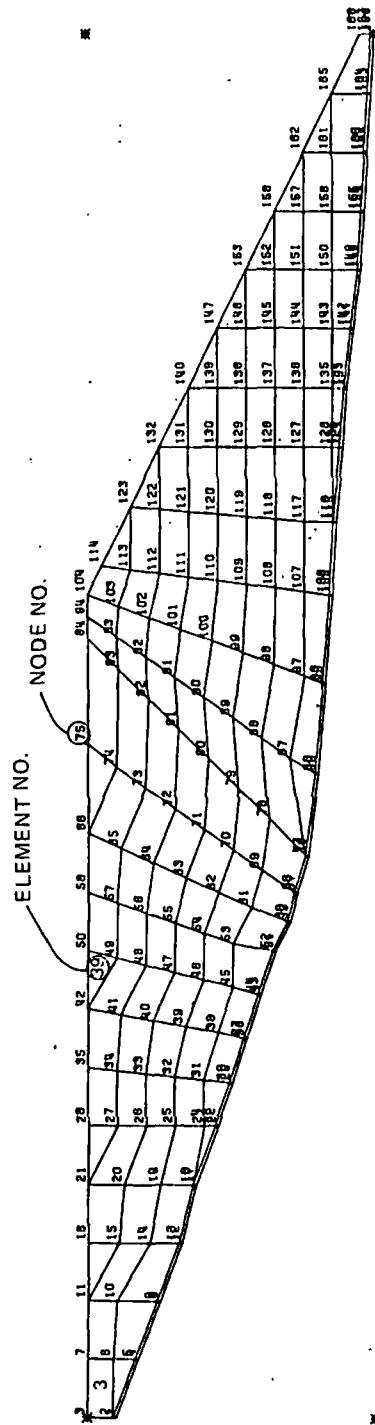
Time after rainfall (hrs.)	Cumulative Leach (liters)	
	Field Data	Simulation
0.0	.00	0.000
.6	.02	0.000
1.9	.06	0.000
3.2	.09	0.71
6.0	.15	0.71
22.7	5.59	0.71
30.2	6.30	0.71
46.7	6.99	0.71
70.7	6.99	0.71
94.7	6.99	0.71

problem was studied under three boundary conditions:

1. A 100 year 1 hour storm (intensity of .95 inches per hour)
2. A 100 year 6 hour storm (intensity of .25 inches per hour)
3. A ponded condition of 1.5 m (5 ft.) of water on surface nodes 3 through 84 and no infiltration or evaporation on the remainder of the pile.

The 100 year storm data is applicable for Northwestern Colorado (9). A seepage surface was allowed at the right side of the mesh (Nodes 186-188) under all these conditions.

The two storm intensities were selected to determine whether rainfall would infiltrate the waste pile, or run off the surface. Results of the two storm simulations were similar. There was no runoff at any time during either storm for the 85 pcf shale. The moisture content in the upper layer increased by about 0.5 percent. This water would be held in the upper layer until evaporated, since it did not seep down into the pile. In both cases there was substantial runoff from the 95 pcf shale (infiltration rate was less than the rainfall rate), and therefore only a slight increase in moisture content was detected. This result indicates a need for berms on the downslope side of the embankment for erosion control, and diversion channels for runoff control. Contamination of surface or ground water from leachate would not appear to be a problem.



SCALE: 1 cm = 24 m

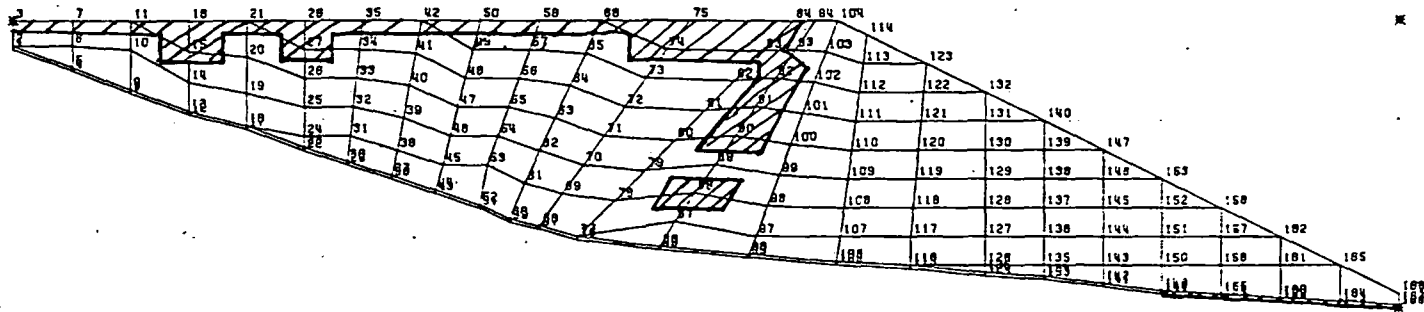
FIGURE 5 - Finite Element Mesh 2-D Waste Shale Pile

In the analysis of the ponded boundary condition, the ponded area extended over the entire surface of the 85 pcf shale (nodes 3 through 84). This problem was studied by simulation for a period of 1 year. The regions that became saturated are indicated in Figure 6. The saturated zone had moved into the shale as much as 12.2 m (40 ft.) from the surface and moved considerably deeper than that at the left end of the 95 pcf shale. With this type of situation, the simulation suggests that the impoundment would become saturated, and protection of surface and ground water would have to be considered.

CONCLUSIONS

The use of finite element simulation has proven effective in analyzing problems involving seepage under saturated conditions, build up of ground water mounds, infiltration due to rainfall, and evaporation from a soil surface. The analyses involving seepage from a saturated pond, and infiltration due to sprinkling a dry pond, provided results which were compared to field measured values. With environmental restrictions concerned with surface and ground water protection becoming more stringent, the methodology of analyzing partially saturated flow conditions will be valuable. Results of this type of analysis are much more realistic than those obtained assuming saturated conditions, and the method allows for an accurate analysis of a wider range of problems, as shown in the example. The good correlation between the results obtained from the computer simulation and the field values lend credence to the overall methodology and provide a verification of the simulation approach.

CROSS HATCHED AREA IS SATURATED



SCALE: 1cm = 24m

FIGURE 6 - Saturated Zones After One Year of Ponding

REFERENCES

- (1) Kealy, C.D. and R.A. Busch, Determining Seepage Characteristics of Mill Tailings Dams by the Finite-Element Method, BuMines RI 7477, 1971.
- (2) Wahler, W.A. and Associates, Engineering Evaluation of Mill Tailings Disposal and Potential Stability Problems in Southwestern U.S., 5 Volumes, NTIS PB-243 073-078, 1974.
- (3) Soderberg, R.L. and R.A. Busch, Design Guide for Metal and Non-metal Tailings Disposal, BuMines IC 8755, 1977.
- (4) Kealy, C.D., R.A. Busch, and M.M. McDonald, Seepage - Environmental Analysis of the Slime Zone of a Tailings Pond, BuMines RI 7939, 1974.
- (5) Neuman, S.P., R.A. Feddes, and E. Bresler, Finite Element Simulation of Flow in Saturated - Unsaturated Soils Considering Water Uptake by Plants. Third Annual Project Report No. AIO-SWC-77. Israel Institute of Technology, Haifa, Israel, 1974.
- (6) Holtz, W.G., Disposal of Retorted Oil Shale from the Paraho Oil Shale Project, NTIS PB-263 793, 1976.
- (7) Corey, A.T., Mechanics of Heterogenous Fluids in Porous Media, Water Resources Publications, Fort Collins, Colorado, 1977.
- (8) Sinclair, L.R., D.W. Fitzsimmons, and G.L. Bloomsburg, Permeability of Unsaturated Field Soils Calculated from Desaturation Data, Transactions ASAE, Vol. 17, No. 3, 1974.
- (9) U.S. Department of Commerce - Weather Bureau (National Weather Service) Technical Paper No. 25, Rainfall Intensity - Duration - Frequency Curves for the United States, 1946-55, Superintendent of Documents, Washington, D.C., 1959.

GEOPHYSICAL INVESTIGATIONS OF THE PULLMAN, WASHINGTON - MOSCOW, IDAHO GROUND-WATER BASIN

By

Muriel S. Robinette
College of Mines and Earth Resources
University of Idaho
Moscow, Idaho

ABSTRACT

Ground-water basins on the Columbia basalt margins have posed interesting questions for the hydrogeologist to answer. Complex interrelationships of basalt flows, dikes, sedimentary interbeds and basement structure affect the ground-water flow regime. Sometimes the collected hydrologic data is insufficient to adequately define the ground-water flow conditions in a basalt margin basin.

The Pullman, Washington - Moscow, Idaho ground-water basin was studied using surface and borehole geophysical methods. This study was undertaken to show that a combination of geophysical methods could define the structural relationships within the local geology which govern ground-water flow in the Basin. The geophysical methods used in the study area were gravity, resistivity, seismic reflection, magnetics, aeromagnetics and borehole geophysics.

A composite interpretation of the geophysical data yields substantial information about the Basin geology. The Bouguer gravity map generated from the gravity data indicate the basement topography while the aeromagnetics information delineate basalt configurations. Resistivity soundings, seismic reflections and borehole geophysics can be correlated to locate sedimentary interbeds and associated aquifer zones. Gravity modeling and trend surface analysis indicate pre-basalt drainages and sedimentary structures. The compilation of the geophysical data gives the hydrogeologist a unique picture of the geohydrology of the Pullman-Moscow ground-water basin.

INTRODUCTION

Purpose and Scope of Study

The Pullman-Moscow ground-water basin has been the subject of intensive study primarily due to declining piezometric levels. Population growth associated with the cities and two major universities has caused increased demand for water supplies. Previous studies approached the problem from a geologic and hydrologic viewpoint in attempts to define the location and movement of ground-water in the basin (Lin, 1967; Walters and Glancy, 1969; Najjar, 1972; Barker, 1977). This study emphasizes a geophysical approach to the study of the ground-water occurrence in the Pullman-Moscow basin. The Pullman-Moscow basin was chosen for the location of the study because of its close proximity to the university and the volume of available hydrologic data. The study was designed to delineate ground-water conditions using surface and borehole geophysical techniques and then compare these conditions to known geohydrologic

features in the basin. Field work included conducting a regional gravity survey, electrical resistivity and induced polarization surveys, a magnetic survey and profiles, a regional well survey, a regional aeromagnetic survey and borehole geophysical logging of selected wells.

Location and Extent of Study Area

The study area is located within two states, in the southeastern part of Whitman County, Washington, and west-central part of Latah County, Idaho -- all within the Pacific Northwest (Figure 1). The basin is bordered by a surface exposure of Pre-Tertiary crystalline rocks on all sides except the west and encompasses approximately 250 square miles (647 square kilometers). The study area lies on the edge of the Columbia Basin Plateau within the "Palouse Country" where the rolling Palouse hills merge with the mountains of northern Idaho.

General Geohydrology of Basin

The basic geologic units in the basin are shown in Figure 2 and are broadly classified into four types: Precambrian Belt rocks, Post-Precambrian intrusive granitic rocks, basalt flows of late Paleogene-Neogene age, and surficial loessal sites of Holocene age. The Belt rocks originated in a nearshore intratidal environment which was uplifted and complexly metamorphosed to produce argillites and quartzites. The Belt rocks were intruded by silicic granitic rocks of the Idaho Batholith and the western Belt margin was inundated by basalt flows which issued intermittently from linear fissure systems to the south and west. The geologic section in the study area is topped with a thick blanket of loessal silts which originated from the southwest.

The ground-water conditions within the study area have been described by Stevens (1960); Foxworthy and Washburn (1963); Crosby and Chatters (1965); Ross (1965); Sokol (1966); Lin (1967); Walters and Glancy (1969); Jones and Ross (1972); Najjar (1972); Brown (1976); and Barker (1977). Ground-water occurs in the study area in three general zones. Small quantities of ground-water are contained with the loess or the loess/basalt contact which are usually sufficient for domestic and stock supplies. The eolian deposits generally have high porosities and low permeabilities and tend to act as a barrier to vertical recharge to the underlying basalt. Primary ground-water occurrence is between basalt flows of the Columbia River Basalt Group. The principal basalt aquifers consist of upper broken parts of basalt flows, unconsolidated sedimentary material between flows and basal parts of flows particularly in pillow structures formed where lava flowed into water and cooled rapidly. The thickness and extent of these sedimentary interbeds have been topics of much study in the Pullman-Moscow basin. Generally, the thicknesses of sedimentary interbeds decrease from east to west in the Pullman-Moscow basin primarily because of thickening of basalt flows and increased distance from topographic uplands where the sediments are derived

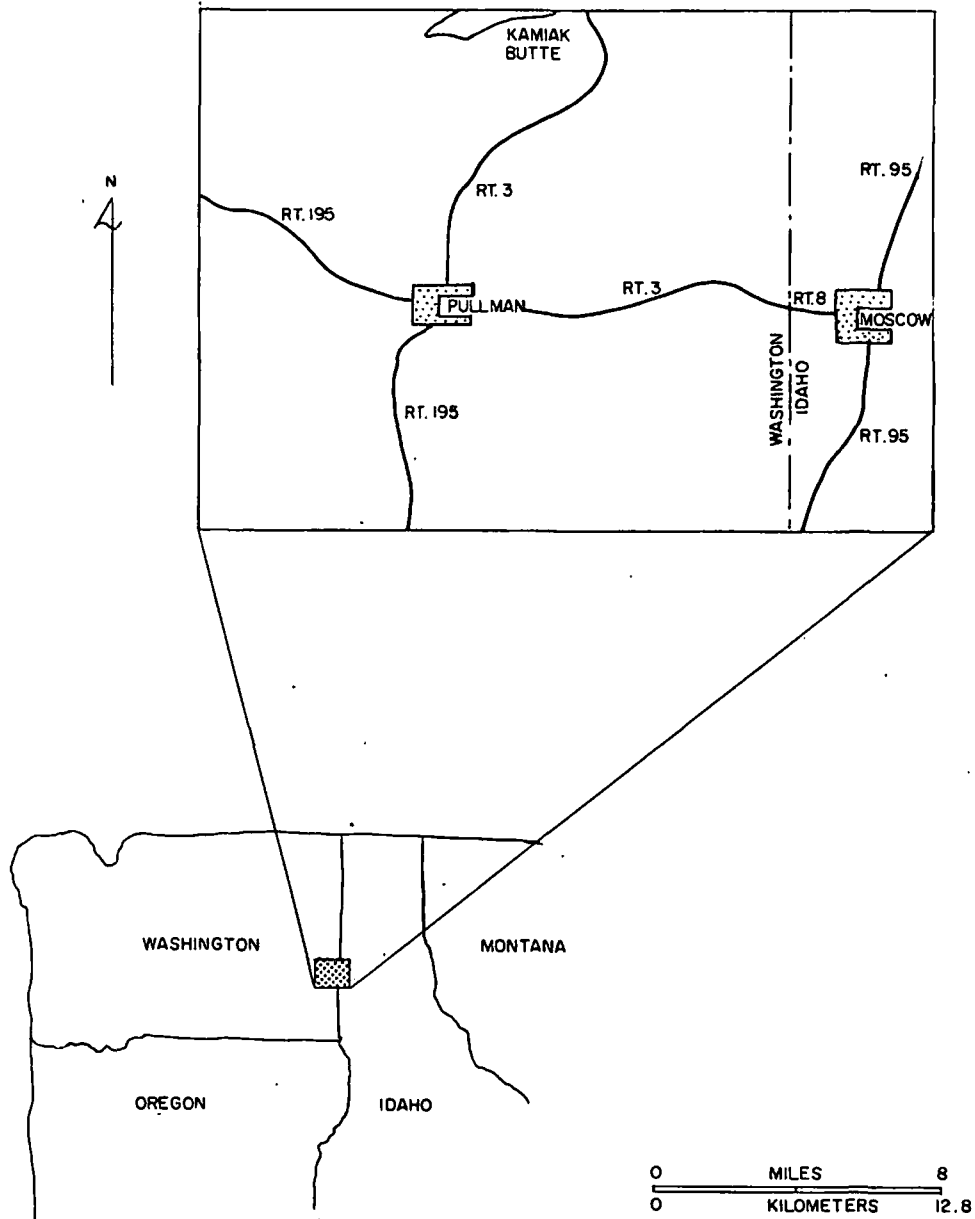


FIGURE 1 - Location Map of the Study Area

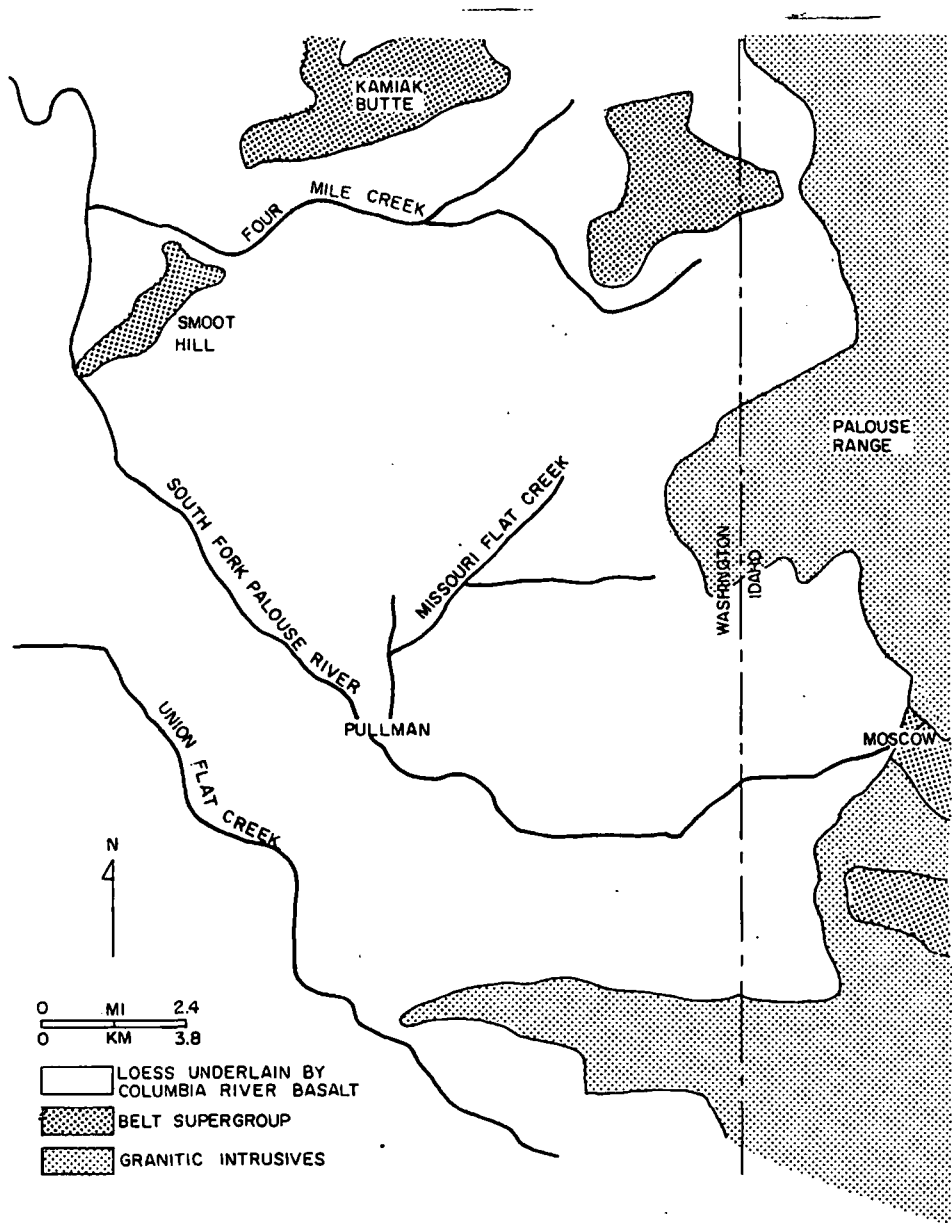


FIGURE 2 - General Geology of the Study Area

(Belt rocks and granitic intrusives to the east). The third zone of ground-water occurrence in the basin is associated with the fractured, weathered contact between the lower-most basalt flow and crystalline basement. Very little hydrologic data have been collected from this zone because of the lack of wells which penetrate to this zone. Figure 3 is a schematic cross section through the study area illustrating the hydrostratigraphic sequences.

Analysis of the geohydrology of the Pullman-Moscow basin has been "handicapped" by lack of deep well data in the majority of the area. Deep wells which penetrate multiple aquifers only occur in the immediate vicinity of Pullman and Moscow, leaving one to speculate on the variations of geohydrologic properties elsewhere within the basin. Some shallow domestic wells are available for study outside of the cities' limits, but they only provide geologic and hydrologic information on a maximum of the upper 250 feet (76 meters) of the hydrostratigraphic column. Consequently, basin-wide hydrogeologic conclusions to date have been drawn from a relatively narrow data base which may have led to a misleading assessment of the total ground-water conditions.

METHOD OF STUDY

Introduction

The field study consisted of extensive data collection using both surface and borehole geophysical instrumentation. Techniques used in the surface geophysical study include gravity, magnetic, resistivity and induced polarization surveys. The following logs were taken during the borehole geophysical section of the study: gamma gamma, neutron gamma, neutron epithermal neutron, natural gamma, caliper, fluid temperature and resistivity, single point resistance and spontaneous potential logs. The aeromagnetic survey was flown by Aerial Surveys of Salt Lake City. A well survey was done to substantiate published well log locations and to locate unused wells for borehole logging. The research effort was designed to generate an extensive network of surface geophysical data which could be interpreted with respect to the basin's geohydrology and substantiated with existing geophysical and well log data.

Surface Geophysical Methods

Three hundred and eighty-two gravity readings were taken in the study area during the summer of 1975. The stations were spaced approximately half to three-quarters of a mile apart and located using United States Geological Survey 7.5 minute quadrangle sheets. A temperature compensated Wordon Master Gravimeter was used for the survey while station elevations were determined with an altimeter having a 1-foot precision. Compensations for meter drift were made by resurveying a reference point every two hours.

Resistivity measurements were taken using a Schlumberger electrode array and a 15 KW Scintrex IPR-8 receiver. Nineteen vertical soundings were completed in the study area over a three week period.

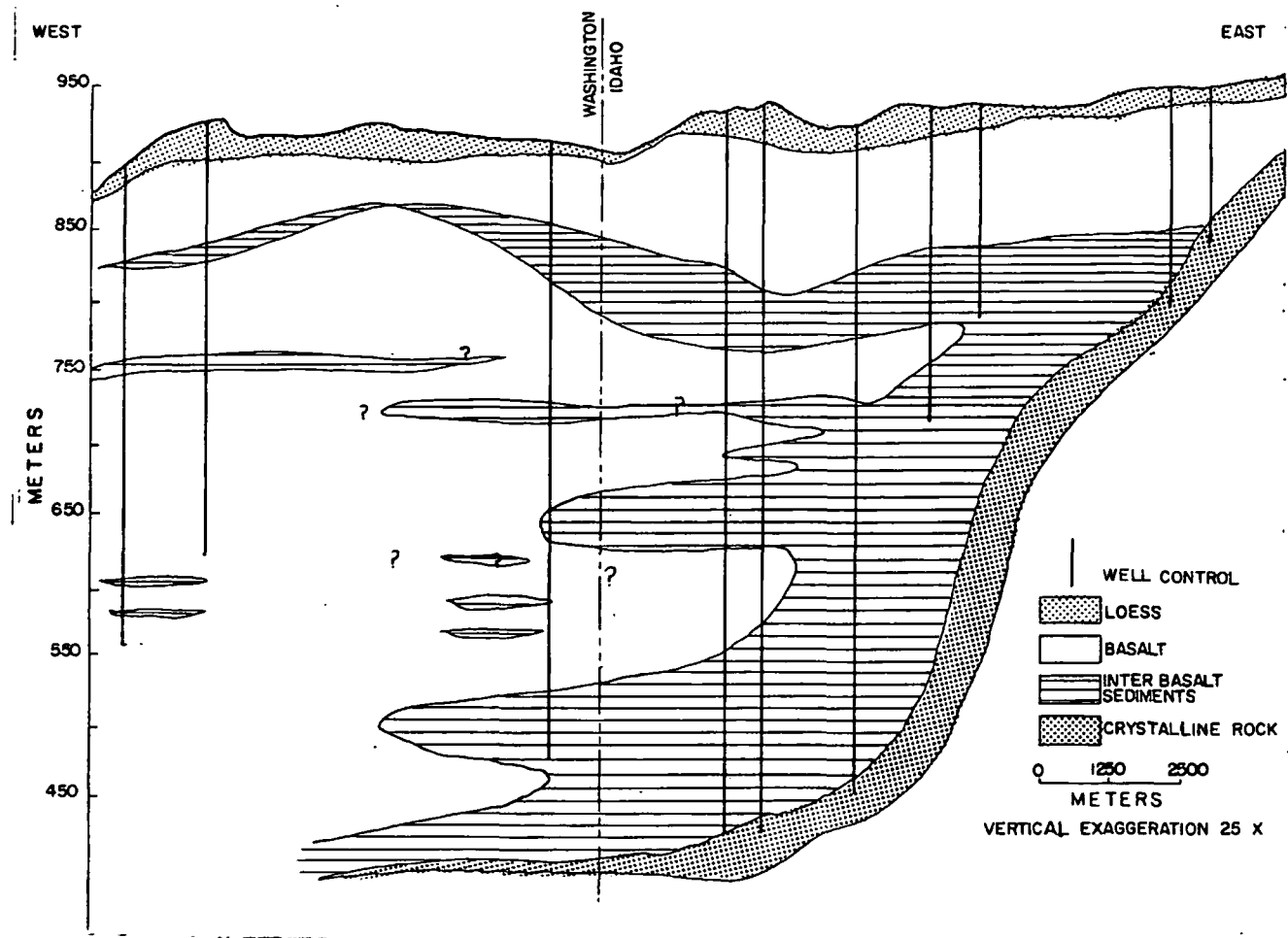


FIGURE 3 - Schematic East-West Section Through the Study Area Illustrating Sedimentary Thinning

The induced polarization measurements were taken during the resistivity survey at all the same stations. The Scientrex IPR-8 receiver integrates the induced polarization response over four current cycles and stores the data in six time modes of 250 milliseconds each. This technique of data collection describes the decay curve as a function of time and is termed time domain or pulse transient measurements.

Borehole Geophysical Methods

Borehole geophysical log information in the Pullman-Moscow basin is concentrated within the two cities. A few, shallow domestic wells have been logged in the outlying areas, but these only provide information about the shallow aquifers. Radiation, fluid and electric logs are available on 11 holes in the study area. Of these, only three wells are deeper than 500 feet (152 meters). Geophysical logs can only be run in a hole without a pump, so this eliminates logging all wells used as a primary water source. Consequently, there is very inadequate subsurface geophysical control in the study area.

Aerial Geophysical Method

The aeromagnetic survey was flown by Gary Garner of Aerial Surveys of Salt Lake City. A GeoMetrics G-803 Proton Precession Magnetometer was used with digital and analog acquisition. The sampling rate was every one-half second with a track photo being taken every four samples for location. The aircraft cruised at an average speed of 175 mph (284 kph) and maintained an altitude of 1,000 feet (305 meters) above the terrain. The survey encompassed approximately 100 line-miles. North-south flight lines were four miles (6.44 kilometers) apart with the east-west tie lines eight miles (12.87 kilometers) apart.

ANALYSIS OF RESULTS AND DISCUSSION

Gravity Survey

Field gravity values are reduced for latitude, elevation and local topographic effects. The reduced gravity data were contoured to produce a Bouguer anomaly map shown in Figure 4. The Bouguer map shows a very strong gradient of 23 milligals trending northeast to southwest. The gradient is steepest in the Moscow area and flattens as it approaches the Pullman area. Steep gravity gradients can be produced by an offset due to a fault or abrupt change in subsurface density. This density variation could be due to compressional folding or shearing due to Yate's Trans-Idaho Discontinuity (Harrison et al., 1974) and Savage's (1973) Idaho-Washington Disturbed Belt which traverse the study area from Paradise Ridge to Smoot Hill. This discontinuity is all part of a large disturbed system known as the Lewis and Clark Line trending southeast to northwest through northern Idaho. The Disturbed Belt is evidenced in the area as producing major fault blocks in the basement (Kamiak Mountain and Smoot Hill) (Savage, 1973), so possibly it could cause a 0.1 gm/cm^3 density change in the basement.

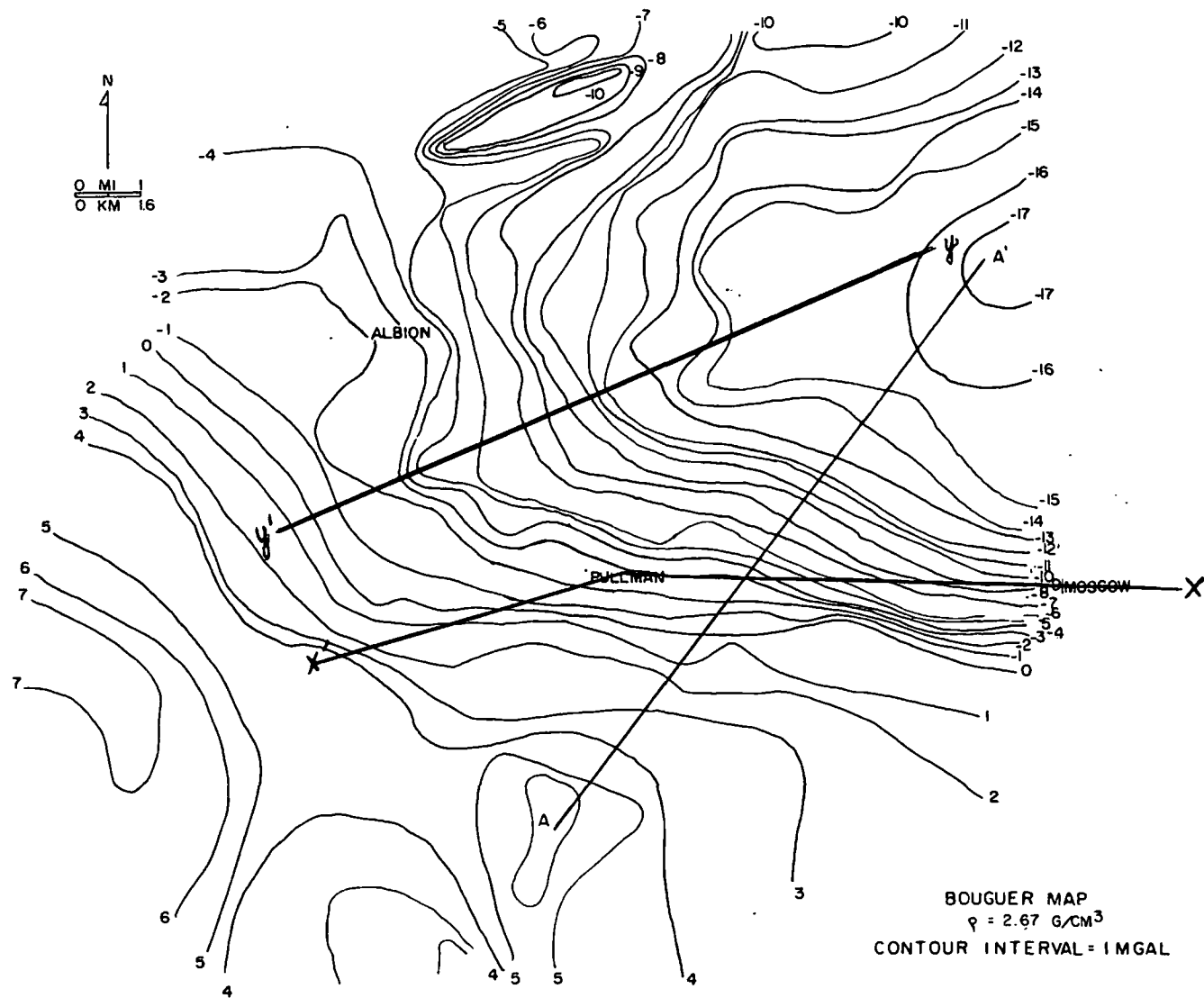


FIGURE 4 - Bouguer Anomaly Map Using $\rho = 2.67 \text{ gm/cm}^3$

The best fit trend surface for the study area appears to be of the third order with a correlation coefficient of 81 percent. Figure 5 shows the contoured residuals and associated local anomalies. The regional trend due to the basement has been removed and major highs are seen north of Albion and south of Pullman and Moscow. The high surrounding Kamiak Butte northeast of Albion is most probably associated with recent valley filling basalt flows. The low in the central portion of the basin coincides with a drainage configuration superimposed on the basement surface.

Resistivity Survey

Geoelectric models from resistivity soundings can be correlated within the study area. These responses can be correlated to show contacts of similar geoelectric layers. Correlation line X-X' (shown on Figure 4) parallels the Pullman-Moscow highway and shows the configuration of the crystalline basement and uppermost basalt surface (Figure 6). Comparisons of the geoelectric models, available well and geophysical logs show good correlation. An east-west correlation line of well and geophysical logs along the Pullman-Moscow highway shows the thinning of basalt flows to the west and increased predominance of sediments in the Moscow area (Figure 7). Figure 8 shows a crystalline basement of considerable relief in the basin. It generally is steeply dipping from east to west, but rises again west of Pullman. This map was generated using basement elevations interpreted from resistivity and induced polarization soundings.

The elevation of the uppermost basalt surface is shown in Figure 9. This surface was determined by resistivity and induced polarization soundings with quite a bit of well control. The basalt/loess contact is generally quite near the surface, so many domestic wells penetrate to this zone. The upper basalt surface shows considerable relief indicating a well developed east-west drainage system with a maximum relief of approximately forty meters.

Induced Polarization Survey

Field transient voltage curves were analyzed for chargeability variations with depth. Chargeability is a measure of the polarizability of a medium. In the study area, very low, consistent chargeabilities are seen in the loess while very high chargeability gradients are typical of basalt. The crystalline basement chargeabilities are generally high, but irregular. A northeast/southwest correlation line (along Y-Y' in Figure 4) of induced polarization soundings shows very consistent responses across the study area (Figure 10). Contacts are very distinct and the basement configuration readily apparent.

Figure 11 illustrates the variation in chargeability due to basalt influences. The features of primary importance in Figure 11 are the high chargeabilities associated with the greatest basalt thicknesses in the central basin and the low chargeability trends in the east and southwest. Basalt thicknesses are known to decrease in the Moscow area so a decrease in chargeability is expected there, but the gradient of high to low chargeabilities in the southwest

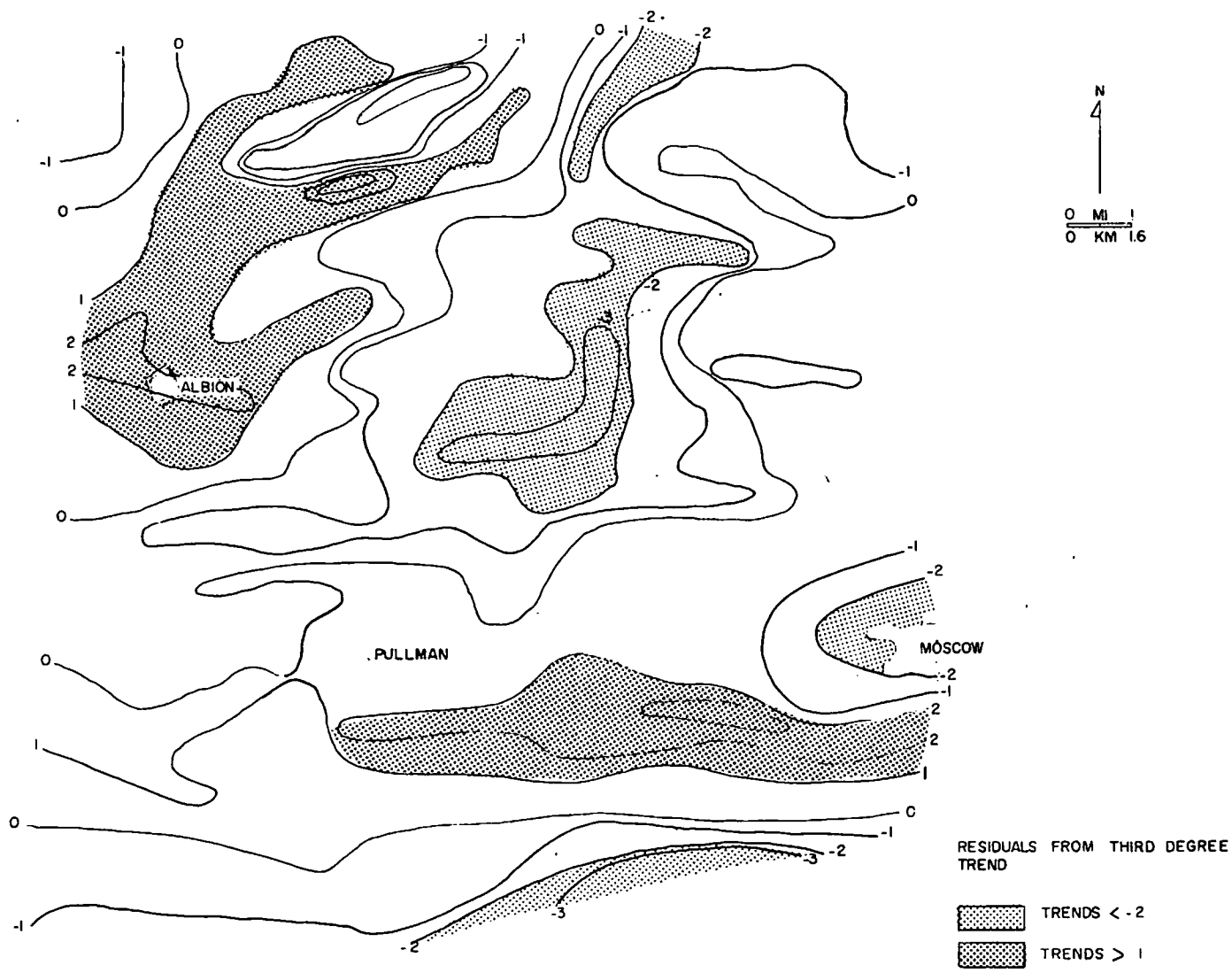


FIGURE 5 - Contoured Residuals of a Third Degree Trend Surface

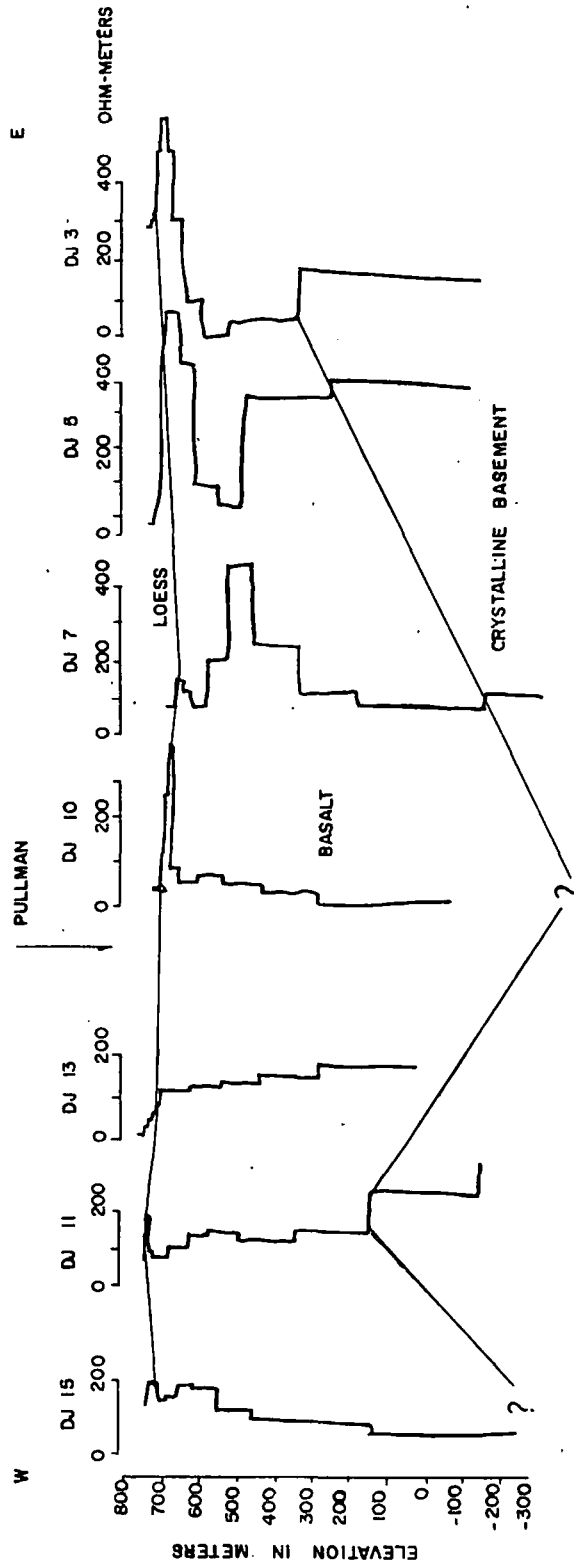


FIGURE 6 - Geoelectric Correlation Line Along X-X'

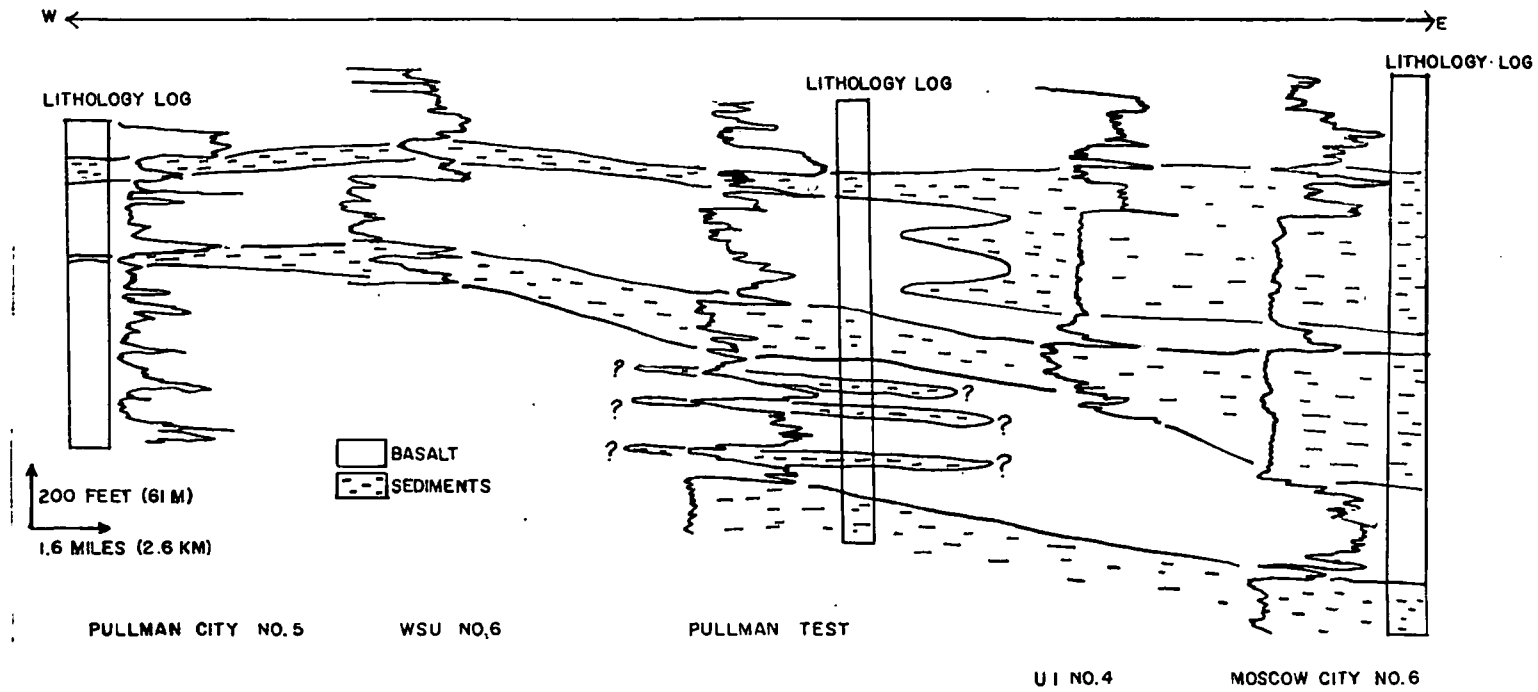


FIGURE 7 - Borehole Geophysical Log (Neutron Epithermal Neutron) Correlation Line Along X-X'

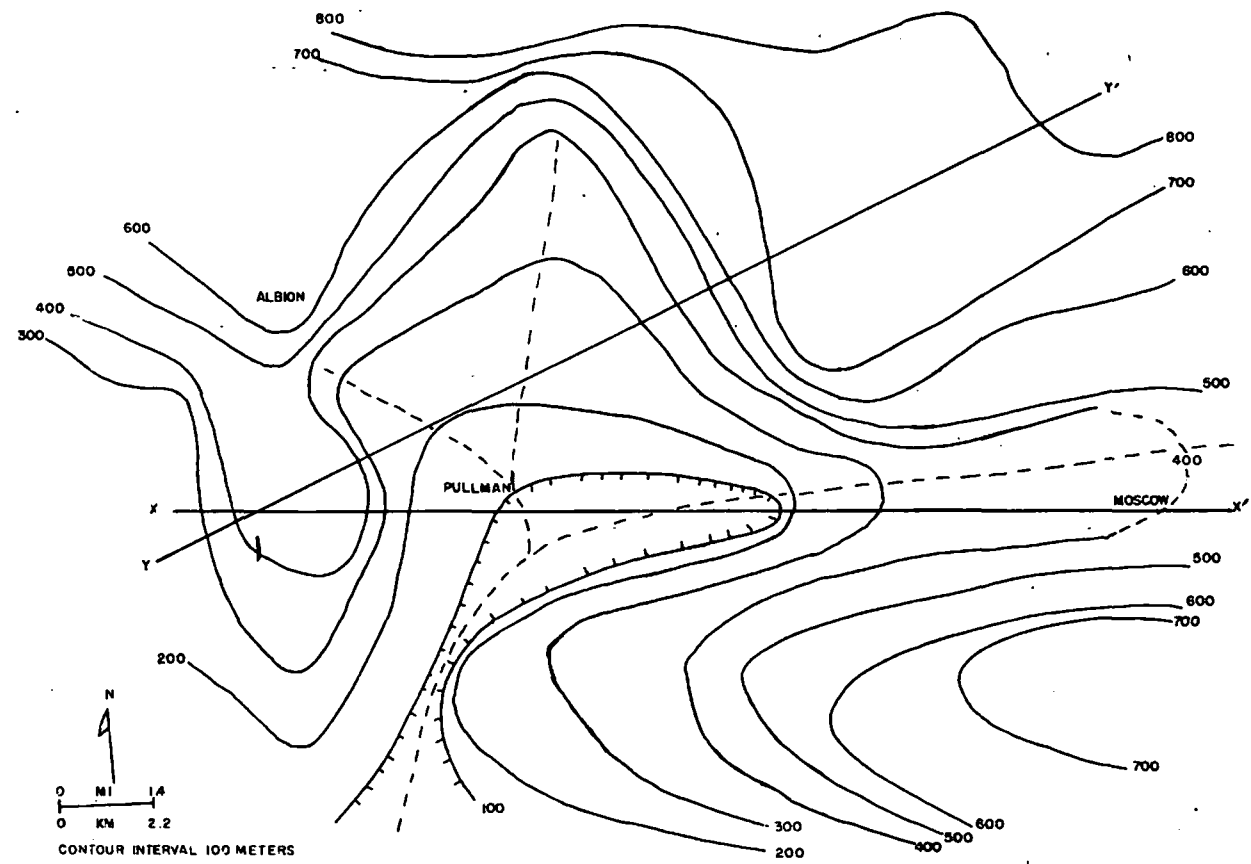


FIGURE 8 - Crystalline Basement Topography Determined from Wells and Geoelectric Soundings

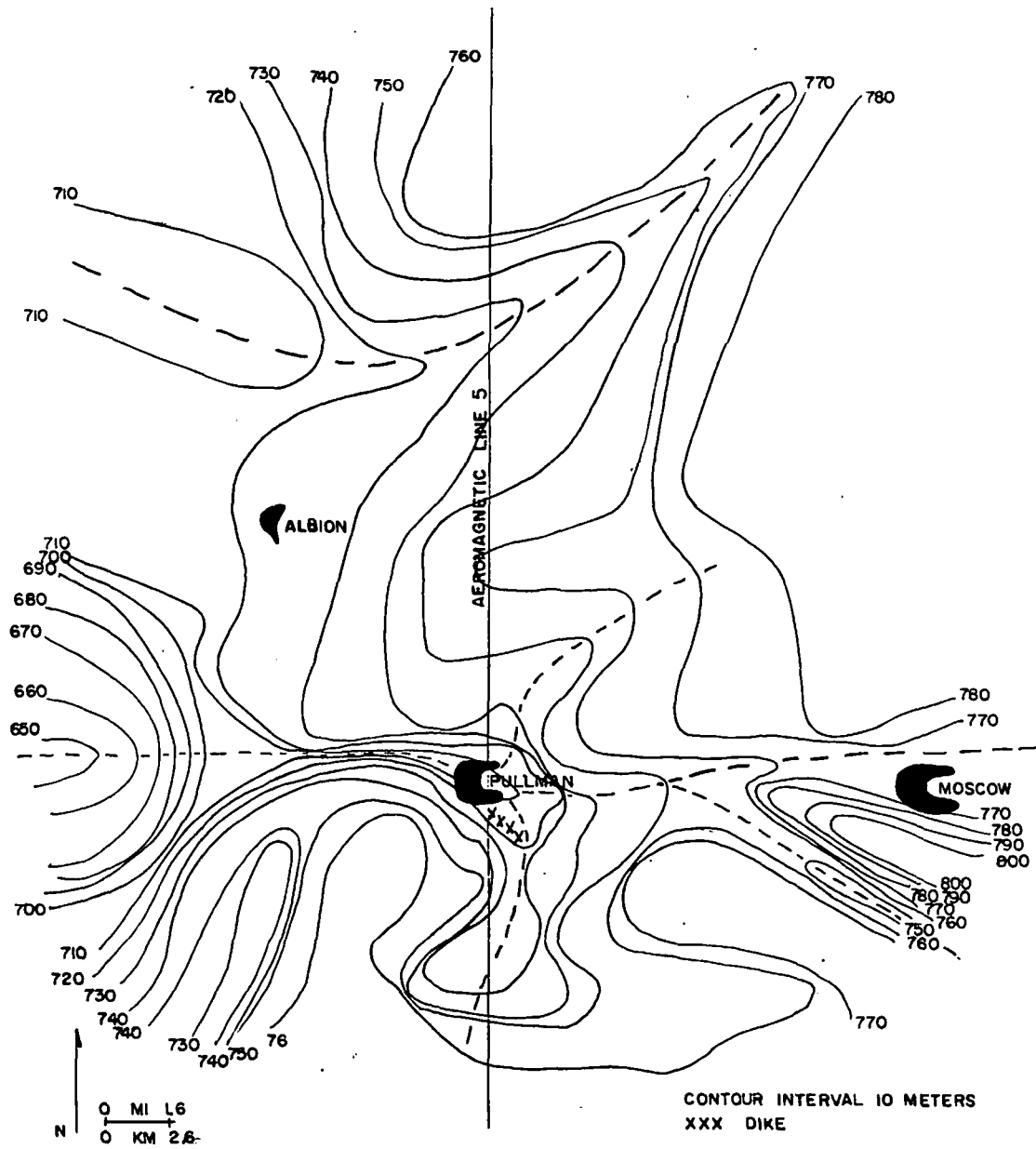


FIGURE 9 - Topography of Uppermost Basalt Surface Determined from Wells and
Geoelectric Soundings

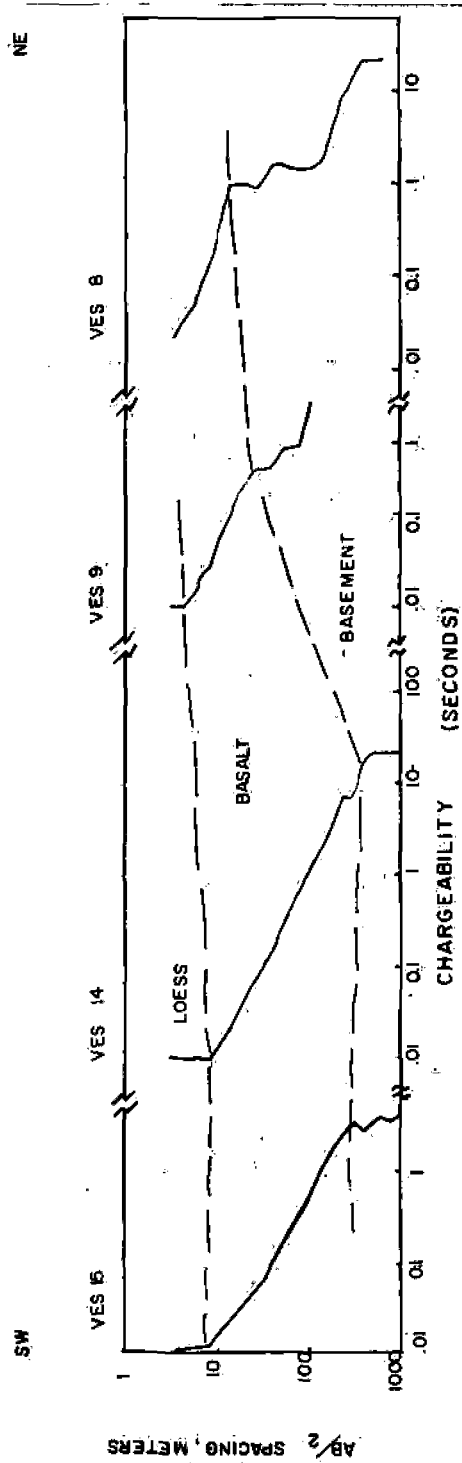


FIGURE 10 - Correlation Line of Induced Polarization Soundings Along Y-Y'

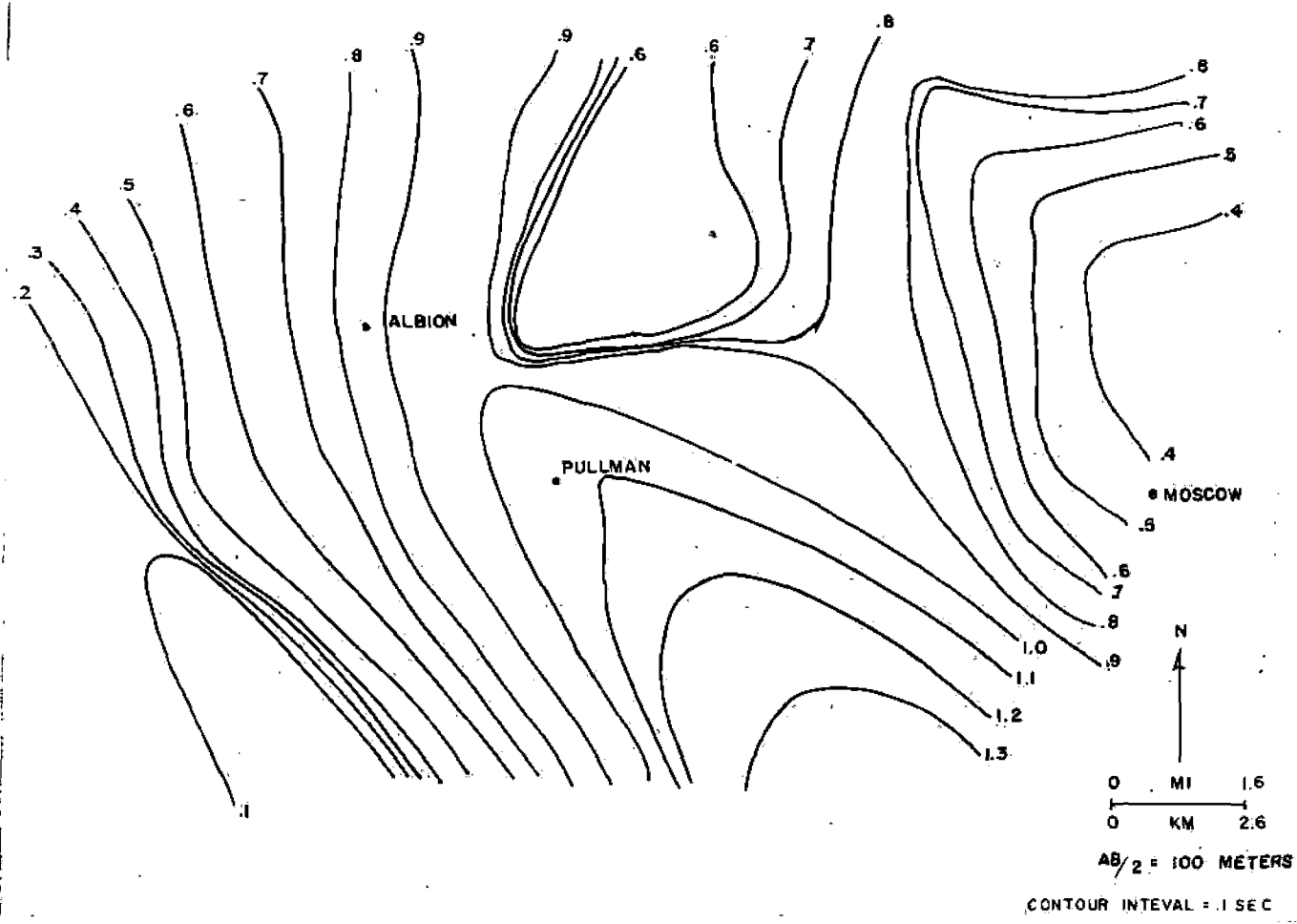


FIGURE 11 - Contoured Chargeabilities at the 100 Meter Level

corner of the study area indicate similar basalt thinning. The chargeability gradient is hypothesized to be a function of basalt filling in the ancient drainage channels on the crystalline basement.

Aeromagnetic Survey

The aeromagnetic survey was flown as a general reconnaissance technique to detect major variations or trends in the study area. In general, the most obvious magnetic trend in the study area is the east to west increasing magnetic trend interpreted as a response to a thickening basalt sequence. Figure 12 shows a typical east/west aeromagnetic profile showing the consistent magnetic responses of the Belt rocks and increased magnetic response due to basalt thickening.

Probably the most distinct feature of the aeromagnetic profile is the irregularity of the data which closely correspond to topographic irregularities. Positive or negative magnetic anomalies would be generated over an area depending on the exposure of normal or reversed basalt flows. In the study area, a reversed flow (Priest Rapids) overlies a normal flow (Grand Ronde) (Swanson et al., 1977) so positive anomalies correspond to erosional features which expose the normal flows. Figure 13 shows a comparison of the sub-loess basalt topography and aeromagnetic line three. A major positive anomaly occurs in the Pullman area as a function of the positive dike and erosional exposure of normal basalt flows. A depressed magnetic anomaly is associated with a reversed polarity basalt high in the central basin. A very high magnetic anomaly is associated with the erosional feature of Rose Creek (past and present) and a depression of the measured magnetics occurs with a rise in basalt elevation and reversed flow.

CONCLUSIONS

The composite geophysical analysis of the study area delineates the configuration of the major ground-water environments described by previous investigators for the Pullman-Moscow area. The major ground-water zone (basalts) is shown to vary substantially in thickness and have associated sedimentary zones which become less significant with distance westward from the eastern margins of the basin. The boundary between the basaltic ground-water zone and crystalline basement is not distinct due to substantial erosion and relief of the lower unit. It is suggested that substantial ground-water may be associated with this zone particularly in the central and western areas of the basin where maximum relief occurs.

The geophysical data delineate a basement high in the southwest portion of the basin which may be partially responsible for controlling ground-water flow in the lower aquifers. The surficial survey techniques are not capable of tracing distinct aquifer zones within the basalts but, instead, delineate

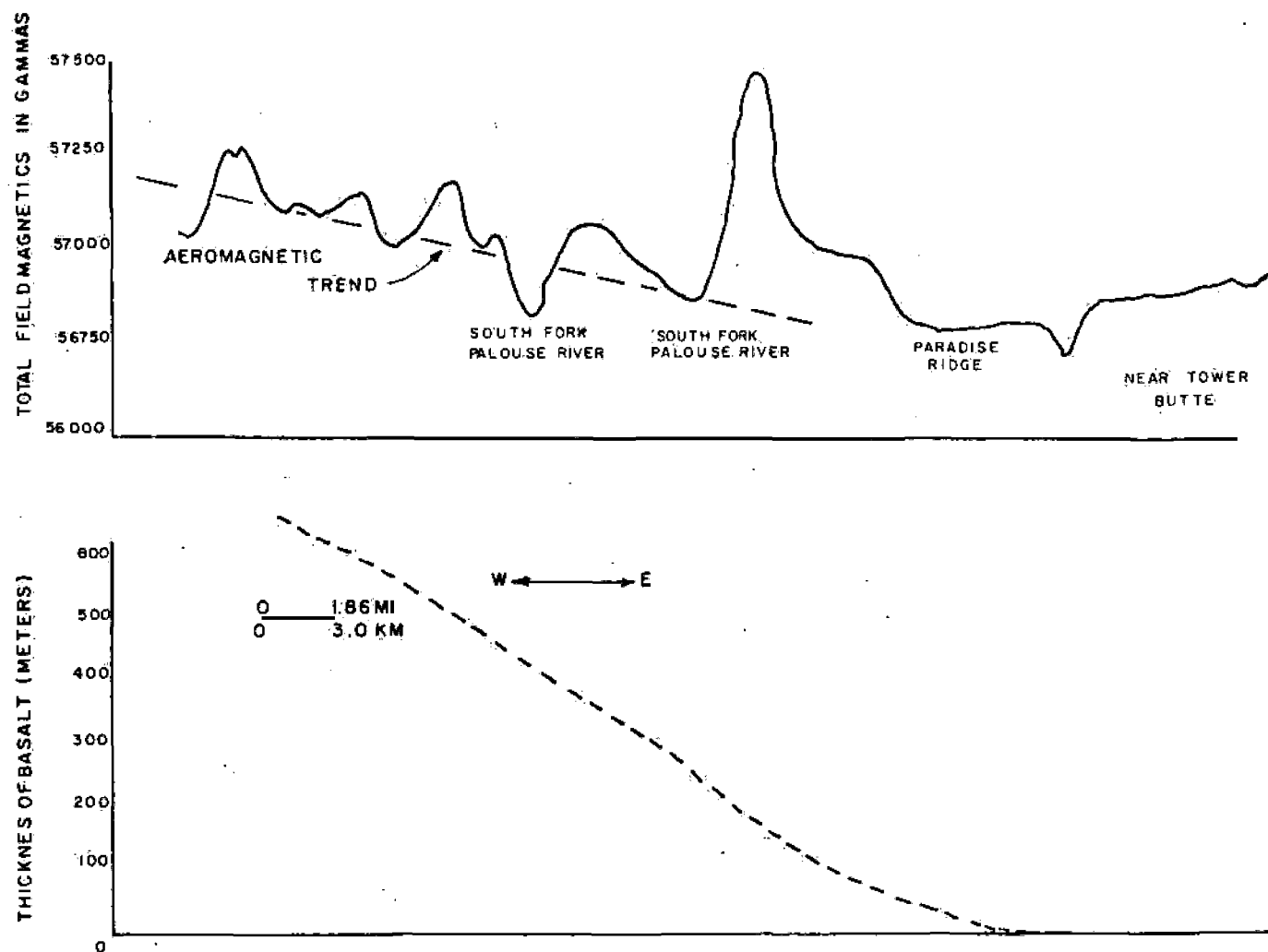


FIGURE 12 - Aeromagnetic Profile Showing Basalt Thickening

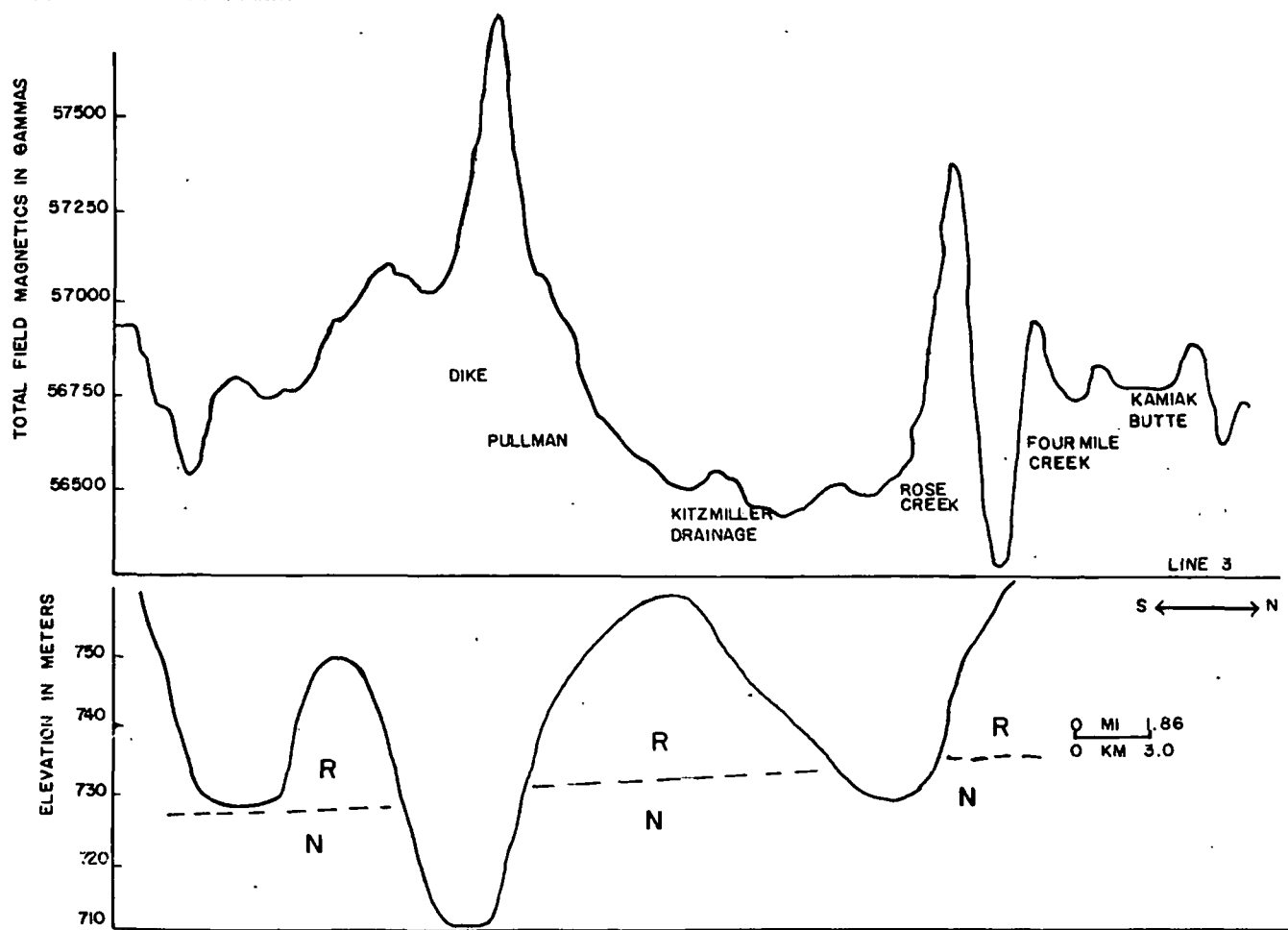


FIGURE 13 - Comparison of Sub-loess Basalt Topography and Aeromagnetic Line Three

the configuration of the major hydrostratigraphic units defined earlier as the loess/basalt zone, interbasaltic zone, and basalt/crystalline basement zone.

REFERENCES

- Barker, R.A., "Ground-Water in the Columbia River Basalt of the Moscow-Pullman Basin," U.S. Geol. Survey Open File, 1977, 144 p.
- Brown, J.C., "Well Construction and Stratigraphic Information: Pullman Test and Observation Well, Pullman, WA," Wash. State Univ. College of Engineering Research Report 76/15-6, 1976, 35 p.
- Crosby, J.W. III and Chatters, R.M., "Water Dating Techniques as Applied to the Pullman-Moscow Ground-Water Basin," Wash. State Univ. College of Engineering Bull. 296, 1965, 21 p.
- Foxworthy, B.L. and Washburn, R.L., "Ground-Water in the Pullman Area, Whitman County, Washington," U.S. Geol. Surv. Water Supply Paper 1655, 1963, 71 p.
- Harrison, J.E., Griggs, A.B., and Wells, J.D., "Tectonic Features of the Precambrian Belt Basin and Their Influence on Post-Belt Structures," Geol. Surv. Prof. Paper 866, 1974.
- Jones, R.W. and Ross, S.H., "Moscow Basin Ground-Water Studies," Idaho Bur. Mines and Geology Pamph. 153, 1972, 95 p.
- Lin, Chang-Lu, "Factors Affecting Ground-Water Recharge in the Moscow Basin, Latah County, Idaho," M.S. thesis, Wash. State Univ., 1967, 86 p.
- Najjar, I.M., "Distribution of Trace Elements in the Ground-Water of the Moscow-Pullman Basin, Idaho, Washington," M.S. thesis, University of Idaho, 1972, 189 p.
- Ross, S.H., "Contributions to the Geohydrology of the Moscow Basin, Latah County, Idaho," Idaho Bureau of Mines and Geology Open-File Report, 1965, 119 p.
- Savage, C.N., Geological Field Trip in Benewah and Whitman Counties, Idaho and Washington in Dept. of Geology and Idaho Bureau of Mines and Geology Belt Symposium, Vol. 1, 1973, pp. 265-317.

Geophysical Investigations of the Pullman, Washington -
Moscow, Idaho Ground-Water Basin
By Muriel S. Robinette
Page 21

- Sokol, D., "Interpretation of Short Term Water Level Fluctuations in the Moscow Basin, Latah County, Idaho," Idaho Bureau of Mines and Geology Pamph. No. 137, 1966, 42 p.
- Stevens, P.R., "Ground-Water Problems in the Vicinity of Moscow, Latah County, Idaho," U.S. Geol. Surv. Water Supply Paper 1460-H, 1960, 32 p.
- Swanson, D.A., Wright, T.L., Byerly, G.R., "Complex Tectonic Setting of the Columbia Plateau," (abs.), Geol. Soc. Am. Abstracts with Programs, V. 9, No. 7, 1977, p. 1194
- Walters, K.C., and Glancy, P.A., "Reconnaissance of Geology and of Ground-Water Occurrence Development in Whitman County, Washington," U.S. Geol. Surv. Water Supply Paper 26, 1969, 169 p.



SIMPLE STATISTICS FOR ELASTIC PROPERTIES FROM SEISMIC ANALYSIS

By

Lee Robinson
Idaho State University
Pocatello, Idaho

ABSTRACT

In last year's Symposium the speaker presented some simple statistics to estimate error in determinations of velocity and depth from refraction seismic data. This paper extends those methods to estimates of error in Poisson's Ratio, Modulus of Elasticity and Young's Modulus as calculated from seismic data. The error estimates thus calculated can help the user identify cases where results are inconsistent and can help him verify the assumption of elasticity.

INTRODUCTION

The most common use of the refraction seismic timer is to determine the compression wave velocity in soil layers by which the depth to underlying layers may be determined. However, it is also possible with refraction equipment to measure either the shear wave velocity or the Rayleigh (surface) wave velocity from which elastic properties may be determined. A previous paper (1) presented statistical methods for estimating error in velocity and depth determinations. This paper extends those methods to estimate error in elastic property determinations.

Elastic properties of soil or rock can be considered an interrelated set: the compression wave velocity, V_p , the shear velocity, V_s , the Rayleigh wave velocity, V_r , Poisson's Ratio, ν , the modulus of rigidity, G , and the modulus of elasticity, E . In theory, if any two of these properties are known, the others may be determined. Actually, the accuracy and validity of such a determination depends on whether the material does indeed act elastically, and whether the elastic properties are constant throughout the material.

The common method of seismic determination (2) is to measure V_p and V_s and calculate ν , E and G . Either computation scheme of Table 1, Col. 2 may be used; i.e., calculate G from V_s then E from G , or calculate E from V_p then G from E .

An alternate method (3) is to measure V_p and V_r and calculate ν , E and G . Since the Rayleigh wave is a surface wave, this second method is limited to the near-surface material (approximately the upper 5 to 15 ft.). A convenient approach to this method is to note that the elastic equations provide single-valued relations between V_r and V_s (Figure 1). With V_r/V_p determined from field data V_s/V_p and V_r/V_s may be scaled from Figure 1. V_s can then be calculated and either of the computation schemes of Table 1 can then be followed.

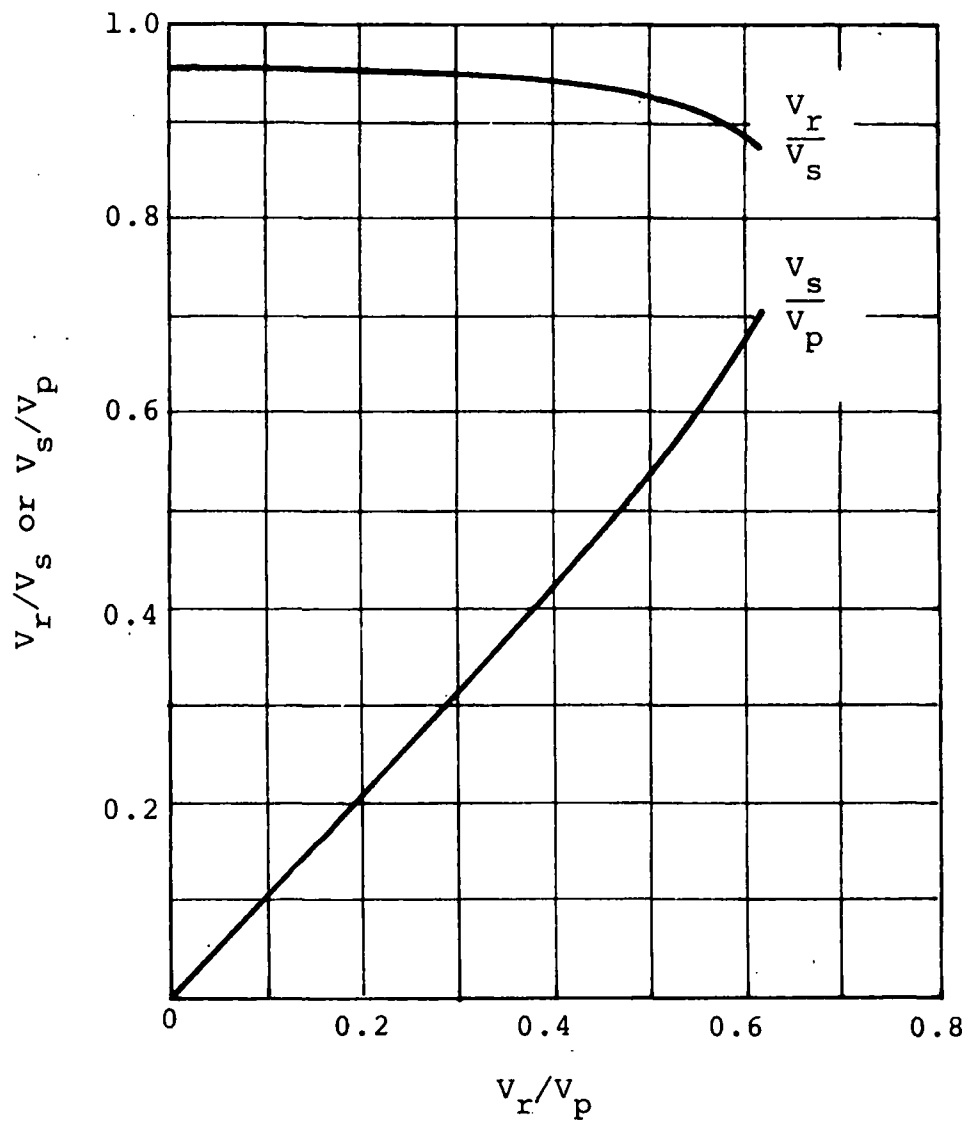


FIGURE 1 - Relations Among Elastic Velocities

TABLE 1

Elastic Parameters and Their Standard Errors Estimated from Seismic Velocities

Parameter (1)	Equation for Determination (2)	Error Estimator Equations Based on		
		Compression (3)	Shear (4)	Rayleigh (5)
Poisson's Ratio	$\nu = \frac{\left(\frac{V_s}{V_p}\right)^2 - 1/2}{\left(\frac{V_s}{V_p}\right)^2 - 1}$	$s_\nu = A \frac{s_{Vp}}{V_p} \quad (a)$	$s_\nu = A \frac{s_{Vs}}{V_s}$	$s_\nu = A \frac{s_{Vr}}{V_r}$
Modulus of Rigidity	$G = \rho V_s^2$ or $G = \frac{E}{2(1+\nu)}$	$s_G = 2G \frac{s_{Vp}}{V_p}$	$s_G = 2G \frac{s_{Vs}}{V_s}$	$s_G = 2G \frac{s_{Vr}}{V_r}$
Modulus of Elasticity	$E = \frac{(1-2\nu)(1+\nu)}{(1-\nu)} \rho V_p^2$ or $E = 2(1+\nu)G$	$s_E = 2E \frac{s_{Vp}}{V_p}$	$s_E = 2E \frac{s_{Vs}}{V_s}$	$s_E = 2E \frac{s_{Vr}}{V_r}$
(a)	$A = \frac{4(1-\nu)}{1 - (V_s/V_p)^2} \left(\frac{V_s}{V_p}\right)^2$			

ERROR ESTIMATION

The author's earlier paper (1) developed a relation to estimate the standard error in seismic velocity determination:

$$s_v = 8.33V^2 \frac{u c}{N^2 \bar{x}} \quad [1]$$

in which V is the velocity, u is the maximum time deviation of data points from the line on a travel time plot, N is the number of points, and \bar{x} is the average distance to the plotted points. The coefficient c is a constant related to point spacing ($c = 0.67$ for 10 unit spacing, 1.0 for 5 unit spacing, 1.5 for 2.5 unit spacing). Eq. 1 applies to shear and Rayleigh wave velocities as well as compression wave velocity.

Relationships for the standard error in ν , E and G may be determined by propagation of variance methods (4). The analysis is complicated by the fact that the elastic properties are all interrelated. Thus, the derivations are too cumbersome to present here. (The method of derivation is outlined in Appendix 1.) The results, however, are simple and are given in Table 1, Cols. 3, 4 and 5. A group of terms used in determination of s_v has been grouped for convenience as a quantity, A . For ease of evaluation Figure 2 gives A as a function of V_s/V_p and V_r/V_p .

If ν is constant through the material then it can be shown that

$$\frac{s_{Vp}}{V_p} = \frac{s_{Vs}}{V_s} = \frac{s_{Vr}}{V_r} \quad [2]$$

Eq. 2 can be evaluated using Eq. 1 to estimate the s 's and taking the V 's from the field data. (Normally only two of the three ratios will be determined.) In such an evaluation, the three ratios will commonly be found to be unequal due to several possible reasons: 1) errors in estimates of the s 's and V 's, 2) non-constancy of ν , 3) inelastic behavior of the material. When Eq. 2 is met, the error estimates from Cols. 3, 4 and 5 of Table 1 give identical results, otherwise each column gives a different estimate.

MONTE CARLO ANALYSIS

It is instructive to apply simulation techniques to some hypothetical data. If we assume that field determined values of V_p and V_s are normally distributed, then values can be selected at random from the normal distributions and used to compute ν , G and E . Histograms of the computed values may then be constructed.

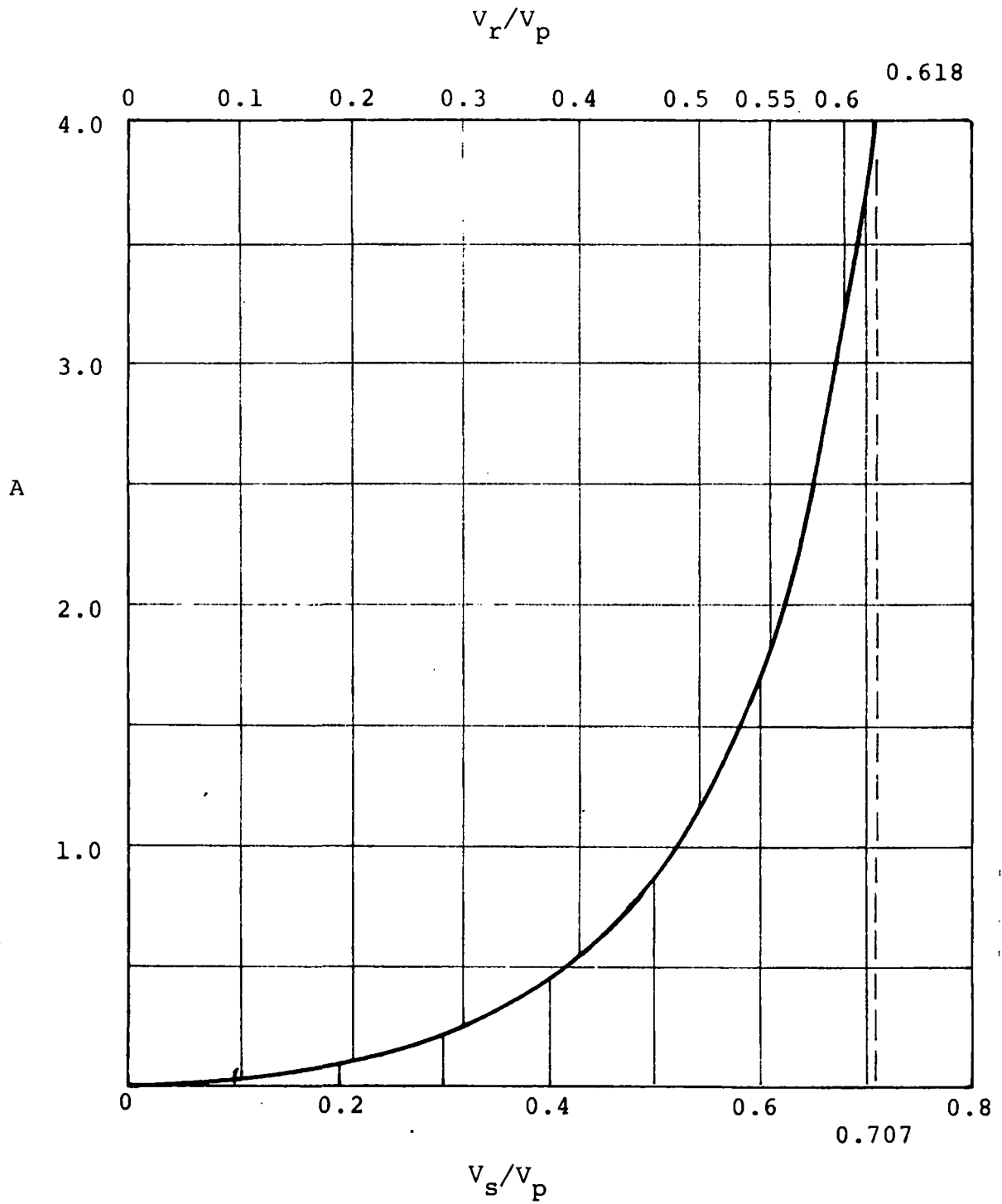


FIGURE 2 - Quantity A Expresses as a Function of Seismic Velocities

Figure 3 shows the histograms for 1,000 random selections, for a case where Eq. 2 is met. Mean values and standard errors as calculated from Table 1 (at top, with tildes), and mean values and standard errors as calculated from the sample are shown above each histogram. It is evident that for this case the sample statistics correspond closely to the calculated estimates from Table 1. Note that although the Poisson Ratio histogram is narrow, large errors in G/ρ and E/ρ are quite common.

Figure 4 shows what happens with the same case, except that Eq. 2 is not met. Here there are two Table 1 estimates of error from the Col. 3 equations and the Col. 4 equations. The sample standard error approaches the larger of the two Table 1 estimates for G/ρ and E/ρ , while the standard error is about equal to the average of the Table 1 estimates for Poisson's Ratio standard error. Note that even though the sample mean corresponds quite closely with the Table 1 G/ρ and E/ρ values, a wide range of values are about equally common. There is, in fact, some question whether it is practical to determine G or E in this case.

Figure 5 shows another case, similar to that of Figure 3, but with a lower mean value of v_p . Eq. 2 is met. Here, it is evident that a wide variation exists in the determined values of Poisson's Ratio. Negative ν values occur a significant part of the time even though the correct value of ν is about 0.3. The apparent skewness of the histogram also indicates that calculated ν values are more likely to be larger than the correct value. But when they are smaller they may well be a lot smaller than the correct value. (In the previous examples, the probability density function is also skewed, but the fact is masked by the small variability.) The large variability of ν does not seem to imply a proportionately large variability in G/ρ or E/ρ estimates for this case.

Figure 6 shows what happens to the case of Figure 5 when Eq. 2 is not met. The variability of ν , G/ρ and E/ρ all grow so large that the practicality of estimating any of them with any degree of certainty becomes questionable. Again, as for Figure 4, the larger Table 1 estimates of standard error of G/ρ and E/ρ are similar to the sample estimates, while the average of the Table 1 estimates of s_ν is reasonably close to the sample estimate.

CONCLUSIONS

1. If Eq. 2 is met, Cols. 3, 4 and 5 of Table 1 all give the same estimates of standard error. If Eq. 2 is not met, the average value of s_ν from Table 1 should be used and the largest value of s_G and s_E should be used to estimate reliability of results.

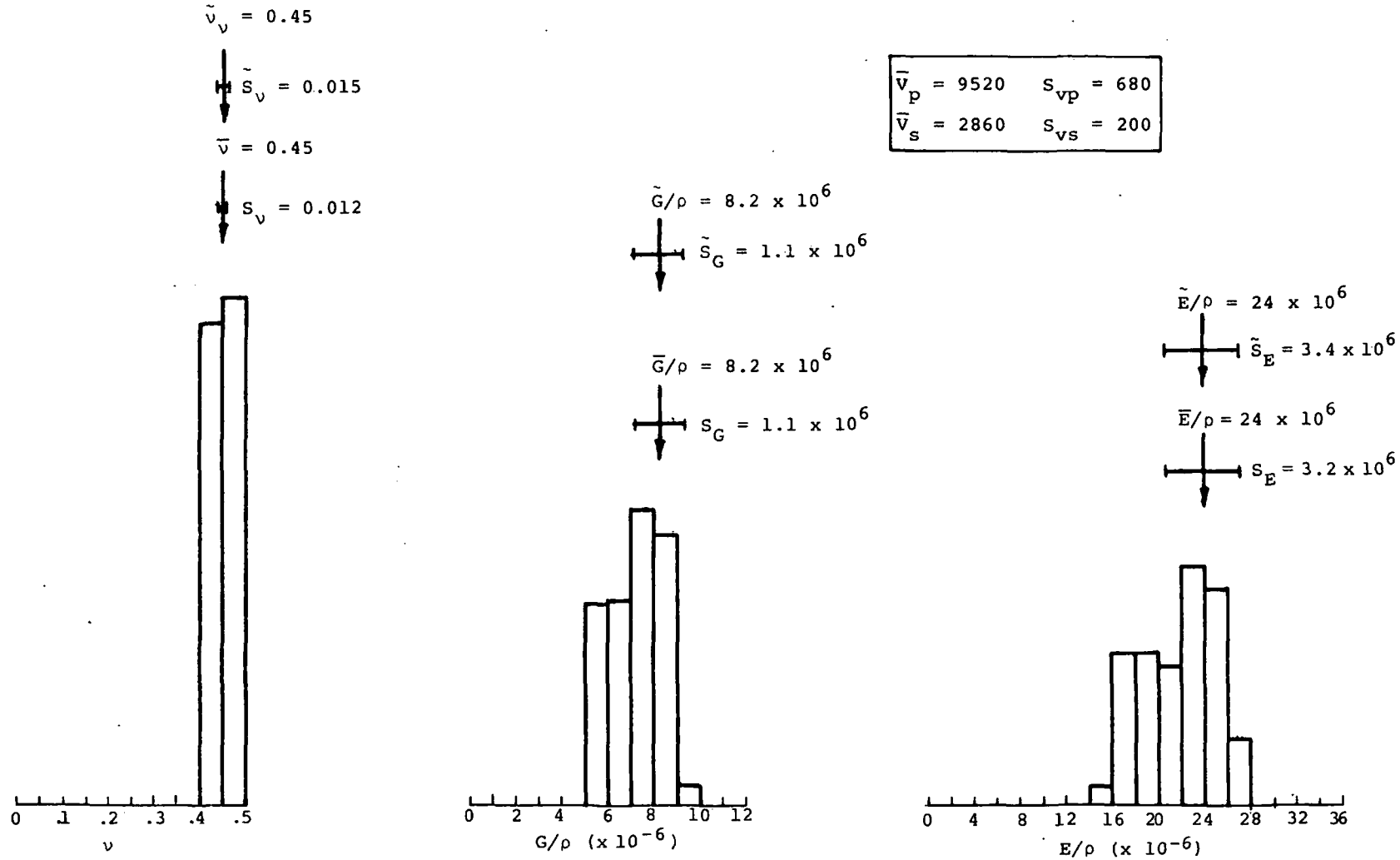


FIGURE 3 - Histograms of Elastic Properties Calculated from Normally Distributed Compression and Shear Velocities. Case 1: Eq. 2 met, Large v .

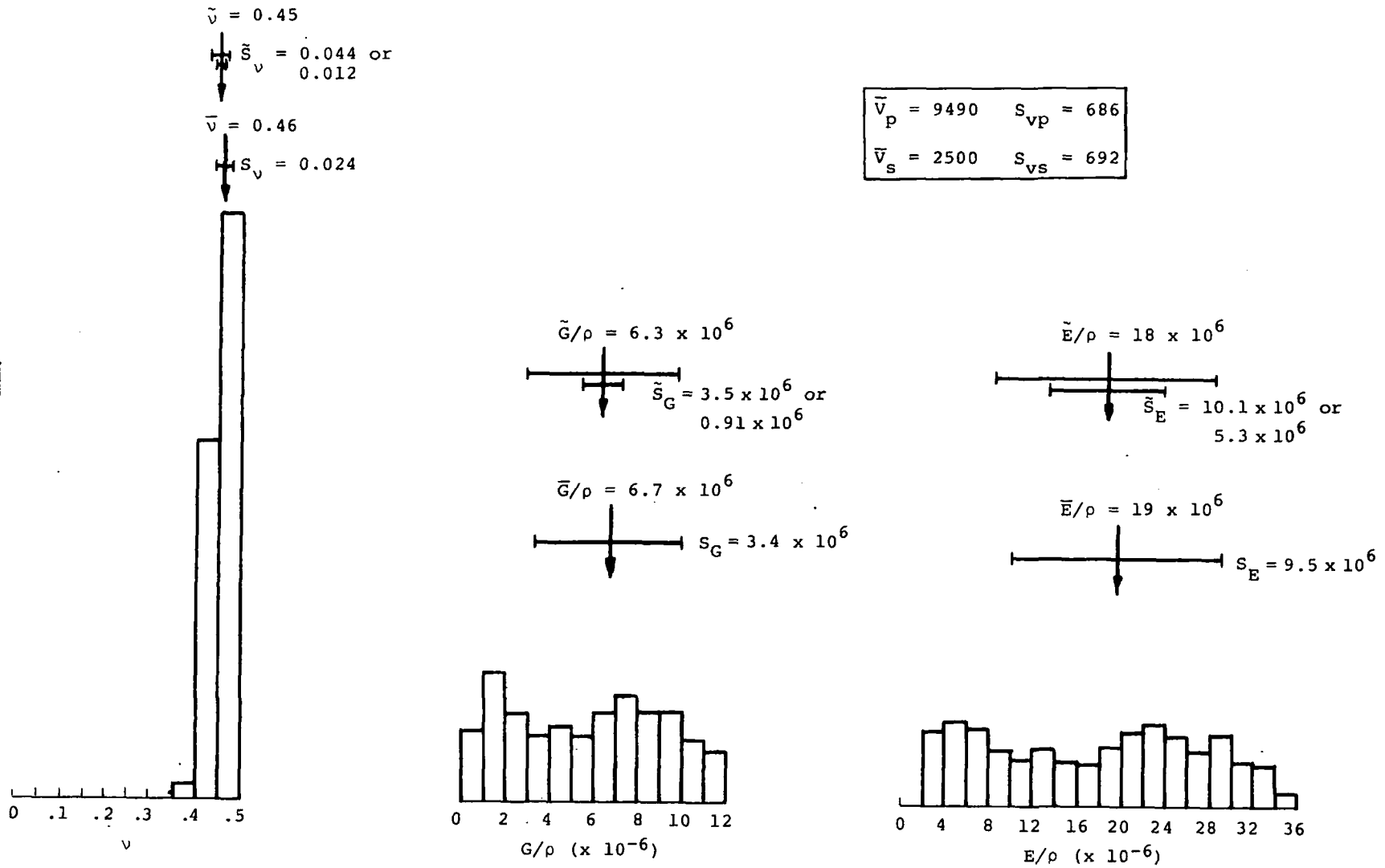


FIGURE 4 - Histograms of Elastic Properties Calculated from Normally Distributed Compression and Shear Velocities. Case 2: Eq. 2 not met, Large v .

$\bar{v}_P = 5520$	$s_{vp} = 680$
$v_S = 2860$	$s_{vs} = 692$

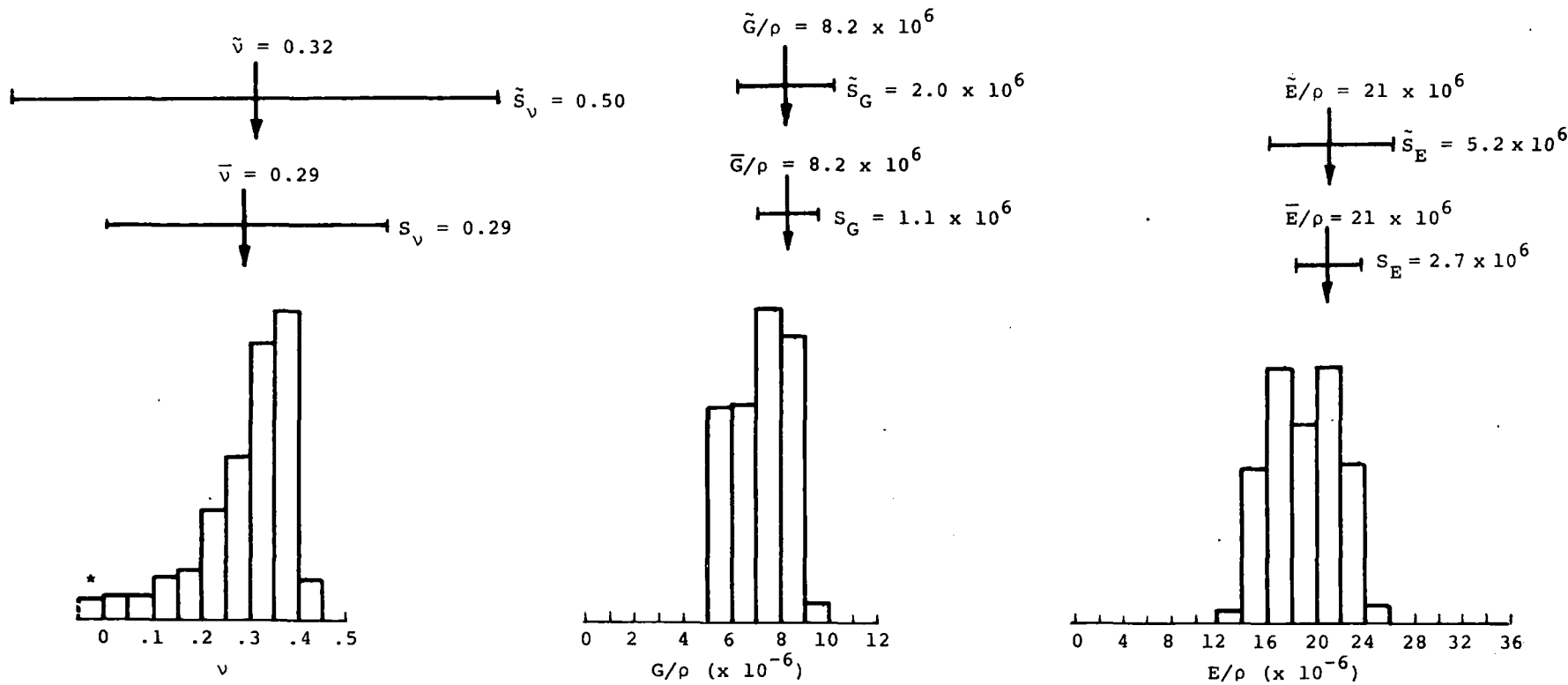


FIGURE 5 - Histograms of Elastic Properties Calculated from Normally Distributed Compression and Shear Velocities. Case 3: Eq. 2 met, small v (* all Negative Values this Bar).

$\bar{v}_p = 5490$	$S_{vp} = 686$
$\bar{v}_s = 2500$	$S_{vs} = 692$

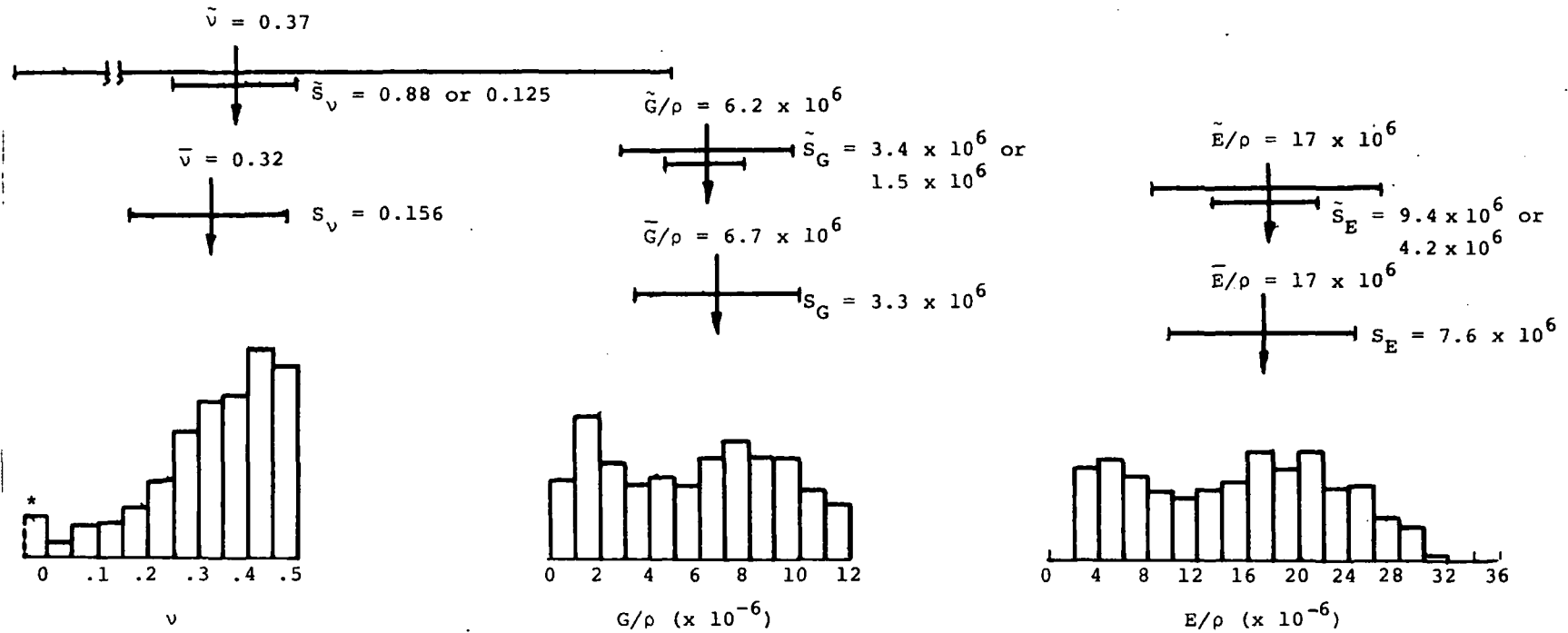


FIGURE 6 - Histograms of Elastic Properties Calculated from Normally Distributed Compression and Shear Velocities. Case 4: Eq. 2 not met, Small v (* all Negative Values this Bar).

2. Eq. 2 not being satisfied is presumptive evidence of non-constant elastic properties (non-homogeneity) or inelasticity of the material. However, high measurement error could be indicated if any of the standard error of velocity estimates is especially large.

3. When the equalities of Eq. 2 are not met, the possibility of not being able to reliably estimate elastic properties is raised. Table 1 estimates of the standard error can be used to decide whether calculation of the elastic properties is feasible.

EXAMPLE

Travel time plots for two ends of a seismic line are shown in Figure 7. The soil is a silt-size loess. Lines were fitted to the data points by the method of least squares. Using Table 1, Col. 2 and Figure 1 elastic properties were calculated from the Compression and Rayleigh wave velocities. Using Eq. 1, s_{vp} and s_{vr} were determined. Then, estimates of the standard error of elastic properties were computed from Table 1, Cols. 3 and 5. As recommended above, the average value of the Col. 3 and 5 estimates is adopted for standard error of Poisson's Ratio, and the maximum of the Col. 3 and 5 estimates are adopted for s_g and s_e . The results of these computations are listed in Table 2.

Notice that although the plots are qualitatively similar, the accuracy of determination is much better for the left-end of the line. If an error analysis were not made, the elastic property estimates would probably be considered to be of equal accuracy.

The standard error-velocity ratios are not equal for the right-end data (see Table 2). In this case the inequality is thought to be due to non-homogeneous material or error in the velocity data, rather than inelastic behavior, since the left-end data exhibits standard-error-velocity ratios which are about equal.

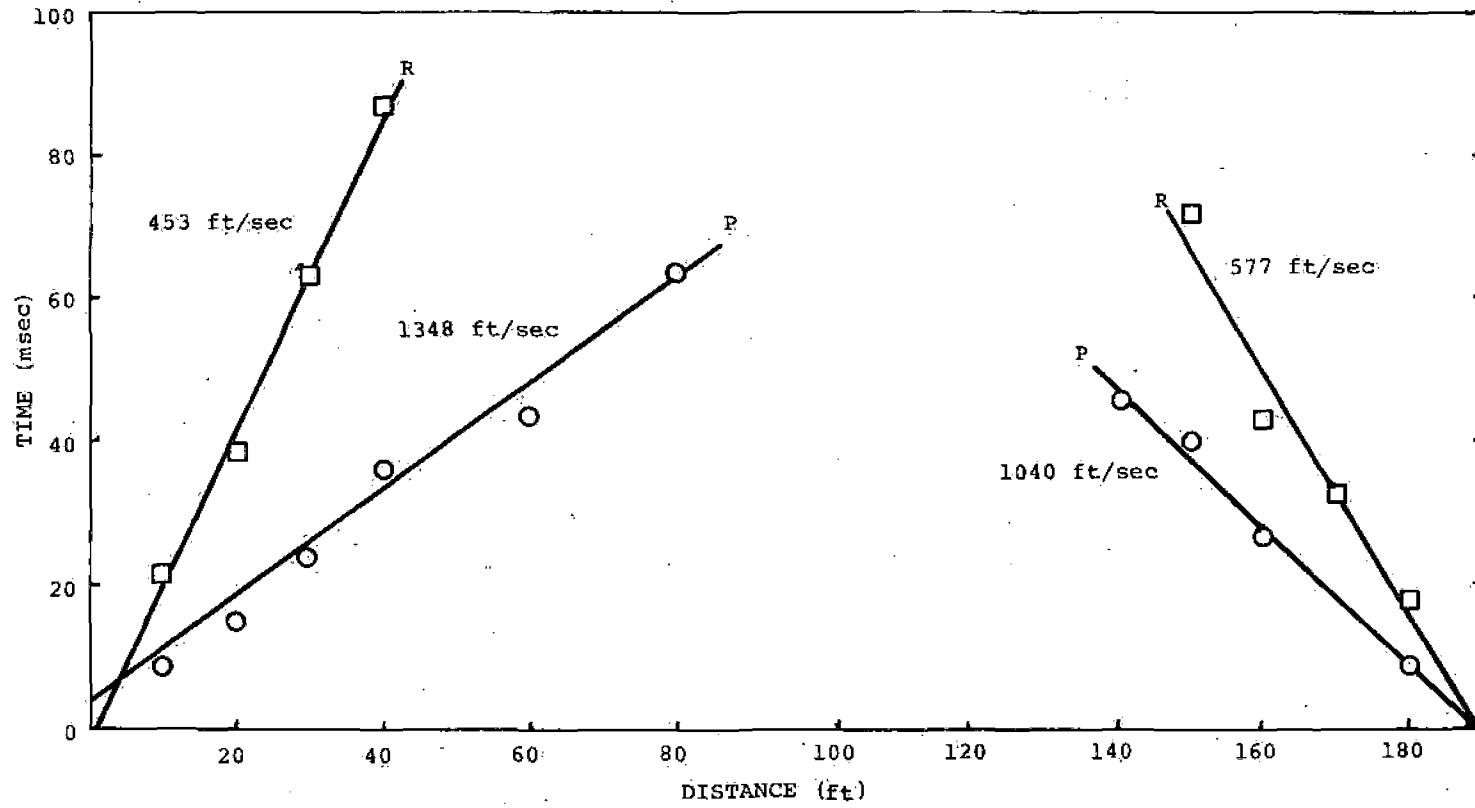


FIGURE 7 - Seismic Data for Error Estimation Example.

TABLE 2
 Calculated Elastic Parameters for Example

Property	Left End (Value \pm s)	Right End (Value \pm s)
ν	0.43 \pm 0.04	0.28 \pm 0.41
G (PSF)	6.4 $\times 10^5 \pm 1.4 \times 10^5$	9.4 $\times 10^5 \pm 5.3 \times 10^5$
E (PSF)	1.84 $\times 10^6 \pm 4.0 \times 10^5$	2.4 $\times 10^6 \pm 1.3 \times 10^5$
s_{V_P} / V_P	0.108	0.15
s_{V_r} / V_r	0.094	0.28

APPENDIX - METHOD OF VARIANCE PROPAGATION

If a function can be written

$$w = f(x,y) \quad [3]$$

an expression for the variance of w resulting from a large number of determinations using values of x and y with given variances can be obtained as follows:

Step 1: Determine the first and second partial derivatives of w with respect to x and y.

Step 2: Write a Taylor expansion in two variables for $w - \bar{w} = \Delta w$; i.e.,

$$\Delta w = \frac{\partial w}{\partial x} \Delta x + \frac{\partial w}{\partial y} \Delta y + \frac{1}{2!} \left(\frac{\partial^2 w}{\partial x^2} (\Delta x)^2 + 2 \frac{\partial^2 w}{\partial x \partial y} \Delta x \Delta y + \frac{\partial^2 w}{\partial y^2} (\Delta y)^2 \right) + \dots \quad [4]$$

in which $\Delta x = x - \bar{x}$ and $\Delta y = y - \bar{y}$.

Step 3: Substitute the Taylor expansion into the definition of variance of w

$$s_w^2 = \frac{\Sigma (\Delta w)^2}{n} \quad [5]$$

in which n = number of values in summation.

Step 4: Expand the resulting expression to a form similar to Eq. 7B-2 in Ref. 4. Substitute in the expressions for the partial derivatives.

Step 5: Neglect any terms which are at least one order of magnitude smaller than the largest term. If x and y are uncorrelated, the cross-products terms (containing both Δx and Δy) go to zero by definition. When x and y are correlated (as they are for the elastic properties considered herein), the cross-product terms only can be disregarded if they can be shown of a smaller order of magnitude than the largest term.

The expression which results from the five steps will be a first-order approximation for the variance in w .

NOTATION

- A = a convenient grouping of terms for s_w calculation (see Table 1)
- c = spacing coefficient
- E = modulus of elasticity
- G = modulus of rigidity
- N = number of points establishing line on travel time plot
- SE = standard error in modulus of elasticity

Simple Statistics for Elastic Properties
From Seismic Analysis
By Lee Robinson
Page 15

- s_G = standard error in modulus of rigidity
 s_{V_p} = standard error in compression wave velocity
 s_{V_r} = standard error in Rayleigh wave velocity
 s_{V_s} = standard error in shear wave velocity
 s_v = standard error in Poisson's Ratio
 u = maximum time deviation of points from line on travel time plot
 V_p = compression wave velocity
 V_r = Rayleigh wave velocity
 V_s = shear wave velocity
 \bar{x} = average distance to plotted points on travel time plot
 v = Poisson's Ratio
 ρ = mass density (bulk) of soil material

REFERENCES

- (1) Robinson, Lee, "Simple Statistics to Improve Refraction Seismic Results," Sixteenth Annual Engineering Geology and Soils Engineering Symposium, Idaho Transportation Dept., Div. of Highways, Boise, Idaho, (1978), p. 183-199.
- (2) Mooney, H.M., Handbook of Engineering Geophysics, Bison Instruments Inc., (1977), Ch. 6.
- (3) Johnson, W.E., "Determination of Elastic Moduli Using a Digital Display Seismograph and Rayleigh Waves," Twelfth Annual Engineering Geology and Soils Engineering Symposium, Idaho Transportation Dept., Div. of Highways, Boise, Idaho, (1974), p. 25-36.
- (4) Hahn, G.J. and S.S. Shapiro, Statistical Models in Engineering, John Wiley & Sons, New York, (1967), Ch. 7 (esp. 7-B).

SOIL CLASSIFICATION BY SEISMIC REFRACTION

By

Michael L. Hiner, Andres Garcia and Dan Herold
Department of Geology and Geophysics
Boise State University
Boise, Idaho

ABSTRACT

Velocity ratios and elastic moduli have been shown to vary proportionately with different rock types. Our research has taken this one step further in an attempt to apply the concept to identifying site specific soil types, based on their physical properties. Through the use of seismic refraction techniques, compressional and shear wave velocities and bulk density were measured and these resulting data were used to calculate Shear, Young's, and Bulk moduli as well as Poisson's Ratio. These data were compared to the Unified Soil Classification for correlation.

The test sites were located in Ada County, near Boise, Nampa, and Kuna. Selection was based upon the diversity of clay and sand content. The results showed that for an area, velocity ratios could be correlated to the relative percentage of clay and sand. With further testing, this process will be able to aid the engineer and the geologist in acquiring information relating to slope and soil stability, and foundation or fill testing at greater cost savings than can now be realized.

INTRODUCTION

The classification of soils and the subsequent determination of their elastic parameters, is often the focus of many geotechnical studies for engineering purposes. This paper presents an illustration of a technique which, with further study, may prove to be a useful and cost effective tool for determining soil type and character.

The elastic moduli can be derived from complex relationships of the velocities of the compressional and shear waves, and soil density. The wave velocities and soil density are controlled by soil type, and the relative percentage of sand and clay. Therefore, the relationship of the elastic moduli should be useful in predicting the relative percentage of sand and clay in a soil. However, soil density is a laborious and expensive value to obtain. If a ratio of the shear and compressional wave velocities without density, adequately approximates the elastic moduli, the ratio should also predict the relative percentage of sand and clay in a soil. This would provide a direct and cost effective approximation of the elastic parameters of the soil.

This study had two purposes -- first, to establish a correlation between the elastic moduli and the ratio of shear-wave velocity (V_s) to compressional wave velocity (V_p). The second part of the project was to determine if cross plots of the elastic moduli and the ratios of V_s/V_p could predict the percentage of sand and clay in a soil.

METHODS AND PROCEDURES

Eighteen sites in the Boise area, having contrasting soil types, were used in the project. The soils at nine of the test sites were predominantly sand. The soils at six other test sites had soil types composed of mixtures of sand and clay. At each test site three parameters were measured -- shear-wave velocity, compressional wave velocity, and soil density, Figure 1. The wave velocities were measured independently from analog wave forms recorded by a Nimbus six-channel engineering seismograph. The method of seismic refraction was employed, using geophone spacings of both 1 and 5 feet. The different geophone spacings were used to determine soil depth, and first layer velocity.

The shear waves were generated by striking the end of a shear wave generator placed at the end and perpendicular to the geophone spread. The shear wave generator consisted of pieces of 2-inch angle-iron bolted to the bottom of a 4 in. by 6 in. by 4 ft. plank. To further enhance the shear-wave arrival, a technique using reversed wave polarity, and horizontal geophones was employed. The reversed polarity of the shear-waves was produced by striking opposite ends of the plank. The horizontal component phones, besides recording the shear-wave components, also minimized the vertical components of the signal. The compressional waves were generated by striking a shot put with a sledge hammer. Vertical component geophones were used to record the compressional wave. The density of the soil at each location was determined by a portable, nuclear-soil densometer.

The shear and compressional wave velocities for each soil type were calculated by linear regression. Figures 2 and 3 show typical plots of velocity profiles for one location. Figure 3 also illustrates the effectiveness of shear-wave polarity reversal. The parallel slopes of the arrival times for normal and reversed records indicate that there was no change in the picked phase of the shear-wave arrival.

The elastic parameters for each soil type were calculated using the relationship including the Lamè coefficient (λ) and the Bulk modulus or modulus of compression (K). From these two values, the other elastic parameters of Young's Modulus, Poisson's Ratio, and shear modulus can be calculated (Figure 4). The calculated values of the shear modulus for each location were then plotted as a function of the ratio of V_s/V_p . From the plot, distinct zones were found to exist for each soil type, based on approximate percentages of sand and clay (Figure 5). Using classifications found in the Unified Soil Classification scheme, the boundaries of each zone were tested and verified by computer approximation of the constants in the elastic moduli.

The next phase of analysis involved cross plotting the velocity of the shear-wave against the ratio V_s/V_p for each location (Figure 6). The resulting graph shows strong correlation, and suggests that interpretation of a particular soil type can be based upon the relationship of the velocities without going into a detailed calculation of the elastic moduli.

FIGURE 1 - DATA TABLE

P-WAVE	S-WAVE	DENSITY	SHEAR MODULUS
1000.0	526.3	122.5	33931482.025
898.9	666.0	115.7	51319429.200
714.3	465.1	122.4	26477324.424
930.2	1095.9	118.2	141957822.942
909.1	1081.0	117.2	136955349.200
1363.6	625.0	113.4	44296875.000
934.5	405.4	115.2	18933023.232
992.5	722.9	117.2	61245198.386
1000.0	461.5	117.8	25089309.050
295.5	289.8	87.0	7306611.480
631.5	336.1	88.0	9940762.480
695.0	563.0	89.5	28368725.500
495.0	326.0	91.5	9724254.000
473.0	327.8	83.8	9004547.992
684.9	300.0	93.9	8451000.000
754.0	355.0	114.0	14366850.000
666.7	363.0	116.8	15390619.200
740.0	440.0	112.6	21799360.000
ft./s	ft./s	p.c.f.	M-b

FIGURE 2 - TIME DISTANCE PLOT OF P-WAVE ARRIVAL

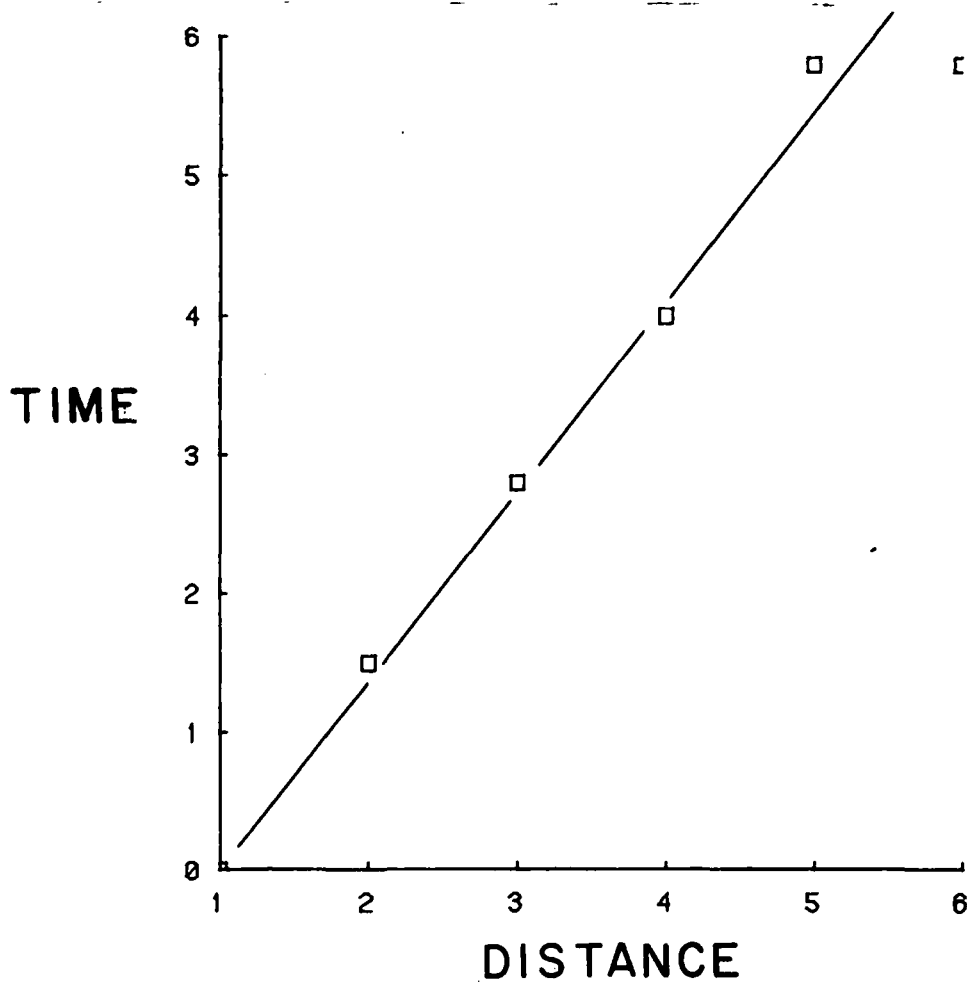


FIGURE 3 - TIME DISTANCE PLOT OF S-WAVE ARRIVAL
 AND REVERSED POLARITY ARRIVAL

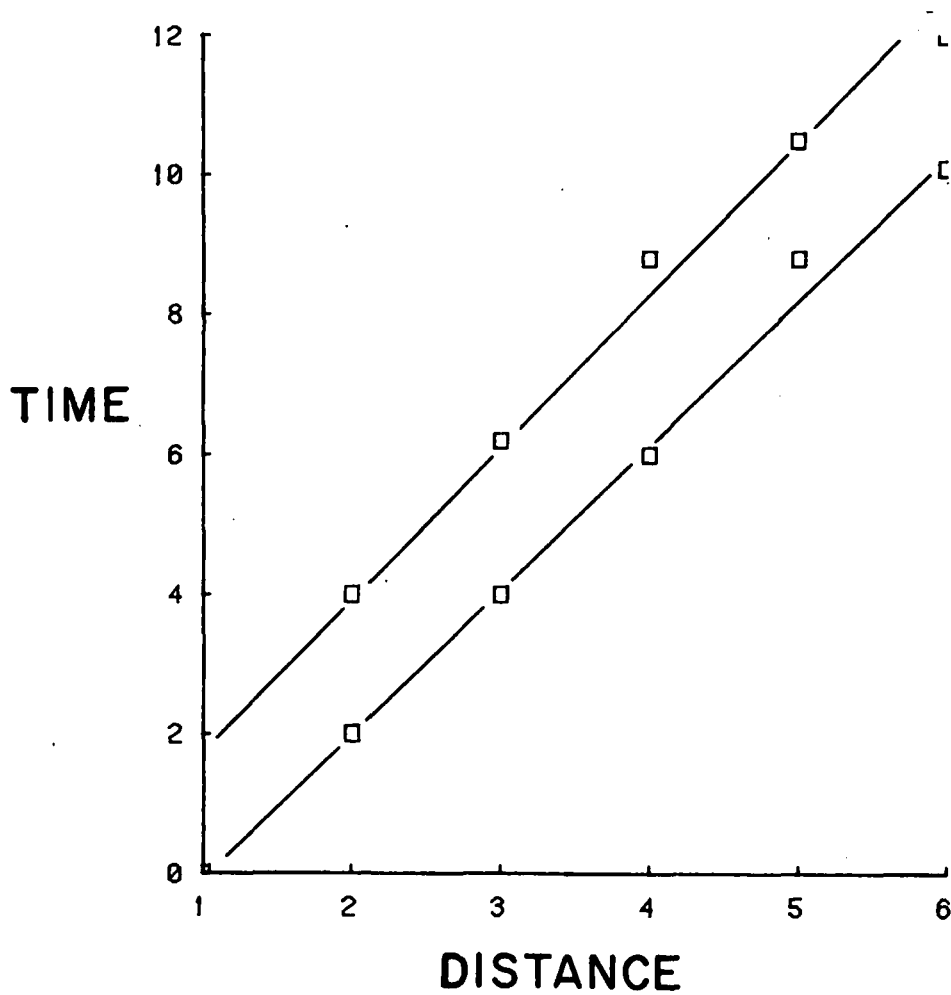


FIGURE 4 - FORMULAS USED TO CALCULATE ELASTIC MODULI

$$V_p = \sqrt{\frac{\lambda + 2\mu}{\rho}} \quad ; \quad \sigma = \frac{1 - 2(V_s/V_p)^2}{2 - 2(V_s/V_p)^2}$$

$$V_s = \sqrt{\frac{\mu}{\rho}} \quad ; \quad \mu = \frac{E}{2 + 2\sigma}$$

$$K = \rho(V_p^2 - 4V_s^2/3) \quad ; \quad \lambda = \rho(V_p^2 - 2V_s^2)$$

$$E = \frac{9K(K - \lambda)}{3K - \lambda}$$

FIGURE 5 - CROSS-PLOT OF SHEAR MODULUS VERSUS V_s/V_p

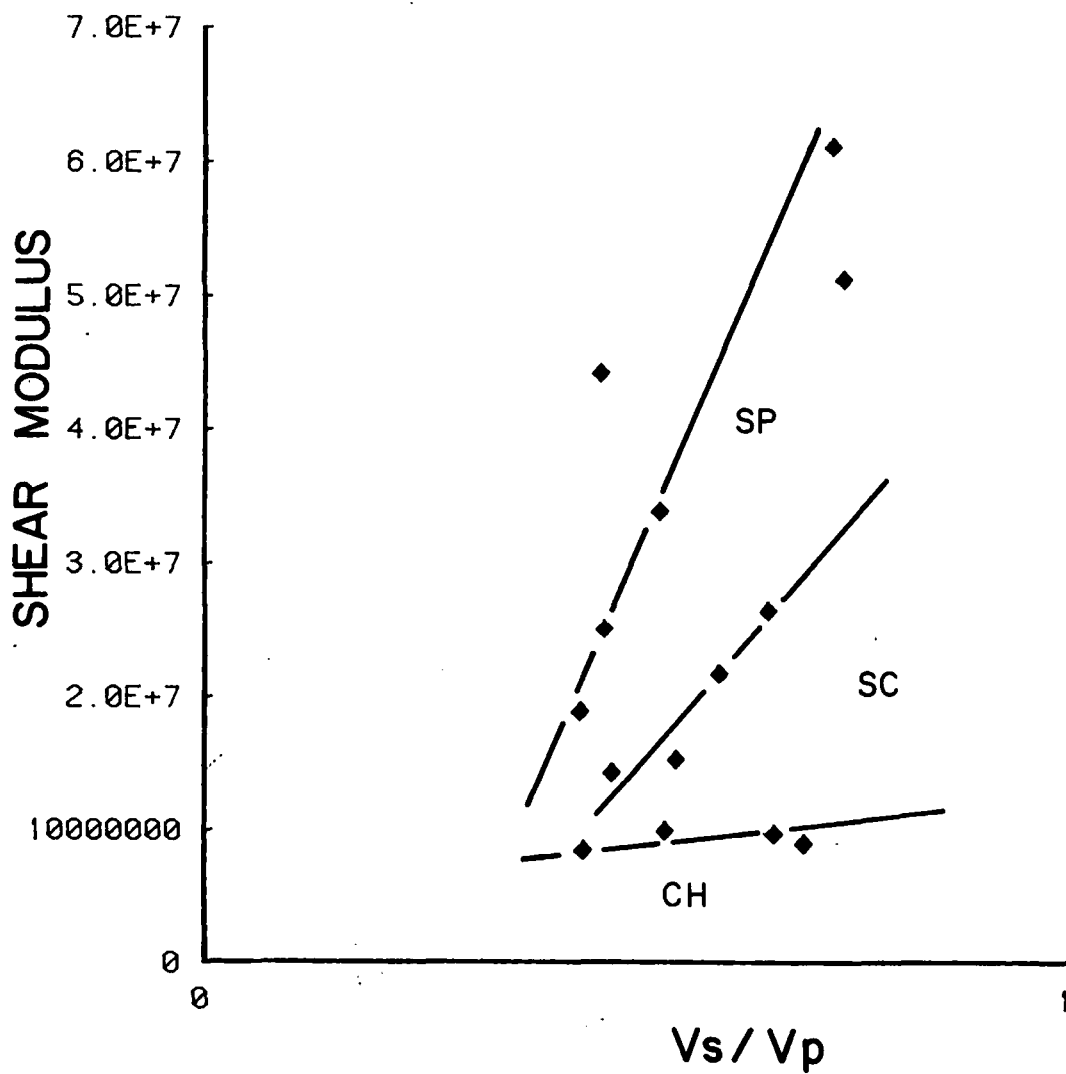
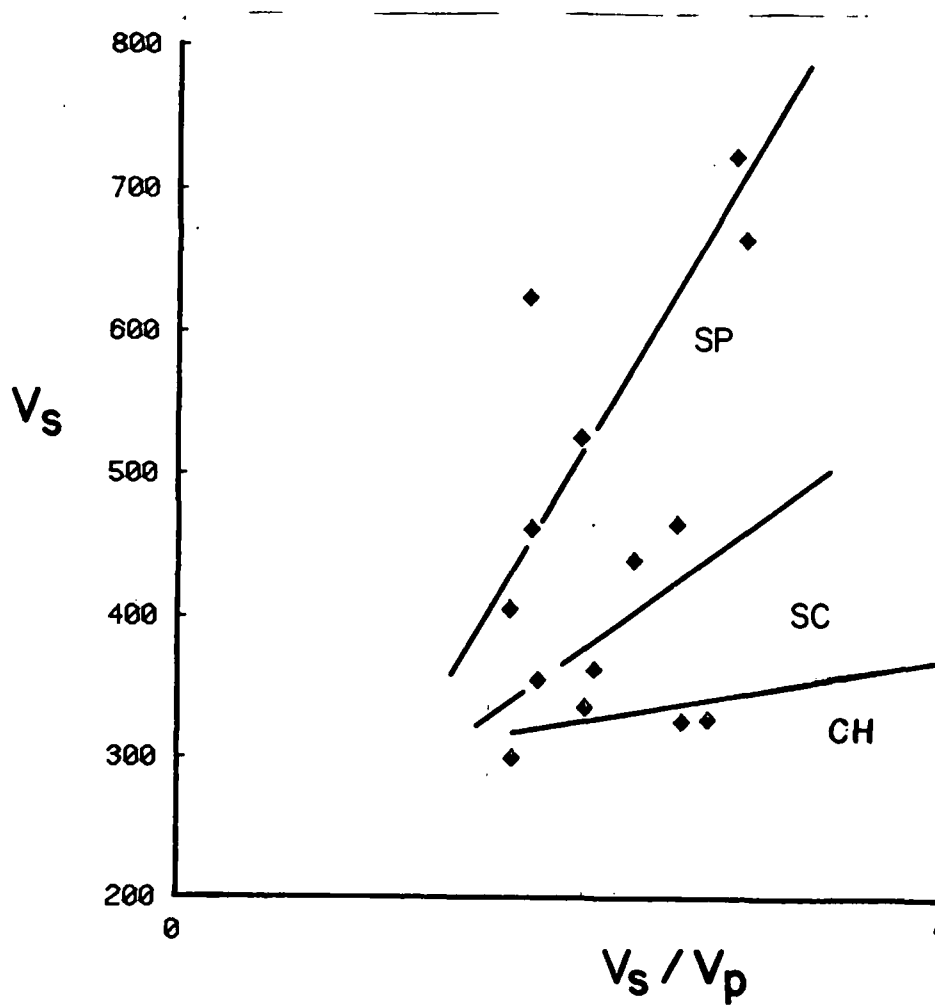


FIGURE 6 - CROSS-PLOT OF V_s VERSUS V_s/V_p



The concept was further tested by plotting both the bulk modulus and compressional-wave against the ratio V_s/V_p . Again, distinct soil type trends in the data were found. The separation of the different soil types into distinct trends can be seen in Figure 7. These are further enhanced by linear, computer approximations of the trends.

One area of concern is the validity of data that exceeds the theoretical limits of Poisson's ratio at .7, and whether the data is due to the soil type being anisotropic and inelastic. It is suggested that plots of Poisson's ratio versus the ratio V_s/V_p for each soil type, will show such anomalous data points as having negative values of Poisson's ratios. Such data points will also have V_s/V_p ratios greater than .7 (Figure 8).

CONCLUSIONS

From this study, it was found that plots of V_s versus V_s/V_p allows for soil typing in given locations. The ratios of V_s/V_p can then be used to directly approximate the values of the elastic moduli. In addition, it was found that density and moisture content values were not needed for soil typing (Figure 9 and 10).

With further testing, this technique should prove useful in evaluating soil types in engineering studies for site selection and analysis, and will provide a means of directly approximating the elastic parameters of different soil types with less time spent in the field and laboratory.

FIGURE 7 - CROSS-PLOT OF BULK MODULUS VERSUS V_s/V_p

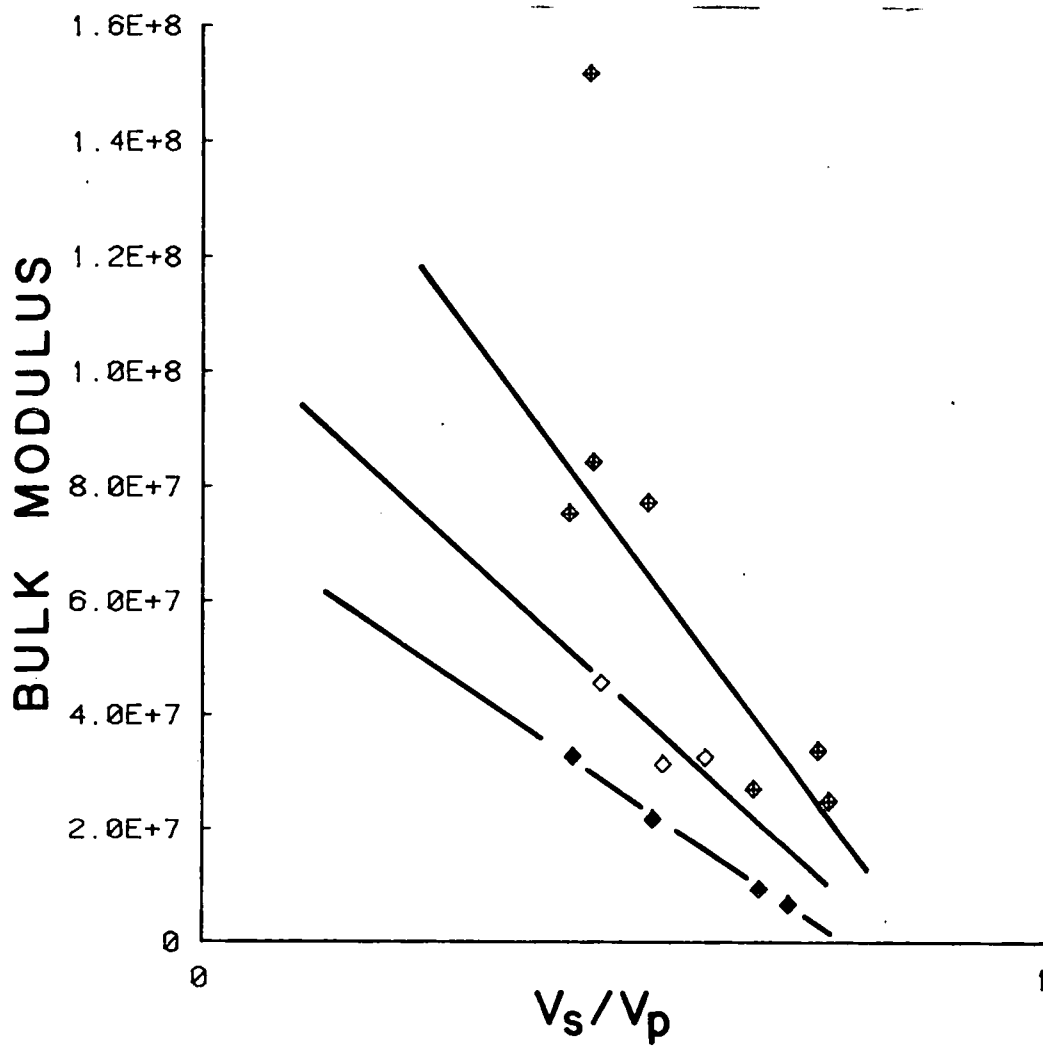


FIGURE 8 - PLOT OF POISSON'S RATIO VERSUS V_s/V_p

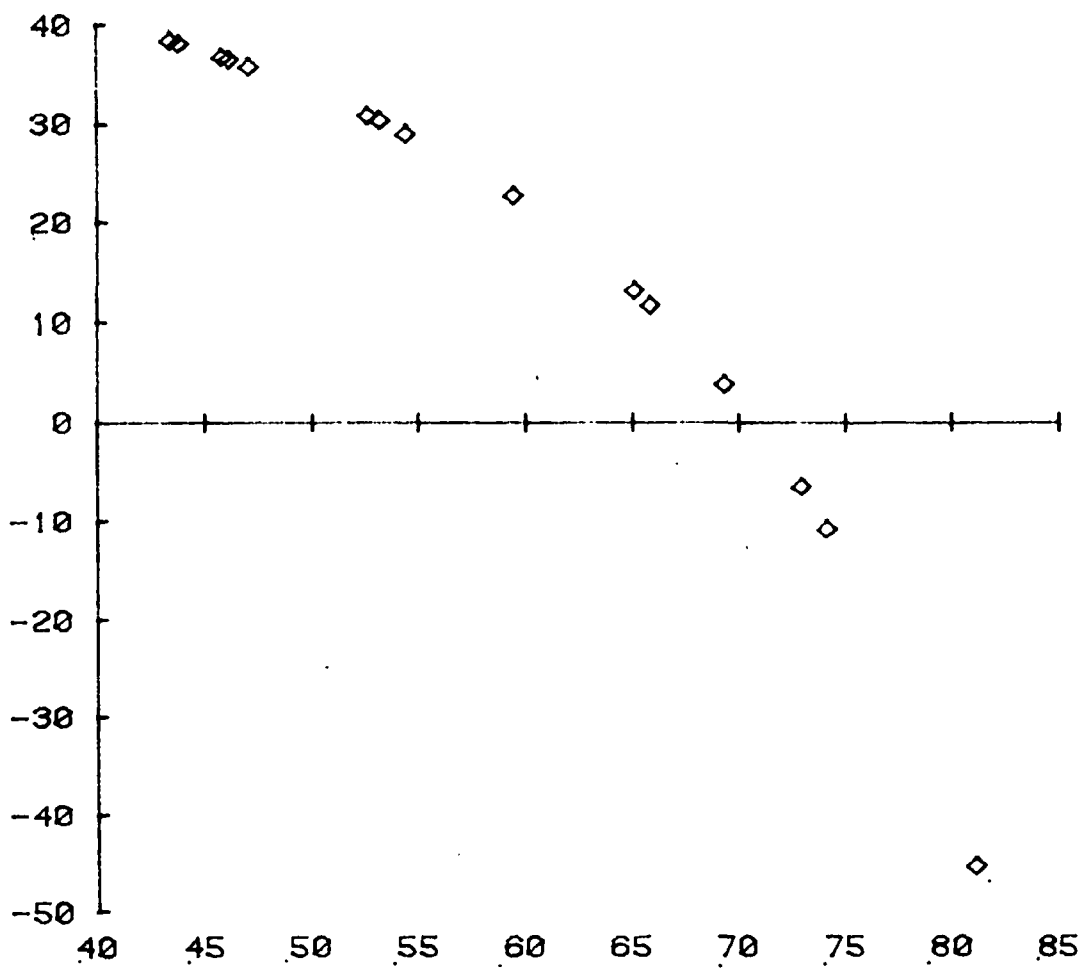


FIGURE 9 - PLOT OF DENSITY VERSUS V_s/V_p

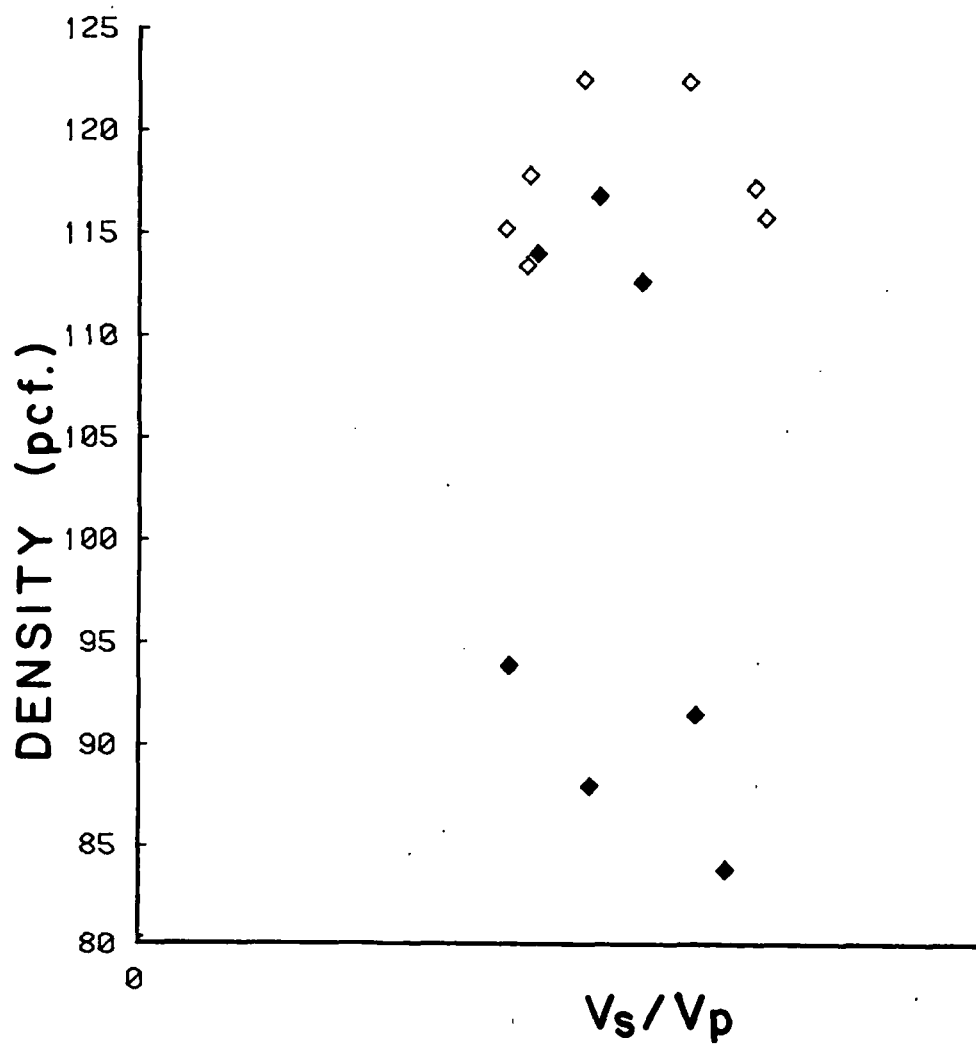
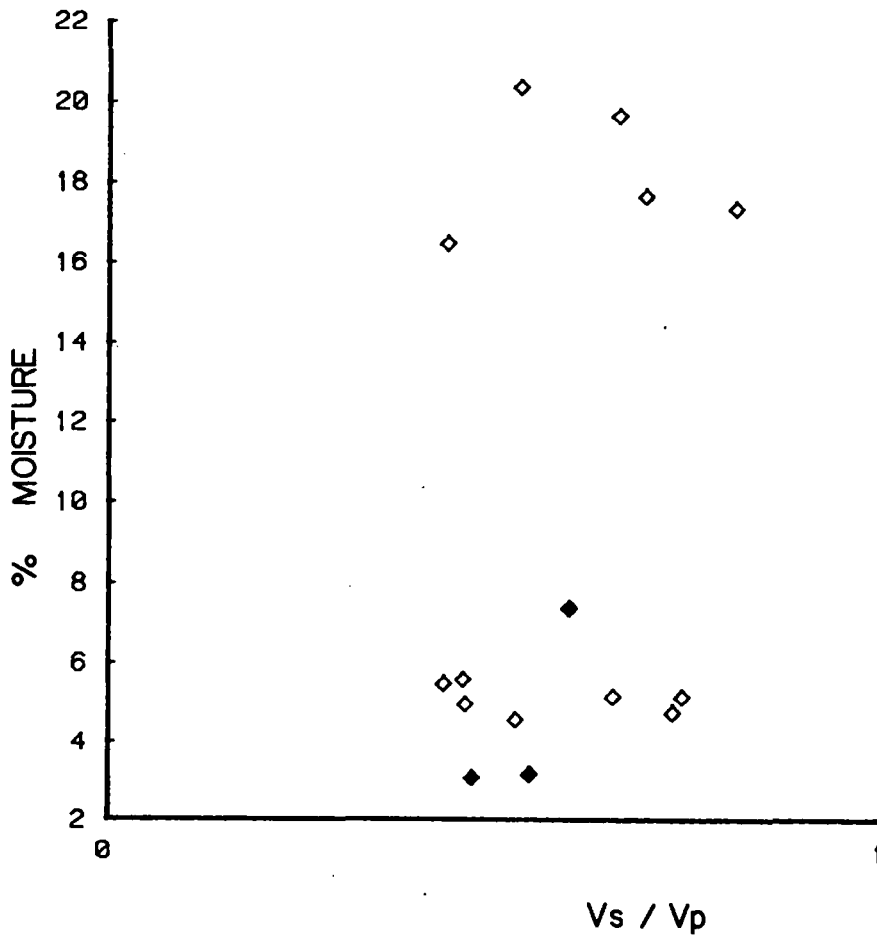


FIGURE 10 - PLOT OF MOISTURE CONTENT VERSUS V_s/V_p



REFERENCES

- Applegate, J.K., 1974a, A Torsional Seismic Source: Ph.D. Thesis, T-1635, Colorado School of Mines, Golden, Colorado.
- Applegate, J.K., 1974b, The Variability of Dynamically-Determined Poisson's Ratios and Some Factors that May Affect the Variability: Proceedings of the 12th Annual Symposium on Engineering Geology and Soils Engineering, Boise, Idaho.
- Fry, A.B., "A Procedure for Determining Elastic Moduli of Soils by Field Vibratory Techniques," Miscellaneous Paper S-72-36, U.S. Army Engineers Waterways Experiment Station, CE, Vicksburg, Miss., June 1973.
- Johnson, W.E., 1976, Seismic Detection of Water Saturation in Unconsolidated Material: Proceedings of the Fourteenth Annual Symposium on Engineering Geology and Soils Engineering, Boise, Idaho.
- Schlumberger, Inc., "Log Interpretation", Vol. II - Applications, New York 1974.
- Telford, W.M., Geldart, L.P., Sheriff, R.E., Keys, D.A., "Applied Geophysics", Cambridge University Press, Cambridge 1976.
- Waters, K.H., "Reflection Seismology", John Wiley & Sons, Inc., New York 1978.

A SIMPLIFIED PRELOAD DESIGN

By

Thomas M. Gurtowski and Thomas E. Kirkland
Shannon & Wilson, Inc.
Seattle, Washington

ABSTRACT

Frequently consulting geotechnical engineers must design foundations for relatively large in area, moderately loaded warehouses, at sites that are underlain by compressible, normally consolidated alluvium. The alluvium can consist of loose silts, sands, and soft organic and/or non-organic clayey silts. In the majority of cases structurally supporting an entire warehouse on pile foundations is expensive and preloading the building site is generally more cost effective.

This paper summarizes the procedures used in our office for designing preloads based on limited soil test data. The procedures in the design involve estimating allowable soil bearing pressures, determining preload dimensions, making initial approximate 'time-of-removal' estimates, corrections to 'time-of-removal' based on field settlement measurements, and estimating the amounts of post-construction settlement. Limited data is presented from an actual preload design.

INTRODUCTION

Frequently, consulting geotechnical engineers must design foundations for relatively large area, moderately loaded warehouses, at sites that are underlain by compressible, normally consolidated, alluvium. The alluvium can consist of loose silts, sands, and soft organic and/or non-organic clayey silts. In most cases, pile supporting a large warehouse is not feasible and preloading provides a more viable solution.

The title of this paper is not to suggest that designing a preload is a simple procedure; it implies providing a client with a cost effective preload design within a limited budget. Consequently, the engineer must thoroughly research the geology of the area and use his experience in selecting the most effective boring locations, boring depths, and representative samples for strength and consolidation tests. Before making these decisions, however, it is advisable to find out the dimensions of the warehouse, maximum live floor load, interior and exterior footing loads, and finished floor grade. Without knowing these parameters before making the explorations, the soils engineer may find out later, during his studies, that borings have not been made deep enough.

Boring depths should be estimated by distributing the live floor load over the warehouse area and determining the resulting stresses in the subsoil. In general, the depth to drill and sample is that depth where the additional increase in stress is less than 10 percent of the existing overburden pressure. The depth of borings may also be controlled by a more shallow depth to bedrock, glacially preconsolidated soil, etc.

A Simplified Preload Design

By Thomas M. Gurtowski and Thomas E. Kirkland

Page 2

It has been our experience that settlements of normally consolidated soil can be estimated to a satisfactory degree by one-dimensional consolidation theory from oedometer tests for cohesive soils (8, 9), and Standard Penetration Resistance (N-value, blows per foot) elastic modulus correlations (1, 5) for cohesionless soils. We generally estimate settlements of a non-preloaded site to emphasize to the client that preloading is required prior to constructing a warehouse. The alluvial deposits we design for are generally non-homogeneous, i.e., various types of soils and thicknesses, making accurate settlement predictions difficult. With this in mind, sophisticated settlement analysis methods are usually not warranted. However, we do determine a maximum-minimum range of total and possible differential settlements. Note that for preloaded sites, the actual settlements with time would be measured from the settlement plates.

The rate of settlement for alluvium is difficult to predict from laboratory tests. Many variables are involved, such as: (a) the ordinary theory of consolidation used for analysis applies essentially for vertical drainage, whereas alluvial deposits may also exhibit some horizontal drainage, (b) accurate layer thicknesses, length of drainage paths and the coefficients of consolidation of good undisturbed samples must be evaluated, (c) corrections for gradual load application and pressure distribution are needed, and (d) various types and thicknesses of soils are usually involved. Except where drainage is controlled, as in sand drain installations, the predicted time-settlement rate from laboratory tests tends to be slower than the actual rate. However, a time-settlement design estimate for a preload can and should be made; this will be discussed later. Past experience with similar soils will generally prove to be the most reliable estimate.

To estimate allowable soil bearing pressures for shallow foundations founded within normally consolidated alluvium, we determine the undrained strength from unconfined compression tests, unconsolidated-undrained tests, pocket shear torque and/or hand penetrometer tests, Standard Penetration tests, and correlations thereof. We use a lower bound average to estimate bearing capacity.

ALLOWABLE SOIL BEARING PRESSURES

Quite often the near-surface soils will not provide enough strength to support conventional spread or wall footings and/or the soil is too compressible, yielding intolerable settlements, even after preloading. This problem is approached two ways: first, over-excavate enough soft or loose alluvium beneath the footing to produce a prism of compacted structural fill, which with sufficient thickness would limit settlements and not allow overstressing of the underlying alluvium beyond its allowable bearing capacity; and second, assuming that the near-surface soils are uniform and normally consolidated, develop a representative undrained strength from, for example, a c/\bar{p}_n ratio (6) in order to estimate the increase in strength from the preload stress. For this latter approach, a series of consolidated undrained

A Simplified Preload Design

By Thomas M. Gurtowski and Thomas E. Kirkland

Page 3

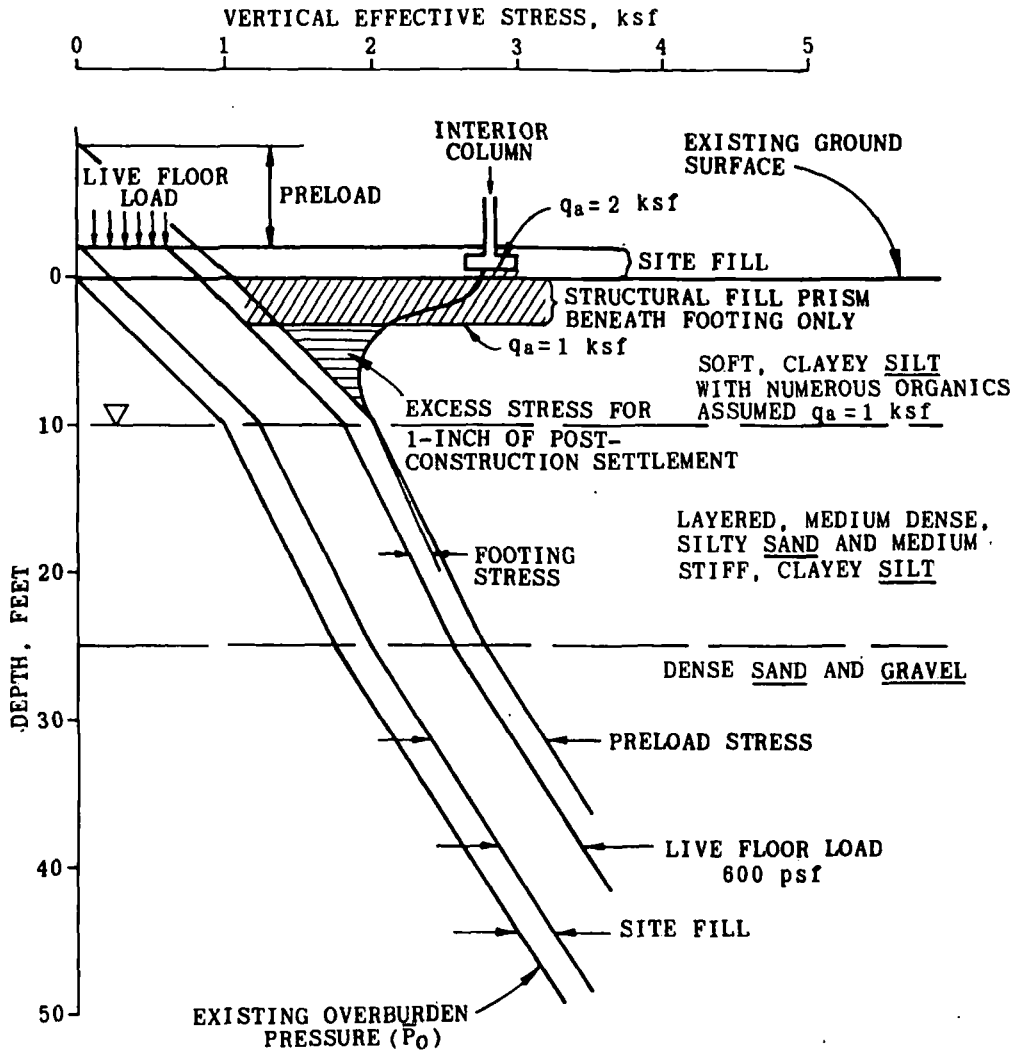
triaxial tests may be required to develop a strength envelope. Note that if the near-surface soils are variable across the proposed site, more than one series of tests may be required. This can become costly. Alternatively, soil samples could be obtained from borings, or test pits excavated to test strength by hand penetrometer, torvane, unconfined compression, etc., after the preload is removed. However, even with increased strength, settlement may control an allowable bearing pressure and should be checked.

With the majority of our preload designs, we establish the allowable soil pressure by the first method. We assume that net soil pressure for footings on compacted structural fill to be in the order of 1.5 to 3 kips per square foot (ksf), generally 1.5 to 2 ksf, and then size the footing from the column or wall load. Obviously the relatively low bearing pressure on the structural fill may mean a large footing, but the lower pressure generally causes less settlement in the underlying alluvium. Using the known footing size and bearing pressure, we estimate the stress on the alluvium for different thicknesses of structural fill. The stresses within the subsoils are determined by conventional methods (7). The required depth of over-excavation is to where the stress at the bottom of the compacted structural fill is equal to or less than the allowable soil pressure of the alluvium or to that depth where computed settlements are within a tolerable limit. It should be realized that the thicker the prism the less settlement, and as can be recognized later, the smaller the preload.

DETERMINING PRELOAD DIMENSIONS

Basically the preload serves three functions: first, to pre-settle the building site to reduce final building total and differential settlements to about an inch or less; second, to attempt to eliminate all primary consolidation and some secondary compression under final load (permanent site fill and live floor load); and third, to accomplish the first two within a relatively short time frame. Preload time-settlement will be discussed in a later section.

A method to reduce structural settlement to an inch or less is presented on Figure 1. Included is a stress profile with depth at the center of a typical warehouse. The soil conditions depicted on the figure are hypothetical and are for the purpose of discussion. The near-surface soft, clayey silt is assumed to have a relatively low shear strength. A structural fill prism is shown beneath the footing only, in order to reduce the stress on the clayey silt. It is apparent from the stress distribution that the prism also reduces footing settlement. The prism thickness can be varied to decrease settlements. However, this depth would depend upon the cost of over-excavation, backfill, compaction and dewatering. The combination of the floor live load, assumed to be 600 pounds per square foot (psf), and interior footing load could cause substantial settlement. Assuming that these settlements are intolerable, preloading would then be required. The preload would be designed to eliminate most of the settlement, except for about an inch or less. This is illustrated on Figure 1. If column spacings are sufficiently wide, pyramids of fill could be designed and placed above the surcharge for the floor load at column locations to reduce footing settlements. Continuous wall footing surcharges could be designed similarly.



NOTE

WAREHOUSE IS ASSUMED TO BE LARGE, SUCH THAT STRESS FROM LIVE FLOOR LOAD DOES NOT DECREASE WITH DEPTH.

STRESS PROFILE - WAREHOUSE CENTER

FIGURE 1

A stress profile at the side midpoint of the warehouse is illustrated on Figure 2. The subsurface soil conditions are the same as on Figure 1. Normally a loading dock will be along at least one exterior side of the warehouse. In this case, the wall footing would be deeper than an interior footing and may possibly bear within the alluvium. For these deep exterior footings we normally recommend a lower allowable soil pressure than for interior footings, in order to develop less stress and less settlement. The stress caused by the same footing in Figure 1, with a soil pressure of 2 ksf, is plotted on Figure 2 for comparison purposes; with this higher soil pressure, more settlement and consequently more preload would be required.

Another difference at the side midpoint of a warehouse is that only one-half of the floor live load stresses the ground (flexible foundation assumed). However, if the preload were only to extend to the edge of the warehouse, only half of the stress would be effective and settlements greater than 1 inch could result from exterior footings. This is illustrated on Figure 2. Therefore, in order to provide more overstressing for the wall footing, the surcharge must extend beyond the building line or "overlap" the building line.

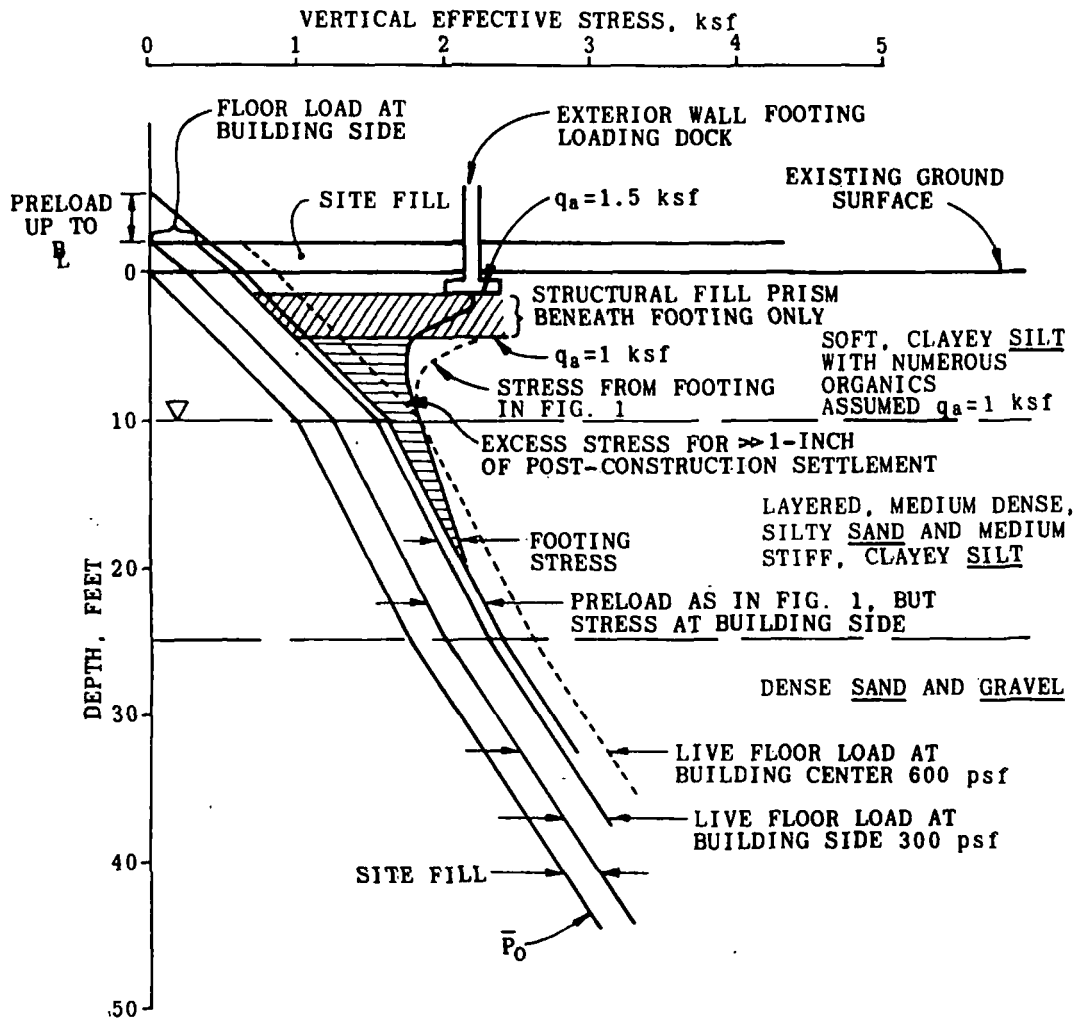
A method to determine the stresses from overlapping is illustrated on Figure 3. The method involves calculating the stresses with depth at the side of a strip for various widths of overlap B, and adding them by superposition (8) to the side of the warehouse. It should be noted that if compressible stratum is relatively deep, wide crest to crest overlaps could result.

As illustrated on Figure 4, a crest to crest preload overlap of about 10 feet would be required to reduce final building settlements to an inch or less.

The method illustrated on Figure 3 could also be applied to preloading a warehouse in sections, if the availability of preload material is limited or construction schedule is short. For instance, after a section of the site is preloaded, monitored and removed, construction could start while the other section is being preloaded. It has been our experience that if compressible soil is deep and the warehouse large, crest to crest overlaps in excess of 40 feet could result because the stress required near the center of the warehouse is higher than the side. Also, some soil would be stressed longer beneath portions of the overlap and cause more settlement. If particular sections of the warehouse carry different floor loads, various preload heights could be used. However, the section with a higher floor load will require some overlap.

INITIAL TIME-OF-REMOVAL ESTIMATE

Obviously, an important factor with a preload design is this question: how long would the site require preloading before the start of building construction? If the preloading time is too long, the site may be deemed unsuitable. Also, if the approximate length of time needed for preloading is not

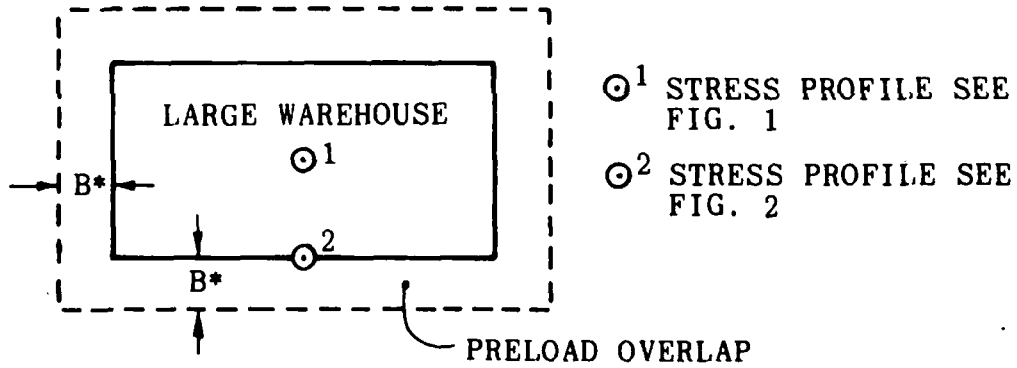


NOTE

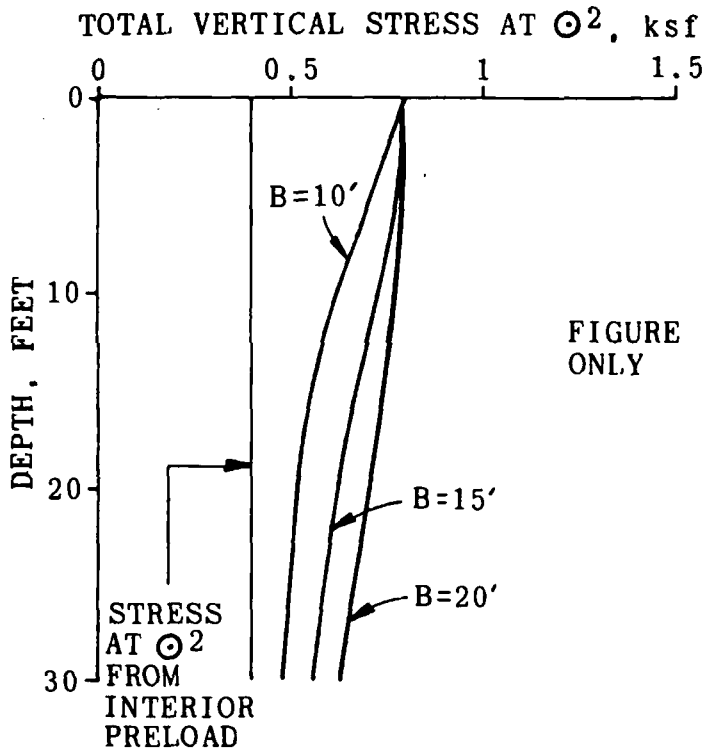
WAREHOUSE IS ASSUMED TO BE LARGE, SUCH THAT STRESS FROM LIVE FLOOR LOAD DOES NOT DECREASE WITH DEPTH.

STRESS PROFILE - WAREHOUSE SIDE MIDPOINT

FIGURE 2



FOR EXAMPLE: PRELOAD = 800 psf



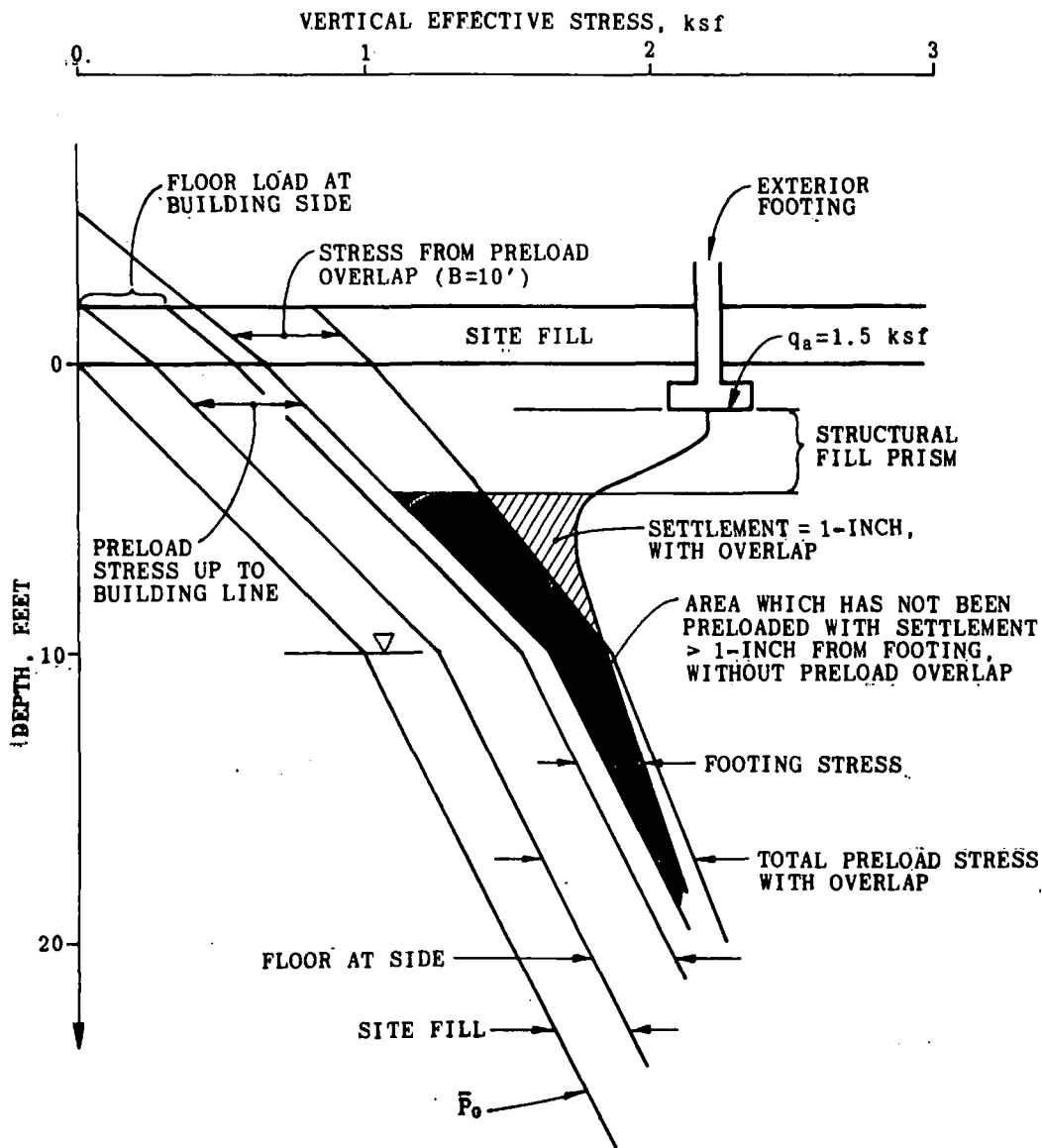
NOTE

FIGURE IS ILLUSTRATIVE ONLY

*THE LENGTH OF B IS DEPENDENT UPON THE DEPTH OF COMPRESSIBLE SOIL AND SIZE OF WAREHOUSE.

PRELOAD OVERLAP

FIGURE 3



STRESS PROFILE AT WAREHOUSE SIDE WITH PRELOAD OVERLAP.

FIGURE 4

A Simplified Preload Design

By Thomas M. Gurtowski and Thomas E. Kirkland

Page 9

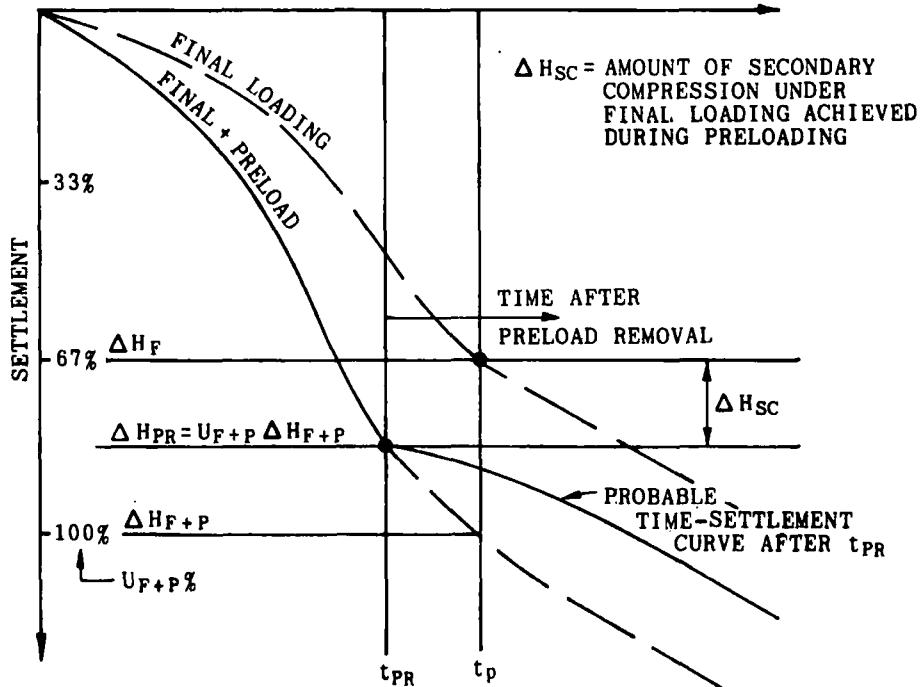
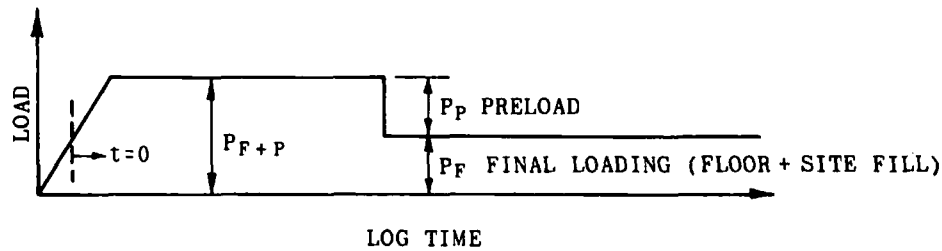
judged correctly, a site may not be ready when construction is scheduled to begin. However, with suitable evaluation made beforehand, the preloading time could be shortened when desired by adding more preload.

With reference to Figure 5, a design time-of-removal estimate for our purposes means evaluating the time at which a specific degree of consolidation (U_{F+P}) would occur under the final and preload fill (P_{F+P}) which would eliminate all primary consolidation and some secondary compression of the design final loading. The design final loading consists of permanent site fill plus live floor load (PF). With this specific degree of consolidation, an estimate can then be made for the time-of-removal. These estimates are possible if certain items are known or determined by testing, such as: 1) the coefficient of consolidation compatible with the maximum effective stresses to be imposed; 2) pore pressure distribution; and 3) layer thickness and length of drainage paths. Without these items, an estimate of time is primarily a guess, although experience in an area can provide a satisfactory estimate for the time-of-removal.

A method to estimate time of removal is presented on Figure 5. This figure was adopted from Johnson, 1970 (3) and is presented elsewhere (2). As shown, at the time of preload removal, (t_{PR}), all primary and some secondary settlement under final load (PF) had been eliminated. Note that the time to the end of primary consolidation (t_p) is assumed to be the same under the final load and final plus preload. An equation to estimate the degree of consolidation and hence, time-of-removal, under final plus preload is presented on the figure. Symbols in this equation, not defined on Figure 5, are as follows: \bar{p}_0 - existing overburden pressure, e_0 - void ratio in situ, t_{SEC} - time to completion of specific amount of secondary compression, C_c - compression index, C - coefficient of secondary compression. It is apparent from this equation that the degree of consolidation can be varied with the amount of preload (e.g., more preload less time). When estimating preload time-of-removal for a warehouse, at least one log cycle of time for secondary compression (t_{SEC}) should be compensated. The preload as recommended in the previous section should be considered a minimum surcharge. With this minimum surcharge, a rough estimate of the time-of-removal can be made.

One limitation of this method is that the shape of the time-settlement curve, after the preload is removed, is not usually evaluated by standard consolidation testing. Special, long-term testing would be needed, using the proposed design loadings. In addition, it has been our experience that the in situ rate of secondary compression is generally greater than determined from short-term oedometer tests. Consequently, the actual rate from settlement plate readings during preloading should be used to estimate future settlements.

With respect to our experience in the Seattle area, we have found that preloads should remain at full height on typical warehouse sites for a period of about 1 to 3 months.



- | | |
|--|---|
| t_{PR} - TIME OF PRELOAD REMOVAL | ΔH_F - PRIMARY SETTLEMENT (CONSOLIDATION) UNDER FINAL LOADING |
| t_p - TIME TO END OF PRIMARY (ASSUMED TO BE EQUAL FOR FINAL & FINAL + PRELOAD) | ΔH_{F+P} - PRIMARY SETTLEMENT UNDER FINAL + PRELOAD |
| U_{F+P} - DEGREE OF CONSOLIDATION UNDER P_{F+P} | ΔH_{PR} - SETTLEMENT AT FINAL + PRELOAD REMOVAL |

INITIAL PRELOAD TIME-OF-REMOVAL ESTIMATE

(AFTER JOHNSON, JANUARY 1970 (3))

EQUATION TO DETERMINE A DEGREE OF CONSOLIDATION (U_{F+P}) AT THE CENTER OF THE COMPRESSIBLE LAYER UNDER FINAL + PRELOAD LOAD (2):

$$U_{F+P} \text{ LOG } \left[1 + \frac{P_F}{P_0} \left(1 + \frac{P_P}{P_F} \right) \right] = \left[1 - C_\alpha \text{ LOG } \frac{t_{SEC}}{t_p} \right] \text{ LOG } \left(1 + \frac{P_F}{P_0} \right) + \frac{C_\alpha}{C_c} (1 + e_0) \text{ LOG } \frac{t_{SEC}}{t_p}$$

FIGURE 5

A Simplified Preload Design

By Thomas M. Gurtowski and Thomas E. Kirkland

Page 11

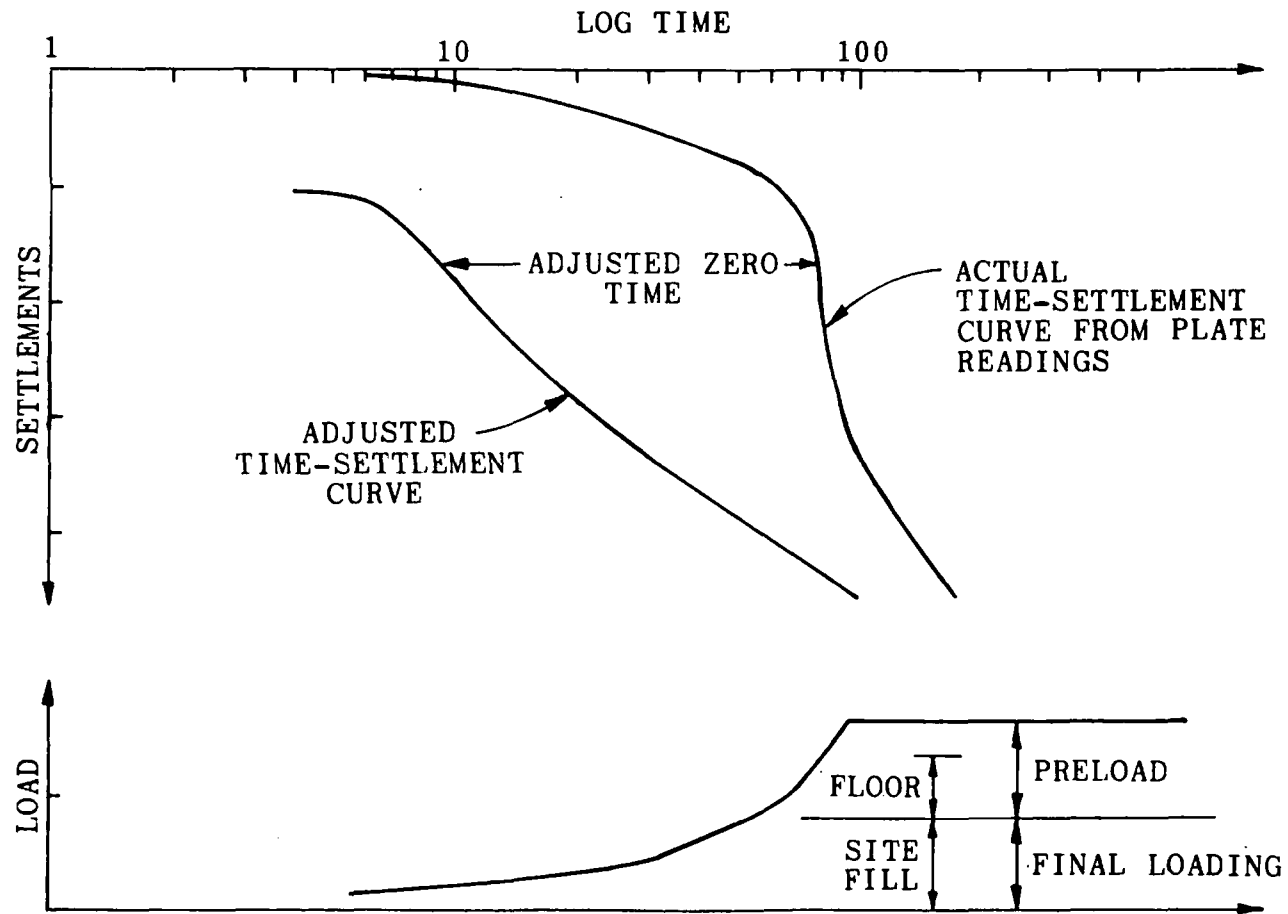
POST-CONSTRUCTION SETTLEMENT ESTIMATES

One of the most important aspects of preload projects is monitoring settlement plates during filling and preloading. The plates should be located strategically, such as near the center, sides, and corners of the preloaded area. If settlement plates are not constantly maintained and measured during filling and preloading, post-construction settlement estimates and the time of preload removal cannot be accomplished.

We determine the time of preload removal from the settlement plate readings. The preload is removed when settlements indicate a linear rate when plotted on a log time scale. This log time is adjusted, and then used to estimate post-construction settlements.

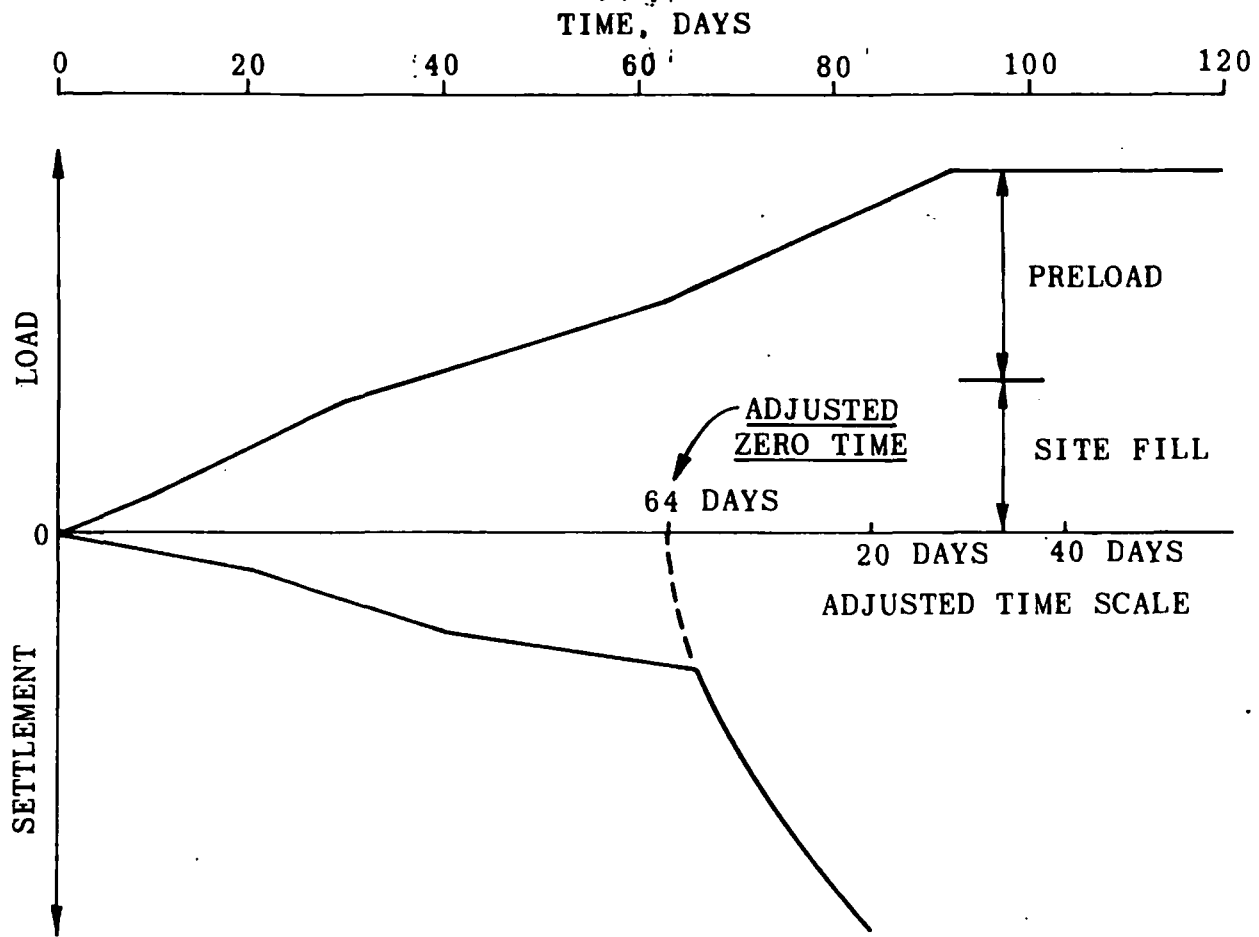
In order to theoretically predict post-construction settlements, a correction should be applied to the actual settlement plate readings to account for the gradual application of loads. The general theory of consolidation assumes instantaneous loading, so that an adjusted zero time is required. Various methods of determining this correction are available (2, 3, 8, 9). An approximate, simplified method is presented herein. The results of typical settlement plate readings before the preload was removed are presented on Figure 6. Two time-settlement curves are shown - actual and adjusted. Figure 7 illustrates the approximate method of determining an adjusted zero time. The same settlement plate readings from Figure 6 are plotted on an arithmetic scale as shown on Figure 7. The adjusted zero time is approximate by drawing a continuous curve up to the actual time scale. This time is the adjusted zero time. As shown on Figure 6, the actual plate readings are then shifted left to develop the adjusted time-settlement curve. This adjusted curve is then used to estimate the post-construction settlements.

As mentioned, when the adjusted log time-settlement curve develops a linear relationship, post-construction settlements can be estimated. Note that for this relationship the degree of consolidation for the final load and preload (U_{F+p}) is assumed to have reached 100 percent and secondary compression is assumed to develop. An approximate method for estimating post-construction settlements is illustrated on Figure 8. For this example, it is assumed that the site is raised with fill to support the floor slab (site fill). At the time of preload removal (t_{PR}), the settlements for the site fill only ($PF - floor$), and site fill plus floor live load (PF) are assumed to be directly proportional to the total settlement (ΔH_{PR}) from the site fill plus preload ($PP + PF$). From these estimated settlements, log time-settlement lines are drawn parallel to the developed adjusted curve. Where they intersect the total settlement (ΔH_{PR}), a construction period correction is applied as shown. From this, the post-construction settlements are estimated. It is apparent from this figure that the longer the preload remains on the site, the lower the post-construction settlements will be, since the estimated time zero would be shifted further right on the log time scale.



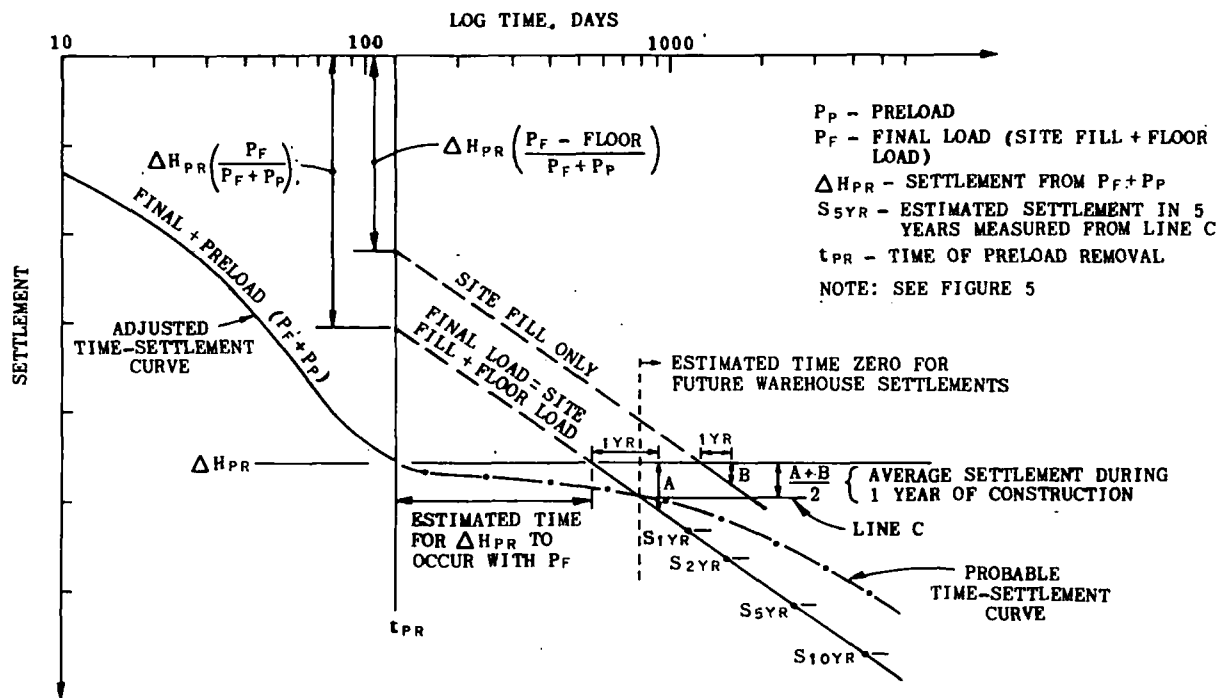
ACTUAL AND ADJUSTED TIME - SETTLEMENT CURVES

FIGURE 6



APPROXIMATE METHOD TO DETERMINE ADJUSTED ZERO TIME

FIGURE 7



ESTIMATING POST - CONSTRUCTION SETTLEMENTS

FIGURE 8

The assumption that these design load curves are parallel to the actual adjusted time-settlement curve is probably conservative. The probable time-settlement curve is expected to be as shown on Figure 5 and 8. The initial decrease would be due to the stress reduction from the higher preload surcharge to the actual building load (3). The compressible layer would be in effect over-consolidated after the preload is removed. With time, however, the rate of secondary compression is expected to increase and become parallel to the original secondary rate. Data presented by Mesri and Godlewski, 1977 (4) indicate that for an over-consolidated deposit, secondary compression increases with time. Considering the non-homogeneity of typical alluvial deposits and the present state-of-the-art with respect to actual long-term settlement readings for preloaded sites, a more accurate prediction of the actual secondary rate after preload removal is not justified at this time. It would be more appropriate at this time to estimate post-construction settlements as illustrated and assume that after about 20 years the actual settlements would be about 3/4 of the estimated values.

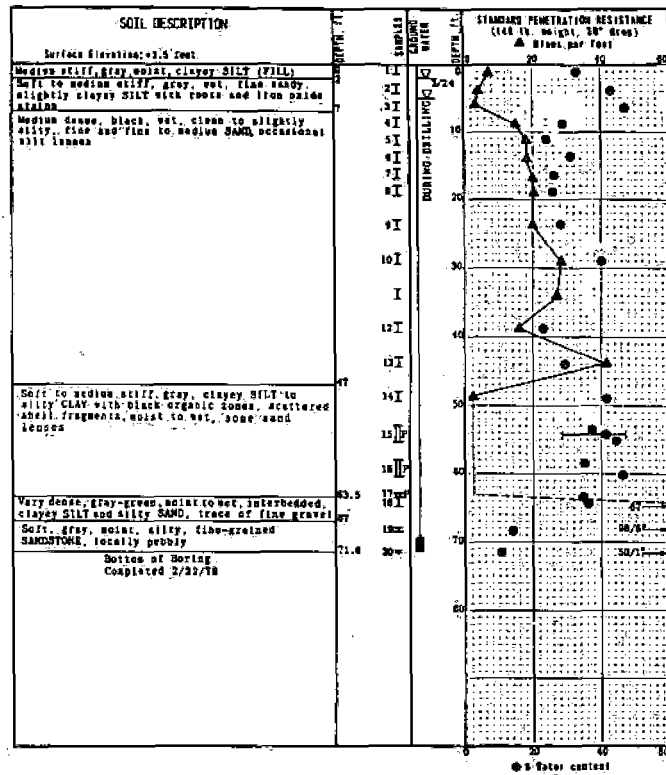
To further the current state-of-the-art for preload design, long-term building settlements should be maintained along with sufficient subsurface soil data including oedometer tests with long-term time-settlement relationships.

LIMITED PRELOAD DATA

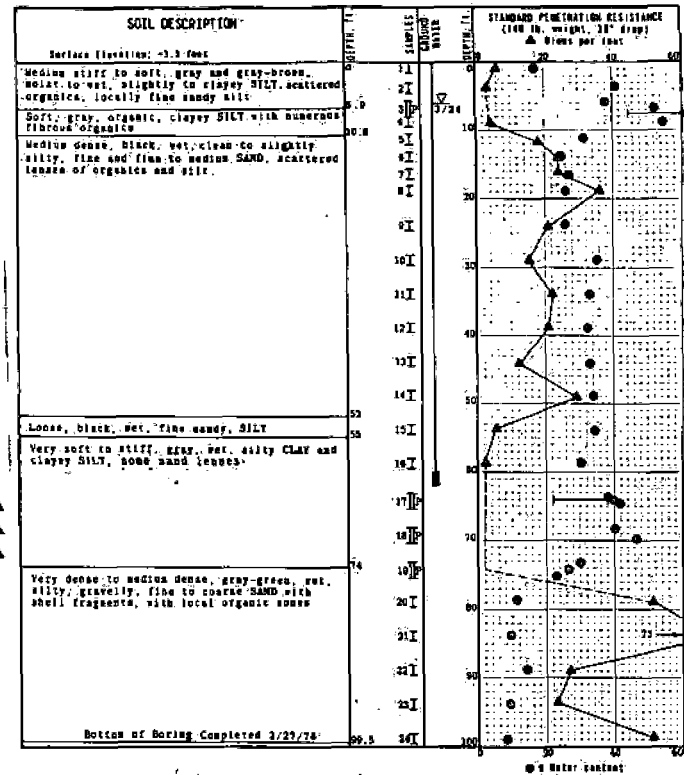
Limited results of two preload designs are presented. Limited implies that settlement plate readings were taken up to the time of preload removal. Settlement of the structures is not available since they are still under construction. Also, due to time limitations of the design phase, long-term oedometer time-settlement curves at various anticipated effective stress levels were not accomplished.

A client wished to construct a grocery storage and shipping warehouse approximately 360 by 810 feet in plan dimension. About 7 feet of structural fill was required within portions of the warehouse area to establish the grade desired for the slab-on-grade floor. The maximum live floor load for preload design was 750 pounds per square foot (psf). However, the post-construction settlements were estimated from an estimated average floor load of 400 psf. Some of the eastern and southern sections of the site were previously filled with rubble, which was removed prior to construction. The approximate locations of the rubble fill, the warehouse and the toe of the preload are shown on Figure 9a.

Three borings were accomplished for this project. Their relative locations and logs are presented on Figures 9a, 9b, 10a and 10b. Basically, the site consisted of three relatively distinct soil layers: an upper clayey silt to sandy silt with scattered fibrous organics, overlying fine to medium sand with local silt lenses, overlying clayey silt to silty clay with organic zones and shell fragments. The upper and lower cohesive soils were soft to medium stiff and the sand layer was generally medium dense with an average N-value



LOG OF BORING B-2



LOG OF BORING B-3

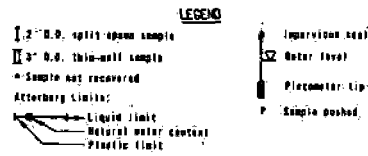


FIGURE 10a

FIGURE 10b

of around 20 blows per foot. A generalized subsurface profile is presented on Figure 11.

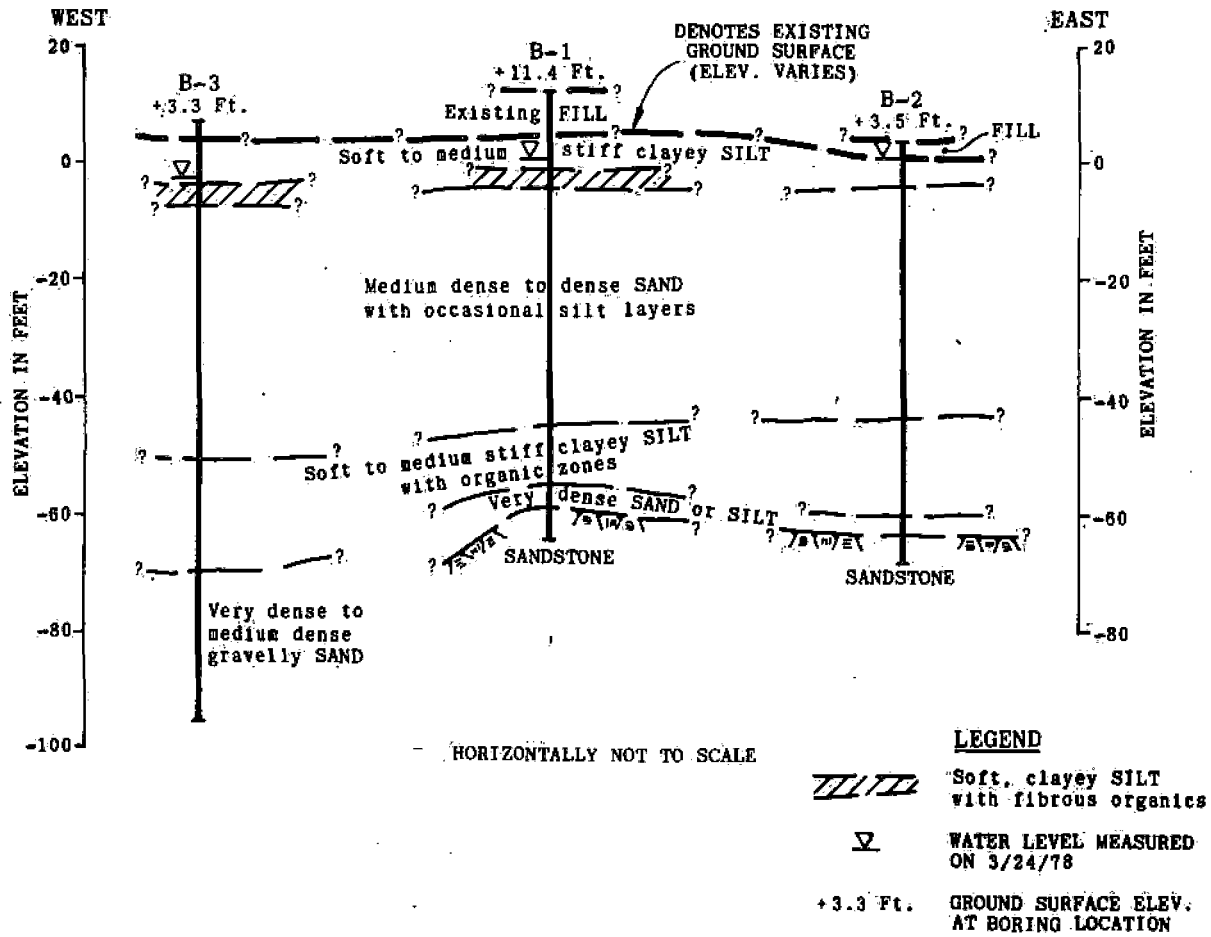
Four consolidation tests were accomplished on representative samples of cohesive soils. The results are presented on Figure 12. The variability of the physical characteristics of the alluvial deposits at this site is apparent from the range in compressibility indicated on the figure.

Considering the variable soil conditions at the site, as revealed by the borings and seven shallow backhoe test pits, the alluvium was estimated to have a minimum allowable bearing capacity of 800 psf before preloading. Without a structural fill prism, footing settlements were estimated to be greater than 1.5 inches for the structure load only, even neglecting settlements due to site fill and live floor loads. Consequently, interior and exterior spread footings were provided with a 4.5-foot thick prism of compacted structural fill and designed for an allowable net soil pressure of 2 ksf. An exterior loading dock continuous footing was designed for 1.5 ksf with a 3-foot thick structural fill prism. The decision was made to over-excavate and backfill any applicable footing pads during initial site grading and filling. In this regard, accurate locations for the excavations were necessary. This scheme was deemed more economical than excavating through all or part of the 7 feet of floor fill after the preload was removed.

Without preloading, untreated site settlements were estimated by using conventional one-dimensional consolidation theory based on the results of carefully conducted oedometer tests (Figure 12), and an assumed modulus for the middle sand layer. Total structure and floor settlements were estimated to range from 6 to 14 inches for the interior, 5 to 8 inches along the side, and 3 to 5 inches at the corner. Differential settlement possibilities were numerous. These settlements assumed that the site fill, foundations and live floor load would be applied within a relatively short time.

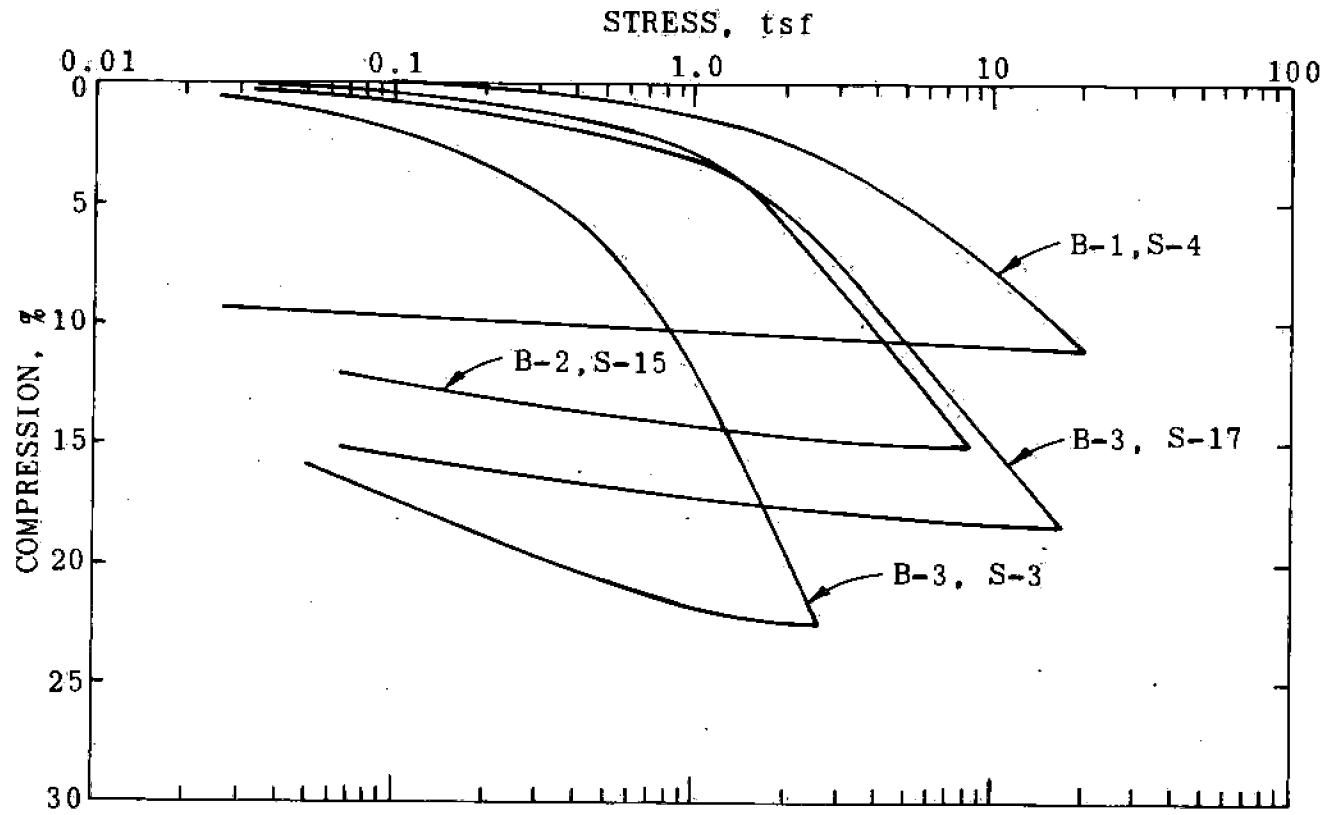
An 8-foot high preload fill, equivalent to about 1,100 psf, was designed and applied to the entire site as shown on Figure 9a, to reduce footing and floor differential settlements to approximately 1-inch. The crest of the preload was designed to overlap or extend beyond building lines by 15 feet with an exterior slope of 1 Vertical on 1.5 Horizontal. Based upon our experience with similar soils and projects, and a rough approximation using the method previously described, a minimum preload period of 2 months at full height was estimated.

The results of the settlement plate readings are presented on Figure 13. As shown the total settlement at the various settlement plates ranged from 3.5 to 12.8 inches. The agreement with the untreated site settlement estimates was excellent. It took a month to remove the preload and it remained on the site at full height for about 3 months instead of the estimated 2 months. As illustrated on Figure 13 this longer period was required in order to develop a linear log time-settlement curve for estimating post-



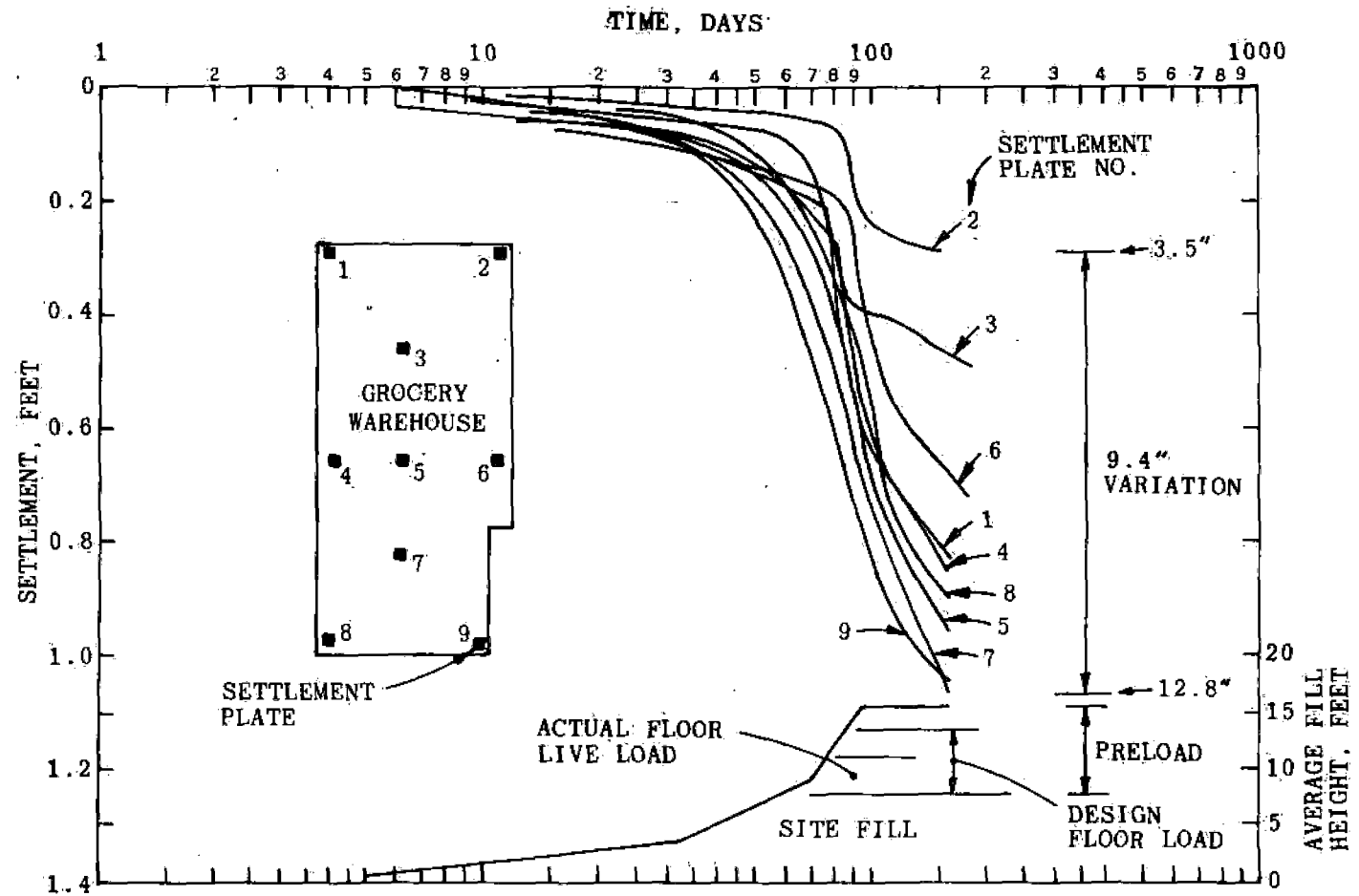
GENERALIZED SUBSURFACE PROFILE

FIGURE 11



CONSOLIDATION TESTS

FIGURE 12



ACTUAL SETTLEMENT PLATE READINGS
 GROCERY WAREHOUSE

FIGURE 13

A Simplified Preload Design

By Thomas M. Gurtowski and Thomas E. Kirkland

Page 22

construction settlements. As shown, plates 2, 3, 6, 1 and 4 started to develop a linear trend after about 40 days at full preload height, but the other plates took longer. It was decided to remove the preload after adjusting all curves and estimating future settlements, after about 80 days of preloading.

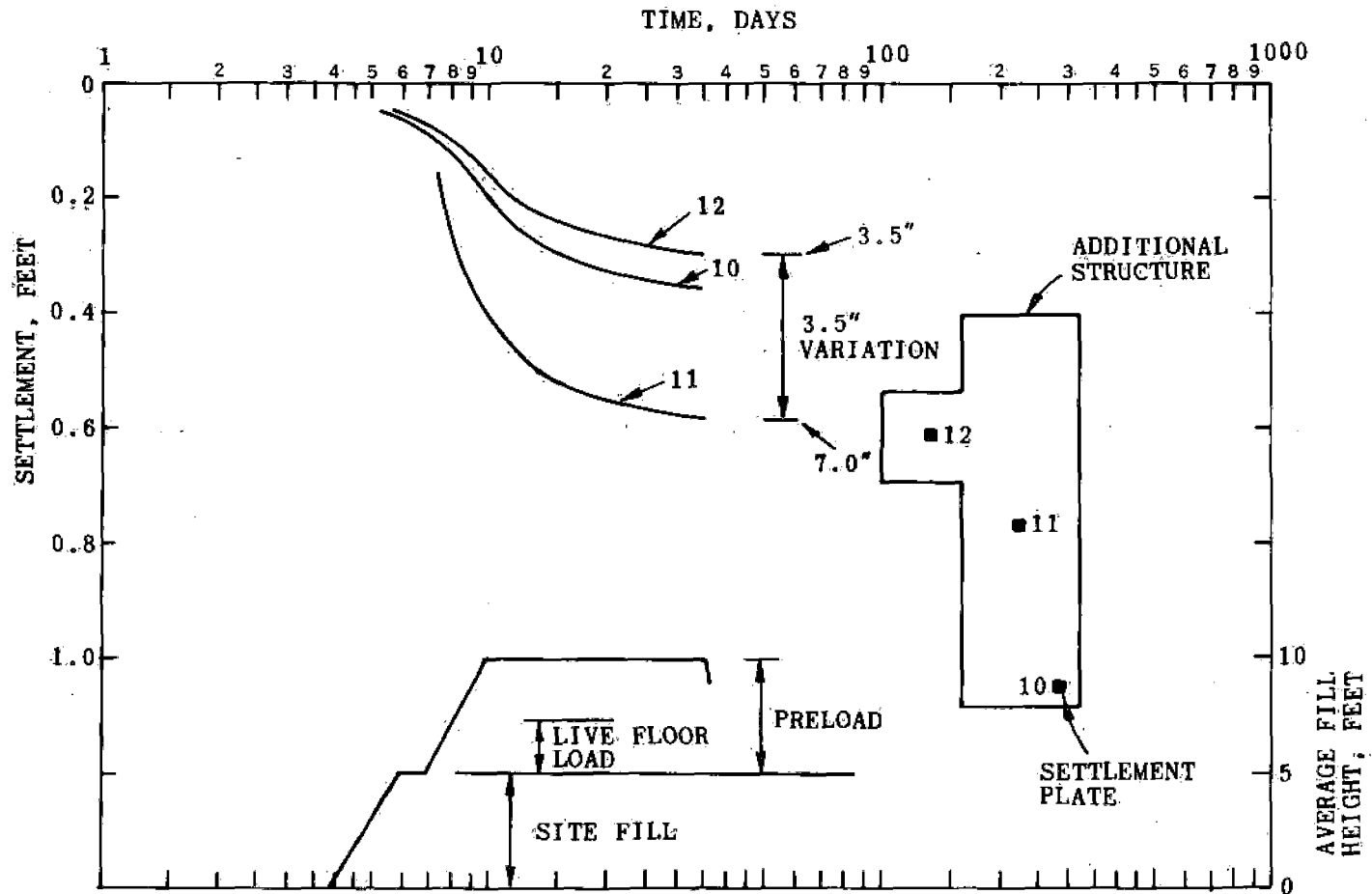
After an estimated one year of construction and floor loading, we estimated that settlements could vary at plate locations from 1/2 to 1 1/2 inches. This includes footing settlement. Twenty years after completion, total area settlements could vary from 1 to 6.5 inches. In other words, the entire site would settle in a dish-shaped pattern. Although this area settlement would seem intolerable, the maximum differential footing settlement with 40-foot bays would be less than about 1 1/2 inches, as determined for the two plates (3 and 5) which showed the maximum difference in estimated settlement after 20 years.

Another structure was also preloaded near the grocery warehouse. A brief summary follows. The building is 60 by 205 feet in plan dimension with a 300 psf floor live load. Soil conditions at this site were similar to the grocery warehouse. Untreated site settlements were estimated to vary from 3.5 to 7.5 inches. The preload was overlapped 10 feet beyond the building lines. The site was preloaded with 5 feet of fill (675 psf) for 26 days. Settlements measured from three plates ranged from 3.5 to 7 inches at the time of preload removal. The results of the settlement plate readings are presented on Figure 14. Post-construction total settlements were estimated to vary from 3/4-inch after 2 years to 2 inches after 30 years. Differential settlements were estimated to be about 1.3 inches along 60 feet in 30 years.

CONCLUSIONS

Preloading is an effective means to provide foundation support for a relatively large, moderately loaded warehouse, upon what may appear to be an otherwise unsuitable site. The procedures described for designing a preload indicate that:

1. Proper footing sizes, allowable bearing pressures and thickness of structural fill beneath a footing is an effective means of supporting structures on loose and/or soft compressible soil after preloading.
2. A preload should be designed to reduce future footing differential settlements to about an inch. Also, the preload should overlap the building lines if the exterior footing settlements have not been compensated by the interior preload fill.
3. Approximate preload time-of-removal estimates and adjustments thereof, can be made if the engineer has confidence in his data. Past experience with similar soils would be more effective.



ACTUAL SETTLEMENT PLATE READINGS
 ADDITIONAL STRUCTURE

FIGURE 14

A Simplified Preload Design

By Thomas M. Gurtowski and Thomas E. Kirkland

Page 24

4. Preloads must be monitored effectively with a sufficient number of settlement plates in order to determine actual preload settlements, time for removal and to estimate future building settlements.

5. The actual preload time-of-removal should be determined after the settlement plate readings develop a linear log time-settlement curve and the estimated post-construction settlements are tolerable.

6. A simplified approximate method to estimate post-construction settlements is proposed. Long-term settlement records of structures on preloaded sites should be maintained to evaluate the proposed method and further the current state-of-the-art.

REFERENCES

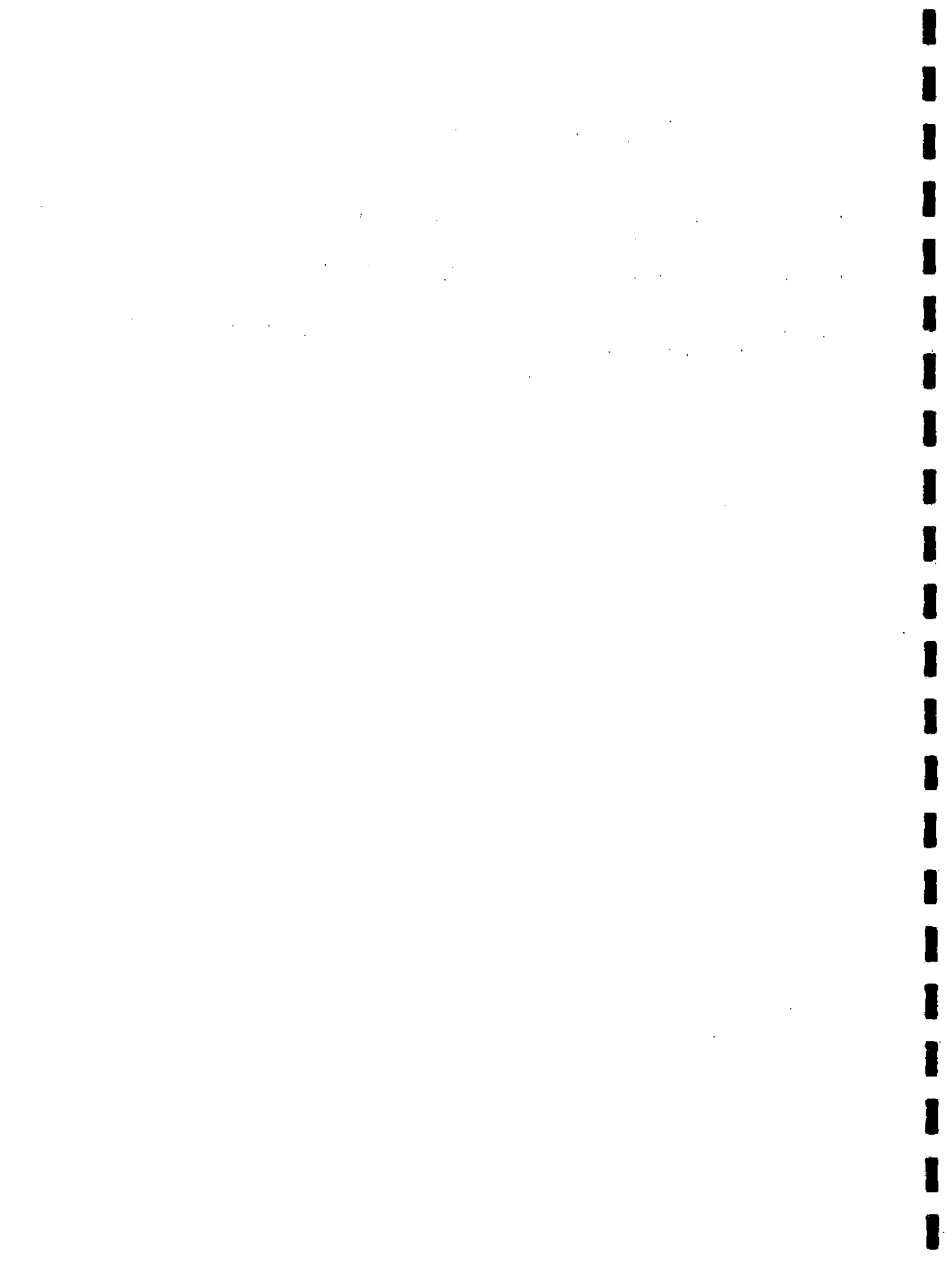
- (1) Bowles, J.E., - Foundation Analysis and Design, 2nd Edition, McGraw-Hill, New York, 1977, pp. 159-165.
- (2) Department of the Navy, Bureau of Yards and Docks, - "Soil Mechanics - Foundations and Earth Structures," Design Manual Navdocks DM-7, 1974.
- (3) Johnson, S.J., - "Precompression for Improving Foundation Soils," Journal of the Soil Mechanics and Foundation Division, ASCE, Vol. 96, No. SM1, January 1970.
- (4) Mesri, G. and Godlewski, P.M., - "Time-and Stress-Compressibility Interrelationship," Journal of the Geotechnical Engineering Division, ASCE, Vol. 103, No. GT5, May 1977.
- (5) Mitchell, J.K., and Gardner, W.S., - "In-Situ Measurement of Volume Change Characteristics," Proceedings of the Conference on In-Situ Measurement of Soil Properties, ASCE, North Carolina State University, Raleigh, N.C., 1975, Vol. 2, pp. 279-345.
- (6) Peck, R.B., Hanson, W.E., and Thornburn, T.H., - Foundation Engineering, 2nd Edition, John Wiley and Sons, New York, 1974, pp. 93.
- (7) Poules, H.G., and Davis, E.H., - Elastic Solutions for Soil and Rock Mechanics, John Wiley and Sons, New York, 1974.

A Simplified Preload Design

By Thomas M. Gurtowski and Thomas E. Kirkland

Page 25

- (8) Taylor, D.W., - Fundamentals of Soil Mechanics, John Wiley and Sons, New York, 1948, pp. 290.
- (9) Terzaghi, K., - Theoretical Soil Mechanics, John Wiley and Sons, New York, 1943.
- (10) Terzaghi, K., and Peck, R.B., - Soil Mechanics in Engineering Practice, 2nd Edition, John Wiley and Sons, New York, 1967.



ACTIVE FAULT ZONES AND REGIONAL SEISMICITY IN WESTERN NEVADA

By

David K. Rogers¹, David B. Simon² and John Stellar³

ABSTRACT

The majority of active faulting in Western Nevada occurs along several, relatively wide structural zones. These consist of three major geomorphic and tectonic elements of the region (the Sierra Nevada frontal fault system, the Fairview-Dixie Valley fault zone, and the Walker Lane fault zone), and several minor transverse structural elements of the region (the Truckee-Olinghouse fault zone; the Carson Lineament, the Yerington-Rawhide Lineament and the Mono Basin-Excelsior Mountains structural zone). Along the various fault zones, photogeologic interpretation of recent low altitude, low-sun angle aerial photography, high altitude color IR and RADAR imagery reveals numerous, previously undetected fault segments displacing Quaternary alluvium and older bedrock. Comparisons of scarp morphology between the various fault zones suggest that the transverse zones have the least amount of activity. Maximum credible earthquakes in the range of 7.1 to 7.3 can be expected to occur along the major active fault zones while the minor, transverse fault zones are capable of generating 6.5 to 6.7 magnitude earthquakes.

INTRODUCTION

This paper summarizes the results of a comprehensive literature review and remote sensing analysis in Western Nevada. Field verification, and the remote sensing analysis covered two study areas at a scale of 1:250,000 consisting of more than 9,200 square kilometers which included four detailed areas at a scale of 1:12,000 covering about 4,500 square kilometers. The literature review, tectonic model, and remote sensing areas are within a circular regional study area 320 kilometers in diameter. Many of the features identified in the remote sensing analysis have been verified in the field.

The types of remote sensing imagery analyzed included computer-enhanced LANDSAT scenes, high-altitude color infrared photography, Side-Looking Airborne Radar (SLAR), and low-sun angle black and white photography. The fundamental results of the imagery analysis are:

- 1) the location of previously unmapped faults,
- 2) the location of the boundaries of the active portions of major fault zones, and

¹ Converse-Ward-Davis-Dixon, San Francisco, California

² Harding Lawson Associates, Reno, Nevada

³ Converse-Ward-Davis-Dixon, Pasadena, California

Active Fault Zones and Regional Seismicity
in Western Nevada

By David K. Rogers, David B. Simon and John Stellar

Page 2

- 3) the identification of lineaments that may or may not be associated with faulting.

For clarification, the term "lineation" as used in this paper is defined by O'Leary and others (1976) as a geomorphic feature:

"A lineament is a mappable, simple or composite linear feature of a surface whose parts are aligned in a rectilinear or slightly curvilinear relationship and which differs distinctly from the patterns of adjacent features and presumably reflects a sub-surface phenomenon."

TECTONIC SETTING

The two study areas are near the western edge of the seismically active Basin-and-Range Province. Figure 1 "Regional Geology," shows the location of the ranges (rock areas) and the basins (alluvium), and the boundaries of the Copper Valley and Churchill Butte study areas. Figure 2 "Regional Faults and Epicenters," shows the general location of major faults, fault zones and earthquake epicenters as discussed in this paper.

The western edge of the Basin-and-Range Province is dominated by structural relationships that are described by various writers, including Shawe (1955), Gilbert and Reynolds (1973), Steward (1973), Slemmons (1967), Wright (1976), and Slemmons and others (in press). Some of these relationships are:

- a) a region characterized by progressive extensional break-up of the Basin-and-Range Province that was initiated about 15 million years ago with the concomitant tilting and uplift of the Sierra Nevada to the west;
- b) a period of regional uplift that has been correlated by Atwater (1970) to the continental North America Plate overriding the East Pacific Rise with a change in tectonic style from compressional tectonics to one of extensional tectonics;
- c) three main geomorphic and structural elements of the region (the Sierra Nevada frontal fault system; the Fairview-Dixie Valley fault zone; and the Walker Lane fault zone (a right-slip fault system within the Basin-and-Range Province);
- d) several minor transverse structural elements of the region (the Truckee-Olinghouse fault zone, the Carson Lineament, the Yerington-Rawhide Lineament and the Mono Basin-Excelsior Mountains structural zone).

These structural elements, described in the following sections, can be grouped into three categories: fault zones that trend north-south, northwest and northeast.

Active Fault Zones and Regional Seismicity
in Western Nevada
By David K. Rogers, David B. Simon and John Stellar
Page 3

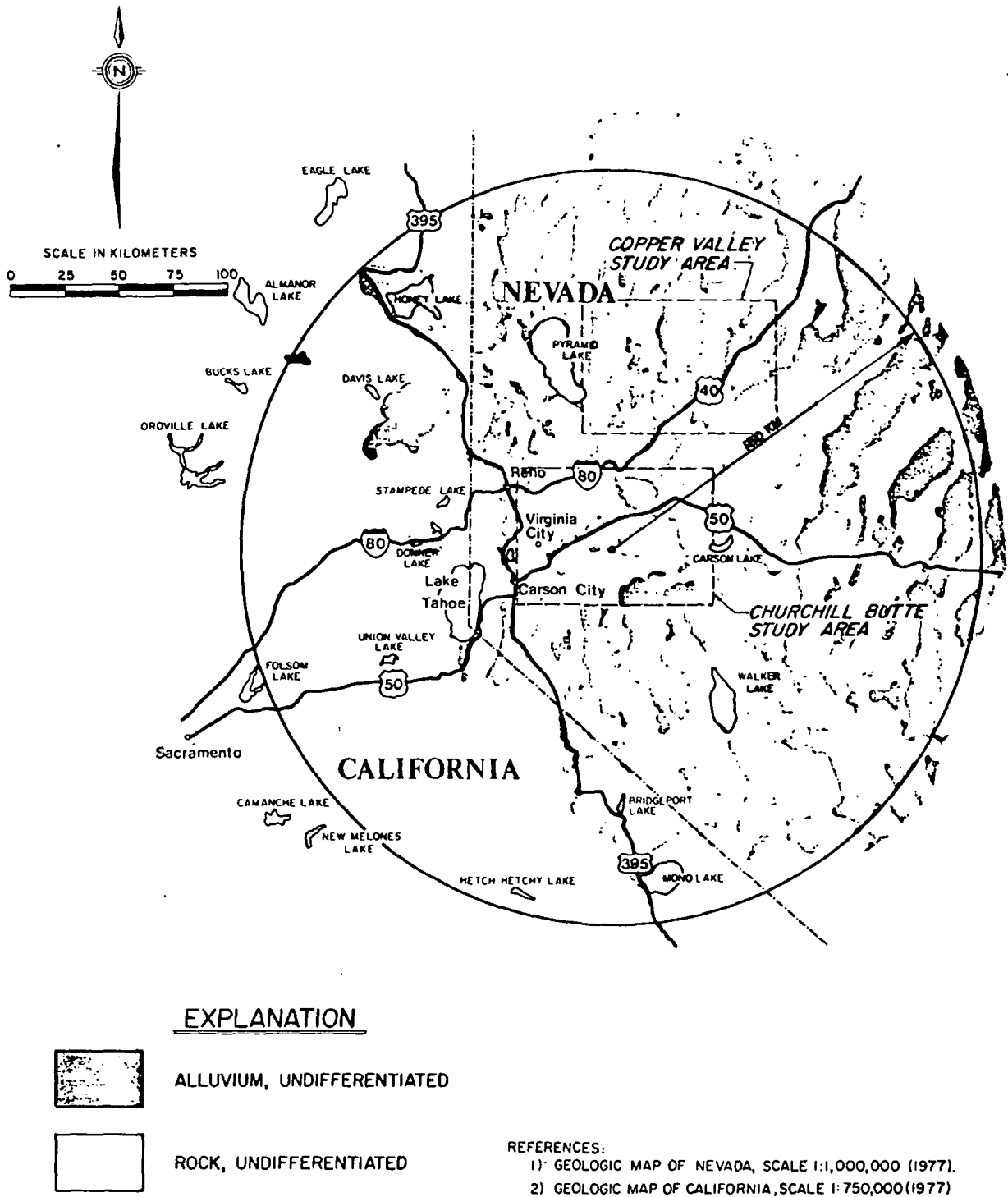


FIGURE 1 - Regional Geologic Map

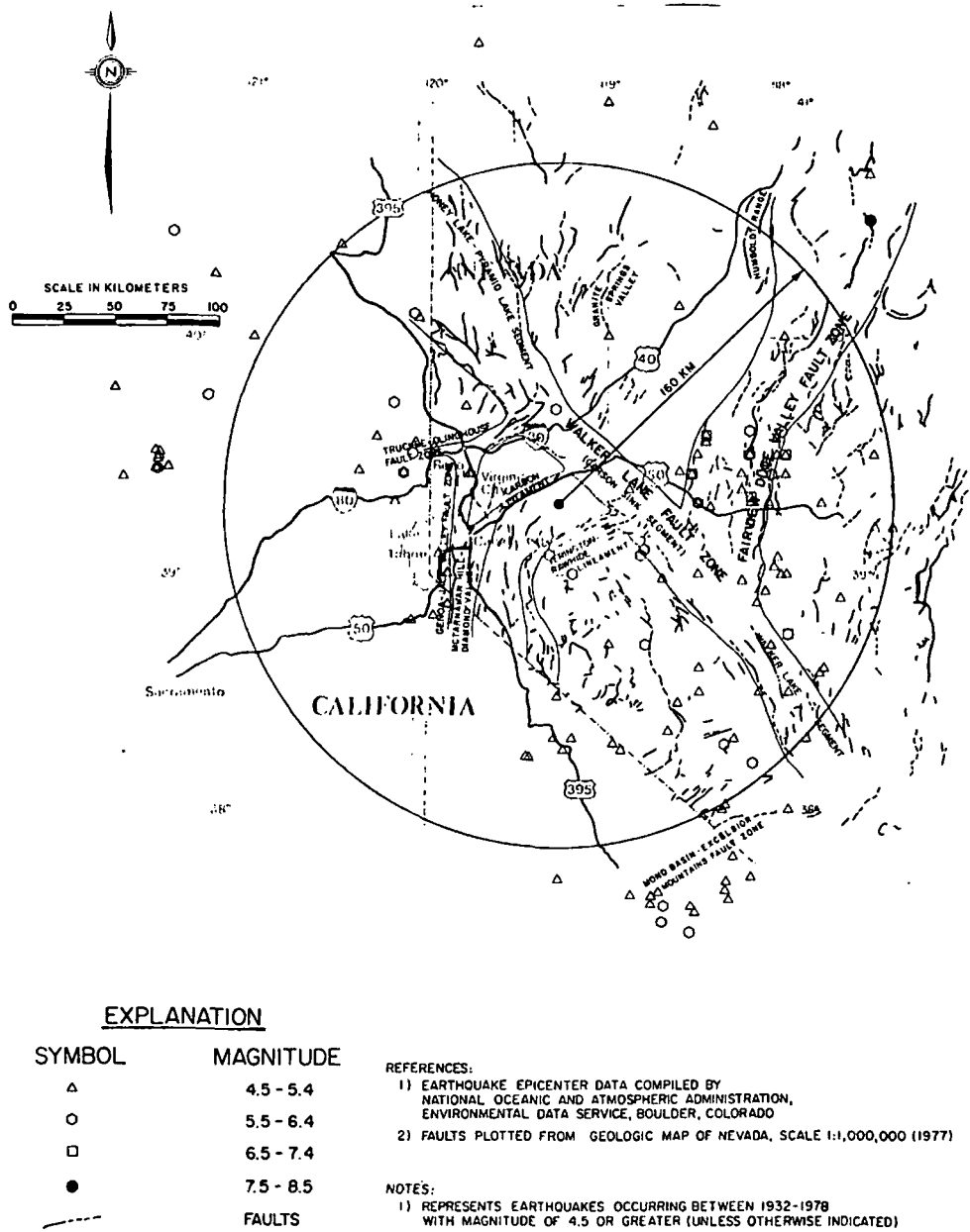


FIGURE 2 - Regional Fault and Epicenter Map

Active Fault Zones and Regional Seismicity
in Western Nevada

By David K. Rogers, David B. Simon and John Stellar
Page 5

North-South Trending Fault Zones

The north-south trending fault zones include the Genoa-Jack Valley, McTarnahan Hill-Diamond Valley, Fairview-Dixie Valley, and Granite Springs Zones of active faulting. These zones are described as follows:

a) Genoa-Jack Valley Fault Zone

The Genoa-Jack Valley fault zone is a north-trending, zigzag pattern of faults along the east side of the Carson Range. These impressive fault scarps along the eastern flank of the Sierra Nevadas can be followed from the community of Woodfords near U.S. Highway 88 northward where they splay into an en echelon pattern near the Mount Rose Highway, a few miles south of Reno, Nevada.

On the southern end, from Woodfords north to Stewart, an impressive fault scarp several thousand feet high overshadows the Carson Valley. At the base of this scarp is a recent fault scarp about 13 meters high and inclined 36° to 60° east (Moore, 1969). This recent scarp is clearly visible for about 16 kilometers northward to the town of Genoa. According to Moore (1969), the time of the formation of this scarp is very recent, yet it was present in 1854 when the first settlers arrived.

Aerial reconnaissance flights and imagery analysis show that the active fault traces of this zone are confined to a single fault along the east flank of the Carson Range except where it splays into broad northeast-trending patterns through Carson City and again towards the north near Reno, Nevada.

Northward from the town of Stewart, the faulting becomes more complex near Carson City. Rather than a single fault scarp, a pattern of en echelon, right-stepping fault scarps can be followed towards Lakeview Summit. Here the Hartford Hill Rhyolite Tuff (renamed by Bingler, 1977) has been displaced vertically about one kilometer since late Oligocene time (Lagenheim and Larson, 1973), about 20 to 28 million years ago (Silberman and McKee, 1974).

Stemmons and others (1977) believe that one-half of this deformation may have occurred within the last five million years.

North of Lakeview Summit, the east front of the Carson Range appears to be controlled by simple frontal faulting west of Washoe Lake. This normal faulting then splays into numerous, en echelon faults that displace alluvial fans near the Mount Rose Highway. Many of these fault scarps are multi-faceted (Cordova, 1969), suggesting recurrent movement in the recent geologic past.

Active Fault Zones and Regional Seismicity
in Western Nevada

By David K. Rogers, David B. Simon and John Stellar

Page 6

Greensfelder (1974) shows the Jack Valley fault with a maximum credible earthquake of 7.0 magnitude. Using fault length and displacement relationships by Slemmons (1977), the Genoa-Jack Valley fault zone may be capable of generating a 7.2 magnitude earthquake.

b) McTarnahan Hill-Diamond Valley Fault Zone

McTarnahan Hill is the northern boundary of a zone of north-south trending faults beginning near the California-Nevada border about 35 kilometers to the south. Numerous subdued and highly weathered north-south trending fault scarps are seen about 4 kilometers east of the Minden-Gardnerville area. Most of these normal faults are down-dropped to the east, having scarps several meters high. South of Hot Springs Mountain, several faults displace younger alluvium northeast of the Douglas-Tahoe airport. The McTarnahan zone appears much less active than the Genoa-Jack Valley zone; however, the sediments and alluvial materials forming the fault scarps weather faster than bedrock and other alluvial scarps along the Carson Range front. Presently, detailed studies of the fault scarp morphology south of Carson City are being conducted by Pease (1979).

Recent work by Van Wormer and others (1979) shows a clustering of microseismicity along north-south trends in the vicinity of the southern end of the McTarnahan-Diamond Valley Fault Zone. On September 4, 1978, an earthquake sequence began in Diamond Valley, California. The two largest events had a magnitude of 4.5 and 5.0 and were felt in the Carson Valley area.

The largest recorded event possibly associated with the McTarnahan Hill-Diamond Valley zone is a 5.0 to 5.9 magnitude earthquake with an epicenter just south of Gardnerville.

Based on worldwide relations of earthquake magnitude to length of the fault zone, individual fault rupture lengths within the zone and displacements compiled by Slemmons (1977), the McTarnahan fault zone may be capable of generating a 6.0 to 6.5 magnitude event. An estimated slip rate of 0.01 cm per year is assumed due to the lack of precise activity determinations.

c) Fairview-Dixie Valley Fault Zone

According to Coffman and Von Hake (1973), on December 16, 1954, two strong earthquakes of magnitude 7.1 and 6.8 were felt over a large area of the western United States.

Active Fault Zones and Regional Seismicity
in Western Nevada

By David K. Rogers, David B. Simon and John Stellar

Page 7

The earthquakes of December 16, 1954, were accompanied by offsets along segmented faults in four main zones of a larger north-trending belt 96 kilometers long by 32 kilometers wide. Minor geologic effects included: changed flow of springs and wells, formation of water fountains and craters, landslips, landslides, mudflows, and rockfalls, and secondary fracturing of unconsolidated sediments.

The fault displacements were mainly along normal, oblique-slip faults of the Basin-Range type in the following zones:

- west of Dixie Valley
- southeast of Dixie Valley
- east of Fairview Peak
- east of Stinger Valley

The maximum strike-slip component was 3.6 meters (right-lateral) at Fairview Peak, and the maximum vertical-slip component was about 3.6 meters at Bell Flat. Most of the faults are at or near the alluvium-bedrock contact.

Although east of the study areas, aerial reconnaissance flights were conducted in Dixie Valley to compare the recent fault scarp morphology with other fault zones and selected detailed study areas. In addition, a comparison of LANDSAT imagery of the Fairview-Dixie Valley Fault Zone and the study areas was made. The main frontal fault scarp along the west side of Dixie Valley is clearly visible due to high spectral reflectance in Band 7 of the LANDSAT scenes. Another major fault having similar LANDSAT reflectance and fresh scarp morphology was observed along the east side of Granite Springs Valley in Pershing County.

d) Granite Springs Valley Fault Zone

A striking fault scarp bordering the east flank of the Shawave Mountains can be observed on LANDSAT imagery, from aerial reconnaissance flights, and from the ground. The north-south trending fault begins near Copper Valley where alluvium is displaced in a left-stepping en echelon fashion and continues northward in a zigzag pattern for about 45 kilometers. Towards the northern end, the fault trends northeast, displacing alluvium. Field inspection of the fault shows the scarp to be inclined about 25° and down-dropped to the east. With the exception of a short northeast-trending fault in Copper Valley, no other faults in the area of Granite Springs Valley have fresh scarps or appear to be aligned with any of the active fault traces.

Active Fault Zones and Regional Seismicity in Western Nevada

By David K. Rogers, David B. Simon and John Stellar

Page 8

Using the state-of-the-art fault length-displacement and earthquake magnitude relationships compiled by Slemmons (1977), the fault along the west side of Granite Springs Valley may be capable of generating a 7.0 magnitude earthquake. An assumed slip rate of 0.01 cm per year is estimated for this fault.

Other north-south faults with fresh bedrock scarps or displacements in alluvium are located both west and east of Granite Springs Valley. Along the western and northeastern flanks of the Nightingale Mountains about 16 to 25 kilometers west of Granite Springs Valley, less defined fault scarps appear on the LANDSAT imagery. Apparently less active, the Nightingale Mountain faults may be capable of earthquakes in the same range as faults in Granite Springs Valley; i.e., about 7.0 magnitude. Wallace (1977, 1978) and Slemmons (1979) discussed a north-south trending frontal fault system along the west flank of the Humboldt Range which is located about 48 kilometers east of the Granite Springs Valley. The maximum credible earthquake associated with the faulting along the west flank of the Humboldt Range has been estimated by Wallace (1978) to be 7.3 magnitude.

Northwest Trending Fault Zones

The Walker Lane fault zone is a major, but discontinuous, right-slip fault zone of northwest trend in the western part of the Basin-and-Range Province (see Figure 2). It extends more than 640 kilometers from the Likely Fault in northeastern California to the Las Vegas shear zone near Las Vegas, Nevada. The main effect of this zone is to separate the north-northeast trending, long horst and grabens of the eastern Basin-and-Range Province from a series of irregular but partly northwest-southeast trending blocks of the western Basin-and-Range Province.

The zone has approximately 48 kilometers of cumulative right-slip offset during the last 22 million years (Hardyman and others, 1975). The zone appears to become more distributed in northern California (Pease, 1969). Fault segments, lying within the Walker Lane are the Honey Lake-Pyramid Lake, Carson Sink and Walker Lake Segments. These are described as follows:

a) Honey Lake-Pyramid Lake Segment

As reported by Bell and Slemmons (1977), the following conclusions relating to the Honey Lake-Pyramid Lake fault segment (shown on Figure 2) are:

Active Fault Zones and Regional Seismicity
in Western Nevada

By David K. Rogers, David B. Simon and John Stellar

Page 9

- 1) The site-specific diagnostic evidence of late Cenozoic strike-slip faulting includes: sag ponds, en echelon fault scarps, elongate depressions and troughs, offset stream channels vegetation alignments, transcurrent buckles, and rhomb- and wedge-shaped depressions.
- 2) The regional and site-specific major fault features disrupt late Pleistocene to Holocene and, possibly, historic deposits and landforms.
- 3) The fault zone has a similar orientation to the San Andreas fault system and displays right-lateral strike-slip displacements.
- 4) The active portion of the fault zone has a maximum observable width of 4 to 5 kilometers and a maximum observable length of 60 kilometers. The Pyramid Lake lineament suggests a projection of the fault zone approximately 30 kilometers to the southeast, or 90 kilometers total length.
- 5) The historic seismic activity in the vicinity of the fault zone includes microseismic events and several events of magnitude 4.0 to 5.9. The mid-1800's earthquake reported for the Pyramid Lake-Stillwater area and estimated to have had a Richter Magnitude of 7.0 may also be related to this zone. Reconnaissance examination of fault scarp morphology, however, suggests that displacements along the Pyramid Lake fault zone are neo-historic rather than historic.
- 6) Based on worldwide relations of earthquake magnitude to length of the zone of surface rupture, the fault zone is inferred to be capable of generating a 6.7 to 7.2 magnitude event for a half-length of approximately 30 kilometers.

An earthquake, which may be related to the Pyramid Lake fault zone, apparently occurred near Pyramid Lake in 1852 with an estimated Richter Magnitude of 7.0 (Stemmons and others, 1965). The location and date of occurrence of this event are based on Paiute Indian accounts of ground cracks, water spouts, and ground shaking observed in the Pyramid Lake and Carson Sink areas. Ryall (1977) reports a date of 1845 for the same earthquake and places the epicenter in the Stillwater area based on an 1869 Gold Hill News item indicating that the shock knocked down people in the Carson Sink area, that river banks were shaken down in the vicinity of Stillwater, and that the river changed its course.

A moderate earthquake of magnitude 5.2 occurred on February 22, 1979 in the southeast portion of Honey Lake Valley (Bryant, 1979). His-

torical seismicity of the Honey Lake region prior to 1900 includes a magnitude 6.0 in 1875, a magnitude 5.6 in 1885 and a 5.5 magnitude in 1889 near Susanville and Jamesville (Topozada and others, 1979). In 1950, a magnitude 5.6 earthquake occurred in the Fort Sage Mountains, producing up to 20 cm of ground displacement.

b) Carson Sink Segment

The Carson Sink segment (Figure 2) has many short faults of various orientations but has no single, through-going faults exposed at the surface. There are a few, short fault scarps of possible Holocene age. The lack of surface expression and evidence of activity of this segment may be related to the tectonic activity bypassing this section via the Fairview Peak, Dixie Valley and Carson Sink areas, or to detachment faulting of the type described by Hardyman and others (1975), for some of the Walker Lane branches in the Walker Lake area. The short active faults of this segment of the Walker Lane could have developed from earthquakes of 6.5 to 6.7 magnitude, with major deformation bypassed through the Carson Sink. If detachment faulting exists, this zone may be capable of generating a 7.3 magnitude earthquake, based on half-length relationships for continuous segments.

Although there are no single through-going faults exposed at the surface, the combined analysis of LANDSAT, Radar and color infrared imagery shows several long lineaments trending northwest within the Walker Lane. One lineament starts in the center of the Dead Camel Mountains and is nearly continuous for 40 kilometers in a northwest direction. Several other Radar imaged lineaments are aligned extensions of mapped faults and show continuous trends of up to 20 kilometers. Based on the Radar imagery and published geologic reports, the Carson Sink segment of the Walker Lane is about 22 kilometers wide between Fallon and Silver Springs.

Many of the Radar imaged lineations which are located within the Walker Lane or northeast of Reno or in the Virginia Range, are aligned with elongate, closed aeromagnetic contours (Nevada Bureau of Mines, 1977) or coincide with truncated aeromagnetic contours. This correlation suggests that many of the lineaments may be associated with basement faulting, particularly those lineaments located within the Walker Lane.

c) Walker Lake Segment

The Walker Lake segment is shown on Figure 2. The data of Hardyman and others (1975) indicate a total strike-slip separation rate of over 2 mm/yr. across the section of the Walker Lane opposite the Walker Lake segment. At least five major strands of the Walker

Active Fault Zones and Regional Seismicity
in Western Nevada

By David K. Rogers, David B. Simon and John Stellar

Page 11

Lane fault zone are present in the Walker Lake area, and the slip rates for individual branches are about 0.5 mm/yr., averaged over the last 22,000,000 years. Current rates have not been established but may be higher (Slemmons, 1978).

Transverse Northeast-Trending Fault Zones

The western Basin-and-Range Province is a region of conjugate active faults (Wright, 1976) with northwest-trending faults having right-slip displacements similar to the San Andreas fault system and northeast-trending faults having left-slip components similar to the Garlock fault zone. The mountains and valleys of this area are controlled by short horst and graben blocks or northerly trend and conjugate left-slip and right-slip faults of northwest and northeast trend, respectively. The strike-slip faults have cumulative displacements of up to a few kilometers. There are three main conjugate zones of northeast trend in the study area. They include:

- the Truckee-Olinghouse zone of approximately 96 kilometers length
- the Carson Lineament of approximately 56 kilometers length
- the Yerington-Rawhide zone of approximately 50 kilometers length

Two other conjugate zones of northeast trend outside and south of the study area include the Mono Basin-Excelsior Mountains structural zone (Gilbert and Reynolds, 1973) which includes the Candelaria Hills faulting described by Speed and Cogbill (1979).

The three main conjugate zones, illustrated on Figure 2 are described as follows:

a) Truckee-Olinghouse Fault Zone

The Truckee-Olinghouse fault zone is the more structurally prominent zone, with historic seismic activity. This zone has a series of en echelon northeast trending faults with up to 3.7 meters of left-slip offset on the Olinghouse fault of 1869 (Sanders and Slemmons, in press) and an associated 6.7 magnitude earthquake. The Olinghouse fault can be traced for most of its length from its geomorphic expression in the hilly terrain and is hidden only where overlain by recent alluvial sediments. Numerous features characteristic of strike-slip faulting can be observed along the fault, including: scarps, vegetation lines, sidehill and shutter ridges, sag ponds, offset stream channels and stone stripes, enclosed rhombohedral and wedge-shaped depressions, and en echelon fractures.

In the Truckee area where the 1966 magnitude 5.7 earthquake occurred, Van Wormer and others, (1979) found a zone of current seismicity distributed over a northeast-trending zone about 25 kilometers long. In their report, they state:

"This zone follows a structural low from Donner Pass through Donner Lake, then turns north through Bennett Flat northwest of Truckee, and continues to the northeast through a structural depression north of Prosser Hill to Hobart Mills. There the zone is spread in a northwest-southeast direction, which may be related to the aftershock zone of the 1966 earthquake. The fault that runs northeast from this epicentral zone is the one that ruptured in 1966; it passes through one of the abutments of Stampede Dam and continues through Hoke Valley and Dog Valley for another 10 km to intersect with the Last Chance fault."

b) Carson Lineament

The Carson Lineament has been referred to only briefly in the literature with regard to the regional Basin-and-Range tectonics by Shawe (1965), and Gilbert and Reynolds (1973). Shawe first named this major structural trend as the "Carson Lineament." The southwestern end of the Carson Lineament near Carson City and the community of New Empire have been investigated by Rogers (1975), and Trexler and Bingler (1977). The first comprehensive investigation of the entire length of the Carson Lineament was conducted by Simon and Mason (1978) under the direction of Dr. David B. Slemmons at the University of Nevada, Reno. Simon is presently conducting detailed analysis of scarp morphology along the Carson Lineament (personal communication, 1979).

There is no compelling geologic, geophysical or seismologic evidence for designating the Carson Lineament as a continuous fault zone. However, some evidence is suggestive that the discontinuous segments are seismogenic structures. The lineament was first discussed by Shawe (1965) mainly for its imagery and topographic character. The current status of evidence relating to the lineament, including geophysical and seismological evidence, is summarized under each topic below.

Geologic Evidence: The geologic map of Nevada (Stewart and Carlson, 1977) and the county maps of the Nevada Bureau of Mines and Geology covering the Carson Lineament show no evidence of a well-defined fault zone for either the Truckee-Olinghouse zone or the Carson Lineament. Both zones appear to change the overall pattern of distribution of geologic units to the north and south of each of these lineaments. The pattern and position of faults is changed; but the effect is a subtle, irregular one suggesting that the main effect is the presence of less granitic and metamorphic rocks in the area between the two lineaments.

Active Fault Zones and Regional Seismicity
in Western Nevada

By David K. Rogers, David B. Simon and John Stellar

Page 13

Faults of the Zone: The geologic mapping and the imagery analysis of this zone clearly show a dispersed and irregular pattern of young faults, with no through-going faults of lengths more than about 10 kilometers. The irregular pattern of short fault segments suggests that there is not a deep basement fault, or the basement fault is detached from the surface by horizontal or bedding plane detachment faults, or by plastic deformation and folding accompanying the faulting.

Seismicity: The historic seismic activity suggests a lower than normal seismicity along the zone. Recent work by Van Wormer and others (1979) shows that a cluster of epicenters located between 1970-77 lies east and northeast of Carson City in the northern end of the McTarnahan Hill-Diamond Valley zone. A few epicenters trend northeast along the Carson Lineament; however, the largest swarm of earthquakes in July, 1976 occurred near Virginia City, north of the intersection of the north-south-trending McTarnahan Hill-Diamond Valley zone and the Carson Lineament. Of additional interest is the lineament extension of several mapped faults based on the Radar imagery interpretation near the end of McTarnahan Hill-Diamond Valley zone and northward towards Virginia City.

Gravity Anomalies: The recent Reno Gravity Map (Erwin and Berg, 1977) shows a vague pattern that follows the Truckee-Olinghouse trend and the Carson Lineament. The gradients are broad and vague, suggesting that the effects of the three domains, north of the Olinghouse zone between the two lineaments and to the south of the Carson Lineament, are not sharp or major boundaries. The gravity data are not definitive but are suggestive of a non-fault origin for the Carson Lineament.

Aeromagnetic Anomalies: The recent Aeromagnetic Map for the Reno Sheet (Nevada Bureau of Mines and Geology Map 54) shows a similar vague pattern along the two main lineaments: the Truckee-Olinghouse and the Carson. Neither has major gradients that indicate the presence of shallow faults of any considerable length along these two zones, although lengths of up to about 10 to 15 kilometers are present. The data are not definitive but are suggestive of a non-fault origin for the Carson Lineament.

Although the Carson Lineament may not represent a through-going fault zone, the individual segmented faults have lengths up to 10 kilometers, suggesting a maximum credible earthquake magnitude of 6.2 to 6.5 (using Figure No. 27 of Slemmons, 1977).

The maximum earthquake for the Truckee-Olinghouse zone is assigned a value of 6.7, based on the 1869 earthquake. Due to similar tectonic features, the Carson Lineament is likewise assigned a maximum value of 6.7, with associated left oblique-slip offsets.

c) Yerington-Rawhide Lineament

A northeast trending zone of discontinuous faults, small intrusives, and major metallic ore deposits define a zone informally designated as the Yerington-Rawhide Lineament by Bingler (1971). The active portion of the structure, similar to the Carson Lineament, has a length of about 50 kilometers and passes just north of Wabuska (see Figure 2). The dominant active faults within the zone strike northeast, dip steeply north and have an exposed strike parallel to Churchill Canyon for at least 15 kilometers.

Essentially, the same geologic, aeromagnetic, gravity evidence for non-continuity that was discussed for the Carson Lineament can be applied to the Yerington-Rawhide zone. In addition, the lack of any micro- or macro-seismicity suggests the two zones may be tectonically similar.

Based on this preliminary analysis, the Yerington-Rawhide Lineament is assigned a maximum credible earthquake magnitude of 6.5.

SUMMARY OF REGIONAL FAULTING IN WESTERN NEVADA

Figure 2, "Regional Faults and Epicenters," shows the generalized location of the regional fault zones and the recorded epicenters from 1932 to 1978 for earthquake magnitudes of 3.8 and greater. Twelve historic earthquakes have associated surface faulting in the Basin-and-Range Province. The active fault zones listed in Table 1, as follows, were selected as those most likely to influence a planned facility within the study area. To clarify definitions, an active fault, as defined in this paper, is "one that can be shown to exhibit displacement at or near the ground surface at least once within the past 10,000 years; i.e., Holocene displacement."

The maximum credible earthquake for a particular fault, as defined in this paper, is the largest magnitude event which can be reasonably postulated to occur, based upon existing geologic and seismologic evidence. Note: the maximum credible earthquakes may not include the maximum possible earthquake because the known geologic framework may not be complete.

CONCLUSIONS

The combined use of special LANDSAT, Side-Looking Airborne Radar, and color IR imagery with specially flown low altitude, low-sun angle aerial photography resulted in the detection of numerous, previously unknown active fault scarps in Western Nevada. Many of these features were checked by aerial and ground reconnaissance and found to offset Lake Lahonton age shorelines and sediments (12,000 years before present).

TABLE 1
ESTIMATED SEISMIC CHARACTERISTICS OF ACTIVE FAULT¹ ZONES

<u>NAME</u>	<u>TOTAL² ZONE LENGTH (KM)</u>	<u>MAXIMUM³ CREDIBLE EARTHQUAKE MAGNITUDE</u>	<u>APPROXIMATE⁴ SLIP RATE (CM/YR)</u>	<u>AGE OF⁵ MOST RECENT DISPLACEMENT</u>
Genoa-Jack Valley	80	7.2	.01/.02	Holocene
McTarnahan Hill-Diamond Valley	35	6.5	.01	Late Pleistocene
Fairview-Dixie Valley	96	7.1	.1	Historic
Granite Springs Valley	45	7.0	.01	Holocene
Walker Larie				
Honey Lake-Pyramid Lake Segment	90	7.3	.1	Holocene
Carson Sink Segment	85	7.3	.1	Late Pleistocene
Walker Lake Segment	90	7.3	.2	Historic
Truckee-Olinghouse	96	6.7	.01	Historic
Carson Lineament	56	6.7	.01	Late Pleistocene
Yerington-Rawhide	50	6.5	.01	Late Pleistocene

- ¹ Active fault, as defined in this report, is one that exhibited displacement at or near the ground surface at least once within the past 10,000 years; i.e., Holocene.
- ² Due to many discontinuous fault segments, total zone length not used exclusively to determine maximum credible earthquake magnitude.
- ³ Maximum credible earthquakes estimated based on fault zone length, fault displacement, historic earthquakes, experience and judgement.
- ⁴ Slip rates estimated from geologic evidence.
- ⁵ Displacement age estimated from geologic evidence.

The identification of these fault scarps greatly refines the boundaries of the active fault zones from what is shown on Figure 2 when the scarps are located on base topographic map at scales of 1:250,000 and 1:62,500.

Projects located within the seismically active Basin-and-Range Province, may be subjected to ground motion from several structural zones. Three of the major zones are the Sierra Nevada frontal fault system, the Walker Lane fault zone, and the Fairview-Dixie Valley fault zone. Transverse to these major areas of active faulting are zones capable of generating 6.5 to 6.7 magnitude earthquakes, while earthquakes along the major zones may be in the 7.1 to 7.3 magnitude range.

REFERENCES

- Atwater, T., 1970. Implications of Plate Tectonics for the Cenozoic Evolution of Western North America: *Geol. Soc. America Bull.*, v. 81, p. 3513-3536.
- Bell, E.J., and Slemmons, D.B., 1977. Recent Crustal Movement in the Central Sierra Nevada-Walker Lane Region of California-Nevada: Part II, The Pyramid Lake Right-slip Fault Zone Segment of the Walker Lane: *Tectonophysics*. (In press).
- Bingler, E.C., 1971. Major East-west (Yerington-Rawhide) Lineament in West-Central Nevada: *Geol. Soc. America Abst.*, v. 3, Cordilleran Sec., p. 83.
- _____, 1978. Abandonment of the Name Hartford Hill Rhyolite Tuff and Adoption of New Formation Names for Middle Tertiary Ashflow Tuffs in the Carson City-Silver City Area, Nevada: *USGS Bull.* 1457-D.
- Bryant, W.A., 1979. Earthquakes near Honey Lake, Lassen County, California: *California Geology*, v. 32, no. 5, p. 106-109.
- Coffman, J.L. and Von Hake, C.A., 1975. United States Earthquakes, 1973: U.S. Dept. of Commerce and U.S. Geological Survey NOAA, 112 p.
- Cordova, T., 1969. Active Faults in Quaternary Alluvium and Seismic Regionalization, in a Portion of the Mount Rose Quadrangle, Nevada: Univ. of Nevada, Reno, M.S. Thesis, 60 p., Map Scale 1:63,400.

Active Fault Zones and Region Seismicity
in Western Nevada

By David K. Rogers, David B. Simon and John Stellar

Page 17

- Erwin, J.W. and Berg, J.C., 1977. Bouger Gravity Map of Nevada, Reno Sheet: Nevada Bur. of Mines and Geology Map 58, 1:250,000 Scale.
- Gilbert, C.W., and Reynolds, M.W., 1973. Character and Chronology of Basin Development, Western Margin of the Basin-and-Range Province: Geol. Soc. America Bull. v. 84, p. 2489-2510.
- Greensfelder, R.W., 1974. Maximum Credible Rock Acceleration from Earthquakes in California: California Div. Mines and Geology Map Sheet 23.
- Hardyman, R.F., Ekren, E.B., and Byers, F.M., 1975. Cenozoic Strike Slip, Normal and Detachment Faults in Northern Part of the Walker Lane, West-Central Nevada: Geol. Soc. America Abs., 7 (7) 1:1,100.
- Langenheim, R.L. and Larson, E.R., 1973. Correlations of Great Basin Stratigraphic Units: Nevada Bur. Mines and Geology Bull. 72, 36 p. with Correlation Charts.
- Moore, J.G., 1969. Geology and Mineral Resources of Lyon, Douglas and Ormsby Counties, Nevada: Nevada Bur. Mines and Geology Bull. 75, 45 p.
- Nevada Bureau of Mines, 1977. Aeromagnetic Map of Nevada, Reno Sheet, Map 54, Scale 1:250,000.
- O'Leary, D.W., Friedman, J.D., Pohn, H.A., 1976. Lineament, Linear, Lineation: Some Proposed New Standards for Old Terms: Geol. Soc. America Bull., v. 87, p. 1463-1469.
- Pease, R.W., 1969. Normal Faulting and Lateral Shear in Northern California: Geol. Soc. America Bull. 80, p. 715-720.
- Pease, R.B., 1979. Fault Scarp Degradation in Alluvium Near Carson City, Nevada: Geol. Soc. America Abst., v. 11, no. 3, Cordilleran Sec. p. 121.
- Rogers, D.K., 1975. Environmental Geology of Northern Carson City: Univ. of Nevada, Reno, M.S. Thesis, 133 p. with Maps, 1:12,000.
- Ryall, A., 1977. Earthquake Hazard in the Nevada Region: Bull. Seismological Soc. of America. v. 67, no. 2, p. 517-532.
- Sanders, C.O. and Slemmons, D.B., 1977. Recent Crustal Movements in the Central Sierra Nevada-Walker Lane Region of California-Nevada: Part III, the Olinghouse Fault Zone: Tectonophysics, (in press) 14 p.
- Shawe, D.R., 1965. Strike-slip Control of Basin-Range Structure Indicated by Historical Faults in Western Nevada: Geol. Soc. of America Bull. v. 76, no. 12, p. 1361-1378.

Active Fault Zones and Region Seismicity
in Western Nevada

By David K. Rogers, David B. Simon and John Stellar

Page 18

Silberman, M.L. and McKee, E.H., 1974. Ages of Tertiary Volcanic Rocks and Hydrothermal Precious-metal Deposits in Central and Western Nevada in Guidebook to the Geology of Four Tertiary Volcanic Centers in Central Nevada: Nevada Bur. of Mines Rept. 19, p. 67-72.

Simon, D.B., 1979. Personal Communication.

Simon, D.B. and Mason, C.H., 1978. Fault Analysis of the Carson Lineament, Nevada and its Relation to Basin-and-Range Structure: Univ. of Nevada, Reno, Student Report, 41 p. with Map 1:62,500.

Slemmons, D.B., 1967. Pliocene and Quaternary Crustal Movements of the Basin-and-Range Province, USA: Jour. of Geoscience, Osaka City Univ., Japan, v. 10, Part 1-11.

_____ 1977. Personal Communication.

_____ 1977. State-of-the-art for Assessing Earthquake Hazards in the United States in Rept. 6, Faults and Earthquake Magnitude: U.S. Army Engineer Waterways Experiment Station, Contract No. DACW39-76-C-0009, 129 p, Appendix, 37 p.

Slemmons, D.B., Jones, A.E., Gimlett, J.I., 1965. Catalog of Nevada Earthquakes, 1852-1960: Seismological Soc. of America, Bull. 55, p. 537-583.

Slemmons, D.B., Van Wormer, D., Bell, E.J., Silberman, M.L., 1977. Recent Crustal Movements in the Sierra Nevada-Walker Lane Region of California-Nevada: Part I, Rate and Style of Deformation: Tectonophysics 7 p. (In press).

Speed, R.C. and Cogbill, A.H., 1979. Candelaria and Other Left-oblique Slip Faults of the Candelaria Region, Nevada: Geol. Soc. America Bull. pt. I, v. 90, p. 149-163.

Steward, J.H., 1971. Basin-and-Range Structure: A System of Horsts and Grabens Produced by Deep Seated Extension: Geol. Soc. of America Bull., v. 82, no. 4, p. 1019-1043.

Stewart, J.H. and Carlson, J.E., 1977. Geologic Map of Nevada: U.S. Geol. Survey Misc. Field Studies Map MF-609.

Topozada, T.R., Real, C.R., Bezore, S.P., and Parke, D.L., 1979. Compilation of Pre-1900 California Earthquake History: Sacramento, California Div. Mines and Geology Open-File Rept. 79-6.

Active Fault Zones and Region Seismicity
in Western Nevada

By David K. Rogers, David B. Simon and John Stellar
Page 19

Trexler, D.T. and Bingler, 1977. Earthquake Study in the Carson City, Nevada Area: U.S. Geol. Survey Final Technical Report, Grant No. 14-08-0001-G-248, 62 p.

Van Wormer, J.D., Ryall, A., Mohler, A., Ryall, F., 1979. Seismic Hazard Evaluation of Large Known and Suspected Faults in Western Nevada in Nevada Bur. Mines and Geology, Seismological Laboratory, Second Annual Technical Report: U.S. Geological Survey Contract No. 14-08-0001-16744, 55 p.

Wallace, R.E., 1977. Profiles and Ages of Young Fault Scarps, North-central, Nevada: Geol. Soc. of America Bull. v. 88, pp. 1267-1281.

_____, 1978. Size of Larger Earthquakes, North-Central Nevada: Seismol. Soc. America Abst., 73rd Ann. Meeting, v. 49, no. 1, p. 23.

_____, 1978. Patterns of Faulting and Seismic Gaps in the Great Basin Province: U.S. Geol. Sur. Open-File Rept. 78-943, 9 p.

Wright, L., 1976. Late Cenozoic Fault Patterns and Stress Fields in the Great Basin and Westward Displacement of the Sierra Nevada Block: Geology, v. 4, p. 489-494.

VIBRATORY CORE SAMPLING IN THE MISSOURI RIVER

By

Marvin W. Taylor
Geology Section, Foundation Materials Branch
Engineering Division, Omaha District
U.S. Army Corps of Engineers
Omaha, Nebraska

ABSTRACT

Vibratory core sampling is a method of continuous sampling using a vibratory core barrel under water. Penetration of the sampler is provided by compressed air. This method was used to obtain continuous samples of the bed material of the Missouri River from Yankton, South Dakota to Plattsmouth, Nebraska. The samples are used to provide information as to the character of the bed material for a degradation study in this reach of river. The study is being conducted to determine the ultimate bed levels of the river. This determination is necessary to assess the impact these levels will have on bridges, decks, water intakes, and other river facilities. Vibratory core sampling proved to be an excellent method of acquiring continuous samples for this project.

INTRODUCTION

The Missouri River drains the upper Great Plains region, it is the second largest river in the United States being 2,315 miles long. The river provided a route for Lewis and Clark in 1804. Today, the main stem dams provide flood control and vast amounts of electricity in Montana, North and South Dakota. The degradation study is being conducted to determine the ultimate bed levels of the river. By contract, a sampling program using a vibratory sampler started at Yankton, South Dakota about 800 river miles above the mouth of the Missouri and continued 200 miles downstream to Plattsmouth, Nebraska, see Figure 1.

BACKGROUND

Vibratory sampling of sediments is a method of obtaining continuous samples below the water bottom with vibration and weight as the driving mechanism. It uses an air driven piston to provide the vibration and weight to drive the sampler into the river bottom material.

A vibratory sampler consists of a core barrel powered by a vibrating head run by compressed air. The core barrel has a plastic liner. The mechanism slides up and down on an H-beam. This means of sampling has been used successfully for some time in coastal regions.

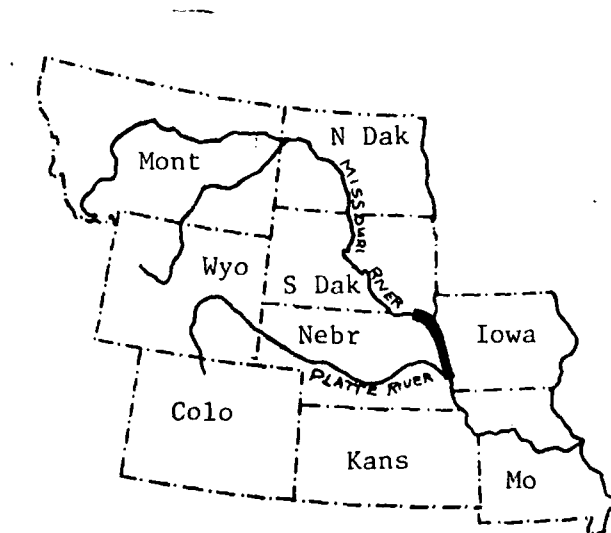


FIGURE 1 - Study Area Shown in Heavy Line

The first use of vibratory sampling by the Corps of Engineers was in Savannah Harbor, Savannah, Georgia in 1967. It was an air powered vibrator and had a 20 foot long drive pipe sampler. This project was successful with 100 cores 20 feet long being taken in twenty days (U.S. Army Corps of Engineers, Savannah District 1967).

Vibratory sampling has been used predominately in the shallow regions of the ocean and in bays. It has been used for dredging exploration, sand inventory and foundation investigation. In dredging exploration, it is used to determine the type of materials to be dredged. Sand inventory is finding source areas of suitable material to be borrowed for beach replenishment. Foundation investigation involves exploration of underlying materials at the site of a proposed structure. Most of this work has been done in or adjacent to the ocean. Sand exploration has been done in Great Lakes.

Vibratory samplers now use hydraulic or electric power in addition to compressed air. Different lengths of sample pipe are used from short 6' and 10' lengths to 20', 30', and 40' lengths. The operating principles and geometry of the system are the same no matter which power system and what length sampler are being used.

The degradation study being conducted on the Missouri River will predict the ultimate bed levels of the river and determine the impact these levels will have on bridges, docks, marinas, water intakes, recreation areas, and other river facilities. The study is complex and involves many disciplines such as hydraulics, sedimentation, and hydrology. These disciplines

require that the nature of the material of the river-bed be determined. The HEC 6 computer model from the Hydraulic Engineering Center of Berkeley, California, is being used in this study. The computer model requires input of the gradation of the bed material. In order not to miss any zone within the vertical column a continuous sample is required. The vibratory sampling technique can provide the necessary samples. In addition, experience had been gained from a previous sampling program, a year earlier, which used a conventional truck-mounted drill rig on a barge and a 3" split spoon sampler. This earlier program resulted in only sampling certain points along the vertical column of the site. One of the deficiencies in this earlier program was that only specific intervals were sampled. Another deficiency was poor recovery. The point is that the intervals not sampled or recovered may be the most important.

OPERATIONS

The work force required for this project consisted of an individual in charge of the entire sampling operation. One or two assistants were needed to take care of the logging and storage of the samples and to put new liners into the sampling barrel. The operation of the floating plant required a general foreman, a push boat operator, crane operator, machinery operator, a welder, and a driver who remained on shore. The foreman was in charge of all the floating plant and personnel. The machinery operator ran the air compressor, water pump and generator. The welder made repairs plus generally helped out. The driver would deliver everyone to the river near the barge in the morning, and pick up everyone at the end of the day near where the work stopped for the day.

The floating plant consisted of a barge with two spuds on one side, a push boat, a crane, air compressor, large volume water pump, and an electrical generator. Additional miscellaneous equipment included a welding machine, fuel tanks and shack.

The vibratory sampler is self-supporting with an aluminum H-beam forming the support and guide tower for the vibrator. The H-beam is held vertical by four support legs and feet which extend in each direction, 10 feet from the center of the bottom of the beam. The legs attach to a cross brace 12 feet up from the bottom of the beam. The rear support foot and leg can be collapsed to allow the rig to lie flat on the deck. This permits removal of the sample tube through the bottom of the base plate. The core pipe is driven into the sediment by an air driven vibrator powered by the air compressor (250 cfm, 100 psi). The air is fed to the rig through a 1.25" ID hose and vented through two additional hoses of the same diameter, with all three bound in an array. The vibrator, working like a double action pile driver, drives a piston up and down about 600 strokes per minute. The vibrator holds the core barrel and slides up and down on the front flange of the H-beam (Dill 1978), see Figure 2.

Penetration both rate and absolute depth is measured electrically by a potentiometer on the vibratory head and a strip chart recorder. The potentiometer is a continuous turn potentiometer connected to a small-link ladder chain

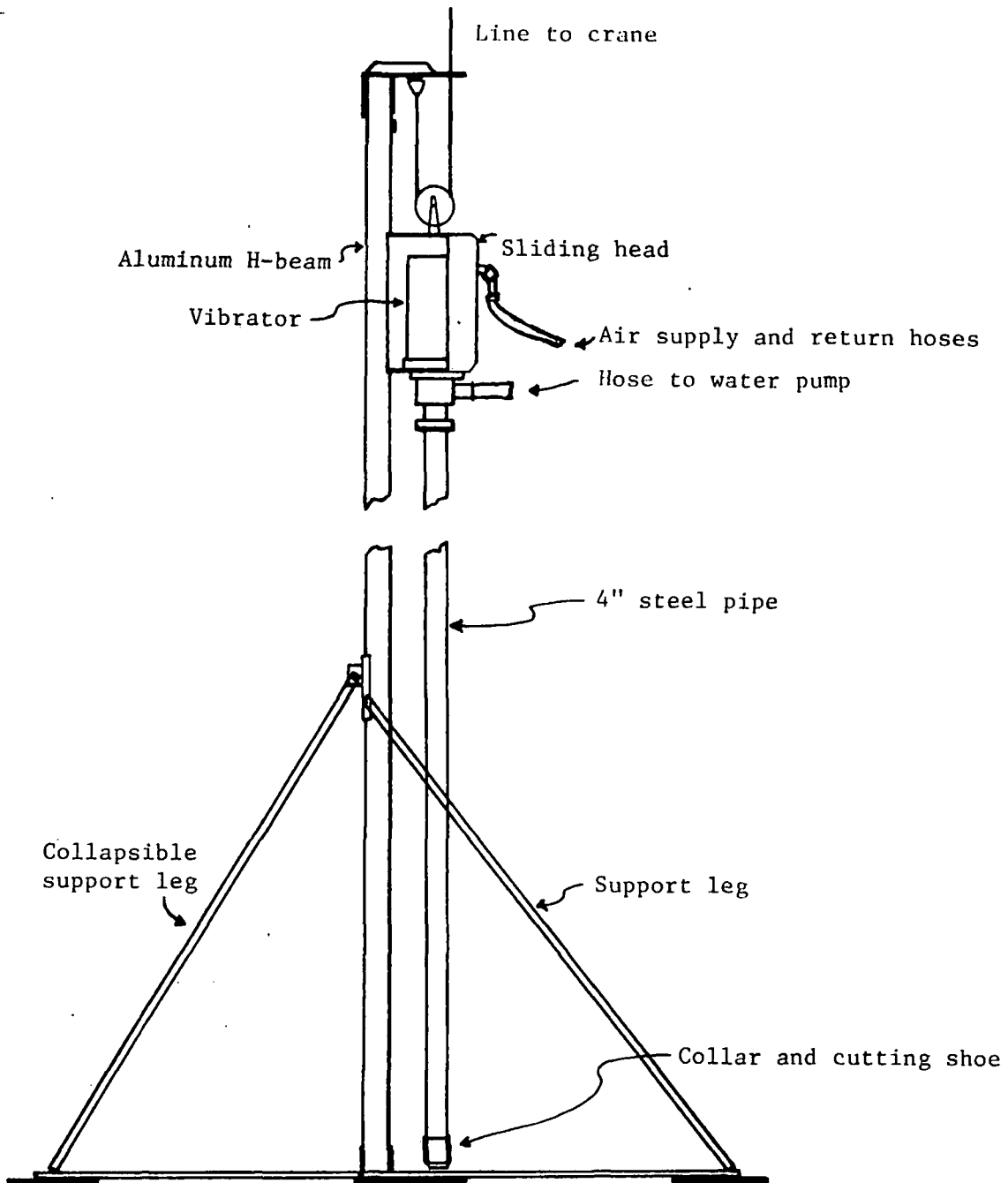


FIGURE 2 - Generalized Diagram of a Vibratory Core Sampler

Vibratory Core Sampling in the Missouri River

By Marvin W. Taylor

Page 5

stretched the length of the aluminum H-beam. Each foot of penetration of the vibratory head makes the potentiometer rotate one complete revolution. Each turn makes the needle on the strip chart move once across the chart. Thus the rate of penetration and depth of penetration of the core barrel are continuously monitored (Dill 1978).

Typical operations at a drilling on a station was as follows: The station was selected by a scout boat ranging upstream and downstream from the designated point to find the low spot between the sand dunes along the river bottom. After having traveled downstream, the push boat would turn the barge around so that it was pointed upstream. The upstream spud would be lowered into the river-bed followed by the downstream spud. The crane would lift up the assembly so that it was vertical on deck. It would then lift the assembly over the side and place it into the water and down onto the river-bed.

After determining that the assembly was stable in the current, the air valve would be opened allowing the compressed air to drive the sampling barrel and tube into the river-bed the required depth. Upon reaching the full depth, the air valve would be closed and the barrel would be pulled out of the bed material. Pulling of the sampler was facilitated by a 2 to 1 mechanical advantage from a pulley and line arrangement between the top of the H-beam and the vibratory head.

The assembly was then lifted up onto the deck and laid down on its collapsible backleg. The drive shoe was unscrewed and the plastic liner removed. A new liner and drive shoe was inserted and screwed onto the drive barrel and the mechanism was ready for another operation.

The time required to retrieve a sample was really quite short. It only took from 5 to 10 minutes for the complete operation for most single attempts. However, at most of the sites, due to the nature of the sediments, it almost always took two to three attempts to get 20 feet of sample. When this occurred, the procedure was to require successive attempts. The second attempt would start just above where the first attempt left off. This would be accomplished by pumping water down through the tube and drive barrel. This washed the drive pipe down to the proper level at which the pump would be cut off and the compressed air valve turned on. This procedure was followed on successive attempts until a satisfactory length of sample was obtained.

When removed from the barrel, the sample within the plastic tube was examined, briefly logged, cut into 4-foot lengths, capped, and then stored until transfer to the laboratory.

In the laboratory the tubes were split in half lengthwise, photographed and a detailed log prepared. The material was analyzed by mechanical sieving and hydrometer analysis.

PROBLEMS

The greatest problem in drilling in the Missouri River was the swift current. The current would cause the assembly to tilt as soon as it started into the water. Then, when it was setting on the bottom, it would tend to tip over. To correct this, a rope was tied to the top of the assembly. During withdrawal from the water, the assembly would again tilt with the bottom sliding downstream. This placed a great burden upon the crane operator to insure that the equipment was not damaged.

Recovery was a problem also as previously mentioned. The sampler would be driven to its full 20-foot depth but core recovery would range from 7 to 12 feet in spite of the core retainer being in place. It was assumed that the top material was in the liner and that the underlying material did not have enough compressive strength to push the material already in the tube upward. The sampler then became a vibrating pipe pile.

At a few locations where successive attempts were required to get a complete sample, overlaps in sample occurred. This was because the jetting down of the next attempt was always halted above the bottom of the previous sample to assure coverage. The overlap itself was not a problem but in a few instances different material was found in the overlap.

At a few locations, rock layers were encountered at shallow depths.

CONCLUSION AND RECOMMENDATION

Continuous sampling by the vibratory method proved to be an excellent method of obtaining the samples for this project. It provided a continuous sample of the material encountered. The early program of conventional drilling only provided samples from part of the bed material. Vibratory sampling is a good method when sample disturbance can be tolerated.

REFERENCES

- Babcock, F.M. and Miller, H.J., 1972, A Correlation of the Standard Penetration Test and the Vibracore Sampler, in Underwater Soil Sampling, Testing and Construction Control, ASTM Special Technical Publication 501.
- Dill, C.E., 1978, Final Report, Vibracore Sampling Project, Missouri River Degradation Survey Mile No. 805 and 585, November, 1978.

Vibratory Core Sampling in the Missouri River
By Marvin W. Taylor
Page 7

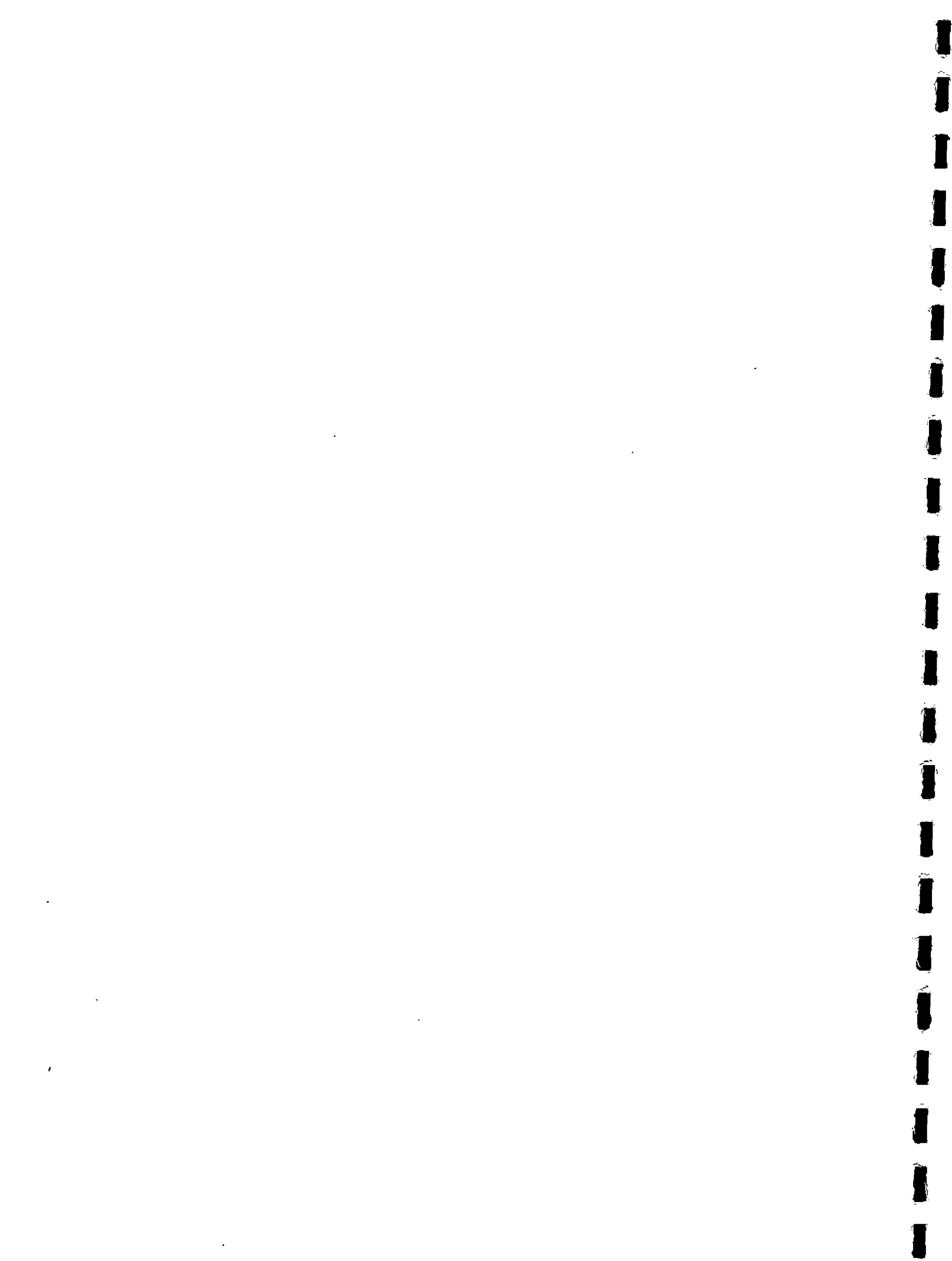
Noorany, I., 1972, Underwater Soil Sampling and Testing-A State-of-the-Art Review, in Underwater Soil Sampling, Testing and Construction Control, ASTM Special Technical Publication 501.

Ocean/Seismic/Surveys, Inc., Norwood, New Jersey, 1978, Capabilities Booklet.

Tirey, G.B., 1972, Recent Trends in Underwater Soil Sampling Methods, in Underwater Soil Sampling, Testing, and Construction Control, ASTM Special Technical Publication 501.

U.S. Army Corps of Engineers, Savannah District, 1967, Vibratory Sampling Program, Savannah Harbor, Georgia, Report, 18 p.

Woodward-Clyde Consultants, Plymouth Meeting, Pennsylvania 1978, Capabilities Folder.



INVENTORY AND CLASSIFICATION OF ABANDONED MINE TAILINGS

By

Mike Gross, Christos Ioannou and Dale R. Ralston
University of Idaho
Moscow, Idaho

ABSTRACT

Abandoned mine tailings in the Coeur d'Alene Mining District are a major non-point source of water quality degradation. The quality of the South Fork of the Coeur d'Alene River has greatly improved in recent years with the control of point sources of poor quality discharge. Continued improvement in water quality is dependent upon reclamation of abandoned mine tailings sites.

A recently completed study of abandoned mine tailings piles in the district included an inventory and classification of these wastes. Tailings piles were classified as controlled or uncontrolled sites based upon evidence of an original dike or embankment. A total of seventeen controlled and fourteen uncontrolled tailings piles were identified in the mining district.

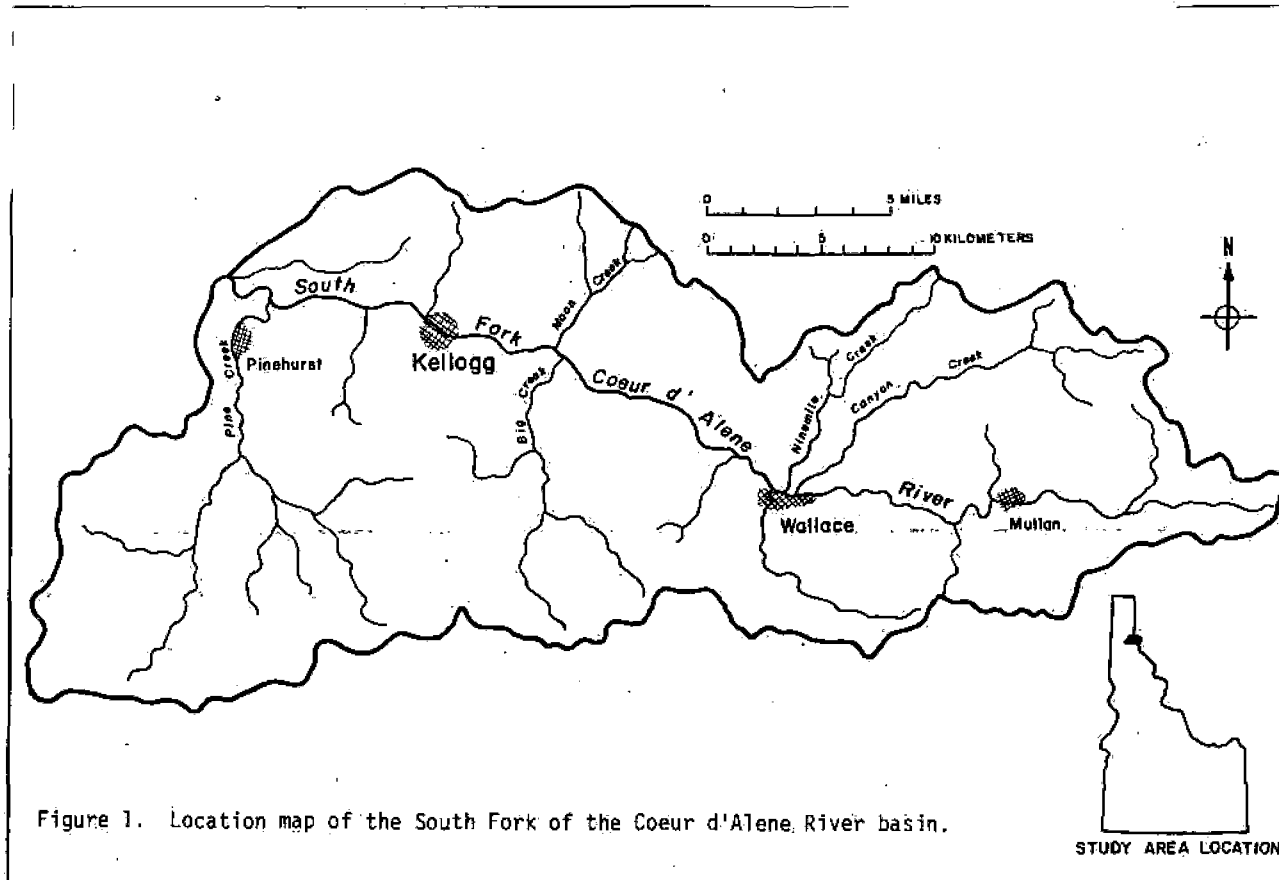
The sites were further classified based on the potential for physical or chemical transport. Some of the piles are eroded heavily by normal spring runoff while others are susceptible only to wind erosion. Only a few of the sites have an identified potential for major chemical leaching of metals.

Plans for reclamation of abandoned mine tailings sites must be based upon an accurate identification of potential problems. This study has established that base for the wastes in the Coeur d'Alene District.

INTRODUCTION

The Coeur d'Alene Mining District in northern Idaho is one of the world's premium areas for the production of silver, lead and zinc (Figure 1). Mining and milling activity has been the dominant force in the region's economy since 1884, when miners from the gold camps at Prichard and Murray first began to stake claims in the valley of the South Fork (Hawley, 1920). Construction of ore concentrating mills proceeded rapidly, and the South Fork and its tributaries became convenient disposal systems for tailings, the term for crushed-rock waste material from the concentrators. By 1943, partly as a result of the demand for metals to aid the war effort, a total of 30 mills were operating in the District (Campbell, 1943).

These mills produced tailings of differing size and chemical composition, depending on the type of metal recovery process employed and the mineralogy of the ore. Early gravity-process mills used "jig" tables in which rather coarsely ground ore was separated by taking advantage of the higher specific gravity of lead-rich grains. Waste material from such mills was typically coarse-grained angular gravels, some with a maximum dimension of 3/4 inch. These gravels were usually deposited in unprotected piles along stream beds and are frequently rich



in heavy metals. By about 1916, milling operations in the district were using a combination of gravity and "froth flotation" techniques to recover metals. The flotation process produced tailings of a much smaller grain size which were transported by slurry pipeline from the mill and either piled behind a protective embankment or deposited directly in a stream.

The accumulation of large quantities of tailings in the valley which covered the natural river alluvium and the thoughtless discharge of other wastes from the mining and smelting activities before the 1960's resulted in heavily polluted streams and unstable channel conditions. During high flows, the streams erode the loose tailings, carry and deposit them downstream, thus creating physical, chemical, and aesthetic problems. Some old tailings are rich in heavy metals such as cadmium, lead and zinc, and leaching through the tailings is believed to cause an increase in dissolved heavy metal ions in the river flow (Galbraith and others, 1972).

Strict federal regulations halted direct discharge of tailings into streams in 1968 and thereby brought point discharges from milling operations under control; however, the remaining abandoned tailings represent a significant non-point source of sediments and heavy metals which continue to pollute surface streams (Reece, 1974).

This study, involving the inventory and classification of these abandoned tailings, is part of a larger research project conducted by the University of Idaho for the Idaho Department of Health and Welfare in which reclamation plans for abandoned tailing sites will be drafted. Reclamation of the abandoned sites will further improve water quality throughout the Coeur d'Alene River system.

INVENTORY

An examination of the South Fork Coeur d'Alene and its tributaries was conducted during the summer of 1978 to locate and identify all abandoned tailings sites. The investigations included traveling along all the tributaries and main stream of the Coeur d'Alene River basin. Sites were also located using a small aircraft. The field investigations were augmented with maps showing the distribution of the tailings prepared by Norbeck (1974), stereo air photos for the area taken in selected years since 1932, old photographs of the mills and waste areas, and stereo oblique slides taken during the flights of the areas. Sites were located and mapped using large scale air photos taken in 1976. A total of seventeen abandoned controlled tailing sites were found in the drainage of the South Fork of the Coeur d'Alene River. In addition, fourteen abandoned uncontrolled tailings sites were identified, inventoried and mapped. Sites were defined as controlled if any remnants of constructed embankments could be found.

The controlled sites are in various degrees of site abandonment. Several "abandoned" sites have recently raised embankments and are ready to receive tailings. Both of these serve active mills which have alternate tailings disposal sites and have not received tailings on a regular basis for at least a

year. These sites remain "abandoned" only until the mining companies require their use. A small accumulation of tailings in the braided floodplain of the East Fork of Pine Creek represents the other end of the spectrum of controlled "abandoned" sites. Whatever mill produced the tailings no longer stands and only faint remnants of embankments have survived the series of seasonal floods from which the site has no protection. This site is not likely to be of any use for future tailings disposal due to its precarious location and would be of little economic interest to a mining company even if metals concentrations were high due to the small volume involved.

All of the abandoned uncontrolled tailings sites are located along the course of the South Fork of the Coeur d'Alene River or its tributaries. The sites range from large flood plain deposits of as much as two square miles to small tailings areas of less than 10,000 square feet. The composition of abandoned uncontrolled sites ranges from essentially all flotation or jig tailings to nearly native sediments depending on the degree of mixing with native alluvium.

PROCEDURE FOR CLASSIFICATION OF SITES

The criteria for classification of the abandoned controlled and uncontrolled tailings sites can be divided into three categories representing the identified factors important in site abandonment. Physical, chemical and aesthetic factors were considered separately in the examination of each site. The general classification system is outlined below.

Chemical Factors

- (1) Acid production potential for the site based on the presence of pyrite in the mine wastes and the presence of acid neutralizing agents within the tailings. This factor would be measured by the quantity of iron evident from chemical analysis of the sediment and any historic water quality data or indications of drainage water quality.
- (2) Presence of a fluctuating ground water system within a tailings pile of known chemical acid production potential. This factor deals with water as a flushing agent from either precipitation and direct infiltration or from ground water movement into the tailings.

Physical Factors

- (1) The potential for an immediate and massive physical failure of the tailings pile thereby releasing all previously impounded sediments into a stream drainage area.

- (2) The potential for the direct erosion of tailings by seasonal floodwaters from an established stream or streams. This is controlled primarily by the sites location within the floodplain and the structural integrity of whatever protective embankment exists.
- (3) The sites potential for sediment contribution to surface streams due to sheet wash from hillsides or direct precipitation on tailings surface and from wind erosion of the material. This reflects the amount and effectiveness of the vegetative cover on the site and the existence or potential of drainage of the site which would facilitate the movement of sediment into nearby streams.

Aesthetic Factors

- (1) Public visibility of the site reflected in its proximity to public roads and communities.
- (2) An assessment of the visual quality of the site especially the presence or absence of vegetation and the overall shape and orientation with respect to surrounding topography.

LOCATION AND CHARACTERISTICS OF ABANDONED CONTROLLED SITES

The location of identified abandoned controlled tailings sites within the drainage of the South Fork of the Coeur d'Alene River are shown on Figure 2. As may be seen, most of the abandoned controlled sites are located in major tributary valleys of the South Fork of the Coeur d'Alene River. The classification of the seventeen sites for physical and chemical problems is presented on Table 1. Potential physical hazards were sub-divided into: (1) massive failure, (2) erosion by surface streams, and (3) sheet wash and wind erosion. Each site was classified into one of five states based upon an on site field investigation. The potential was noted as follows:

- I. No significant potential for physical movement of wastes regardless of reclamation condition.
- II. Potential exists, but present reclamation procedures are adequate to control any physical problems.
- III. Potential exists, reclamation is inadequate.
- IV. High potential exists, no reclamation attempted.
- V. Very high potential exists, need for corrective measures obvious.

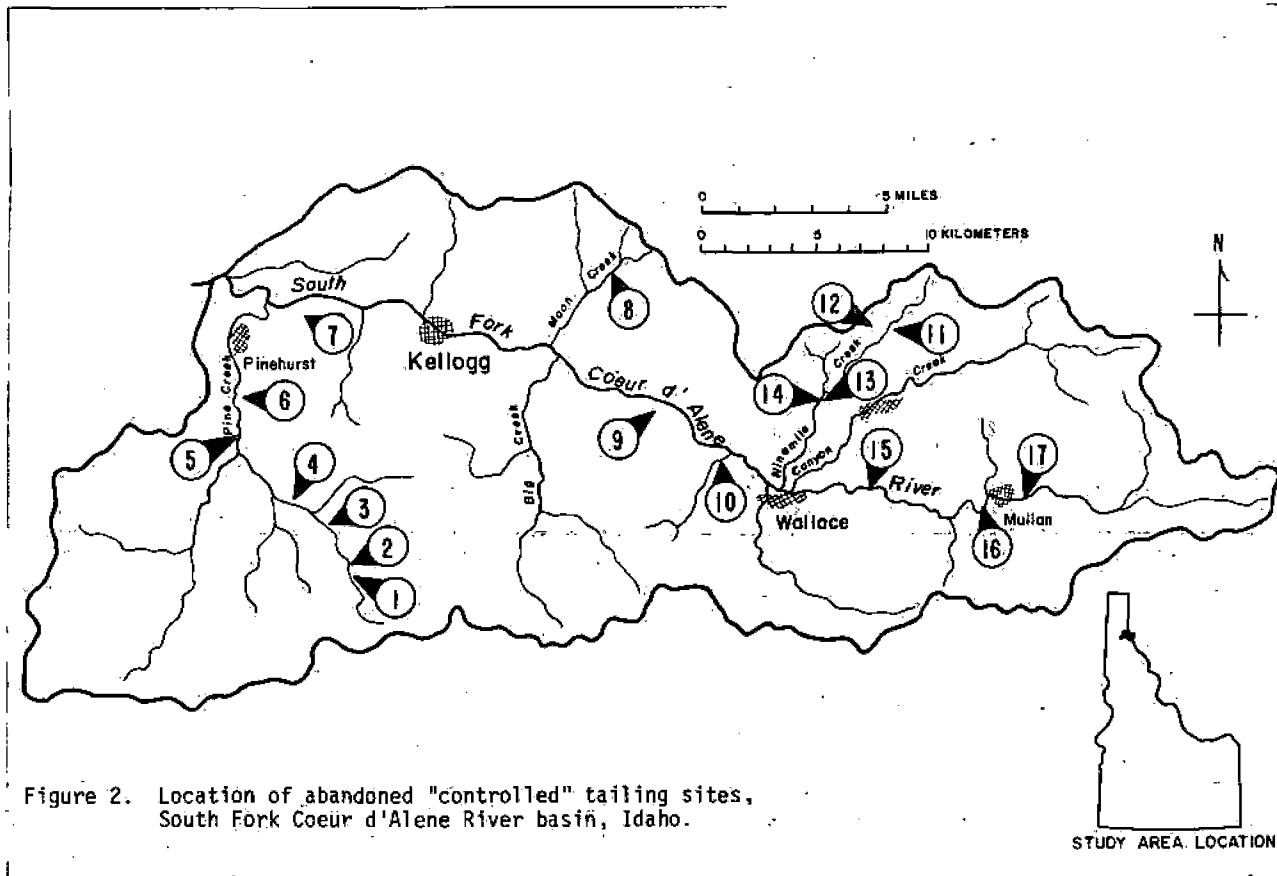


Figure 2. Location of abandoned "controlled" tailing sites, South Fork Coeur d'Alene River basin, Idaho.

TABLE 1
TAILING SITE CLASSIFICATION ACCORDING TO HAZARD TYPE AND POTENTIAL FOR POLLUTION *

Site	Drainage	No. of Piles	HAZARD CLASS				
			A Potential for Acid Production; Long Term Water Pollution Problem		B Potential Physical Hazard (Massive Failure)	C Potential for Erosion by Surface Streams	D Potential for Sheet Wash and Wind Erosion
			Sufficient Data Available	Insufficient Data Available			
1	Pine Creek	2	-	-	III	IV	V
2	Pine Creek	1	-	-	I	IV	III
3	Pine Creek	2	-	-	III	V	IV
4	Pine Creek	2	-	-	I	IV	IV
5	Pine Creek	1	-	-	I	IV	IV
6	Pine Creek	2	-	-	I	III	III
7	South Fork	1	V	-	II	I	III
8	Moon Creek	6	-	-	III	V	IV
9	South Fork	2	-	-	I	I	III
10	Lake Creek	3	I	-	II	II	III
11	Ninemile Creek	1	-	-	III	IV	V
12	Ninemile Creek	1	-	-	V	III	III
13	Ninemile Creek	1	-	-	II	I	II
14	Ninemile Creek	3	-	-	I	II	II
15	South Fork	1	-	-	I	II	III
16	South Fork	1	I	-	II	I	III
17	South Fork	2	-	-	I	I	III

- * I. No significant potential for physical movement of wastes regardless of reclamation condition.
 II. Potential exists, but present reclamation procedures are adequate to control any physical problems.
 III. Potential exists, reclamation is inadequate.
 IV. High potential exists, no reclamation attempted.
 V. Very high potential exists, need for corrective measures obvious.

As can be seen, most of the sites have a low potential for major massive failure; however, a number of the sites are susceptible to erosion by surface streams with potential for sheet wash and wind erosion to a lesser extent.

The chemical hazards of these sites were similarly evaluated. An accurate assessment of the chemical potential of these sites was limited because of an insufficient data base. One of the three sites for which data were available had a high potential for water quality problems.

The tailings site classification according to aesthetic factors important in abandonment is presented in Table 2. Each site was rated according to public visibility and visual quality based on the following scale: (A) most aesthetically favorable condition through (D) most aesthetically unfavorable condition.

LOCATION AND CHARACTERISTICS OF ABANDONED UNCONTROLLED SITES

Eleven of the identified uncontrolled abandoned tailings sites are located along the course of the South Fork of the Coeur d'Alene River; two are located along Ninemile Creek and one occupies the flats of the lower part of the Canyon Creek valley (Figure 3). The large number of custom and other types of mills that operated in the Coeur d'Alene Mining District, the number of common tailing disposal sites, the transport of ore from a mine to a custom mill in another part of the district and the later reworking of the old tailings deposits for metal extraction render any attempt to link a particular abandoned uncontrolled site with a particular mill impossible. In a general way, however, it seems probable that the tailings present in the valley bottom are probably associated with mining activities carried out upstream of the site of the deposits. It is thus most likely that the tailings north-east of Mullan are associated with mining activities in the Hunter District, those in Canyon Creek with the Lelande District, the Osburn tailings with the Evolution District and the escapes from the Hunter and Lelande Districts and the wastes in the Smelterville Flats associated with the Yreca District and waste transported from the other upriver districts.

The abandoned uncontrolled tailings sites were classified according to physical, chemical and aesthetic problems in a similar manner as that described for controlled sites. The physical and chemical classification of uncontrolled tailings sites is presented in Table 3. The evaluation of aesthetic factors for each inventoried uncontrolled site is shown in Table 4. Many of these sites are continually eroded by surface streams, sheet wash and wind action. Available chemical data show that at least two of the areas present a major water pollution problem from chemical activities. Similarly many of the sites are aesthetically displeasing because of both public visibility and visual quality.

TABLE 2
 TAILING SITE CLASSIFICATION ACCORDING TO AESTHETIC FACTORS
 IMPORTANT IN ABANDONMENT

Site	PUBLIC VISIBILITY		VISUAL QUALITY		Composite Aesthetic Rating
	Proximity to Public Roads	Proximity to Communities and Residences	Landscape Continuity	Presence of Vegetation	
1	B	A	C	C	B-
2	B	A	B	D	B
3	C	A	C	C	C
4	C	A	C	C	C
5	C	C	D	C	C-
6	C	B	B	B	B
7	D	C	D	D	D
8	B	B	D	C	C+
9	A	C	B	C	B-
10	C	A	C	B	B-
11	B	A	C	D	C+
12	B	A	B	D	B-
13	C	B	B	B	B
14	C	B	B	C	B-
15	D	B	C	C	C
16	D	D	B	B	C
17	C	C	A	B	B-

Explanation of Symbols:

- A . . . Most aesthetically favorable condition
 - far from public view or hidden by vegetation or landforms, or
 - in harmony with landscape, or
 - covered by a sustained growth of vegetation.
- B . . . Less aesthetically favorable condition
 - visible from unpaved Forest Service or county road, or
 - residences nearby, but not within sight, or
 - pile placed along hillside, not occupying entire valley, or
 - vegetation is successful on embankments, some present on tailing surface.
- C . . . Aesthetically unfavorable condition
 - visible from paved, well-traveled road, or
 - visible from at least one residence, or
 - occupying a large portion of the valley and dominating the visual scene, or
 - vegetation beginning to encroach on site without modification.
- D . . . Most aesthetically unfavorable condition
 - visible from major interstate highway, or
 - visible from an established community, or
 - an obvious contradiction to natural landscape, or
 - no vegetation on the site.

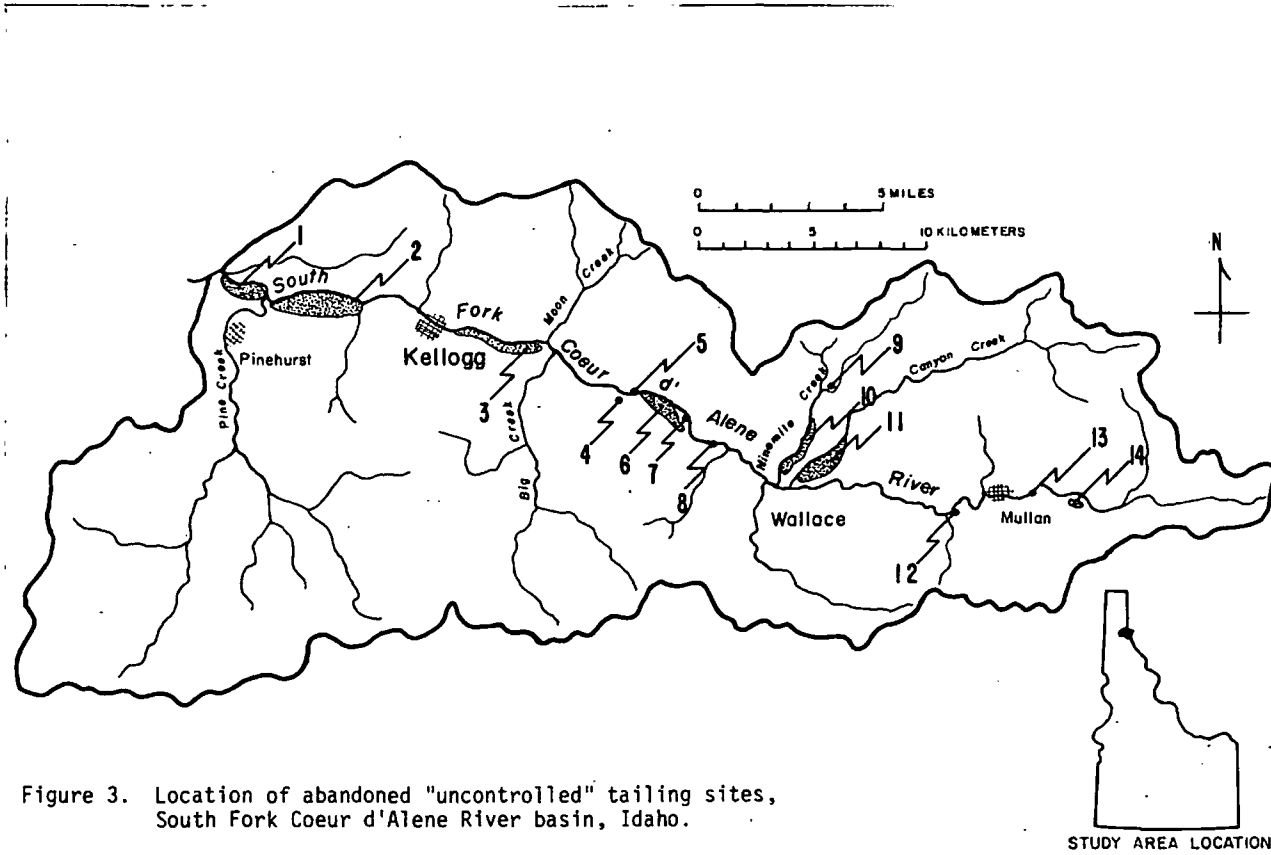


Figure 3. Location of abandoned "uncontrolled" tailing sites, South Fork Coeur d'Alene River basin, Idaho.

TABLE 3
TAILING SITE CLASSIFICATION ACCORDING TO HAZARD TYPE AND POTENTIAL FOR POLLUTION *

Site	No. of Piles	HAZARD CLASS				
		A Potential for Acid Production; Long Term Water Pollution Problem		B Potential Physical Hazard (Extensive Erosion)	C Potential for Erosion by Surface Streams	D Potential for Sheet Wash and Wind Erosion
		Sufficient Data Available	Insufficient Data Available			
1 Enaville Flats	-		-	III	IV	IV
2 Smeltonville Flats	-	V	-	III	V	V
3 Flood plain area between Ross Gulch and Moon Creek	-		-	III	III	V
4 Osburn Site 1	1		-	I	I	II
5 Osburn Site 2	2		-	I	I	III
6 Osburn Flats	-		-	III	IV	V
7 Nuckols Gulch Site	1		-	IV	IV	V
8 Silverton Site	1		-	III	IV	V
9 Ninemile Creek, East Fork		IV		III	IV	V
10 Ninemile Creek Flats			-	III	III	III
11 Canyon Creek Flats		V		III	IV	V
12 Near the mouth of Gold Creek	1		-	I	I	III
13 Near the mouth of Gold Hunter Gulch	1		-	I	I	I
14 Near the mouth of Daizy Gulch	1		-	III	III	III

- * I. No significant potential for physical movement of wastes regardless of reclamation condition.
 II. Potential exists, but present reclamation procedures are adequate to control any physical problems.
 III. Potential exists, reclamation is inadequate.
 IV. High potential exists, no reclamation attempted.
 V. Very high potential exists, need for corrective measures obvious.

TABLE 4
 TAILING SITE CLASSIFICATION ACCORDING TO AESTHETIC FACTORS
 IMPORTANT IN ABANDONMENT

Site	PUBLIC VISIBILITY		VISUAL QUALITY		Composite Aesthetic Rating
	Proximity to Public Roads	Proximity to Communities and Residences	Landscape Continuity	Presence of Vegetation	
1	B+	A	B	B	B+
2	D	D	D	C-	D
3	D	C	C	B-	C
4	B	B	C	C	C+
5	C	C	D	C	C-
6	D	D	D	D	D
7	C	C	D	C-	C-
8	B	B	C	C	B-
9	C	B-	D	C-	C
10	D	C	D	C	C-
11	D	D	D	D	D
12	A	A	B+	B	B
13	A	A	B	B	B
14	C-	B	C	B	C

Explanation of Symbols:

- A . . . Most aesthetically favorable condition
 - far from public view or hidden by vegetation or landforms, or
 - in harmony with landscape, or
 - covered by a sustained growth of vegetation.
- B . . . Less aesthetically favorable condition
 - visible from unpaved Forest Service or county road, or
 - residences nearby, but not within sight, or
 - pile placed along hillside, not occupying entire valley, or
 - vegetation is successful on embankments, some present on tailing surface.
- C . . . Aesthetically unfavorable condition
 - visible from paved, well-traveled road, or
 - visible from at least one residence, or
 - occupying a large portion of the valley and dominating the visual scene, or
 - vegetation beginning to encroach on site without modification.
- D . . . Most aesthetically unfavorable condition
 - visible from major interstate highway, or
 - visible from an established community, or
 - an obvious contradiction to natural landscape, or
 - no vegetation on the site.

CONCLUSIONS

Abandoned tailings resulting from nearly a hundred years of mining activity in the South Fork, Coeur d'Alene River basin pose a serious threat to the quality of surface and ground waters of the area. These abandoned tailing sites vary widely in size, form, chemical composition, type of material involved, and position with respect to surface drainages. This study includes a classification of sites according to potential for pollution and aesthetic factors important in abandonment.

With the completion of the inventory and classification of abandoned tailing sites, a data base has been established from which permanent clean up operations can proceed. Those sites exhibiting only physical problems can be hauled away to a more easily protected site, used in construction, or regraded and seeded. Chemical reclamation procedures can be implemented where needed, and aesthetic ratings can be used in assigning priorities for reclamation action.

Although the mandatory controls on point discharges from mines and mills since 1968 have resulted in an obvious improvement in water quality and even though the great majority of "controlled" tailing sites seem to pose no chemical threat, the mixture of tailings and alluvium which covers nearly every floodplain in the basin provides a source for a background water quality which cannot compare with a virgin stream. Water quality can be improved from its present condition. Sediment loading can be reduced by stream channel modifications and revegetation of abandoned tailing sites. Care can be taken to prevent leaching of metals in the more obvious problem sections of the floodplain. Finally, the combination of these techniques cannot help but make the overall environment of the South Fork more aesthetically pleasing.

REFERENCES

- Campbell, A., 1943, 45th Annual Report of the Mineral Industry in Idaho.
- Galbraith, J.H., R. Williams and P. Seims, 1972, Migration and Leaching of Metals from Old Mine Tailings Deposits: Ground Water, May/June, Vol. 10, #3.
- Hawley, J.H., 1920, History of Idaho, Vol. 1: S.J. Clarke Publishing Company, Chicago.

Inventory and Classification of Abandoned Mine Tailings
By Mike Gross, Christos Ioannou and Dale R. Ralston
Page 14

Norbeck, P.L., 1974, Water Table Configuration and Aquifer and Tailings Distribution, Coeur d'Alene Valley, Idaho: M.S. Thesis, University of Idaho, Moscow, 1974.

Reece, D.E., 1974, A Study of Leaching of Metals from Sediments Ores and the Formation of Acid Mine Water in the Bunker Hill Mine: M.S. Thesis, University of Idaho, Moscow, 1974.

DESIGN CONSIDERATIONS FOR EMBANKMENT CONSTRUCTION ON A LOESS FOUNDATION IN SOUTHEASTERN IDAHO

By

Fred Y.M. Chen and Stanley H. Kline
International Engineering Company, Inc.
San Francisco, California

ABSTRACT

A waste water impoundment is planned for construction on the Pocatello East Bench in southeastern Idaho at a site which consists of about 80 feet of loessial soil underlain by gravel and basalt. Soils investigations and laboratory consolidation tests have shown that the silt deposit at the site has the potential for sudden settlement upon saturation and loading, a characteristic of many low density, naturally dry loess deposits. This characteristic is often termed hydrocompaction. Engineering analyses have shown that large settlements will occur upon foundation saturation and embankment loading, and that these settlements will occur rapidly if saturation occurs following embankment loading.

Based on the foundation conditions discovered, special design considerations were given to the construction of the reservoir which will impound 860 acre-feet of water. Preconstruction wetting of foundation soils was recommended in order to initiate settlement at the beginning of embankment construction. Careful monitoring of foundation settlements during and after embankment construction was recommended.

INTRODUCTION

An earth embankment to impound waste water has been planned for construction on the Pocatello East Bench in southeastern Idaho on a foundation of loessial soil. Special design considerations were given to the construction of the reservoir and embankment because of the characteristics of the foundation soils. These design considerations are the subject of this paper along with a description of the area geology, a description of the soil properties, and a comparison with other findings about loessial soils.

Loess is characteristically a tan, unstratified silt with a variable percentage of sand and clay content. True loess is a loose, wind-deposited soil that has never been saturated. It is generally a very uniform deposit, the particles of which are bonded together with relatively small fractions of clay to form its typical low density structure. Loess often has natural moisture contents which are quite low. Loess deposits cover large areas of several continents, including North America. Figure 1 shows the major loess deposits in the United States.

Naturally dry loess usually has a high shearing resistance and can support large loads without significant settlement provided the natural moisture contents are not increased. Upon wetting, however, the bonds between particles in the soil matrix are weakened, causing the loess deposit to undergo settlement or collapse. This behavior is often termed hydrocompaction and is of

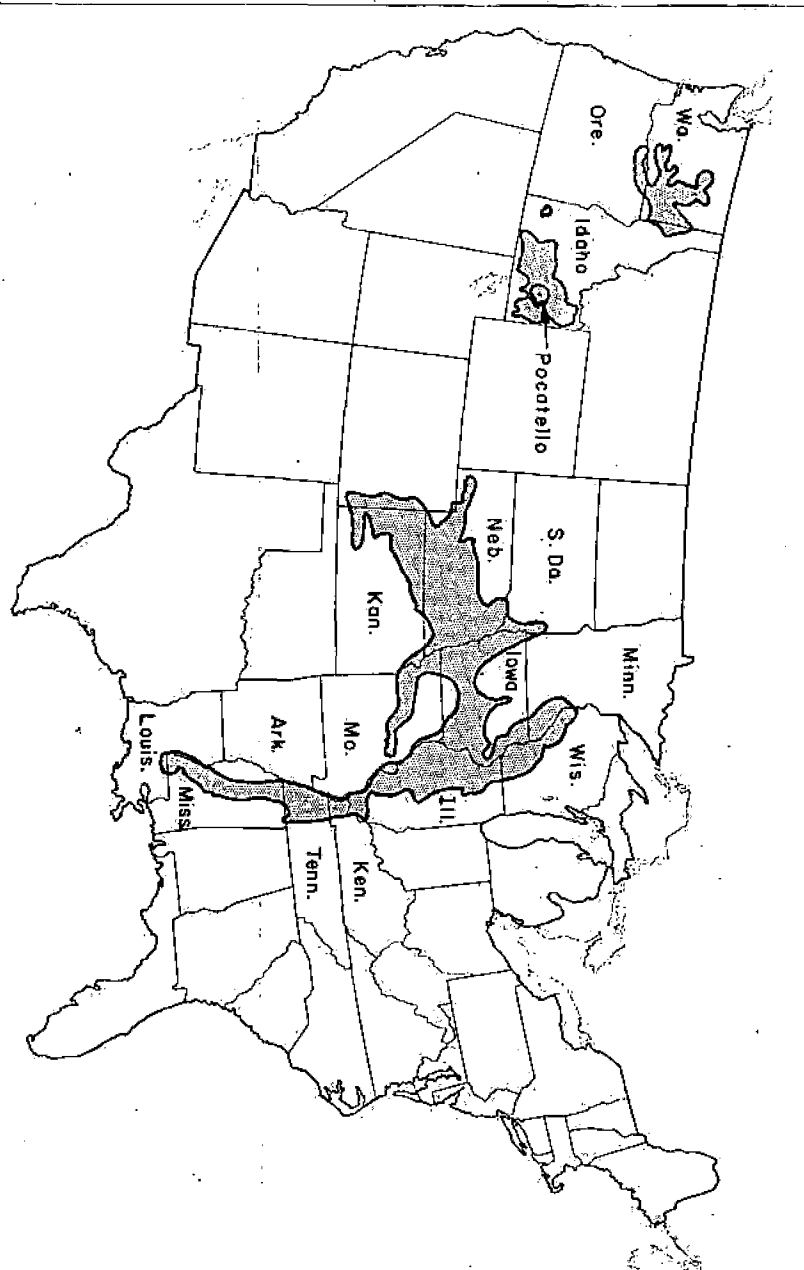


FIGURE 1 - Major Loess Deposits in the United States

particular concern to hydraulic structures that eventually saturate portions or all of their foundations. This potential problem was recognized for the project discussed herein and a preconstruction wetting program was developed to treat the foundation soils.

PROJECT DESCRIPTION

The proposed project referred to herein is the Pocatello Effluent Irrigation System, a proposed system designed to provide water for land irrigation. The owner and developer of the project is the J.R. Simplot Company. The effluent water from the J.R. Simplot Company fertilizer plant in Pocatello, Idaho and the domestic waste water from the City of Pocatello secondary sewage treatment facility, both of which are presently being discharged into the Portneuf River will be utilized for land irrigation. During winter non-irrigation months, plant effluent will be pumped to and stored in an 860 acre-foot reservoir. The reservoir is to be created by the construction of an embankment with native materials obtained from excavations for the reservoir.

Geotechnical investigations were carried out at the site of the proposed embankment in 1977 followed by the design of the impoundment reservoir system. The project site is located about four miles north of Pocatello adjacent to the Interstate 15 Highway (I-15). Figure 2 indicates the project location on a key map and the location of the impoundment site on the Pocatello East Bench in relation to Pocatello and the other project features. Pertinent embankment engineering data are presented in Table I.

GEOLOGIC AND SITE CONDITIONS

Impoundment Site Conditions

The impoundment site, located on the Pocatello East Bench, is situated on the west side of a gently rolling hill bounded by drainage draws to the north and south and I-15 to the west. The ground surface slopes to the west at about 4 percent. Field explorations revealed the impoundment site to be underlain by a thick accumulation of very uniform, dry, wind-deposited silt varying from 64 to over 100 feet thick with an average thickness of approximately 80 feet. The silt deposit is underlain by gravels, below which occurs a basalt interval.

Geology

The project lies within two distinct physiographic regions. The lowlands are part of the Eastern Snake River Plain section of the Columbia Plateau physiographic province, and the adjacent uplands are part of the Basin and Range province. These two regions were created during the late Tertiary Period by a massive downdropped block which formed the plain, truncating the valleys and mountains to the south.

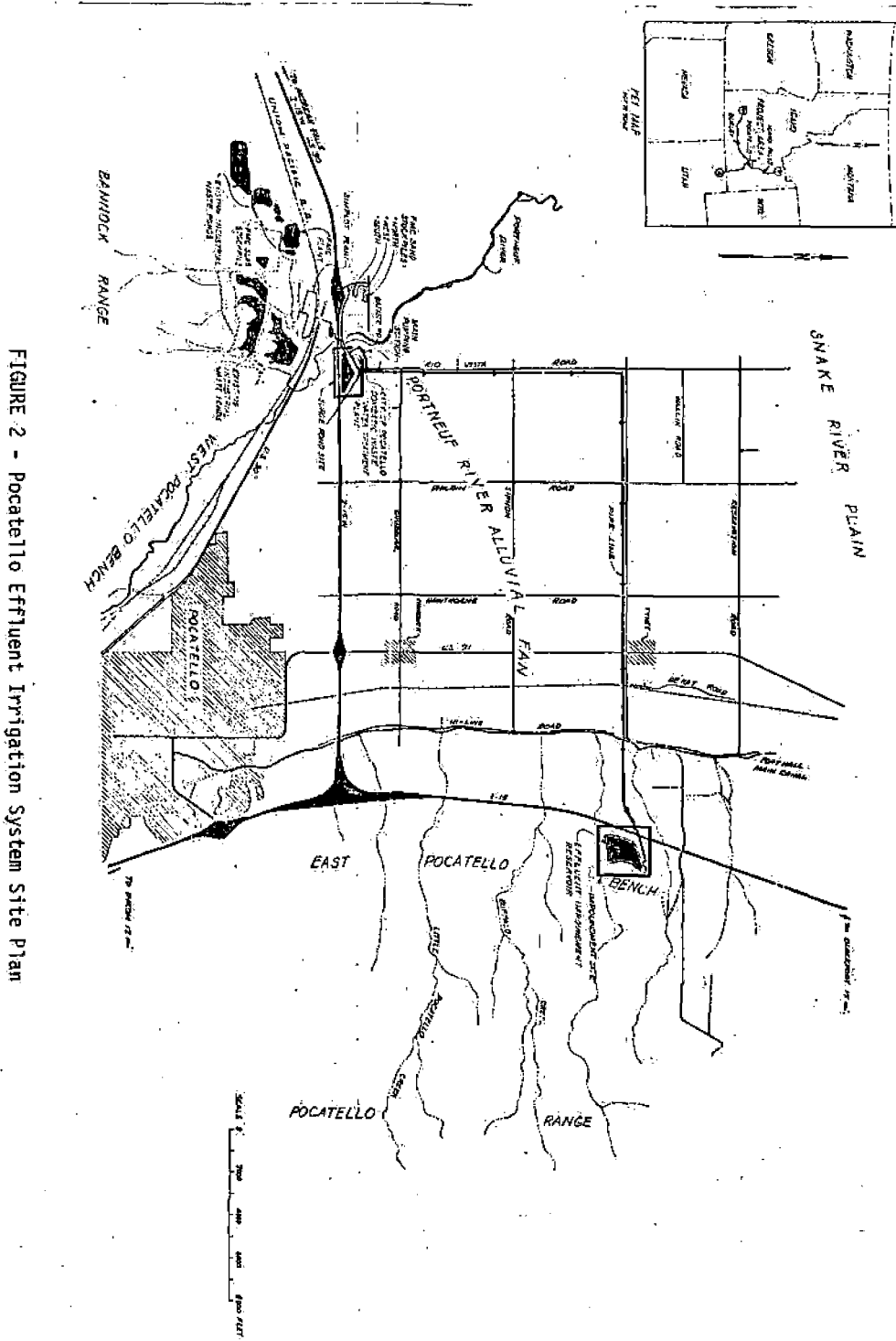


FIGURE 2 - Pocatello Effluent Irrigation System Site Plan

TABLE I
 IMPOUNDMENT
 EMBANKMENT ENGINEERING DATA

Item	Data
Maximum Height of Embankment	38 feet
Upstream or Interior Slope	4.0H:1.0V
Downstream or Exterior Slope	3.5H:1.0V
Crest Width	20 feet
Crest Length	3,926 feet
Embankment Volume	625,000 cubic yards
Foundation Area	20 acres
Reservoir Area @ Maximum Water Level	38.8 acres
Crest Elevation (without camber)	E1. 4678.5
Maximum Water Surface Elevation	E1. 4675.0
Overflow or Spillway Crest Elevation	E1. 4674.25
Storage Capacity @ Maximum Water Level	860 acre-feet

Later in the Tertiary Period, deep-seated volcanic activity occurred and during the last few million years was responsible for damming the Snake River and creating a huge lake that eventually accumulated over 200 feet of sediment. Erosion finally breached the dam formed from the volcanic flows and the lake was drained. The fine sediments of the lake bed were then blown by the wind to adjacent areas and redeposited as thick accumulations of loess such as found at the impoundment site.

Approximately 50,000 years ago, volcanic flows again blocked the Snake River and formed a Pleistocene lake in the vicinity of the American Falls Reservoir. The waters of the lake cut benches in the loess along its margins, and tributary streams were entrenched into the surrounding loess-covered pediment surfaces, resulting in the deposition of about 80 feet of sediments into the lake.

The last major geological event occurred about 30,000 years ago when Lake Bonneville, which was located south of the project in Utah, broke through a drainage divide and caused a flood of catastrophic proportions as it flowed down the Portneuf Valley and emerged onto the Snake River Plain, engulfing the American Falls Lake, and depositing a great deltaic fan of boulders and gravel. The flood waters soon broke through the basaltic dam and dissected the flood deposits until a stable level of dissection was reached, which is recorded as terrace levels along the valley.

Subsequent erosion of the Snake River Valley has left remnants of lower terrace levels, but since the spillover of Lake Bonneville, the only major geological activity of the area has been the continued downcutting of the Snake River Valley, the local deposition of sand dunes, accumulations of thin loess deposits, and the deposition of alluvium and alluvial fans.

Geologic units within the project area are Quaternary age alluvial and wind-blown deposits, a basalt layer that outcrops near the impoundment site, and a tertiary formation of interstratified layers of tuff, basalt, sand, gravel, and in some places, limestone, called the Starlight Formation. The impoundment site is within an area where the geology has been previously mapped and described (Trimble, 1976). Reconnaissance geologic mapping was performed during the field geotechnical investigations to confirm the earlier work.

Figure 3 shows the surficial geology of the impoundment site and surrounding area. A generalized geologic cross section of the impoundment site developed from the surficial geology, local water well logs, and the impoundment site exploratory boring logs is shown on Figure 4. No ground water exists within the loess deposit at the impoundment site.

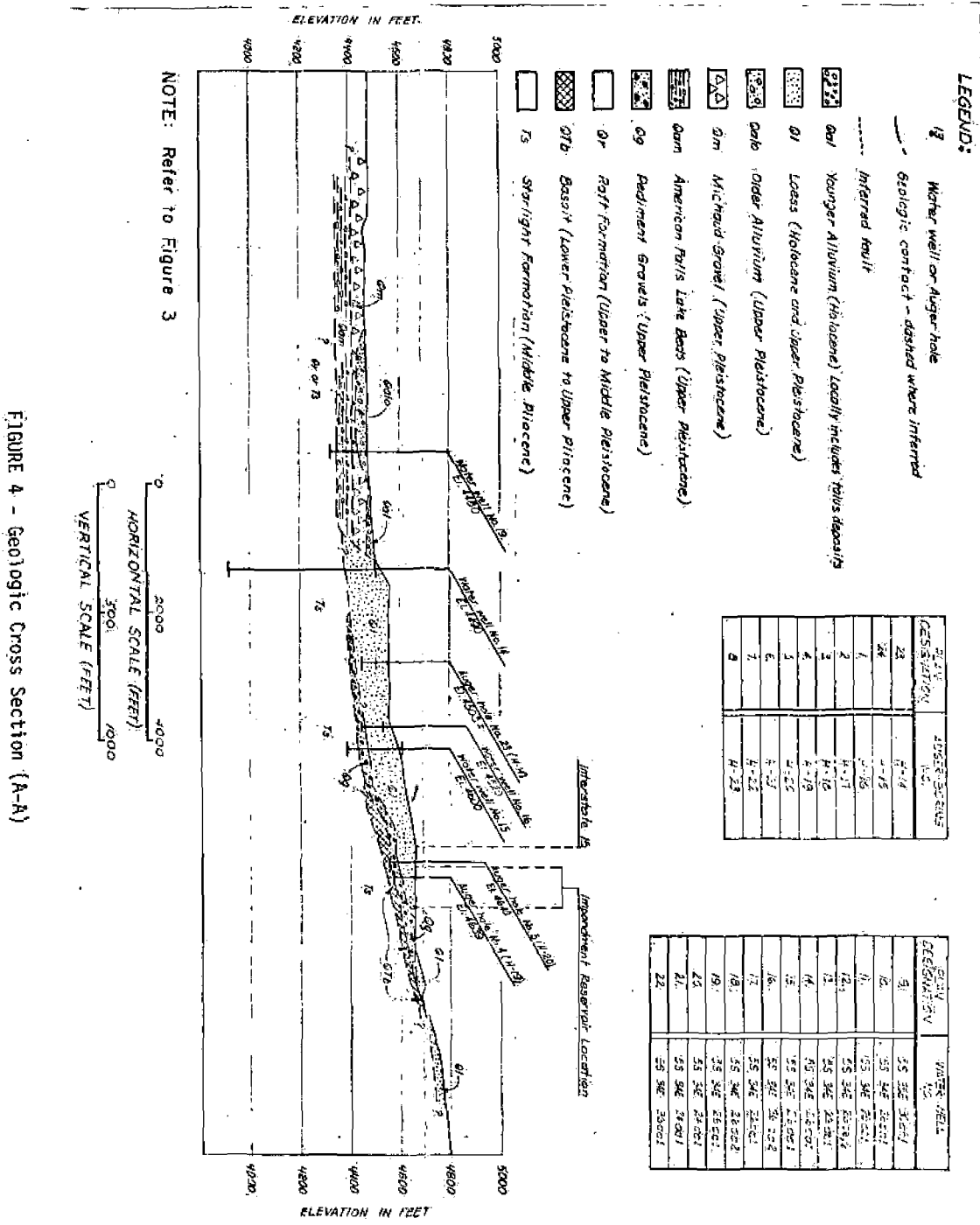


FIGURE 4 - Geologic Cross Section (A-A)

LOESS SOIL CHARACTERISTICS

Physical Properties

Based on laboratory testing performed on undisturbed and remolded samples of the loess taken from the impoundment site, design parameters were selected for the natural foundation soils and the recompacted native soils as presented in Tables II and III, respectively. Figure 5 is a compilation of eight typical grain size curves from gradation analyses performed on samples from the site. The figure shows the uniformity of the loess and that it consists of mostly silt sized particles. Figure 6 shows the compaction characteristics for the subject loess, and the results of direct shear tests performed on inundated samples of undisturbed and recompacted loess are given on Figure 7.

Upon suspicion that the foundation soils at the proposed site might be susceptible to sudden settlements upon wetting, special procedures were used for consolidation testing. Three standard consolidation tests were performed on samples taken from one bore hole at different depths. The samples were inundated toward the beginning of each test. The void ratio versus log of pressure plots for these tests are shown on Figure 8. A fourth consolidation test was performed by loading the sample, at its dry natural condition, to a maximum pressure approximately equal to the sample's in situ overburden pressure plus the maximum weight of the embankment. After equilibrium was reached at the natural water content, the sample was inundated. The purpose of this consolidation test was to determine the soil's potential for settlement upon wetting. The results of this test are also presented on Figure 8.

The results showed that the percent compression at the total load of 8 ksf at the natural moisture content was 1.4 percent. Upon wetting, an instantaneous increase in percent compression occurred. Three minutes after wetting, the percent compression had increased to 8.2 percent, and at the end of a 24-hour period, it had stabilized at 9.7 percent. The percent compression after equilibrium of the other three samples (#57, #60, #68) at the same load of 8 ksf ranged from 5.6 percent to 10.7 percent. These samples, as stated earlier, were inundated toward the beginning of each test. These results confirmed the characteristic behavior of the loessial soil at the impoundment site. The soil exhibited the ability to support large loads without significant settlement at its natural moisture content, but upon wetting, sudden settlement was caused by the loss of strength of the soil skeleton. Both types of consolidation tests resulted in comparable ultimate settlements, but the rate at which settlement occurred was dependent upon when the soil was inundated and at what load the soil was subjected to when inundation occurred.

A majority of the publications and information found about the properties and characteristics of loessial soil as a foundation material present the experiences obtained by the United States Department of the Interior Bureau of Reclamation (USBR) relative to the construction of earth dams in the Missouri

TABLE II
NATURAL FOUNDATION SOILS
SELECTED DESIGN PARAMETERS

Parameters	Impoundment Site Silt Overburden
Dry Density, γ_d (pcf)	90
Moist Density, γ_m (pcf)	95
Saturated Density, γ_{sat} (pcf)	117
Natural Water Content, w_n (%)	6
Specific Gravity, G_s	2.68
Friction Angle, θ (degrees)	0' - 40':26 > 40':30
Cohesion, c (psf)	0
Permeability, k (cm/sec)	1×10^{-4}
Compression Index, C_c	0.29
Swelling Index, C_s	0.016
Coefficient of Consolidation, C_v (cm ² /sec)	0.17

TABLE III
RECOMPACTED NATIVE SILT
SELECTED DESIGN PARAMETERS

Parameter	Impoundment Site Recompacted Silt
Maximum Dry Density, γ_d max (pcf)	107
Optimum Water Content, w_{opt} (%)	16
Dry Density, γ_d (pcf)*	102
Moist Density, γ_m (pcf)*	118
Saturated Density, γ_{sat} (pcf)*	126
Friction Angle, ϕ (degrees)*	28
Cohesion, c (psf)*	0
Permeability, k (cm/sec)*	1×10^{-5}

* The parameters in this table are based on laboratory tests on remolded soil samples that were compacted to 95% of the Standard Proctor maximum density at the optimum moisture content.

POCATELLO EFFLUENT IRRIGATION SYSTEM
IMPOUNDMENT SITE SOILS

COMPILATION OF FOLLOWING GRADATION CURVES:

Boring	Sample No.	Depth
H-16	15	0'-5.0'
H-17	16	0'-5.0'
H-17	18	7.5'-9.0'
H-17	20	17.5'-19.0'
H-17	22	27.5'-29.0'
H-18	33	0'-5.0'
H-19	45	0'-5.0'
H-23	109	0'-3.0'

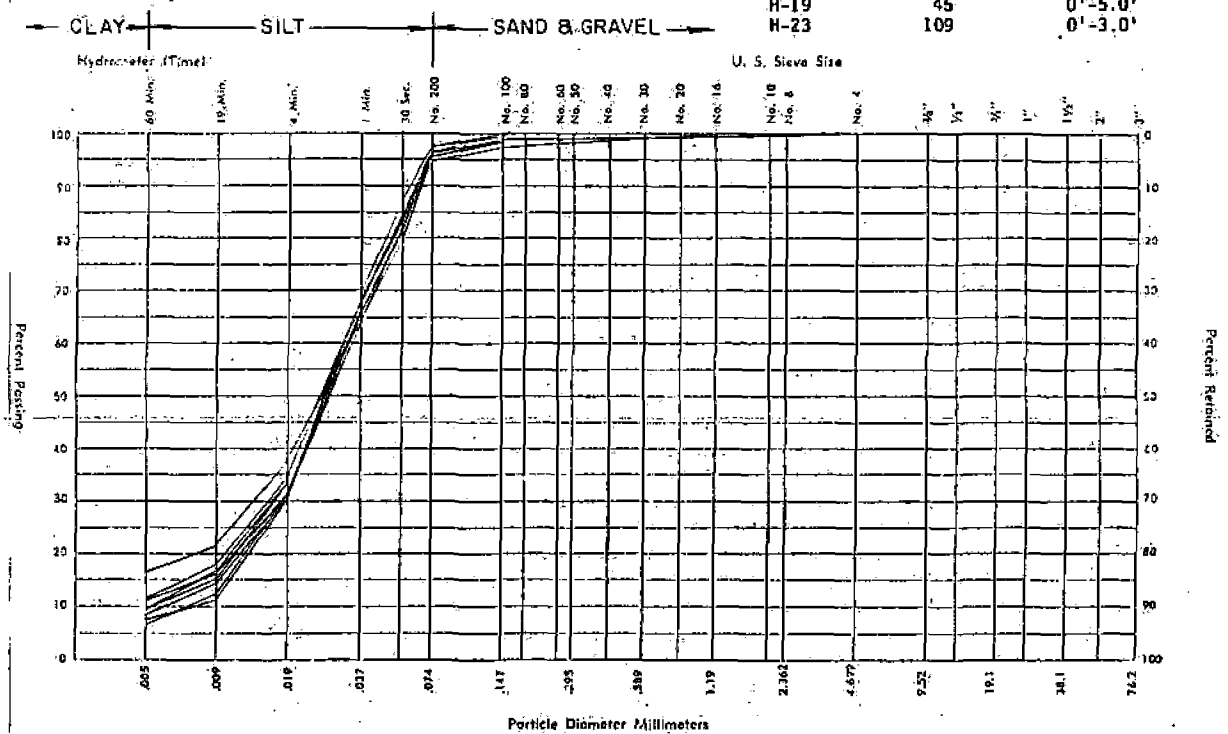
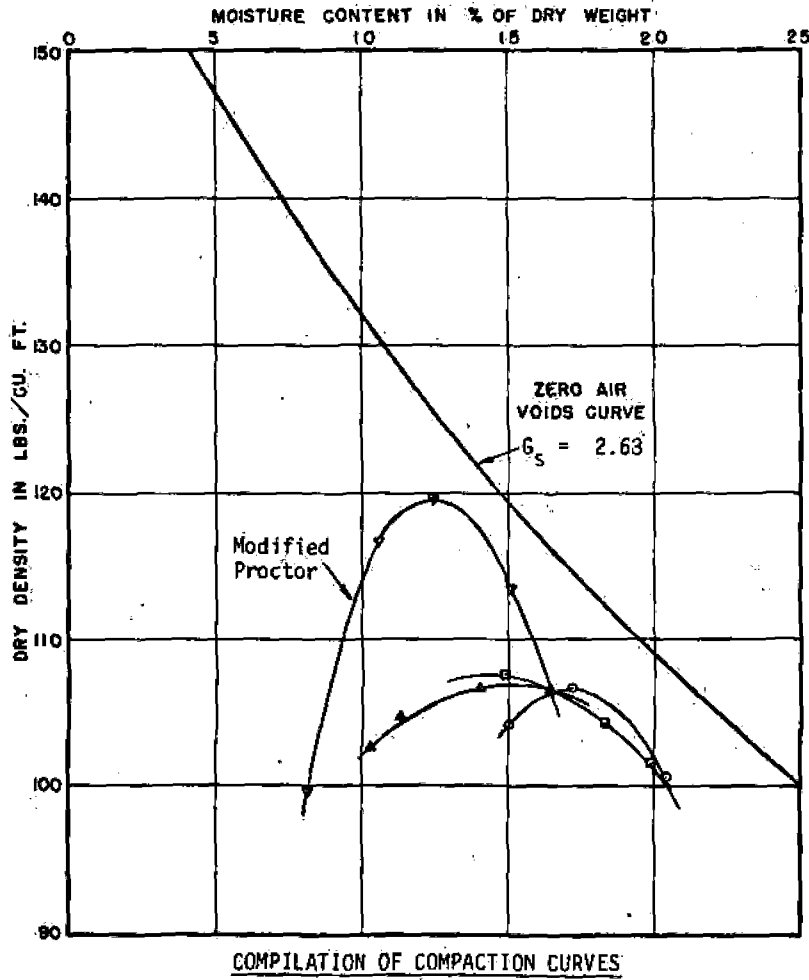


FIGURE 5 - Pocatello Impoundment Site Loess - Gradation Characteristics



COMPACTION TEST DATA

<u>STANDARD PROCTOR</u>	•	K-16	Sample No. 15	0'-5.0'	$w_{opt} = 17.6\%$, $\gamma_d \text{ max.} = 106.7 \text{ pcf.}$
	■	H-17	Sample No. 16	0'-5.0'	$w_{opt} = 15\%$, $\gamma_d \text{ max.} = 107.4 \text{ pcf.}$
	▲	H-18	Sample No. 33	0'-5.0'	$w_{opt} = 15.3\%$, $\gamma_d \text{ max.} = 106.6 \text{ pcf.}$
<u>MODIFIED PROCTOR</u>	•	H-23	Sample No. 109	0'-5.0'	$w_{opt} = 12.7\%$, $\gamma_d \text{ max.} = 119.4 \text{ pcf.}$

FIGURE 6 - Pocatello Impoundment Site Loess - Compaction Characteristics

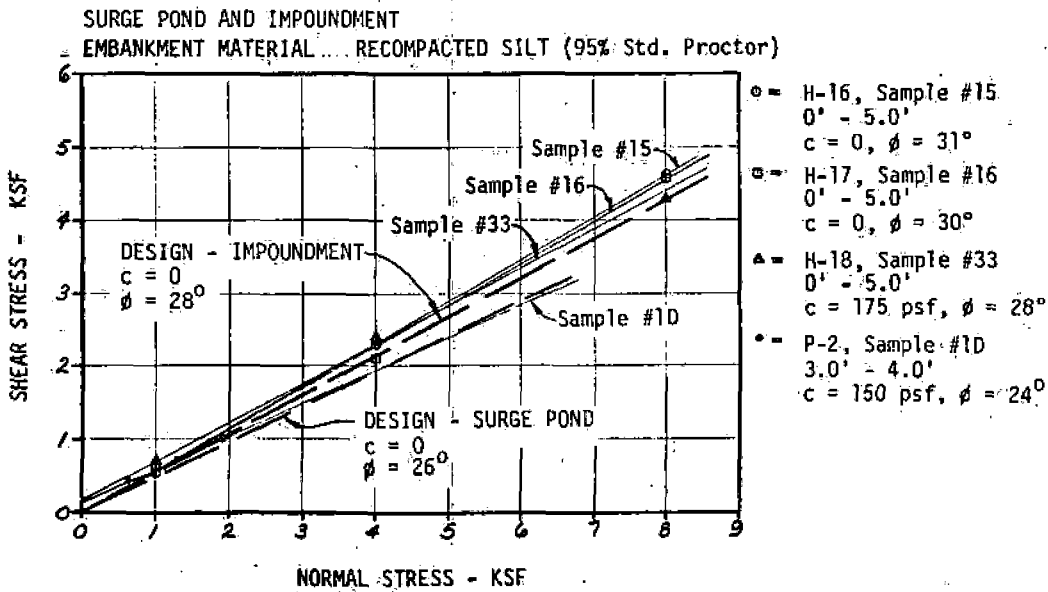
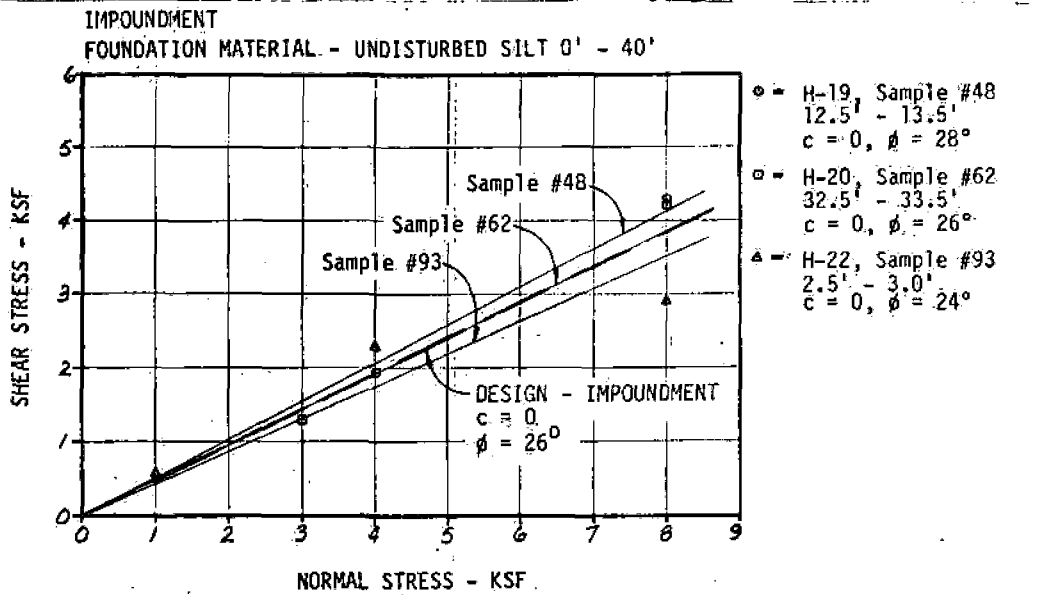


FIGURE 7 - Pocatello Impoundment Site Loess - Strength Characteristics

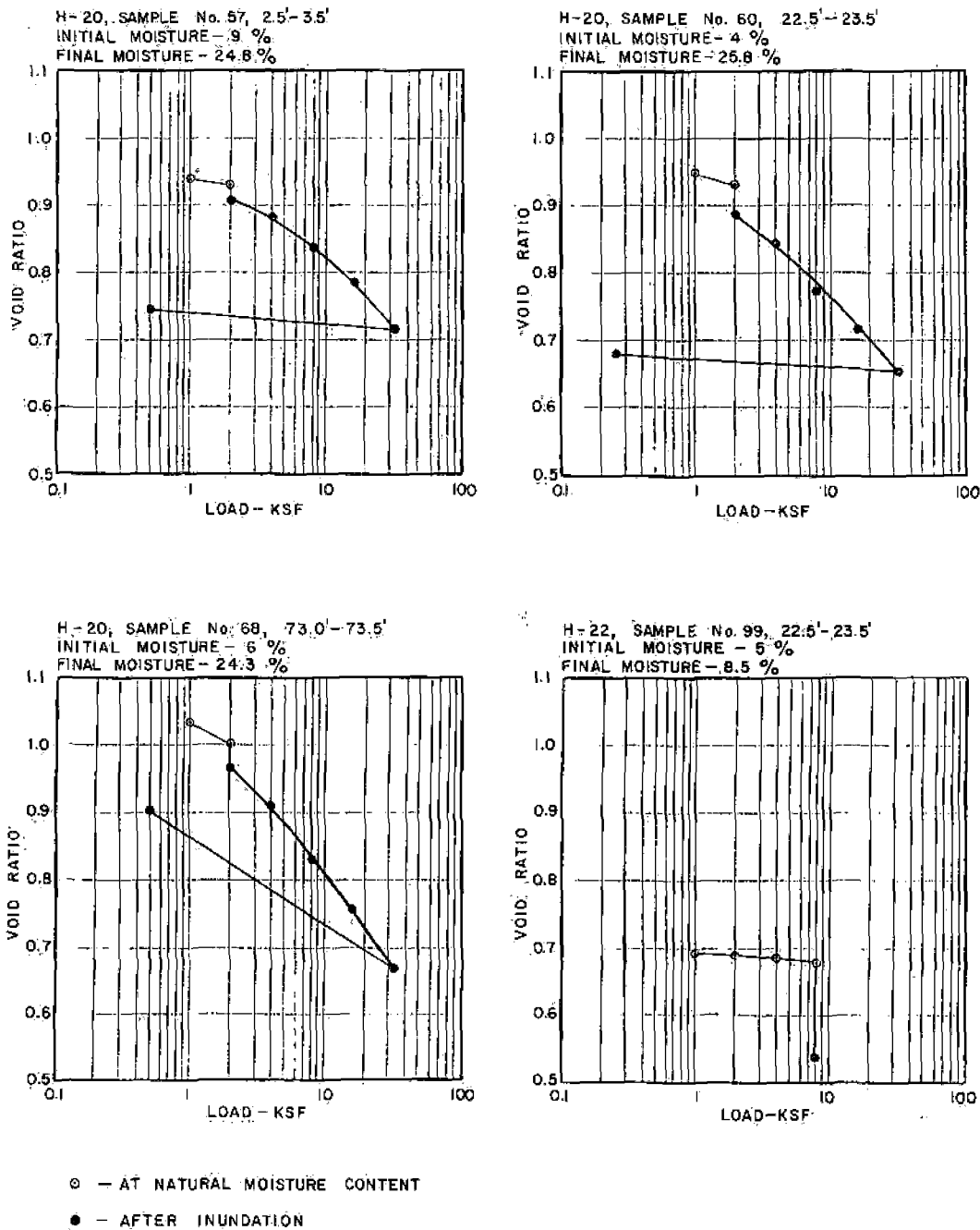


FIGURE 8 - Pocatello Impoundment Site Loess - Consolidation Characteristics

River Basin states of Nebraska and Kansas. Efforts were made to compare the properties and behavior of the loessial soil at the impoundment site in southeastern Idaho with the findings reported from other projects. A few of these comparisons are presented in the following paragraph.

A great similarity exists between the grain size distribution for the subject loess and the gradation trends for Missouri River Basin loess as reported by the USBR in their Engineering Monograph No. 28 (Gibbs & Holland, 1960). This comparison is shown on Figure 9. A comparison was also made between the consolidation tests performed on the Pocatello loess and the consolidation trends for Missouri River Basin loess also presented in the USBR Engineering Monograph No. 28. This comparison is also shown on Figure 9. The three consolidation tests performed on inundated samples #57, #60, and #68 have characteristics similar to the trends indicated for wetted loess tested at moisture contents above 20 percent. The final moisture contents of samples after testing were above 20 percent. The consolidation curve from the unsaturated test conducted at its natural moisture content of 5 percent is comparable to the consolidation trends indicated for dry loess with moisture contents below 10 percent. The settlement upon wetting is also indicated on the void ratio versus log of pressure plot of sample #99.

Mineralogical Properties

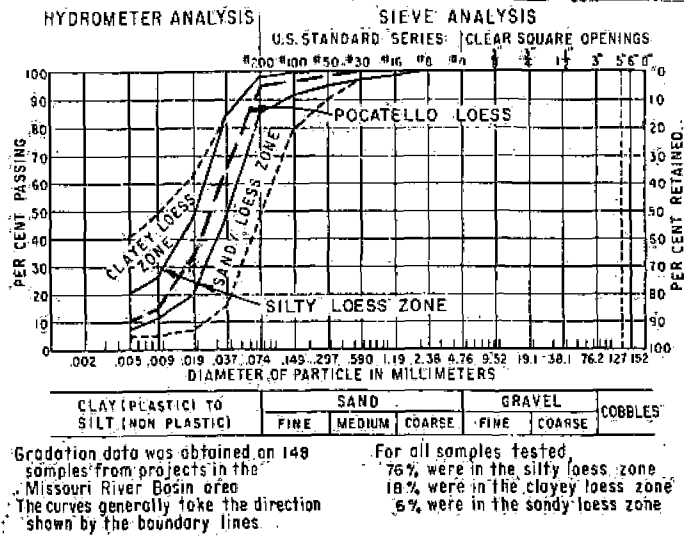
A brief mineralogical study was made on one sample of loess from the Pocatello site. The comparison of mineralogical properties of loess from various sources to the loess found at the Pocatello site is summarized in Table IV.

FOUNDATION TREATMENT

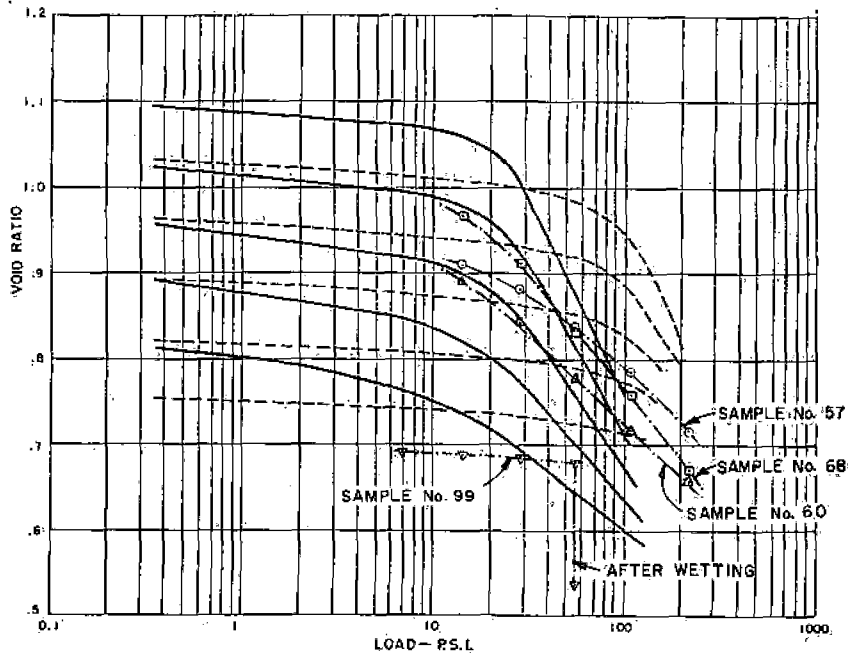
Criterion for Foundation Treatment

As a result of the characteristics found for the loessial foundation soil, a program of foundation saturation prior to construction was incorporated into the design of the impoundment embankment. The practice of pre-wetting of dry foundation soils under earth embankments has been used by the USBR for a number of major earth dams constructed on Missouri River Basin loess, and has proven effective in reducing post-construction settlements and their associated problems. Ponding or irrigation was carried out to some degree prior to the construction of projects such as Medicine Creek Dam, Sherman Dam, Trenton Dam, Enders Dam, and Bonny Dam, all of which are part of the USBR Missouri River Basin Project.

Studies made by the USBR during their work on Missouri River Basin loess have indicated that the major factors influencing the susceptibility of loess to large settlement upon wetting are its density, moisture content, and the magnitude of the applied load. A criterion was developed by the USBR



GRADATION CHARACTERISTICS



MISSOURI RIVER BASIN LOESS **POCATELLO LOESS**
 ——— Wetted Loess (above 20% moisture) ——— Wetted Loess (above 20% moisture)
 - - - - Dry Loess (below 10% moisture) - - - - Dry Loess (below 10% moisture)

CONSOLIDATION CHARACTERISTICS

FIGURE 9 - Comparison of Pocatello Loess and Missouri River Basin Loess

TABLE IV
COMPARISON OF MINERALOGICAL PROPERTIES OF LOESS FROM VARIOUS SOURCES

Mineralogy (Average Ranges-in.%)	USBR Dams, Missouri River Basin, Kansas & Nebraska (ML-CL)	Teton Dam, Idaho (ML)	Simplot Impoundment Pocatello, Idaho (ML)	State Highway Commission of Kansas Research Depart- ment, Northern Kansas (CL-ML)
Quartz	25-37	30-35	30	30-38
Feldspar	10-22	20-25	20	30-33
Calcite	5	15-20		
Dolomite		5-10		
Kaolinite		2-3		1-4
Illite-mica	4-6	2-3	10	3-7
Montmorillonite	15	1-2		12-24
Chlorite		1-2		
Hornblende & Chalcedony	2	2		5
Glass shards, pumice	8			0-5
Plant opal				1
Minor and unidentified		10		
Carbonate			40	

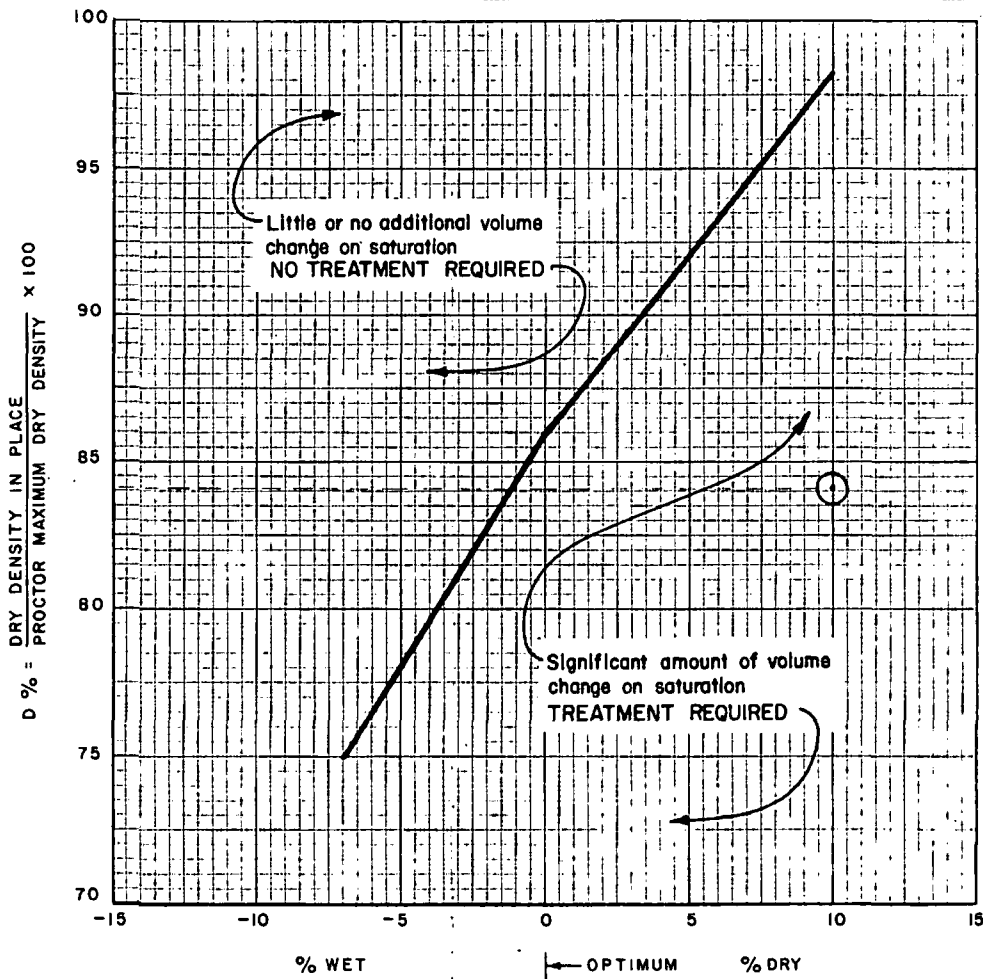
for determining the need for foundation treatment based on 112 tests made on samples of undisturbed foundation soils (Design of Small Dams, 1974). This criterion is presented here as Figure 10. The criterion is based on the ratio of the natural dry density to the proctor maximum dry density, and the difference between the optimum water content and the natural water content. The silt soil from the Pocatello site falls within the zone indicating treatment required.

Another significant comparison was made between Missouri River Basin loess and Pocatello loess and is presented as Table V. Table V summarizes partial laboratory test results on undisturbed samples of loess taken from the foundation of the USBR's Medicine Creek Dam (Design of Small Dams, 1974). The table shows the ratios of the natural dry densities to the proctor maximum dry densities and the differences between the optimum water contents and the natural water contents, the properties that the criterion in Figure 10 is based on. Also, shown is the percent compression under a total load of overburden plus fill at the natural moisture content and after wetting. Added to this table is the data from the four consolidation tests performed on loess from the impoundment site. The data has many similarities.

Foundation Prewetting Program

In order to attempt to saturate the impoundment embankment foundation, a prewetting scheme was developed whereby the embankment foundation area would be irrigated and the surface kept saturated for a minimum period of 60 days preceding construction. Figure 11 shows the estimated quantity of water required to saturate the foundation to various depths as a function of soil permeability and time of treatment. This was based on the foundation area of about 20 acres, and an initial void ratio of 0.9 and an initial natural moisture content of 5 percent determined from laboratory testing. The natural soil permeability in the vertical direction was estimated to be approximately 1×10^{-4} cm/sec. Saturation of the foundation to a depth of about 40 feet was considered adequate since the majority of the settlement would occur in this zone, thus the 60 day prewetting period was chosen.

Figure 12 shows a graph of the design prewetting program and the actual program carried out in terms of water quantity applied versus days of treatment. The design quantity of 2.03 mgd (70 gpm/acre) for 60 days was based on the maximum estimated amount of water that could be absorbed by the loess foundation surface without excess runoff. This was determined from the estimated vertical permeability of 1×10^{-4} cm/sec. from laboratory testing. The actual prewetting program was carried out over a period of 87 days. The initial quantities of water applied were considerably less than that recommended; however, toward the end of the operation, water was being applied at about the maximum rate possible without producing excess runoff. This rate estimated from the graph was about 1.8 mgd (62 gpm/acre) which is quite close to the design quantity, suggesting that the estimated in situ vertical permeability of 1×10^{-4} cm/sec. was probably quite accurate. The resulting total quantity of water applied to the foundation, 93.5 million gallons, was not too different from the recommended design quantity, 122 million gallons.



$W_0 - W = \text{OPTIMUM WATER CONTENT} - \text{NATURAL WATER CONTENT}$

POCATELLO LOESS: $\left. \begin{array}{l} \gamma_d (\text{natural}) = 90 \text{ pcf} \\ \gamma_d \text{ max (Std. Proctor)} = 107 \text{ pcf} \end{array} \right\} D = 84.1 \%$
 $\left. \begin{array}{l} W (\text{natural}) = 6 \% \\ W_0 (\text{optimum}) = 16 \% \end{array} \right\} W_0 - W = 10 \%$

FIGURE 10 - Foundation Treatment Criterion

TABLE V
 PROPERTIES OF LOESSIAL FOUNDATION SOILS

Approximate sample depth (feet)	Natural water content (percent)	Average $w_0 - w$ (percent)	In-situ dry density (pcf)	Average D^2 (percent)	Total load, fill plus overburden (psi)	Compression at total load	
						At natural moisture (percent)	After wetting (percent)
MEDICINE CREEK DAM							
5	8.8	7.4	79	75	25	8.4	10.9
17	9.7	6.5	77	74	33	1.3	9.1
19	9.6	6.6	81	77	34.5	1.0	3.9
50	6.6	8.7	92	83	55	1.5	6.5
POCATELLO IMPOUNDMENT EMBANKMENT							
3 (#57)	9	7	92	86	33	—	3.9
23 (#60)	4	12	89	83	46	—	8.9
73 (#68)	6	10	87	81	79	—	12.3
23 (#99)	5	11	87	81	56 ³	1.4	9.7

- 1 - $w_0 - w$ = optimum water content for Proctor maximum dry density minus natural water content.
 2 - $D(\%)$ = $(\text{in-situ dry density} \div \text{Proctor maximum dry density}) \times 100$.
 3 - Load is 10 psi greater than actual expected total load of fill plus overburden.

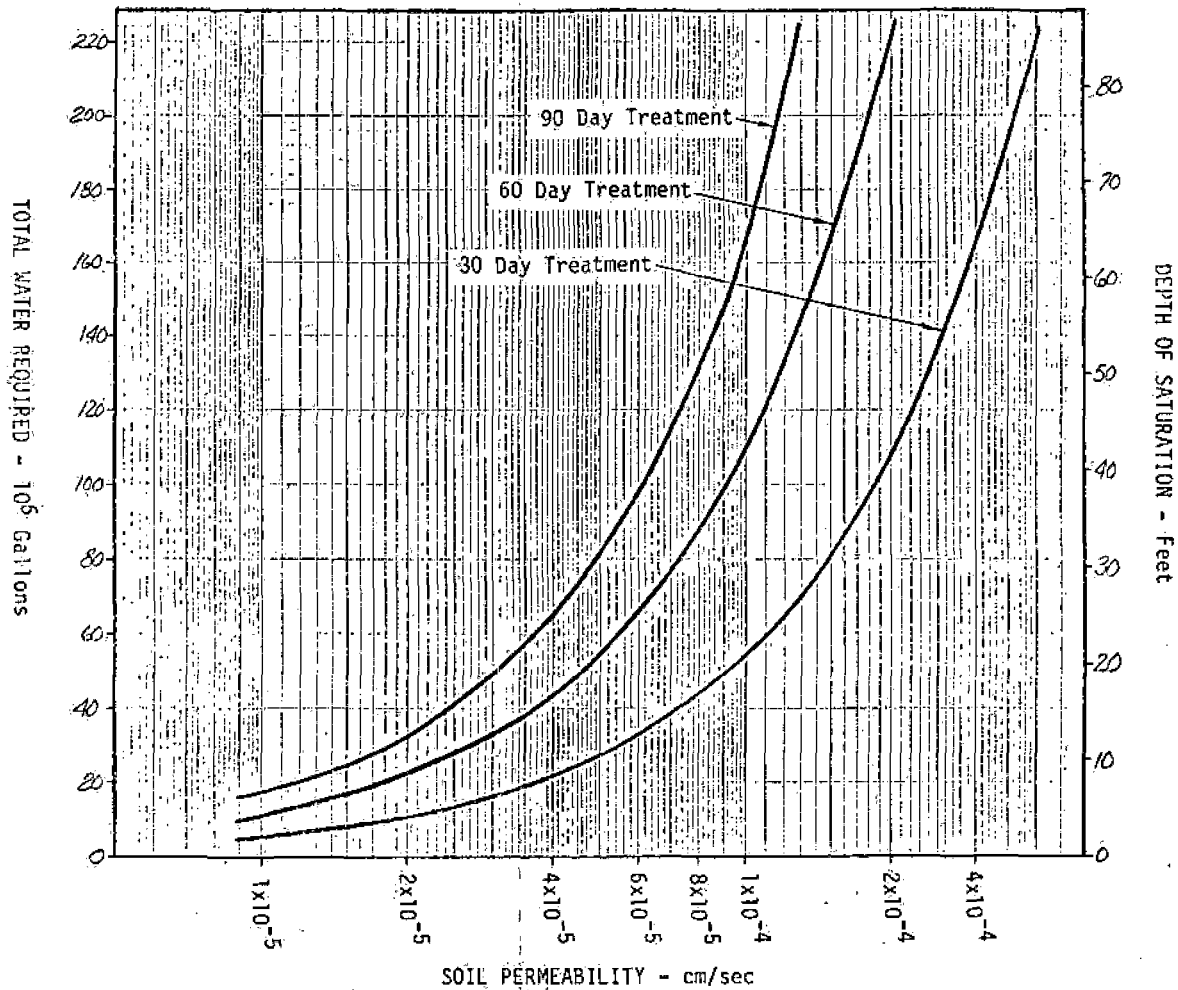


FIGURE 11 - Pocatello Impoundment Foundation Prewetting Water Quantity and Depth of Saturation vs. Soil Permeability and Treatment Time

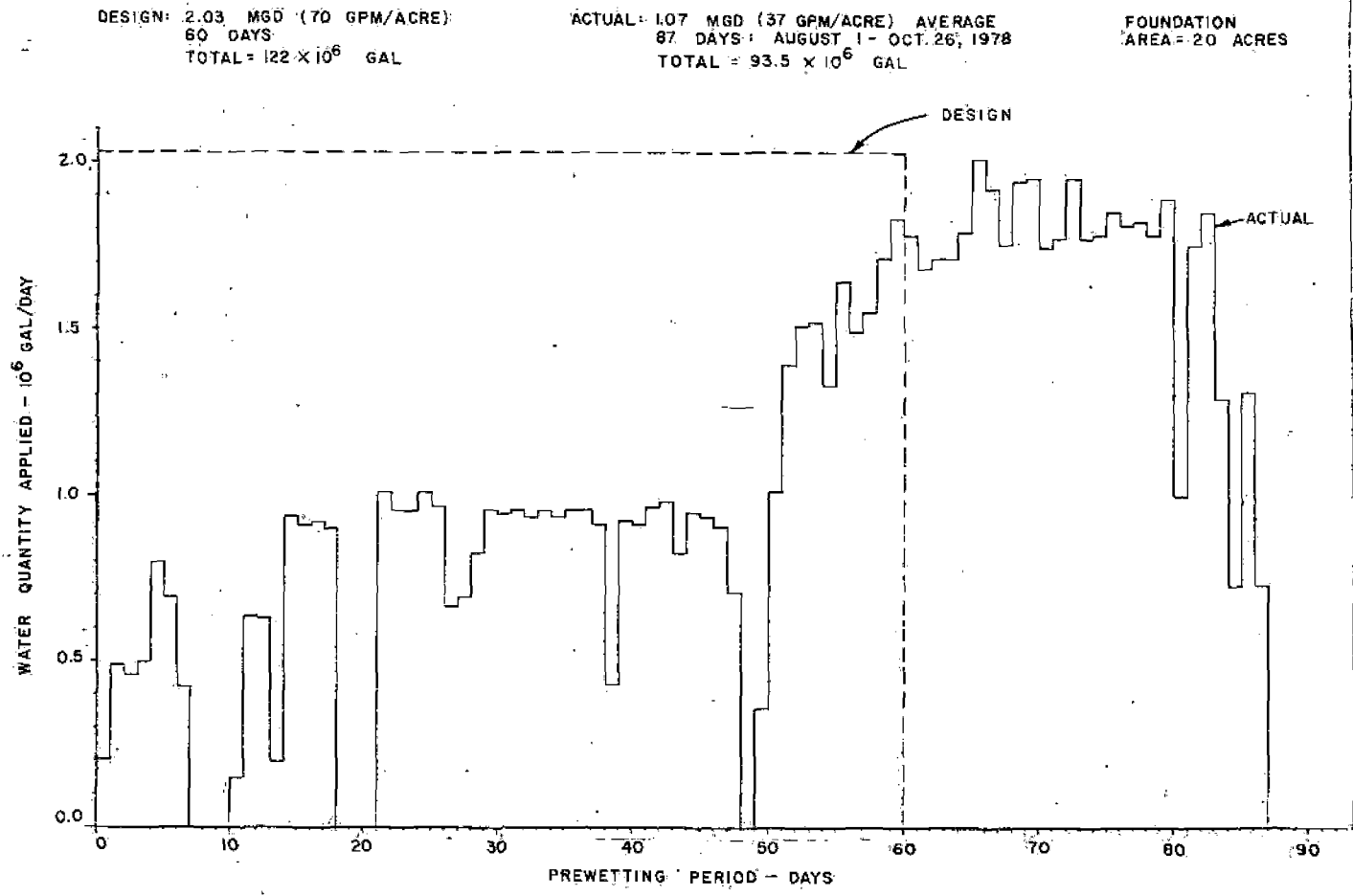


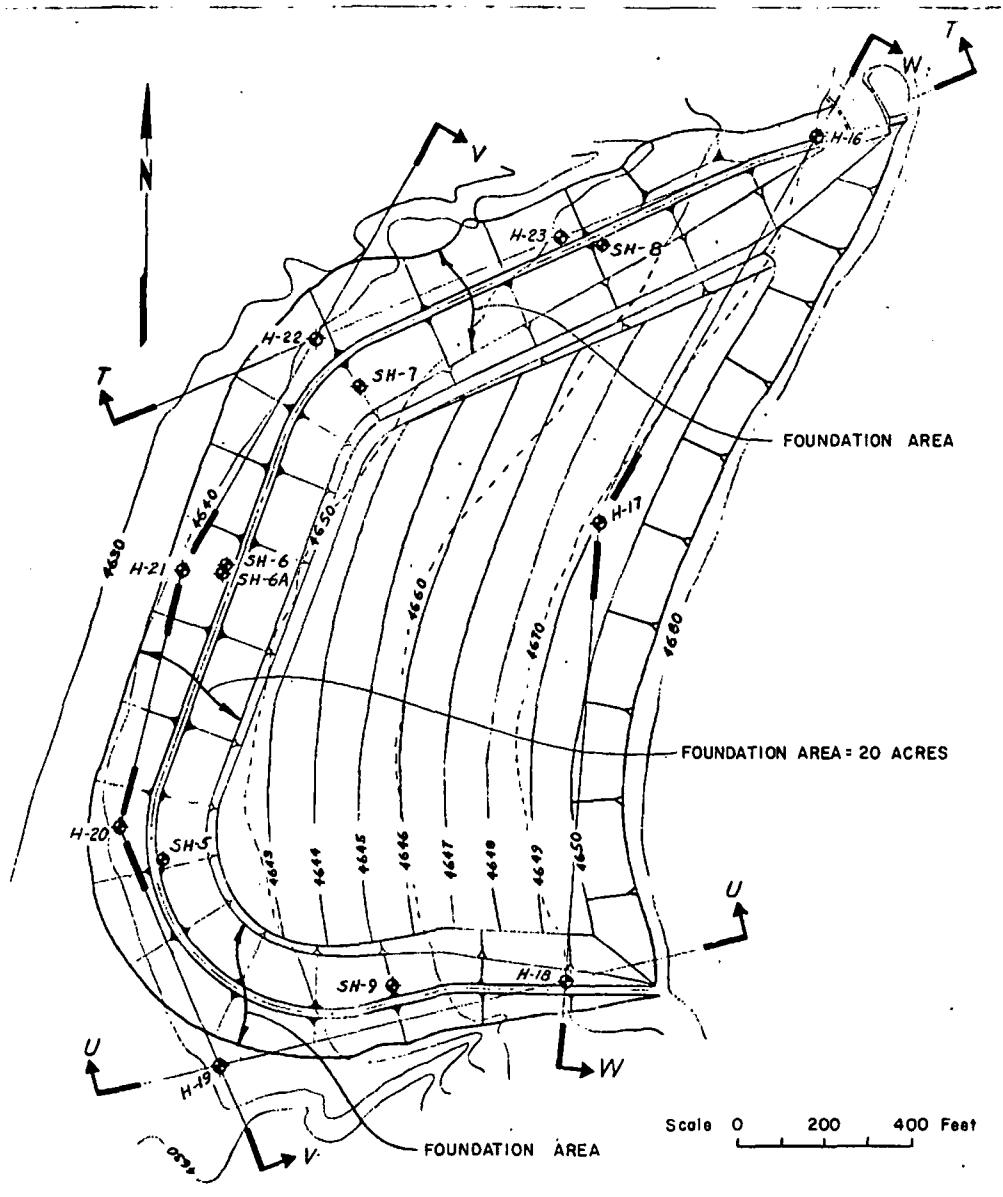
FIGURE 12 - Pocatello Impoundment Embankment Foundation Prewetting Program

Part of the recommendations for the prewetting operation included the drilling of test holes for moisture content tests to determine the moisture penetration depth and the effectiveness of the prewetting. Figure 13 shows a plan of the impoundment embankment and reservoir with the foundation area, original bore hole locations, and test hole locations after prewetting indicated. Profile plots of in situ moisture contents prior to and after foundation prewetting are presented on Figure 14. Also, indicated on the profiles is the average estimated moisture content at saturation. The results showed that the prewetting treatment increased moisture in the naturally dry loess to an overall average moisture content of about 20 to 25 percent in the top 40 feet. Below 40 feet, moisture contents dropped sharply back to the levels encountered from original explorations. These findings suggest that although the prewetting program was not carried out exactly as conceived, the total quantity of water applied was not too different than that recommended to achieve saturation to a depth of 40 feet, and in fact moisture contents were increased considerably in the upper 40 feet. Although the design curves presented in Figure 11 are based on saturated flow and complete saturation was not achieved from the prewetting, they provided a good estimate of moisture penetration depth.

At the time of this writing, construction of the impoundment embankment has not begun. Because of delays in the start of embankment construction, it has been recommended that further foundation treatment be performed prior to construction. Moisture contents determined from samples retrieved at the end of March 1979 showed a decrease in moisture content to an average of about 13 percent as shown on Figure 14. The moisture content desired in the foundation soils at the start of embankment construction is preferably 25 percent and no less than 20 percent to ensure effectiveness. Settlement criteria established for Kansas-Nebraska loess by the USBR, based on moisture content, classifies loess with less than 10 percent moisture as very dry, of maximum dry strength, and highly resistant to settlement; loess with 10 to 15 percent moisture as still quite dry and of rather high dry strength; loess with 15 to 20 percent moisture as approaching moist conditions; and loess with more than 20 percent moisture as rather wet to moist and generally will permit full consolidation to occur under load. USBR experience with Missouri River Basin loess has shown that moisture contents in the range of 25 to 28 percent could easily be obtained by surface ponding and sprinkling, and about 35 percent moisture, depending on natural density, would be required for complete saturation (Holtz and Hilf, 1961). These findings are again quite similar to the characteristics of the loess encountered in Pocatello, Idaho.

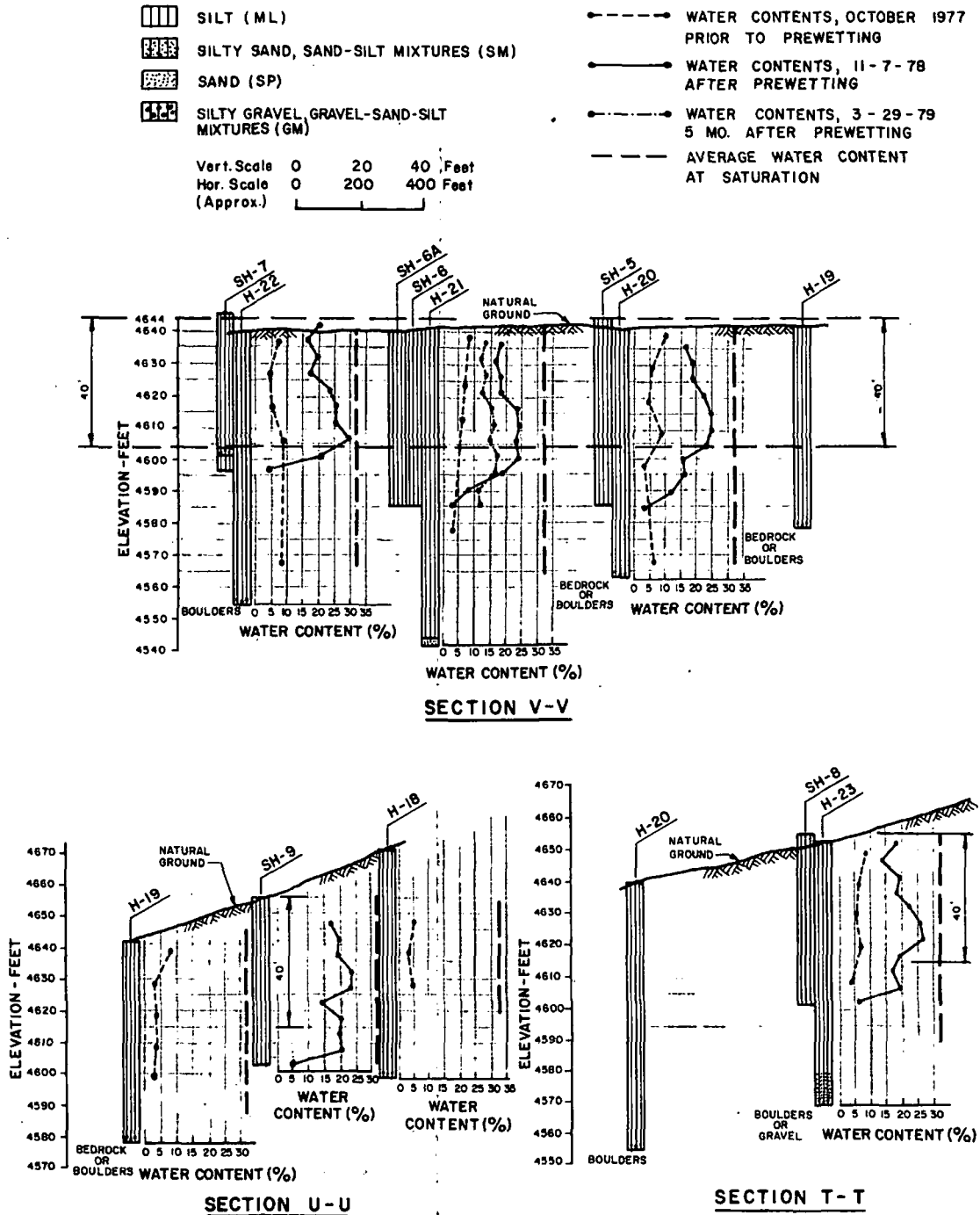
FOUNDATION MONITORING

For proper monitoring, the installation of foundation settlement plates are recommended. Accurate settlement monitoring is required to determine the effectiveness of the foundation treatment in minimizing post-construction settlements. Eleven foundation settlement plates were installed at various positions along the impoundment embankment centerline and at various offsets



ORIGINAL FIELD INVESTIGATION: H-16 - H-23, OCTOBER 1977
 TEST HOLES AFTER PREWETTING: SH-5 - SH-9, 11-7-78
 TEST HOLES AFTER PREWETTING: SH-6A, 3-29-79
 NOTE: REFER TO FIGURE 14

FIGURE 13 - Pocatello Impoundment Plan



NOTE: REFER TO FIGURE 13

FIGURE 14 - Foundation Prewetting Moisture Penetration Water Content vs. Depth

from the centerline. The settlement markers will be carried up through the embankment as construction progresses. Data obtained from surveying the foundation markers will show the progress of foundation settlements along the embankment and across its section during the foundation prewetting period, during embankment construction, and during reservoir operation. This data is important to verify settlement predictions and to observe any unexpected behavior.

Unlike other soils susceptible to settlement upon wetting which exhibit this behavior without the influence of additional load applied, loess characteristically will not settle significantly upon wetting in its undisturbed state without the addition of load. Experience obtained by the USBR from dam construction on Missouri River Basin loess has shown this, and experience obtained thus far from Pocatello loess has shown the same behavior. Settlement data accumulated thus far has shown that essentially no settlement has occurred to date as a result of the 87-day period of foundation irrigation, as expected. Recommendations were made to continue settlement monitoring on a regular basis during the additional recommended foundation prewetting, during embankment construction, and during reservoir operation.

CONCLUSIONS AND RECOMMENDATIONS

Loess, a uniform, wind-deposited soil typically having low natural densities and moisture contents, is found over large areas of several continents, including many of the central states and parts of Idaho and Washington in the United States. Loess is characteristically susceptible to sudden settlements upon wetting under load, a behavior often called hydrocompaction. The loess encountered at the Pocatello impoundment site was found to exhibit these characteristics, and a program of preconstruction wetting of the foundation soils was recommended for foundation treatment.

It is important to recognize the characteristics of loessial soils when they will provide the foundation for structures. Certain soil properties and laboratory testing procedures were used to evaluate the impoundment site soil's susceptibility to settlement upon wetting. Consolidation testing showed the capability of the Pocatello loess to support large loads at its natural moisture content, but undergo large sudden settlement upon wetting. Comparison of natural dry density to proctor maximum density and natural water content to optimum water content according to a foundation treatment criterion developed by the USBR from their experiences with Missouri River Basin loess indicated that the impoundment site loess required treatment. Comparisons of gradation, consolidation, and other characteristics between Missouri River Basin loess and Pocatello loess showed many similarities.

Foundation saturation prior to construction by ponding or irrigation has been found to be an applicable method for the treatment of loessial foundation soils under earth embankments. A prewetting program was recommended for the impoundment embankment foundation and was carried out by irrigation over an 87-

day period. Test holes were drilled after prewetting to verify the estimated depth of moisture penetration and to evaluate the effectiveness of the treatment. The application of 93.5 million gallons of water to the foundation area of 20 acres resulted in an increase in moisture content from an average of 6 percent to an average of 20 to 25 percent in the top 40 feet. Subsequent determinations of field moisture five months after prewetting showed that moisture contents in the top 40 feet had dropped to an average of about 13 percent. As a result of this and delays in the start of embankment construction, further prewetting was recommended. It was determined that a minimum of 20 percent moisture content in the top 40 feet of foundation soils should be achieved prior to embankment construction to ensure effective treatment.

The main objective in prewetting the loessial foundation soil is to minimize post-construction settlements. Without prewetting, the impoundment embankment would not experience appreciable settlement until reservoir filling. As the foundation became partially or fully saturated, the embankment would be subject to rapid settlements due to weakening of the soil particle bonds in the loose skeleton structure. Prewetting does not reduce the magnitude of the ultimate settlement, but it causes settlement to occur during embankment construction upon application of the first loading. Prewetting, by filling soil voids with water, and by weakening the soil structure prior to loading, allows settlement to occur during construction and causes settlement to occur at a slower rate which can be estimated by consolidation theory. It is expected that about 25 percent of the ultimate settlement of the impoundment embankment will occur during an estimated 4-month construction period, and that post-construction settlements will occur at an acceptable rate.

Settlement monitoring was recommended during the prewetting operation, during embankment construction, and during reservoir operation. This is an important follow-up to the foundation treatment program, and it will verify its effectiveness as well as point out any unexpected behavior. Foundation settlement markers were installed at the impoundment site prior to prewetting and have indicated no settlement to date, as expected. They will be observed throughout construction and periodically during reservoir operation.

ACKNOWLEDGEMENTS

The authors gratefully acknowledge the support of the J.R. Simplot Company in the preparation of this paper. The cooperation and efforts of Mr. James A. Higgins, Senior Division Engineer of the Minerals and Chemicals Division of J.R. Simplot Company, in providing the necessary data for this report are especially appreciated.

Design Considerations for Embankment Construction
on a Loess Foundation in Southeastern Idaho
By Fred Y.M. Chen and Stanley H. Kline
Page 29

REFERENCES

- Clevenger, William A., "Experiences with Loess as a Foundation Material", Transactions, ASCE, Vol. 123, (1958), pp. 151-180.
- Crumpton, Carl F. and Badgley, William A., A Study of the Clay Mineralogy of Loess in Kansas in Relation to its Engineering Properties, State Highway Commission of Kansas Research Department, (1965).
- Denisov, N.J., "Settlement Properties of the Loessial Soils", Soviet Science, USSR Government Publishing Office, Moscow, (1946), (Abstracted and Translated by K.P. Karpoff and H.J. Gibbs, Bureau of Reclamation, June 1951).
- Dudley, John H., "Review of Collapsing Soils", Journal of the Soil Mechanics and Foundation Division, ASCE, Vol. 96, No. SM3, (May 1970), pp. 925-947.
- Gibbs, H.J. and Bara, J.P., Predicting Surface Subsidence from Basic Soil Tests, U.S. Department of the Interior Bureau of Reclamation, Soils Engineering Report No. EM-658, Denver, Colorado, (25 June 1962).
- Gibbs, H.J. and Holland, W.Y., Petrographic and Engineering Properties of Loess, U.S. Department of the Interior Bureau of Reclamation, Engineering Monograph No. 28, Denver, Colorado, (November 1960).
- Holtz, W.G. and Gibbs, H.J., "Consolidation and Related Properties of Loessial Soils", ASTM Symposium on Consolidation Testing of Soils, Special Technical Publication No. 126, (1951), pp. 9-33.
- Holtz, W.G. and Hilf, J.W., "Settlement of Soil Foundations Due to Saturation", Proceedings - 5th International Conference on Soil Mechanics and Foundation Engineering, Vol. 3, (1961), pp. 673-679.
- Jennings, J.E. and Knight, K., "The Additional Settlement of Foundations Due to a Collapse of Structure of Sandy Subsoils on Wetting", Proceedings - 4th International Conference on Soil Mechanics and Foundation Engineering, Vol. 3a/12, (27 August 1957), pp. 316-319.
- Malde, H.E., The Catastrophic Late Pleistocene Bonneville Flood in the Snake River Plain, Idaho, U.S. Geological Survey Professional Paper 596, (1978).
- Mitchell, J.K., Fundamentals of Soil Behavior, John Wiley and Sons, Inc., New York, (1976), p. 79.
- Sherard, Woodward, Gizienski, Clevenger, Earth and Earth-Rock Dams, John Wiley and Sons, Inc., New York, (1963), pp. 447 and 448.

- Studley, G. and Gardinelli, A., The Geology of the Pocatello West Bench, Study for the City of Pocatello by the Department of Geology, Idaho State University, (20 January 1976).
- Studley, G. and Wieland, E., The Surficial Geology of the Pocatello East Bench and its Environmental Implications, Study for the City of Pocatello by the Department of Geology, Idaho State University, (10 April 1975).
- Trimble, Donald E., Geology of the Michaud and Pocatello Quadrangles, Bannock and Power Counties, Idaho, U.S. Geological Survey Bulletin 1400, (1976).
- U.S. Department of the Interior Bureau of Reclamation, Design of Small Dams, U.S. Government Printing Office, Washington, D.C., (1974), pp. 246-254.
- U.S. Department of the Interior Bureau of Reclamation, Enders Dam Technical Record of Design and Construction, Denver, Colorado, (April 1958).
- U.S. Department of the Interior Bureau of Reclamation, Medicine Creek Dam Technical Record of Design and Construction, Denver, Colorado, (1955).
- U.S. Department of the Interior Bureau of Reclamation, Sherman Dam Technical Record of Design and Construction, Denver, Colorado, (February 1964).
- U.S. Department of the Interior Bureau of Reclamation, Trenton Dam Technical Record of Design and Construction, Denver, Colorado, (1957).
- U.S. Department of the Interior Bureau of Reclamation, Soil Samples - Teton Dam - Teton Project, Idaho, U.S. Government Memorandum, Denver, Colorado, (14 April 1978).

TUNNEL BORING MACHINES FOR AQUEDUCTS AND SUBWAYS

By

Richard J. Proctor
Engineering Geology Branch
The Metropolitan Water District of Southern California
Los Angeles, California.

ABSTRACT

Tunneling technology is undergoing a revolution. Tunnel boring machines (TBM's or "moles") were introduced in the middle 1950's for soft-rock tunneling; since then more than 400 tunnels have been excavated in the world with TBM's, by more than two dozen TBM manufacturers. Rates of tunneling advance continue to set records; with 100 to 200 feet per day commonplace. Long aqueduct tunnels built mainly in the 1960's have shown the way to economies for rapid transit construction. Brief examples of recent subway construction at San Francisco and Washington, D.C., are compared to proposed subway construction in Los Angeles.

INTRODUCTION

The technology transfer of low-cost large aqueduct tunnels--built generally in the southwestern U.S. by high-speed TBM's--has not been fully implemented with regard to urban subway construction. Tunnel excavation rates as high as 200 to 400 feet per day have been achieved by the Metropolitan Water District of Southern California and by the U.S. Bureau of Reclamation. However, TBM excavation rates for subways have rarely exceeded 100 feet per day, and the costs have been much higher.

Two reasons for the differences in cost and excavation speed are:

1. Subway contracts have commonly been let from station to station--only one-half to one mile apart. The high cost of a TBM (\$2 to \$5 million) cannot be amortized over this short distance, and the contractor cannot be sure he will obtain another contract to use the same TBM again. Moreover, the contractor is just getting underway in the first 2,000 feet of tunneling, with all his start-up problems being worked out. In contrast, an aqueduct tunnel contract is let for several miles of construction. Why not for subways also? This means tunneling through the station sites and excavating them later from within the tunnel, as described by Walton and Proctor (1976).
2. Recent urban subways in the U.S. have been built in cities with poor subsurface geology--Boston, Baltimore, New York, Washington and San Francisco. In most of these cities the cut-and-cover method of subway construction down city streets has been preferred, because deep tunneling by TBM would encounter difficult conditions, such as mixed-face of hard and soft rock, or wet running ground, or squeezing ground. However, a few cities are planning rapid transit and have good tunneling ground for TBM's--essentially firm soil or sedimentary rock above the permanent

Tunnel Boring Machines for Aqueducts and Subways

By Richard J. Proctor

Page 2

water table. Some of these cities are Los Angeles, Minneapolis-St. Paul, Denver, Dallas, Kansas City, Milwaukee, Cincinnati and Indianapolis. Table 1 shows the 33 largest U.S. Standard Metropolitan Statistical Areas (SMSA) (over 1,000,000 population) and their rapid transit status. Also, shown are the major rock types that underlie each city and an indication as to which are feasible for low-cost mole tunneling.

RECENT TBM AQUEDUCT TUNNELS IN SOUTHERN CALIFORNIA

The Metropolitan Water District (MWD) is responsible for the distribution of wholesale water to 11 million people in six counties of Southern California. This is accomplished through the Colorado River Aqueduct (built in the late 1930's) and the California Aqueduct (Feather River Project water, completed in the early 1970's). During the last major construction period, from 1965 to 1974, the MWD built 25 miles of tunnels in hard and soft rock, using six different types of TBM's, as well as conventional drilling and blasting techniques.

The most noteworthy construction was the San Fernando Tunnel in the City of Los Angeles. It is 5.5 miles long with a bore diameter of 22 feet. A Robbins backhoe type tunneling machine within a shield advanced through firm alluvium, sandstone and siltstone, both wet and dry, by pushing hydraulic rams against previously installed precast concrete segments, which were the primary supports. The segments are 4 feet wide by 10 inches thick, with four comprising a ring. A ring was installed in just 15 minutes by an erector arm at the tail of the shield. The installed segmented support system cost only about \$150 per foot of tunnel. At an average depth of 140 feet below residential San Fernando Valley, the residents were unaware of tunneling beneath their homes.

The rate of tunnel construction exceeded 3,500 feet in one month, and the progress of 277 feet in one day for a 22-foot diameter fully-supported tunnel is a world record. (This diameter is more than enough for a single track subway or an electric busway).

BAY AREA RAPID TRANSIT (BART)

BART is a 75-mile-long new rail mass transit system combining elevated, surface and subways (Figure 1). The route and modes of construction were selected on the basis of socio-economic benefits and impacts, but the geologic conditions were a dominant factor in the final construction cost (Taylor and Conwell, 1979).

The San Francisco Bay area can be viewed as an old eroded bedrock surface, partly covered by sediments derived from rivers, the ocean, and man-made fill. It is traversed by active faults associated with historic earthquakes

TABLE 1
 URBAN GEOLOGY FOR UNDERGROUND CONSTRUCTION

1970 SMSA metropolitan area (1)	Rock types ^a (2)	Rapid transit status ^b (3)	Total mileage/subway mileage (planned) (4)
New York	HR—granite; schist; clay	1, 2	240/137
Los Angeles	M—sandstone, shale	3	(232/35)
Chicago	M—clay, limestone	1, 2	89/10
Philadelphia	HR—granite, schist	1, 2	45/18
Detroit	M—clay, sandstone, limestone	3	(25/11)
San Francisco	M—clay, sandstone, shale	1	75/21
Washington	HR and M—clay, sandstone, granite	1, 2	98/48
Boston	HR and M—clay, argillite, volcanic, granite	1, 2	39/18
Pittsburgh	M—sandstone, shale, limestone	3	(50/4)
St. Louis	M—limestone, clay	3	(86/69)
Baltimore	HR—clay, granite, schist	2	28/9
Cleveland	M—sandstone, clay, till	1	20/0
Houston	M—sand, clay (saturated)	3	?
Newark	M—clay, sandstone	1	13/4
Minneapolis-St. Paul	M—sandstone, till	3	56/33
Dallas	M—limestone		
Seattle	M—clay, till, sandstone	3	46/4
Anaheim	M—sandstone, sand		
Milwaukee	M—limestone, clay, till	3	?
Atlanta	HR and M—granite, clay	2	56/9
Cincinnati	M—limestone, till		
Paterson	M—sandstone, basalt		
San Diego	M and HR—clay, sandstone, granite	3	?
Buffalo	M—limestone, sandstone	3	(13/4)
Miami	Sand (saturated)	3	(54/0)
Kansas City	M—limestone, shale	3	?
Denver	M—sandstone, shale	3	(55/2)
Riverside-San Bernardino	M and HR—soft sandstone, granite		
Indianapolis	M—limestone, till		
San Jose	Sand (saturated)	3	?
New Orleans	Clay (saturated)	3	?
Tampa	Sand (saturated)		
Portland	M and HR—basalt, soft sandstone		

^aM = typical "mole" ground; HR = hard rock.

^b1 = area that has rapid transit; 2 = area that has rapid transit funded or under construction; 3 = area that has rapid transit proposed.

REFERENCE: Walton, Matt S., and Proctor, Richard J., "Urban Tunnels—An Option for the Transit Crisis," *Transportation Engineering Journal*, ASCE, Vol. 102, No. TE4, Proc. Paper 12532, November, 1976, pp. 715-726.

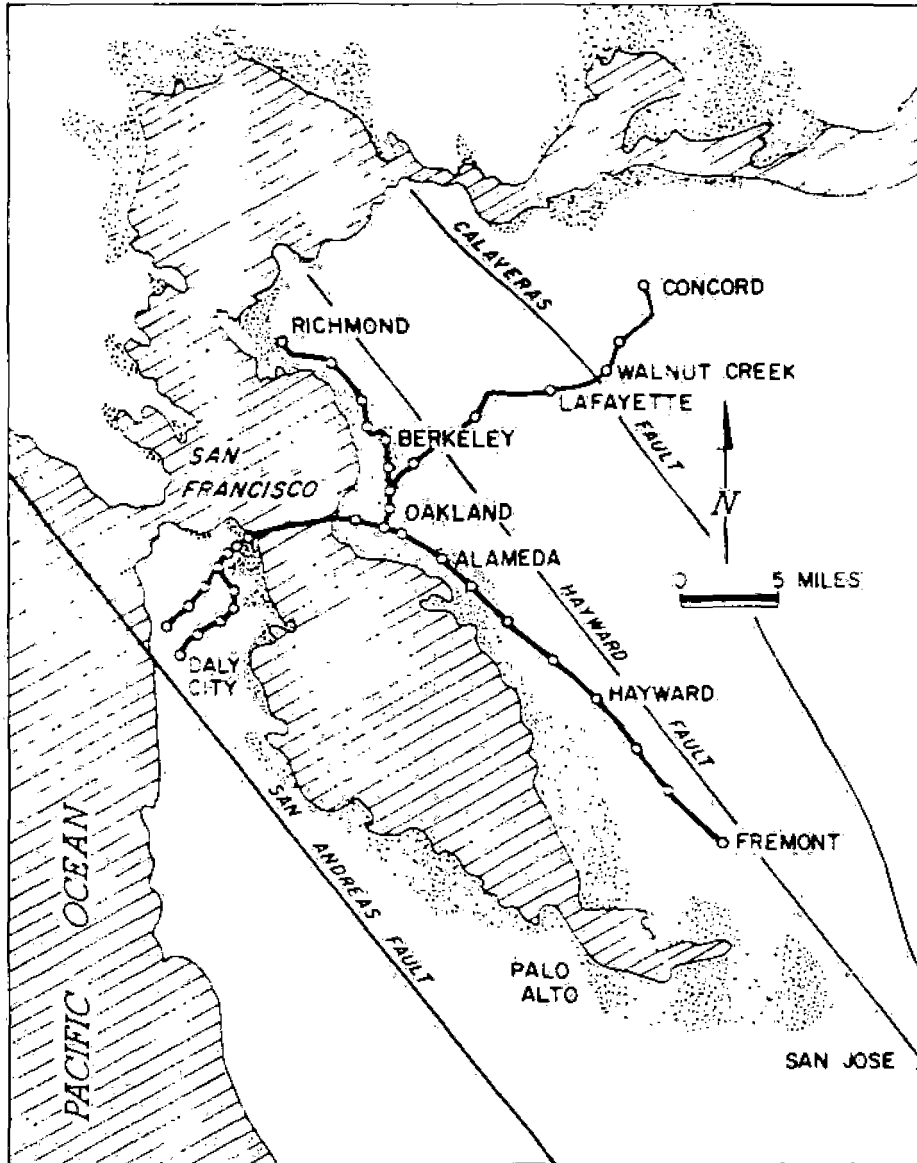


FIGURE 1 - The 75-mile Bay Area Rapid Transit (BART) System. Subways Comprise 20 Miles Including 10 Miles Tunnled, 6 Miles Cut-and-cover, and 4 Miles of Sunken Tube Under the Bay. Striped Areas are Bay Mud.

Tunnel Boring Machines for Aqueducts and Subways

By Richard J. Proctor

Page 5

(see later discussion on earthquake hazards). The dominant bedrock is the Franciscan Formation, consisting of folded and sheared sandstone, shale, andesite, serpentine, chert, and limestone. Overlying this, at the margins of the Bay, are unconsolidated sediments, Bay Mud, and artificial fill; it was these materials that required costly compressed air tunneling conditions.

Partly because of having to use compressed air for tunnel excavation in the gooey Bay Mud, BART purchased and specified that the contractors install special steel liner plates for primary supports. These cost an average of \$400 per foot of tunnel and took 45 minutes to install a ring (Kuesel, 1969). Although this gave all tunnels a known support strength and watertightness, it denied contractors the liberty to use alternative or innovative tunnel supports that might have been less expensive.

TBM performance was predictably costly and slow because of the generally poor geology here. Even so, the 5-year-long cut-and-cover subway excavation down Market Street was extremely expensive in terms of "hidden costs" (Proctor and Hoffman, 1974, pg. 54), such as lost business, traffic disruption, noise, dust, utility interruption and relocation, etc.

WASHINGTON METROPOLITAN AREA TRANSIT AUTHORITY (WMATA)

Several miles of this rapid transit system, the newest in the U.S., began operation in 1976. About half of the total 97 miles (see Figure 2) will be underground in a variety of hard and soft rock, similar to BART excavation, but not quite as difficult (Bock, 1979). A major part of the subway excavation was by cut-and-cover adjacent to old, historic buildings. As a result, many buildings had to be underpinned for lateral support which added as much as 42% to the cost of some subway contracts. This cost would have been unnecessary if the subway were built in deep tunnels, well beneath the influence of the building foundations. However, subway excavation at depth would be in mixed hard and soft, fractured, crystalline rock, deemed not suitable for economical TBM excavation.

PROPOSED SUBWAY FOR LOS ANGELES

Los Angeles is one of the world's largest cities in area with a span of 44 miles between its north and south limits. The population in Los Angeles Basin exceeds 9 million people.

The Southern California Rapid Transit District (SCRTD) Board of Directors voted in late 1978 to build an 18-mile "Starter Line" subway system (see Figure 3). The route chosen along Wilshire Boulevard currently has the most bus patronage, and the extension northward through Hollywood to San Fernando Valley should alleviate the automobile congestion on the Hollywood Freeway.

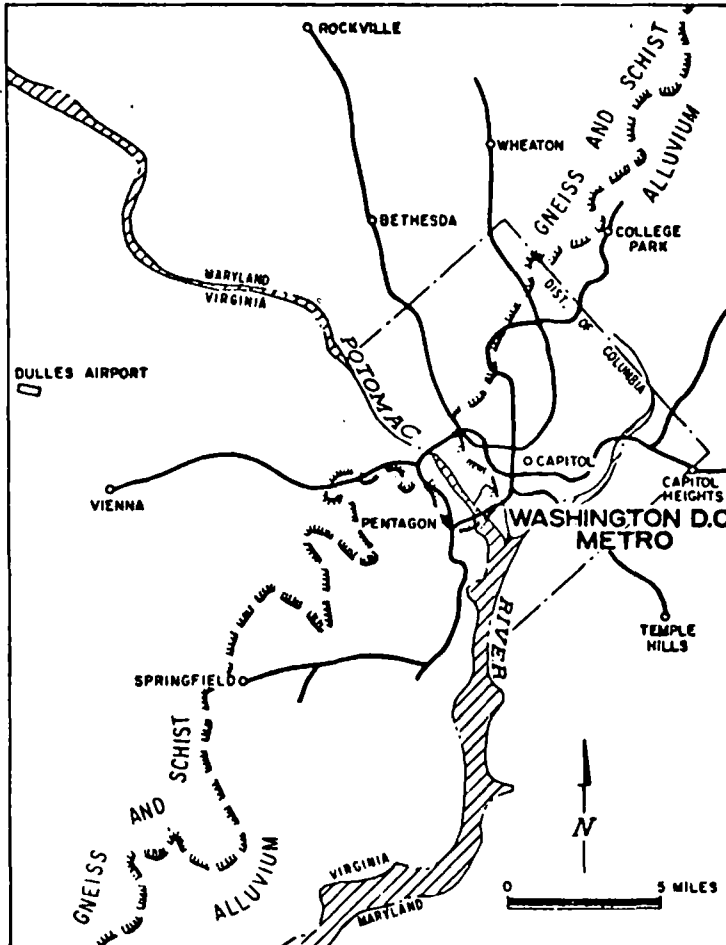


FIGURE 2 - The 97-mile Washington Metropolitan Area Transit Authority (WMATA) System. About One-third is now Completed (1979). Almost 45 Miles are in Subway. The Hachured Line is the "Fall Line" Separating Crystalline Rock from Alluvium.

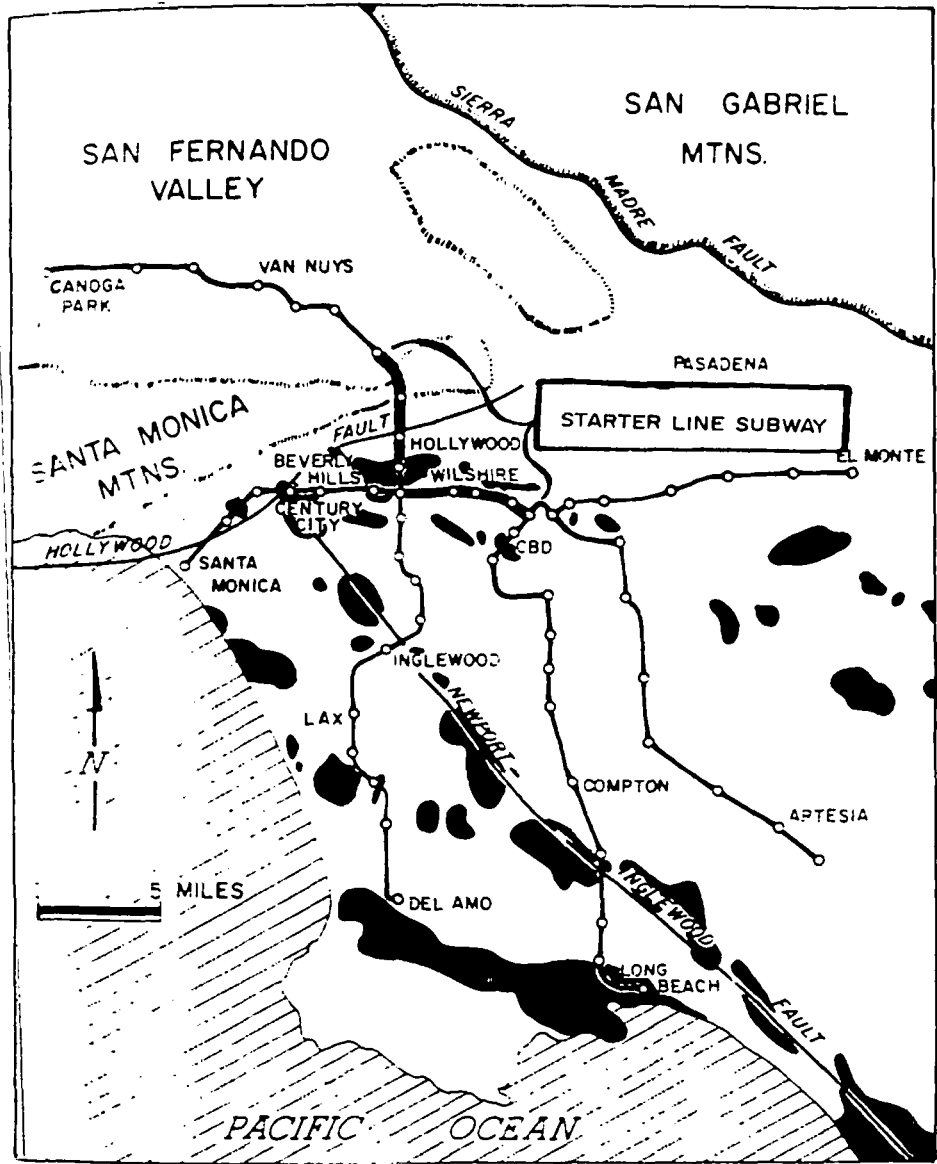


FIGURE 3 - The Proposed 116-mile Southern California Rapid Transit District System. The 18-mile Starter Line Subway is Bracketed Along Wilshire Blvd. North to the San Fernando Valley. Dark Areas are Oil Fields.

Downtown Los Angeles is perched on low hills of sandstone, shale and siltstone of the Puente and Fernando Formations (Lamar, 1970). Westward and southward from the CBD the hills are buried by old alluvium that consists of compacted and slightly cemented sand, silt and gravel. The groundwater table is below 200 feet, for the most part, making these sediments ideal for excavation by softground TBM's. Locally perched groundwater lenses exist, but these are of limited extent spacially.

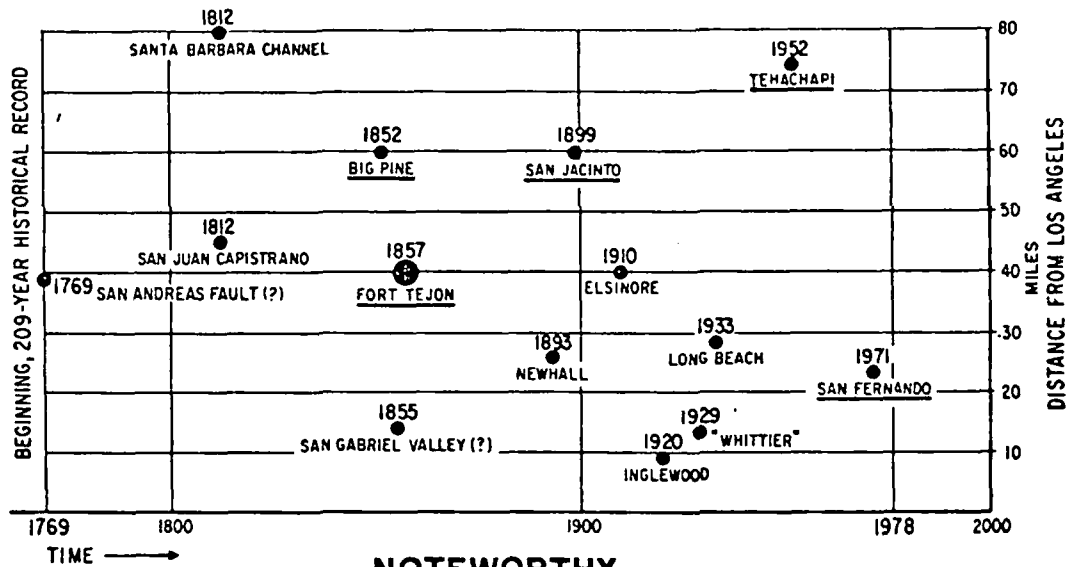
Ten cored borings were recently drilled by the SCRDT, some to a depth of 200 feet. Their cores substantiate the firm nature of these soft rocks and sediments, and also confirmed the deep water table, as most of the holes were dry.

The locations where the future rapid transit subway routes cross oil fields could cause gassy tunneling. Of particular note are the La Brea Tar Pits, which overlie a part of the Old Salt Lake oil field. Experience with previous gassy tunnels in the greater Los Angeles area shows that tunnels can be completed safely if precautions are taken. Abundant ventilation is the main solution.

In general, the geologic conditions in Los Angeles are favorable for deep tunnel subways to be excavated by boring machines (Yerkes and others, 1977). Possibly the fastest construction period and most economical new mass transit system could be built in Los Angeles, see Figure 4.

EARTHQUAKE HAZARDS

Some comments on seismic hazards may be helpful relative to subways. The greatest damage in any earthquake is due to ground shaking, not geologic fault rupture. A route may cross several potentially active earthquake faults, but the probability of a given fault causing surface rupture during the life of a facility is remote. What is more probable, indeed, even expected in California, is strong ground shaking caused by an earthquake on a nearby fault. In such an event, a large area is subjected to strong shaking, and history has shown that tunnels (and deep caves) are less damaged than surface or elevated facilities (Richter and Lindvall, 1978). This is logical because a tunnel is surrounded by the medium that is moving, and moves with it. At the surface, where a ground/air interface exists, and other seismic waves come into play, the shaking and the resultant damage is more significant. Thus, earthquake hazard considerations strongly favor deep tunnels. The randomness of earthquakes in the Los Angeles area is depicted in Figure 5.



**NOTEWORTHY
 EARTHQUAKES THAT HAVE DAMAGED LOS ANGELES**

FIGURE 4 - This Graph Shows that the Distribution of Damaging Earthquakes have been Random in both Time and Distance, as Regards Los Angeles. Only Six Earthquakes, are Considered to have Caused Serious Damage, which Yields an Average Recurrence of 35 Years

**ASSESSMENT OF IMPACTS OF TRANSIT CONSTRUCTION
 IN THE URBAN ENVIRONMENT**

CONSTRUCTION METHOD	NOISE	TRAFFIC DISRUPTION	SURFACE WATER DISPOSAL	VIBRATION	UTILITIES RELOCATION	RIGHT-OF-WAY COSTS	COMMUNITY DISRUPTION	CONSTRUCTION COSTS
CUT-AND-COVER	●	●	●	●	●	○	●	● ₁
MOLE TUNNELING	○	○	●					○ ₃
HARD-ROCK TUNNELING	○	○	●	●				● ₂
ELEVATED GUIDEWAY	●	●				●	●	○ ₄

● HIGH COST OR SERIOUS IMPACT
 ○ LOW COST OR IMPACT
 BLANK NEGLIGIBLE COST OR IMPACT

Ⓐ

FIGURE 5

REFERENCES

- "BART" Special Issue of Western Construction, April 1973.
- Bock, Carl, (in press) "WMATA--Influence of Geology on Construction Conditions and Costs," Proceedings, Rapid Transit Construction Costs Related to Local Geology: DOT-Sponsored Symposium, March 23, 1978 at Caltech. (To be published in 1979 by the DOT Transportation Systems Center, Cambridge, Massachusetts).
- Cushing, E.M., and R.M. Barker, 1974, "Summary of Geologic and Hydrologic Information Pertaining to Tunneling in Selected Urban Areas", National Technical Information Service Report DOT-TST-75-49. Report for Department of Transportation by U.S. Geological Survey.
- Kuesel, T.R., 1969, "BART Subway Construction: Planning and Costs," Civil Engineering, March 1969.
- Lamar, Donald, 1970, "Geology of the Elysian Park-Repetto Hills Area, Los Angeles", California Division Mines and Geology Special Report 101.
- Proctor, R.J., 1969, "Performances of Tunnel Boring Machines," Bulletin of the Association of Engineering Geologists, Volume 6, No. 2, p. 105-117.
- Proctor, R.J., 1973, "Geology and Urban Tunnels, Including a Case History of Los Angeles," p. 187-199, in Geology, Seismicity, and Environmental Impact, Association of Engineering Geologists Special Publication, Los Angeles.
- Proctor, R.J., and G.A. Hoffman, 1974, "Planning Subways by Tunnel or Cut-and-Cover--Some Cost-Benefit Comparisons," p. 51-63, Proceedings of the 1974 Rapid Excavation and Tunneling Conference, AIME and ASCE, New York.
- Richter, Charles F., and C.E. Lindvall, January 1978, Letter-report to Richard Gallagher, Chief Engineer of the SCRTD, on Earthquake Hazard Comparison of Subways vs. Surface Facilities.
- Taylor, C.L., and F.R. Conwell, (in press) "Influence of Geology on BART Construction Costs," Proceedings, Rapid Transit Construction Costs Related to Local Geology: DOT-Sponsored Symposium, March 23, 1978 at Caltech. (To be published in 1979 by the DOT Transportation Systems Center, Cambridge, Massachusetts).
- "Tunneling Machine Holes Through Four Months Early," Engineering News-Record, March 6, 1969, p. 26-27. (MWD Tunnel near Los Angeles).

Tunnel Boring Machines for Aqueducts and Subways
By Richard J. Proctor
Page 11

Walton, Matt S., and R.J. Proctor, 1976, "Urban Tunnels--An Option for the Transit Crisis," Transportation Engineering Journal, ASCE, Volume 102, No. TE4, November, 1976, p. 715-726.

Yerkes, R.F., J.C. Tinsley, and K.M. Williams, 1977, "Geological Aspects of Tunneling in the Los Angeles Area", U.S. Geology Survey Map MF-866.

ROCK ENGINEERING AT BROWNLEE DAM

By

Nestor T. Mirafuente
Rock Mechanics and Geophysics
International Engineering Company, Inc.
San Francisco, California

ABSTRACT

Rock engineering for a complicated rock excavation at Brownlee Dam, Idaho, incorporated the application of state-of-the-art techniques in (a) rock mechanics for stability analysis and design of rock support systems; (b) vibration control engineering for blast design and safe vibration limits; and (c) rock instrumentation for monitoring rock behavior during construction and to check adequacy of design support requirements for the slopes and underground openings as long-term permanent support systems.

Two factors were unique in this project: First, in order to accommodate a much larger 240-MW unit instead of the 90-MW unit planned for the project, the existing intake structure had to be modified and the originally designed power tunnel had to be radically changed to handle increased volume of water. Second, limited space between the existing powerhouse-tailrace and a high, steep rock slope on the Idaho side of the Snake River required properly and carefully controlled rock excavation.

INTRODUCTION

Brownlee Dam, with four 90-MW power plant units, owned and operated by Idaho Power and Light Company, is located on the Snake River between Idaho and Oregon. When the 395 ft. rockfill dam and four-unit power plant were built during the mid-50's, Idaho Power and Light Company's planners knew that power demands would increase significantly within two decades. For this reason, an area was reserved for a fifth 90-MW turbine-generator unit to be built at a future date. During construction, a power intake structure was built for the future power tunnel.

Twenty years later, triggered by the expected demand for clean power and the high cost of alternative power, the installation of a larger generating unit was considered. This unit had to be accommodated in the space originally reserved for the fifth 90-MW unit. Innovative and creative design, backed by economic analyses of trade-offs, resulted in the selection of a 240-MW power unit, nearly three times the originally planned size.

Two major problems had to be overcome as a result of the decision to build a much larger power plant: First, a space problem on how to fit a 240-MW unit into a site originally planned for a 90-MW unit; and, second, site problems in excavating an opening for the large fifth unit and a tailrace channel. The opening for the power unit had to be excavated at the base of the right abutment of the dam and adjacent to the existing powerhouse, which had to be kept in operation. The new unit required a separate tailrace channel to be located between an existing

tailrace and a steep 250 ft. high rock slope. The rock rib left between the two tailraces was very narrow, with a minimum width of 25 feet.

This paper describes the practical application of rock mechanics, blast and vibration control, and rock instrumentation to geotechnical problems encountered in this project.

International Engineering Company, as the engineer-designer for the project, has won an "Honorable Mention" during the 1977 Engineering Excellence Awards Competition of the Consulting Engineers Association of California. As a result of this award, the company is being considered for the National Grand Conceptor Award sponsored by the American Consulting Engineers Council.

General Geology

The geologic formations at Brownlee Dam consist of Columbia River Basalts, which compose the walls of the Snake River canyon. Columbia River Basalt refers to those lavas, predominantly of Miocene age, which cover a large portion of Western Idaho, Eastern and Central Oregon, and Southern Washington.

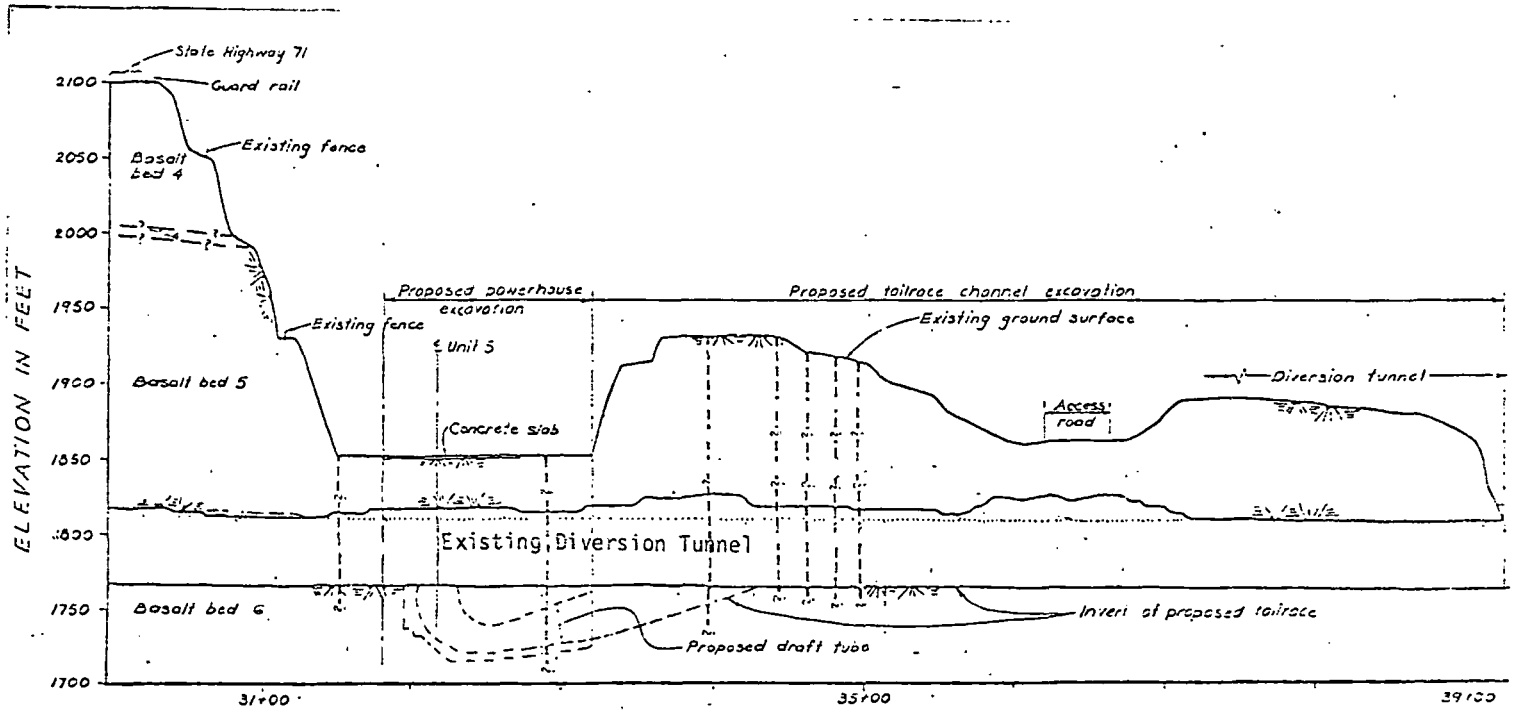
At Brownlee, there are six flows dipping approximately 13° west and forming the easterly limit of the large syncline. The lavas at the site are generally hard, dense and massive rocks. Some flows are feldsparporphyritic and some non-porphyritic. Feldspar phenocrysts up to 1" long are common in some flows.

Beds of fine-grain tuff a few inches to several meters thick, which in a few places contain very thin bituminous layers, lie between the flows. A few dikes and a few faults of small displacement cut across the site (Figure 1).

EXCAVATION PLAN

The following major excavations were conducted for Unit 5 of Brownlee, as shown in Figure 2:

- a) Near the powerhouse, the lower 70 ft. of the existing 250 ft. high steep slope were cut back to approximately 1/4:1.
- b) A 1,400 ft. long, 46 ft. wide and 135 ft. deep open channel was excavated for the new tailrace at a slope of approximately 1/7:1.
- c) A vertical cut 95 ft. wide and 137 ft. deep was opened for the new powerhouse.
- d) A new power tunnel was driven 32 feet in diameter and 660 ft. in length.



(Section on Centerline of Existing Diversion Tunnel and New Tailrace)

FIGURE 1 - Brownlee Unit #5 General Geologic Cross Section

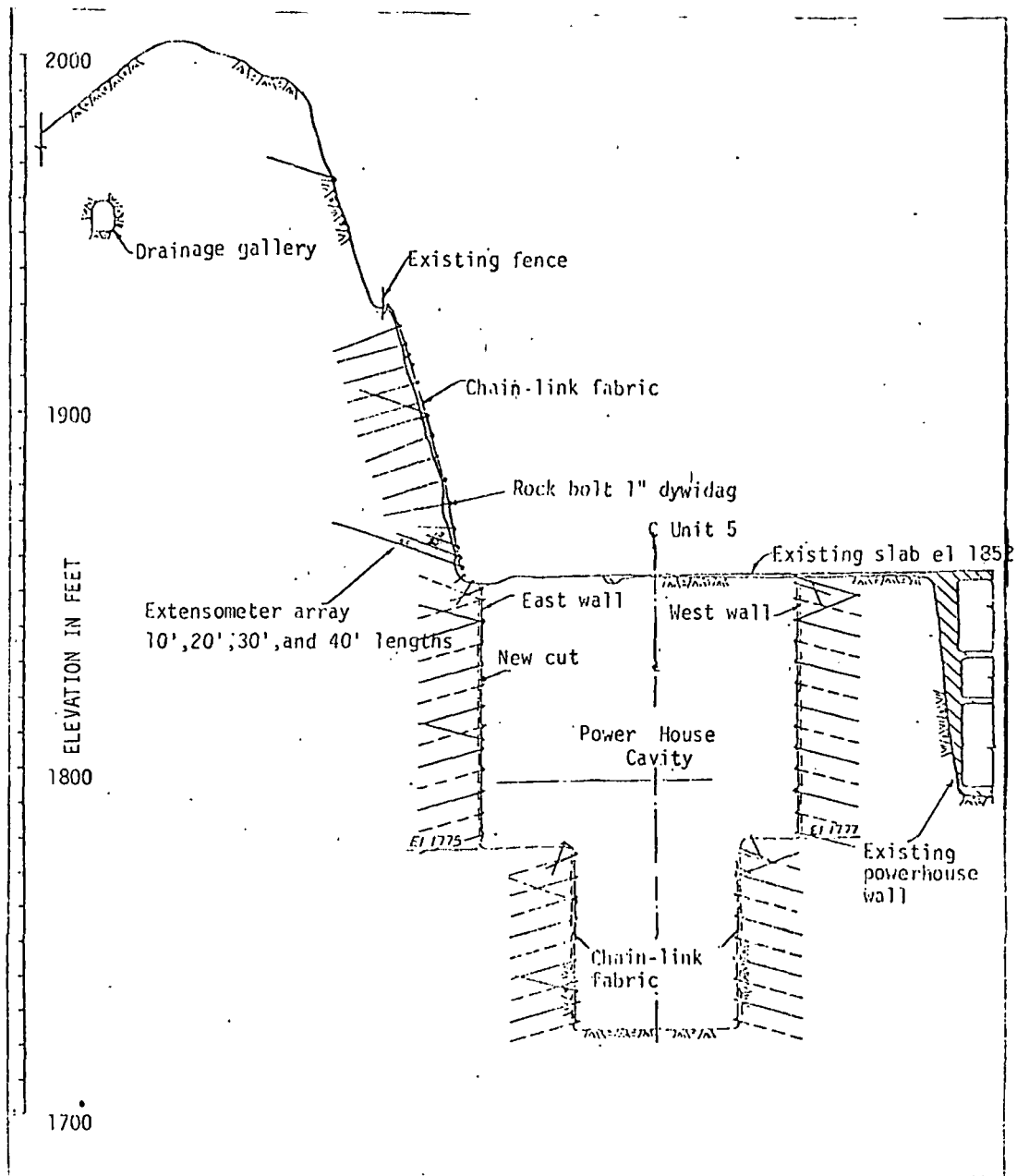


FIGURE 2 - Rock Slope and Powerhouse - Rock Bolting

ROCK MECHANICS DESIGN METHODS

Slope Stability Analysis and Slope Support System

Rock mechanics techniques and methods used for slope stability analysis and design of support systems incorporate detailed structural geologic mapping, laboratory tests of rock cores, and the use of limiting equilibrium principles.

Since stability of rock slopes in general depends mainly on the orientation of discontinuities relative to the free face or slope cut and on mechanical properties of such discontinuities, a detailed structural geological study was performed for this project. After identification of all major joints and fractures, rock wedges were identified, and their possible displacements analyzed to determine whether failure along these joints was kinematically possible with respect to the proposed cuts.

Support System for Cut Slopes

From the results of all the rock mechanics studies performed for the slopes, it was determined that large, massive failure of the rock mass was not possible. However, small local blocks of rock could fail during excavation and, for this reason rock bolts on a 12 x 12 ft. staggered pattern were used to stabilize the blocky and fractured areas. Rock bolt lengths were 20 ft. to 30 ft. Where the lava flows were more massive and less fractured, rock bolts were installed as required. Figure 2 shows a typical cross section of the rock slope at Brownlee Dam and the rock bolts installed.

Two-dimensional sliding wedge analyses were performed for the high and narrow rock rib created by the new tailrace channel excavation. The analyses were performed prior to excavation using established values of rock strength parameters ϕ (friction angle) and C (cohesion) for a weak tuff layer dipping into the excavation. Since results showed that the rock rib would remain stable, the only concern was that small rock slabs could be loosened during excavation. For this reason, the same 20 or 30 ft. long rock bolts on a 12 x 12 ft. pattern were used for the rock rib. Again, where the rock was massive and less fractured, bolting was only done as required. In addition, the obviously loose rock blocks on the west wall of the rock rib facing the existing tailrace were rock bolted prior to excavation of the new tailrace channel.

Power Tunnel Stability and Support Systems

Rock mechanics principles and rock support design techniques applied to the power tunnel at Brownlee Dam Unit No. 5 have been described by world-renowned authors in rock mechanics, such as Kastner, Coates, Talobre, Terzaghi and many others. Depending upon the size and geometry of an underground opening, the two most important parameters necessary for design of support requirements are: (a) condition of loading and (b) rock strength. As an example, Terzaghi's loading criteria determination was applied to the Brownlee Dam power tunnel which has an essentially circular cross section, 32 ft. in diameter. Conservatively assuming

a blocky and fractured rock condition, the amount of rock load would be in the order of 70 ft. Under this load condition, for rock of moderately high strength with a modulus of elasticity of 4×10^6 psi and a modulus of rupture of 1500 psi the required rock beam or arch would be approximately 9 ft. thick. This was calculated using the elastic beam and arch theory:

$$L = \sqrt{\frac{2 T t}{(pg+p/t)F}}$$

where:

- L = Span of opening
- T = Modulus of rupture
- pg = Weight-density of rock
- p = Rock load
- F = Factor of Safety
- t = Beam thickness

An analysis using Fenner's equation and Talobre's principles would give comparable results. The same results could also be achieved using Kastner and Coates' determination of tension zone configuration over a tunnel with circular cross section. Using either the tension zone of Kastner or Coates or the over-strained zone from Fenner's equation, design rock loads can be determined and proper rock bolt lengths can be calculated.

Support System for the Power Tunnel

From an analysis made using rock mechanics principles and design techniques, the final support design for the Brownlee Dam power tunnel consisted of 1" ϕ Dywidag bolts, 15 ft. long and spaced 6 ft. apart. A typical cross section of the tunnel and rock bolts installed is shown in Figure 3. In addition, rock support design was established for the rock wedge between the old diversion tunnel and the new power tunnel. Studies indicated that this portion of the power tunnel, with a minimum width of only 4 ft. could not withstand blast vibration. In addition, rock in this location is highly fractured. Collapse of this rock wedge would present serious stability problems of the rock slope above the power tunnel portal and the powerhouse cavity itself. Figure 4 shows the rock bolt pattern and the concrete plug installed inside the diversion tunnel prior to excavation of the new power tunnel.

BLASTING AND VIBRATION CONTROL

Blast damage and vibration levels can be accurately defined in terms of peak particle velocities. Vibration caused by blasting can be controlled and safe limits established if handled with caution and a good understanding of the factors affecting vibration. The four most important variables, Oriard (1972), used in vibration control and the factors used in controlling these variables are:

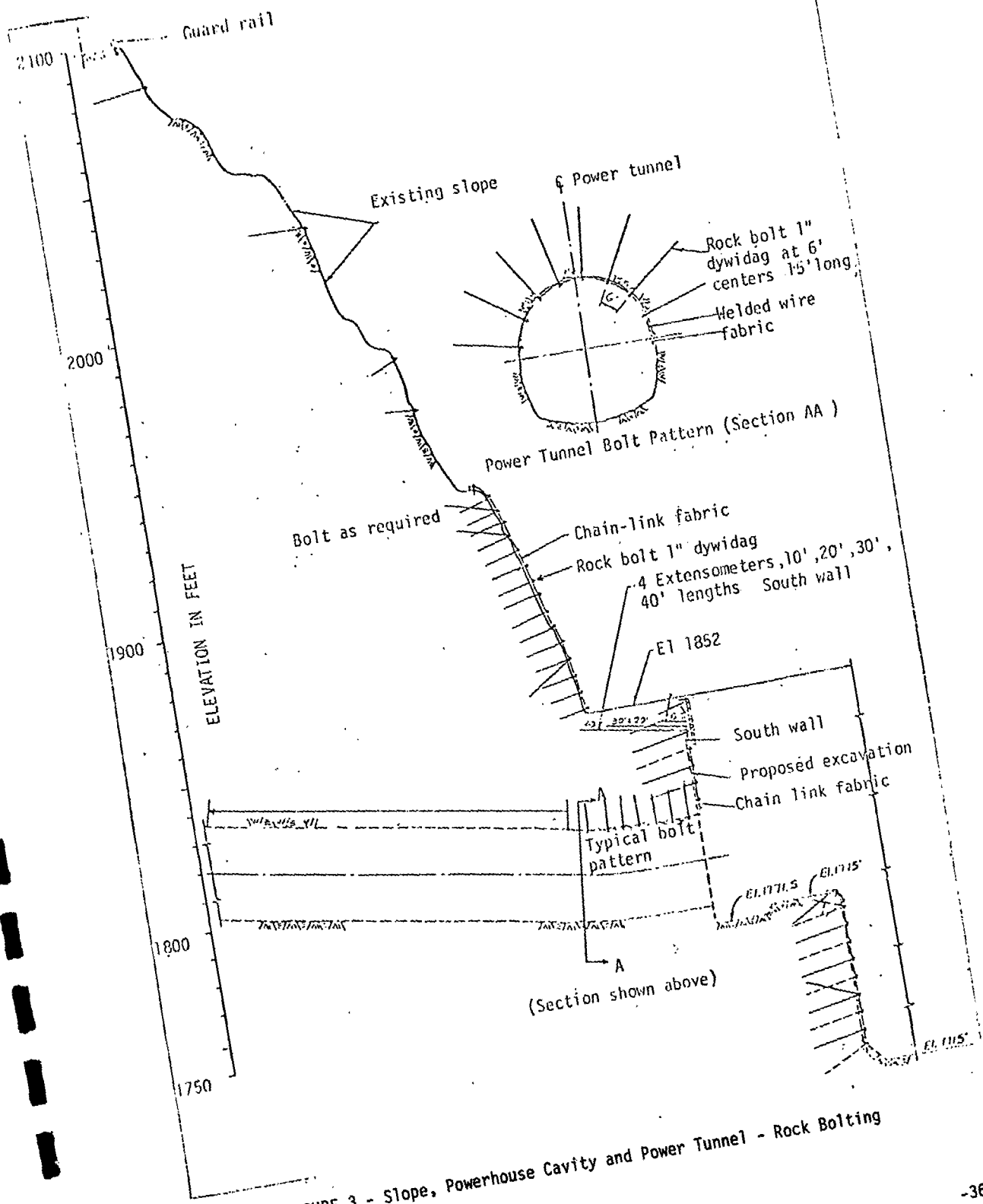


FIGURE 3 - Slope, Powerhouse Cavity and Power Tunnel - Rock Bolting

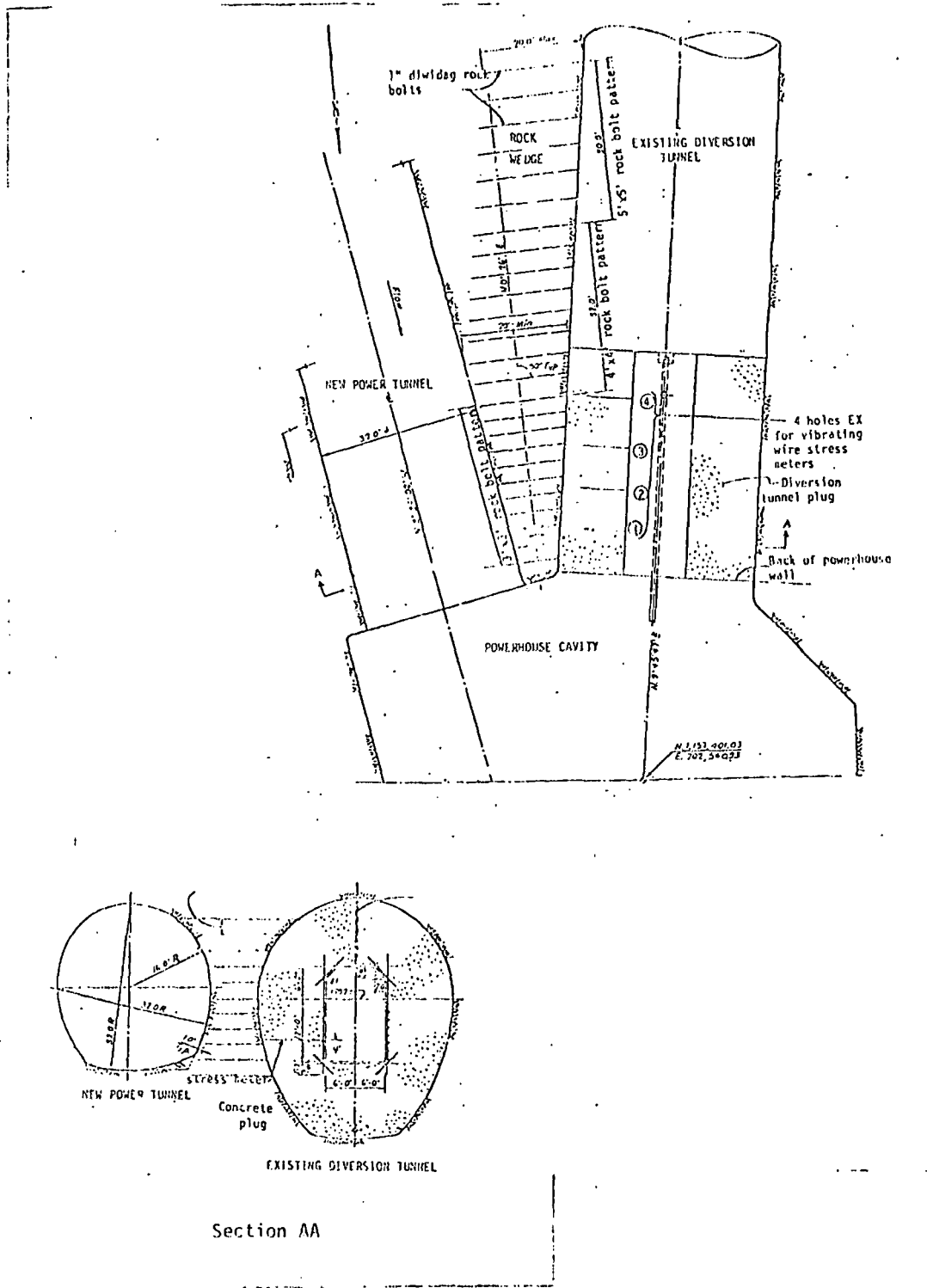


FIGURE 4 - Rock Wedge Reinforcement

A. Time Dispersion

- Conventional delay sequence
- Dispersive delay sequence
- Firing time scatter
- Travel time scatter

B. Spatial Dispersion

- Orientation
- Geometry

C. Charge Concentration

- Drill size
- Depth of lift
- Charge distribution

D. Charge Confinement

- Burden
- Spacing
- Powder factor

At Brownlee Dam, vibration had to be carefully controlled during excavation for Power Unit 5 for the following reasons:

- Blasting for the new powerhouse cavity was to be performed adjacent to existing powerhouse walls.
- Blasting was to be performed adjacent to an existing underwater intake structure for the new power tunnel and penstock.
- Blasting was to be performed without loosening blocks of rock on existing high and steep rock slopes.
- To prevent power interruption, blasting was to be performed without tripping sensitive override mercury switches on generators and other sensitive instruments inside the powerhouse.
- Blasting was to be performed without any fly rock that could damage high tension transmission cables close to and above the planned excavation.
- Blasting for the new tailrace channel was to be performed without creating stability problems on the high and narrow rock rib that would be left by the excavation between the new and old tailrace channels.

At the onset of the project, when excavation for the access roads and upper benches was still far from the powerhouse, continuous vibration measurements were made using vibration seismographs. Three Sprengnether VS 1200 and two Dallas Instrument Company VS 3 seismographs were used. These instruments were strategically located at different distances from the blasts. Different powder weights were recorded per delay and peak particle velocities vs scaled distances were plotted. As the shots approached the critical excavation area, enough vibration data had been studied to be able to predict safe vibration levels. Figure 5 shows peak particle velocities plotted against scaled distances. For prediction of safe vibration levels for the critical blasts, the upper limit of the band was used. The data points shown in Figure 5 are from results of approximately 500 blasts. Except for a few data points above the upper band limit, all points were well within the band. In addition, these data points were studied immediately following the shots.

In some instances, it was determined that there were discrepancies on actually recorded weights of powder used per delay. This means that if the amount of powder used had been accurately recorded, these data points would have been within the band. Figure 6 shows a typical blast design pattern used for the tailrace and powerhouse cavity. It should be noted that, even if there are only seven delays used in the pattern, full production can still be achieved even though shallow lifts are used. With good planning of the firing time sequence and trunkline connection, as shown in Figure 6, the delay sequence can be repeated to cover a large area. Thereby, the volume of excavated rock for shallow lifts can be made equal to that of deep lifts to achieve good production while maintaining safe vibration levels. For other critical areas where deeper holes were required, "deck loading" was used to limit vibration. "Deck loading" consists of using three or four delays in deep holes fired at different intervals.

For the power tunnel excavation, the typical design blast pattern is shown in Figure 7. It can be seen from the pattern of holes that the tunnel was driven "top heading" first and benching was done later for the final excavation. For the downstream portal of the power tunnel close to the powerhouse and for the last few shots adjacent to the underwater intake structure, vibration levels were controlled to avoid any damage to the existing structures by limiting hole depths and subsequently limiting burden and powder weights.

ROCK INSTRUMENTATION

An instrumentation program was carried out for the project to monitor rock behavior during construction and to check the adequacy of designed support systems, both for the rock slopes and the underground openings.

Extensometers

For the slopes, a series of rock bolt type extensometers was used.

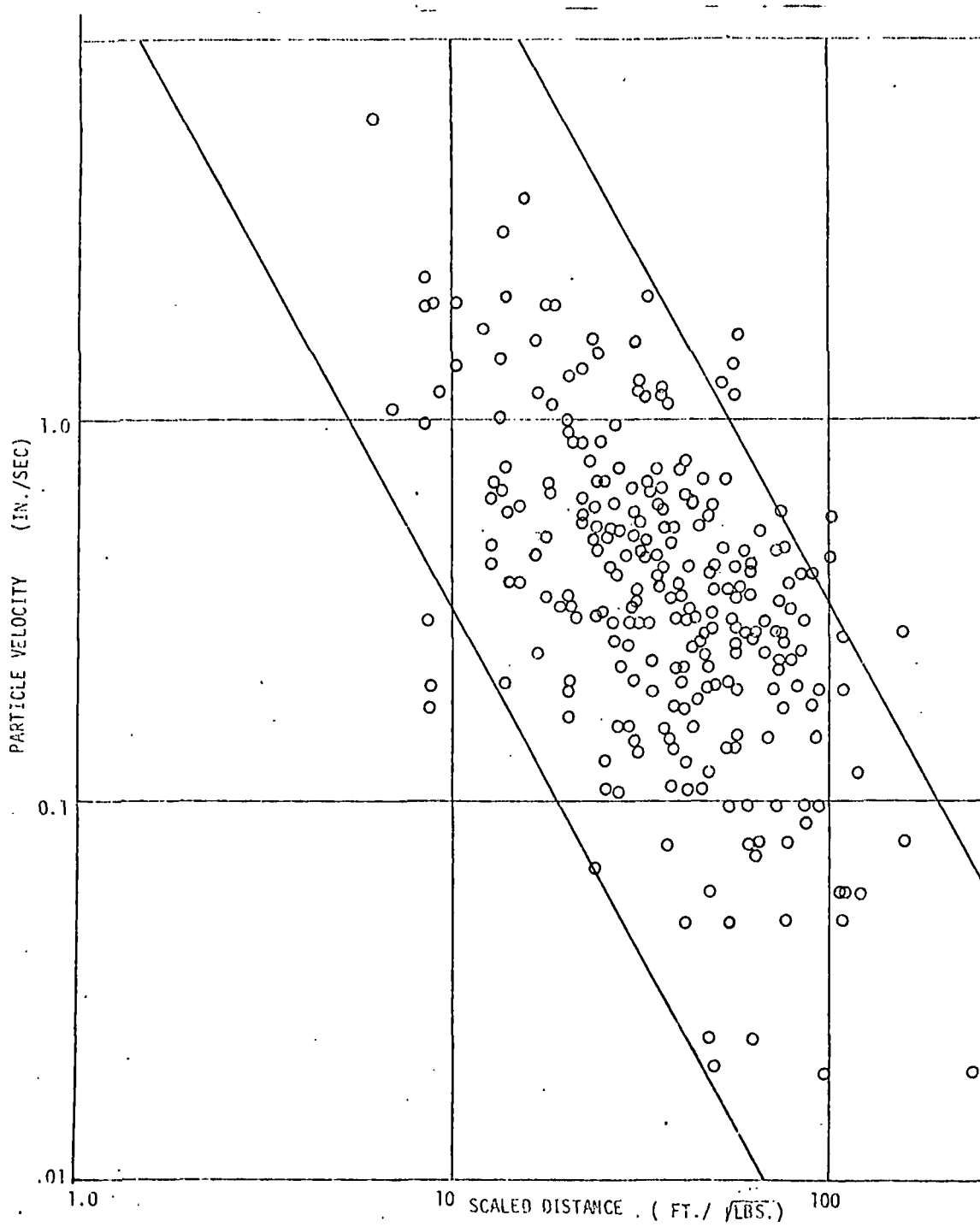
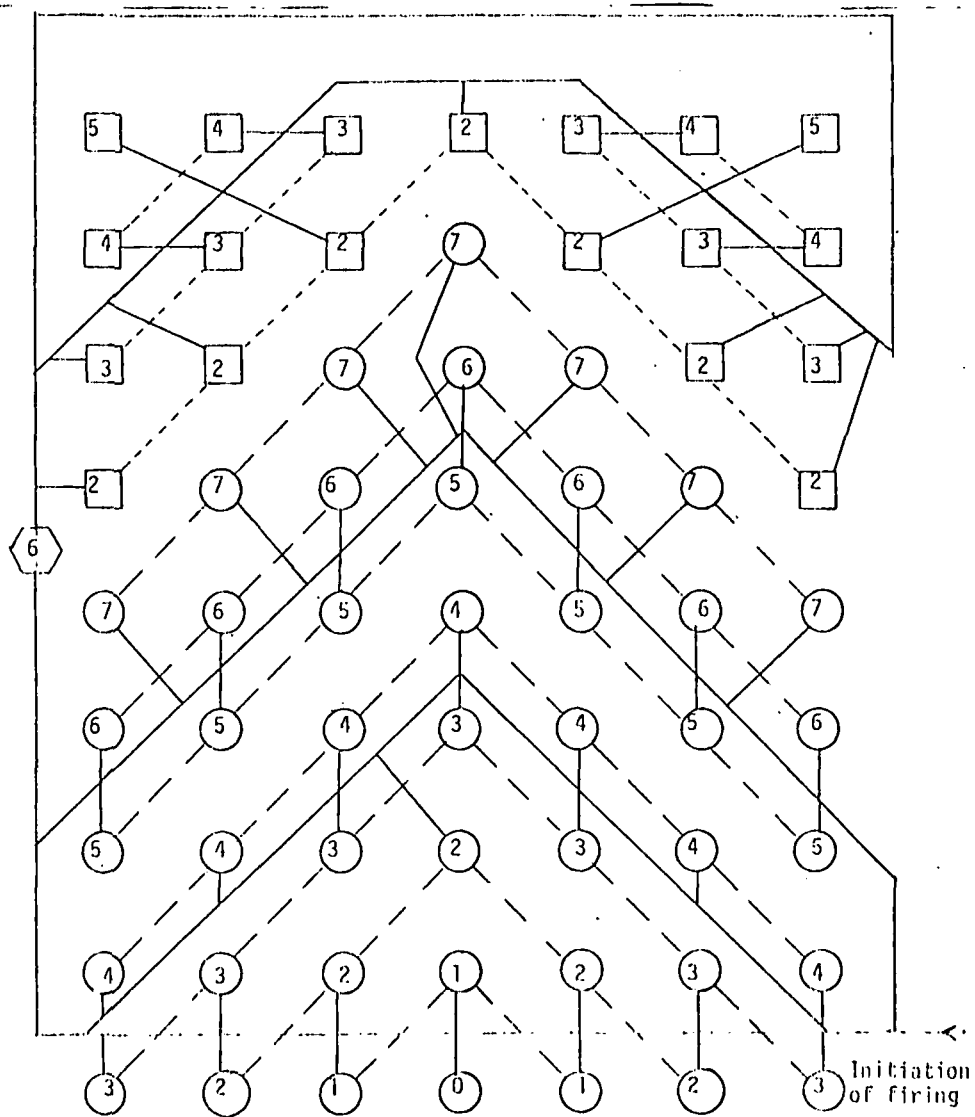


FIGURE 5 - Brownlee Dam Unit #5 - Vibration Data



TIME DELAY

0 - 0 ms	6+2 - 200 ms
1 - 25 ms	6+3 - 225 ms
2 - 50 ms	6+4 - 250 ms
3 - 75 ms	6+5 - 275 ms
4 - 100 ms	
5 - 125 ms	
6 - 150 ms	
7 - 175 ms	

FIGURE 6 - Hole Pattern Delay Sequence

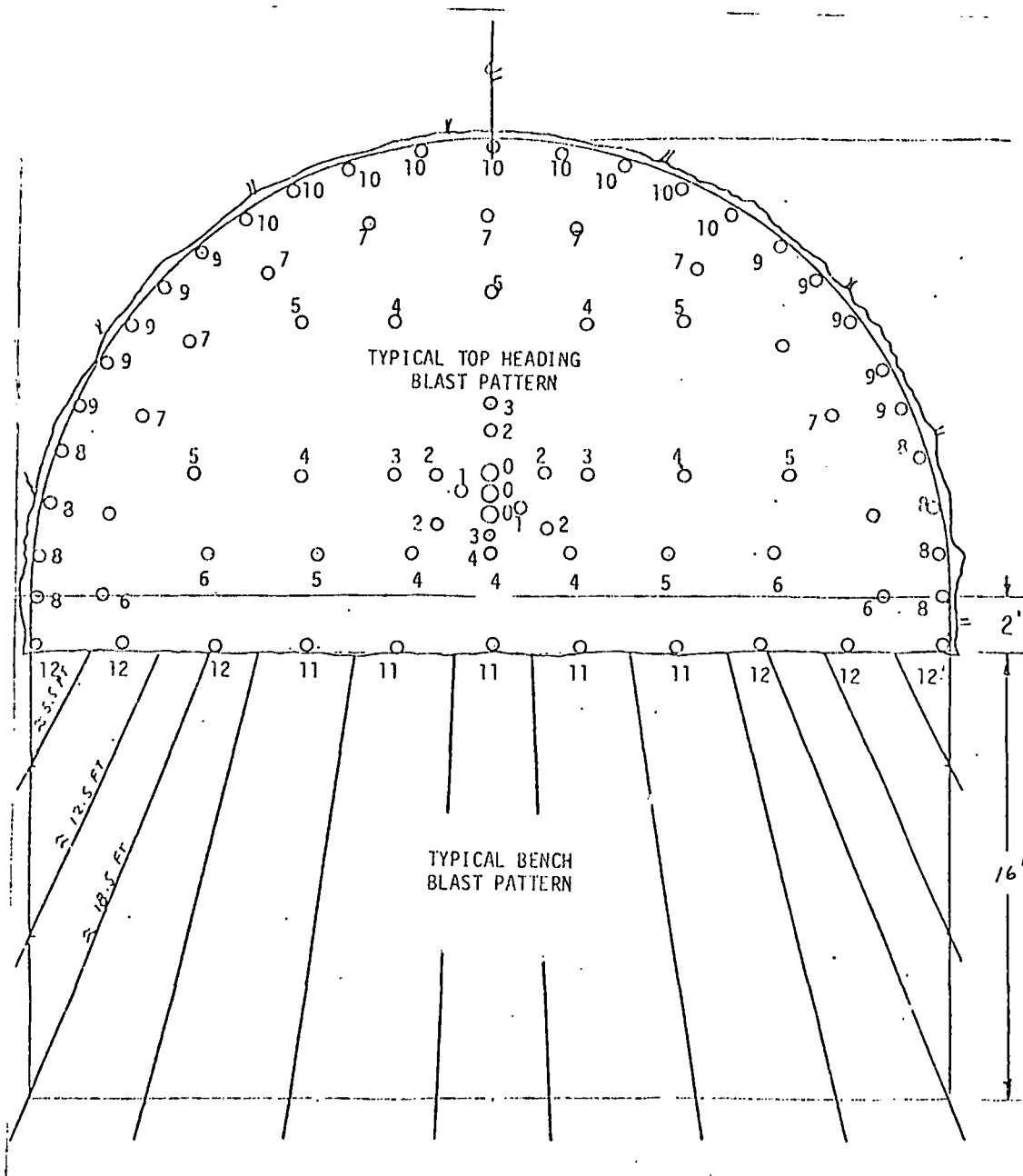


FIGURE 7 - Blast Design Pattern - Power Tunnel

Four-depth arrays of 40, 30, 20, 10 ft. long rock bolt extensometers were installed in four locations along the base of the existing 250 ft. high east slope prior to excavation. During excavation for the 135 ft. tailrace channel, three arrays of extensometers were installed on the left wall. This left wall was on the narrow rock rib between the existing tailrace and the new tailrace channel mentioned earlier in this paper. For the powerhouse cavity, one array of extensometers was installed immediately above the downstream portal of the power tunnel. Figures 2, 3, 4 and 8 show typical extensometer arrays installed at Brownlee. Inside the power tunnel one array was installed at the crown during excavation to determine tunnel crown behavior and tunnel closure.

During and after final excavation of the tailrace channel, powerhouse cavity and power tunnel, none of the extensometers recorded any appreciable rock movements, indicating that the design rock support systems were adequate.

Inclinometers

Two vertical inclinometers as shown in Figure 8 were also installed in the rock rib between the new and existing tailrace channels. The purpose of these inclinometers was to determine the behavior of the rock rib during excavation of the new tailrace channel and to cross-check horizontal movements of the rock rib with movements registered by the extensometer arrays installed in its left wall.

Results of the inclinometer readings were in good agreement with measured movements registered by extensometers in the rock rib. Analysis of these movements show normal rib reactions during excavation for the tailrace channel.

Vibrating Wire Stress Meters

Vibrating wire stress meters were used during excavation for the new power tunnel to monitor load transfer and load intensity on the concrete plug installed inside the existing diversion tunnel. Eight vibrating wire stress meters were installed in four boreholes in the concrete plug as shown on Figure 4. Inside each of the two outer holes, one horizontal, one inclined 45° and one vertically oriented stressmeter were installed. In the two inner drill holes, only vertical stressmeters were installed.

Results of stress measurements during excavation of the power tunnel show good agreement with predicted values of the load being carried by the power tunnel rock mass prior to excavation, and of the transfer of this load to the rock wedge. The load was almost entirely transferred to the concrete plug due to the fractured and weak nature of the rock wedge. Because of this, it was concluded that without the rock reinforcements installed in this location, the rock wedge would not have sustained the load imposed on it during the power tunnel excavation.

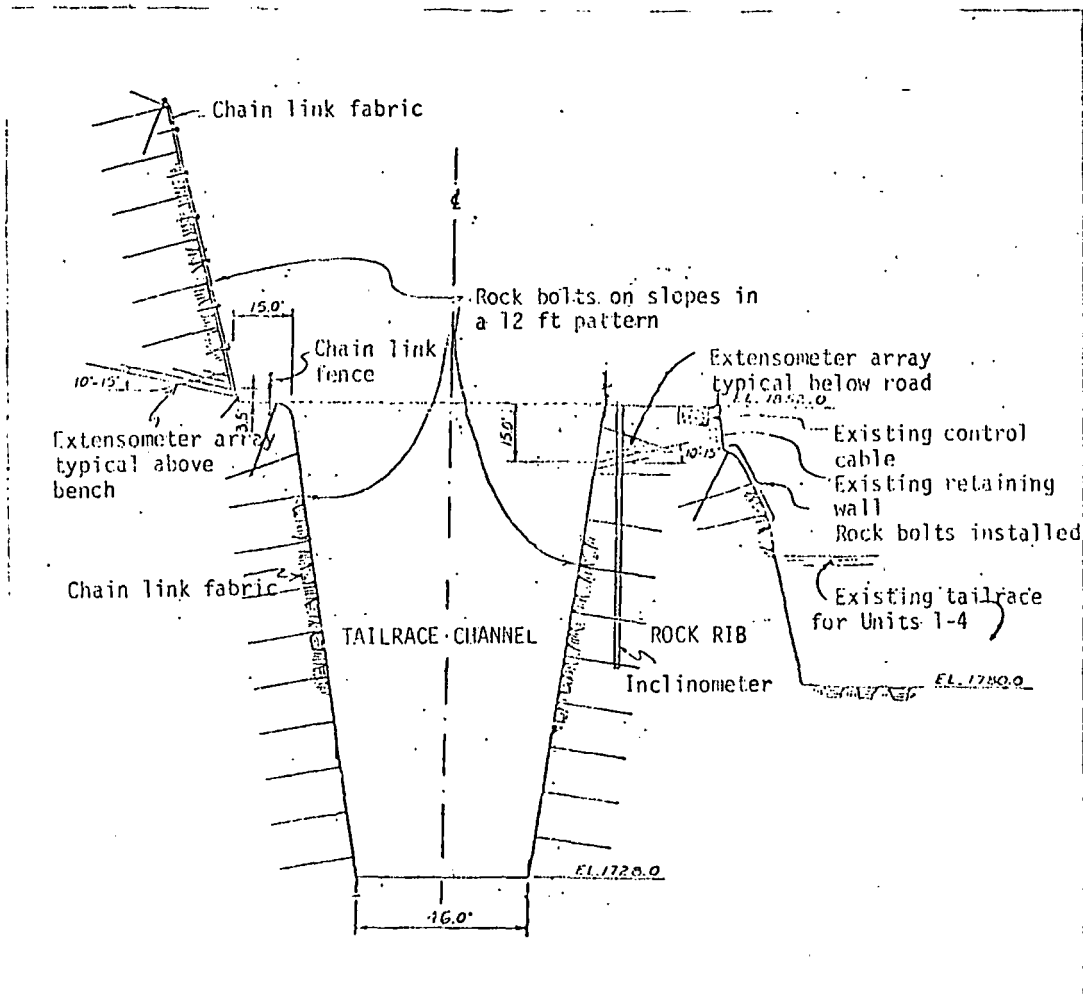


FIGURE 8 - Rock Rib Reinforcement and Instrumentation

Survey Brass Points

In addition to extensometers and inclinometers, four survey brass points on a straight line were installed along an existing concrete wall between the new and old tailrace channels. An additional four points were installed along the abutment of the new bridge. The purpose of these survey points was to monitor movements along the top of the rock rib and to determine horizontal and vertical displacements of the bridge abutments during excavation of the new tailrace channel.

All movements registered by the survey points show normal rock reactions during excavation.

CONCLUSIONS

Close coordination between Idaho Power personnel, design engineers and the contractor to handle specific design problems during construction has yielded excellent results. Brownlee Project Unit Number 5 has progressed according to schedule; no delay is anticipated, and the following constraints and requirements have been met:

- There has been no damage to any of the existing structures, facilities or equipment during excavation.
- Except for anticipated small loose blocks of rock and some minor raveling rock fragments, no significant rockfalls have occurred.
- No significant rock movements have been recorded.
- There has been no significant interruption of power production and no interruption of power flow to customers.
- Project costs have remained within the budget.

Brownlee Project Unit Number 5 has demonstrated that greater potential for hydroelectric power development can be realized through creative and sound engineering practice. At the Brownlee site, these practices have resulted in safe and economical operations during construction of an additional power generating unit which is larger and more efficient than the unit that was originally planned.

ACKNOWLEDGEMENTS

The author expresses his gratitude to Messrs. G. Condit, R. Clemens and R. Stewart of Idaho Power and Light Company, for their full cooperation during the various construction stages of this project. Gratitude is also expressed to Dan Stover of Idaho Power and Light Company, who as Resident Engineer for the project contributed valuable and practical advice and assistance to both engineers and contractor.

Special mention should also be given to J.A. Rapp, who performed blast vibration and instrumentation monitoring for this project, to E.G. Zurflueh and D.A. Baskin, all of International Engineering Company, Inc., for their advice and critique during the writing of this paper.

REFERENCES

- Coates, D.F. (1965), "Rock Mechanics Principles", Dept. of Mines and Tech. Surveys, Mines Branch Monograph 874, Ottawa.
- Fenner, R. (1938), "Rock Mechanics and Engineering," Cambridge University Press, 1972.
- Heuze, F. and Goodman, R.E. (1971), "Three Dimensional Approach to the Design of Cuts in Jointed Rock," Proc. 13th Symposium of Rock Mechanics, ASCE.
- Kastner, H. (1962), "Statik des Tunnel-und Stollenbaues, Springer-Verlag, Berlin.
- Kovari, K. and Fritz, P. (1977), "Stability Analysis of Rock Slopes for Plane and Wedge Failure with the Aid of a Programmable Pocket Calculator," Proc. 16th Symposium on Rock Mechanics, ASCE.
- Obert, L., Duvall, W.I. and Merrill, R.H. (1960), "Design of Underground Openings in Competent Rock", Bulletin of U.S. Bureau of Mines No. 587.
- Oriard, L. (1972), "Blasting Operation in the Urban Environment," Bulletin of AEG, Vol. IX, No. 1.
- Terzaghi, K. (1966), "Introduction to Tunnel Geology," Rock Tunneling with Steel Supports by Proctor and White, Commercial Shearing and Stamping Co., Youngstown, Ohio.

Rock Engineering at Brownlee Dam
By Nestor T. Mirafuente
Page 18

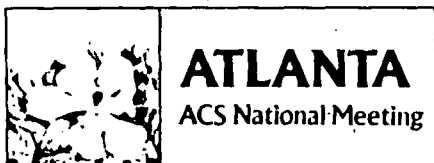
Tolobre, J. (1957), "La Mecanique des Roches," Dunod, Paris.

Tom, E., Mirafuente, N.T. and Estrella E. (1976), "Stability Study of a
Concrete Arch Dam Abutment," Rock Engineering for Foundation and
Slopes, ASCE.

APR 30 1981

Fresh look at geochemistry for oil searching

Increasing oil costs and dwindling known reserves have sparked renewed interest in geochemical methods for petroleum exploration



One of the oldest methods of locating oil and gas deposits is having a revival. The method is surface geochemistry. Long eclipsed by more purely geological procedures, such as seismic testing, geochemistry is still the stepchild among the high-technology petroleum exploration methods. But rising oil costs and shrinking known reserves have rekindled interest among oil exploration companies in tracking down the clues to unknown deposits that geochemical techniques can provide.

A look at what the science has to offer and how one oil company in particular is employing these techniques comes from a symposium on advances in geochemical techniques for oil exploration sponsored by the Division of Geochemistry. (The division was elevated from probationary to full divisional status by the ACS Council during its meeting in Atlanta.)

Analyzing the ground surface for signs of oil or other hydrocarbons that seeped up from deposits below is probably the oldest method of locating oil deposits. However, as very shallow deposits were depleted, obvious surface signs of oil below became unusual. Prospectors began instead to study the subsurface geology looking for formations that could trap oil or natural gas in reservoirs, particularly in regions where other geologic markers showed conditions would have been right for petroleum formation. Usually such conditions induce an impermeable capping layer, which, many prospectors believed, would prevent seepage of hydrocar-

bon molecules from the oil deposit to the surface.

Now that picture is changing. Few rocks are entirely impermeable, and improved analytical techniques now allow detection of indicator molecules at the parts-per-million level in ground and water samples. According to one current theory, hydrocarbons are most likely to escape from the edges of a subsurface deposit, creating a characteristic "halo" of increased hydrocarbons in the soil gases above a deposit.

Although soil bacteria and other factors unrelated to subsurface oil deposits also can put hydrocarbons into the soil, these confounding factors generally can be separated out—by isotopic analysis, for example. In fact, the techniques for detecting and identifying surface hydrocarbons are now so good, says Victor T. Jones, director of the physical geochemistry and minerals section of Gulf Research & Development Co., that "the geochemical evidence is irrefutable if you have hydrocarbons at the surface. The only question is where the source is." However, he adds, it is dangerous to condemn a project on the basis of a lack of geochemical evidence that something is there.

Gulf Research & Development is using surface geochemical techniques to search for oil in several ways. Ted J. Weismann, manager of the firm's geochemistry and minerals department, outlined some of the ways the company uses surface geochemistry. The presence of relatively high concentrations of hydrocarbons in soil gases indicates a petroleum deposit somewhere below the surface, he says. In addition, the relative abundance of different hydrocarbons gives an indication of the chemical composition of the deposit below.

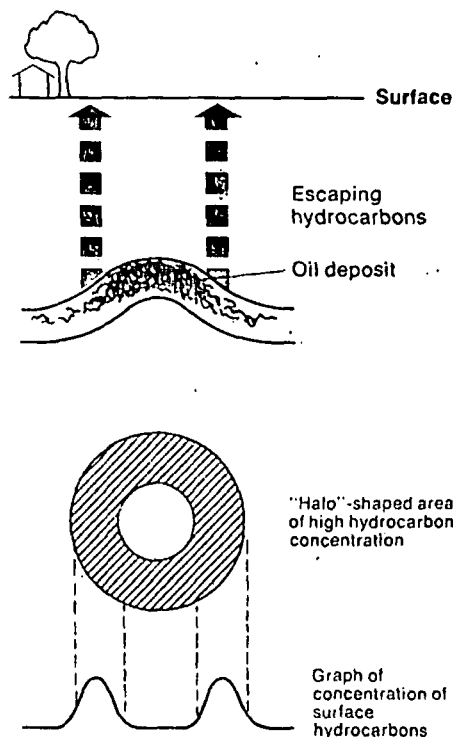
For instance, analysis of near surface gases at the predominantly oil producing Permian Basin in West Texas, the oil condensate region of the Alberta Foothills, and the dry methane gas production of Sacramento Valley, Calif., give quite different ratios of methane to propane and ethane to butane, explains senior geologist Gregory J. Pazdersky. Such surface gas analysis might be useful for exploration, particularly in regions

where no earlier wells have been drilled, he suggests.

Deposits in the offshore continental shelf also send up hydrocarbon markers that can be measured in the water column above them, says Gulf's John C. Williams, supervisor of the marine geochemistry section. Gulf's research vessel, the *Hollis Hedberg*, samples ocean water at three depths—the surface, 450 feet down, and as much as 600 feet down. The samples are analyzed for methane and propane and compared with average concentrations for these compounds in open ocean water.

In areas that are known to contain petroleum deposits, the levels of the measured hydrocarbons are much greater than the average ocean value, he finds. For example, in the Gulf of Mexico, 22% of the samples taken have more than 2 nanoliters of propane per liter of seawater, compared to an open ocean average of 0.34 nanoliter. For methane, 80% of the Gulf of Mexico samples show more

Hydrocarbon "halos" can mark oil deposits below



than 100 nanoliters per liter, compared to 8% of open ocean samples.

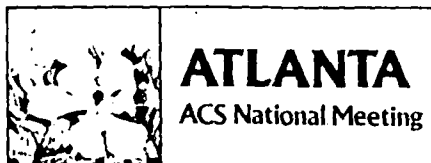
Although there are many examples of a correlation between high hydrocarbon measurements and successful drilling, Williams points out that there also have been some failures. The area off the Washington-Oregon coast, for example, has very high methane and moderately high propane levels in the seawater, but 14 exploratory wells have shown only minor gas and oil deposits. The Gulf of Alaska, too, should have petroleum deposits, based on hydrocarbons found in the water, but drilling to date has not located deposits.

A preliminary look at what happens to hydrocarbons as they migrate from the source deposit to the surface comes from Gulf's Richard J. Drozd, research geochemist, and colleagues at West Virginia University. High bicarbonate and methane concentrations in water taken from aquifers near the surface are an indication of hydrocarbon migration from gas reservoirs below, Drozd says. The migrating hydrocarbons would lead to increased evaporation of the water. This, in turn, leads to an isotopic fractionation of the oxygen and an increase in ^{18}O . The process also involves an enrichment in ^{12}C in the carbon dioxide that is released, with a resulting increase in ^{13}C in the residual dissolved carbonate.

Monitoring the soil and ocean water for indicator gases does have some drawbacks, however: "The correspondence is not one-to-one between soil gas anomalies and oil deposits below," Weismann says. Sometimes geologic features deflect the gases as they migrate to the surface, so that a well sunk where the gases reach the surface may fail to tap the petroleum source they come from. A history that includes a few such misses is one reason why geochemical techniques are not being used more widely in today's exploration.

There are two important factors needed to decide whether an oil source can be tapped profitably that surface gas analysis does not provide. Surprisingly, it does not give much information on the size of a deposit. The concentration of gases in the soil is more a function of the ease of migration through the material that separates the source from the surface than it is of the size of the oil reservoir, Weismann says. And the technique does not tell how deep the deposit may be. Some early dry holes dug on the basis of geochemistry may have failed to tap oil because they did not go deep enough. □

Trace organics are thrust of water cleanup



For the past five to 10 years, scientists and engineers have been laying the groundwork for the technology of treating drinking water with granular activated carbon. That technology promises to form the basis for a new phase in water treatment history. First came the removal of particulates, then the removal of bacteria, and now the removal of trace organic compounds, particularly trihalomethanes.

As evidenced by a three-and-a-half-day Division of Environmental Chemistry symposium on treatment of water by granular activated carbon, work has been progressing along a broad front, ranging from carbon adsorption theory to commercial economics. Three studies described at

the symposium point up the variety of work currently under way at an applications level.

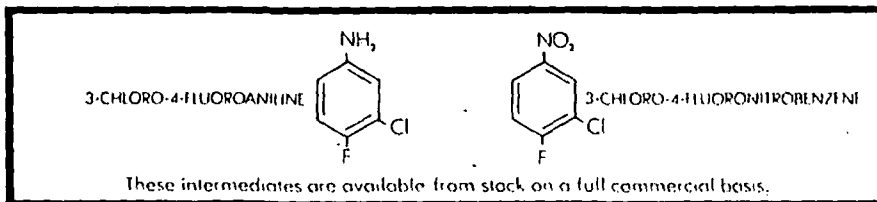
In Florida, researchers have been studying the removal of trihalomethanes in a 150,000 gal-per-day pilot plant with bacteria-activated towers. The project has been funded and operated jointly by the Environmental Protection Agency's Municipal Environmental Research Laboratory, Miami-Dade Water & Sewer Authority, Dade County Department of Public Health, and the Drinking Water Research Center at Florida International University.

Paul Wood of the Florida International research center noted that granular-activated carbon can't be used economically for removal of trihalomethanes, formed during chlorination from generally natural precursor substances. Thus, the objective of the pilot plant is to see whether bacteria-activated towers of granular activated carbon would be suitable for removing precursors.

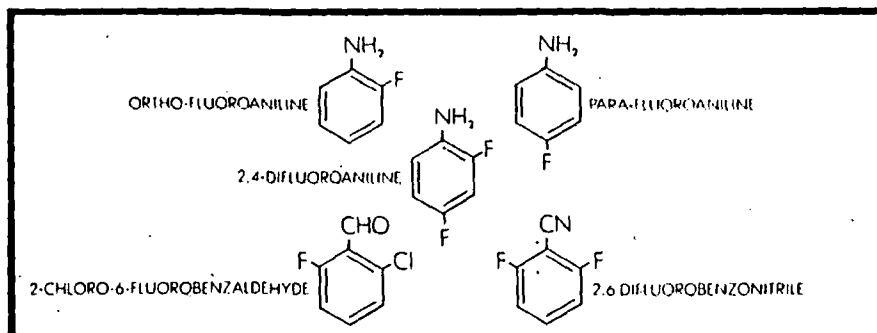
The pilot plant includes an ozone generating and contacting section. The study is seeking to determine if ozonation of the water will modify

Fluoroaromatics

COMMERCIALY AVAILABLE



DEVELOPMENT CHEMICALS



Now available from one of the world's largest plants for the manufacture of these fluoroaromatics, which are finding increasing application in agricultural and pharmaceutical fields. Please contact

biddle sawyer
CORPORATION

2 Penn Plaza, New York, N.Y. 10121 • Telephone: (212) 736-1580

GEOLOGICAL AND GEOCHEMICAL RELATIONSHIPS AT THE GETCHELL MINE
AND VICINITY, HUMBOLDT COUNTY, NEVADA

Byron R. Berger

**UNIVERSITY OF UTAH
RESEARCH INSTITUTE
EARTH SCIENCE LAB.**

Introduction

The Getchell gold mine, located in eastern Humboldt County, Nevada (Figure 1), was a producer of gold bullion intermittently between 1938 and 1967. This occurrence is one of several disseminated-type gold deposits in the western United States, including Carlin, Cortez, Gold Acres, Jerrett Canyon, Mercury, and numerous smaller deposits (Roberts and others, 1971). The geological and geochemical characteristics of these deposits are similar; high gold to silver ratio, associated arsenic and mercury, carbonaceous limy host rocks, associated intrusive igneous rocks, and extensive silica replacement.

The purposes of this report are to describe the geologic relationships at the Getchell mine and their effects on the localization of gold mineralization, and to present data concerning the geochemical characteristics of the ore bodies and the consequent ramifications for exploration.

GENERAL GEOLOGIC SETTING

The Getchell mine is located in the Potosi mining district on the eastern flank of the Osgood Mountains, about 70 km northeast of Winnemucca, Nevada (Figure 1). Initial geologic mapping in a portion of the Osgood Mountains was done by Hobbs (1948), followed by a study of the entire Osgood Mountains 15-minute quadrangle by Hotz and Willden (1964).

Studies of the mineral deposits of the Potosi mining district include Hobbs and Clabaugh (1946), Joralemon (1949, 1951, 1975), Cavender (1963), Hsu and Galli (1973), Silberman and others (1974), Taylor (1974), Berger (1975), Berger and others (1975), Berger (1976), and Taylor and O'Neil (1977).

In the vicinity of the Getchell mine (Figure 2 and 3), lower Paleozoic sedimentary rocks are intruded by a granodiorite stock of Cretaceous age (Silberman and McKee, 1971). The oldest rocks are Middle and Upper Cambrian carbonaceous shale and thin-bedded limestone, in part intercalated, called the Preble Formation (Hotz and Willden, 1964). The shale beds are commonly phyllitic, and appear light-greenish in the near surface weathered zone. The Preble Formation is unconformably overlain by a sequence of intercalated dolomitic limestone and chert, shale, siltstone, and mafic volcanic rocks belonging to the Comus Formation of Early and Middle Ordovician age. The mafic volcanic rocks are in part intrusive into the intercalated dolomitic limestone and chert, although vesicular textures, pillow-like structures, and interbedded shale indicate that they are mainly submarine flows. All of these lower Paleozoic rocks are isoclinally folded, with the fold axes overturned to the west (Erickson and Marsh, 1974). This style of folding is not seen in younger rocks. North of the mine area, Etchart Limestone and chert, shale and quartzite of the Farrel Canyon Formation are imbricately thrust over the older Paleozoic rocks. The Etchart Limestone is similar to the Highway and Antler

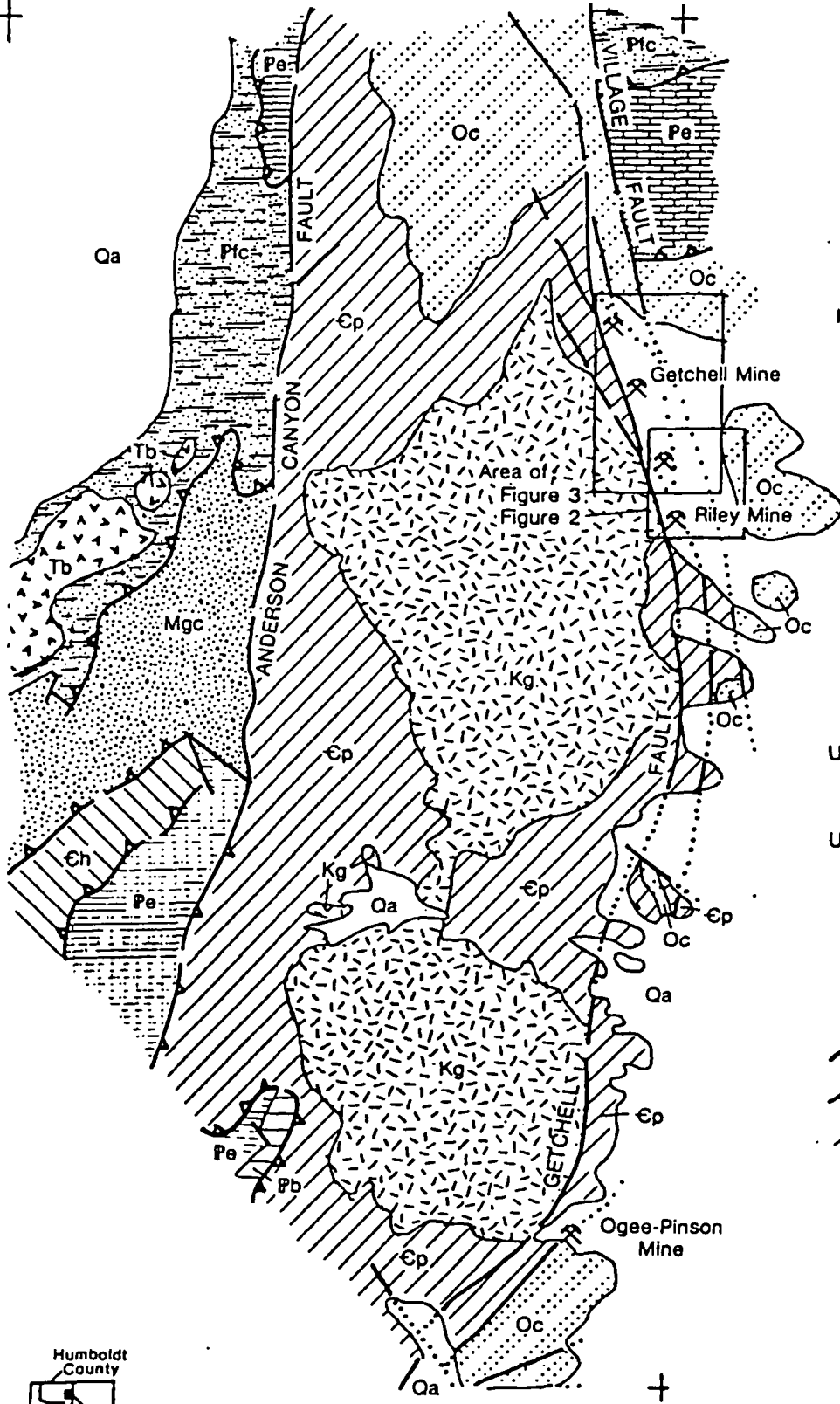
Au^o 10ppm

11
115

0718

117°20'
41°15'

117°15'



EXPLANATION		
Qa	Alluvium	QUATERNARY
UNCONFORMITY		TERTIARY
Tb	Olivine basalt	
UNCONFORMITY		CRETACEOUS
Kg	Granodiorite	
INTRUSIVE CONTACT		
Pe	Etchart Limestone	PENNSYLVANIAN OR PERMIAN(?)
UNCONFORMITY		
Pb	Battle Formation	MISSISSIPPIAN
THRUST CONTACT		
Pfc	Farrel Canyon Formation	ORDOVICIAN
THRUST CONTACT		
Mgc	Goughs Canyon Formation	CAMBRIAN
THRUST CONTACT		
Oc	Comas Formation	
UNKNOWN CONTACT		
Ch	Harmony Formation	
UNKNOWN CONTACT		
Ep	Preble Formation	
Mine		
Normal fault		
Thrust fault		
Lithologic contact		

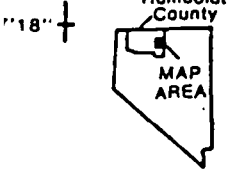
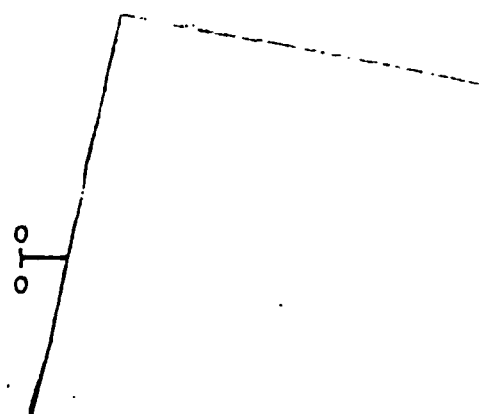





FIGURE 1



- EXPLANATION**
- CRETACEOUS
 - Kp Porphyritic dacite dikes
 - Kg Granodiorite
 - ORDOVICIAN
 - Ov Comus Formation
 - Ols Ov-volcanic rocks
 - Ols Ols-limestone
 - CAMBRIAN
 - Cls Preble Formation
 - Csh Cls-limestone
 - Csh Csh-shale
-  Major faults and related gouge zones
 -  Lithologic contact
 -  Outline of open pit
 - X** K-Ar age date

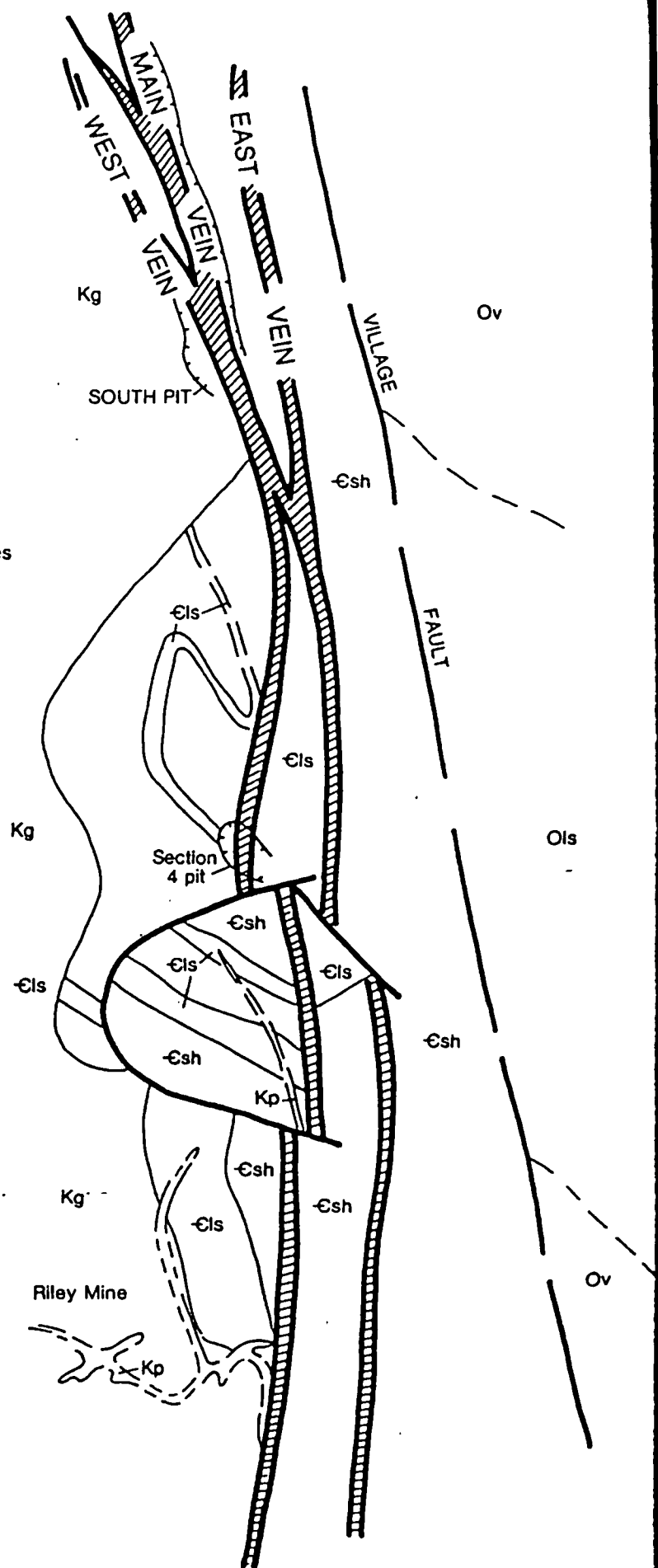
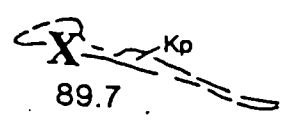
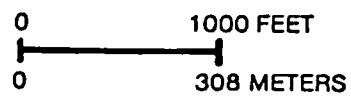


FIGURE 2

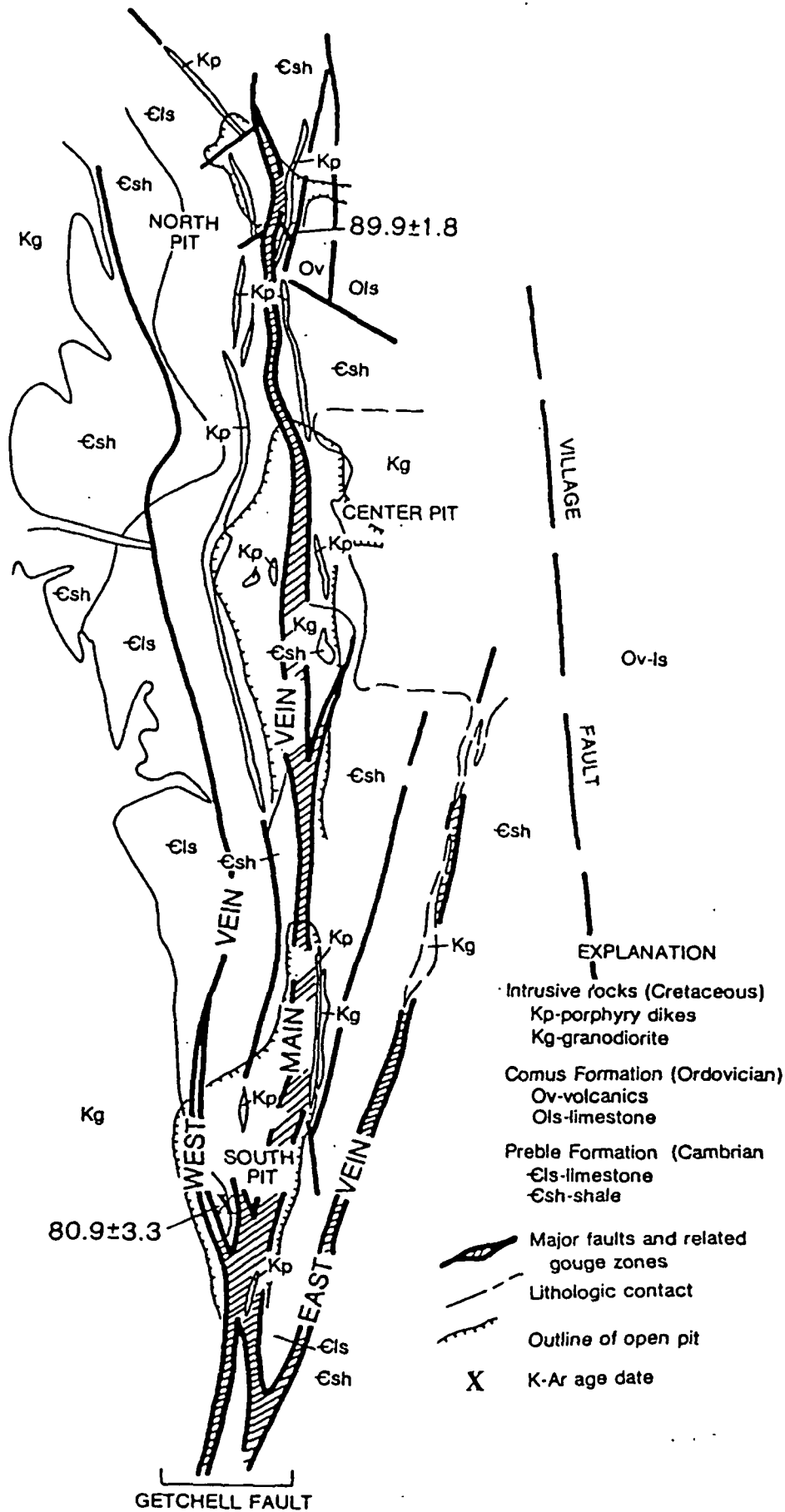


FIGURE 3. Geologic map of Getchell mine area. Revised from Silberman, Berger, and Koski (1974, after Joralemon, 1951).

Peak Formations found elsewhere in the region, and contains rocks of Middle to Late Pennsylvanian or Early Permian age (Hotz and Willden, 1964). The Farrel Canyon Formation of Pennsylvanian (?) to Permian age resembles the Havallah and Pumpnickel Formations found to the south and southeast of the Osgood Mountains.

The Cretaceous Osgood Mountains biotite granodiorite and related dike rocks intrude all of the Paleozoic rocks. The stock is an homogenous, coarse body of variable grain size. The dikes consist of both granodiorite and dacite porphyry. The stock is symmetrical, and appears to dip outward 45°-60° on both east and west flanks (Continental Oil Co., unpublished aeromagnetic data, 1973). There is a metamorphic aureole around with the intrusion with a mineral assemblage in shaly rocks consisting of cordierite-, biotite-, and andalusite-hornfels. Locally limy beds are recrystallized and calc-silicate minerals are developed.

The imbricate thrust faults juxtaposing the early and late Paleozoic formations have been interpreted by Erickson and Marsh (1974) in the Edna Mountain area south of the Osgood Mountains as representing two distinct episodes of deformation--Late Pennsylvanian to Early Permian and Late Permian to Early Triassic (Sonoma orogeny). The Getchell fault zone, an anastomosing system of high-angle, dip-slip faults, cuts the thrust faults along the eastern margin of the Osgood Mountains and the zone is a clearly younger feature. Hobbs (1948) and Joralemon (1951) felt that the Getchell fault system postdated the granodiorite stock, and that the earliest sense of movement on the fault was lateral based on presumed mullion structures and horizontal slickensides. Berger and Taylor (1974) re-evaluated the field evidence and concluded that the displacement has been predominantly vertical, and that the fault system controlled the emplacement of the granodiorite stock and related dikes. The fault system has been active to the present as evidenced by the displacement of Quaternary(?) alluvium in the mine area.

MINERALIZATION IN THE OSGOOD MOUNTAINS

Mining activity in the Osgood Mountains has been described by Hotz and Willden (1964). For completeness, a brief summary of the types of deposits other than disseminated gold and the geochemical characteristics of some is presented here.

Barite is a widespread gangue mineral in many of the hydrothermal mineral deposits in the Osgood Mountains. In addition, barite commonly occurs as rosettes in carbonate beds of the Ordovician Comus and Cambrian Preble Formations, and massive, bedded barite deposits are known in sec. 12, T. 37 N., R. 41 E., sec. 32, T. 38 N., R. 42 E., and sec. 30, T. 39 N., R. 42 E. Silver-bearing quartz veins cross-cut the bedded barite, but otherwise there is no hydrothermal sulfide mineralization accompanying the barite.

Metasomatic skarn deposits occur in carbonate host rocks around the periphery of the Osgood Mountains granodiorite. A number of the skarns have been mined for tungsten, with the most active periods being 1942-1945 and 1951-1957. Copper is a minor accessory element in most of the deposits, and molybdenum is a significant co-product of the Moly tungsten mine (figure 2). Tin is present in garnet-pyroxene skarn as an accessory trace element.

Disseminated sulfides occur in the granodiorite stock in two places, one within each of the exposed lobes. Hotz and Willden (1964) referred to the zone in the central part of the northern lobe west of the Riky mine as the Section 5 pit (sec. 5, T. 38 N., R. 42 E.), and at this locality tungsten occurs with quartz in a matrix of quartz sericite and pyrite. The second zone is located at the north end of the southern lobe (secs. 19, 20, T. 38 N., R. 42 E.) and was described by Neuerburg (1966) as consisting of "thin seams of iron sulfides along subparallel irregular fractures." Molybdenum and tin occur in trace amounts in these altered zones.

Small silver-bearing quartz veins occur at numerous localities throughout the range. The veins are fault controlled, and are also common in the broken noses of plunging antiformal structures. Lead and zinc are associated with the silver, and secondary oxides of these elements are common in outcrop. Gold is present in amounts subordinate to the silver.

Minor manganese sulfide and oxide prospects occur at several localities in the range. Most are in chert of the Farrel Canyon Formation as coatings along fractures and as a matrix cementing breccia fragments.

GEOLOGY AT THE GETCHELL MINE

The geology of the Getchell mine area is shown on Figure 3. The alluvium and dump materials have been omitted to better illustrate the geologic relationships.

The Getchell fault system generally consists of two persistent gouge zones referred to locally as the "footwall strand" (Joralemon, 1951) and the "hangingwall strand" (Berger and Taylor, 1974). However, a single fault is not consistently present in either position for the entire length of the range (Figure 1). In the mine area, the Getchell fault exclusive of the Village fault has been simplified into three main strands that are of importance in the localization of the mineralization. These are the West, Main, and East veins (Figure 2 and 3). Ancillary faults do contain gold mineralization, although this mineralization is of limited economic importance.

At the mine, the Getchell fault system consists of a series of anastomosing, east-dipping, normal faults. The dip of the faults varies from about 30° to 60°, with the eastern strand generally dipping more steeply than the western strands. In spite of a thick gouge zone along the Main vein of the Getchell fault (Figure 3), the greatest vertical displacement appears to have taken place to the east along the Village fault, although the absolute displacement is unknown. This interpretation is based on the stratigraphic continuity of the Preble Formation limestone across the Main vein of the fault system in the Getchell mine workings and on drill data south of the workings and along the Village fault (unpublished data, Continental Oil Co.).

Limestone of the Preble Formation is the most important host rock for gold mineralization in the mine area. Arenaceous limestone beds (1-2" thick) are intercalated with equally thick carbonaceous shale beds. The shales are in part limy, particularly in the North Pit area. Thick shale units lie both stratigraphically above and below the predominantly limestone portion of the formation. Against the intrusion the shales are metamorphosed to cordierite-

andalusite hornfels. Biotite hornfels appears along some faults and biotite schist appears along others. Berger and Taylor (1974) interpreted these biotite-rich areas as faults ancestral to the present day Gatchell system. The shale and limestone beds strike northerly and dip 30°-50° to the east. Outside the zone of contact metamorphism Pre-Cretaceous regional metamorphism has converted the Preble shales into phyllitic rocks.

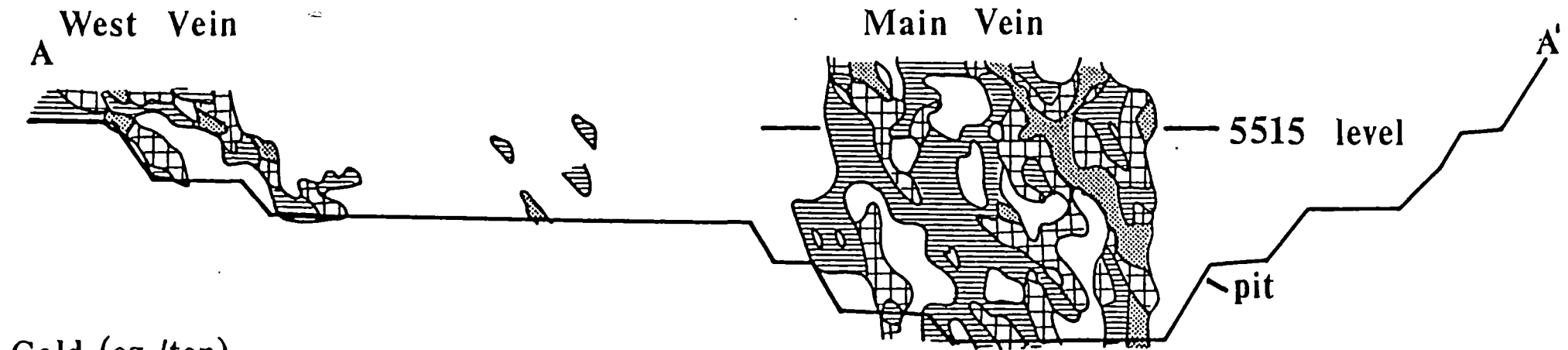
The main mass of the granodiorite stock is located along the west side of the mine area (Figure 3). It forms the footwall of the West vein of the Gatchell fault system in the South pit. Another large mass is located in the hangingwall of the Main vein to the east of the Center pit. Hotz and Willden (1964) suggested that the latter mass was offset approximately 0.7 miles laterally from the main stock. However, an intricate set of offshoot granodiorite dikes along the East vein and to the north of the body along the Main vein imply that the body was emplaced along the faults and is not an offset portion of the main stock. Three- to ten-foot wide granodiorite and dacite porphyry dikes also were emplaced along the Main vein. All of the intrusive dikes are of Cretaceous age (Silberman and McKee, 1971; Silberman and others, 1974).

Several sequences of Tertiary and Quaternary alluvial deposits cover most of the eastern portion of the mine area. These deposits have been unaffected by hydrothermal activity. A rhyolitic ash is incorporated in the oldest alluvium exposed in the North, Center, and South pit areas. The ash units are found in the alluvium in the east wall of all of the open pits and about two miles north of the mine along the Village fault. The largest exposure of ash is adjacent to the North pit entrance ramp. Joralemon (1951, 1975) felt the ash adjacent to the North pit was genetically related to the gold mineralization. However, eroded fragments of mineralized rock occur in alluvium beneath the ash beds, and portions of the ore zones are truncated by alluvium-filled channels which contain the ash beds.

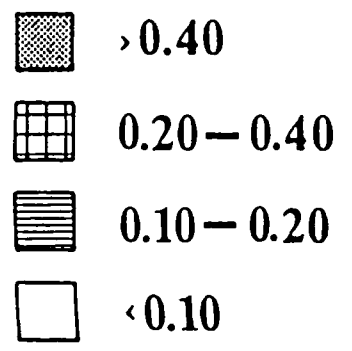
GEOLOGIC RELATIONS OF THE GOLD MINERALIZATION

Gold was discovered at Gatchell in 1934. Open-cut and underground production of primarily oxide ore commenced in 1938 and continued to 1950. The gold was extracted using the cyanide process. Sulfide ores, mined from three open pits, were primarily treated during a later stage of mining (1962-1967) using a fluid-bed roast to oxidize the ores prior to cyanidation. The bullion production record for both periods of mining is given in Table 1.

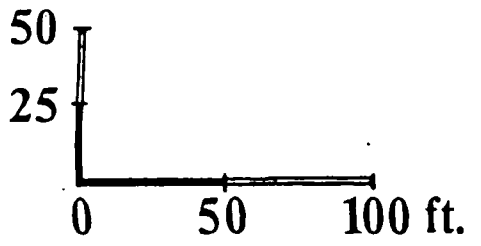
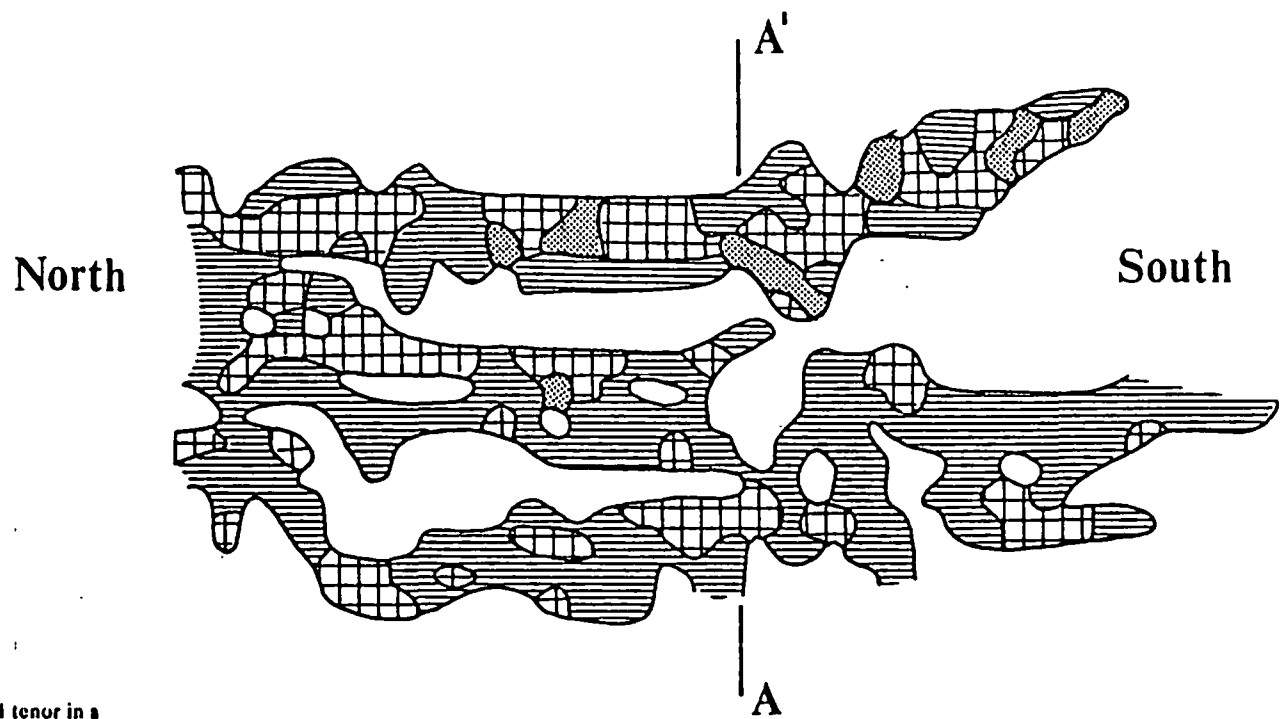
The gold ore deposits are low temperature (Nash, 1972) replacements of limestone along the Gatchell fault zone with the faults serving as conduits for the ore solutions. Typical of many epithermal deposits, the ore bodies form irregular pods of erratic grade (Figure 4). Mining widths averaged 12 meters (Joralemon, 1951), although zones as much as 61 meters wide were mined. Deep explorations shows that the mineralization persists at least 1 kilometer down-dip on the Gatchell fault system and also occurs along the parallel Village fault (Berger, 1976). Although the major strands of the Gatchell fault appear to converge down-dip, the complex pattern of mineralization remains consistent to considerable depths, and there is still more than one persistent mineralized structure at the deepest levels investigated.



Gold (oz./ton)



Cross Section S-11



Plan 5515 Level

FIGURE 4. Plan and cross-sectional views of gold tenor in a portion of the South Pit.

118

TABLE 1. Gold production at the Gatchell mine*
1938-1950

<u>Year</u>	<u>Ounces</u>	<u>Value</u>
1938	24,818	\$ 868,632
1939	49,135	1,719,740
1940	63,385	2,218,467
1941	59,515	2,083,033
1942	49,168	1,720,868
1943	34,949	1,223,232
1944	35,536	1,243,760
1945	9,925	347,375
1946-47	No Production	
1948	10,754	376,390
1949	18,758	656,530
1950	<u>32,090</u>	<u>1,123,150</u>
TOTAL	388,033	\$13,581,177

1962-1967

	<u>Tons</u>	<u>Ounces/Ton</u>
North Pit	804,130	0.33
Center Pit	396,100	0.25
South Pit	879,400	0.23
Section 4	33,400	0.23
	<u>2,113,030</u>	<u>0.271</u>

*Data compiled as shown from annual reports of Gatchell Mine, Incorporated.

Alteration and Ore Mineralogy

Hydrothermal alteration consists chiefly of decarbonatization accompanied by silicification of the limestone beds. Some portions of the limestone have been completely altered to fine, granular quartz. Secondary quartz is also present in all other rock types in the mineralized zone. Where relict bedding is preserved, the quartz is very fine grained, and the grains are elongated parallel to the bedding. Where silicification is more intense, the quartz is fine to medium grained, and grew obliquely to the bedding. All of the secondary quartz grains display an irregular outline in contrast to the equant, mosaic texture found in the unmineralized metamorphosed rocks. Polished section examination has shown some native gold to be jacketed by and along the margins of quartz grains (Joralemon, 1949). Amorphous and/or cryptocrystalline masses of silica referred to as "jasperoid" have only been found in oxidized portions of the mineralized zones and are probably supergene in origin.

Some of the silicified zones are surrounded by pods of carbonaceous material. The carbon has probably been in part remobilized from limestone and shale by the hydrothermal solutions, and is a mixture of amorphous carbon, organic carbon complexes (B. R. Berger, unpublished data), and graphite (Botinelly and others, 1973). The most carbonaceous zones occur where shale made up a significant proportion of the host rock. Where the bedding has been preserved, the carbonaceous material forms thin laminae paralleling quartz layers. The carbon often surrounds the quartz, but is not, in general, adjacent to subhedral pyrite grains which form elongate clots parallel to the bedding. The pyrite is intergrown with larger quartz grains and commonly contains blebs or rims of arsenopyrite. Joralemon (1949, 1951) found some visible gold in association with pyrite, arsenopyrite, and carbonaceous material. Where silicification is more intense, the carbonaceous material forms irregular, intergranular mattes surrounding quartz grains. However, the sulfides again tend to be enclosed by elongate quartz grains and not carbonaceous material, implying that there is a closer relationship of gold to quartz and sulfide than to carbonaceous material (Wells and others, 1969). Depending on the original host rock mineralogy, other alteration products include sericite, clay, and chlorite. Cordierite, andalusite, and biotite are altered to sericite and/or chlorite. Feldspar is argillized and/or sericitized. X-ray data from an altered granodiorite mass in the South pit indicate that the clay is primarily kaolinite.

As₂S₃ As₂S₃
Realgar and orpiment are late-stage products of the hydrothermal activity. They are generally interstitial to other ore and gangue minerals along veins, fractures, or bedding planes. In rocks with considerable carbonaceous material, realgar and orpiment are surrounded by dense mattes of late-stage remobilized carbon.

The igneous dikes and portions of the main stock are altered. Plagioclase is altered to sericite and kaolinite; biotite is altered to sericite, chlorite, and pyrite. Stockwork quartz veins cut the igneous bodies, and these veins are cut by calcite-dolomite veins in the South pit. Realgar occurs along the stockwork veins and around the boundaries of altered feldspar grains. Much of the groundmass of the porphyritic intrusions is altered to quartz and clay. Joralemon (1949) suggested that the alteration of the igneous dikes may be deuteric. The only deuteric alteration noted during the present study consisted of partial sericitization of biotite in dikes crosscutting tactite in the Riley mine to the south of the Getchell mine (Figure 2). Intense argillic alteration and pervasive quartz and sericite along dike boundaries are found only in dikes located in areas having gold mineralization. Away from the ore bodies or within the granodiorite, dikes are fresh; even a short distance from the Getchell fault they do not show alteration of any sort.

Minor ore minerals include cinnabar, stibnite, and occasional chalcopyrite and sphalerite. In addition to quartz and calcite, gangue minerals include marcasite, magnetite, barite, fluorite, and chabazite. Stibnite is most common in the South pit ore body and along the East vein. Fluorite occurs in the North pit ore body as do the rare minerals getchellite (Sb₃As₂S₃) and galkhaite (Hg,Cu,Tl,Zn)(As,Sb)S₂ (Botinelly and others, 1973).

Stratigraphic and Structural Ore Controls

The Getchell and Village faults are the primary loci of mineralization. Alteration and metallizations string out along minor structures into the hangingwall or footwall only a few meters. The hydrothermal solutions mineralized all rock types in the mine area, although economic mineralization for the most part appears to be restricted to the limestone and limy portions of the shale of the Preble Formation.

The strike and dip of the bedding in the Preble Formation are subparallel to the Getchell fault; as a result the replacement ore bodies in plan view are thin and sheet-like zones along the fault. Isoclinal folding of the sedimentary rocks also controls the mineralization: (1) the folds have duplicated the relatively thin limestone member of the Preble Formation resulting in a thicker mineralized zone transected by the fault zone; and (2) increased permeability in the crushed noses of the folds allowed the mineralization to follow the plunge, increasing ore length. However, the folds do not carry the mineralization away from the main fault zone more than a few meters. Depending on the position of the limy rocks relative to the fault the mineralization can occur either against the footwall or adjacent to the hanging wall.

The geometry of the ore bodies is shown in Figure 4. Both cross sectional and plan views are shown from the South pit (Berger, 1975). The higher grade bodies form scattered pods and narrow, continuous shoots down the dip of the vein. Although in the interior of the veins ore grade generally decreases gradually away from high-grade bodies, locally it decreases abruptly. The high-grade bodies commonly persist to the margin of the vein, where grade drops off abruptly.

Joralemon (1975) reported that for ore grades exceeding 0.10 ounces per ton the ore bodies apex within 9 to 15 meters of the present-day land surface, reflecting current topographic highs and lows and implying a very young age for the deposit. Berger and others (1975) found that for the minimum grade of 0.10 ounces per ton gold, the relation between the top of the north ore body and the surface prior to mining is as shown in Figure 5. Small pods of ore and altered rocks cropped out or were exposed in shallow trenches along ancillary faults in the footwall of the North pit ore body (Witt, 1936b). Where the Center Pit is now located, silicified gold-bearing ledges up to 45 m high and 24 m thick were traceable for over 900 m to the south (Witt, 1936a) to the South Pit (Figure 3). Mine reports indicate that an ore width of over 31 m was covered directly by 1 to 6 m of unaltered, unmineralized alluvium in the South Pit area (unpublished data, Getchell Mine, Inc., 1934). Five hundred meters south of the South pit over 15 m width of ore cropped out, and gold ore crops out at the Riley tungsten mine, 2 km south of Getchell. The mineralization is pervasive along parts of the Getchell fault, and what constitutes ore is wholly dependent upon the economics of mining and recovery. As a result, the geometry of ore pods can vary depending on the chosen cutoff grade, and no age can be inferred from the ore geometries.

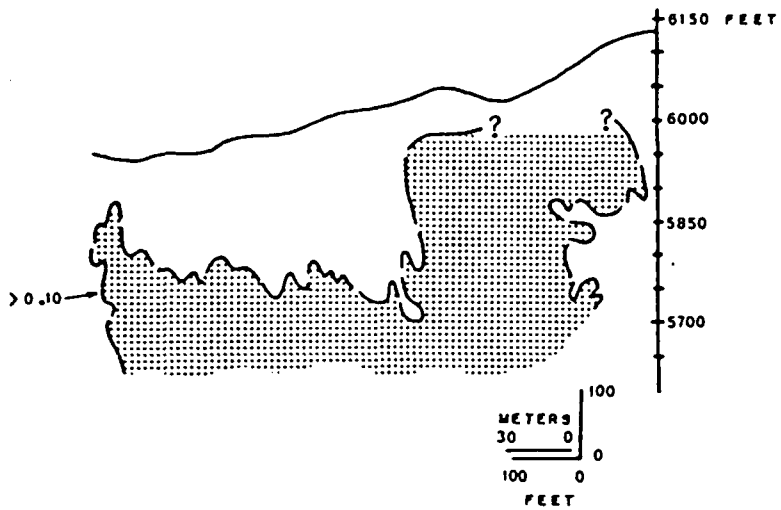


FIGURE 5. Longitudinal, vertical projection of ore apex (greater than 0.10 oz/ton) North Pit orebody, Getchell mine. Taken from Getchell mine cross sections N19-N36.

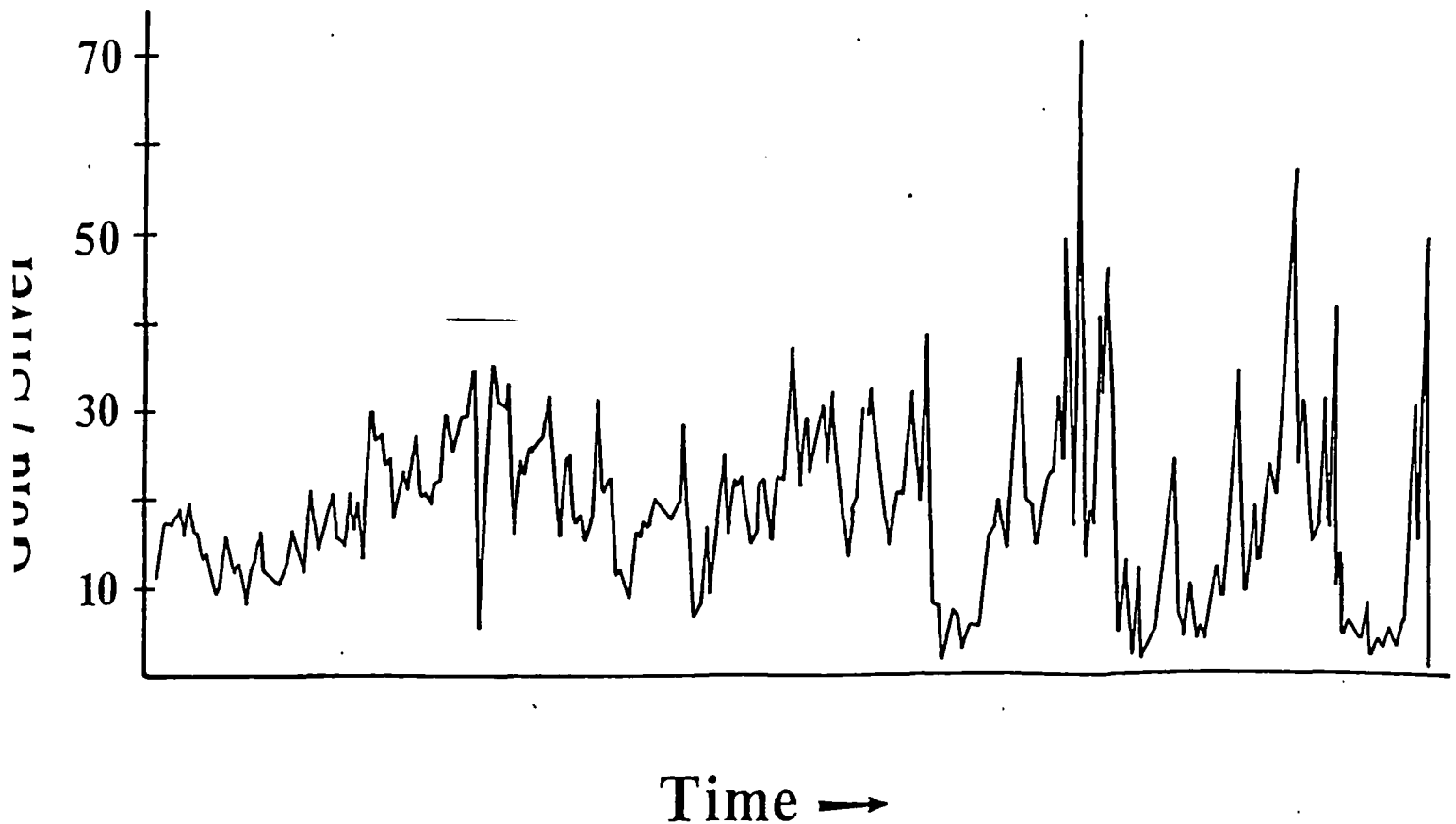


FIGURE 6. Gold to silver ratios for bullion produced at Getchell for the period 1938-1945. Unpublished data, Getchell Mine, Inc.

GEOCHEMICAL NATURE OF THE MINERALIZATION

Gold occurs in the native state as micrometer- to submicrometer sized particles. Unpublished electron microprobe data (A. Radtke, personal commun.) show the gold to occur in association with carbonaceous material, within sulfide minerals, and as particles within and between quartz and clay grains. The average grade of the exploited Getchell ore bodies was about 9 to 10 ppm (Table 1). The subeconomic mineralization ranges from 0.02 ppm to 3 ppm gold. Silver is generally less than 1 ppm in the ore zones, but ranges from 0.2 ppm to 16 ppm in samples taken for this study. The gold to silver ratio in bullion for the period 1938 to 1945 is shown in Figure 6. Presuming that the mining progressed to greater depths with time, there is no discernible systematic trend to increased gold/silver ratios with depth in the oxidized parts of the ore bodies which made up the bulk of the ores mined. Cycles of progressively higher ratios followed by progressively lower ratios possibly reflect the somewhat irregular grade distributions shown in Figure 4, and the poor gold-silver correlations shown in Table 4 also corroborates this interpretation.

Erickson and others (1964) suggest that the trace element suite found at the Getchell deposit is similar to that found at the Carlin gold mine (Hausen, 1967; Radtke and others, 1972) and other disseminated gold deposits (Ferguson, 1924; Gilluly, 1932; Wells and others, 1969). Arsenic, mercury, and antimony are most closely associated with gold mineralization. Erickson and others (1964) also suggested that tungsten may be anomalous in the Getchell ore, though any genetic relationship is obscured by the proximity of tungsten-bearing tactites to the main productive gold zones.

The average trace element content of the Getchell gold deposit based on 50 samples collected for this study is shown in Table 2. The most notably enriched elements are arsenic, antimony, and mercury. The low concentration of copper, zinc, and lead is conspicuous and characteristic of the disseminated gold deposits along the Getchell fault. There appear to be trace element variations between the north, center, and south ore zones (Table 3) although the population of 50 samples evenly divided for each pit is not large enough to statistically validate the differences shown. Nevertheless, the geological relationships in the pits provide corroborative evidence to the geochemical variations shown. Silver, molybdenum, and tungsten are highest in the South pit (Figure 3) where the most pre-gold calc-silicate is in evidence. Disseminated molybdenite can be found in the granodiorite stock adjacent to tungsten-bearing skarn along the West Vein, and granodiorite dikes in the east wall of the pit are spatially associated with the alteration of some of the Preble Formation limestone to a garnet-pyroxene skarn. The average mercury abundance increases from about 15 ppm in the North pit to over 80 ppm in the South pit. The highest mercury values occur as cinnabar in association with antimony. The footwall of the Center pit is siliceous hornfels, which may explain the generally lower concentrations of copper, lead, and zinc in the central ore zone. However, the concentrations of these base metals are uniformly low and the differences between the pits minor.

TABLE 2a. Average trace element content of the Getchell gold deposit.

Element	Average abundance (%)	Element	Average abundance (%)
Arsenic	0.285	Nickel	<0.0018
Boron	0.0052	Lead	0.0018
Barium	0.019	Antimony	<0.0935
Cobalt	<0.0009	Strontium	<0.0186
Chromium	0.0031	Titanium	0.103
Copper	0.0047	Vanadium	0.034
Gallium	<0.0016	Tungsten	0.0016
Lanthanum	0.0028	Yttrium	<0.0015
Manganese	0.0113	Zinc	0.0050
Molybdenum	0.001		

TABLE 2b. Abundance of arsenic, mercury, and antimony in ore and unmineralized host rock.

[Numbers in parantheses show the sample population size]

Element	Ore	Background
Arsenic	0.285% (181)	0.0003% (74)
Mercury	0.0022% (181)	0.000007% (50)
Antimony	0.0325% (36)	0.0007% (40)

TABLE 3. Trace element variations in parts per million between mining areas at the Getchell mine.

[All samples other than Oxide Zone represent primary sulfide ore]

Location	Ag	Cu	Pb	Zn	Mo	As	W	Hg
North Pit	2.3	84	27	99	22	2,800	26	15
Center Pit	1.9	69	14	69	13	2,800	19	30
South Pit	7.4	44	42	98	208	2,800	33	88
Oxidized Ores	--	169	59	--	18	900	--	14

The results of a correlation analysis of selected elements in ores are shown in Table 4. The ore samples were collected from all of the mining areas including the Section 4 pit south of the South pit and north of the Riley mine (T. 38 N., R. 42 E.). The relatively higher correlations between gold and molybdenum and gold and tungsten are interesting in light of the trace-element chemistry of disseminated molybdenite and scheelite-bearing skarn mineralization in the area. These correlations suggest that the gold, molybdenum and tungsten were deposited in response to different geochemical parameters than the arsenic, mercury, antimony, and thallium. Arsenic, mercury, antimony, and thallium are closely related, with thallium also showing a dependent relationship with molybdenum. The fluorine content is linearly independent of all of the elements except arsenic. The lack of correlations between gold, arsenic, mercury, and antimony with copper, lead, and zinc underscore the deficiency of base metals as a characteristic of the disseminated gold ore bodies.

TABLE 4. Table of correlation coefficients for selected elements in ores from the Getchell mine.

		Number of Qualified Pairs											
		Au	Ag	As	Hg	Sb	W	Tl	F	Mo	Cu	Pb	Zn
CORRELATION COEFFICIENT	Au		78	67	77	44	81	42	37	57	56	48	49
	Ag	.11		66	77	44	78	43	34	59	60	51	52
	As	.13	.20		72	37	69	40	30	46	46	44	46
	Hg	.20	.29	.73		36	82	40	30	57	57	56	58
	Sb	.004	.60	.91	.69		37	37	38	15	16	9	8
	W	.24	.09	.33	.27	.37		47	37	59	58	50	52
	Tl	.14	.33	.71	.73	.72	.38		37	17	17	8	10
	F	-.10	-.05	.50	.13	-.04	-.07	-.04		7	7	0	0
	Mo	.50	.32	.08	.03	-.20	.38	.75	-.26		66	58	59
	Cu	-.10	.19	-.03	-.05	-.13	-.008	-.35	-.15	.05		58	59
	Pb	-.02	.48	-.01	-.08	.14	-.08	-.21		.05	.13		58
	Zn	-.10	.09	-.03	-.11	-.26	.13	.41		.21	.38	.55	

There is no strong evidence, however, for mechanical or chemical supergene leaching and enrichment of gold at the base of the oxidized zone. Some depletion of arsenic and mercury has taken place in the oxidized, mineralized zones (Table 3) but no enriched areas are recognizable. The abundances for arsenic and mercury from selected samples are given in Table 5. Therefore, observed arsenic and mercury dispersion halos are primarily hypogene features, a fact which is useful in applying these data to exploration.

TABLE 5. Representative arsenic and mercury data from oxidized ores.

[Data from Erickson and others (1964)]

Sample No.	Arsenic	Mercury	Sample No.	Arsenic	Mercury
252	700	3	216-G	500	9
250	30	<2	216-H	300	6
212	3,000	3	216-J	1,000	5
214-C	1,000	10	216-K	700	9
245	2,000	2	216-R	40	8
246	1,000	8	216-S	1,000	30
251	500	<2	216-T	500	14

Major element redistribution accompanying hydrothermal alteration is illustrated in Table 6. In the limestone calcium, carbon dioxide, and magnesium were removed and silica, aluminum and iron were added. There was a loss in the granodiorite of silica, ferrous iron, and sodium. Since there was a decrease of bulk density during alteration, there was probably a significant loss of aluminum. Titanium, phosphorus, and manganese were essentially unchanged. There was an increase in ferric iron, magnesium, calcium, potassium, water, and carbon dioxide.

Trace element halos around the ore bodies are not extensive except where the rock is strongly fractured. Erickson and others (1964) demonstrated that calcite and quartz veinlets and limonite-coated fractures away from the pervasive hydrothermal alteration represent leakage halos and may contain pathfinder elements leading to buried mineralization. The present study has found that arsenic and mercury have moved along fractures for several hundreds of meters laterally and vertically from the ore zones. Within the pervasively altered zones and in fractured rock away from the main faulting, arsenic and mercury anomalies are scarcely broader than the areas with detectable concentrations of gold (more than 0.02 ppm).

TABLE 6. Whole rock analyses of altered and unaltered rock types in the Gatchell mine area.

	1	2	3	4	5	6	7	8	9	10
SiO ₂	67.6	68.4	65.9	44.0	5.8	2.4	53.1	83.4	76.4	59.0
Al ₂ O ₃	16.8	16.8	16.8	16.8	.80	.34	26.4	4.2	5.1	10.4
Fe ₂ O ₃	1.3	1.6	1.5	2.3	.43	.10	3.0	1.70	.11	1.30
FeO	1.6	1.4	2.0	.96	.01	.02	5.3	2.60	1.20	1.90
MgO	1.0	1.2	1.4	2.4	.26	.42	1.7	.13	.21	.83
CaO	4.0	4.0	4.3	10.4	52.7	54.9	.19	.92	1.10	1.60
Na ₂ O	3.5	3.5	3.6	.06	.07	.06	1.0	.01	.01	.05
K ₂ O	2.8	2.8	2.8	7.8	.12	.02	3.9	1.10	1.30	2.60
TiO ₂	.42	.40	.53	.62	.04	.02	.87	.23	.35	.38
P ₂ O ₅	.22	.22	.19	.27	.09	.10	.14	.25	.70	.09
MnO	.10	.09	.07	.10	--	.01	.11	.30	.077	.097
CO ₂	.05	.05	--	10.1	40.1	42.6	.05	--	--	--
H ₂ O ⁺	--	--	}	3.3	.01	.02	5.1	.80	1.50	1.20
H ₂ O ⁻	--	--						2.30	9.80	19.0
F(%)								.12	.15	.13
Au (ppm)	--	--		7.8				9.3	.08	6.2
As (%)	--	--		.50				.39	3.6	14.5
Hg (ppm)	--	--		19.5				101.8	110.6	112.5
Sb (%)	--	--		.001				.005	.068	.17
Tl (ppm)	--	--		--				80	50	69

- 1, 2 Granodiorite--unaltered, Hotz and Willden (1964)
 3 Granodiorite--unaltered, Silberman and others (1974)
 4 Granodiorite--altered, Silberman and others (1974)
 5, 6 Preble Formation--limestone, Hotz and Willden (1964)
 7 Preble Formation--phyllite, Hotz and Willden (1964)
 8, 9, 10 Preble Formation--altered limestone, this study

The variation of total sulfur and total carbon (carbonate and organic) with gold, arsenic, and mercury contents in ores is shown in Table 7. There is no apparent correlation between the gold tenor and the sulfur or carbon contents, suggesting that gold was introduced at a different stage in the alteration-metallization paragenesis. An increase occurred in sulfur introduced as pyrite in the sedimentary rocks during hydrothermal activity. The hydrothermal solutions apparently removed virtually all the carbonate from intensely altered limestone (see CO₂ analyses for altered and unaltered limestone, Table 4). Assuming that these solutions were just as effective in removing carbonate from other rock types as well, the carbon analyses shown for altered rock in Table 7, which are total carbon determinations, represent mainly carbonaceous material rather than carbonate.

TABLE 7. Sulfur and carbon data for selected ore and host-rock samples showing correlation between sulfur, carbon, gold, arsenic, and mercury.

	Gold oz/ton	Arsenic ppm	Mercury ppm	% Sulfur	% Carbon	
SOUTH PIT	Carbonaceous (oxidized)	0.023	700	100.9	0.10	0.90
	Carbonaceous	0.006	640	72.6	0.74	1.17
	Carbonaceous	0.05	0.16%	45.8	0.89	1.42
	Carbonaceous	0.029	0.84%	641.8	1.28	0.97
	Carbonaceous	0.006	2.1%	67.9	2.46	1.10
	Siliceous	0.006	380	69.0	1.27	0.46
	Siliceous, arsenical	0.131	12.8%	248.9	6.7	0.23
	Siliceous, arsenical	0.015	5.7%	400.1	6.9	0.34
CENTER PIT	Argillic, arsenical	0.175	6.4%	93.9	4.5	0.20
	Argillic, arsenical	0.090	7.8%	89.3	7.7	0.51
NORTH PIT	Carbonaceous	0.114	0.28%	57.6	1.12	2.29
	Carbonaceous, arsenical	0.073	4.8%	467.8	2.88	1.72
	Carbonaceous limestone (unmineralized)	----	0.012%	0.505	0.44	10.9
	Limestone (unmineralized)	----	0.007	0.82	0.18	7.13
	Carbonaceous shale (unmineralized)	----	0.0480	0.86	0.16	3.55

AGE AND ORIGIN OF THE MINERALIZATION

Age Relationships

Controversy has surrounded discussions concerning the ages of the various disseminated gold deposits. Associations of mineralization with Basin-Range faults and Tertiary volcanic rocks have led several workers to assume a late Tertiary to Quaternary age for all of the disseminated gold occurrences (Joralemon, 1951; Hotz and Willden, 1964; Hardie, 1966). At most of the occurrences, geologic relationships are obscure, allowing only maximum age estimates.

Silberman and others (1974) and Berger and others (1975) interpreted the age of the Getchell deposit to be Cretaceous based on both field and laboratory evidence. Alteration assemblages associated with gold mineralization yielded K-Ar ages of 80 to 96 m.y., and the mineralization is consistently associated with intrusive dikes of the same age. Granodiorite and/or porphyry dikes of similar or equivalent composition occur in all of the mineralized areas along the Getchell fault trend including the Hansen Creek (3 km south of Getchell), Summer Camp Creek (5 km south), Ogee-Pinson mine (10 km south), and Preble prospect (32 km south). A discordant Cretaceous age obtained using K-Ar was found for sericite from a granodiorite dike in the Preble deposit (M. L. Silberman, personal commun.). Oxidation of the dike rocks inhibits using radiometric age dating techniques on most samples. Further investigations of the age relationships are currently being done by B. R. Berger and R. P. Ashley of the U.S. Geological Survey. Fission track studies on apatite from the granodiorite stock in the South Pit indicate a major thermal event during the Miocene. The significance and precision of this event need to be assessed before a better understanding of the relationship of the age to the gold mineralization can be reached.

Character of the Hydrothermal Solutions

Discussion of the geochemistry of the ore-forming solutions is tenuous due to the lack of detailed laboratory studies relevant to the Getchell deposit. The ore mineral suite (Au-As-Hg-Sb) and alteration assemblage (quartz-clay-K-mica) suggest one possible interpretation that the mineralization took place from near-neutral to slightly alkaline, low salinity solutions (Tunell, 1964; Barnes and Czamanske, 1967; Seward, 1973; Learned and others, 1974). Fluid inclusion studies by Nash (1972) suggest that the temperature of formation may have been as high as 200°C, and the salinity of the fluid about 6% (NaCl equivalent by weight). The character of the products of alteration and metallization, taken together with properties of the fluid, suggest that the ore constituents may have been transported as sulfide complexes in solutions of low ionic strength (F. W. Dickson, personal commun.). Fluids having these properties are found in presently active hot springs systems. Joralemon (1951) noted the similarities between present-day hot springs systems and the alteration and mineralization at Getchell. Hausen and Kerr (1967) suggested a similar origin for the Carlin deposit and the stable isotope data of Rye and others (1974) are consistent with a thermal spring origin for the Cortez deposit.

EXPLORATION GUIDES

The Getchell gold deposits contain many of the characteristics that typify the Carlin-type disseminated gold occurrences. They are as follows:

- (1) Moderate to low temperature hydrothermal replacement-type deposits;
- (2) They are best developed in thin-bedded, carbonaceous, sandy carbonate rocks;
- (3) Intrusive igneous rocks of intermediate granitic composition are present as dikes or sills;
- (4) Gold predominates over silver in abundance, and the gold is associated with arsenic, mercury, and antimony and to a lesser extent with thallium, fluorine, tungsten, and molybdenum; and
- (5) High-angle faults serve as conduits for the ore-forming solutions.

These characteristics are the best exploration guidelines. The geochemical studies at Getchell suggest several other relationships that may be useful in regional exploration programs.

There is a consistent trace-element suite through all of the skarn, stockwork sulfide, and disseminated gold deposits in and around the Osgood Mountains stock. This is the suite Mo-W+Sn. This fact of occurrence suggests that irrespective of the relative ages of the various types of deposits, the same trace-element suite is being produced by hydrothermal activity, implying that the crustal source of magmas is the same through time or the crust is uniform in composition, giving rise to a consistent trace-element suite through time. This is particularly exemplified if one considers the disseminated gold mineralization to be much younger (e.g., Miocene) than the skarn formation which has been interpreted to be Cretaceous by Silberman and others (1974). An analogous magma to-hydrothermal situation has been inferred by the present author from studies by Shawe (1977) in the Round Mountain, Nevada, 7 1/2-minute quadrangle, where the trace-element suite of Mo-Sn-W is associated with four separate episodes of igneous activity spanning the time interval from approximately 90 m.y. to at least 26 m.y. B.P. Additionally, Joralemon (1978) documents a Carlin-type gold deposit in the area; the fact of this occurrence again underlines the possible importance of the Mo-Sn-W trace-element suite as an exploration guide.

The whole-rock chemistry of the Osgood Mountains stock may provide some clues as to the types of igneous rocks that may be related to the disseminated gold deposits. Neuerburg (1966) found the stock to be higher than normal granitic rocks in its gold content, and showed that the gold content was highest near the eastern contacts with the sedimentary rocks. Berger (1979) reported that the trace-element suite Mo-Sn-W is found associated with leucocratic batholithic rocks in southwestern Montana that have low K_2O/Na_2O ratios and low calcium contents. The data in Table 6 show the Osgood Mountains stock to also be somewhat sodium-rich relative to potassium, further suggesting that the whole-rock chemistry may provide clues to the species of metals associated with specific igneous complexes.

Berger (1976) and Brooks and Berger (1978) investigated two approaches to exploration in the Getchell area. The presence of potassium-rich alteration phases and thallium in the ores suggested that radiometric surveys may be of some value in exploration. Figure 7 shows the results of an aeroradiometric survey over the Getchell mine area. A trend clearly outlines the fault zone,

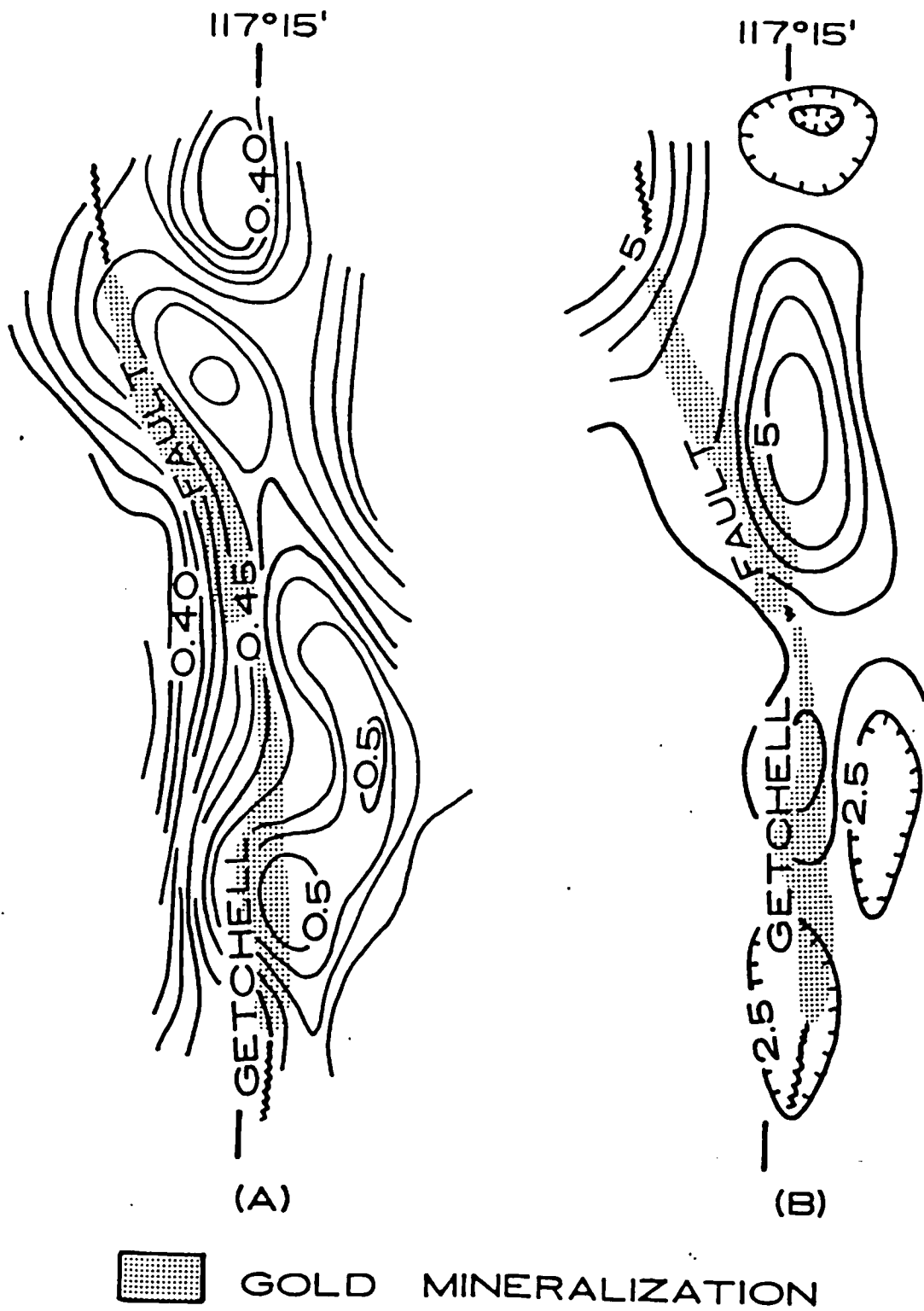


FIGURE 7. $\text{Bi}^{214}/\text{K}^{40}$ ratios (A) and Tl^{208} radiation (B) over gold mineralization at the Getchell mine. Data from Berger (1976).

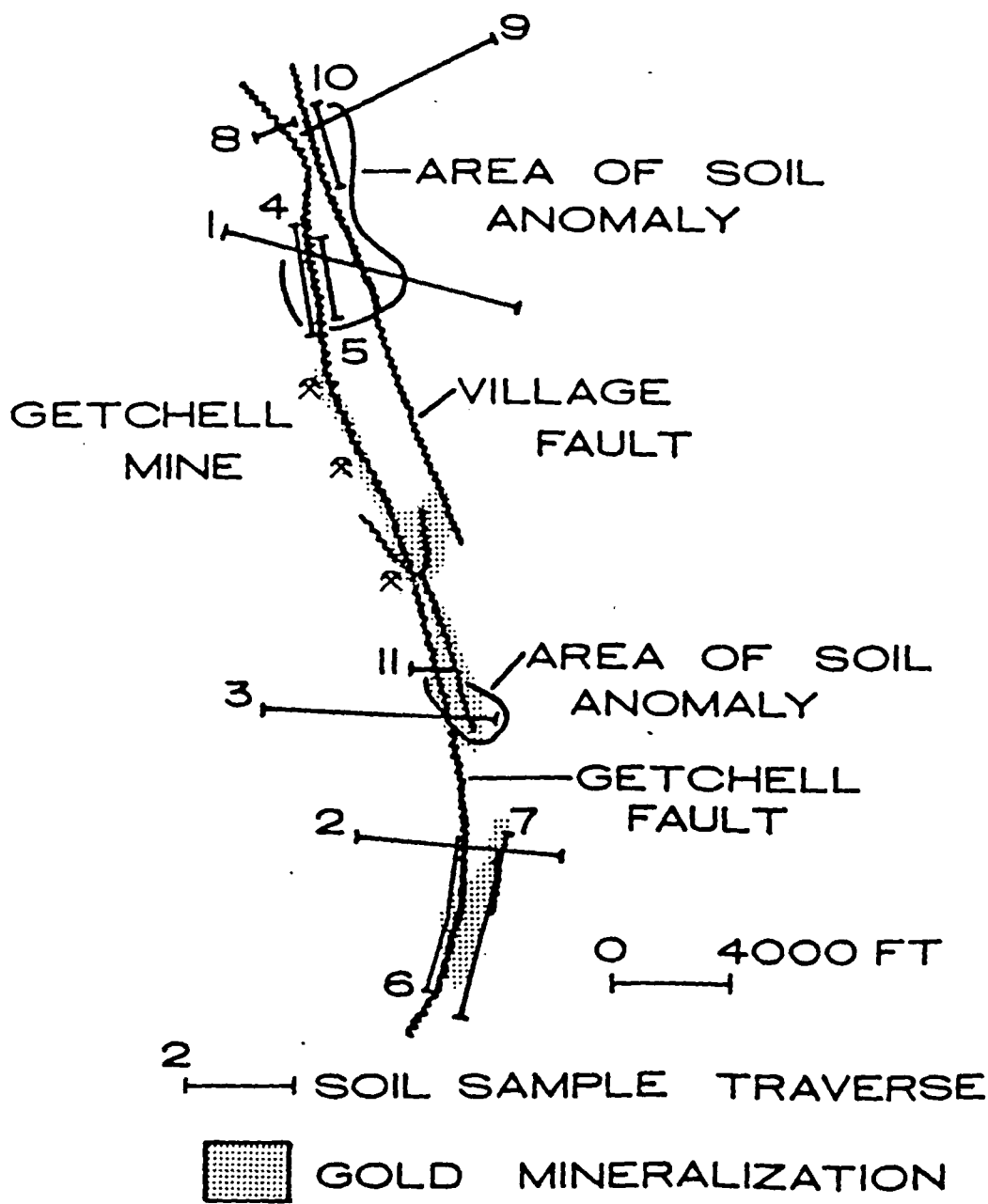


FIGURE 8. Relationship of anomalous concentrations of arsenic in soil to gold mineralization at the Getchell mine. Data from Brooks and Berger (1978).

but the locations of ore grade mineralization are not detected. Figure 8 shows a summary of the findings of Brooks and Berger (1978) wherein they found that arsenic and mercury in soils may be anomalous in the vicinity of gold mineralization, but the soil type plays a stronger role in arsenic and mercury entrapment than the presence or absence of arsenic and mercury in mineralized rock beneath the soil. Thus high-organic soils can lead to partial or displaced anomalies.

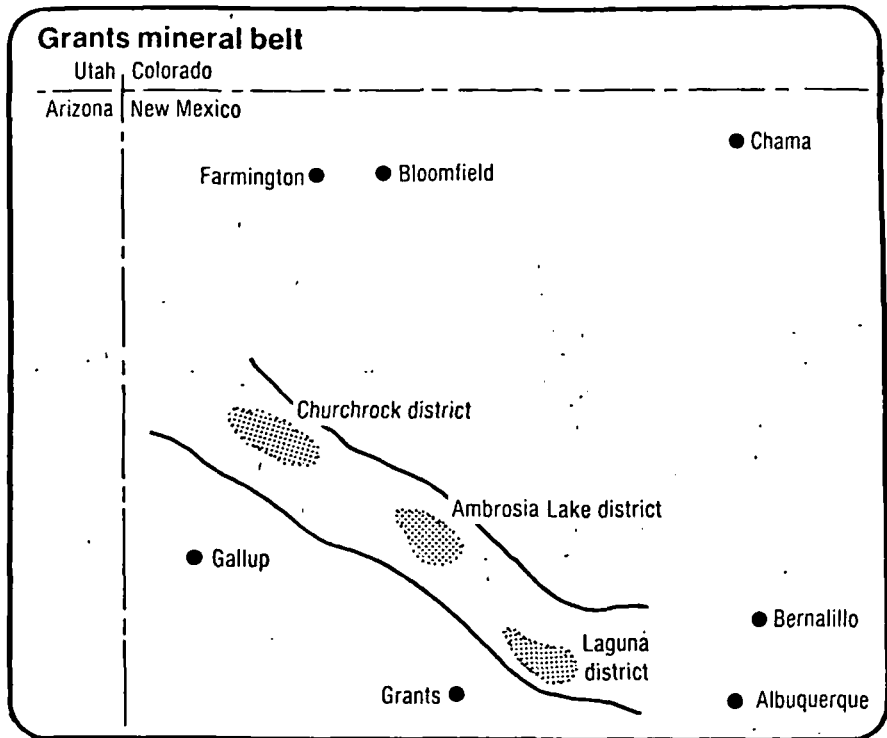
REFERENCES

- Barnes, H. L., and Czamanske, G. K., 1967, Solubilities and transport of ore minerals, in Barnes, H. L., ed., *Geochemistry of hydrothermal ore deposits*: New York, Hold, Rinehart, and Winston, Inc., p. 334-381.
- Berger, B. R., 1975, *Geology and geochemistry of the Getchell disseminated gold deposits, Humboldt County, Nevada*: Am. Inst. Mining, Metall. and Petroleum Engineers Preprint No. 75-I-305.
- _____, 1976, *Geology and trace element variations at the Getchell mine, Humboldt County, Nevada* [Abs.]: Symposium on the Geology and Exploration Aspects of Fine-Grained, Carlin-type Gold Deposits, Univ. Nevada, Reno.
- _____, 1979, *Applications of exploration geochemistry in regional resource studies* [Abs.]: Geol. Soc. America Abs. with Programs, v. 11, no. 7, p. 387.
- Berger, B. R., Silberman, M. L., and Koski, R. A., 1975, K-Ar age relations of granodiorite emplacement and tungsten and gold mineralization near the Getchell mine, Humboldt County, Nevada--a reply: *Econ. Geol.*, v. 70, p. 1487-1491.
- Berger, B. R., and Taylor, B. E., 1974, Pre-Cenozoic age for "basin-range" faulting, Osgood Mountains, north-central Nevada [Abs.]: *Geol. Soc. America, Cordilleran Section, Las Vegas, Nevada*.
- Botinelly, Theodore, Neuerburg, G. J., and Conklin, N. M., 1973, Galkhaite, (Hg,Cu,Tl,Zn)(As,Sb)S₂, from the Getchell mine, Humboldt County, Nevada: *U.S. Geol. Survey Jour. Research*, v. 1, no. 5, p. 515-517.
- X Brooks, R. A., and Berger, B. R., 1978, Relationship of soil-mercury values to soil type and disseminated gold mineralization, Getchell mine area, Humboldt County, Nevada: *Jour. Geochem. Exploration*, v. 9, p. 186-194.
- Cavender, W. S., 1963, *Integrated mineral exploration in the Osgood Mountains, Humboldt County, Nevada*: Unpublished Ph.D. Thesis, Univ. Calif., Berkeley, 225 p.
- Erickson, R. L., Marranzino, A. P., Uteana, O., and James, W. W., 1964, *Geochemical exploration near the Getchell mine, Humboldt County, Nevada*: *U.S. Geol. Survey Bull.* 1198-A, 26 p.
- Erickson, R. L., and Marsh, S. P., 1974, *Paleozoic tectonics in the Edna Mountain quadrangle, Nevada*: *U.S. Geol. Survey Jour. Research*, v. 2, no. 3, p. 331-337.

Subj
GEOL
GDPU

UNIVERSITY OF UTAH
RESEARCH INSTITUTE
EARTH SCIENCE LAB.

E&Mj EXPLORATION ROUNDUP



Grants district: Publication updates geology and exploration technology

The Grants district, located in northwestern New Mexico, is the principal source of US uranium and is expected to remain such for some time. It contains several of the world's largest uranium orebodies. In 1963, the New Mexico Bureau of Mines & Mineral Resources published Memoir 15, *Geology and Technology of the Grants Uranium Region*. Subsequent developments in the area, including much well-financed exploration and development by oil companies, has led to an increase in both reserves and understanding of the geology. The need for a new, up-to-date volume has now been filled by Memoir 38, *Geology and Mineral Technology of the Grants Uranium Region, 1979*. It consists of 49 papers, most of which were presented at a symposium in Albuquerque in 1979 and have just recently been issued in memoir form.

Included papers will be useful to people new to the district and to those already familiar with it. A good introduction is David C. Fitch's "Exploration for Uranium Deposits, Grants Mineral Belt." He describes the general features of the deposits of the belt, ore guides, theory of origin, and methods of exploration. Ore is confined to the Brushy Basin, Westwater Canyon, and Recapture members of the Jurassic Morrison formation.

Fitch describes the usual three-stage exploration drilling program:

- Delineation stage, in which holes are drilled 1/2 mi to several miles apart.
- Mineralization search using five to 10 drill holes per square mile.
- Closely spaced drilling in mineralized

areas to define ore zones.

While Fitch's paper is a good introduction to the area, a paper by John B. Squyres on "Origin and Significance of Organic Matter in Uranium Deposits of Morrison Formation, San Juan Basin, New Mexico," might be considered a review paper for someone already acquainted with the area who wants the latest thought on the most widely accepted theory of Grants area ore genesis. Several lines of evidence suggest the age of the ore is about the same as the age of the host rock. According to the prevalent model, "humic acids were leached from buried plant debris by groundwater, during or shortly after Morrison sedimentation. The acids migrated with the groundwater and eventually consolidated into streamlined, interstitial humate [the solid or semisolid equivalents of humic acids] masses. Uranium in the groundwater was chelated by the humates and subsequently reduced."

Squyres' detailed examination of the evidence, with accompanying photos and diagrams, is followed by conclusions and inferences. Two of the inferences are that "ore occurrences will not be confined to the margins of the San Juan Basin. Additional trends or belts of ore deposits deeper in the Basin are likely to be arranged in a radial pattern with a hub in the general area of the Westwater Canyon fan apex," and "Jordisite-impregnated sandstone is a strong indicator of ore in the immediate vicinity."

The historical side of the Grants region

(Continued on p 31)

is presented in "Exploration in Grants Uranium Region Since 1963," by William L. Chenoweth and Harlen K. Holen. The nature of the Morrison formation as several large, low-gradient, humid-region alluvial fans is described by William E. Galloway. He gives special attention to the Westwater Canyon member. Frank G. Ethridge, et. al., did laboratory flume studies to determine the effect of variable flow rates, porous-media layering, baffles (mudstone lenses), fluid density differences, and geochemical reactions. Similarities between flume results and effects observed in deposits in the field suggest that the laboratory studies can be useful in predicting the shape and distribution of tabular orebodies and the relationship between these bodies and groundwater flow patterns.

A detailed description of one deposit as viewed through the generally accepted organic hypothesis is "Sedimentary Controls of Uranium Ore at L-Bar Deposits, Laguna District, New Mexico," by L. C. Jacobsen. A somewhat different ore genesis is presented in an abstract by Douglas G. Brookins of a paper entitled "Geochemical and Clay Mineralogical Studies, Grants Mineral Belt," in which he writes that "Uranium for the deposits of the Grants mineral belt was most likely carried in solution as an oxyion . . . although organic transport cannot be entirely ruled out."

James W. Melvin, in "Uranium Royalties and Severance Taxes in the Grants Region, with Examples of their Effects on Minimum Producing Grade," examines eight actual royalty agreements and relates cutoff grade to royalty and severance taxes applied to an actual orebody.

A paper by Dean S. Clark describes an orebody in the Nose Rock area of the San Juan Basin, the furthest down-dip deposit of the Grants area. Memoir 38 is 400 pp and costs \$18.00. Write to New Mexico Bureau of Mines & Mineral Resources, Socorro, N.Mex. 87801. ■

Ongoing projects

Sweden: Boliden has announced discovery of an 800,000 mt orebody containing 2-3% lead, 1% copper, and 5-6% zinc at its Saxberget mine in central Sweden. A new level will be opened at 665 m, and there will be exploration drilling to 900 m. The mine has been in production 100 yrs, producing a complex copper-lead-zinc ore.

Canada: Dynamic Mining Exploration Ltd. has announced that it has entered into an option agreement to purchase claims covering about 511 acres in the Bird River and Euclid Lake areas of Manitoba. Diamond drilling on the prop-

erties by other owners has indicated about 13 million st of low-grade chromite reserves.

US: Kerr-McGee Corp. has announced that while it has discontinued efforts to find commercial uranium in Wisconsin's Florence Co., it will continue exploration for base metals in northern Wisconsin. The company has obtained mineral rights in Florence, Forest, Langlade, Oneida, and Vilas Counties through an agreement with the Chicago and North Western Railroad.

Australia: US-owned Newmont Holdings Pty. Ltd. has taken a 60% stake in a mineral prospect, Location 50, near Kalgoolie in Western Australia. As manager of a joint venture, it has agreed to spend the first \$2.9 million within the first four years of exploration.

US: The Goldfield Corp. says it has found a silver deposit at a depth of 100-400 ft on its St. Cloud property in New Mexico. One hole showed 31.79 oz/st silver over 14.3 ft with additional values in copper and other base metals.

Texasgulf Inc. has acquired a two-year option on another Goldfield Corp. property in New Mexico, the San Pedro property, operated as a copper mine and mill prior to 1976.

US: The Minnesota Dept. of Natural Resources, Div. of Minerals, has recently completed a ground EM and magnetic survey and limited drilling over the Greenwood Lake anomaly in Lake County. The single drill hole, completed this year, penetrated 113 ft of glacial drift and 26 ft of bedrock. The bedrock consisted of banded trocolite gabbro with disseminated sulphides throughout. Details are available from David Meineke at the Div. of Minerals, P.O. Box 567, Hibbing, Minn. 55746.

Australia: Endeavour Resources Ltd. has entered into an option agreement for a 50% stake in gold mining leases at Barry's Reef and Simmon's Reef in Victoria. The area is said to have been worked for gold intermittently since the middle of the last century, and records show that some workings reached a depth of 300 m.

Canada: Thunderwood's Malartic, Que., property adjoining Camflo has received final assays indicating an 8.5-ft section starting at 244.5 ft, assaying 0.54 oz gold per st. On a different zone 1,400 ft to the northeast, a hole cut 5 ft, starting at 174.3 ft, that assayed 0.286 oz/st. Gold Hawk Resources (Ont.) Ltd. will acquire a 50% interest in the property. Additional drilling is planned for the very near future.

Australia: UNC Resources Inc. has sold a 50% interest in its Australian exploration venture, Teton Exploration Drilling Co. Pty. Ltd., to North Kalgurli for \$5.8 million. As part of the agreement, Teton will undertake general mineral exploration throughout Australia that UNC will fund jointly with North Kalgurli. Teton Australia is a wholly owned subsidiary of Teton Exploration Drilling Co., Inc., which in turn is a subsidiary of United Nuclear Corp., the operating company for UNC Resources.

US: Sunshine Mining Co. has said that three new drill holes completed by Sunshine on ground leased to it by Chief Consolidated Mining Co. in the East Tintic mining district of Utah encountered significant mineralization at depths between 1,500 and 1,600 ft beneath the surface, including 8 ft containing 12.8% lead, 4.1% zinc, 4.0 oz/st silver, and 0.07 oz/st gold; another hole with 41 ft of mineralization assayed 23.6% lead, 1.8% zinc and 19.8 oz/st silver and a trace of gold; and the third hole has 37 ft containing 13.8% lead, 3.4% zinc, 32.6 oz/st silver, and trace gold. According to Chief Mining, Sunshine intends to reopen the Apex No. 2 shaft on the property in preparation for further underground drilling as well as testing of ground and water conditions. The block Chief Mining leases includes the now-inactive Burgin mine, previously operated by Kennecott Corp. during the period 1966-1978.

US: Spearhead Energy Inc., of Casper, Wyo., has signed an exploration and option agreement with Texaco that will permit Texaco to purchase all or part of about 50,000 acres of uranium leases in Wyoming's Powder River Basin.

Australia: Utah Development Co. and Gold Copper Exploration Ltd. have entered into a joint venture to explore a tungsten-molybdenum prospect near Cairns in northern Queensland. The venture will test leases held by Gold Copper and a mining lease application by Utah for a 425-hectare area west southwest of Cairns. Gold Copper will be the operator of the venture and plans to undertake a major diamond drilling program. The area is to be assessed as a potential large-tonnage, low-grade deposit suitable for open-pit mining.

US: Operating plans for stepped-up exploration this summer in the platinum and palladium mineral zone of the Stillwater Complex in southern Montana are being reviewed by officials of the Custer and Gallatin National Forests.

Stillwater PGM Resources, a joint venture of Chevron USA Inc. and Johns-

(Continued on p 201)

(Continued from p 31)

Manville Sales Corp., is proposing construction of an exploratory adit at least 750 ft long, drilling of 25 more exploratory core holes, and construction of a 5-mi extension from a new US Forest Service road under construction. Johns-Manville has actively explored in the area since 1967. Operations accelerated after the company entered the agreement with Chevron.

In the same district, Dewey Whittaker, a Seattle independent operator, is proposing drilling 16 exploratory holes on his claims. The PGM and Whittaker operating plans are under review by the Forest Service's Big Timber District. Ranger John McCulloch said he has not completed study of the plans but "there does not seem to be anything in them that would significantly disturb any area."

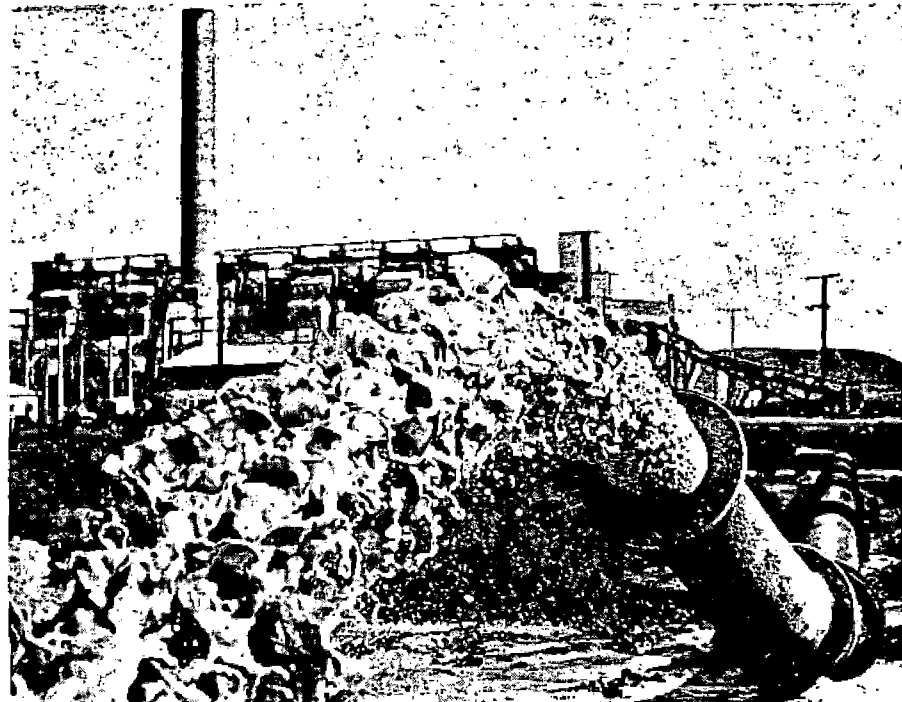
Anaconda Co., which is exploring in the Bear Tooth District of the Custer National Forest, is proposing to deepen by more than 2,000 ft an existing exploratory adit driven about 3,000 ft in the past two summer seasons. Anaconda is also proposing 20-24 exploratory drill holes.

PGM said it expects to reach a decision in early 1983 on whether to go ahead with a commercial development. In late April, the first public meeting was held in Big Timber to determine the scope of an Environmental Impact Statement to be prepared by the Forest Service and Montana state agencies during the next 18 months. PGM will contribute at least \$1 million toward the cost of the study. PGM officials said if a decision is made to go ahead with commercial development, it could be on the order of 1,000-3,000 st of ore milled per day. An operation of 2,000 st/d would produce 60 st of concentrate, which would be hauled to a smelter to be constructed at Big Timber.

Canada: Pearl Resources Ltd., a Vancouver, B.C., exploration and development company, plans a diamond drilling program to explore the potential of the Union Mine gold property near Franklin Camp, B.C. The property was leased last August from Hecla Mining Co. of Wallace, Ida. Hecla operated the property prior to 1935.

Yugoslavia: Government geologists have finished the first stage of exploration of accumulations of alluvial material near the bed of Timok River in eastern Serbia. The deposits are reported to have potential as a titanium-manganese ore.

India: The Indian government has launched an intensive five-year gold exploration program in the states of Karnataka, Andhra Pradesh, Bihar, Orissa, Kerala, and Maharashtra, to be jointly executed by the Geological Survey of



ABRESIST The Lining That LASTS!

Abresist . . . the hardest, most durable lining material ever developed to resist sliding abrasion. This is the time-tested conclusions of major industries throughout the world.

Abresist . . . far superior to metallic alloys in abrasion resistant qualities.

Abresist . . . no observable wear after 20 years' use in transporting fly ash in a German mine.

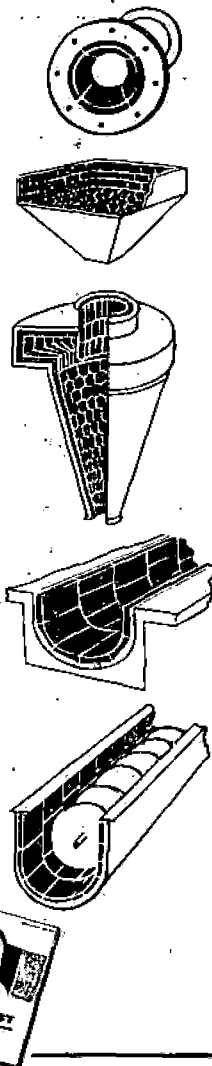
Uniformly adaptable to both hydraulic and pneumatic system, Abresist pipe systems come complete and ready to install.

Complete range of sizes and special fabrications—with bends, elbows, tees, reducers and branches—plus rotating flanges for easy alignment and connection.

Transports all types of abrasive materials—dust, coal, sand, tailings, slurries, grain, etc.—in sluices, flumes, cyclones, conveyors, bins, hoppers.

Historically outwears steel linings by a ratio of 6 to 1. Test applications and engineering assistance available.

Send for Abresist Bulletin AB-64

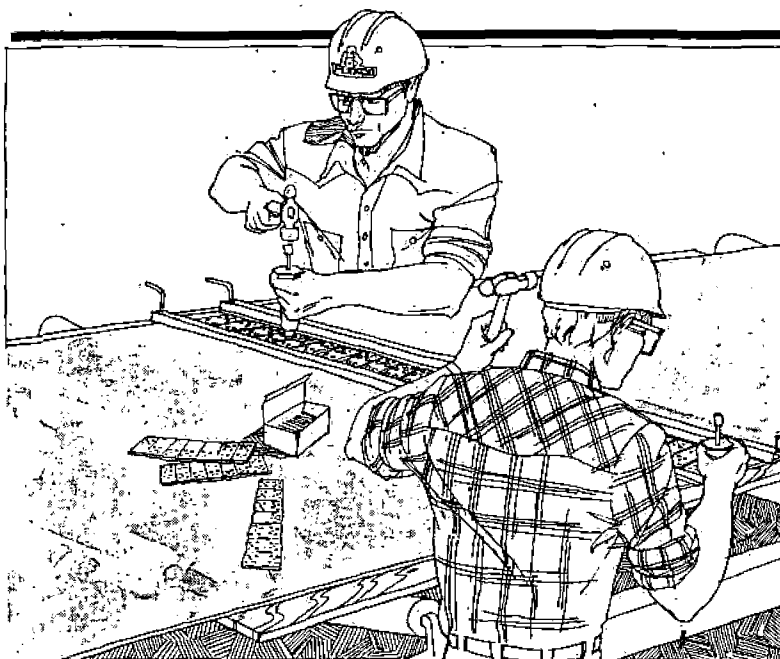


M.H. DETRICK CO.

20 NO. WACKER DRIVE, CHICAGO, ILL. 60606

Exclusive Licensee in the U.S. and Canada for ABRESIST, the International Answer to Sliding Abrasion
CIRCLE 123 ON READER SERVICE CARD

Now you can splice a 48-inch belt in less than an hour... with tough Flexco® rivet fasteners



Fast, easy belt splicing. That's what you need to minimize conveyor downtime. And that's what you get with the patented Flexco rivet system.

Flexco rivet fasteners are provided in strips. A portable tool holds belt and fasteners in proper alignment. Rivets are driven and set in one step. And a new "multiple rivet driver" lets you load 20, 40, or more rivets at once.

What's more—the staggered rivet pattern gives you greater holding power than any other belt fastener. And that means longer-lasting splices in high tension belting.

For information on both hinged and solid-plate Flexco rivet fasteners, write or call the address/phone below.

FLEXCO®

FLEXIBLE STEEL LACING CO.

2525 Wisconsin Ave., Downers Grove, IL 60515

Phone (312) 971-0150



**INDUSTRIAL
DISTRIBUTORS**

Belt fastening products
in stock at your local distributor.



EXPLORATION ROUNDUP

India (GSI) and Mineral Exploration Corp. (MEC). The program calls for drilling 44,300 m, exploratory mining of 5,460 m, analysis of 45,000 samples, and mapping.

The GSI, in coordination with Hutti Gold Mines (HGM), will explore the Manglur, Wandalli, and Toppaldoddi areas with integrated surveys. Exploratory mining by MEC is proposed at the Budhini block, explored earlier by GSI.

Another belt in Karnataka known as the Gadag belt will also be investigated by GSI, whose work will be followed up by exploratory mining and detailed drilling by MEC in the Hosur-Champion and Mysore Mines.

In the state of Andhra Pradesh, the Ramagiri Gold Mines closed since 1929, are now being reopened. GSI estimates 1.64 million mt of gold-bearing rock in the area. In the Chittoor district of Andhra Pradesh, south of the Anantapur district, some 0.3 million mt of gold-bearing rock with 5.5 gm/mt of gold have been identified.

US: Wendover Queen Mine Corp., a closely held private company based in Ogden, Utah, reports reserves of micro-fine gold and silver near Wendover, Nev. LeGrant E. Shreeve, president, said the assays show gold yields of 0.18-1.08 oz/st and silver yields of 0.51-7.82 oz/st. The assays are a low average of eight series of core drilling programs taken over the last 12 yrs on at least 2/3 of Wendover's 42 claims, which cover 840 acres. Shreeve said the deposit could total 3.5 million oz of gold and 14 million oz of silver.

Australia: Bridge Oil Ltd. has reported that uranium ore grades ranging between 1.08 and 3.96 lb of U₃O₈ per lt have been found in four drill holes on the Pandanus Creek uranium prospect in the Northern Territory. One of the samples also assayed 10 gm/mt gold and 1 gm/mt silver. The prospect covers an area of 68.5 km² and is close to the Queensland border, 400 km northwest of Mt. Isa.

Australia: Eastmet Ltd. and Aberfoyle Ltd. have discovered a significant sulphide tin deposit below the oxidized zone on their Doradilla prospect near Bourke, New South Wales. The oxidized zone extends to a depth of 80 m with grades up to 0.85% tin.

New Zealand: Amax Exploration (New Zealand) Inc. is manager of a joint venture with Mineral Resources (N.Z.) Ltd. and Green and McCahill Mining Ltd. and is maintaining an exploration program at Martha Hill, Waihi, North Island. Diamond drilling is in progress and earlier holes assay up to 37.0 gm/mt silver and 4.2 gm/mt gold. ■